

AFRL-RX-WP-TR-2020-0110

ADVANCED MATERIAL CHARACTERIZATION AND STRUCTURAL CERTIFICATION (AMCSC)

Volume 1 of 2

Waruna Seneviratne, John Tomblin, and Ruchira Walimunige
National Institute for Aviation Research (NIAR)
Wichita State University (WSU), Wichita, Kansas

17 December 2020
Final Report

DISTRIBUTION STATEMENT A.
Approved for public release: distribution is unlimited.

AIR FORCE RESEARCH LABORATORY
MATERIALS AND MANUFACTURING DIRECTORATE
WRIGHT-PATTERSON AIR FORCE BASE, OH 45433-7750
AIR FORCE MATERIEL COMMAND
UNITED STATES AIR FORCE

NOTICE AND SIGNATURE PAGE

Using Government drawings, specifications, or other data included in this document for any purpose other than Government procurement does not in any way obligate the U.S. Government. The fact that the Government formulated or supplied the drawings, specifications, or other data does not license the holder or any other person or corporation; or convey any rights or permission to manufacture, use, or sell any patented invention that may relate to them.

This report is the result of contracted fundamental research deemed exempt from public affairs security and policy review in accordance with SAF/AQR memorandum dated 10 Dec 08 and AFRL/CA policy clarification memorandum dated 16 Jan 09. This report is available to the general public, including foreign nationals.

Copies may be obtained from the Defense Technical Information Center (DTIC) (http://discover.dtic.mil).

AFRL-RX-WP-TR-2020-0110 HAS BEEN REVIEWED AND IS APPROVED FOR PUBLICATION IN ACCORDANCE WITH ASSIGNED DISTRIBUTION STATEMENT.

MOLLENHAUER.DAVID.H.1230181590
Digitally signed by MOLLENHAUER.DAVID.H.1230181590
Date: 2021.05.21 13:04:59 -04'00'

DAVID MOLLENHAUER
Program Manager
Composites Branch
Structural Materials Division
Materials and Manufacturing Directorate

ROGERS.BRET.ZACHARY.1265647924
Digitally signed by ROGERS.BRET.ZACHARY.1265647924
Date: 2021.05.21 17:56:52 -04'00'

BRET ROGERS
Section Chief
Composites Branch
Structural Materials Division
Materials and Manufacturing Directorate

This report is published in the interest of scientific and technical information exchange and its publication does not constitute the Government's approval or disapproval of its ideas or findings

REPORT DOCUMENTATION PAGE

Form Approved
OMB No. 0704-0188

The public reporting burden for this collection of information is estimated to average 1 hour per response, including the time for reviewing instructions, searching existing data sources, gathering and maintaining the data needed, and completing and reviewing the collection of information. Send comments regarding this burden estimate or any other aspect of this collection of information, including suggestions for reducing this burden, to Department of Defense, Washington Headquarters Services, Directorate for Information Operations and Reports (0704-0188), 1215 Jefferson Davis Highway, Suite 1204, Arlington, VA 22202-4302. Respondents should be aware that notwithstanding any other provision of law, no person shall be subject to any penalty for failing to comply with a collection of information if it does not display a currently valid OMB control number. **PLEASE DO NOT RETURN YOUR FORM TO THE ABOVE ADDRESS**.

1. REPORT DATE *(DD-MM-YY)*	2. REPORT TYPE	3. DATES COVERED *(From - To)*
17 December 2020	Final	23 January 2018 – 17 November 2020

4. TITLE AND SUBTITLE
Advanced Material Characterization & Structural Certification (AMCSC)
Volume 1 of 2

5a. CONTRACT NUMBER
FA8650-18-C-5289

5b. GRANT NUMBER

5c. PROGRAM ELEMENT NUMBER
62102F

6. AUTHOR(S)
Waruna Seneviratne, John Tomblin, and Ruchira Walimunige

5d. PROJECT NUMBER
4347

5e. TASK NUMBER

5f. WORK UNIT NUMBER
X1EJ

7. PERFORMING ORGANIZATION NAME(S) AND ADDRESS(ES)
National Institute for Aviation Research (NIAR)
Wichita State University
1845 Fairmount St
Wichita, KS 67260-0093

8. PERFORMING ORGANIZATION REPORT NUMBER

9. SPONSORING/MONITORING AGENCY NAME(S) AND ADDRESS(ES)
Air Force Research Laboratory
Materials and Manufacturing Directorate
Wright Patterson Air Force Base, OH 45433-7750
Air Force Materiel Command
United States Air Force

10. SPONSORING/MONITORING AGENCY ACRONYM(S)
AFRL/RXCC

11. SPONSORING/MONITORING AGENCY REPORT NUMBER(S)
AFRL-RX-WP-TR-2020-0110

12. DISTRIBUTION/AVAILABILITY STATEMENT
DISTRIBUTION STATEMENT A. Approved for public release: distribution is unlimited..

13. SUPPLEMENTARY NOTES
Volume 1 of 2. Report contains color.

14. ABSTRACT *(Maximum 200 words)*
Fatigue evaluation and progressive damage growth inspections using X-ray computed tomography (CT) for IM7/5302-1 UNI, IM7/5250-4 UNI, and T650/5320-1 8HS fabric material systems were carried out. Open-hole (OH), interlaminar tension (ILT), double-notch shear (DNS), and short-beam shear (SBS) failure modes were selected for the test program. Tension-tension open-hole fatigue specimens indicated all runouts, even at stress levels (SLs) as high as 90 percent of quasi-static strength. Higher SLs indicated significant amounts of delamination, but minimal damages were noted (microcracks around the hole) for SLs less than or equal to 80 percent. Typical operational conditions for aircraft are significantly less than these SLs, thus tension-tension fatigue is not a concern. Only the ILT failure mode for all three material systems indicated relatively low values of shape parameters, indicating a higher data scatter than the other failure modes investigated in this study. This is primarily due to sensitivity of this failure mode to manufacturing defects in the curved portion of test specimens. The load-enhancement factors (LEFs) calculated for these materials indicate significant reduction due to the improvement in materials and processes.

15. SUBJECT TERMS
Fatigue of composites, X-ray CT inspections, load-enhancement factor, LEF

16. SECURITY CLASSIFICATION OF:			17. LIMITATION OF ABSTRACT:	18. NUMBER OF PAGES	19a. NAME OF RESPONSIBLE PERSON (Monitor)
a. REPORT	b. ABSTRACT	c. THIS PAGE			David Mollenhauer
Unclassified	Unclassified	Unclassified	SAR	392	19b. TELEPHONE NUMBER *(Include Area Code)* (937) 904-4394

TABLE OF CONTENTS

Section **Page**

LIST OF FIGURES ..... **iii**

LIST OF TABLES ..... **xiv**

1. INTRODUCTION **1**
1.1 Advanced Material Characterization 2
1.2 Durability and Damage Tolerance Test Substantiation 7
1.3 Certification Testing of Hybrid Structures 8
1.4 Characterization of Progressive Damage Growth of Composites 9

2. CERTIFICATION TESTING OF COMPOSITE STRUCTURES **11**
2.1 Reliability (Scatter) Analysis for Fatigue Life Determination 11
2.2 Life Factor Approach 12
2.3 Load-Enhancement Factor Approach 15
2.4 Certification Testing of Composite-Metal Hybrid Structures 20
2.5 Multi-LEF Approach 25
2.6 Deferred Severity Spectrum 28

3. COMPOSITE DATA ANALYSIS **36**
3.1 Individual Weibull Method 37
3.2 Joint Weibull Method 38
3.3 Sendeckyj Equivalent Wearout Model 39
3.4 Scatter Analysis Software 40

4. EXPERIMENTAL PROCEDURES **44**
4.1 Panel Fabrication 45
4.2 Test Matrices 51
4.2.1 Open-Hole Tension/Open-Hole Compression Testing 51
4.2.2 Interlaminar Tension Testing 55
4.2.3 Double-Notch Shear Testing 56
4.2.4 Short-Beam Shear Testing 57

5. STATIC TEST DATA ANALYSIS **58**
5.1 Solvay 5320-1/ IM7 Unidirectional Tape 58
5.2 Solvay 5320-1/ T650 8-Harness Satin Weave Fabric 59
5.3 Solvay 5250-4 (BMI)/ IM7 Unidirectional Tape 59
5.4 Summary 60

DISTRIBUTION STATEMENT A
Approved for public release: distribution is unlimited.

6. FATIGUE TEST DATA ANALYSIS 62
6.1 Solvay 5320-1/ IM7 Unidirectional Tape 62
6.1.1 IM7/5320-1 UNI Open-Hole Compression/Tension 62
6.1.2 IM7/5320-1 UNI Double-Notch Shear 69
6.1.3 IM7/5320-1 UNI Interlaminar Tension 71
6.1.4 IM7/5320-1 UNI Short Beam Shear 72
6.2 Solvay 5320-1/ T650 8-Harness Satin fabric 75
6.2.1 T650/5320-1 8HS Open-Hole Compression/Tension 75
6.2.2 T650/5320-1 8HS Double-Notch Shear 81
6.2.3 T650/5320-1 8HS Interlaminar Tension 82
6.2.4 T650/5320-1 8HS Short Beam Shear 82
6.3 Solvay 5250-4 (BMI)/ IM7 Unidirectional Tape 85
6.3.1 IM7/5250-4 UNI Open-Hole Compression/Tension 85
6.3.2 IM7/5250-4 UNI Double-Notch Shear 91
6.3.3 IM7/5250-4 UNI Interlaminar Tension 92
6.3.4 IM7/5250-4 UNI Short Beam Shear 92
6.4 Load-Enhancement Factor 95
7. COMPOSITE DEFECTS AND FAILURE ANALYSIS 99
7.1 Post-Processing of X-ray Computed Tomography Data 103
7.2 Investigation of Resin-Rich Areas 105
7.3 Visible Fiber Gaps 107
7.4 Interlaminar-Tension Specimen Quality 108
7.5 Effects of Extended Post-Cure 114
7.6 Damage Growth under Open-Hole Tension-Tension Fatigue 122
7.6.1 IM7/5320-1 UNI OHT-T 122
7.6.2 IM7/5250-4 OHT-T 130
7.6.3 T650/5320-1 OHT-T 136
8. CONCLUSIONS 141
9. REFERENCES 144
APPENDIX A - S/N DATA AND SENDECKYJ ANALYSIS 147
APPENDIX B - PROGRESSIVE DAMAGE GROWTH 221
LIST OF SYMBOLS, ABBREVIATIONS, AND ACRONYMS 372

DISTRIBUTION STATEMENT A
Approved for public release: distribution is unlimited.

LIST OF FIGURES

Figure **Page**

Figure 1. Composite and metal fatigue behavior [1]. 1
Figure 2. Material characterization time and cost [3]. 3
Figure 3. Effects of sample size on design allowables. 4
Figure 4. B-basis allowable generation. 5
Figure 5. Example of probability density functions of constituent property for multiple batches of materials tested over several years of production runs. 6
Figure 6. Comparison of LEFs developed for historical and modern materials. 8
Figure 7. Progressive damage growth of IM7/5320-1 24-ply quasi-isotropic open-hole specimen (R = 0.1) monitored across one million cycles [14]. 10
Figure 8. Life factor approach. 13
Figure 9. Influence of fatigue life shape parameter on B-basis life factor. 14
Figure 10. Derivation and application of life and load-enhancement factors through scatter analysis of composite test data 17
Figure 11. Influence of strength and life parameter on LEF 18
Figure 12. Influence of MSSP and MLSP on LEF (combined load-life approach). 18
Figure 13. Combined load-life approach for composite structures 19
Figure 14. Composite-metal fatigue data [10]. 20
Figure 15. Failure modes for single-shear double-fastener hybrid joint. 21
Figure 16. Fatigue SN data for metal single-shear double-fastener hybrid joint. 22
Figure 17. Spectrum fatigue test results for F/A-18 wing-root stepped lap joint [12] 22
Figure 18. Failure modes for TDFS [12]. 23
Figure 19. Composite and metal spectrum requirements 24
Figure 20. Multi-LEF approach for hybrid structures. 26
Figure 21. Comparison of application of combined load-life approach for hybrid structures (assume $N_F = 5$). 27
Figure 22. Multi-LEF example for hybrid structures 28
Figure 23. Full-scale test substantiation using deferred severity spectrum approach [18]. 29
Figure 24. Illustration of hybrid spectrum development for deferred severity spectrum approach (assume $N_F = 5$). 32
Figure 25. Fiber failure of spectrum loading near endurance limit [20]. 34
Figure 26. Certification of composite-metal hybrid structures using deferred severity spectrum. 35
Figure 27. Scatter analysis using Weibull distribution of shape parameters. 37
Figure 28. Example of Sendeckyj curve fit. 40
Figure 29. Scatter analysis software module. 41
Figure 30. Process for obtaining fatigue life shape parameters for individual test configuration. 42
Figure 31. Process for generating static strength and fatigue life shape parameters. 43
Figure 32. Specimen selection for evaluating batch variability in static and fatigue tests. 44
Figure 33. Cure cycle for 5320-1. 47
Figure 34. Cure cycle for 5250-4. 48
Figure 35. Viscoelastic properties for T650/5320-1. 50
Figure 36. OHT test setup with extensometer. 51
Figure 37. OHC test setup with extensometers. 54
Figure 38. OHC fixture preparation for fatigue test. 55

DISTRIBUTION STATEMENT A
Approved for public release: distribution is unlimited.

Figure 39. ILT test setup with deflectometer and microscope. 56
Figure 40. Double-notch shear test specimen configuration. 57
Figure 41. SBS test setup with microscope. 57
Figure 42. Summary of shape parameters for quasi-static data. 61
Figure 43. Sendeckjy analysis prediction for IM7/5320-1 UNI, OHC, 10/80/10, R = 5. 63
Figure 44. Summary of shape parameters for IM7/5320-1 UNI SN data. 64
Figure 45. Comparison of quasi-static strength and pooled Sendeckyj equivalent strength for IM7/5320-1 UNI material system. 65
Figure 46. IM7/5320-1 UNI, OH, 50/40/10 fatigue data—measured. 66
Figure 47. IM7/5320-1 UNI, OH, 50/40/10 fatigue data—normalized. 67
Figure 48. IM7/5320-1 UNI, OH, 25/50/25 fatigue data—measured. 67
Figure 49. IM7/5320-1 UNI, OH, 25/50/25 fatigue data—normalized. 68
Figure 50. IM7/5320-1 UNI, OH, 10/80/10 fatigue data—measured. 68
Figure 51. IM7/5320-1 UNI, OH, 10/80/10 fatigue data—normalized. 69
Figure 52. IM7/5320-1 UNI, DNS fatigue data—measured. 70
Figure 53. IM7/5320-1 UNI, DNS fatigue data—normalized. 70
Figure 54. IM7/5320-1 UNI, ILT fatigue data—measured. 71
Figure 55. IM7/5320-1 UNI, ILT fatigue data—normalized. 72
Figure 56. IM7/5320-1 UNI, 100/0/0, SBS, fatigue data. 73
Figure 57. Comparison between DNS and SBS for IM7/5320-1 UNI data—normalized. 73
Figure 58. Representative SBS failure modes for IM7/5320-1 UNI, 100/0/0. 74
Figure 59. Representative DNS failure modes for IM7/5320-1 UNI, 10/80/10 and 50/40/10. 74
Figure 60. Summary of shape parameters for T650/5320-1 8HS SN data. 76
Figure 61. Comparison of quasi-static strength and pooled Sendeckyj equivalent strength for T650/5320-1 8HS. 77
Figure 62. T650/5320-1 8HS, OH, 40/20/40 fatigue data—measured. 78
Figure 63. T650/5320-1 8HS, OH, 40/20/40 fatigue data—normalized. 78
Figure 64. T650/5320-1 8HS, OH, 25/50/25 fatigue data—measured. 79
Figure 65. T650/5320-1 8HS, OH, 25/50/25 fatigue data—normalized. 79
Figure 66. T650/5320-1 8HS, OH, 10/80/10 fatigue data—measured. 80
Figure 67. T650/5320-1 8HS, OH, 10/80/10 fatigue data—normalized. 80
Figure 68. T650/5320-1 8HS, DNS fatigue data—measured. 81
Figure 69. T650/5320-1 8HS, DNS fatigue data—normalized. 82
Figure 70. T650/5320-1 8HS, ILT fatigue data—measured. 83
Figure 71. T650/5320-1 8HS, ILT fatigue data—normalized. 83
Figure 72. T650/5320-1 8HS, 100/0/0, SBS, fatigue data. 84
Figure 73. Comparison between DNS and SBS for T650/5320-1 8HS data—normalized. 84
Figure 74. Summary of shape parameters for IM7/5250-4 UNI SN data. 86
Figure 75. Comparison of quasi-static strength and pooled Sendeckyj equivalent strength for IM7/5250-4 UNI. 87
Figure 76. IM7/5250-4 UNI, OH, 50/40/10 fatigue data—measured. 88
Figure 77. IM7/5250-4 UNI, OH, 50/40/10 fatigue data—normalized. 88
Figure 78. IM7/5250-4 UNI, OH, 25/50/25 fatigue data—measured. 89
Figure 79. IM7/5250-4 UNI, OH, 25/50/25 fatigue data—normalized. 89
Figure 80. IM7/5250-4 UNI, OH, 10/80/10 fatigue data—measured. 90
Figure 81. IM7/5250-4 UNI, OH, 10/80/10 fatigue data—normalized. 90

DISTRIBUTION STATEMENT A
Approved for public release: distribution is unlimited.

Figure 82. IM7/5250-4 UNI, DNS fatigue data—measured. 91
Figure 83. IM7/5250-4 UNI, DNS fatigue data—normalized. 92
Figure 84. IM7/5250-4 UNI, ILT fatigue data—measured. 93
Figure 85. IM7/5250-4 UNI, ILT fatigue data—normalized. 93
Figure 86. IM7/5250-4 UNI, 100/0/0, SBS, fatigue data. 94
Figure 87. Comparison between DNS and SBS for IM7/5250-4 UNI data—normalized. 94
Figure 88. LEF curves for various scatter analysis methods of SN data. 98
Figure 89. Ply-by-ply XCT damage progression data for IM7/5250-4 UNI, 50/40/10 layup, OHT, R = 0.1. 101
Figure 90. Damage area percent increase for IM7/5250-4 UNI, 50/40/10 layup, OHT, R = 0.1. 102
Figure 91. Ply-by-ply scan for IM7/5250-4 UNI, 50/40/10 layup, OHT, R = 0.1. 103
Figure 92. (a) Histogram adjustment and (b) line profile evaluation for thresholding. 104
Figure 93. a) Cropped volume with filtering applied and (b) demonstration of Microsoft Excel spreadsheet documenting slice-to-ply correlations for each inspection interval. 104
Figure 94 – Interface for viewing processed data through in-house software. 105
Figure 95. Resin-rich areas observed in XCT scans of OH UNI specimens. 106
Figure 96. Photomicrographs of resin-rich areas in IM7/5320-1 UNI. 106
Figure 97. Inspections of gaps in IM7/5250-4 UNI. 107
Figure 98. Representative porosity levels in IM7/5250-4 UNI. 110
Figure 99. Representative porosity levels in IM7/5320-1 UNI. 110
Figure 100. Representative porosity levels in T650/5320-1 8HS. 111
Figure 101. (a) pre-test manufacturing defects and (b) post-test damage overlay along critical void locations. 111
Figure 102. Example of quantifying of critical void location(s). 112
Figure 103. IM7/5320-1 UNI, 50/40/10, ILT fatigue data with XCT. 113
Figure 104. IM7/5320-1 UNI 100-hour EPC for (a) flat panels and (b) curved panels. 114
Figure 105. IM7/5250-4 UNI 100-hour EPC for (a) flat panels and (b) curved panels. 115
Figure 106. Thermal analysis of EPC for IM7/5320-1 UNI. 116
Figure 107. Baseline and EPC SN data for IM7/5320-1 UNI, R = 5, OHC-C. 118
Figure 108. Baseline and EPC SN data for IM7/5320-1 UNI OH. 118
Figure 109. Baseline and EPC SN data for IM7/5250-4 UNI OHC. 119
Figure 110. Baseline and EPC SN data for IM7/5320-1 UNI DNS. 120
Figure 111. Baseline and EPC SN data for IM7/5250-4 UNI DNS. 120
Figure 112. Baseline and EPC SN data for IM7/5320-1 UNI ILT. 121
Figure 113. Baseline and extended post-cure SN data for IM7/5250-4 UNI ILT. 121
Figure 114. OHT-T SN data for IM7/5320-1 UNI, 50/40/10. 122
Figure 115. OHT-T stiffness degradation (normalized) for IM7/5320-1 UNI, 50/40/10. 123
Figure 116. OHT-T residual strength increase for IM7/5320-1 UNI, 50/40/10. 124
Figure 117. XCT damage indications near hole for IM7/5320-1 UNI, 50/40/10. 124
Figure 118. OHT-T fatigue damage increase for IM7/5320-1 UNI, 50/40/10, SL4. 125
Figure 119. Fiber splitting in 0° ply and delaminations near off-axes plies. 125
Figure 120. Simple laminate sizing chart [37]. 127
Figure 121. OHT-T SN data for IM7/5320-1 UNI, 25/50/25. 127
Figure 122. OHT-T stiffness degradation (normalized) for IM7/5320-1 uni, 25/50/25. 128
Figure 123. OHT-T residual strength increase for IM7/5320-1 uni, 25/50/25. 129

DISTRIBUTION STATEMENT A
Approved for public release: distribution is unlimited.

Figure 124. XCT damage indications near hole for IM7/5320-1 UNI, 25/50/25 OHT-T. 129
Figure 125. OHT-T fatigue damage increase for IM7/5320-1 UNI, 25/50/25, SL4. 129
Figure 126. OHT-T SN data for IM7/5250-4 UNI, 50/40/10. 130
Figure 127. OHT-T stiffness degradation (normalized) for IM7/5250-4 UNI, 50/40/10. 131
Figure 128. OHT-T residual strength increase for IM7/5250-4 UNI, 50/40/10. 131
Figure 129. XCT damage indications near hole for IM7/5250-4 UNI, 50/40/10 OHT-T. 132
Figure 130. OHT-T fatigue damage increase for IM7/5250-4 UNI, 50/40/10, SL3. 133
Figure 131. OHT-T SN data for IM7/5250-4 UNI, 25/50/25. 134
Figure 132. OHT-T stiffness degradation (normalized) for IM7/5250-4 UNI, 25/50/25. 134
Figure 133. OHT-T residual strength increase for IM7/5250-4 uni, 25/50/25. 135
Figure 134. XCT damage indications near hole for IM7/5320-1 UNI, 25/50/25 OHT-T. 135
Figure 135. OHT-T fatigue damage increase for IM7/5250-4 UNI, 25/50/25, SL3. 135
Figure 136. OHT-T SN data for T650/5320-1 8HS, 40/20/40. 136
Figure 137. OHT-T stiffness degradation (normalized) for T650/5320-1 8HS, 40/20/40. 137
Figure 138. OHT-T residual strength increase for T650/5320-1 8HS, 40/20/40..... 137
Figure 139. XCT damage indications near hole for T650/5320-1 8HS, 40/20/40 OHT-T. 138
Figure 140. OHT-T SN data for T650/5320-1 8HS, 25/50/25. 138
Figure 141. OHT-T stiffness degradation (normalized) for T650/5320-1 8HS, 25/50/25. 139
Figure 142. OHT-T residual strength increase for T650/5320-1 8HS, 25/50/25..... 139
Figure 143. XCT damage indications near hole for T650/5320-1 8HS, 25/50/25 OHT-T. 140

Figure A.1 – SN data for IM7/5320-1, 50/40/10, R=0.1, OHT-T. 148
Figure A.2 – SN data with Sendeckyj fitting model for IM7/5320-1, 50/40/10, R=5, OHC-C. 150
Figure A.3 – SN data with Sendeckyj fitting model for IM7/5320-1, 50/40/10, R=-1, OHC-T. 152
Figure A.4 – SN data for IM7/5320-1, 25/50/25, R=0.1, OHT-T. 154
Figure A.5 – SN data with Sendeckyj fitting model for IM7/5320-1, 25/50/25, R=5, OHC-C. 156
Figure A.6 – SN data with Sendeckyj fitting model for IM7/5320-1, 25/50/25, R=-1, OHC-T. 158
Figure A.7 – SN data with Sendeckyj fitting model for IM7/5320-1, 10/80/10, R=0.1, OHT-T. 160
Figure A.8 – SN data with Sendeckyj fitting model for IM7/5320-1, 10/80/10, R=5, OHC-C. 162
Figure A.9 – SN data with Sendeckyj fitting model for IM7/5320-1, 10/80/10, R=-1, OHC-T. 164
Figure A.10 – SN data with Sendeckyj fitting model for IM7/5320-1, 50/40/10, R=0.1, DNS. 166
Figure A.11 – SN data with Sendeckyj fitting model for IM7/5320-1, 10/80/10, R=0.1, DNS. 168
Figure A.12 – SN data with Sendeckyj fitting model for IM7/5320-1, 50/40/10, R=0.1, ILT. . 170
Figure A.13 – SN data with Sendeckyj fitting model for IM7/5320-1, 10/80/10, R=0.1, ILT. . 172
Figure A.14 – SN data with Sendeckyj fitting model for IM7/5320-1, 100/0/0, R=0.1, SBS.... 174
Figure A.15 – SN data for T650/5320-1, 40/20/40, R=0.1, OHT-T. 176
Figure A.16 – SN data with Sendeckyj fitting model for T650/5320-1, 40/20/40, R=5, OHC-C. 178
Figure A.17 – SN data with Sendeckyj fitting model for T650/5320-1, 40/20/40, R=-1, OHC-T. 180
Figure A.18 – SN data for T650/5320-1, 25/50/25, R=0.1, OHT-T. 181
Figure A.19 – SN data with Sendeckyj fitting model for T650/5320-1, 25/50/25, R=5, OHC-C. 183

DISTRIBUTION STATEMENT A
Approved for public release: distribution is unlimited.

Figure A.20 – SN data with Sendeckyj fitting model for T650/5320-1, 25/50/25, R=-1, OHC-T. 184
Figure A.21 – SN data with Sendeckyj fitting model for T650/5320-1, 10/80/10, R=0.1, OHT-T. 186
Figure A.22 – SN data with Sendeckyj fitting model for T650/5320-1, 10/80/10, R=5, OHC-C. 188
Figure A.23 – SN data and Sendeckyj fitting model for T650/5320-1, 10/80/10, R=-1, OHC-T. 190
Figure A.24 – SN data with Sendeckyj fitting model for T650/5320-1, 40/20/40, R=0.1, DNS. 192
Figure A.25 – SN data with Sendeckyj fitting model for T650/5320-1, 10/80/10, R=0.1, DNS. 194
Figure A.26 – SN data with Sendeckyj fitting model for T650/5320-1, 40/20/40, R=0.1, ILT. 196
Figure A.27 – SN data with Sendeckyj fitting model for T650/5320-1, 10/80/10, R=0.1, ILT. 198
Figure A.28 – SN data with Sendeckyj fitting model for T650/5320-1, 100/0/0, R=0.1, SBS. . 200
Figure A.29 – SN data for IM7/5250-4, 50/40/10, R=0.1, OHT-T. 201
Figure A.30 – SN data with Sendeckyj fitting model for IM7/5250-4, 50/40/10, R=5, OHC-C. 203
Figure A.31 – SN data with Sendeckyj fitting model for IM7/5250-4, 50/40/10, R=-1, OHC-T. 205
Figure A.32 – SN data with Sendeckyj fitting model for IM7/5250-4, 25/50/25, R=0.1, OHT-T. 206
Figure A.33 – SN data with Sendeckyj fitting model for IM7/5250-4, 25/50/25, R=5, OHC-C. 208
Figure A.34 – SN data with Sendeckyj fitting model for IM7/5250-4, 25/50/25, R=-1, OHC-T. 209
Figure A.35 – SN data with Sendeckyj fitting model for IM7/5250-4, 10/80/10, R=0.1, OHT-T. 210
Figure A.36 – SN data with Sendeckyj fitting model for IM7/5250-4, 10/80/10, R=5, OHC-C. 211
Figure A.37 – SN data with Sendeckyj fitting model for IM7/5250-4, 10/80/10, R=-1, OHC-T. 212
Figure A.38 – SN data with Sendeckyj fitting model for IM7/5250-4, 50/40/10, R=0.1, DNS. 214
Figure A.39 – SN data with Sendeckyj fitting model for IM7/5250-4, 10/80/10, R=0.1, DNS. 216
Figure A.40 – SN data with Sendeckyj fitting model for IM7/5250-4, 50/40/10, R=0.1, ILT. . 217
Figure A.41 – SN data with Sendeckyj fitting model for IM7/5250-4, 10/80/10, R=0.1, ILT. . 219
Figure A.42 – SN data with Sendeckyj fitting model for IM7/5250-4, 100/0/0, R=0.1, SBS.... 220

Figure B.1 – Ply-by-ply damage growth and area increase for IM7/5320-1, 50/40/10, R=0.1, SL1. 223
Figure B.2 – Ply-by-ply damage growth and area increase for IM7/5320-1, 50/40/10, R=0.1, SL2. 224
Figure B.3 – Ply-by-ply damage growth and area increase for IM7/5320-1, 50/40/10, R=0.1, SL3. 226

DISTRIBUTION STATEMENT A
Approved for public release: distribution is unlimited.

Figure B.4 – Apparent stiffness change during fatigue (normalized by initial compliance) for IM7/5320-1 UNI, 50/40/10 layup, OHT-T, R=0.1. 227
Figure B.5 – Ply-by-ply damage growth and area increase for IM7/5320-1, 50/40/10, R=5, SL1. 228
Figure B.6 – Ply-by-ply damage growth and area increase for IM7/5320-1, 50/40/10, R=5, SL2. 229
Figure B.7 – Ply-by-ply damage growth and area increase for IM7/5320-1, 50/40/10, R=5, SL3. 230
Figure B.8 – Apparent stiffness change during fatigue (normalized by initial compliance) for IM7/5320-1 UNI, 50/40/10 layup, OHC-C, R=5..... 232
Figure B.9 – Ply-by-ply damage growth and area increase for IM7/5320-1, 50/40/10, R=-1, SL1. 233
Figure B.10 – Ply-by-ply damage growth and area increase for IM7/5320-1, 50/40/10, R=-1, SL2. 234
Figure B.11 – Ply-by-ply damage growth and area increase for IM7/5320-1, 50/40/10, R=-1, SL3. 235
Figure B.12 – Apparent stiffness change during the tension fatigue (normalized by initial compliance) for IM7/5320-1 UNI, 50/40/10 layup, OHC-T, R=-1. 236
Figure B.13 – Apparent stiffness change during the compression fatigue (normalized by initial compliance) for IM7/5320-1 UNI, 50/40/10 layup, OHC-T, R=-1. 236
Figure B.14 – Ply-by-ply damage growth and area increase for IM7/5320-1, 25/50/25, R=0.1, SL1. 238
Figure B.15 – Ply-by-ply damage growth and area increase for IM7/5320-1, 25/50/25, R=0.1, SL2. 239
Figure B.16 – Ply-by-ply damage growth and area increase for IM7/5320-1, 25/50/25, R=0.1, SL3. 240
Figure B.17 – Apparent stiffness change during fatigue (normalized by initial compliance) for IM7/5320-1 UNI, 25/50/25 layup, OHT-T, R=0.1. 242
Figure B.18 – Ply-by-ply damage growth and area increase for IM7/5320-1, 25/50/25, R=5, SL1. 243
Figure B.19 – Ply-by-ply damage growth and area increase for IM7/5320-1, 25/50/25, R=5, SL2. 244
Figure B.20 – Ply-by-ply damage growth and area increase for IM7/5320-1, 25/50/25, R=5, SL3. 245
Figure B.21 – Apparent stiffness change during fatigue (normalized by initial compliance) for IM7/5320-1 UNI, 25/50/25 layup, OHC-C, R=5..... 246
Figure B.22 – Ply-by-ply damage growth and area increase for IM7/5320-1, 25/50/25, R=-1, SL1. 247
Figure B.23 – Ply-by-ply damage growth and area increase for IM7/5320-1, 25/50/25, R=-1, SL2. 248
Figure B.24 – Ply-by-ply damage growth and area increase for IM7/5320-1, 25/50/25, R=-1, SL3. 249
Figure B.25 – Apparent stiffness change during the tension fatigue (normalized by initial compliance) for IM7/5320-1 UNI, 25/50/25 layup, OHC-T, R= -1. 250
Figure B.26 – Apparent stiffness change during the compression fatigue (normalized by initial compliance) for IM7/5320-1 UNI, 25/50/25 layup, OHC-T, R= -1. 250

DISTRIBUTION STATEMENT A
Approved for public release: distribution is unlimited.

Figure B.27 – Ply-by-ply damage growth and area increase for IM7/5320-1, 10/80/10, R=0.1, SL1. 252
Figure B.28 – Ply-by-ply damage growth and area increase for IM7/5320-1, 10/80/10, R=0.1, SL2. 253
Figure B.29 – Ply-by-ply damage growth and area increase for IM7/5320-1, 10/80/10, R=0.1, SL3. 254
Figure B.30 – Apparent stiffness change during fatigue (normalized by initial compliance) for IM7/5320-1 UNI, 10/80/10 layup, OHT-T, R=0.1. 255
Figure B.31 – Ply-by-ply damage growth and area increase for IM7/5320-1, 10/80/10, R=5, SL1. 256
Figure B.32 – Ply-by-ply damage growth and area increase for IM7/5320-1, 10/80/10, R=5, SL2. 257
Figure B.33 – Ply-by-ply damage growth and area increase for IM7/5320-1, 10/80/10, R=5, SL3. 258
Figure B.34 – Apparent stiffness change during fatigue (normalized by initial compliance) for IM7/5320-1 UNI, 10/80/10 layup, OHC-C, R=5. 260
Figure B.35 – Ply-by-ply damage growth and area increase for IM7/5320-1, 10/80/10, R=-1, SL1. 261
Figure B.36 – Ply-by-ply damage growth and area increase for IM7/5320-1, 10/80/10, R=-1, SL2. 262
Figure B.37 – Ply-by-ply damage growth and area increase for IM7/5320-1, 10/80/10, R=-1, SL3. 263
Figure B.38 – Apparent stiffness change during the tension fatigue (normalized by initial compliance) for IM7/5320-1 UNI, 10/80/10 layup, OHC-T, R= -1. 264
Figure B.39 – Apparent stiffness change during the compression fatigue (normalized by initial compliance) for IM7/5320-1 UNI, 10/80/10 layup, OHC-T, R= -1. 264
Figure B.40 – Shear gauge damage growth and area increase for IM7/5320-1, 50/40/10, R=0.1, SL1. 266
Figure B.41 – Shear gauge damage growth and area increase for IM7/5320-1, 50/40/10, R=0.1, SL2. 267
Figure B.42 – Shear gauge damage growth and area increase for IM7/5320-1, 50/40/10, R=0.1, SL3. 268
Figure B.43 – Apparent stiffness change during fatigue (normalized by initial compliance) for IM7/5320-1 UNI, 50/40/10 layup, DNS, R=0.1. 269
Figure B.44 – Shear gauge damage growth and area increase for IM7/5320-1, 10/80/10, R=0.1, SL1. 270
Figure B.45 – Shear gauge damage growth and area increase for IM7/5320-1, 10/80/10, R=0.1, SL2. 271
Figure B.46 – Shear gauge damage growth and area increase for IM7/5320-1, 10/80/10, R=0.1, SL3. 272
Figure B.47 – Apparent stiffness change during fatigue (normalized by initial compliance) for IM7/5320-1 UNI, 10/80/10 layup, DNS, R=0.1. 273
Figure B.48 – Ply-by-ply damage growth and area increase for T650/5320-1, 40/20/40, R=0.1, SL1. 275
Figure B.49 – Ply-by-ply damage growth and area increase for T650/5320-1, 40/20/40, R=0.1, SL2. 276

DISTRIBUTION STATEMENT A
Approved for public release: distribution is unlimited.

Figure B.50 – Ply-by-ply damage growth and area increase for T650/5320-1, 40/20/40, R=0.1, SL3. 277
Figure B.51 – Apparent stiffness change during fatigue (normalized by initial compliance) for T650/5320-1 8HS, 40/20/40 layup, OHT-T, R=0.1. 278
Figure B.52 – Ply-by-ply damage growth and area increase for T650/5320-1, 40/20/40, R=5, SL1. 279
Figure B.53 – Ply-by-ply damage growth and area increase for T650/5320-1, 40/20/40, R=5, SL2. 280
Figure B.54 – Ply-by-ply damage growth and area increase for T650/5320-1, 40/20/40, R=5, SL3. 281
Figure B.55 – Apparent stiffness change during fatigue (normalized by initial compliance) for T650/5320-1 8HS, 40/20/40 layup, OHC-C, R=5. 282
Figure B.56 – Ply-by-ply damage growth and area increase for T650/5320-1, 40/20/40, R=-1, SL1. 283
Figure B.57 – Ply-by-ply damage growth and area increase for T650/5320-1, 40/20/40, R=-1, SL2. 284
Figure B.58 – Ply-by-ply damage growth and area increase for T650/5320-1, 40/20/40, R=-1, SL3. 285
Figure B.59 – Apparent stiffness change during the tension fatigue (normalized by initial compliance) for T650/5320-1 8HS, 40/20/40 layup, OHC-T, R=-1..... 287
Figure B.60 – Apparent stiffness change during the compression fatigue (normalized by initial compliance) for T650/5320-1 8HS, 40/20/40 layup, OHC-T, R=-1..... 287
Figure B.61 – Ply-by-ply damage growth and area increase for T650/5320-1, 25/50/25, R=0.1, SL1. 289
Figure B.62 – Ply-by-ply damage growth and area increase for T650/5320-1, 25/50/25, R=0.1, SL2. 290
Figure B.63 – Ply-by-ply damage growth and area increase for T650/5320-1, 25/50/25, R=0.1, SL3. 291
Figure B.64 – Apparent stiffness change during fatigue (normalized by initial compliance) for T650/5320-1 8HS, 25/50/25 layup, OH, R=0.1. 292
Figure B.65 – Ply-by-ply damage growth and area increase for T650/5320-1, 25/50/25, R=5, SL1. 293
Figure B.66 – Ply-by-ply damage growth and area increase for T650/5320-1, 25/50/25, R=5, SL2. 294
Figure B.67 – Ply-by-ply damage growth and area increase for T650/5320-1, 25/50/25, R=5, SL3. 295
Figure B.68 – Apparent stiffness change during fatigue (normalized by initial compliance) for T650/5320-1 8HS, 25/50/25 layup, OHC-C, R=5. 296
Figure B.69 – Ply-by-ply damage growth and area increase for T650/5320-1, 25/50/25, R=-1, SL1. 297
Figure B.70 – Ply-by-ply damage growth and area increase for T650/5320-1, 25/50/25, R=-1, SL2. 298
Figure B.71 – Ply-by-ply damage growth and area increase for T650/5320-1, 25/50/25, R=-1, SL3. 299
Figure B.72 – Apparent stiffness change during the tension fatigue (normalized by initial compliance) for T650/5320-1 8HS, 25/50/25 layup, OHC-T, R=-1..... 300

DISTRIBUTION STATEMENT A
Approved for public release: distribution is unlimited.

Figure B.73 – Apparent stiffness change during the compression fatigue (normalized by initial compliance) for T650/5320-1 8HS, 25/50/25 layup, OHC-T, R=-1..... 300
Figure B.74 – Ply-by-ply damage growth and area increase for T650/5320-1, 10/80/10, R=0.1, SL1..... 302
Figure B.75 – Ply-by-ply damage growth and area increase for T650/5320-1, 10/80/10, R=0.1, SL2..... 303
Figure B.76 – Ply-by-ply damage growth and area increase for T650/5320-1, 10/80/10, R=0.1, SL3..... 304
Figure B.77 – Apparent stiffness change during fatigue (normalized by initial compliance) for T650/5320-1 8HS, 10/80/10 layup, OHT-T, R=0.1. 305
Figure B.78 – Ply-by-ply damage growth and area increase for T650/5320-1, 10/80/10, R=5, SL1. 306
Figure B.79 – Ply-by-ply damage growth and area increase for T650/5320-1, 10/80/10, R=5, SL2. 307
Figure B.80 – Ply-by-ply damage growth and area increase for T650/5320-1, 10/80/10, R=5, SL3. 308
Figure B.81 – Apparent stiffness change during fatigue (normalized by initial compliance) for T650/5320-1 8HS, 10/80/10 layup, OHC-C, R=5. 309
Figure B.82 – Ply-by-ply damage growth and area increase for T650/5320-1, 10/80/10, R=-1, SL1. 310
Figure B.83 – Ply-by-ply damage growth and area increase for T650/5320-1, 10/80/10, R=-1, SL2. 311
Figure B.84 – Ply-by-ply damage growth and area increase for T650/5320-1, 10/80/10, R=-1, SL3. 312
Figure B.85 – Apparent stiffness change during the tension fatigue (normalized by initial compliance) for T650/5320-1 8HS, 10/80/10 layup, OHC-T, R=-1..... 313
Figure B.86 – Apparent stiffness change during the compression fatigue (normalized by initial compliance) for T650/5320-1 8HS, 10/80/10 layup, OHC-T, R=-1..... 313
Figure B.87 – Shear gauge damage growth and area increase for T650 5320-1, 40/20/40, R=0.1, SL1..... 315
Figure B.88 – Shear gauge damage growth and area increase for T650 5320-1, 40/20/40, R=0.1, SL2..... 316
Figure B.89 – Shear gauge damage growth and area increase for T650 5320-1, 40/20/40, R=0.1, SL3..... 317
Figure B.90 – Apparent stiffness change during fatigue (normalized by initial compliance) for T650/5320-1 8HS, 40/20/40 layup, DNS, R=0.1. 318
Figure B.91 – Shear gauge damage growth and area increase for T650 5320-1, 10/80/10, R=0.1, SL1..... 319
Figure B.92 – Shear gauge damage growth and area increase for T650 5320-1, 10/80/10, R=0.1, SL2..... 320
Figure B.93 – Shear gauge damage growth and area increase for T650 5320-1, 10/80/10, R=0.1, SL3..... 321
Figure B.94 – Apparent stiffness change during fatigue (normalized by initial compliance) for T650/5320-1 8HS, 10/80/10 layup, DNS, R=0.1. 322
Figure B.95 – Ply-by-ply damage growth and area increase for IM7/5250-4, 50/40/10, R=0.1, SL1. 324

DISTRIBUTION STATEMENT A
Approved for public release: distribution is unlimited.

Figure B.96 – Ply-by-ply damage growth and area increase for IM7/5250-4, 50/40/10, R=0.1, SL2. 325
Figure B.97 – Ply-by-ply damage growth and area increase for IM7/5250-4, 50/40/10, R=0.1, SL3. 326
Figure B.98 – Apparent stiffness change during fatigue (normalized by initial compliance) for IM7/5250-4 UNI 50/40/10 layup, OHT-T, R=0.1. 327
Figure B.99 – Ply-by-ply damage growth and area increase for IM7/5250-4, 50/40/10, R=5, SL1. 328
Figure B.100 – Ply-by-ply damage growth and area increase for IM7/5250-4, 50/40/10, R=5, SL2. 329
Figure B.101 – Ply-by-ply damage growth and area increase for IM7/5250-4, 50/40/10, R=5, SL3. 330
Figure B.102 – Apparent stiffness change during fatigue (normalized by initial compliance) for IM7/5250-4 UNI, 50/40/10 layup, OHT-T, R=5. 331
Figure B.103 – Ply-by-ply damage growth and area increase for IM7/5250-4, 50/40/10, R=-1, SL1. 332
Figure B.104 – Ply-by-ply damage growth and area increase for IM7/5250-4, 50/40/10, R=-1, SL2. 333
Figure B.105 – Ply-by-ply damage growth and area increase for IM7/5250-4, 50/40/10, R=-1, SL3. 335
Figure B.106 – Apparent stiffness change during the tension fatigue (normalized by initial compliance) for IM7/5250-4 UNI, 50/40/10 layup, OHC-T, R= -1. 336
Figure B.107 – Apparent stiffness change during the compression fatigue (normalized by initial compliance) for IM7/5250-4 UNI, 50/40/10 layup, OHC-T, R=-1. 336
Figure B.108 – Ply-by-ply damage growth and area increase for IM7/5250-4, 25/50/25, R=0.1, SL1. 338
Figure B.109 – Ply-by-ply damage growth and area increase for IM7/5250-4, 25/50/25, R=0.1, SL2. 339
Figure B.110 – Ply-by-ply damage growth and area increase for IM7/5250-4, 25/50/25, R=0.1, SL3. 340
Figure B.111 – Apparent stiffness change during fatigue (normalized by initial compliance) for IM7/5250-4 UNI, 25/50/25 layup, OHT-T, R=0.1. 341
Figure B.112 – Ply-by-ply damage growth and area increase for IM7/5250-4, 25/50/25, R=5, SL1. 342
Figure B.113 – Ply-by-ply damage growth and area increase for IM7/5250-4, 25/50/25, R=5, SL2. 343
Figure B.114 – Ply-by-ply damage growth and area increase for IM7/5250-4, 25/50/25, R=5, SL3. 344
Figure B.115 – Apparent stiffness change during fatigue (normalized by initial compliance) for IM7/5250-4 UNI, 25/50/25 layup, OHC-C, R=5. 345
Figure B.116 – Ply-by-ply damage growth and area increase for IM7/5250-4, 25/50/25, R=-1, SL1. 346
Figure B.117 – Ply-by-ply damage growth and area increase for IM7/5250-4, 25/50/25, R=-1, SL2. 347
Figure B.118 – Ply-by-ply damage growth and area increase for IM7/5250-4, 25/50/25, R=-1, SL3. 348

DISTRIBUTION STATEMENT A
Approved for public release: distribution is unlimited.

Figure B.119 – Apparent stiffness change during the tension fatigue (normalized by initial compliance) for IM7/5250-4 UNI, 25/50/25 layup, OHC-T, R=-1. 349
Figure B.120 – Apparent stiffness change during the compression fatigue (normalized by initial compliance) for IM7/5250-4 UNI, 25/50/25 layup, OHC-T, R=-1. 349
Figure B.121 – Ply-by-ply damage growth and area for IM7/5250-4, 10/80/10, R=0.1, SL1. .. 351
Figure B.122 – Ply-by-ply damage growth and area for IM7/5250-4, 10/80/10, R=0.1, SL2. .. 352
Figure B.123 – Ply-by-ply damage growth and area increase for IM7/5250-4, 10/80/10, R=0.1, SL3. 353
Figure B.124 – Apparent stiffness change during fatigue (normalized by initial compliance) for IM7/5250-4 UNI, 10/80/10 layup, OHT-T, R=0.1. 354
Figure B.125 – Ply-by-ply damage growth and area increase for IM7/5250-4, 10/80/10, R=5, SL1. 355
Figure B.126 – Ply-by-ply damage growth and area increase for IM7/5250-4, 10/80/10, R=5, SL2. 356
Figure B.127 – Ply-by-ply damage growth and area increase for IM7/5250-4, 10/80/10, R=5, SL3. 357
Figure B.128 – Apparent stiffness change during fatigue (normalized by initial compliance) for IM7/5250-4 UNI, 10/80/10 layup, OHC-C, R=5. 358
Figure B.129 – Ply-by-ply damage growth and area increase for IM7/5250-4, 10/80/10, R=-1, SL1. 359
Figure B.130 – Ply-by-ply damage growth and area for IM7/5250-4, 10/80/10, R=-1, SL2. 360
Figure B.131 – Ply-by-ply damage growth and area increase for IM7/5250-4, 10/80/10, R=-1, SL3. 361
Figure B.132 – Apparent stiffness change during the tension fatigue (normalized by initial compliance) for IM7/5250-4 UNI, 10/80/10 layup, OHC-T, R=-1. 362
Figure B.133 – Apparent stiffness change during the compression fatigue (normalized by initial compliance) for IM7/5250-4 UNI, 10/80/10 layup, OHC-T, R=-1. 362
Figure B.134 – Shear gauge damage growth and area increase for IM7/5250-4, 50/40/10, R=0.1, SL1. 364
Figure B.135 – Shear gauge damage growth and area increase for IM7/5250-4, 50/40/10, R=0.1, SL2. 365
Figure B.136 – Shear gauge damage growth and area increase for IM7/5250-4, 50/40/10, R=0.1, SL3. 366
Figure B.137 - Apparent stiffness change during fatigue (normalized by initial compliance) for IM7 5250-4 UNI, 50/40/10 layup, DNS, R= 0.1. 367
Figure B.138 – Shear gauge damage growth and area increase for IM7/5250-4, 10/80/10, R=0.1, SL1. 368
Figure B.139 – Shear gauge damage growth and area increase for IM7/5250-4, 10/80/10, R=0.1, SL2. 369
Figure B.140 – Shear gauge damage growth and area increase for IM7/5250-4, 10/80/10, R=0.1, SL3. 370
Figure B.141 – Apparent stiffness change during fatigue (normalized by initial compliance) for IM7 5250-4 UNI, 10/80/10 layup, DNS, R= 0.1. 371

DISTRIBUTION STATEMENT A
Approved for public release: distribution is unlimited.

LIST OF TABLES

Table **Page**

Table 1 – Required test duration for phase 2 after three lifetime tests in phase 1 with LEF = 1.0. 35
Table 2 – Comparison of fatigue scatter analysis techniques. 37
Table 3 – Materials used for laminate panel manufacturing. 45
Table 4 – Laminate stacking sequences. 46
Table 5 – Panel inspection checklist. 49
Table 6 – Static and constant amplitude fatigue test matrix—open-hole. 52
Table 7 – Static and constant amplitude fatigue test matrix—interlaminar tension and shear. 53
Table 8 – Static strength test data and Weibull parameters for IM7/5320-1 UNI. 58
Table 9 – Static strength test data and Weibull parameters for T650/5320-1 8HS. 59
Table 10 – Static strength test data and Weibull parameters for IM7/5250-4. 60
Table 11 – Calculation of modal shape parameters of static data. 61
Table 12 – Fatigue life scatter analysis for IM7/5320-1 UNI. 63
Table 13 – Strength comparison for IM7/5320-1 UNI. 65
Table 14 – Fatigue life scatter analysis for T650/5320-1 8HS. 75
Table 15 – Static strength comparison for T650/5320-1 8HS. 76
Table 16 – Fatigue life scatter analysis for IM7/5250-4 UNI. 85
Table 17 – Static strength comparison for IM7/5250-4 UNI. 87
Table 18 – Calculation of MLSP. 95
Table 19 – Comparison of LEF based on individual Weibull analysis of SN data. 96
Table 20 – Comparison of LEF based on Sendecky analysis (with static) of SN data. 97
Table 21 – Manufacturing improvements with IM7/5320-1 material system. 108
Table 22 – Manufacturing improvements with IM7/5250-4 material system. 109
Table 23 – Summary of porosity assessment and damage characterization for IM7/5320-1 UNI, 50/40/10. 113
Table 24 – Number of EPC test specimens. 115
Table 25 – Comparison of Baseline and EPC for strength data. 117

Table A.1 – SN data for IM7/5320-1, 50/40/10, R=0.1, OHT-T. 147
Table A.2 – SN data for IM7/5320-1, 50/40/10, R=5, OHC-C. 149
Table A.3 – SN data for IM7/5320-1, 50/40/10, R=-1, OHC-T. 151
Table A.4 – SN Data for IM7/5320-1, 25/50/25, R=0.1, OHT-T. 153
Table A.5 – SN data for IM7/5320-1, 25/50/25, R=5, OHC-C. 155
Table A.6 – SN data for IM7/5320-1, 25/50/25, R=-1, OHC-T. 157
Table A.7 – SN data for IM7/5320-1, 10/80/10, R=0.1, OHT-T. 159
Table A.8 – SN data for IM7/5320-1, 10/80/10, R=5, OHC-C. 161
Table A.9 – SN data for IM7/5320-1, 10/80/10, R=-1, OHC-T. 163
Table A.10 – SN data for IM7/5320-1, 50/40/10, R=0.1, DNS. 165
Table A.11 – SN data for IM7/5320-1, 10/80/10, R=0.1, DNS. 167
Table A.12 – SN data for IM7/5320-1, 50/40/10, R=0.1, ILT. 169
Table A.13 – SN data for IM7/5320-1, 10/80/10, R=0.1, ILT. 171
Table A.14 – SN data for IM7/5320-1, 100/0/0, R=0.1, SBS. 173

DISTRIBUTION STATEMENT A
Approved for public release: distribution is unlimited.

Table A.15 – SN data for T650/5320-1, 40/20/40, R=0.1, OHT-T. 175
Table A.16 – SN data for T650/5320-1, 40/20/40, R=5, OHC-C. 177
Table A.17 – SN data for T650/5320-1, 40/20/40, R=-1, OHC-T. 179
Table A.18 – SN data for T650/5320-1, 25/50/25, R=0.1, OHT-T. 181
Table A.19 – SN data for T650/5320-1, 25/50/25, R=5, OHC-C. 182
Table A.20 – SN data for T650/5320-1, 25/50/25, R=-1, OHC-T. 184
Table A.21 – SN data for T650/5320-1, 10/80/10, R=0.1, OHT-T. 185
Table A.22 – SN data for T650/5320-1, 10/80/10, R=5, OHC-C. 187
Table A.23 – SN data for T650/5320-1, 10/80/10, R=-1, OHC-T. 189
Table A.24 – SN data for T650/5320-1, 40/20/40, R=0.1, DNS. 191
Table A.25 – SN data for T650/5320-1, 10/50/10, R=0.1, DNS. 193
Table A.26 – SN data for T650/5320-1, 40/20/40, R=0.1, ILT. 195
Table A.27 – SN data for T650/5320-1, 10/80/10, R=0.1, ILT. 197
Table A.28 – SN data for T650/5320-1, 100/0/0, R=0.1, SBS. 199
Table A.29 – SN data for IM7/5250-4, 50/40/10, R=0.1, OHT-T. 201
Table A.30 – SN data for IM7/5250-4, 50/40/10, R=5, OHC-C. 202
Table A.31 – SN data for IM7/5250-4, 50/40/10, R=-1, OHC-T. 204
Table A.32 – SN data for IM7/5250-4, 25/50/25, R=0.1, OHT-T. 206
Table A.33 – SN data for IM7/5250-4, 25/50/25, R=5, OHC-C. 207
Table A.34 – SN data for IM7/5250-4, 25/50/25, R=-1, OHC-T. 209
Table A.35 – SN data for IM7/5250-4, 10/80/10, R=0.1, OHT-T. 210
Table A.36 – SN data for IM7/5250-4, 10/80/10, R=5, OHC-C. 211
Table A.37 – SN data for IM7/5250-4, 10/80/10, R=-1, OHC-T. 212
Table A.38 – SN data for IM7/5250-4, 50/40/10, R=0.1, DNS. 213
Table A.39 – SN data for IM7/5250-4, 10/80/10, R=0.1, DNS. 215
Table A.40 – SN data for IM7/5250-4, 50/40/10, R=0.1, ILT.Specimen 217
Table A.41 – SN data for IM7/5250-4, 10/80/10, R=0.1, ILT. 218
Table A.42 – SN data for IM7/5250-4, 100/0/0, R=0.1, SBS. 220

DISTRIBUTION STATEMENT A
Approved for public release: distribution is unlimited.

ACKNOWLEDGEMENT

This research program was funded by the Air Force Research Laboratory under contract number FA8650-18-C-5289. The authors would like to acknowledge the guidance and support of Dr. David Mollenhauer, Kara Storage, and Tara Storage of AFRL for their technical guidance and support. In addition, technical guidance and program review from Mr. Jeff Hendrix and industry partners from Boeing, Lockheed, Northrop Grumman, and Spirit Aerosystems is greatly appreciated. The authors also would like to thank NIAR ATLAS and Composites Laboratory staff, especially the test support from John Avino, Reese Avino, and Harishankar Nadason to complete the testing under an aggressive schedule.

This report is 2 Volumes. This is Volume 1 of 2.

DISTRIBUTION STATEMENT A
Approved for public release: distribution is unlimited.

1. INTRODUCTION

Several factors have significantly advanced composite applications in military platforms: life cycle cost reduction due to reduced crew workload for maintenance and repair; advancements in low-cost and high-performance composite materials; and innovative, rapid, and low-cost manufacturing processes. Composite materials have shown superior fatigue performance compared to metals (Figure 1). In some cases, such as open-hole (OH) with tension-tension fatigue, composites have shown a fatigue life over millions of cycles just below the lower bound of the static scatter band. Such observations are dependent on several parameters such as material system, stress ratio (R = min/max stress), layup sequence, etc.

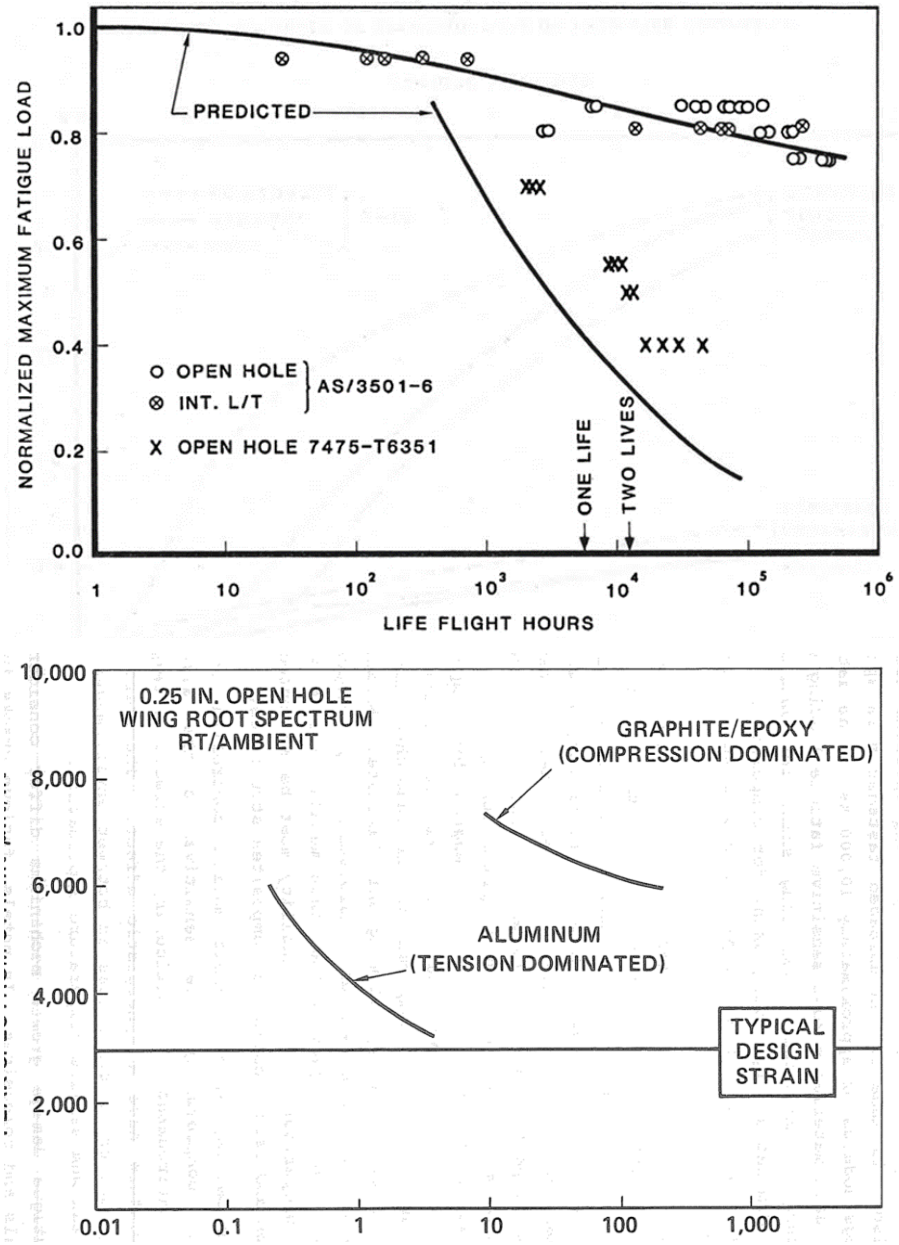


Figure 1. Composite and metal fatigue behavior [1].

DISTRIBUTION STATEMENT A.
Approved for public release: distribution is unlimited.

Although most fatigue stress-to-number of cycles (SN) curves for in-plane fiber-dominant failure modes are considered flat, the matrix-dominant and out-of-plane failure modes have indicated considerable fatigue wearout (reduction is stiffness as the fatigue cycles progresses) [2]. Due to the anisotropy and heterogeneous nature of composites, their fatigue damage growth characteristics are complex, and predictive methodologies are in their infant stages. Therefore, overly conservative assumptions are made for fatigue life assessment without taking full advantage of the fatigue capabilities of composites. In order to design efficient composite structures for future applications, a greater understanding of the fundamentals of fatigue damage initiation and growth characteristics of composites as well as reliable predictive capabilities are needed. The primary goal of this research was to develop techniques to enhance advanced material characterization and structural certification aided by high-fidelity damage modeling and efficient protocol for substantiation of advanced composite structures that weigh both the economic aspects of certification as well as the time frame required for testing, all while ensuring safety. A regularized extended finite element methodology (Rx-FEM), which is a discrete damage modeling (DDM) technology that is currently implemented in the B-spline analysis method (BSAM) software, was used for verification and validation (V&V) exercises on various failure modes and laminate configurations including static and fatigue loading with implementation of geometrically nonlinear regimes and spectrum fatigue loading. Significant advancements of the BSAM software efficiency have taken place at University of Texas at Arlington under Subcontract No. WSU#15662 with the leadership of Dr. Endel Iarve. Discrete modeling of multiple damage modes and their interaction provide a valuable tool in predicting the response of composite structures under variable loading conditions.

1.1 Advanced Material Characterization

Substantiation of composite structures often requires analysis validated by testing conducted at multiple levels of building-blocks of certification (Figure 2). The building-block approach is a rational multi-level analysis and testing development approach used by many aerospace companies to certify metallic and composite structures. Typically, as one proceeds up the building-blocks of testing (BBT) and becomes more confident in the analytical design methods, the number of coupons or replicates is reduced since the structural complexity increases. Costly and time-consuming allowable programs hinder the application of novel composite materials and often force designers to use legacy materials that have established material allowable databases. In order to promote and accelerate the insertion of novel composite material systems into designs, efficient and reliable allowable/screening programs coupled with validated analytical models are required to reduce certification time and cost by ensuring that material performance meets program goals. This enables the expansion of design variables to optimize structural performance and the ability to streamline design changes, thereby reducing the product development cycle. Current certification methodologies account for variability in material properties through numerous tests and analysis/statistical procedures to ensure the safe operation of the aircraft throughout its design service goal (DSG) under standard operating conditions.

DISTRIBUTION STATEMENT A.
Approved for public release: distribution is unlimited.

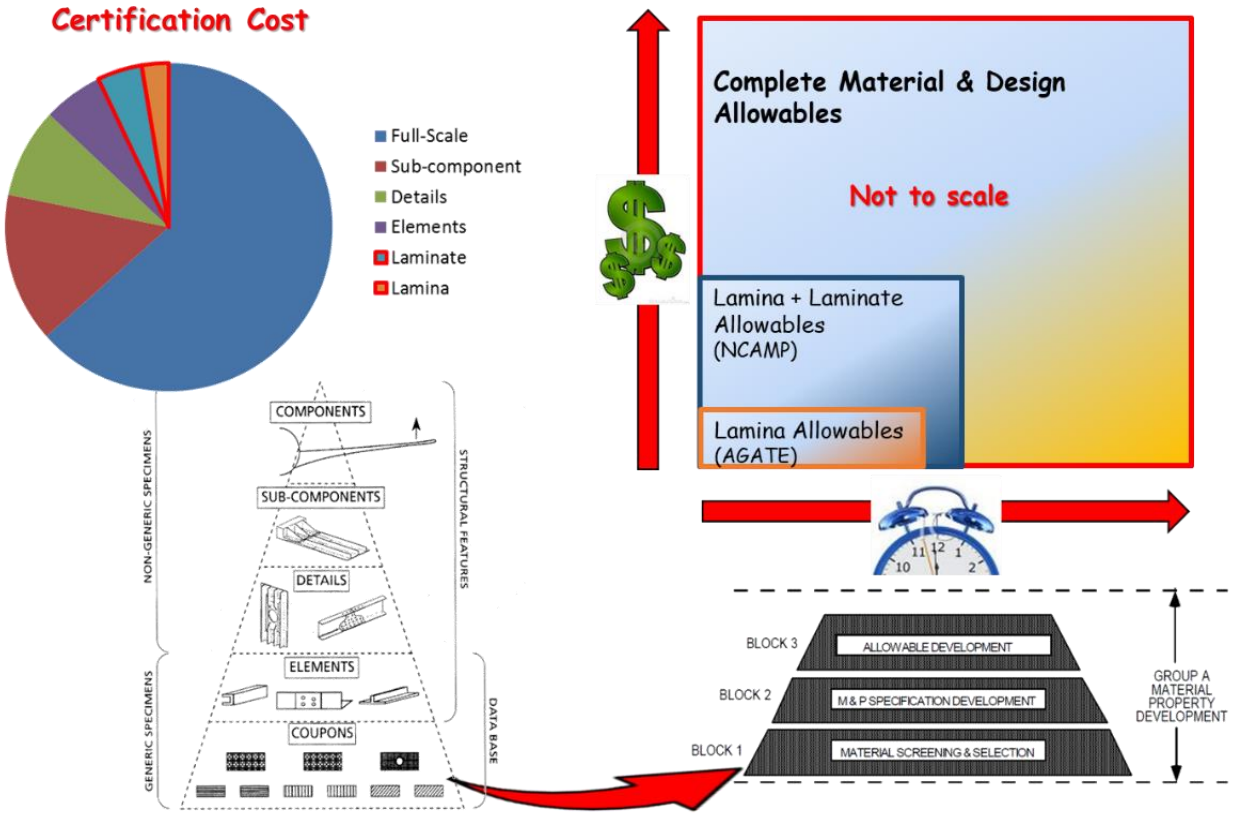


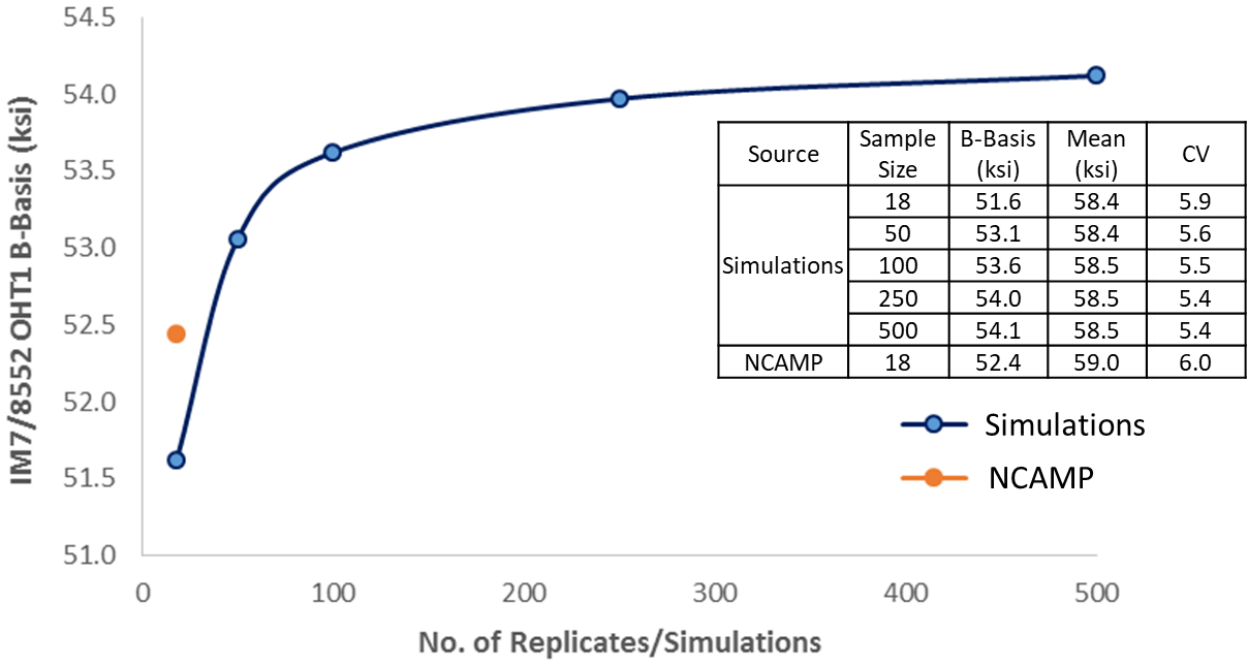
Figure 2. Material characterization time and cost [3].

Composite material design properties used for the analysis of composite structures must be chosen to minimize the probability of structural failure. These design values are currently based on the testing of materials with approved specifications to establish the statistical basis for design allowable generation. Approved design allowables, such as the design values documented in Metallic Materials Properties Development and Standardization (MMPDS) for metals and the Composite Materials Handbook (CMH-17) for composites, require extensive material tests and statistical analyses. Especially for composites, any deviation from the approved material and process specification may require rigorous testing, which is time consuming and costly.

Statistical analyses conducted on composite material data that represent several material and process batches are typically used for generating design allowables and material acceptance limits for production batches (e.g., receiving inspections and quality control). As the complexity of higher-level BBT increases, more variables are introduced, i.e., fastener holes, multi-directional fibers, etc. Currently, there is no standardized statistical methodology that allows progression up the pyramid of tests with a concurrent reduction in the number of tests while maintaining statistical reliability at the lower replicate level. Therefore, conservative approaches are exercised at the lower levels of BBT to attempt to utilize the material variability of lower levels to represent the higher levels. Since a reduction in the number of samples results in excessively low or overly conservative material allowables, as shown in Figure 3 [4], various strategies are employed at

DISTRIBUTION STATEMENT A.
Approved for public release: distribution is unlimited.

lower levels of BBT (lamina and laminate level) in order to develop material allowables. For example, the statistical methodology proposed by Shyprykevich et al. pools data across various test environments for the same failure mode, thus increasing the sample size to estimate material variability for obtaining basis values [5]. Shared databases such as NASA Advanced General Aviation Transport Experiments (AGATE) [6] and the National Center for Advanced Materials Performance (NCAMP) [7] have developed statistical analysis protocols employing such pooling techniques while ensuring that the data satisfies the underlying assumptions in order to take advantage of such pooling techniques.



Source	Sample Size	B-Basis (ksi)	Mean (ksi)	CV
Simulations	18	51.6	58.4	5.9
	50	53.1	58.4	5.6
	100	53.6	58.5	5.5
	250	54.0	58.5	5.4
	500	54.1	58.5	5.4
NCAMP	18	52.4	59.0	6.0

Figure 3. Effects of sample size on design allowables.

B-basis material properties are defined as the tenth percentiles of a material property distribution. However, the true population (probability distribution of an infinite number of samples) is an unknown. By testing *n* specimens, one observes *n* numbers, and if *n* is large enough, then a histogram of these numbers will approximate the unknown probability distribution for the strength property. This probability distribution is referred to as a population, and the *n* numbers are a realization of a random sample of this population. A statistically based B-basis material property is a statistic calculated from a random sample of size *n*, such that if one were to repeatedly obtain random samples of *n* specimens and calculate many of their basis values, 95% of the time the calculated values would fall below the (unknown) tenth percentile (Figure 4). In statistical terminology, basis values are 95% lower confidence limits on prescribed percentiles, which are also sometimes referred to as tolerance limits. Basis values from a set of repeated samples will form a histogram, as shown in Figure 4, rather than a fixed value. If a large number of tests are performed, thereby accounting for variations in constitutive materials and numerous process parameters, then a probability density function (PDF) that closely represents the true

DISTRIBUTION STATEMENT A.
Approved for public release: distribution is unlimited.

population distribution can be obtained. Hypothetically, the B-basis allowable strength can be calculated simply by selecting the strength value corresponding to the tenth percentile of the PDF, as illustrated in Figure 4, instead of conducting statistical analysis.

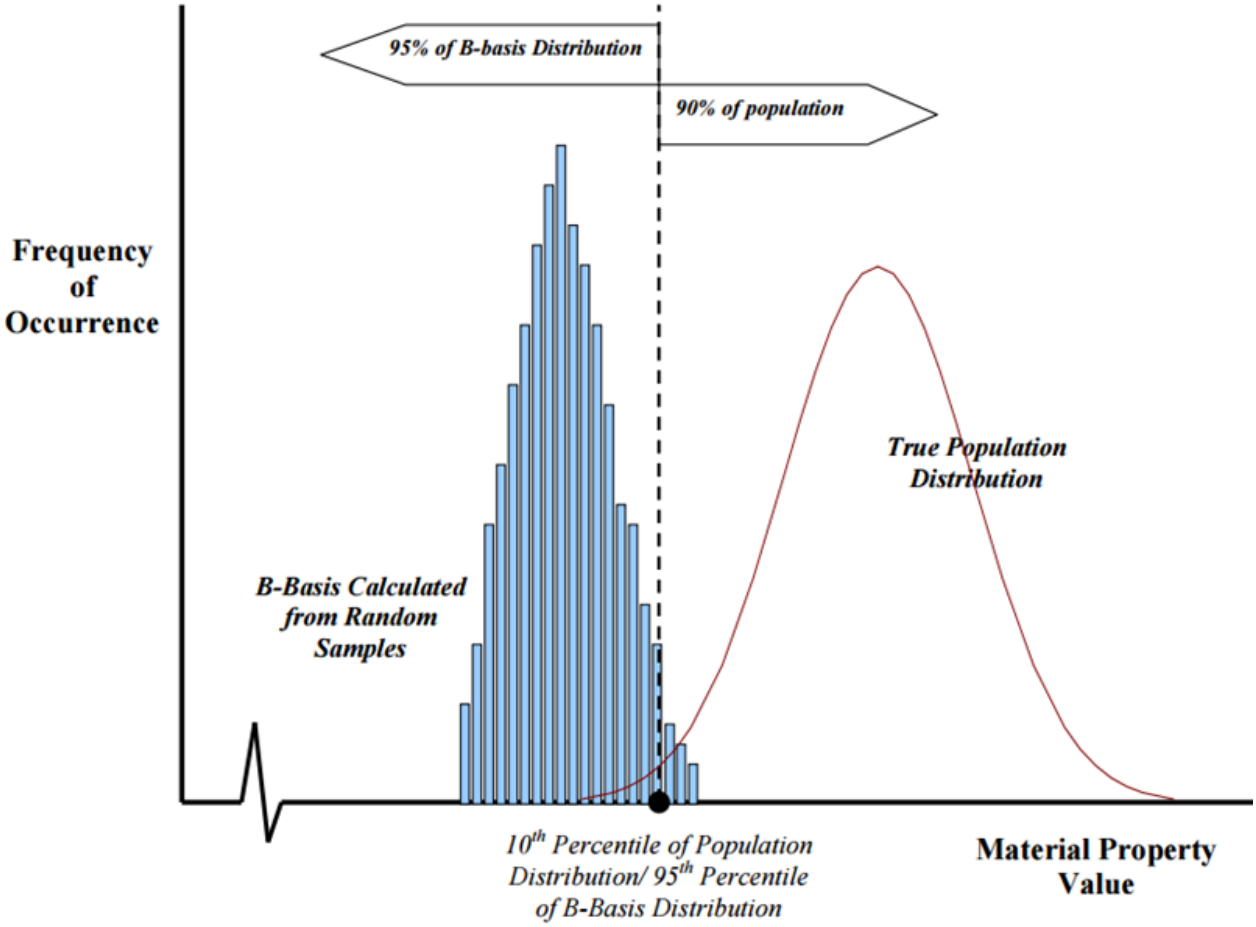


Figure 4. B-basis allowable generation.

Figure 5 illustrates an example of a constitutive property variation over a multi-year production cycle (batches 1 to *n*) and compares that with the property variation of individual batches including the initial three batches used for manufacturing prepreg used for the allowable generation. As can be seen in this illustration, the initial three material batches may not represent the true variability of material over time, because they were produced within a short period of time at early stages of material maturity. Therefore, it is imperative that the material allowables are generated after maturity, thereby demonstrating that the material characteristics are stable. In addition, conservative efforts must be employed to select material batches representative of total population. Currently, the Department of Defense (DOD) and industry programs are using the material allowables in shared databases such as AGATE and NCAMP by simply conducting equivalency tests that accelerate the insertion of composite materials into new applications. Although the shared databases can be used for the material allowables, protocols must be established to monitor the material quality over several years of production cycles so that any

DISTRIBUTION STATEMENT A.
Approved for public release: distribution is unlimited.

deviation from acceptance limits established during initial material qualification can be readily detected to investigate the root cause for drift in material properties over time and remedy the issue(s) by either rejecting materials or, in rare cases, redoing the material allowable calculations based on the larger population of available data.

At the lamina level in the BBT, specimens are selected so that the datasets include batch variability and process variability. The large sample (population) variability for particular failure modes at this level of BBT has implications for the statistical significance of design allowables for higher-level building-block tests, i.e., notched and unnotched laminates, where the number of test samples is small. This laid the foundation for the Lamina Variability Method (LVM) proposed by the authors in their previous work to obtain the B-basis allowable for laminated composites (small datasets) [8]. In order to calculate laminate basis values without generating excessively low B-basis values, the laminate population variation must be assumed or estimated, since it cannot be accurately determined from a small dataset. Basic assumptions for the LVM are that there is substantial related data, e.g., from lamina specimens, and that the intrinsic strength variability of the property for which only a small dataset is available is no greater than the strength variability of the property for which considerable data is available. Extreme care should be taken in applying such small sample analysis methods for high-temperature data as well as for test methods, failure modes, and material types for which there is little experience.

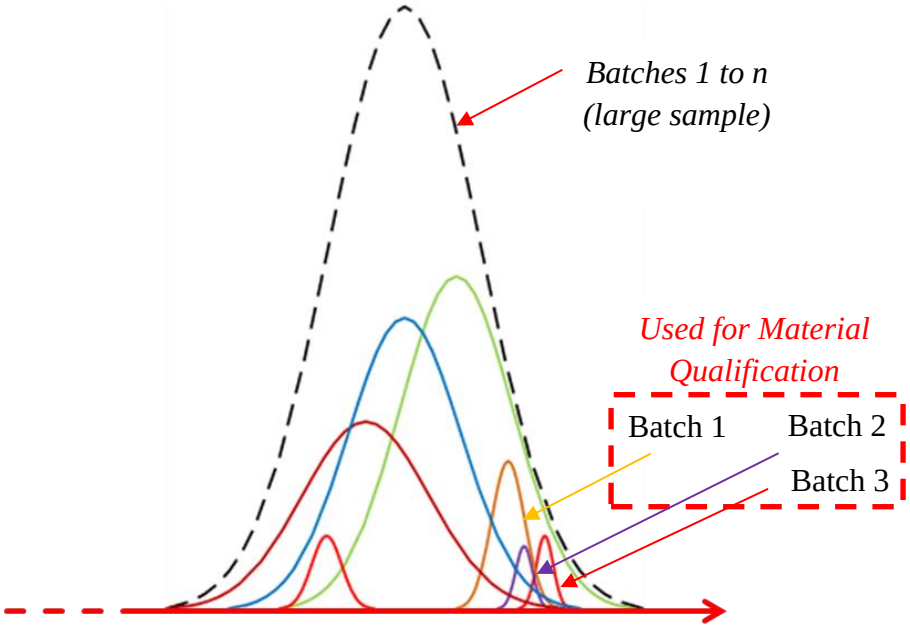


Figure 5. Example of probability density functions of constituent property for multiple batches of materials tested over several years of production runs.

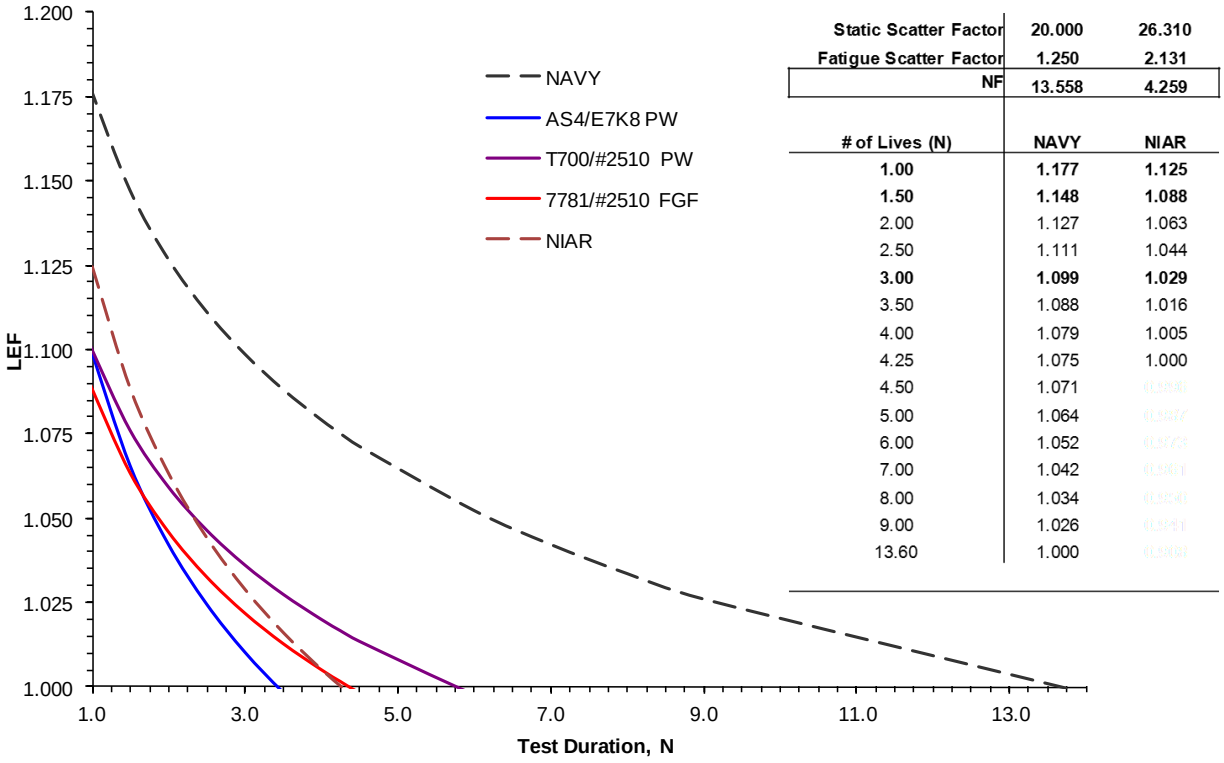
DISTRIBUTION STATEMENT A.
Approved for public release: distribution is unlimited.

1.2 Durability and Damage Tolerance Test Substantiation

Current regulations require airframes to demonstrate adequate static strength, fatigue life, and damage-tolerance capability by testing and/or analysis with a high degree of confidence. These requirements are intended to account for uncertainties in usage and scatter exhibited by materials. The primary means of structural substantiation for most aircraft certification programs is by analysis. It is expected that the analysis will be supported by appropriate test evidence.

Due to the heterogeneous nature of the composite microstructure, material and process variability, and complex interactive damage growth mechanisms, composite fatigue data tend to have a large scatter. This data scatter in composites is related to the reliability of the composite structure through a concept known as the scatter factor, which signifies the relation between the central tendency of a data set (mean) and the extreme statistics (allowables). In order to develop a certification methodology for composite structures that has the same level of reliability as observed in metal certification approaches, accounting for the inherent difference between metal and composites, the FAA and U.S. Navy developed a certification approach for bolted composite structures as part of the F/A-18 certification [1]. This methodology, known as the load-enhancement factor (LEF), was formulated to account for the uncertainties of applied loads as well as the scatter in static strength and fatigue life related to composite structures. This approach requires analysis of data scatter in the static (residual) strength and fatigue life of composites to establish a certification methodology that has the same level of reliability as for metal structures. This approach was developed for what, at that time, was current composite usage and did not explicitly account for the damage in composite structures or structural details such as adhesively bonded and sandwich structures. Over the years, several composite structural certification programs employed this certification methodology, which was developed for materials and test methods that were considered current at the time. Since then, materials and process techniques as well as test methods for evaluating composites have evolved. Consequently, test data often display significantly less scatter with high reliability. The probabilistic approach employed by Whitehead, et al. [1] was reevaluated for several newer material forms and design details/features that are applicable for current DOD applications to obtain improved life and LEFs, as outlined in the WSU principal investigators' previous research work [2], shown in Figure 6.

DISTRIBUTION STATEMENT A.
Approved for public release: distribution is unlimited.



Static Scatter Factor	20.000	26.310
Fatigue Scatter Factor	1.250	2.131
NF	13.558	4.259
# of Lives (N)	NAVY	NIAR
1.00	**1.177**	**1.125**
1.50	**1.148**	**1.088**
2.00	1.127	1.063
2.50	1.111	1.044
3.00	**1.099**	**1.029**
3.50	1.088	1.016
4.00	1.079	1.005
4.25	1.075	1.000
4.50	1.071	
5.00	1.064	
6.00	1.052	
7.00	1.042	
8.00	1.034	
9.00	1.026	
13.60	1.000	

Figure 6. Comparison of LEFs developed for historical and modern materials.

1.3 Certification Testing of Hybrid Structures

When the LEF is applied to a composite-metal hybrid structure during full-scale test substantiation, careful consideration is needed to prevent unintentional damage-growth scenarios and/or load-redistributions that may not be representative of aircraft operational loads. Notch sensitivity and critical loads for composites and metals are significantly different, making the certification testing of hybrid structures challenging, costly, and time consuming, especially at the full-scale structural level.

The large coefficient of thermal expansion (CTE) mismatch between metallic and composite structures induces additional thermal stresses in hybrid structures during flight in a cold environment and extreme ground temperatures that must be investigated during certification [9]. However, such thermal stresses are self-reacting (internal) and thus cannot be applied during full-scale testing that is typically conducted at room-temperature ambient conditions. Normally, thermal stresses are introduced to validate localized models in order to evaluate the cumulative effects of thermo-mechanical loads on the fatigue life of critical design details.

Several test-substantiation approaches can be used for certifying hybrid structures. One approach involves two separate full-scale test articles—one focusing on metal certification and the other focusing on composites certification—to address concerns related to composite components at the lower level of the building-blocks of testing (i.e., pre-production article) and to focus the certification of metallic components at a full-scale level. Often composite structural certification

DISTRIBUTION STATEMENT A.
Approved for public release: distribution is unlimited.

uses LEFs to reduce the test duration. In certain cases, this causes the enhanced load spectrum to have loads beyond the clipping level of metal structural details. Two spectrum modification approaches are discussed in this report for supporting hybrid structural substantiation. The first technique is called a multi-LEF [10], wherein different combinations of life-load factors can be used for different parts of the spectrum so that high loads (that potentially can go beyond clipping level after LEF application) can have a higher life factor and a lower or no LEF. The second concept, referred to as a deferred severity spectrum (DSS) [13], is introduced so that a single test article can be used to substantiate both metals and composites as a two-phase certification methodology with different LEFs. The goal of these approaches is to provide an efficient certification approach that weighs both the economic aspects of certification and the time frame required for certification testing, while ensuring that safety is the key priority.

Both multi-LEF and DSS concepts require significant modifications to the test spectrum. In addition to investigating the sequencing effects at lower levels of the building-blocks of testing, such concepts require greater understanding of material variability and practical bounds of repeated load/life tradeoff (LEF) during structural substantiation to avoid unsafe applications. A series of sequencing studies were conducted to understand the implications of sequencing and spectrum modifications to the overall damage growth mechanism of composites during the next phase of this research under the Modeling for Affordable Sustainable Composites (MASC) project and will be included in a separate report. The spectrum tests under MASC are used for validating the strength tracking method [14], a fatigue life assessment tool for composites under variable-amplitude (spectrum) fatigue loading.

1.4 Characterization of Progressive Damage Growth of Composites

Due to the inherent differences between composite and metals in terms of critical damage modes, there is a need to fully understand the damage growth mechanics in composite materials. More importantly, damage accumulation and growth in composites must be fully characterized to aid in certification as well as establishing damage tolerance testing and analysis protocols. The progressive damage growth of several carbon fiber-reinforced polymer (CFRP) composites that have strategic importance to the DOD was studied using various layup sequences, stress ratios, and failure modes. A database of detailed three-dimensional (3D) X-ray computed tomography (CT) data over fatigue lifetime, referred to as 4D XCT, was developed (see example shown in Figure 7) so that such information can be used for a comprehensive understanding of failure progression and for using validating high-fidelity models and life-prediction tools. Such high-fidelity inspection data can be used for validating progressive damage growth predictions using both discrete damage modeling and continuum damage modeling techniques.

DISTRIBUTION STATEMENT A.
Approved for public release: distribution is unlimited.

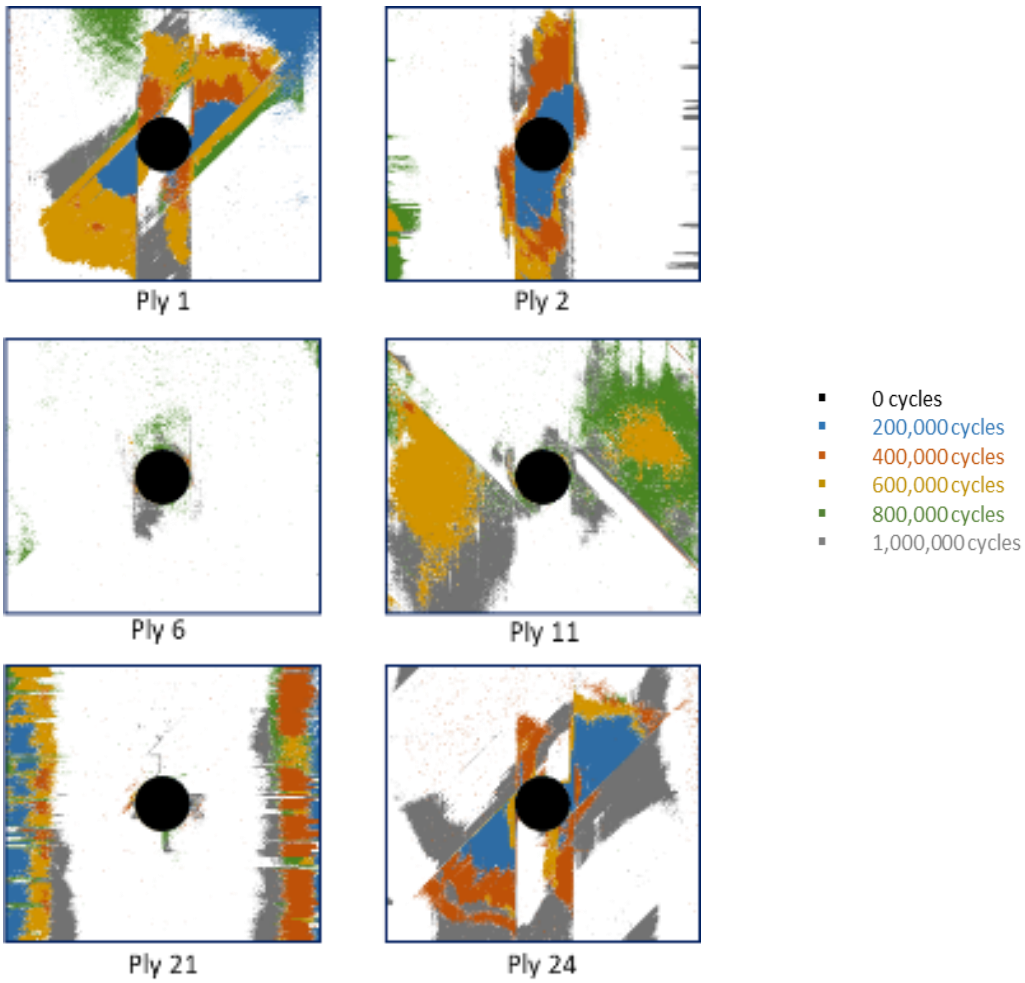


Figure 7. Progressive damage growth of IM7/5320-1 24-ply quasi-isotropic open-hole specimen (R = 0.1) monitored across one million cycles [14].

Typically, nondestructive inspection (NDI) or full-field displacement/strain measurements are not acquired during a fatigue test, because they are time consuming and may not be economical in some cases. As an alternative, the specimen compliance change (or inverse of stiffness) can be calculated by simply outputting data during fatigue testing, without interrupting the fatigue test, and calculating the slope of the load-displacement curve. Thus, it is recommended that specimen compliance, especially for notched specimens, be monitored throughout the fatigue test to better understand the failure mechanism and damage propagation. In addition, high-fidelity nondestructive inspections such as X-ray computed tomography (CT), digital image correlation (DIC) and through-transmission ultrasonic (TTU) for determining the progressive damage growth under fatigue because, unlike metals, the internal composite damages (delaminations, matrix cracks, and fiber breaks) are not visible.

DISTRIBUTION STATEMENT A.
Approved for public release: distribution is unlimited.

2. CERTIFICATION TESTING OF COMPOSITE STRUCTURES

Compared to metal static and fatigue data, composite materials exhibit high data scatter due to their anisotropic heterogeneous characteristics, such as layup, manufacturing defects, imperfections, test complications, environment, etc. In order to interpret this information in a meaningful manner and to incorporate any effects of this into the certification of composite structures, several approaches are used. Life factor, load factor, and load-life combined are three of the commonly used approaches that require composite scatter analysis.

2.1 Reliability (Scatter) Analysis for Fatigue Life Determination

Over the years, composite and hybrid structural certification programs have adopted methodologies utilized for metal structures that are based on several decades of experience in full-scale structural certification and service. Despite the advantages, such as high specific weight, tailorability, and fatigue resistance, composite structural certification becomes challenging due to the lack of experience with large-scale structures, complex interactive failure mechanisms, sensitivity to temperature and moisture, and scatter in the data, especially relative to fatigue. Despite superior fatigue properties, the heterogeneous nature, due to the presence of multiple constituents, and the notch sensitivity of composites resulted in special requirements for the durability and damage tolerance (DaDT) substantiation of composite structures.

In order to develop a certification methodology for composite structures that has the same level of reliability as observed in metal certification approaches, accounting for the inherent difference between metal and composites, the FAA and U.S. Navy developed a certification approach for bolted composite structures [1,15] as part of the F/A-18 certification. This methodology was formulated to account for the uncertainties of applied loads as well as the scatter in static strength and fatigue life related to composite structures. This approach analyzes the data scatter in the static (residual) strength and fatigue life of composites to establish a certification methodology that has the same level of reliability as for metal structures. Furthermore, this approach attempts to address those issues related to hybrid (composite and metallic) structures through a combined method referred to as the load-life approach, which will be discussed further in this report. This approach was developed for what, at the time, was current composite usage and did not explicitly account for the damage in composite structures or adhesively bonded structural details.

Over the years, several composite structural certification programs employed this certification methodology, which was developed for materials and test procedures that were considered current at the time. Since then, materials and process techniques, as well as test methods for evaluating composites, have evolved. Consequently, test data often display significantly less scatter with high reliability. Thus, the probabilistic approach employed by Whitehead et al. [1] can be reevaluated for newer material forms and to represent structural details of current aircraft structures to obtain improved life and load-enhancement factors [2,16,17].

DISTRIBUTION STATEMENT A.
Approved for public release: distribution is unlimited.

2.2 Life Factor Approach

Data scatter in composites is related to the reliability of the composite structure using a concept known as the scatter factor, which signifies the relation between the central tendency of a data set (mean) and the extreme statistics (allowables). The scatter factor shows the penalty paid to gain the required reliability at γ level of confidence from a finite sample size. This is graphically illustrated in Figure 8 in terms of B-basis statistics, i.e., a successful repeated load test to mean fatigue life would demonstrate B-basis reliability on the design lifetime. In terms of static strength and fatigue life, the scatter factor is referred to as the static factor and life factor, respectively.

The life factor approach has been successfully used for metal to assure structural durability. In this approach, the structure is tested for additional fatigue life to achieve the desired level of reliability. The underlying objective of the life factor is to ensure that the design life is representative of the condition of the weakest member of the population after a specified life in service.

The ratio of the mean repeated load life to the A- or B-basis repeated life is defined as the life factor, N_F, and given by

$$N_F = \frac{\Gamma\left(\frac{\alpha_L + 1}{\alpha_L}\right)}{\left\{\frac{-\ln(R)}{\left[\chi^2_\gamma(2n)/2n\right]}\right\}^{1/\alpha_L}} \tag{1}$$

where α_L is the modal life shape parameter (MLSP), n is the number of articles, and R is the reliability. For γ = 0.95, A- and B-basis reliabilities are 0.99 and 0.90, respectively. The term χ^2_γ 2n) is the Chi-square distribution with 2n degrees of freedom at γ level of confidence. Derivation of the MLSP for composite fatigue SN data using several data scatter analysis methods is discussed in detail in Section 3.

Figure 9 shows the influence of the shape parameter on the life factor, which is the ratio between the mean repeated life to B-basis life [1]. This figure shows that the life factor rapidly increases for fatigue life shape parameters that are less than 2. Due to large scatter in the composite test data, the life shape parameter for composite was found to be 1.25 for data analyzed using the Navy approach, while for metal it was found to be 4.00. Therefore, a composite structure is required to test additional fatigue life to achieve the desired level of reliability, i.e., test duration of more than 13 design lifetimes (DLTs) for a composite in contrast to 2 DLTs for metal. As can be seen in equation (1), the life factor is a function of the MLSP. Thus, improvement in the

DISTRIBUTION STATEMENT A.
Approved for public release: distribution is unlimited.

MLSP for newer forms of materials that exhibit less scatter can significantly reduce the life factor.

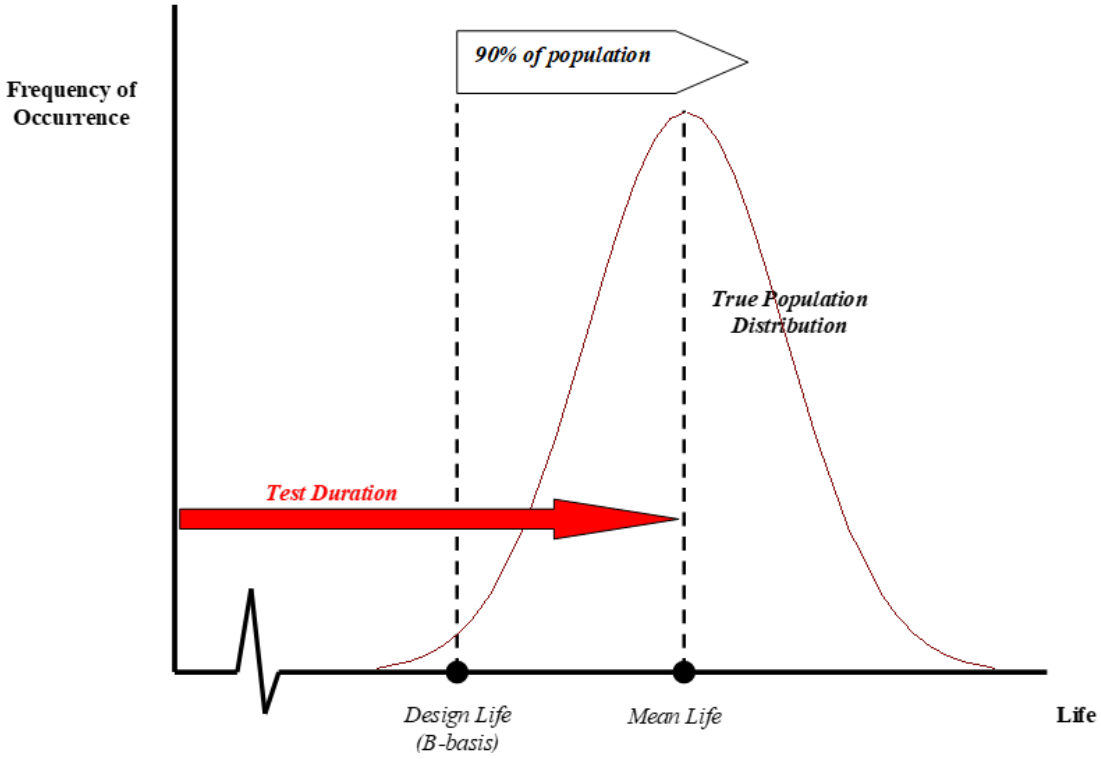
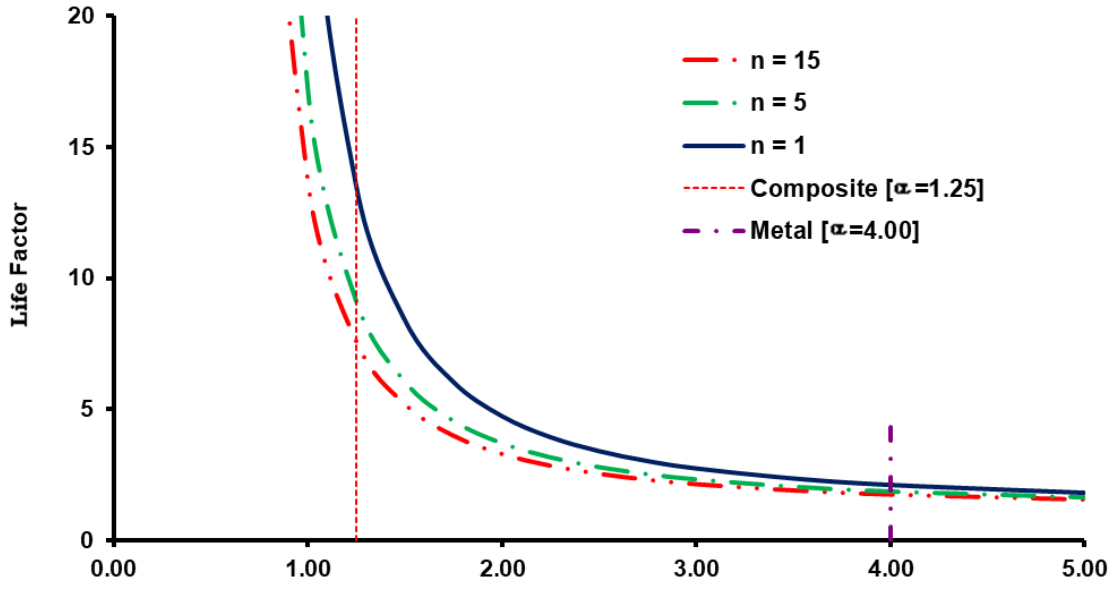


Figure 8. Life factor approach.

DISTRIBUTION STATEMENT A.
Approved for public release: distribution is unlimited.



Modal life shape parameter	Life factor (N_F) for different number of test articles (n)		
	n = 1	n = 5	n = 15
Composites α_L = 1.25	13.558	9.143	7.625
Metals α_L = 4.0	2.093	1.851	1.749

Figure 9. Influence of fatigue life shape parameter on B-basis life factor.

Furthermore, the analysis by Tomblin and Seneviratne [2] shows that the data scatter of notched or damaged composite elements can be significantly less than that of the unnotched composite specimens. Such improvements in the fatigue life shape parameter can significantly reduce the life factor. However, the life factor becomes insensitive to small changes in the life shape parameter beyond a value of 4, which is considered to be the life shape parameter for metal. The composite modal life shape parameter of 1.25, which was used for the Navy approach, lies within the highly sensitive region of life factor vs. shape parameter curve (Figure 9); thus, even a small improvement resulted in a dramatic reduction of the life factor, which reflects the required number of test durations to achieve a certain level of reliability in the design life. The MLSP is obtained from a distribution of shape parameters representing numerous SN curves of different critical structural details. Thus, it is common to have large scatter in the SN data of design details that have competing failure modes and less scatter in notched test data due to stress concentration. For example, a V-notched rail shear test specimen that has a soft (10/80/10) laminate stacking sequence has the majority of its fibers aligned with the tensile and compressive load resultant axes during in-plane shear loading. Although the applied (external) load is an in-plane shear load, the tensile and compressive (internal) loads along with fiber directions often cause a fiber break and fiber buckling, respectively, and significantly contribute to the final failure. In some cases, the competing (tensile and compressive) loading configurations will result in unacceptable failure modes of these in-plane shear specimens. Often, the complex state of

DISTRIBUTION STATEMENT A.
Approved for public release: distribution is unlimited.

stress and these competing failure modes coupled with other variabilities associated with composites such as batch variability, porosity, and fiber misalignments tend to cause large scatter in both static strength and fatigue life. On the other hand, stress concentrations in the notched composite cause the final failure of the specimen, negating or minimizing the collective effects of the above-mentioned secondary variables.

2.3 Load-Enhancement Factor Approach

An alternative approach to the life factor, which requires an excessive test duration, is to increase the applied loads in the fatigue spectrum so that the same level of reliability can be achieved with a shorter test duration [1]. This approach is referred to as the load-enhancement factor or combined load-life approach. A formal relationship between LEF and the test duration, *N*, as shown in equation (2), is formed for composite structural certification [1].

$$LEF(N) = \frac{\Gamma\left(\frac{\alpha_L + 1}{\alpha_L}\right)^{\alpha_L/\alpha_R}}{\left\{\frac{-\ln(R)\cdot N^{\alpha_L}}{\left[\chi^2_\gamma(2n)/2n\right]}\right\}^{1/\alpha_R}} \tag{2}$$

A special case, LEF for a test duration of one design lifetime, referred to as load factor (LF), is calculated as

$$LF = \lambda \cdot \frac{\Gamma\left(\frac{\alpha_R + 1}{\alpha_R}\right)}{\left\{\frac{-\ln(R)}{\left[\chi^2_\gamma(2n)/2n\right]}\right\}^{1/\alpha_R}} \tag{3}$$

where α_R is the modal static strength shape parameter (MSSP), and λ is a function of both the MSSP and the MLSP, as defined in equation (4). Derivation of the MSSP for composite quasi-static test data is discussed in detail in Section 3. Equation (3) has the same form as equation (1), except α_L is replaced by α_R, and the new parameter λ is included so that both life factor and load factor have the same level of reliability.

DISTRIBUTION STATEMENT A.
Approved for public release: distribution is unlimited.

$$\lambda = \frac{\Gamma\left(\frac{\alpha_L + 1}{\alpha_L}\right)^{\alpha_L / \alpha_R}}{\Gamma\left(\frac{\alpha_R + 1}{\alpha_R}\right)} \tag{4}$$

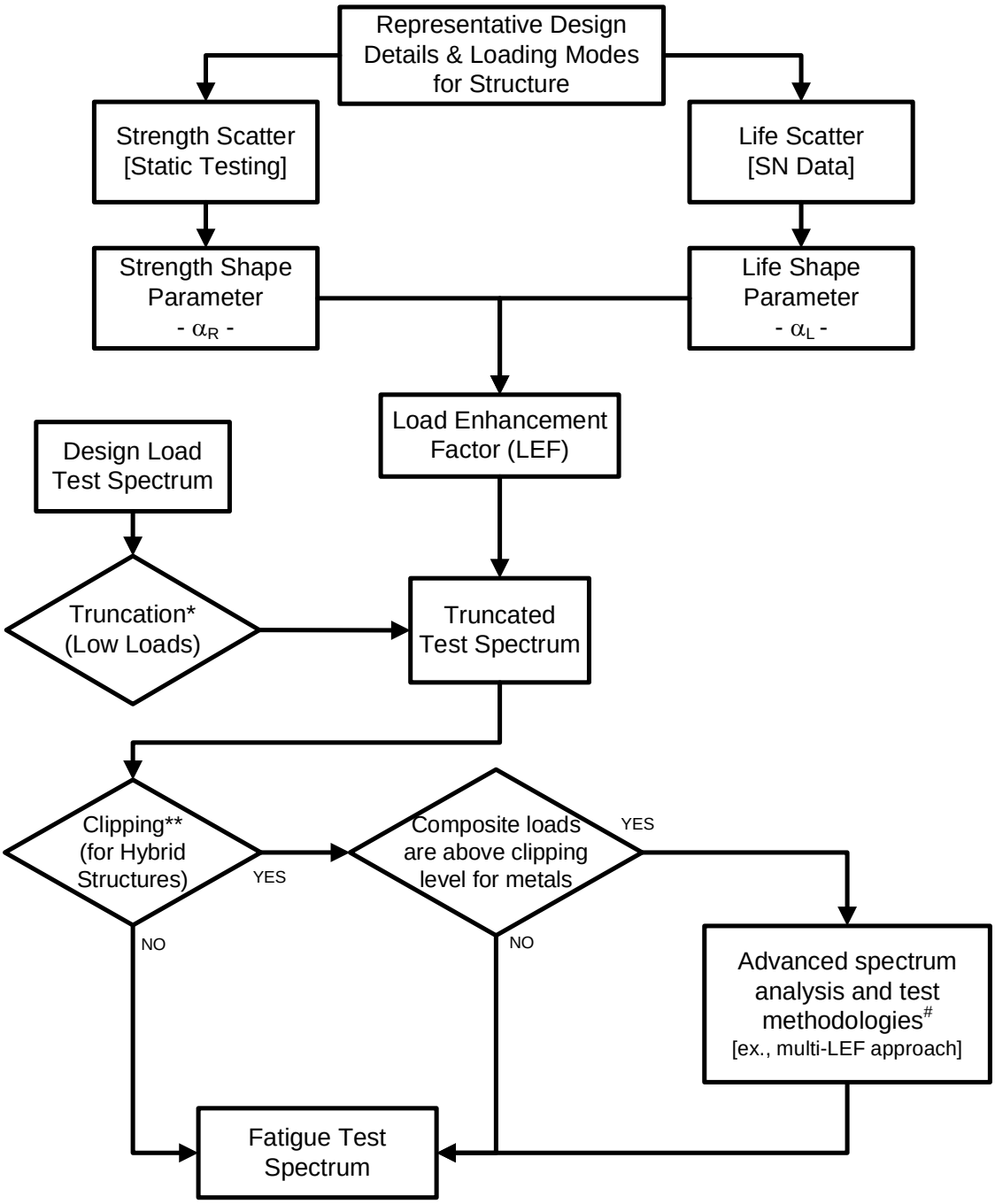
The life factor approach requires an excessive test duration and, by itself, may not be practical for full-scale test demonstrations. In contrast, the load factor approach requires increasing the fatigue loads so that the same level of reliability can be achieved with one test duration. However, for hybrid structures, overloads may cause crack-growth retardation, buckling, and premature failure of some of the metal components. Therefore, the LEF approach given in equation (2) would be to apply a combined load-life factor to achieve a compromise in the full-scale test requirements as well as the load spectrum. This approach allows using a lower load-enhancement factor as a tradeoff for more life cycles, which would reduce the severity of the overload on the metallic parts.

By combining equations (1) and (2), the expression for LEF is simplified in terms of test duration, as shown in equation (5):

$$LEF = \left(\frac{N_F}{N}\right)^{\frac{\alpha_L}{\alpha_R}} \tag{5}$$

Figure 10 shows the general procedure for the derivation of the LEF and the application of the LEF to a full-scale DaDT substantiation of composite structures [17].

DISTRIBUTION STATEMENT A.
Approved for public release: distribution is unlimited.



NOTES:
* Truncation (fatigue endurance) levels for composites and metals are different.
** Clipping of high loads are only required for metals; composite loads should not be clipped
# Further analysis and supporting experiments are required prior to applying these method

Figure 10. Derivation and application of life and load-enhancement factors through scatter analysis of composite test data.

DISTRIBUTION STATEMENT A.
Approved for public release: distribution is unlimited.

As shown in Figure 11, the LEF is significantly influenced by the MSSP and the MLSP. Thus, improvements in these shape parameters for newer forms of materials that exhibit less scatter can significantly reduce the LEF.

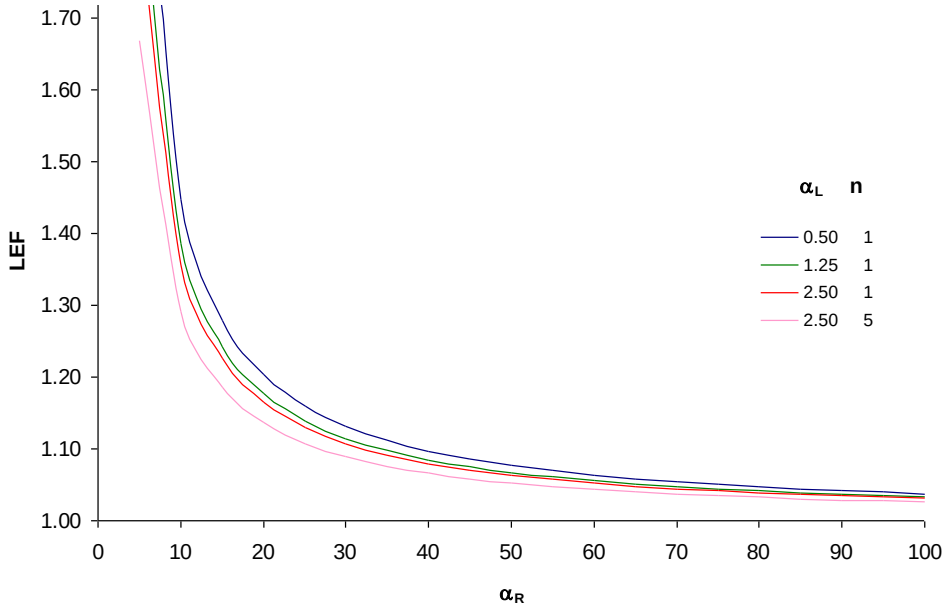


Figure 11. Influence of strength and life parameter on LEF.

As shown in Figure 12, a significant reduction in the LEF is achieved simply by increasing the test duration to 1.5 DLTs. Furthermore, the influence of strength and the life shape parameter on the LEF changes as the test duration is increased. For example, as the test duration is increased, the influence of the fatigue life shape parameter on the LEF increases. This is understood because N_F is only influenced by the MLSP. Also, note that for small test durations, the influence of the MSSP on the LEF is significant due to the increased influence of load factor.

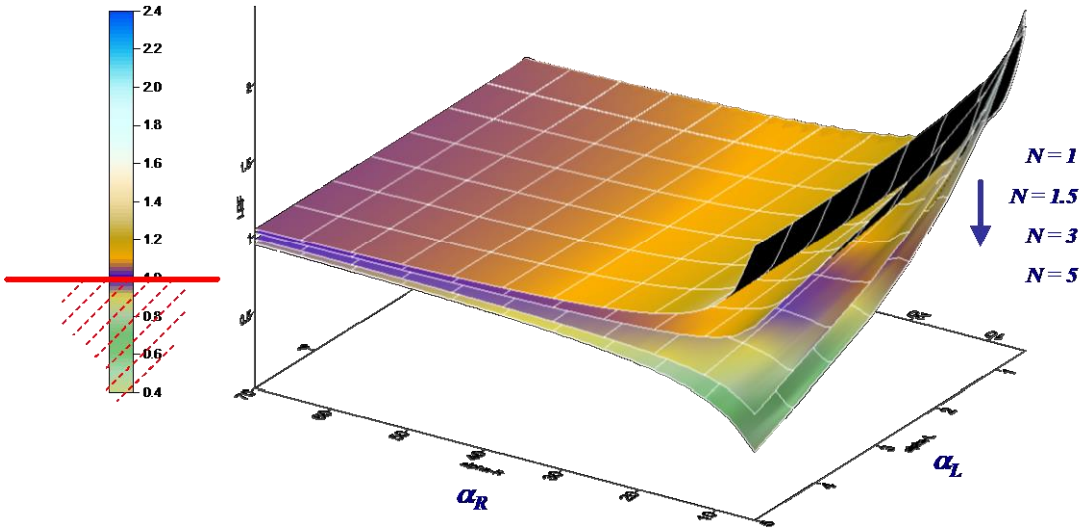


Figure 12. Influence of MSSP and MLSP on LEF (combined load-life approach).

DISTRIBUTION STATEMENT A.
Approved for public release: distribution is unlimited.

Although the LEF relationship can provide a wide range of load and life combinations to achieve the desired reliability, note that life factor (for LEF = 1) and load factor (N = 1) are both practical extremes of the LEF. The fatigue test spectrum loading should always be at least as large as the actual loading on the structure. This has the effect of limiting the LEF to being greater than or equal to 1.0, even if the test is conducted beyond the life factor. In addition, the test duration for a composite structure must be more than one lifetime (N > 1). In addition, for the metallic structure, the test duration should be sufficient to demonstrate that it is free from widespread fatigue damage (WFD) prior to the limit of validity (LOV), as outlined in AC 25.571-1D (Appendix 2), Section 3(d). The LOV is the operational life of the airplane consistent with evaluations accomplished and maintenance actions established to prevent WFD, which is a gradual deterioration of material subjected to repeated loads.

Application of the combined load-life approach is illustrated in Figure 13. The LEF is calculated as the ratio of the maximum applied load to the design maximum fatigue stress. This curve is generated by calculating the LEF for several different test durations. Note that the LEF required for the test duration that is equal to the life factor, N_F, is one, and N_F is obtained from equation (1) for the corresponding fatigue life shape parameter. If the design maximum load in the repeated load test (P_F) is increased to the mean residual strength at one lifetime (P_T), then the A- or B-basis residual strength of the structure would be equivalent to the design maximum fatigue stress. Thus, a successful repeated load test to one lifetime at applied stress, P_T, or a repeated test to N_F at applied stress P_F (no LEF) would both demonstrate the corresponding reliability. Furthermore, a successful repeated load test to a test duration (less than N_F) with the corresponding LEF would demonstrate the same level of reliability on the design lifetime.

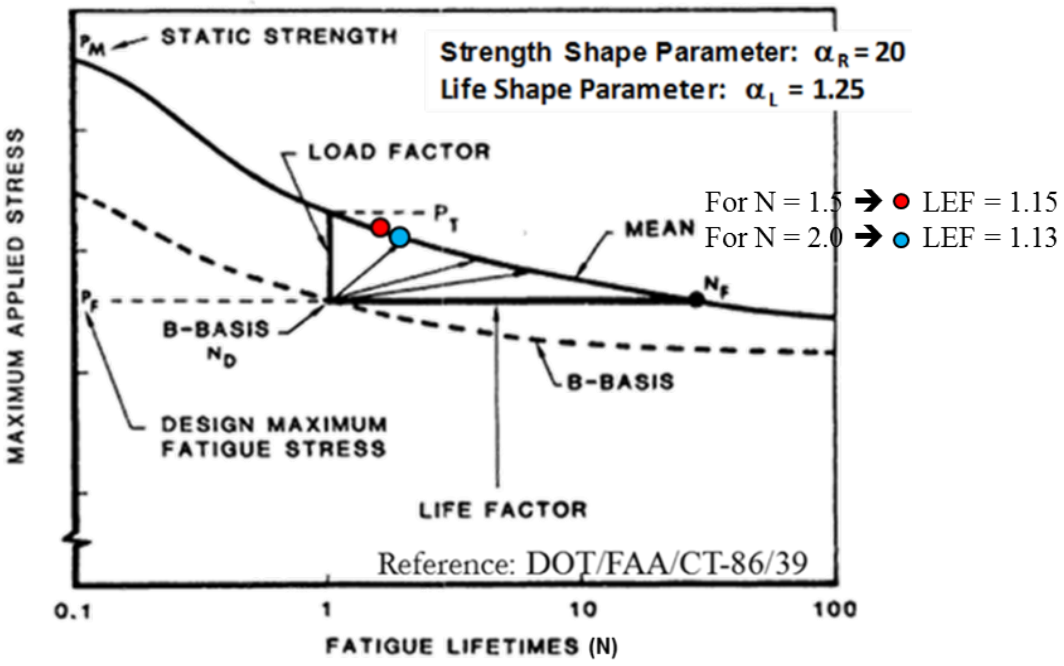


Figure 13. Combined load-life approach for composite structures.

DISTRIBUTION STATEMENT A.
Approved for public release: distribution is unlimited.

2.4 Certification Testing of Composite-Metal Hybrid Structures

The primary goal in a damage-tolerance certification program is to avoid catastrophic failure due to fatigue, corrosion, or accidental damage throughout the operational life of the aircraft. The damage-tolerance philosophy is well established for metallic airframes, where proven methods (structural analysis and inspection procedures) and supporting databases exist to detect damage and predict crack growth and residual strength. Damage-growth mechanics and load spectra for composite and metal structures have significant differences, which make the certification of composite-metal hybrid structures challenging, costly, and time consuming.

Compared to metals, composites are extremely notch/damage sensitive at the high-stress low-cycle region of the SN curve. For example, Figure 14 shows more than a 50 percent reduction in open-hole strength compared to the unnotched strength of the composite, while notched metallic static data show a relatively small reduction in strength. On the other hand, metallic notched data show a significant notch sensitivity at the low-stress high-cycle region of the SN curve, while the composite shows diminishing notch sensitivity at high cycles.

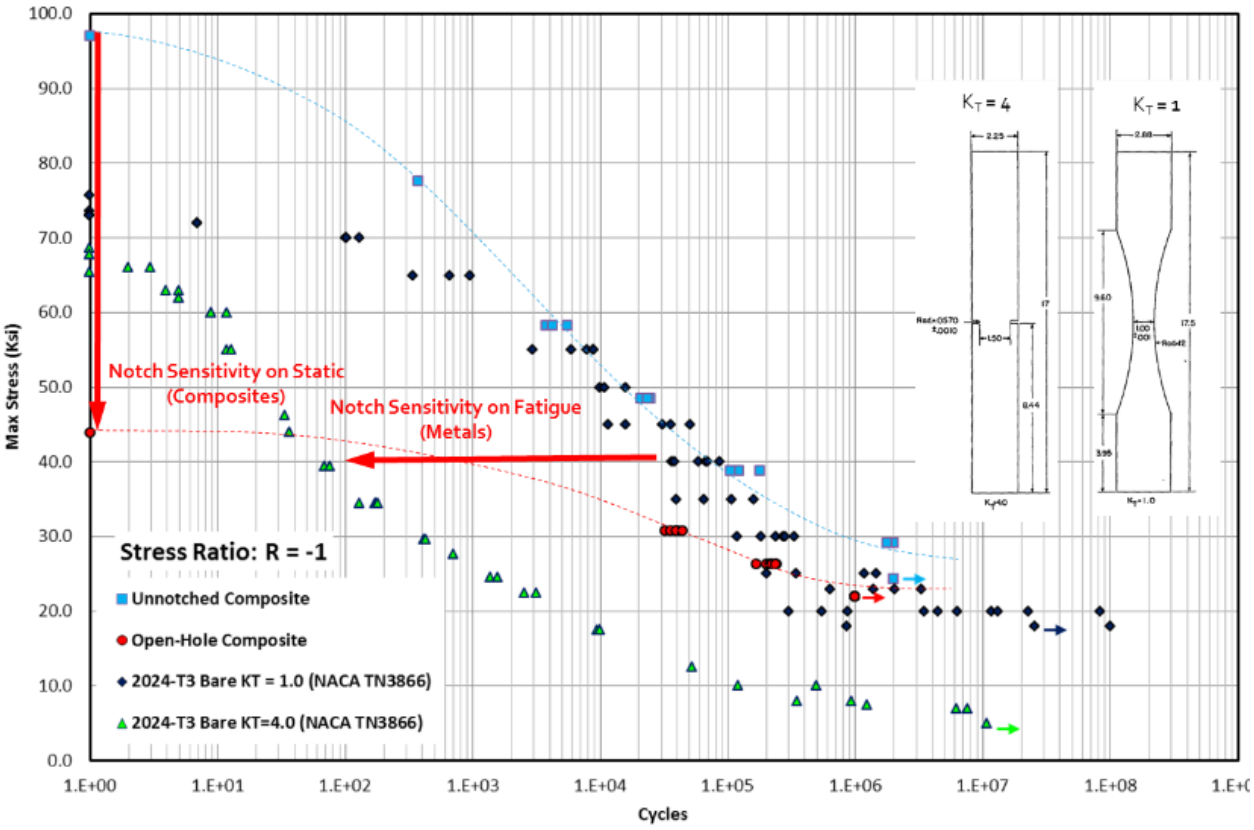


Figure 14. Composite-metal fatigue data [10].

Composite-metal hybrid structures are joined either by adhesive bonding or mechanical fastening. Figure 15 shows a comparison of typical quasi-static and fatigue failure modes for a single-shear double-fastener balanced (similar flexural rigidity [EI] on both metal and

DISTRIBUTION STATEMENT A.
Approved for public release: distribution is unlimited.

composites) hybrid joint. Although some localized plastic deformation near holes in the metal part are observed, the quasi-static failure mode is predominantly driven by the failure in composites due to their notch sensitivity for quasi-static loading. In contrast, the tension-tension fatigue failure is primarily driven by metal crack growth, while no or very minor damage to the composite is observed, indicating notch sensitivity of the metal for fatigue. Therefore, at high-stress low cycles, the fatigue failure mode is composite-dominant, while at low-stress high-cycles, it is metal-dominant. The fatigue SN data shown in Figure 16 indicate that at high stress levels (SLs), metal crack growth is dominant while at lower SLs, fastener fatigue is dominant. Therefore, hybrid tests require careful consideration of both metals and fastener fatigue as well as proper specimen sizing and fastener selection to achieve acceptable specimen failure modes (avoid fastener failure).



(a) Quasi-Static Failure Mode



(b) Fatigue Failure Mode for R = 0.1

Figure 15. Failure modes for single-shear double-fastener hybrid joint.

Aging studies conducted by WSU on decommissioned F/A-18 composite wing skins indicated that there is significant life left on the composite structure with no fatigue wearout, even with environmental conditioning [11-12] (see Figure 17). As shown in Figure 18, failure modes observed for tension-dominant fatigue spectrum (TDFS) tests with significant load severity factors were predominantly due to metal fatigue, while the limited number of failures observed under compression-dominant fatigue spectrum (CDFS) tests was primarily due to local buckling of the test specimens (note that the specimens were extracted from test articles where there were significant ply drop-offs within the specimens).

DISTRIBUTION STATEMENT A.
Approved for public release: distribution is unlimited.

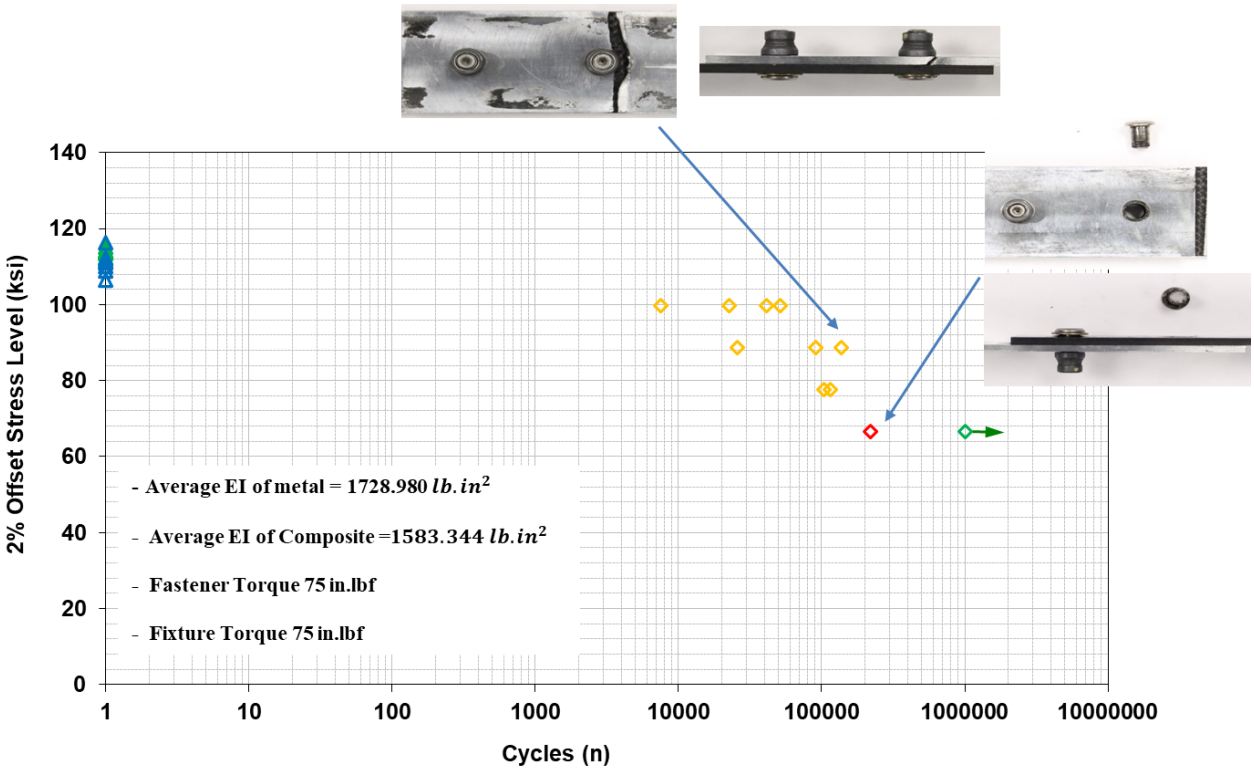


Figure 16. Fatigue SN data for metal single-shear double-fastener hybrid joint.

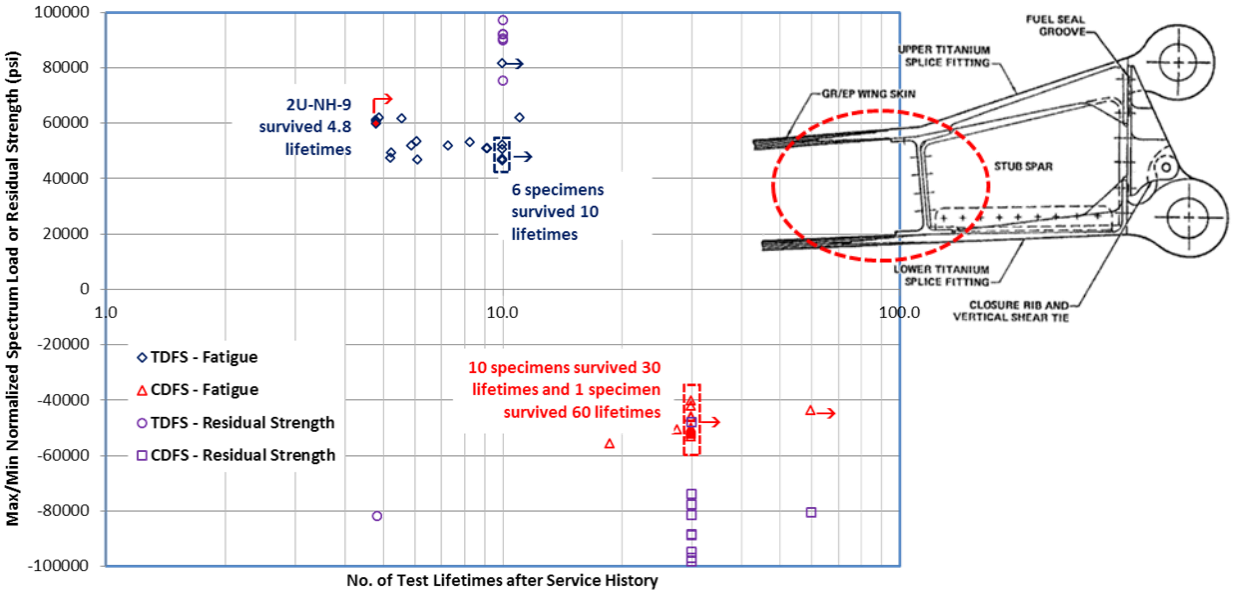


Figure 17. Spectrum fatigue test results for F/A-18 wing-root stepped lap joint [12].

Static strength tests conducted on the specimens extracted from decommissioned F/A-18 inner wing root stepped-lap joints indicated that the load-carrying capacity of the joint is comparable to the test data generated for pristine specimens. This indicates that the service history including environmental exposure has no significant effect on the residual strength of the joint, and the

DISTRIBUTION STATEMENT A.
Approved for public release: distribution is unlimited.

environmental protective scheme is effective. Additional spectrum fatigue tests indicated that the remaining life of the joints is substantial, and that the residual strength was unaffected by the additional fatigue cycles induced under laboratory environmental conditions. When spectrum loads were increased beyond operational stress levels, metallic fatigue failures were observed for the tension-dominant fatigue spectrum. Although significant microcracks were observed at the ply termination of each step, this did not directly impact the progressive damage growth until a crack was formed in the metal. Similar to the observation on mechanical fastened joints, adhesively bonded joint fatigue failure modes are driven by metal crack growth. NDI findings indicated that there is a reasonable window of opportunity to detect microcracks that can cause detrimental localized load redistribution due to softening of the composite structure, which may influence crack migration from the metal to the composite portion of the joint.

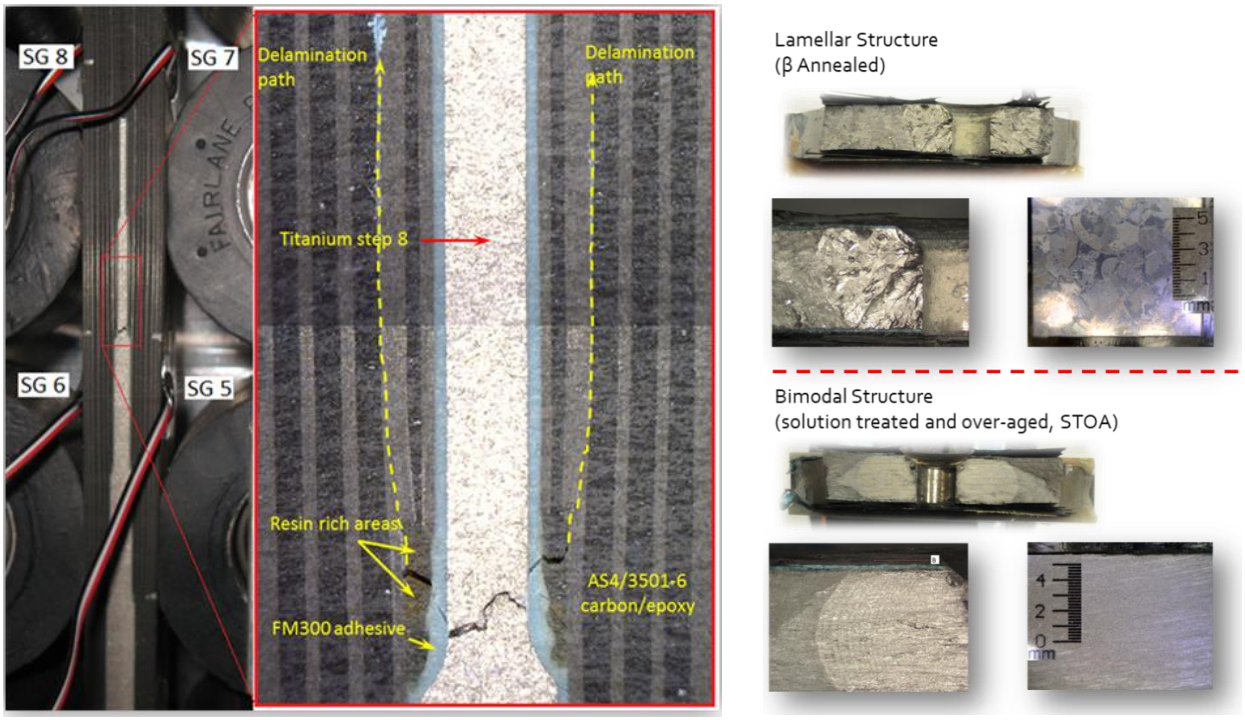


Figure 18. Failure modes for TDFS [12].

Composite damage growth mechanics are influenced by high loads, while low loads can be truncated based on endurance limit (stress level corresponds to infinite life) in order to reduce the test duration. Conversely, metal damage accumulation is influenced by low loads, while high loads must be clipped (i.e., reduce peak loads to clipping level so no loads are omitted) to prevent crack growth retardation and plastic deformation, as shown in Figure 19. However, those high loads significantly contribute to flaw growth in composite structures and reduce the fatigue life. Therefore, the clipping of high fatigue spectrum loads must be avoided during structural testing of composite structures. When load-enhancement factors are applied to the composite load spectrum, test loads can be significantly higher than clipping levels for the metallic components. Furthermore, a significant number of low loads below the composite endurance

DISTRIBUTION STATEMENT A.
Approved for public release: distribution is unlimited.

limit (used for truncating composite spectrum) may still contribute damage growth mechanisms for metals and must be included in the metallic spectrum.

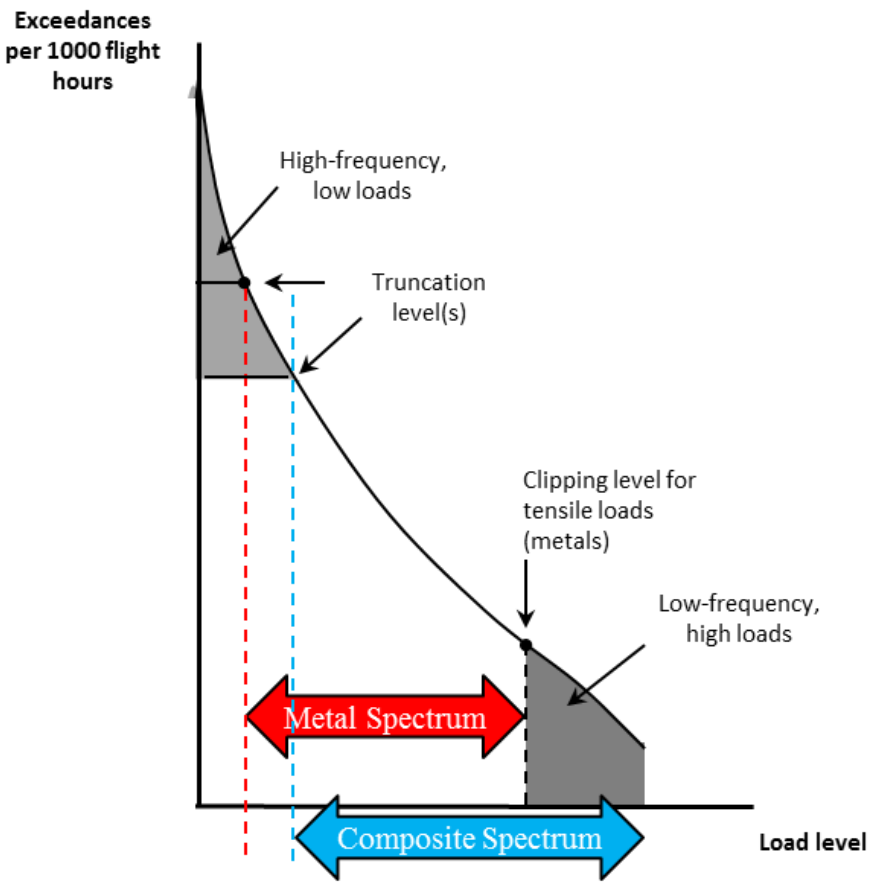


Figure 19. Composite and metal spectrum requirements.

Due to significant differences in damage growth mechanics and load spectra for the composite and metal structure, the certification of composite-metal hybrid structures using a single full-scale test article is challenging, costly, and time consuming. Certification of such a structure typically is achieved by the following:

1. Two separate fatigue test articles, each focusing on the metal and composite spectrums.
2. Pre-production subcomponent repeated load tests primarily focusing on composite structure certification, and full-scale repeated load tests focusing on metal structure certification.
3. Replacement of failed metallic part during repeated load test.

All three approaches are time consuming and costly. The third approach may not be applicable for a metallic-driven design, because multiple-site damage (MSD) and/or multiple element damage (MED) scenarios are not representative for establishing a limit of validity of engineering data that supports the structural maintenance of a metallic structure to avoid wide-spread fatigue

DISTRIBUTION STATEMENT A.
Approved for public release: distribution is unlimited.

damage during service. In addition, the replacement of metallic parts can cause program delays. Reinforcing these members should be avoided to prevent undesirable load distribution around these parts. In order to use a single full-scale test article for both composite and metallic substantiation, the following two approaches are introduced by the authors' previous work:

1. Multi-LEF approach [10]
2. Deferred severity spectrum (DSS) [13]

Please note that these approaches can also be combined in order to develop a hybrid test spectrum while maintaining loads below clipping levels for metals.

2.5 Multi-LEF Approach

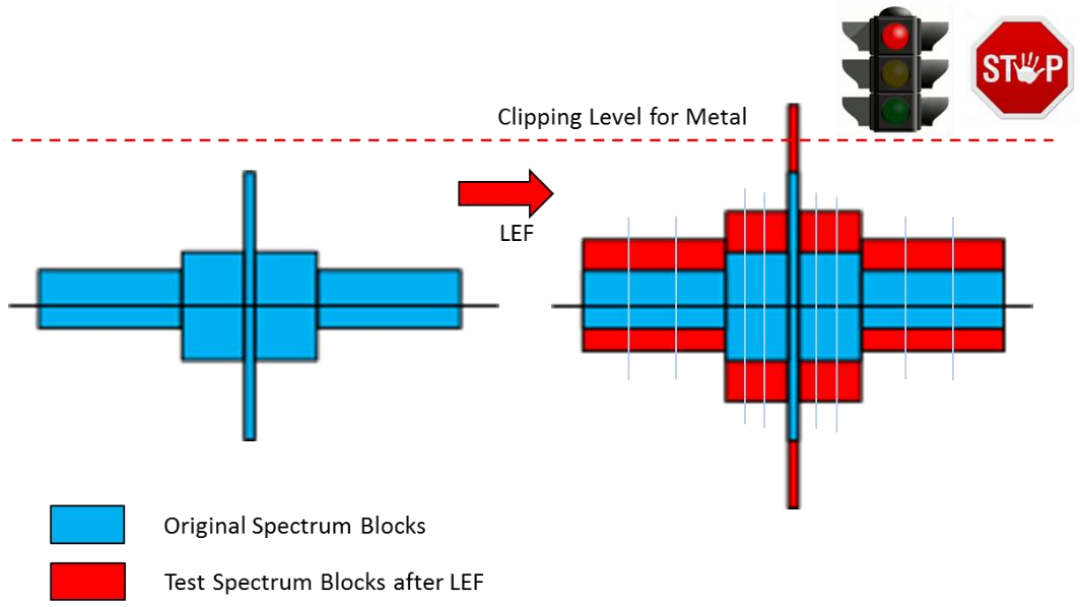
Traditionally, a single LEF value corresponding to a desired test duration (N) is applied to the complete test spectrum, as shown in Figure 20(a), and repeated N times to demonstrate durability of the structure for repeated loading. This approach can cause some of the high loads to go beyond the clipping levels of metal as can be seen in this example. Alternatively, a lower LEF with a longer test duration (note that the LEF is a function of test duration, and the longer the test duration, the smaller the LEF) can be applied to only these high-load blocks and still keep the original LEF for the remainder of the spectrum, as shown in Figure 20(b). Since equation (5) for the LEF is a function of test duration N, $LEF_1(N_1) > LEF_2(N_2)$, where $N_1 < N_2$. For example, $LEF_2(N_2)$ is applied to the high loads, while $LEF_1(N_1)$ is applied to the remaining test spectrum. This is further illustrated in Figure 21 for a composite material with a life factor (N_F) of 5. Note that the life factor is a function of the fatigue modal life shape parameter for a given material system and design details (see Chapter 3 for derivation of the MLSP).

Since the number of occurrences (exceedance) of these high loads is low, applying a longer test duration with lower LEF for just the high loads and not the rest of the test spectrum will not significantly impact the overall test duration. However, the additional repeated high loads corresponding to the low LEF must be spread throughout the spectrum to ensure that the additional high loads do not cause undesirable failures in the metallic structure; a detailed crack growth analysis of metallic parts may be required in order to ensure this.

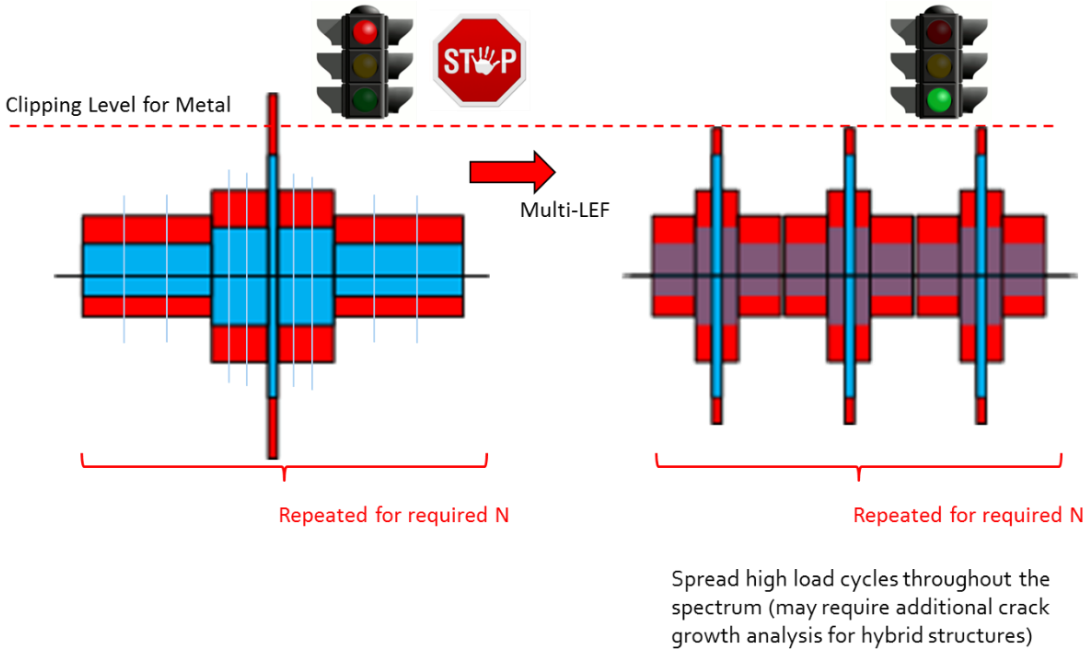
The multi-LEF example shown in Figure 22 indicates that for a test duration of 3, the test spectrum is repeated three times with a corresponding LEF, and only the high loads (red block) are repeated five times with a lower LEF, which corresponds to five test lifetimes. Since the illustration in Figure 21 indicates a life factor (N_F) of 5, for the load blocks with a test duration of 5, the LEF becomes 1. In this example, the additional high loads (two extra red blocks) are spread out during the second test life. Since the multi-LEF approach is a simplistic alternative approach for hybrid structural substantiation using a single test article and does not require additional verification tests, this approach must be considered.

DISTRIBUTION STATEMENT A.
Approved for public release: distribution is unlimited.

Note that the examples in this section use simplified block spectrums, which are not to scale, in order to demonstrate the application of concepts introduced in this report. However, typical test spectrums are complex and may be randomized to address various spectrum development requirements such as sequencing effects. In addition, truncation levels must be selected so that the minimum number of cycles required, especially for metals in order to address fretting, is included in the test spectrum to fully understand the long-term effects.



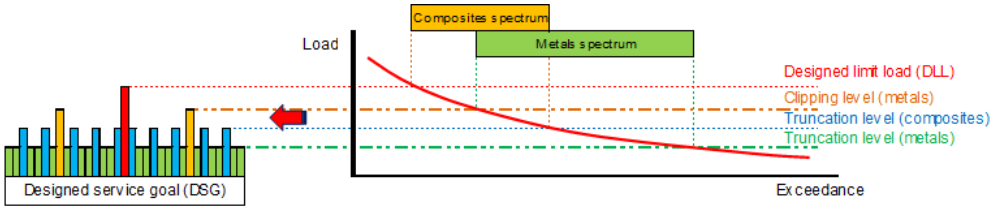
(a) LEF Application



(b) Multi-LEF Application

Figure 20. Multi-LEF approach for hybrid structures.

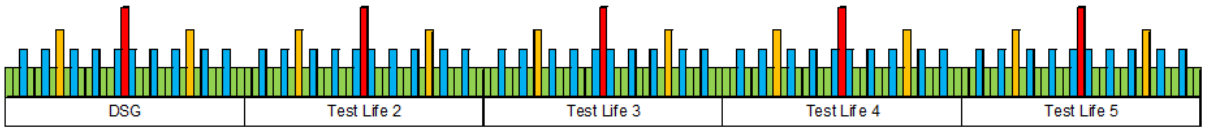
DISTRIBUTION STATEMENT A.
Approved for public release: distribution is unlimited.



Method 1: Life Factor Approach

$N_1 = N_2 = N_3 = \ldots\ldots = N_i = N_F$

➔ $LEF_1 = LEF_2 = LEF_3 = \ldots\ldots = LEF_i = 1.0$

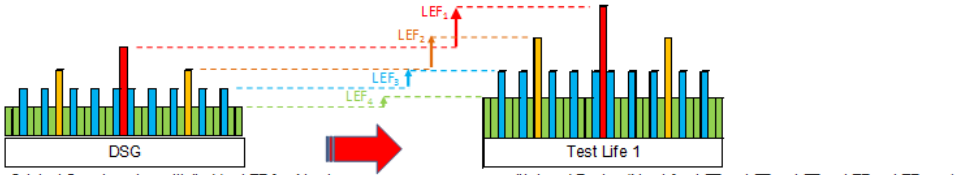


Original spectrum is repeated for Life factor; example (N_F) = 5

Method 2: Load Factor Approach

$N_1 = N_2 = N_3 = \ldots\ldots = N_i = 1$

➔ $LEF_1 = LEF_2 = LEF_3 = \ldots\ldots = LEF_i = LEF_{@N=1}$



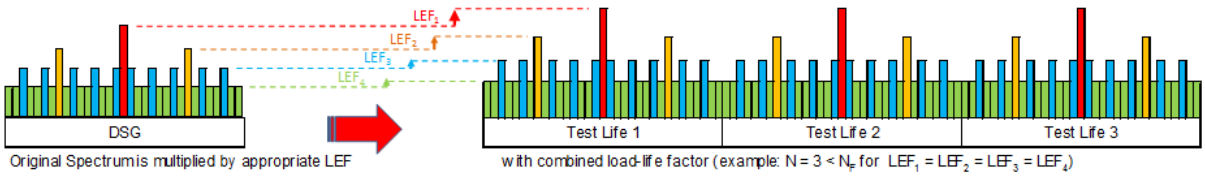
Original Spectrum is multiplied by LEF for N = 1

with Load Factor (N = 1 for $LEF_1 = LEF_2 = LEF_3 = LEF_4 = LEF_{@N=1}$)

Method 3: Combined Load-Life Factor (LEF) Approach

$N_1 = N_2 = N_3 = \ldots\ldots = N_i$

➔ $LEF_1 = LEF_2 = LEF_3 = \ldots\ldots = LEF_i$



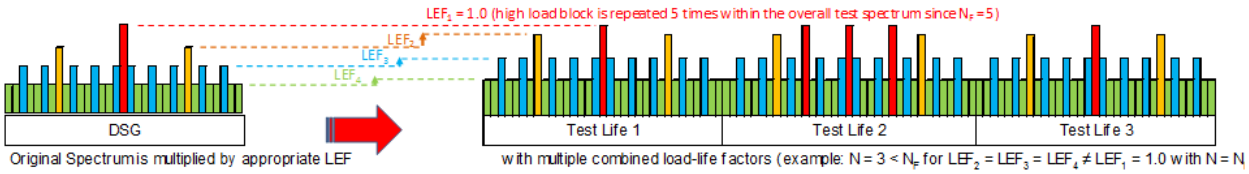
Original Spectrum is multiplied by appropriate LEF

with combined load-life factor (example: $N = 3 < N_F$ for $LEF_1 = LEF_2 = LEF_3 = LEF_4$)

Method 4: Multi Load-Life Factor (multi-LEF) Approach

$N_1 \neq N_2 \neq N_3 \neq \ldots\ldots \neq N_i$

➔ $LEF_1 \neq LEF_2 \neq LEF_3 \neq \ldots\ldots = LEF_i$



Original Spectrum is multiplied by appropriate LEF

with multiple combined load-life factors (example: $N = 3 < N_F$ for $LEF_2 = LEF_3 = LEF_4 \neq LEF_1 = 1.0$ with N = N

Figure 21. Comparison of application of combined load-life approach for hybrid structures (assume $N_F = 5$).

DISTRIBUTION STATEMENT A.
Approved for public release: distribution is unlimited.

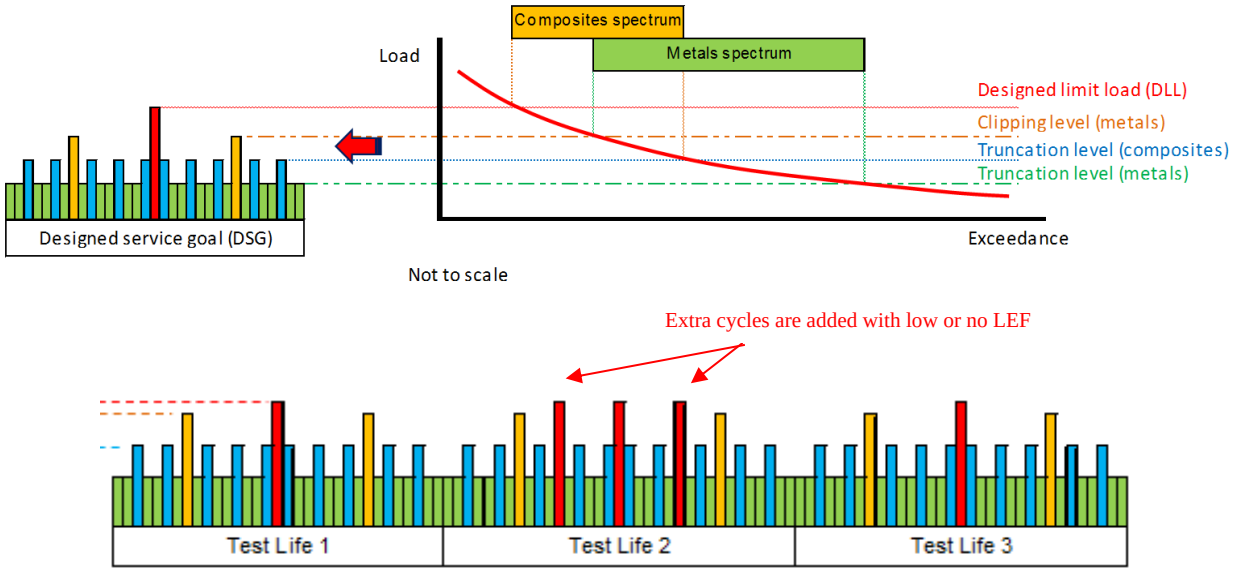


Figure 22. Multi-LEF example for hybrid structures.

2.6 Deferred Severity Spectrum

In addition to the multi-LEF approach, Seneviratne and Tomblin [18] introduced a concept where a single full-scale article is used with a two-phase process. This approach is referred to as the deferred severity spectrum since the high loads above clipping level for metals are moved from the initial metal substantiation phase to the second phase that completes the remainder of the composite loads. As shown in Figure 23, this approach has two major phases:

Phase 1: This initial phase with metal test substantiation focuses on no LEF or multi-LEF to prevent loads above the clipping levels for metals. This phase is further segmented into durability and damage tolerance sections. Phase 1 is carried out as a typical metallic DaDT test (note that the example in Figure 23 uses a 3-lifetime test for metal, but the test duration shall be adjusted accordingly), with the exception of the addition of composite loads below the clipping level for metals. At the end of the metallic substantiation, typically a teardown inspection of the test article is carried out to demonstrate the LOV. Since the same article is used for phase 2, the LOV is demonstrated through a detailed inspection plan for metallic components and/or a limit-load test at the end of phase 1.

Phase 2: The second phase focuses on composite DaDT substantiation with the LEF and composite loads above clipping levels that were deferred during phase 1. Phase 2 is carried out as a typical composite DaDT test, with the exception of modification to the test duration in order to get certification credit for fatigue cycles applied during phase 1.

DISTRIBUTION STATEMENT A.
Approved for public release: distribution is unlimited.

Note that the combined load life approach (including multi-LEF approach) can be applied at any of the above two phases to ensure successful completion of test hybrid test substantiation without unintentional failures.

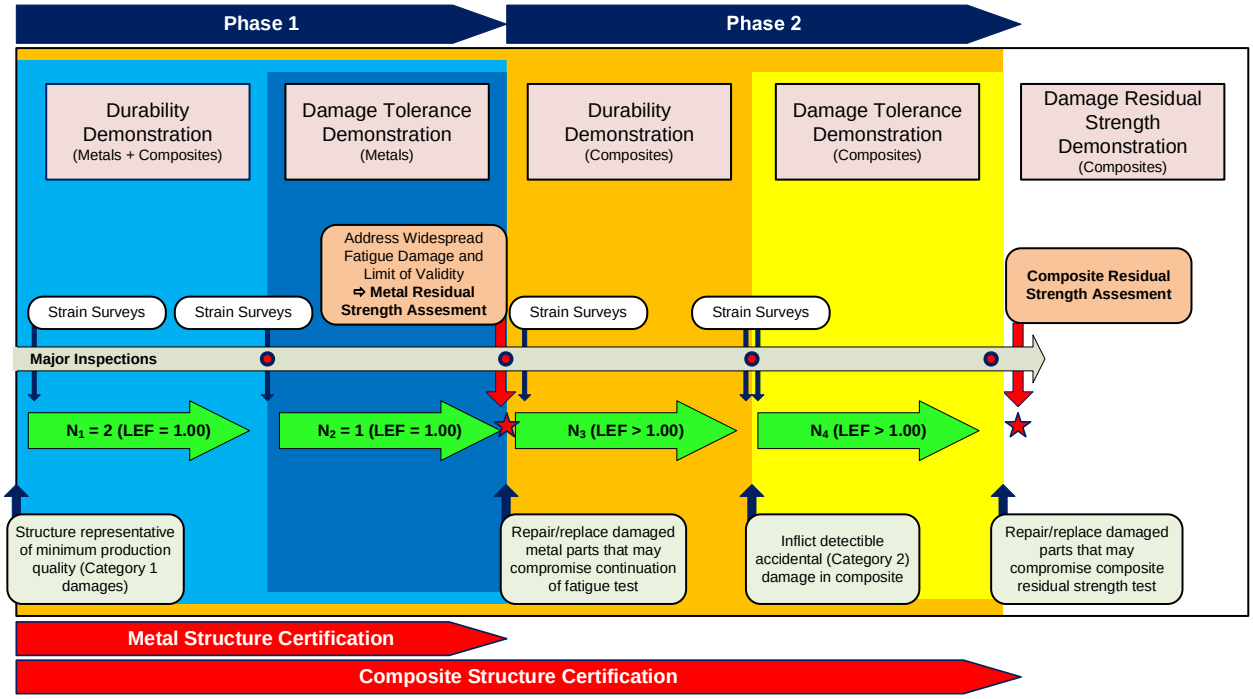


Figure 23. Full-scale test substantiation using deferred severity spectrum approach [18].

The LEF curve is a formal relationship between the LEF and the test duration, as shown previously in Figure 13. When different LEFs are applied to different parts of the same test, an approach called load-life shift is proposed [17], in order to demonstrate the reliability of the DaDT test. This approach combines the required test durations for different phases (with different LEFs) of the same test and demonstrates the required reliability on the design service goal. This load-life shift approach provides a mechanism to obtain credit for the loads applied during the first phase (focusing metal) so that the test duration for the composite certification phase can be reduced. The general form of the load-life shift approach for a multi-phase structural test is

$$\frac{N^T_{LEF_1}}{N^R_{LEF_1}} + \frac{N^T_{LEF_2}}{N^R_{LEF_2}} + \ldots\ldots + \frac{N^T_{LEF_n}}{N^R_{LEF_n}} = \sum_{i=1}^{n} \frac{N^T_{LEF_i}}{N^R_{LEF_i}} \geq 1.0 \qquad (6)$$

where subscripts LEF_i correspond to the test phase i with the corresponding LEF, and superscripts R and T denote the corresponding repeated life (or test duration, N) for a particular LEF and the actual test duration, respectively, to demonstrate reliability of the DSG. In order to show the desired level of reliability on the DSG, the cumulative ratio of test duration for the required repeated life for each corresponding LEF must be greater than (or equal to) 1.0.

DISTRIBUTION STATEMENT A.
Approved for public release: distribution is unlimited.

Equation (6) can be simplified to calculate the required test duration for phase 2 of the DSS approach as follows:

$$N_2^T = \left(1 - \frac{N_1^T}{N_1^R}\right) \cdot N_2^R \tag{7}$$

where subscripts 1 and 2 correspond to the test phases.

Figure 24 illustrates the step-by-step process of generating the deferred severity spectrum for a hybrid structure. In this example, the life factor is assumed to be 5. Therefore, a test duration of five lifetimes does not require the LEF. In order to apply the DSS approach, both metal and composite load spectra must be included during phase 1. During this phase, the truncation of low loads is based on the metal SN data because the metallic truncation level is typically a lower stress level than that for composites. If the composite-critical loads are beyond clipping levels for metals after application of the LEF, then the multi-LEF approach can be implemented. If any of the loads are beyond clipping levels for metal prior to application of the LEF, such loads must be included during the second phase so that the total required number of occurrences for such loads is applied by the end of the second phase. These additional high-load cycles should be interspersed in the spectrum and must be chosen so that the stress ratio is maintained. Since the second phase of the test focuses primarily on composite certification, the truncation of low loads can be based on composite SN data, which typically is a higher stress level than metallic SN data. This allows for the elimination of a significant number of low loads from the remainder of the test, as illustrated in Figure 24.

Upon demonstration of compliance with airworthiness requirements, a type certificate (TC) is issued by the certification authority to signify the airworthiness of an aircraft that is manufactured according to the approved design. Typically, the full-scale fatigue testing is not completed by the time of application for the TC. However, according to the Federal Aviation Regulations (14 CFR 25.571), the TC may be issued prior to completion of full-scale fatigue testing, given the following requirements are met:

> **14 CFR 25.571: § 25.571 Damage—tolerance and fatigue evaluation of structure, Section (b)** *". . . The type certificate may be issued prior to completion of full-scale fatigue testing, provided the Administrator has approved a plan for completing the required tests. In that case, the Airworthiness Limitations section of the Instructions for Continued Airworthiness required by § 25.1529 must specify that no airplane may be operated beyond a number of cycles equal to ½ the number of cycles accumulated on the fatigue test article, until such testing is completed . . ."*

However, the impact of moving the high loads that are in the composite spectrum to phase 2 of the test program may have to be justified, since they are not applied to the test article at the time of the first flight. Information gathered during full-scale static limit-load testing and the low

DISTRIBUTION STATEMENT A.
Approved for public release: distribution is unlimited.

probability of occurrence of such high loads can be used for justifying the deferment of such severe loads.

The test duration for phase 1 must be selected to establish the LOV for a structure susceptible to WFD per recommendations in Advisory Circular 25.571:

> **Advisory Circular 25.571-1D (Appendix 2), Section 3. Elements of a Full-Scale Fatigue-Test Program, (d) Test duration.** *". . . It follows, then, that if one full-scale fatigue-test article maintains the minimum residual-strength requirements of § 25.571(b) for test duration X, one can conservatively assume that the WFD (average behavior) of all WFD-susceptible structure is equal to X. Assuming inspection for MSD/MED is impractical, replacement or modification would be required at X divided by 3 per the guidance in AC 120-104. For areas where inspections for MSD/MED are practical, the applicant may defer replacement or modification until X divided by 2, provided inspections for MSD/MED start at X divided by 3 . . . ."*

DISTRIBUTION STATEMENT A.
Approved for public release: distribution is unlimited.

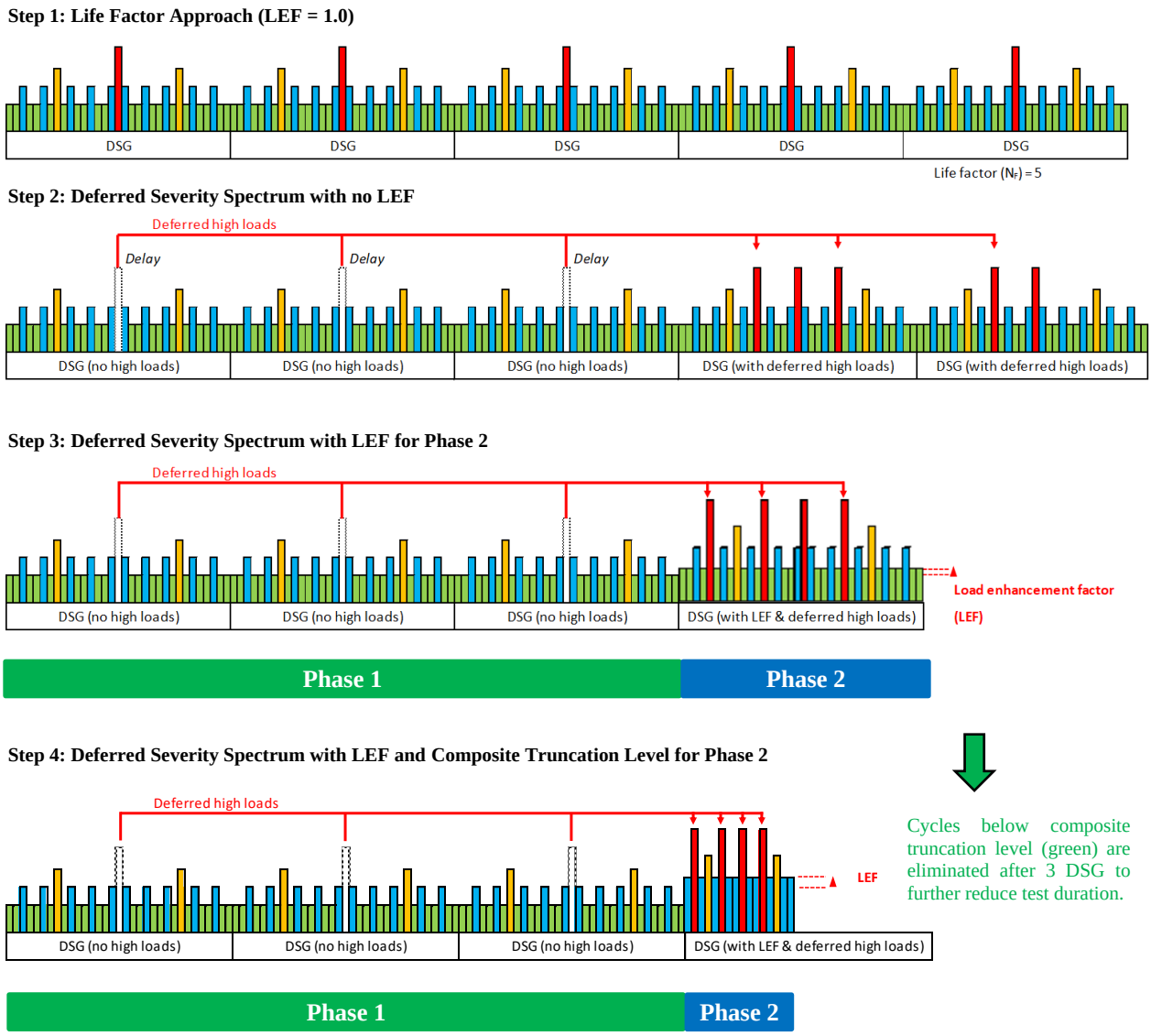


Figure 24. Illustration of hybrid spectrum development for deferred severity spectrum approach (assume N_F = 5).

Demonstration of the LOV for metallic design typically includes a teardown inspection and/or residual strength tests per § 25.571(b) upon completion of the fatigue testing. With the DSS approach, residual strength is demonstrated according to 14 CFR 25.571 in lieu of teardown inspections. Although teardown inspections can be conducted after the completion of phase 2, validity of the results on the metallic fatigue failures must be examined due to additional cycles and any loads above clipping levels for metals that cause crack growth retardation.

The application of multi-LEF and DSS approaches requires demonstrating that the modifications made to the original spectrum do not affect the damage growth mechanism or the failure mode(s). This can be done as an investigation into sequencing effects at coupon- or element-level testing as required. In addition to sequencing effects, the impact of additional cycles and

DISTRIBUTION STATEMENT A.
Approved for public release: distribution is unlimited.

high loads on the metallic structure must be considered through analysis and/or detailed inspections to ensure that any wearout does not alter the load path(s) and cause undesirable or unexpected load redistributions. In the case of the DSS approach, additional cycles beyond the first phase cannot be used for substantiating life extension because the high loads (above clipping level for metals) in phase two or the replacement of metallic parts will invalidate additional cycles on the metallic structure. Because teardown inspections on the metallic structure are delayed until the end of the second phase, the limit of validity (absence of widespread fatigue damage) on the metallic structure must be demonstrated through a limit-load test at the end of the first phase and/or a rigorous inspection plan during phase two, which require approval from certifying agency. Metallic crack growth analysis must be performed to assess the effect of the LEF on metal parts during phase 2. If premature cracking of metal parts is predicted, then agreement may be reached with the certifying agency that test results can be modified analytically to represent the metal part performance under the nominal spectrum up to three test lifetimes, and a rigorous inspection plan must be in place to inspect critical metallic components or replace failed metallic parts at the end of phase 1, the metallic test substantiation.

Development of the hybrid spectrum for phase 1 must adhere to all standard practices for metallic spectrum requirements, since metallic substantiation is the primary focus during this phase. However, during phase 2, since the metallic substantiation is completed in phase 1, the spectrum can be modified to suit composite substantiation requirements, assuming that such modification will not cause metallic failure. If metal part failure is predicted during phase 2, then such components must be replaced to avoid unintentional load redistributions or structural failure.

Metallic damage growth mechanics are highly sensitive to the test spectrum sequence. In order to apply either a multi-LEF or deferred severity spectrum for hybrid structural testing, it is important to demonstrate that the modifications to the test spectrum will not cause unintentional damage growth in the full-scale test article, especially the composite structure, since major modifications to the composite spectrum are required during phase 2 (deferred severity and added high load cycles for multi-LEF). The literature survey indicated mixed observations relative the effects of spectrum sequencing for composite structures. The data [19,20] show that although sequencing effects for composites exist at higher stress levels, they are not a concern because the typical operational SLs for composites are significantly lower than the endurance limits for composites. However, recent findings [20] for T650/5320 unidirectional tape material with a quasi-isotropic layup showed that, when the specimens are tested for a considerable amount of fatigue cycles at spectrum loads near the endurance limit of the composite, fiber failures can occur (Figure 25). In this example, X-ray CT scan inspections carried out after cycling the specimens for 516,340 cycles (400,010 cycles at 40 percent and 116,330 cycles at percent static strength) indicated early fiber breaks that were not visible in the ultrasonic C-scan inspections. Note that the 40 percent SL corresponds to a strain level of about 2,500 microstrain. Typical design limit strain levels are around 3,000 microstrain, and the highest fatigue strain level in a typical spectrum is around 2,500 microstrain. Specimens that were cycled at SLs as

DISTRIBUTION STATEMENT A.
Approved for public release: distribution is unlimited.

high as 70 percent of the static strength for 3,000 cycles only indicated microcracks. Further studies are in progress in collaboration with the Air Force Research Laboratory (AFRL) to fully understand the formation of composite fatigue damage under spectrum fatigue loading. Such phenomenon must be investigated through coupon/element-level testing prior to applying the multi-LEF approach for full-scale structural testing, especially when high loads in the test spectrum are near the endurance limit of composites.

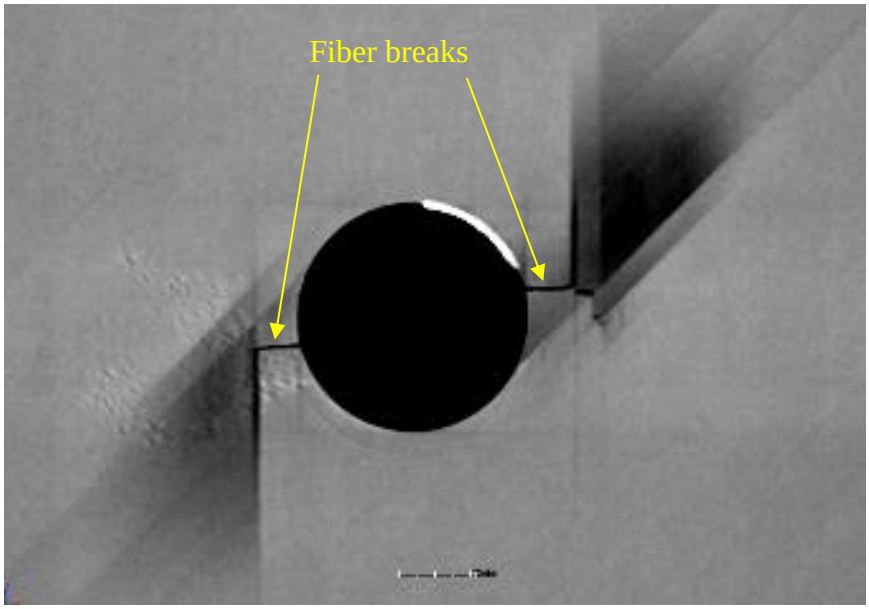


Figure 25. Fiber failure of spectrum loading near endurance limit [20].

The example shown in Figure 26 indicates the test requirements to demonstrate B-basis reliability on life using a single metal-composite hybrid test article. In this example, phase 1 is carried out with no LEF for three lifetimes, primarily focusing on metallic substantiation. In order to continue to the second phase for composite substantiation, several options are given in Table 1 (and illustrated in Figure 26) with corresponding LEFs. The test duration for phase 2 is calculated using equation (6) for each option of the LEF applied during phase 2. For example, after completing three lifetime tests with LEF = 1 in phase 1, if LEF = 1.088 is selected, then the phase 2 test can be completed with an additional 0.5 test lifetime to demonstrate the B-basis reliability on the DSG for the hybrid structure (total test duration is 3.5 lifetimes). Figure 26 also shows the test time reduction (compared to two separate test articles) by using the DSS approach for different LEF requirements.

DISTRIBUTION STATEMENT A.
Approved for public release: distribution is unlimited.

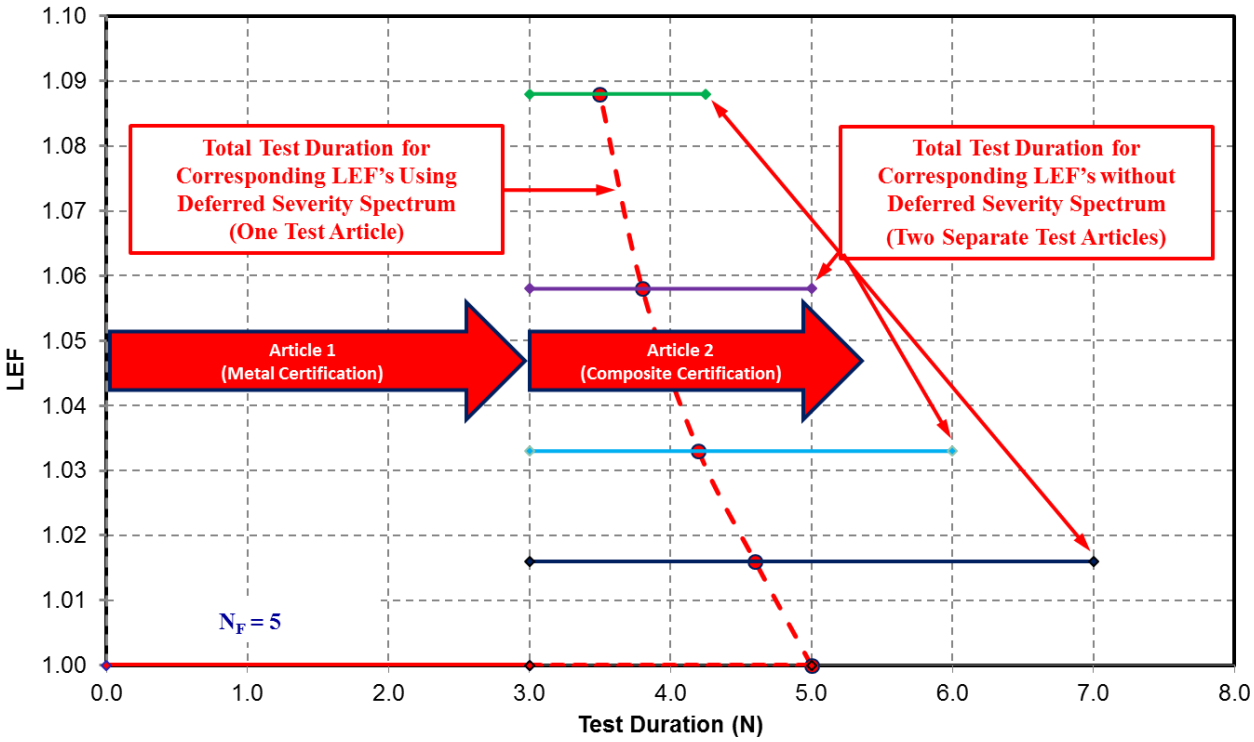


Figure 26. Certification of composite-metal hybrid structures using deferred severity spectrum.

Table 1 – Required test duration for phase 2 after three lifetime tests in phase 1 with LEF = 1.0.

Options for DSS Phase 2	Typical LEF Application		Deferred Spectrum Severity Approach		
	LEF	Test Duration*	Test Duration for Phase 1 (no LEF)	Test Duration for Phase 2 (with LEF)	Total Test Duration for DSS
1	1.000	5.0	3.0	2.0	5.0
2	1.016	4.0		1.6	4.6
3	1.033	3.0		1.2	4.2
4	1.058	2.0		0.8	3.8
5	1.088	1.3		0.5	3.5

*Corresponding to LEF from reference [2] for a typical composite material.

DISTRIBUTION STATEMENT A.
Approved for public release: distribution is unlimited.

3. COMPOSITE DATA ANALYSIS

The primary goal in the scatter analysis of composites is to interpret the data variability obtained at the lower levels of building-block testing and translate the statistical significance of such phenomena into large-scale test substantiation. In order to determine the shape parameters for static strength and fatigue life for the purpose of large-scale test substantiation, test matrices should include design details and loading modes of critical locations of the structure via coupon and/or element tests. The influences of material, layup sequence, loading mode, sandwich construction, joints, environmental effects, etc., are typically considered during static strength scatter analysis. Fatigue analysis includes the influence of the stress ratio, in addition to the above-mentioned design details.

Scatter in composites can be analyzed as either a Weibull, normal, or log-normal distribution. Since the shape parameter provides information with respect to the data scatter, the two-parameter Weibull distribution is commonly used in composite static and fatigue scatter analyses. Fatigue scatter in composite test data can be analyzed using several different techniques but mainly subdivided into two categories: individual analysis and pooling. Joint Weibull and Sendeckyj are two pooling techniques discussed in this section.

First, the shape parameters corresponding to different data sets representing different design details are obtained using Weibull analysis. Then the shape parameters corresponding to their Weibull distributions, referred to as the strength or life shape parameters, are obtained. The lowest of the mean and the modal value is conservatively used (i.e., the modal value of the distribution of shape parameters is selected in the example shown in Figure 27 as the strength or life shape parameter, rather than the mean value), and this is referred to as the modal strength shape parameter or modal life shape parameter, respectively. Note that the mode or modal value is the value that appears most often in a data set.

The determination of fatigue life scatter requires a large number of test replications at different stress levels and stress ratios. To reduce cost and test duration while maintaining the reliability of data analysis, it is recommended that the fatigue scatter analysis be conducted using pooling methods such as the joint Weibull or Sendeckyj wearout analysis. A detailed fatigue life scatter analysis of several composite materials and adhesive systems is included in the work of Tomblin and Seneviratne [2] using individual Weibull, joint Weibull, and Sendeckyj analyses (with and without static data). However, the fatigue life scatter analysis for deriving life- and load-enhancement factors is not limited to these three techniques. Furthermore, different analytical techniques may be required for certain design details, depending on the complexity of the construction and the process techniques used, as outlined in their work [2] (e.g., adhesive joints). A comparison of the three fatigue scatter analysis methods used in this report is shown in Table 2.

DISTRIBUTION STATEMENT A.
Approved for public release: distribution is unlimited.

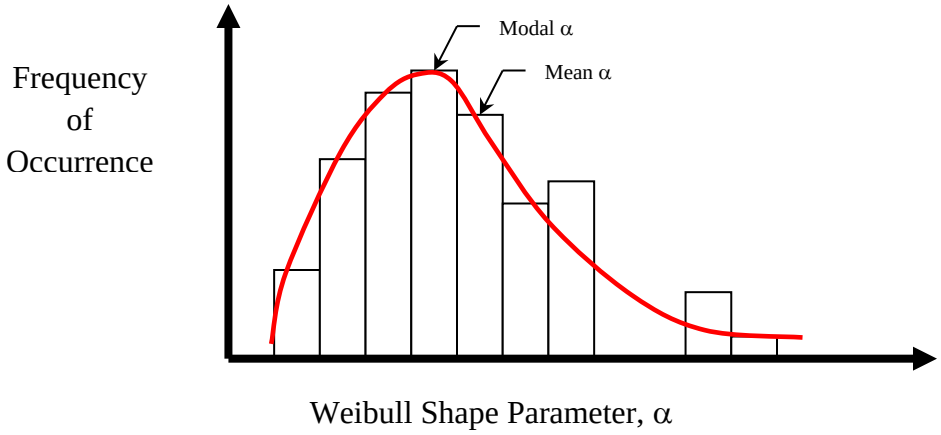


Figure 27. Scatter analysis using Weibull distribution of shape parameters.

Table 2 – Comparison of fatigue scatter analysis techniques.

Analysis Features	Individual Weibull	Joint Weibull	Sendeckyj
Weibull assumptions	x	x	x
Account for effects in multiple stress levels		x	x
Allow unequal replicates per stress level	x	x	x
Accommodate single replicate per stress level		x	x
Allow single stress level test	x	x	
Include runout specimens			x
Include stress levels with all runouts			x
Utilize residual strength from runout coupons			x
Include static specimens			x
Provide information to fit S-N data			x
Provide information to calculate residual strength			x

3.1 Individual Weibull Method

Weibull distribution has been extensively used in life testing and reliability analysis of composites, especially for small samples, due to its simple functionality and ease of interpretation. The commonly used two-parameter Weibull distribution expressed by the cumulative survival probability function is shown as

$$P(X \le x) = e^{-(x/\beta)^{\alpha}} \tag{8}$$

where x is the random variable, α is the shape parameter, and β is the scale parameter.

The population mean, μ, and standard deviation, σ, are calculated with the gamma (Γ) distribution function in equations 9 and 10, respectively.

DISTRIBUTION STATEMENT A.
Approved for public release: distribution is unlimited.

$$\mu = \beta \cdot \Gamma\left(\frac{\alpha+1}{\alpha}\right) \tag{9}$$

$$\sigma = \beta\sqrt{\Gamma\left(\frac{\alpha+2}{\alpha}\right) - \Gamma^2\left(\frac{\alpha+1}{\alpha}\right)} \tag{10}$$

The shape parameter and scale parameter are estimated from an iterative process using either the maximum likelihood estimation (MLE) or rank regression. Rank regression in X (RRX) tends to produce reliable results for small samples, while MLE works well for samples containing more than 20 or 30 data points.

During the individual Weibull analysis of fatigue data, each stress level is analyzed, and then the shape parameters are arithmetically averaged to define life scatter. Since Weibull analysis considers only the data at a certain SL at a time, five or more data points must be included in each SL. For SN data that has less than five data points per SL, either joint Weibull analysis or Sendeckyj analysis must be used.

3.2 Joint Weibull Method

In the joint Weibull analysis, M groups of data having a common shape parameter, but different scale parameters are pooled [22]. The common shape parameter is obtained using the joint maximum likelihood estimate method, as shown in equation (11):

$$\sum_{i=1}^{M}\left\{ n_{fi} \cdot \left[\frac{\sum_{j=1}^{n_i} x_{ij}^{\alpha} \cdot \ln(x_{ij})}{\sum_{j=1}^{n_i} x_{ij}^{\alpha}} - \frac{1}{\alpha} - \frac{\sum_{j=1}^{n_{fi}} \ln(x_{ij})}{n_{fi}} \right] \right\} = 0 \tag{11.a}$$

where n_i is the number of data points in the i^{th} group of data (i = 1, 2, ..., M), and n_{fi} is the number of failures in the i^{th} group of data (i = 1,2, …., M)

For the special case where there is an equal number of failures across all stress levels (i.e., $n_{f1}, n_{f2}, n_{fi} = n_f$), equation (11.a) reduces to the form shown in equation (11.b):

$$\sum_{i=1}^{M}\left[\frac{\sum_{j=1}^{n_i} x_{ij}^{\alpha} \cdot \ln(x_{ij})}{\sum_{j=1}^{n_i} x_{ij}^{\alpha}} \right] - \frac{M}{\alpha} - \sum_{i=1}^{M}\left[\frac{\sum_{j=1}^{n_{fi}} \ln(x_{ij})}{n_{fi}} \right] = 0 \tag{11.b}$$

The common scale parameter for the SN data is obtained using equation (12):

$$\beta_i = \left(\frac{1}{n_{fi}} \cdot \sum_{j=1}^{n_i} x_{ij}^{\alpha} \right)^{1/\alpha} \tag{12}$$

DISTRIBUTION STATEMENT A.
Approved for public release: distribution is unlimited.

3.3 Sendeckyj Equivalent Wearout Model

The Sendeckyj equivalent static strength (wearout) model [23] uniquely relates static strength and residual strength to fatigue life. Thus, the analysis pools static strength, fatigue life, and residual static strength data and converts it into equivalent static strength data. To characterize the SN behavior of composite materials, the Sendeckyj model assumes the following:

- The SN behavior can be determined by a deterministic equation. The equation can be based on theoretical considerations or experimental observations of the fatigue damage accumulation process.
- Static strengths are uniquely related to fatigue lives and residual strengths at runouts. This specific relationship assumes that the strongest specimen has the longest fatigue life or the highest residual strength at runout; fatigue failure is assumed when the residual strength is equal to the maximum amplitude cyclic stress. This assumption may not hold for cases where competing failure modes are observed during fatigue testing.
- The statistical variability of static strength data can be described by a two-parameter Weibull distribution.

The basic Sendeckyj model is presented in the deterministic equation given by

$$\sigma_e = \sigma_a \left[\left(\frac{\sigma_r}{\sigma_a} \right)^{1/S} + \left(n_f - 1 \right) \cdot C \right]^S \tag{13}$$

where σ_e is the equivalent static strength, σ_a is the maximum applied cyclic stress, σ_r is the residual strength, n_f is the number of fatigue cycles, and S and C are Sendeckyj fitting parameters. During scatter analysis of fatigue data, these parameters are recalculated for each fatigue data set (SN curve) and used for developing a fitting curve for each SN curve. Setting the maximum amplitude cyclic stress equal to residual strength for fatigue failures, the power law is obtained as

$$\sigma_a \,.\left(1 - C + C \,.\, N_f\right)^S = \sigma_u \tag{14}$$

where σ_u is the static strength. Using the Sendeckyj analysis, fatigue life, and residual strength, the data for each SN curve are converted into a pool of equivalent static strength data points, as shown in Figure 28. Then, this data set is fitted into a Weibull distribution to obtain the life shape parameter as described by Sendeckyj [23].

DISTRIBUTION STATEMENT A.
Approved for public release: distribution is unlimited.

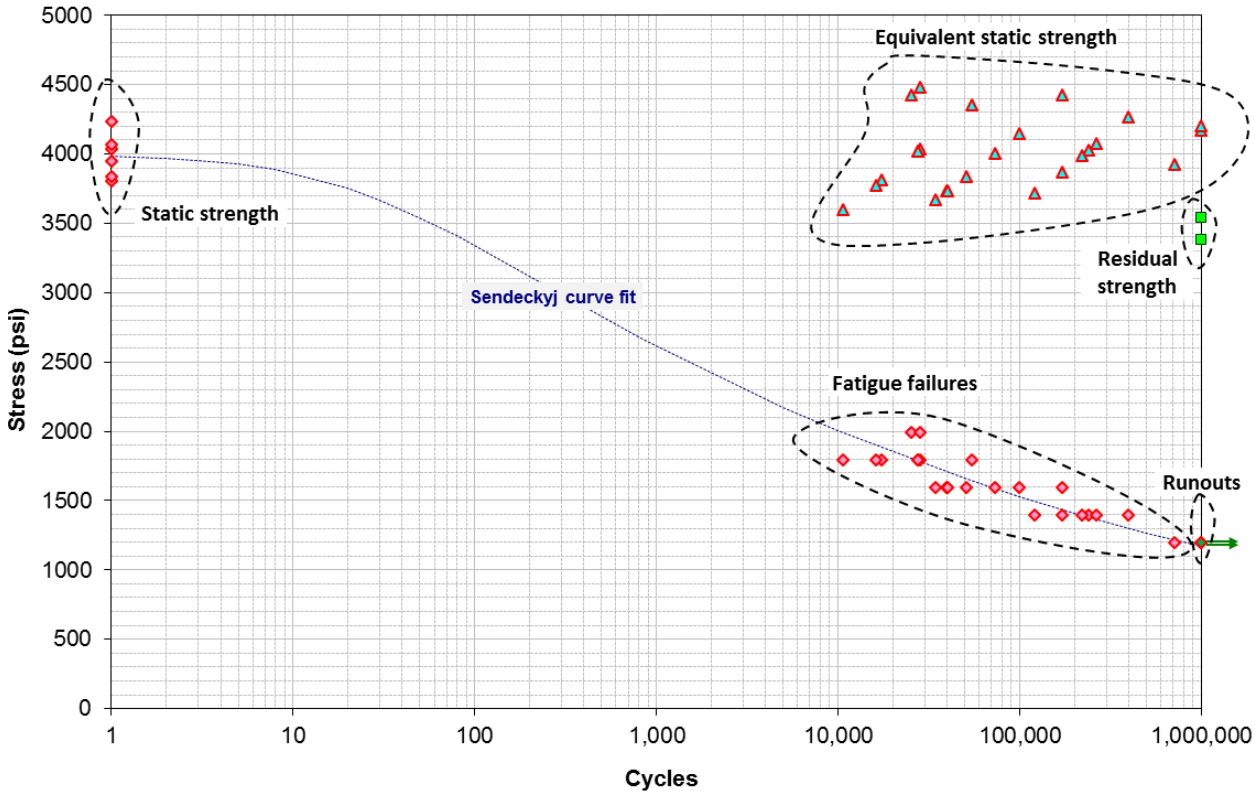


Figure 28. Example of Sendeckyj curve fit.

3.4 Scatter Analysis Software

The scatter analysis software is a NIAR-developed software packaging tool that can be used for analyzing the individual Weibull distribution, joint Weibull distribution, and Sendeckyj equivalent static strength model.

The scatter analysis software was an updated version of the previous NIAR software tool [17] and a combination of Microsoft Excel®, C#®, and ReliaSoft® Weibull software [24]. Sendeckyj analysis was coded in Microsoft C-sharp (C#) programming language. A basic overview of this user-friendly software tool is shown in Figure 29.

DISTRIBUTION STATEMENT A.
Approved for public release: distribution is unlimited.

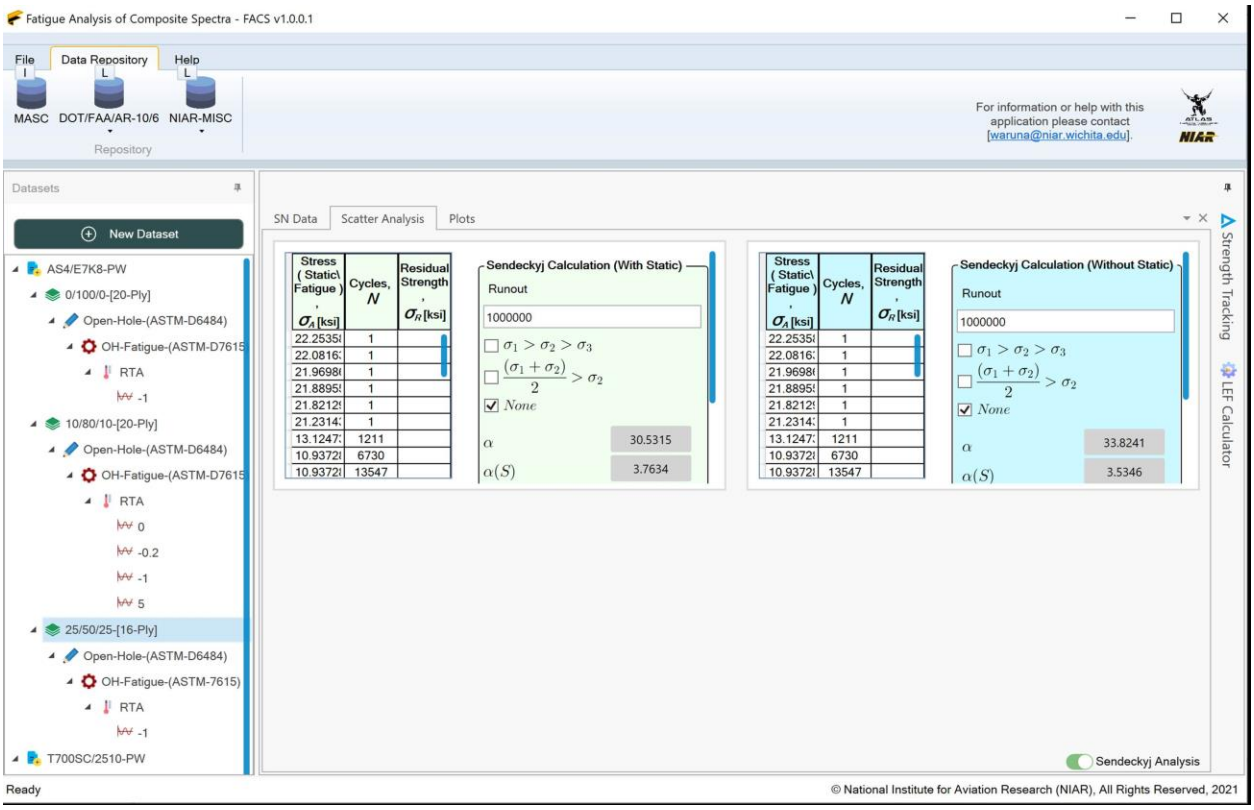


Figure 29. Scatter analysis software module.

Figure 30 illustrates the procedure for analyzing SN data using individual Weibull, joint Weibull, and Sendeckyj analyses for generating the fatigue life shape parameter for a particular test configuration ($\hat{\alpha}_{IW}$, $\hat{\alpha}_{JW}$, and $\hat{\alpha}_{Sendeckyj}$, respectively). As can be seen in this figure, the static data, if applicable, are analyzed using individual Weibull for generating the static strength shape parameter ($\hat{\alpha}_{SS}$) for the same test configuration.

The procedure for generating the static strength (α_R) and fatigue life (α_L) modal shape parameters for calculating the life factor and load-enhancement factors for a particular structure is illustrated in Figure 31. This process requires analysis of static/residual-strength data and fatigue (SN) data for multiple test configurations that represent critical design details of the structure. The fatigue life shape parameter ($\hat{\alpha}_{FL}$) for each design detail or test configuration can be obtained using one of three methods ($\hat{\alpha}_{IW}$,$\hat{\alpha}_{JW}$ or $\hat{\alpha}_{Sendeckyj}$), as shown in Figure 30.

DISTRIBUTION STATEMENT A.
Approved for public release: distribution is unlimited.

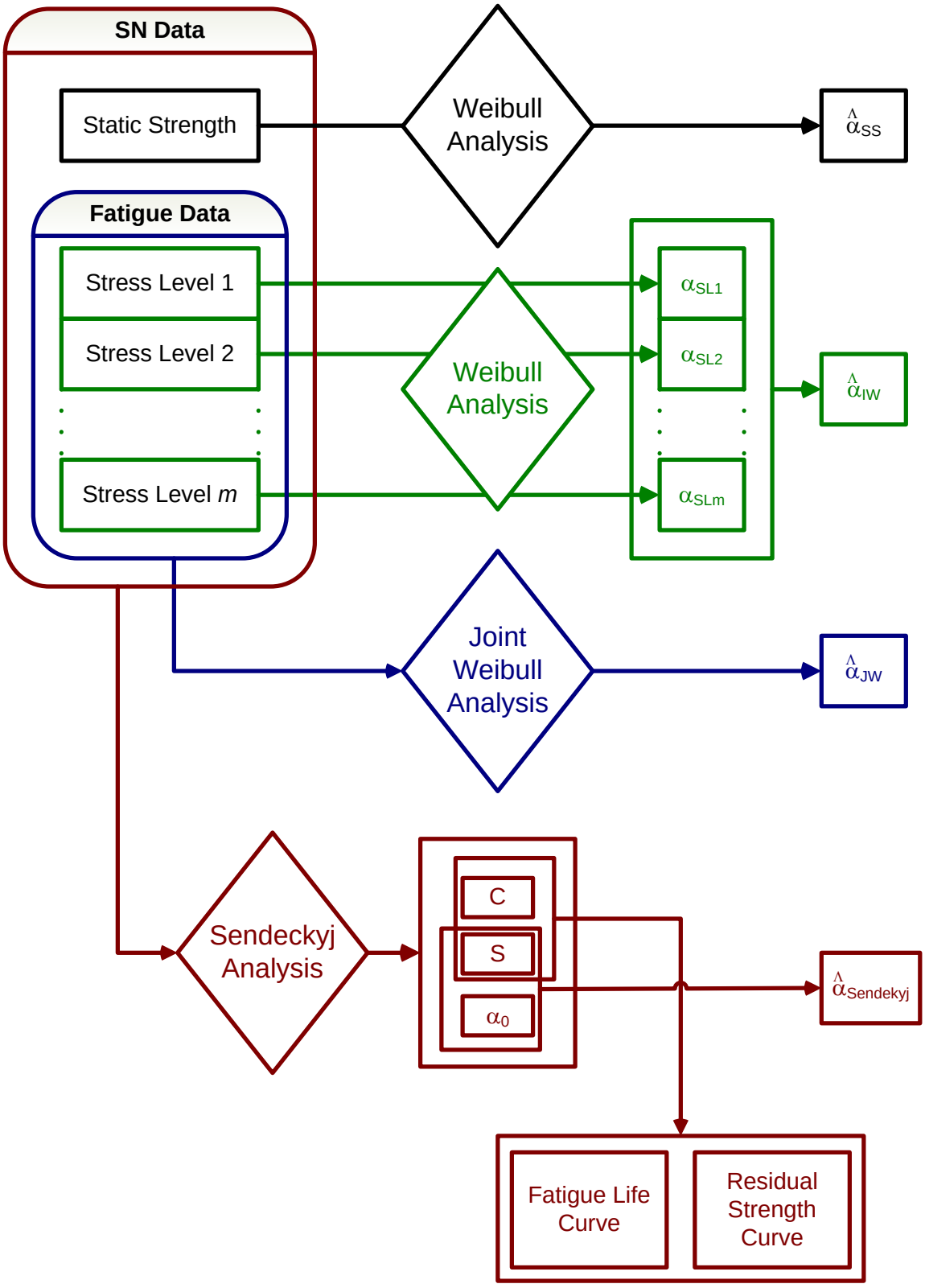


Figure 30. Process for obtaining fatigue life shape parameters for individual test configuration.

DISTRIBUTION STATEMENT A.
Approved for public release: distribution is unlimited.

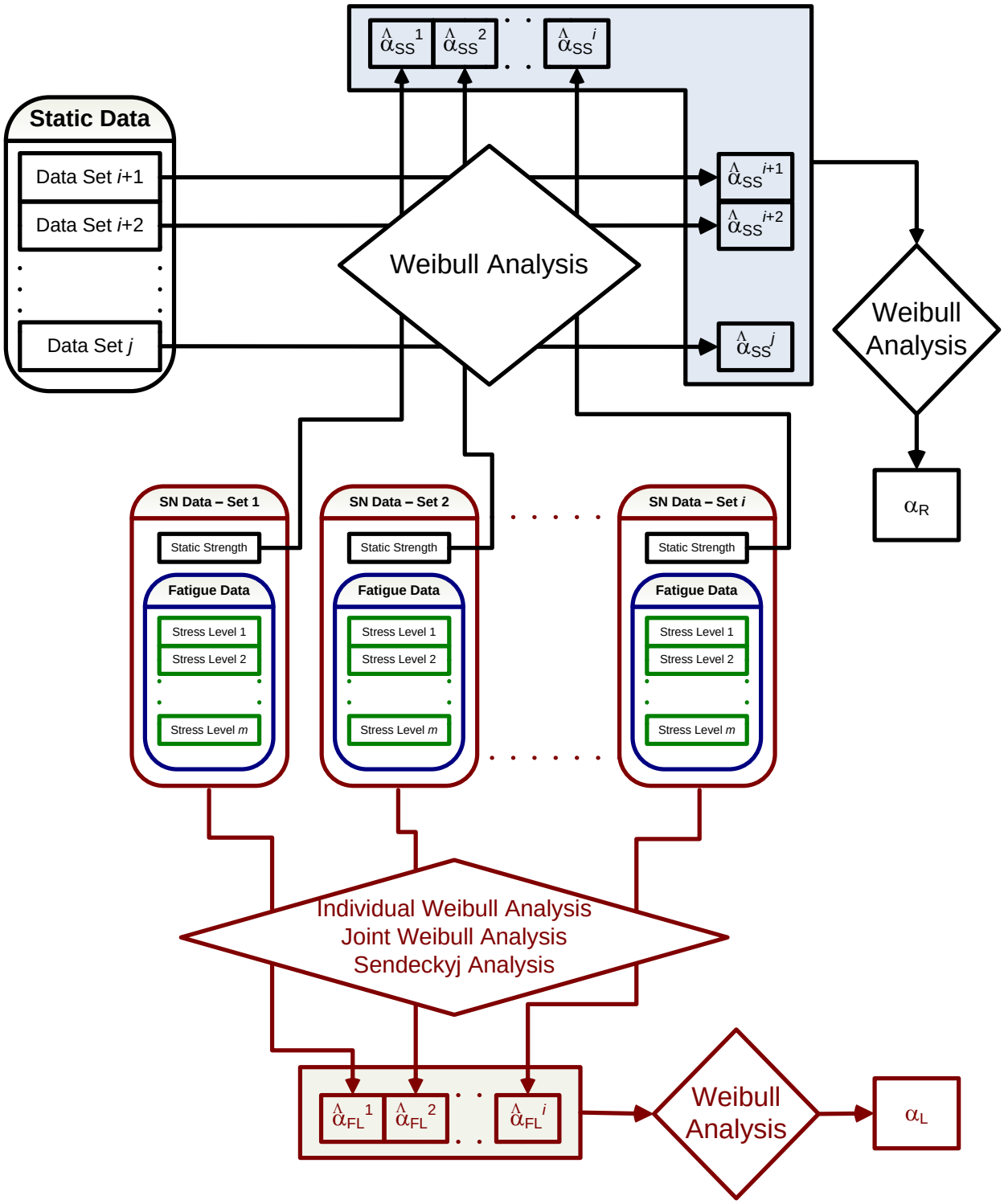


Figure 31. Process for generating static strength and fatigue life shape parameters.

DISTRIBUTION STATEMENT A.
Approved for public release: distribution is unlimited.

4. EXPERIMENTAL PROCEDURES

Test panels were fabricated using three distinct batches of materials for each composite material system selected for this study. Material and process specifications were based on guidance received from the Industry Advisory Board consisting of members from Boeing, Lockheed Martin Corporation, and Northrop Grumman. Since the multi-batch material allowables were already generated for the selected material system, this research focused primarily on the material batch variability on fatigue data, as shown in Figure 32.

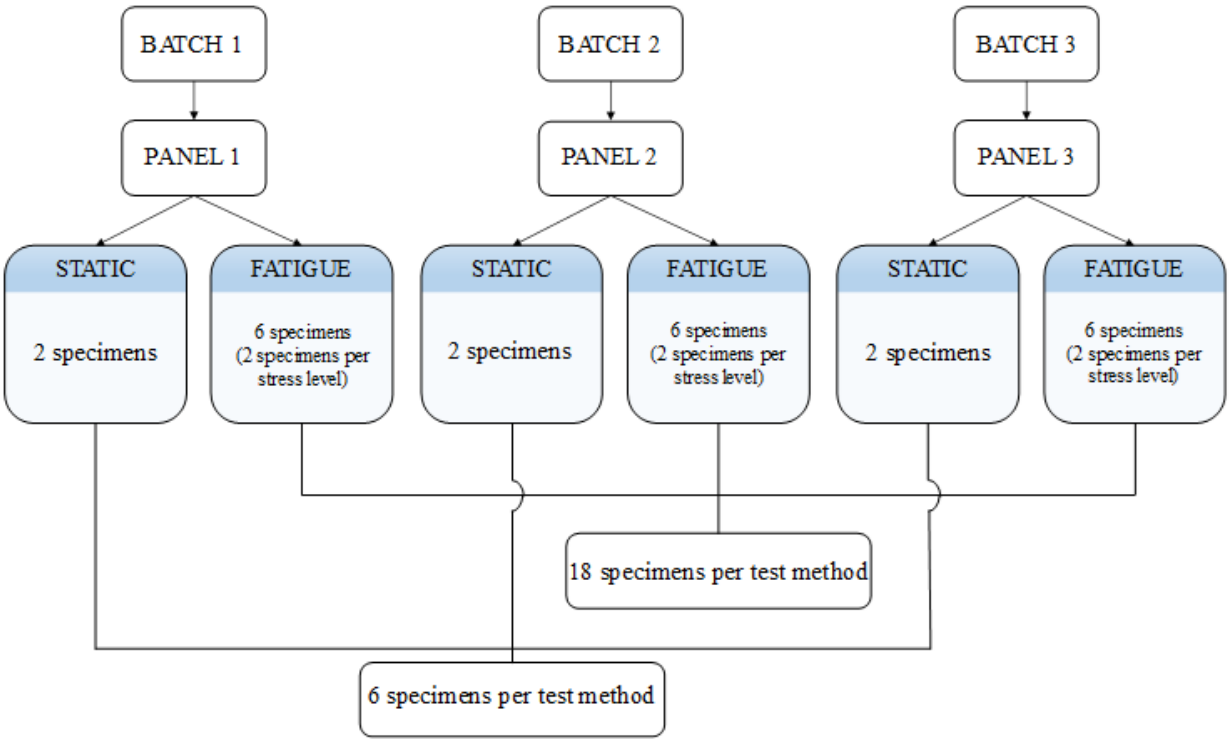


Figure 32. Specimen selection for evaluating batch variability in static and fatigue tests.

Upon completion of the initial static data, fatigue stress levels were selected so that fatigue failures could be observed in multiple SLs between 10,000 and a million cycles to form a SN curve for data scatter analysis. One million cycles were considered runout, and residual strength tests were carried out for runouts.

A minimum of three fatigue stress levels were selected for each SN curve. Typically, an SL of 60 percent of the average quasi-static strength (also referred to as 60% stress level or 60% SL) was selected as the initial stress level. SLs for subsequent fatigue tests were selected based on the outcome of the initial fatigue SL. For example, if runouts (no fatigue failure up to million cycles) were observed for the first fatigue specimen under the first SL, then the SL was increased about 5 to 10 percent for the subsequent SL. If a runout was observed at the second SL, then the fatigue SL was further increased by another 5 to 10 percent. Tension-tension fatigue of hard laminate cases indicated runout at extremely high fatigue stress levels, ex., above 90%. Although these

DISTRIBUTION STATEMENT A.
Approved for public release: distribution is unlimited.

specimens did not indicate the typical two-part failure, high-fidelity inspections carried out on these specimens above an 80% SL indicated significant microcracks and delimitations. Since composite structures are not designed to operate in such high SLs, fatigue damage is not a concern for such failure modes. Thus, further fatigue testing for such cases was halted, and SN curves were not generated.

For each fatigue stress level, at least one specimen was selected to carry out high-fidelity inspections using X-ray computed tomography for characterizing progressive damage growth. An in-house software tool was developed for visualizing XCT data for qualitatively characterizing the progressive damage growth so that users do not have to browse through multiple video files created during XCT reconstruction for determining the damage progression. This tool produces three-dimensional ply-by-ply damage progression over fatigue lifetime. Therefore, the methodology is referred to as 4D damage progression or 4D XCT. The XCT scans were typically accomplished at 150 kV tube voltage and 200 µA target current at 10.01 frames per second and 8.67x magnification with 400 x 400-micron pixel pitch detector (binning) resulting in ~22.76 µm scan resolution.

4.1 Panel Fabrication

The three Solvay material systems shown in Table 3 were selected for the detailed progressive damage growth characterization and scatter analysis. Batch numbers were assigned in the order of receiving them from the material manufacturer.

Table 3 – Materials used for laminate panel manufacturing.

Material System	Material Form	Fiber Areal Weight/Resin Content	Batch	Lot Number
CYCOM® 5320-1/ IM7	Unidirectional Tape - Intermediate Modulus (IM7)	145/33	1	303732609
			2	303732566
			3	301915747
CYCOM® 5320-1/ T650	8 Hardness Satin Fabric (T650)	368/37	1	301915931
			2	301915701
			3	301915702
CYCOM® 5250-4/ IM7-G	Unidirectional Tape - Intermediate Modulus (IM7G)	145/32	1	8037201
			2	8037443
			3	8037457

Static and fatigue testing of CYCOM® 5320-1/Astroquartz® III, an eight-harness satin (8HS) weave quartz fiber-reinforced fabric (Style 4581), and CYCOM® 5320-1/S2, a glass fiber-reinforced fabric (Style 6781) epoxy prepreg with Boeing material specifications, were added to

DISTRIBUTION STATEMENT A.
Approved for public release: distribution is unlimited.

the test program. Those data analyses will be published in a separate report upon completion of the program.

The following three main laminate stacking sequences were used for manufacturing test laminate panels with the stacking sequences shown in Table 4.

- Hard (50/40/10 for unidirectional tape and 40/20/40 for fabric)
- Quasi-Isotropic (25/50/25)
- Soft (10/80/10)

Table 4 – Laminate stacking sequences.

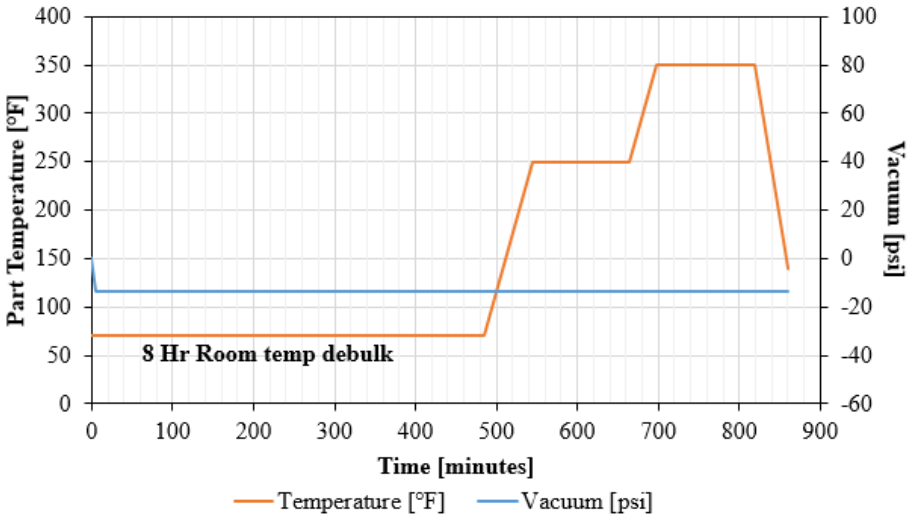
Material System	Test Method	Layup [%] [0°/45°/90°]	Ply Stacking Sequence	Cured Ply Thickness [in]	Total Plies
IM7-5320-1 UNI	Open-Hole	50/40/10	[45/0/-45/0_2/45/90/-45/0_2/45/0/-45/0]ns	0.0054	28
		25/50/25	[45/0/-45/90]ns		24
		10/80/10	[45/-45/45/-45/90/-45/0/45/-45/45/-45/45]ns		24
	Interlaminar Tension	50/40/10	[45/0/-45/02/45/90/-45/02/45/0/-45/0]ns		56
		10/80/10	[45/-45/45/-45/90/-45/0/45/-45/45/-45/45]ns		48
	Double-Notch Shear	50/40/10	[45/0/-45/0_2/45/90/-45/0_2/45/0/-45/0]ns		28
		10/80/10	[45/-45/45/-45/90/-45/0/45/-45/45/-45/45]ns		24
T650-5320-1 8HS	Open-Hole	40/20/40	[0/90/45/0/90]ns	0.0148	10
		25/50/25	[45/0/-45/90]ns		8
		10/80/10	[45/-45/0/45/-45]ns		10
	Interlaminar Tension	40/20/40	[0/90/45/0/90]ns		20
		10/80/10	[45/-45/0/45/-45]ns		20
	Double-Notch Shear	40/20/40	[0/90/45/0/90]ns		10
		10/80/10	[45/-45/0/45/-45]ns		10
IM7-5250-4 Tape	Open-Hole	50/40/10	[45/0/-45/0_2/45/90/-45/0_2/45/0/-45/0]ns	0.0054	28
		25/50/25	[45/0/-45/90]ns		24
		10/80/10	[45/-45/45/-45/90/-45/0/45/-45/45/-45/45]ns		24
	Interlaminar Tension	50/40/10	[45/0/-45/02/45/90/-45/02/45/0/-45/0]ns		56
		10/80/10	[45/-45/45/-45/90/-45/0/45/-45/45/-45/45]ns		48
	Double-Notch Shear	50/40/10	[45/0/-45/0_2/45/90/-45/0_2/45/0/-45/0]ns		28
		10/80/10	[45/-45/45/-45/90/-45/0/45/-45/45/-45/45]ns		24

Detailed process specifications for 5320-1 and 5250-4 can be found in the corresponding manufacturer data sheets. All fabrication tools were prepared as per in-house standard procedures and protocols. For the 5320-1 material system, a pressure debulking was performed after every two plies, and silicone edge dams were placed around the open-hole and double-notch shear flat panel peripheries during debulking to prevent edge compressing, which restricts

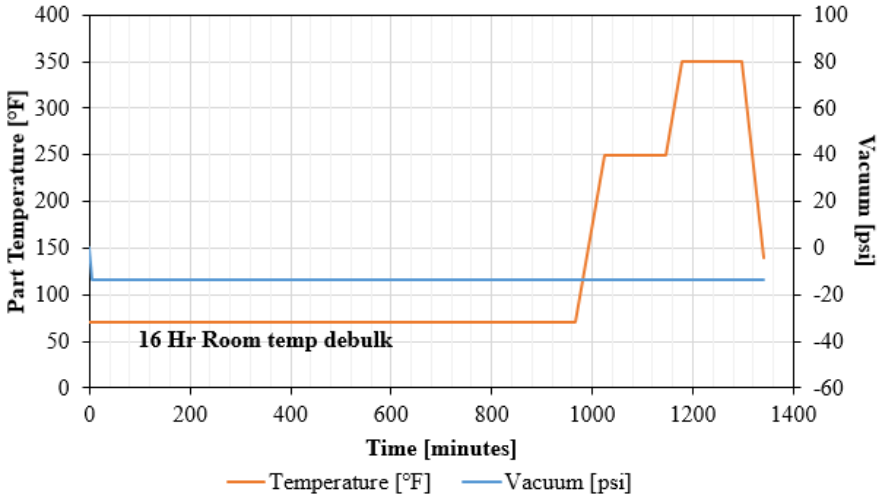
DISTRIBUTION STATEMENT A.
Approved for public release: distribution is unlimited.

air passages. Aluminum caul plates were used during panel consolidation. For the 5320-1 interlaminar tension (ILT) curved panels, a similar procedure was followed, except that the caul plate was made with rubber material. For the panel periphery, silicone dams were placed to prevent resin bleed out. A detailed fabrication process is presented in the 5320-1 process specification [25].

Panels manufactured using the 5320-1 material system were cured under a full vacuum. The flat panels were held under a vacuum for eight hours prior to the cure. Since ILT panels have a significant number of plies, the vacuum duration for them was increased to 16 hours. The baseline cure cycle was a two-step process, with panels cured at 250°F and 350°F for two hours at each stage (Figure 33). Details of the vacuum requirements and the cure process are found in the material process specification.



(a) Flat Panels



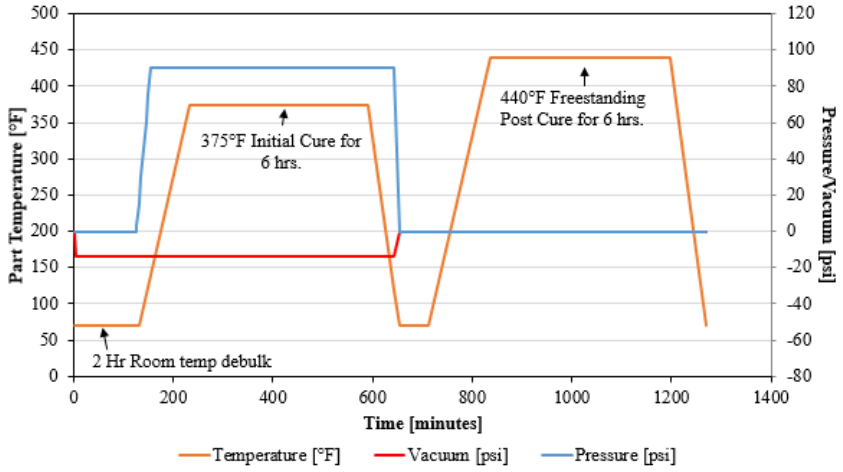
(b) Curved Panels

Figure 33. Cure cycle for 5320-1.

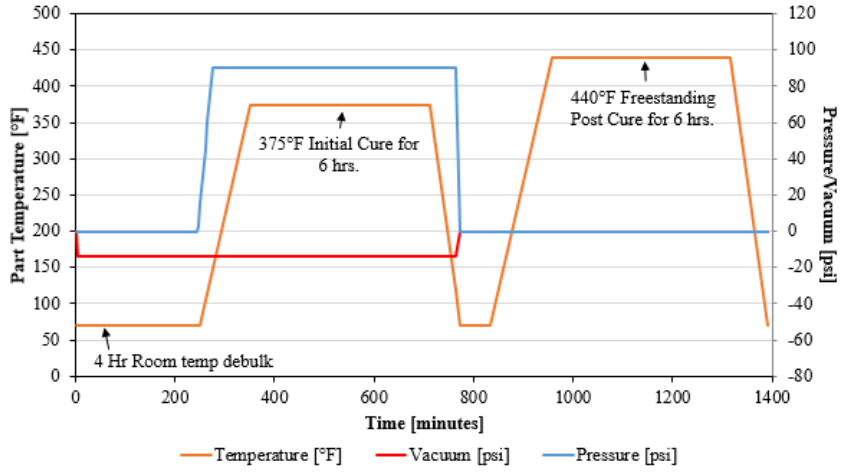
DISTRIBUTION STATEMENT A.
Approved for public release: distribution is unlimited.

The pressure debulking process for the 5250-4 material system was similar to that for the 5320-1 material system, except that debulking was done at every four plies for flat panels and every two plies for curved panels. The caul plate materials were aluminum and rubber for flat and ILT panels, respectively. Sealant tape layers instead of silicone rubber were placed at the periphery of the flat panels to prevent excess resin bleed out. A detailed fabrication process is presented in the 5250-4 process specification [26].

Before curing, the 5250-4 panels were held under a two- and four-hour full vacuum for flat and curved panels, respectively. The baseline cure cycle included an initial one-step cure followed by a free-standing one-step post-cure (Figure 34). These panels were held at 375°F for six hours during the initial cure with 90 psi autoclave pressure and full vacuum throughout the cure. For the post-cure, the panels were held at 440°F for six hours. Details of the vacuum requirements and the cure process are found in the material process specification.



(a) Flat Panels



(b) Curved Panels

Figure 34. Cure cycle for 5250-4.

DISTRIBUTION STATEMENT A.
Approved for public release: distribution is unlimited.

Prior to machining the test specimens, each panel was inspected visually as well as using the through-transmission ultrasonic (TTU) technique in order to determine the quality of each panel. Panels with excessive porosity were rejected and replaced, or the area was marked in order to avoid extracting specimens from such areas. Table 5 summarizes the total number of panels manufactured for each material system and the inspection process.

Table 5 – Panel inspection checklist.

Material System	Panel Type	Number of Panels	Cure Specification	NDI (TTU)	Panel Quality
CYCOM 5320-1/IM7	Curved	13	✓	✓	✓
	Flat	26	✓	✓	✓
CYCOM 5320-1/T650	Curved	10	✓	✓	✓
	Flat	23	✓	✓	✓
CYCOM 5250-4/IM7G	Curved	12	✓	✓	✓
	Flat	26	✓	✓	✓

Rheology is the study of non-Newtonian flow[1] and the deformation of materials under an oscillatory applied force measured using a rheometer. The rheological response of a thermoset composite is continuously measured throughout the cure cycle when the material undergoes changes from the partially to fully cross-linked state. This will provide vital information about different phases of the cure process, which can then be used for controlling the autoclave temperature and pressure set points. For example, the rate of temperature increase at the beginning of the cure must be maintained so that the resin reaches its minimum viscosity and flow prior to acceleration of the cross-linking process, which increases the resin viscosity. Cure recipes for composite materials are based on manufacturer-recommended cure cycle inputs, which are developed as a result of various stochastic cure kinetics models during the development of resin formulation. The time, temperature, pressure, and vacuum integrity are inputs for the autoclave cure, but none of them are direct measurements of the material state and have no direct correlation to viscoelastic characteristics or mechanical performance of the cured material. Measurements of time-dependent viscoelastic properties of polymers can be used for understanding the configurational arrangements and interaction of molecules.

The total stress/strain is assigned as G* or complex shear modulus. Figure 35 shows the viscosity (η*), elastic component of the complex modulus (G'), and loss or viscous component of the modulus (G") for a 5320-1/T650 material sample. The significance of these measurements is that they relate to the change from an essentially viscous state (prepreg) to an elastic state (laminate). Initially, when the temperature is increased, the prepreg starts melting and the resin viscosity is decreased. This improves the resin flow, helps to wet fibers uniformly with resin, and eases the

[1] Fluids whose viscosity changes with the strain rate (shear dependent).

DISTRIBUTION STATEMENT A.
Approved for public release: distribution is unlimited.

outgassing of volatiles. Outgassing is typically augmented by reducing pressure over the prepreg in order to lower the boiling point of residual volatiles that cause migration of the gas within the layup into the lower density air as the result of lowering the pressure in the bag using vacuum. Once volatiles are removed, pressure is applied exterior to the bag containing the prepreg in order to close voids and consolidate the laminate to the desired thickness. It is essential that pressure is applied at the appropriate viscosity in order to cause hydrostatic pressure to build in the resin, thereby closing voids and preventing excessive resin bleed.

An in-situ material state monitoring system outlined in the work of Seneviratne and Tomblin [27] was used with embedded temperature sensors and wireless antennas so that the temperature at the point of interest (in test panel) was transmitted to an external rheometer. Test samples (in rheometer) were prepared with stacking sequences similar to the test panels, and tests were conducted using an encapsulated sample rheometer (ATD 3000) with a controlled strain of 0.7% and a strain rate of 1.667 Hz. Rheological tests were conducted to determine the viscoelastic response and cure kinetics of 5320-1 under the recommended cure cycles.

For this material system, shown in Figure 35, the minimum viscosity occurred at 250°F, and the majority of the elastic modulus, G', buildup occurred during the 250°F temperature hold. The modulus dropped during the second temperature ramp when the material passed the glass transition temperature (Tg) point.

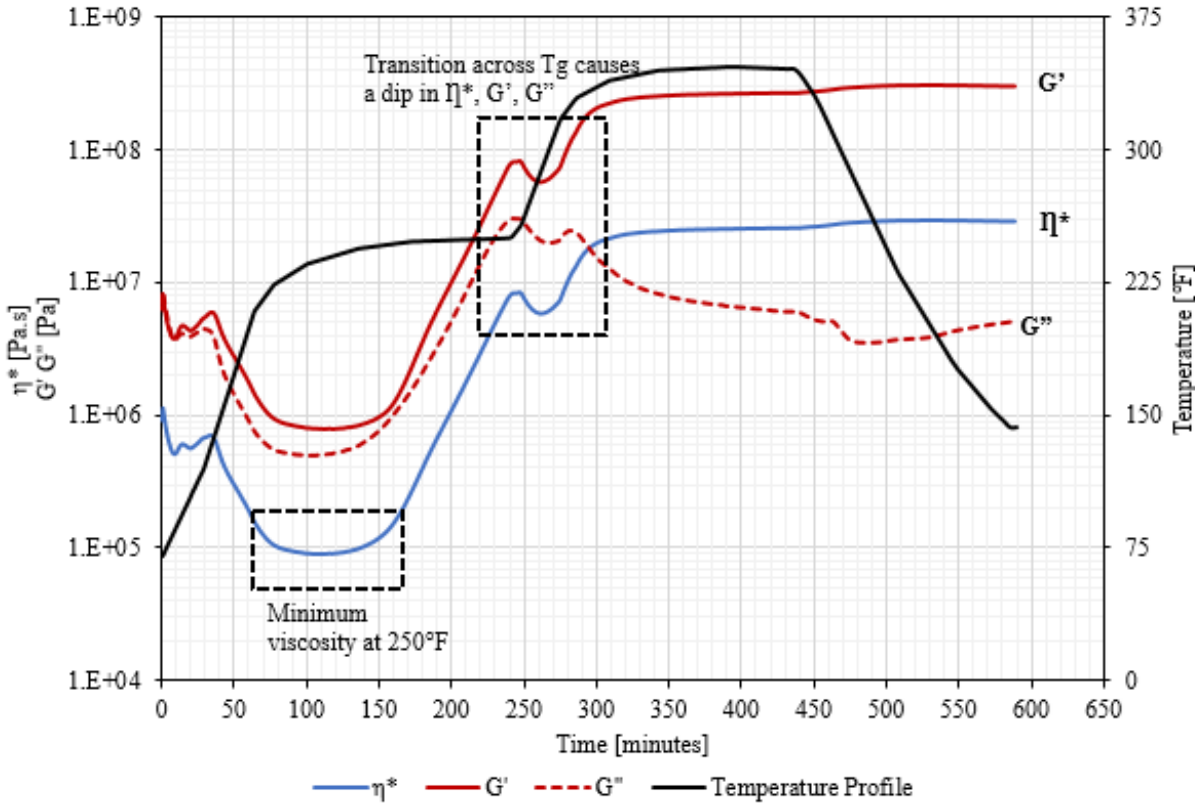


Figure 35. Viscoelastic properties for T650/5320-1.

DISTRIBUTION STATEMENT A.
Approved for public release: distribution is unlimited.

4.2 Test Matrices

In order to obtain a detailed understanding of progressive fatigue damage growth behavior of a composite material system, as shown previously in Table 3, and to generate statistical factors (i.e., life and load-enhancement factors) required for fatigue test substantiation, fatigue SN curves were generated from test specimens obtained for multiple stacking sequences, stress levels, and stress ratios. The test matrix included failure modes representing both in-plane and out-of-plane loading:

- Open-hole tension (OHT)/open-hole compression (OHC)
- Interlaminar tension (ILT)
- Double-notch shear (DNS)
- Short-beam shear (SBS)

Testing included various coupon-level static and constant amplitude fatigue tests and concentrated on generic loading modes representing open-hole in-plane tension and compression (Table 6) as well as interlaminar tension and shear (Table 7). These test matrices were repeated for all three material systems. Each stress level included tests specimens from distinct material batches so that the influence of batch variability could be investigated.

4.2.1 Open-Hole Tension/Open-Hole Compression Testing

Tension-tension open-hole fatigue testing was conducted without an anti-buckling fixture, as shown in Figure 36. A folded emery cloth layer was wrapped around each grip section of the specimen and held using a hydraulic grip assembly with serrated wedges to prevent slippage while preventing damage to the test specimen.

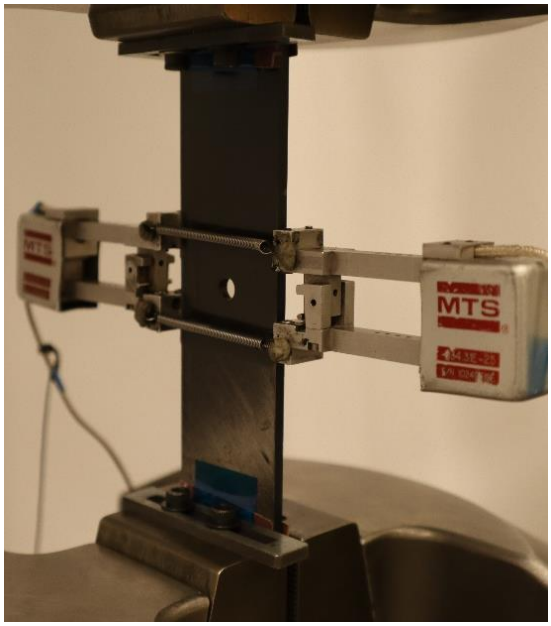


Figure 36. OHT test setup with extensometer.

DISTRIBUTION STATEMENT A.
Approved for public release: distribution is unlimited.

Table 6 – Static and constant amplitude fatigue test matrix—open-hole.

Test Description				Number of Specimens				
Layup	Test Method	R Ratio	Stress Level	Per Batch	Per SL	Per Test	Per MS	Total
50/40/10 (UNI) or 40/20/40 (8HS)	OHT	Quasi-Static		2	6	198	198	594
	OHC			2	6			
	OHT-T	0.1	SL1	2	6			
			SL2	2	6			
			SL3	2	6			
	OHC-C	5	SL1	2	6			
			SL2	2	6			
			SL3	2	6			
	OHC-T	–1	SL1	2	6			
			SL2	2	6			
			SL3	2	6			
25/50/25	OHT	Quasi-Static		2	6			
	OHC			2	6			
	OHT-T	0.1	SL1	2	6			
			SL2	2	6			
			SL3	2	6			
	OHC-C	5	SL1	2	6			
			SL2	2	6			
			SL3	2	6			
	OHC-T	–1	SL1	2	6			
			SL2	2	6			
			SL3	2	6			
10/80/10	OHT	Quasi-Static		2	6			
	OHC			2	6			
	OHT-T	0.1	SL1	2	6			
			SL2	2	6			
			SL3	2	6			
	OHC-C	5	SL1	2	6			
			SL2	2	6			
			SL3	2	6			
	OHC-T	–1	SL1	2	6			
			SL2	2	6			
			SL3	2	6			

SL = Stress Level, MS = Material System

DISTRIBUTION STATEMENT A.
Approved for public release: distribution is unlimited.

Table 7 – Static and constant amplitude fatigue test matrix—interlaminar tension and shear.

Test Description				Number of Specimens				
Layup	Test Method	R Ratio	Stress Level	Per Batch	Per SL	Per Test	Per MS	Total
50/40/10 (UNI) or 40/20/40 (8HS)	ILT	Quasi-Static		2	6	54	132	396
		0.1	SL1	2	6			
			SL2	2	6			
			SL3	2	6			
			SL4	1	3			
10/80/10		Quasi-Static		2	6			
		0.1	SL1	2	6			
			SL2	2	6			
			SL3	2	6			
			SL4	1	3			
50/40/10 (UNI) or 40/20/40 (8HS)	DNS	Quasi-Static		2	6	54		
		0.1	SL1	2	6			
			SL2	2	6			
			SL3	2	6			
			SL4	1	3			
10/80/10		Quasi-Static		2	6			
		0.1	SL1	2	6			
			SL2	2	6			
			SL3	2	6			
			SL4	1	3			
100/0/0	SBS	Quasi-Static		2	6	24		
		0.1	SL1	2	6			
			SL2	2	6			
			SL3	2	6			

SL = Stress Level, MS = Material System

A standard open-hole compression test fixture (Figure 37) was used for fatigue testing for both R = 5 and –1, where compression loads were present. This fixture consisted of two short-grip/long-grip assemblies and two support plates. Ultra-low friction Teflon™ polytetrafluoroethylene (PTFE) tapes were used on the moving surfaces, as shown in Figure 38, to reduce friction during fatigue and to prevent damage to the fixture. The thicker tape on the support plate served to offset the extra thickness added by taping to the gage section of the fixture. In addition, a thin layer of anti-friction Molykote® grease coating was applied to improve surface roughness and to further minimize friction on the wear surfaces and heat generation in between moving parts, even under extreme loads especially for R = –1.

DISTRIBUTION STATEMENT A.
Approved for public release: distribution is unlimited.

During assembly of the specimen into the fixture, the bottom of the fixture and the specimen were placed flush against a steel platen on both ends, and all four bolts were tightened to a torque of 60 in-lb. A nylon insert was used with the special locknuts to ensure that bolts did not loosen during the prolonged cyclic fatigue, and 60 in-lb of torque was maintained throughout the fatigue testing. After the specimen was held at an appropriate grip pressure, an initial compliance check was performed. In order to ensure that the test fixture was assembled/gripped properly and to ensure that there was no slack, the specimen was fatigued for 100 cycles, and then a second compliance check was performed. This value was used as the initial compliance or the reference stiffness value (slope of the load/displacement) for subsequent compliance checks carried out during fatigue in order to monitor stiffness degradation.

Extensometers were used to determine the strain responses during quasi-static loading. For static loading, a displacement rate of 0.05 in/min was used, as recommended in the ASTM D6484 standard [28]. Fatigue tests were conducted in load-control mode at a frequency of 5 Hz per test plan. One million cycles were considered the runout condition. The test was completed when either one million cycles was reached or one of the displacement limits for the interlock was breached for failure modes that exhibit significant stiffness degradation due to widespread fatigue damage. The load frames were tuned before fatigue testing to reach 1% of the peak/valley target loads.

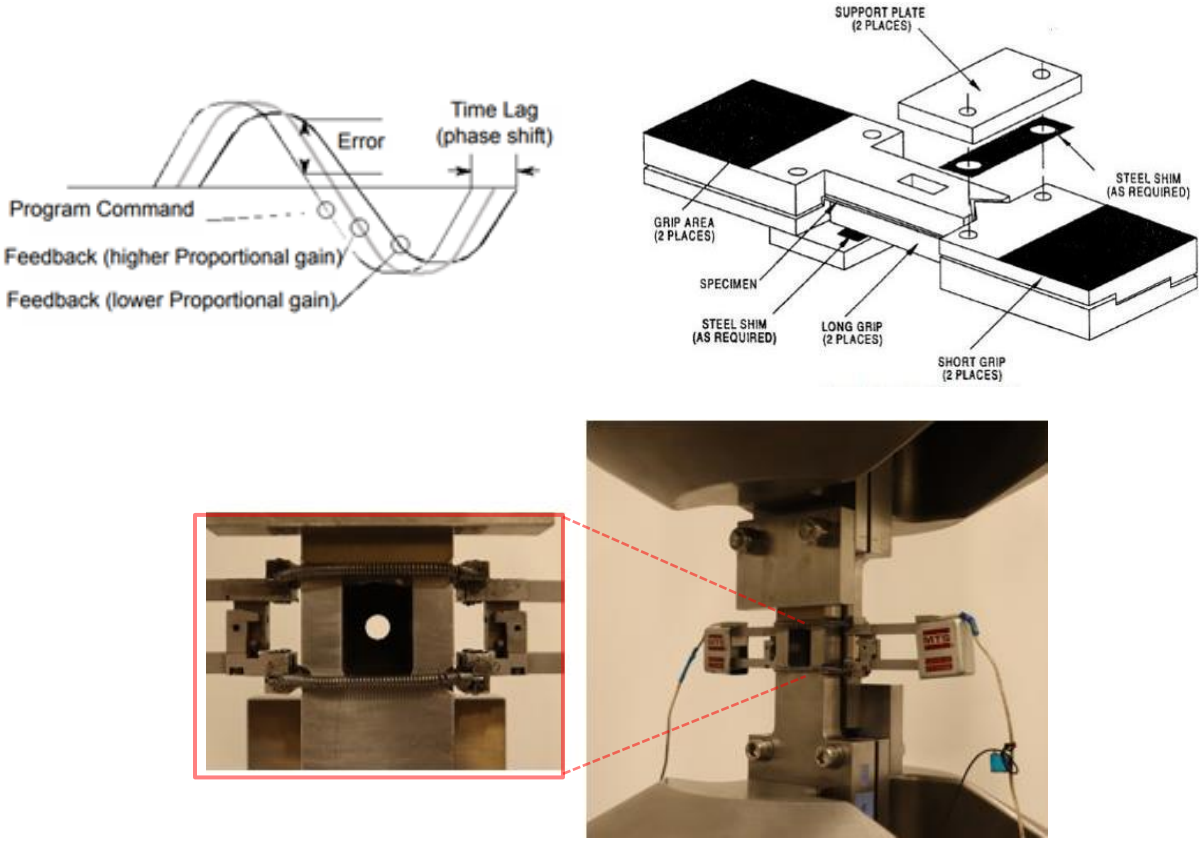


Figure 37. OHC test setup with extensometers.

DISTRIBUTION STATEMENT A.
Approved for public release: distribution is unlimited.

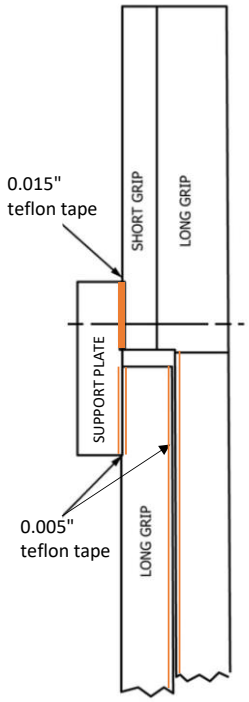


Figure 38. OHC fixture preparation for fatigue test.

4.2.2 Interlaminar Tension Testing

Interlaminar tensile testing was carried out using the recommendations in the ASTM D6415 standard [30] for quasi-static testing. This test, also known as curved-beam strength, was carried out using a four-point bend test fixture, as shown in Figure 39. A preload of 3 lbf was applied first so that the specimen would be in contact with the loading bars. A deflectometer was used to determine the pure deflection responses during quasi-static and fatigue loading. For quasi-static tests, a displacement rate of 0.10 in/min was used, as recommended in the ASTM D6415 standard, to produce failure within 1 to 6 min. Fatigue tests were conducted in load-control mode with a test frequency of 5 Hz.

The curved region of the test specimen was continuously monitored using an in-house designed Automated Microscopic Inspection System (AMIS), which was able to capture delamination/crack growth shown on the side of the test specimens. This system is capable of detecting crack/damage growth by capturing images with a corresponding cycle count. AMIS recordings were validated with several trial tests prior to implementing it for fatigue tests. At the beginning of fatigue, the AMIS takes an initial image for reference with the aid of a high-resolution microscope (Dino-Lite Edge Digital Microscope 5.0MP AM7115MZT). During fatigue, it repetitively compares that image with the real-time frame of the fatigue specimen (curved beam region) in order to detect fatigue damage. If any differences between the current frame and the initial frame are identified, then AMIS saves the image along with the

DISTRIBUTION STATEMENT A.
Approved for public release: distribution is unlimited.

corresponding number of cycles. A brittle white paint was applied to the specimen edges within the curve region to aid in detecting matrix cracks or delamination.

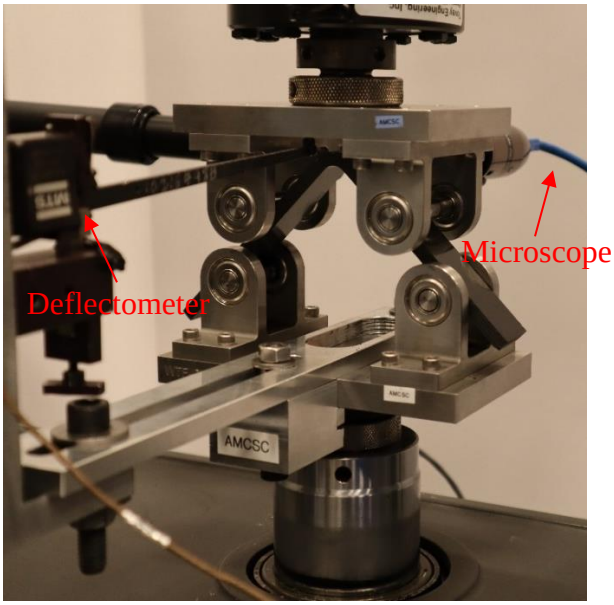


Figure 39. ILT test setup with deflectometer and microscope.

4.2.3 Double-Notch Shear Testing

The double-notch shear test was used for determining the interlaminar shear strength by applying a tensile load to a notched specimen of uniform width. DNS specimen geometry was based on the recommendations of ASTM D3486 standard [29] with an increased shear gage section, as shown in Figure 40. The length and width of the specimen were increased to 12 x 1.5 in, respectively. The modified specimen had an overlap area of 1.5 in^2. The overall dimensions of the specimen were increased to accommodate the open-hole test fixture in order to prevent out-of-plane deformation due to load eccentricity during fatigue loading. A one-inch lap area was centered in the middle of the specimen with two prudently machined notches in opposite directions. Notch depth (d = t/2) and machining quality are crucial for obtaining a proper (shear-dominant) failure mode.

DISTRIBUTION STATEMENT A.
Approved for public release: distribution is unlimited.

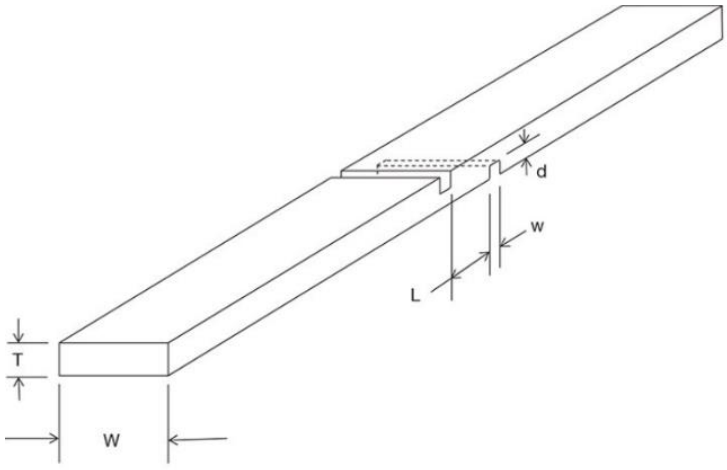


Figure 40. Double-notch shear test specimen configuration.

4.2.4 Short-Beam Shear Testing

Testing of short-beam shear, which is another interlaminar failure mode, is typically used as a quality control test method. Compared to the DNS test method, SBS has limitations and challenges for use as a method for interrogating R-ratio effects. In order to compare the fatigue data scatter between DNS and SBS, a limited number of SBS fatigue tests were added to the test matrix. This test method loads a short-beam specimen in three-point bending, as shown in Figure 41. The goal is to force the short-beam specimen to fail in a shear mode. For quasi-static tests, a displacement rate of 0.05 in/min was used, as recommended in the ASTM D2344 standard [31]. Fatigue tests were conducted in load-control mode at a frequency of 5 Hz.

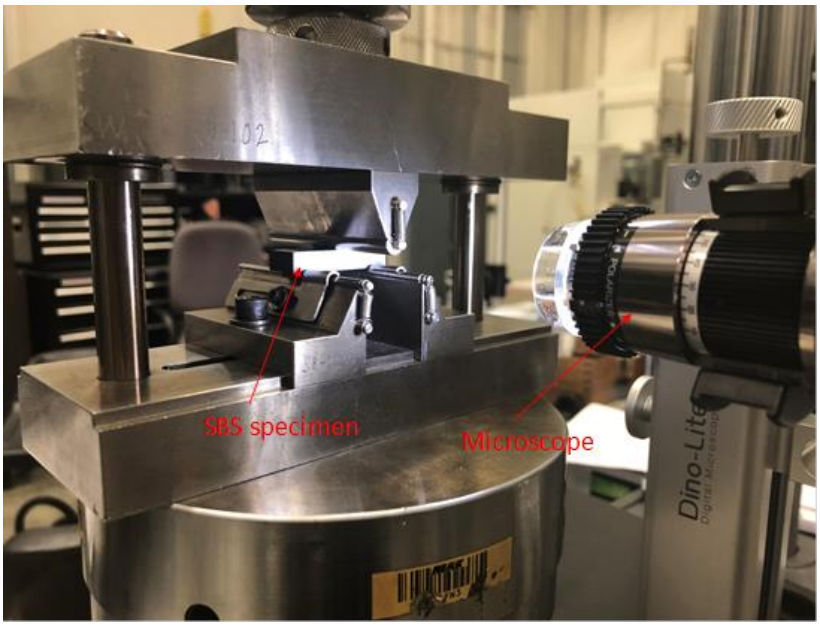


Figure 41. SBS test setup with microscope.

DISTRIBUTION STATEMENT A.
Approved for public release: distribution is unlimited.

5. STATIC TEST DATA ANALYSIS

Data generated from static tests were used to investigate the dependence of the static strength shape parameter, which is a representation of static data scatter. The goal of the static strength data scatter analysis was to produce data for the three material systems used, not only for this program but also for shared databases. For each test method, quasi-static tests were performed to evaluate the ultimate strength properties. A minimum of two specimens from each distinct material batch were included to investigate the batch variability. The two-parameter Weibull analysis was used for the scatter analysis data shown in this section. The following sections include the generation of the shape parameters for three different material systems accounting for the effects of different layups and failure modes.

5.1 Solvay 5320-1/ IM7 Unidirectional Tape

The room-temperature dry (RTD) static strength experimental test results of IM7/5320-1 unidirectional tape is shown in Table 8 along with the Weibull shape parameter (ά) and scale parameter (β) for each test case. A total of 75 quasi-static data points from three different material batches were included in the static data scatter analysis for this material system. Except for the ILT hard laminate, the remaining data indicated a significantly low coefficient of variation (CV), resulting in high shape parameters. Note that the lower the scatter, the higher the shape parameter (opposite behavior compared to CV).

Table 8 – Static strength test data and Weibull parameters for IM7/5320-1 UNI.

Specimen Configuration			RTA Strength (ksi)			Weibull Statistics	
Test Description	Layup	n	Average	STDEV	CV (%)	ά	β (ksi)
OHC	50/40/10	6	69.94	2.35	3.37	41.03	70.93
OHT		6	107.45	6.21	5.78	21.19	110.17
DNS		9	3.35	0.25	7.53	19.16	3.50
ILT		6	11.28	1.79	15.89	6.94	11.91
OHC	25/50/25	6	50.83	0.86	1.69	80.35	51.20
OHT		6	68.46	1.67	2.44	49.49	69.21
DNS		–					
ILT		–					
OHC	10/80/10	6	42.09	0.66	1.57	38.44	41.34
OHT		6	45.10	0.71	1.57	42.21	44.91
DNS		8	3.07	0.14	4.54	24.57	3.14
ILT		6	10.96	0.98	8.98	16.36	11.35
SBS	100/0/0	10	16.30	0.19	1.19	104.37	16.39

n = Number of Specimens, STDEV = Standard Deviation, CV = Coefficient of Variation

DISTRIBUTION STATEMENT A.
Approved for public release: distribution is unlimited.

5.2 Solvay 5320-1/ T650 8-Harness Satin Weave Fabric

The static strength experimental test results of T650/5320-1 8HS fabric and the shape parameters obtained from static strength distributions were analyzed based on the loading mode and the layup configuration scenarios, as shown in Table 9. A total of 76 quasi-static data points from three different material batches were included in the static data scatter analysis for this material system. Most of the test cases indicated very minimal data scatter, resulting in high shape parameters. Both hard and soft ILT test cases indicated scatter resulting from shape parameters just below 20, which is not unusual for this failure mode due to the complexities associated with specimen machining as well as stress concentration at the ends of overlap. Although the OHT test indicated a somewhat higher CV, resulting in a lower shape parameter than what is typically noted for this failure mode, this was not significant.

Table 9 – Static strength test data and Weibull parameters for T650/5320-1 8HS.

Specimen Configuration			RTA Strength (ksi)			Weibull Statistics	
Test Description	Layup	n	Average	STDEV	CV (%)	ά	β (ksi)
OHC	40/20/40	6	58.05	2.51	4.32	26.31	59.18
OHT		6	60.73	4.21	6.94	14.27	62.69
DNS		9	4.21	0.15	3.65	36.00	4.31
ILT		9	6.79	0.45	6.67	18.06	6.99
OHC	25/50/25	6	49.77	1.50	3.02	55.63	50.35
OHT		6	48.50	2.20	4.53	29.93	49.42
DNS		–					
ILT		–					
OHC	10/80/10	6	41.12	0.62	1.50	76.01	41.82
OHT		6	41.48	0.85	2.04	114.63	41.36
DNS		6	4.34	0.04	1.01	121.12	4.36
ILT		6	6.49	0.56	8.62	12.94	6.74
SBS	100/0/0	10	12.44	0.37	2.98	41.52	12.61

n = Number of Specimens, STDEV = Standard Deviation, CV = Coefficient of Variation

5.3 Solvay 5250-4 (BMI)/ IM7 Unidirectional Tape

The static strength experimental test results of IM7/5250-4 unidirectional tape and the shape parameters obtained from static strength distributions were analyzed based on the loading mode and the layup configuration scenarios, and these are shown in Table 10. A total of 69 quasi-static data points from three different material batches were included in the static data scatter analysis for this material system. Similar to the case for IM7/5320-1 UNI, the hard ILT test had a significant CV, resulting in a low shape parameter. Other failure modes had significantly low CVs, resulting in high shape parameters.

DISTRIBUTION STATEMENT A.
Approved for public release: distribution is unlimited.

Table 10 – Static strength test data and Weibull parameters for IM7/5250-4.

Specimen Configuration			RTA Strength (ksi)			Weibull Statistics	
Test Description	Layup	n	Average	STDEV	CV (%)	ά	β (ksi)
OHC	50/40/10	6	69.92	3.39	4.84	24.07	71.43
OHT		6	127.18	3.34	2.63	43.94	128.69
DNS		6	3.65	0.10	2.68	46.68	3.69
ILT		6	10.67	1.25	11.75	10.03	11.18
OHC	25/50/25	6	52.65	2.16	4.11	23.86	53.68
OHT		6	76.48	2.03	2.66	50.85	77.36
DNS		–					
ILT		–					
OHC	10/80/10	6	41.71	0.43	1.03	123.47	41.90
OHT		6	49.12	1.01	2.07	65.66	49.55
DNS		6	3.20	0.16	5.07	35.70	3.29
ILT		6	11.65	0.70	5.97	19.99	11.96
SBS	100/0/0	9	16.44	0.30	1.80	73.55	16.57

n = Number of Specimens, STDEV = Standard Deviation, CV = Coefficient of Variation

5.4 Summary

This exercise was conducted to evaluate the scatter of modern composite quasi-static strength data and to compare the results against the historic value obtained by Whitehead et al. [1] (modal static strength shape parameter of 20). As shown in Figure 42, shape parameters obtained for different test cases indicate significantly low scatter in multi-batch quasi-static data. This can be attributed to the improvements in material and process control of modern composite materials as well as matured test methods. By running a Weibull analysis of shape parameters

Shape parameters (ά values) calculated for various failure modes and layup sequences of each material system were subjected to a Weibull analysis for calculating the modal shape parameter using equation (15):

$$\alpha_{Modal} = \beta \cdot \left(1 - \frac{1}{\alpha}\right)^{1/\alpha} \tag{15}$$

where α and β are the shape and scale parameters corresponding to the Weibull analysis of the collection of shape parameters. Table 11 shows a summary of modal shape parameters for static strength data for each material system as well as a combined analysis of shape parameters for all three material systems. The combined modal value is designated as AMCSC to represent the data in this report.

DISTRIBUTION STATEMENT A.
Approved for public release: distribution is unlimited.

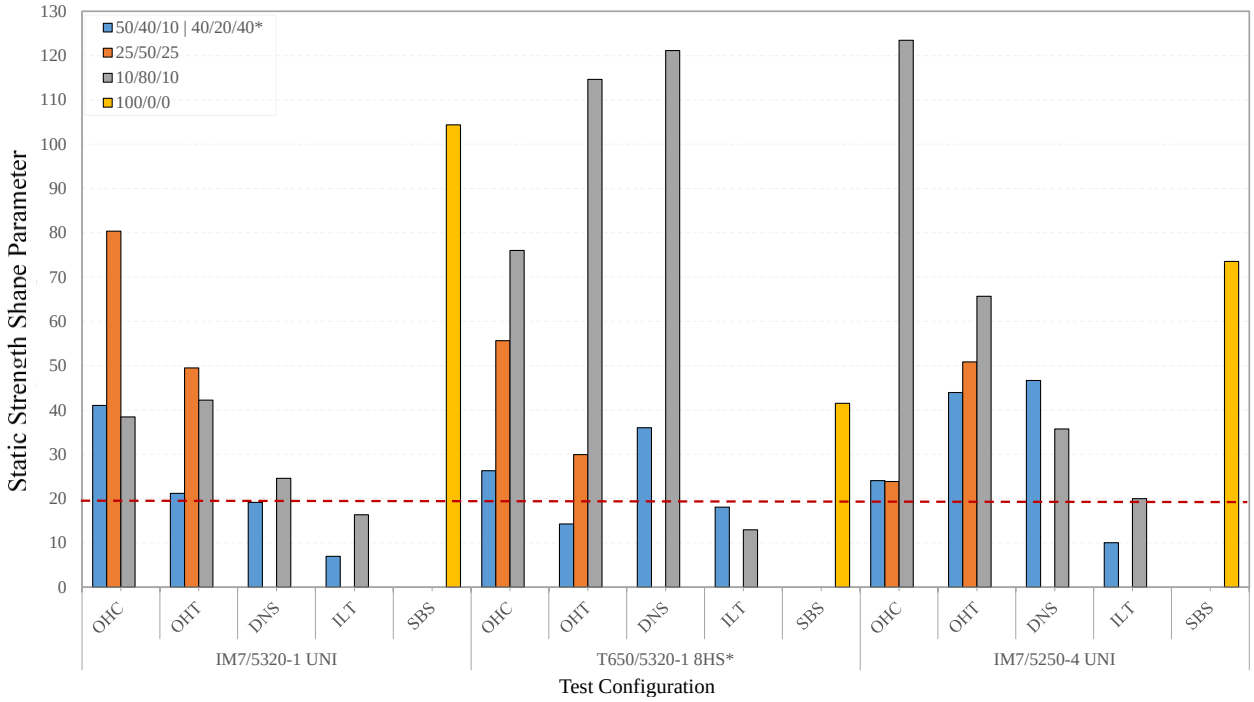


Figure 42. Summary of shape parameters for quasi-static data.

Table 11 – Calculation of modal shape parameters of static data.

Weibull Analysis	IM7/5320-1 UNI (Table 8)	T650/5320-1 8HS (Table 9)	IM7/5250-4 UNI (Table 10)	AMCSC (All data sets)
α	1.534	1.437	1.651	1.517
β	45.090	55.129	52.953	51.037
α Modal	**22.665**	**24.083**	**30.128**	**25.095**
n	11	11	11	33

ILT test data indicated the highest scatter, resulting in shape parameters significantly lower than the history value of 20, especially for UNI material systems. Generally, out-of-plane failure modes have higher scatter than in-plane failure modes. Moreover, ILT failure initiation site(s) and damage growth are influenced significantly by the manufacturing quality of the radius bend, i.e., fiber waviness, resin-rich areas, and porosity, and therefore result in high variability.

Overall, hard laminates indicated higher data scatter, while soft laminates indicated lower data scatter. Short-beam shear strength data also indicated low scatter. Regardless of the complications associated with specimen machining and notch sensitivity of DNS specimens, their shape parameters were near or above 20.

DISTRIBUTION STATEMENT A.
Approved for public release: distribution is unlimited.

6. FATIGUE TEST DATA ANALYSIS

Typically, a stress-to-number of cycles curve contains fatigue failures for multiple stress levels, static strength data points, runouts and residual strength data points. In this paper, the fatigue life scatter was analyzed using individual Weibull, joint Weibull, and Sendeckyj analyses. Only datasets containing more than five specimens within a stress level were included in the individual Weibull analysis. Residual strength data for all runouts were included in the Sendeckyj analysis.

Individual and joint Weibull analyses were conducted using only the fatigue data. At least two specimens from each material batch were included in the three main fatigue stress levels (minimum total of six fatigue failures per stress level) for Weibull analysis. Scatter analysis computer code (SACC) software was used for the Sendeckyj analysis of fatigue data with and without static strength data. Residual strength data of all runout specimens were included in the Sendeckyj analysis.

Fatigue life data scatter analysis of more than seven hundred fatigue data points from three different material systems using individual Weibull, joint Weibull, and Sendeckyj analyses are presented in this chapter. SN data and curves with the Sendeckyj fitting models for all three material systems can be found in Appendix A.

6.1 Solvay 5320-1/ IM7 Unidirectional Tape

6.1.1 IM7/5320-1 UNI Open-Hole Compression/Tension

Fatigue analyses of IM7/5320-1 UNI specimens from 13 data sets are included in this section. Each data set contains static data, fatigue data with a minimum of three fatigue stress levels, and residual strength for runouts, if any. Once the Sendeckyj fitting parameters C and S are determined, the fitting curve for the SN data is obtained, as shown in Figure 43. In addition, the equivalent static strength for each fatigue data point (both failures and runouts) is included in the data summary.

Fatigue life scatter analysis data for IM7/5320-1 UNI OH are summarized in Table 12. The shape parameters corresponding to each SN curve using individual Weibull, joint Weibull, and Sendeckyj scatter analyses are denoted as $\hat{\alpha}_{IW}$,$\hat{\alpha}_{JW}$, and $\hat{\alpha}_{Sendeckyj}$, respectively. Figure 44 provides a summary of the detailed fatigue life scatter analysis conducted on IM7/5320-1 UNI using individual Weibull, joint Weibull, and Sendeckyj analyses (with and without static).

DISTRIBUTION STATEMENT A.
Approved for public release: distribution is unlimited.

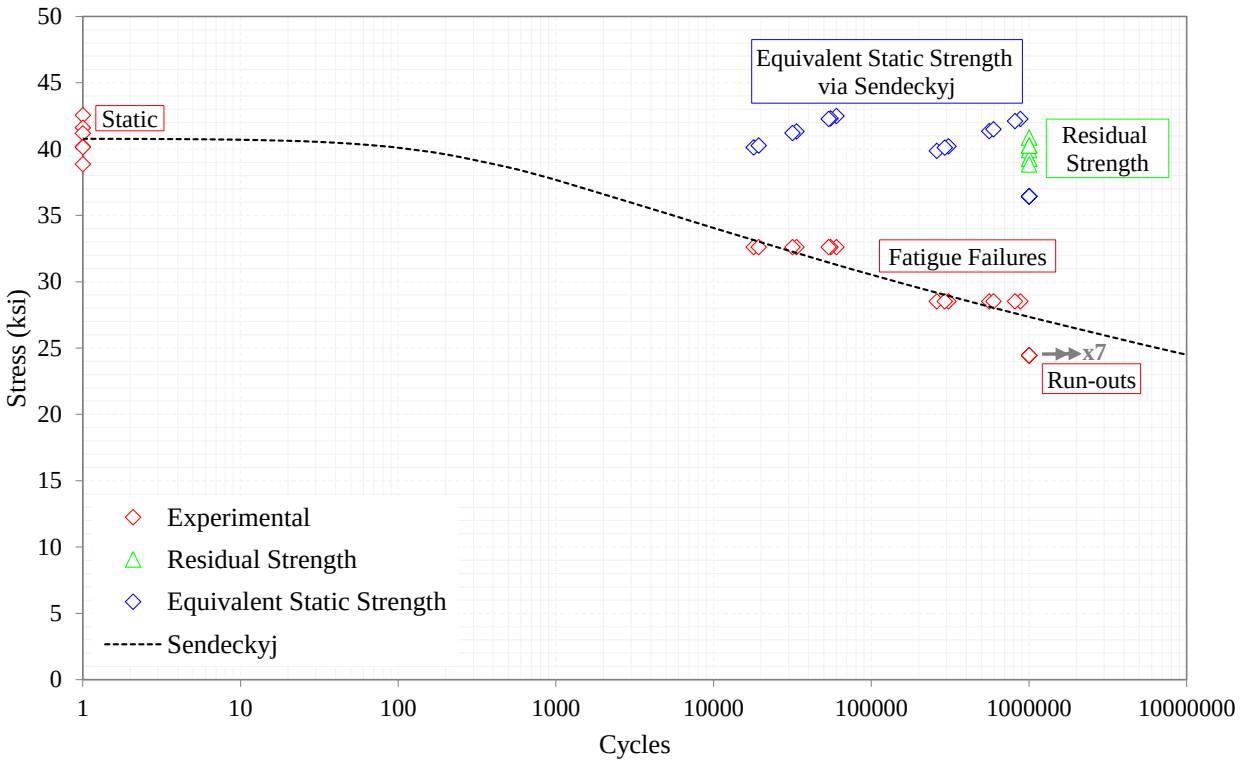


Figure 43. Sendeckjy analysis prediction for IM7/5320-1 UNI, OHC, 10/80/10, R = 5.

Table 12 – Fatigue life scatter analysis for IM7/5320-1 UNI.

Specimen Configuration			Weibull Analysis		Sendeckyj Analysis	
Layup	Test Description	Stress Ratio (R)	$\hat{\alpha}_{IW}$	$\hat{\alpha}_{JW}$	$\hat{\alpha}_{Sendeckyj}$ (w/o static)	$\hat{\alpha}_{Sendeckyj}$ (w/ static)
50/40/10	OHT-T	0.1	All Runouts			
	OHC-C	5	2.090	2.227	2.995	1.019
	OHC-T	–1	4.698	3.857	3.172	1.831
	DNS	0.1	2.882	2.857	3.001	1.751
	ILT	0.1	2.130	1.591	1.655	0.690
25/50/25	OHT-T	0.1	All Runouts			
	OHC-C	5	2.146	1.852	1.738	1.736
	OHC-T	–1	3.550	3.636	3.971	3.317
10/80/10	OHT-T	0.1	4.980	4.646	4.548	1.723
	OHC-C	5	2.570	2.563	2.513	2.244
	OHC-T	–1	5.551	5.528	5.320	3.191
	DNS	0.1	3.649	2.583	2.309	1.611
	ILT	0.1	1.434	1.439	1.493	1.211
100/0/0	SBS	0.1	1.885	1.555	1.651	1.839

DISTRIBUTION STATEMENT A.
Approved for public release: distribution is unlimited.

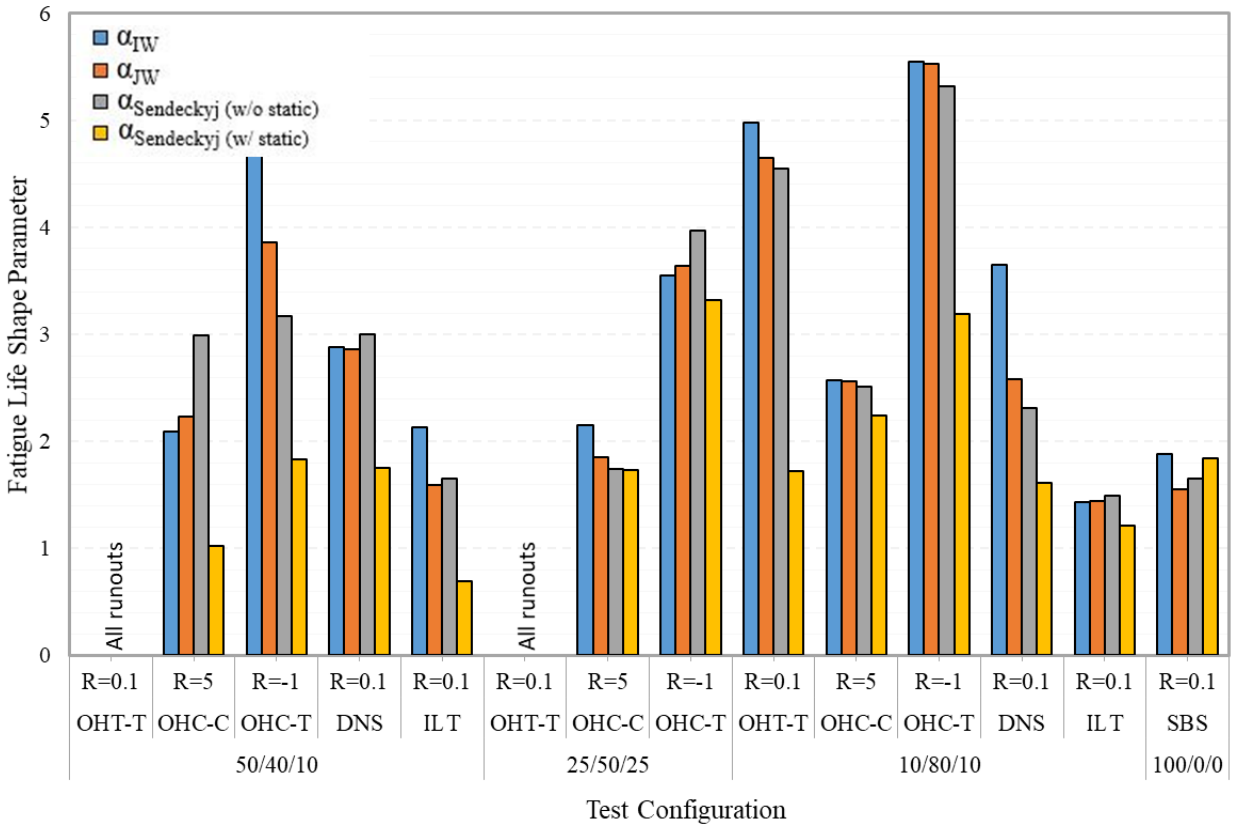


Figure 44. Summary of shape parameters for IM7/5320-1 UNI SN data.

Overall, the individual Weibull analysis provides the highest fatigue life shape parameter, while the Sendeckyj (with static) analysis provides the lowest or conservative fatigue life shape parameter. Results indicate that shape parameters for all SN curves are higher than the historic value of 1.25 for the modal fatigue life shape parameter obtained by Whitehead et al. [1] who used the pooled individual Weibull analysis data. The Sendeckyj analysis includes runout and corresponding residual strength data points. Also, the Sendeckyj analysis produces a higher scatter because it is unbiased compared to the arithmetically averaged individual Weibull shape parameters. In many cases, when the static data are included in the Sendeckyj analysis, the analysis resulted in significantly lower fatigue life shape parameters than that without the static test data, as shown in Figure 44. For example, IM7/5320-1 UNI, 10/80/10, OHT (R = 0.1) SN data resulted in a fatigue life shape parameter of 4.548 for the Sendeckyj analysis without static data, and while the static test data are included in the analysis, this value was reduced to 1.723. Since this is fatigue analysis, one could use the Sendeckyj analysis without static data for generating the modal fatigue life shape parameter.

The average Sendeckyj equivalent strength values calculated for pooled fatigue and residual strength data are compared against the quasi-static strength data along with their CVs in Table 13 and also graphically presented in Figure 45.

DISTRIBUTION STATEMENT A.
Approved for public release: distribution is unlimited.

Table 13 – Strength comparison for IM7/5320-1 UNI.

Specimen Configuration		Static Test		Pooled Sendeckyj Analysis	
Layup	Test Description	Strength (ksi)	CV (%)	Strength (ksi)	CV (%)
50/40/10	OHT	107.455	5.783	105.263	6.127
	OHC	69.938	3.367	69.585	2.915
	OH	69.938	3.367	70.430	4.175
	DNS	3.348	7.534	3.474	4.411
	ILT	11.301	15.152	12.019	10.013
25/50/25	OHT	68.461	2.436	68.645	1.844
	OHC	50.830	1.693	50.423	1.929
	OH	50.830	1.693	50.818	1.612
10/80/10	OHT	45.096	1.572	44.948	6.751
	OHC	42.089	1.570	39.897	5.684
	OH	42.089	1.570	39.348	7.894
	DNS	3.067	4.544	3.039	5.513
	ILT	10.964	8.982	10.914	7.746
100/0/0	SBS	16.300	1.191	16.137	2.046

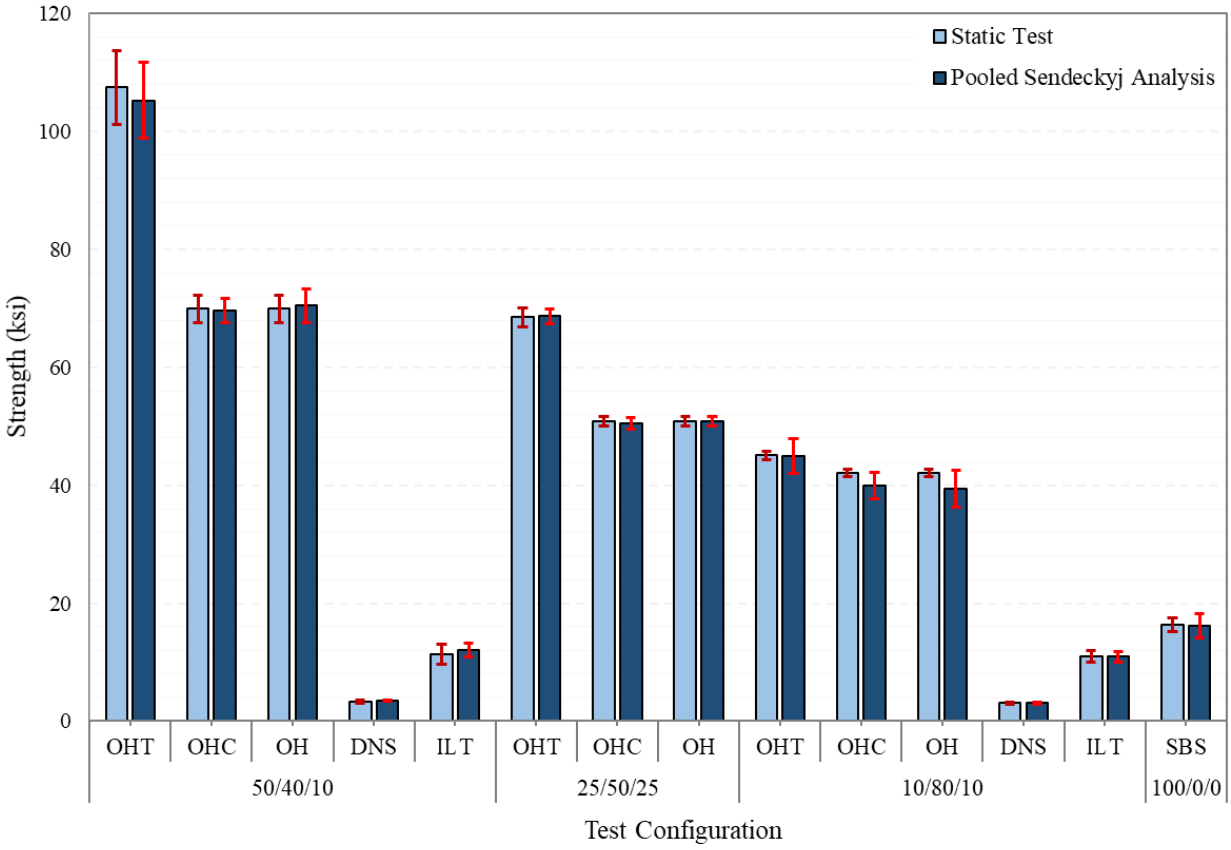


Figure 45. Comparison of quasi-static strength and pooled Sendeckyj equivalent strength for IM7/5320-1 UNI material system.

DISTRIBUTION STATEMENT A.
Approved for public release: distribution is unlimited.

A comparison of OHT (R = 0.1), OHC (R = 5), OHC/T (R = –1) measured and normalized (with respect to the corresponding average ultimate static strength) experimental data for hard (50/40/10), quasi-isotropic (25/50/25), and soft (10/80/10) layup configurations are shown in Figures 46 to 51. SN data shows that both hard and quasi-isotropic layup configurations with the majority of 0° and ±45° plies exhibit great fatigue resistance. Overall, R = –1 data indicated the least fatigue resistance, especially for soft laminates. Tension-tension (R = 0.1) fatigue of hard and quasi-isotropic laminates had all runouts, even at extremely high stress levels, indicating great fatigue resistance. Therefore, no fatigue analysis was conducted for those cases. The residual strength data for runouts at one million cycles indicated a significant increase in static strength, especially for the hard layup.

At least one specimen per each stress level was considered for the high-fidelity XCT inspections for detailed fatigue damage characterization. These high-fidelity inspections indicated microcracks and minor fiber damage around the hold that reduced the stress concentration. This may have caused the residual strength to be higher than the quasi-static strength for stress levels that produced runout without significant fatigue damages.

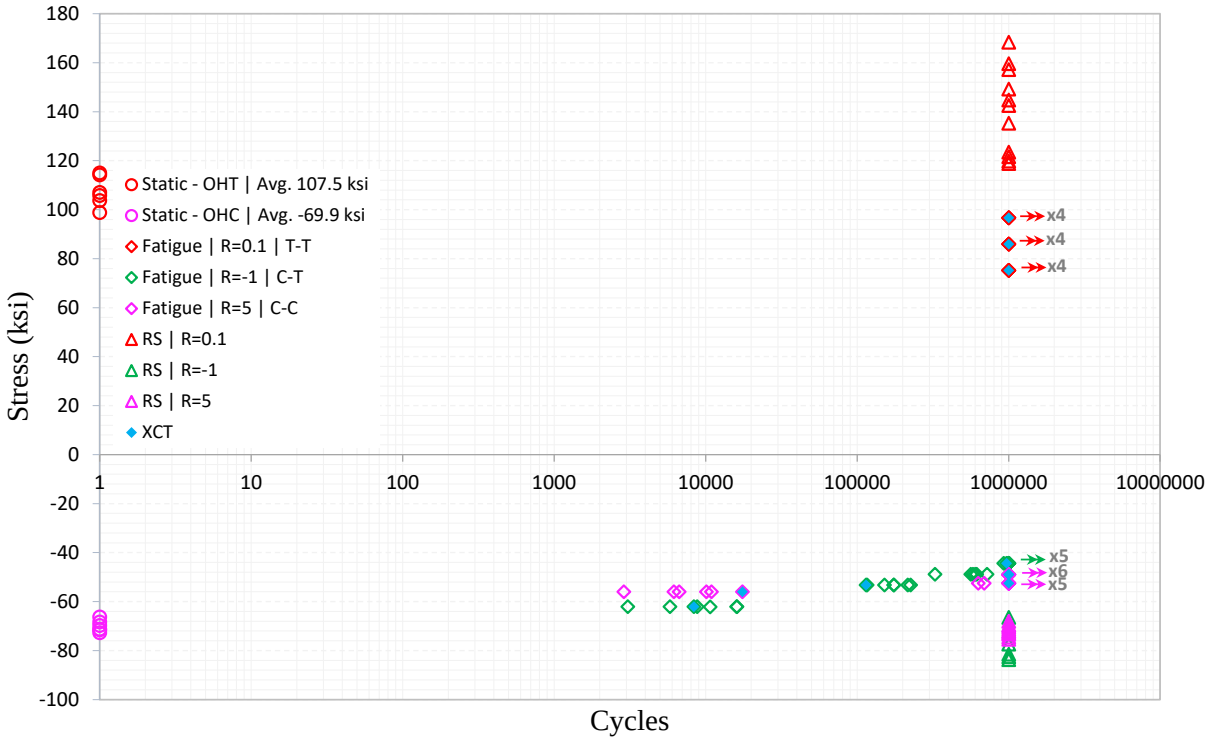


Figure 46. IM7/5320-1 UNI, OH, 50/40/10 fatigue data—measured.

DISTRIBUTION STATEMENT A.
Approved for public release: distribution is unlimited.

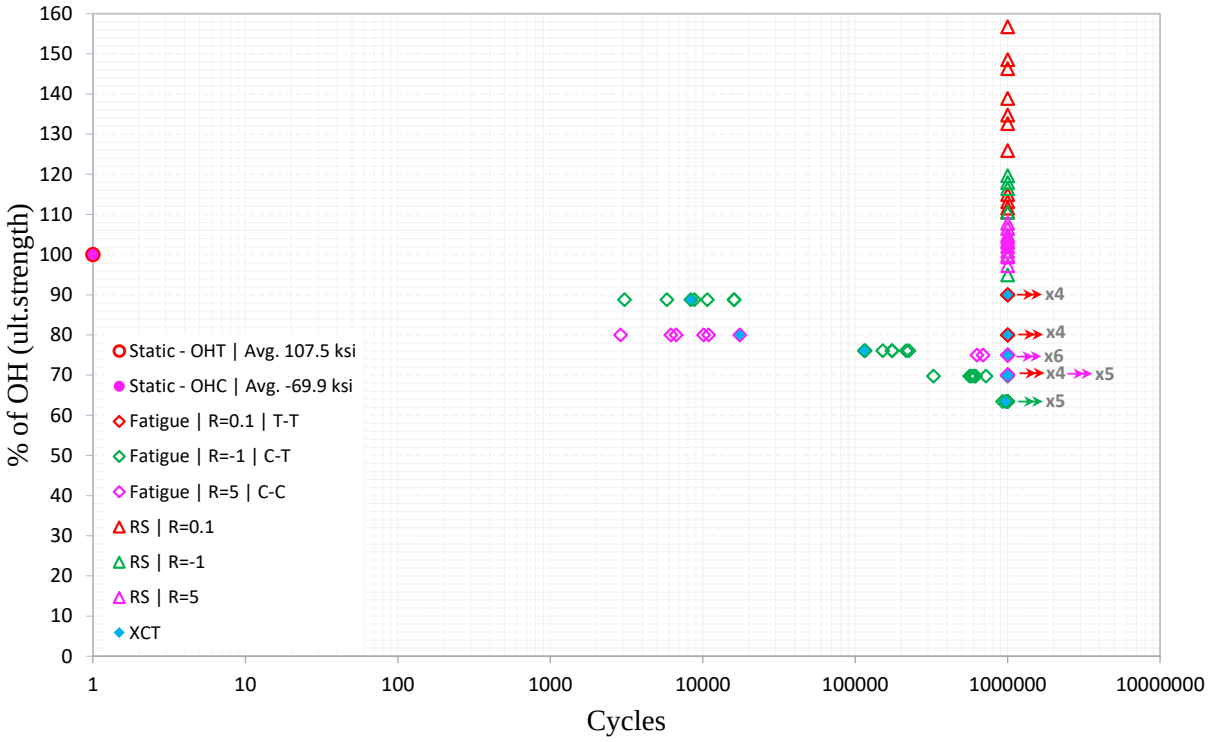


Figure 47. IM7/5320-1 UNI, OH, 50/40/10 fatigue data—normalized.

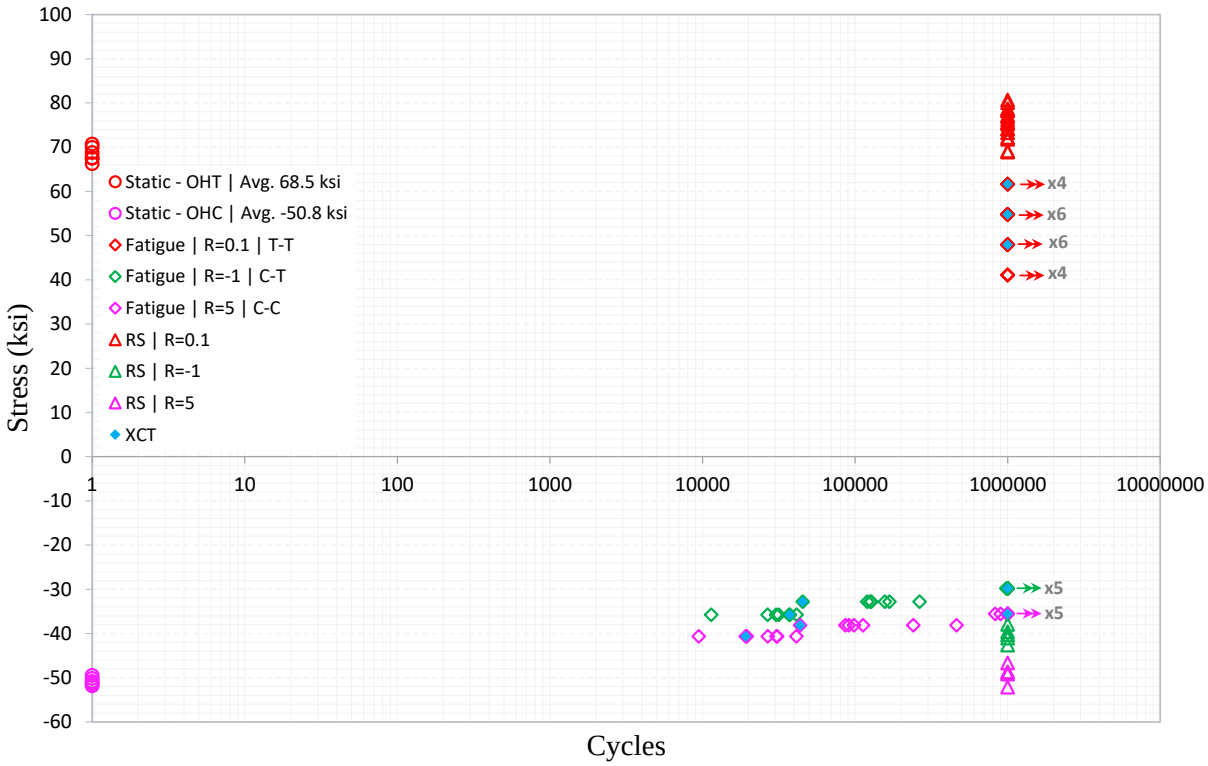


Figure 48. IM7/5320-1 UNI, OH, 25/50/25 fatigue data—measured.

DISTRIBUTION STATEMENT A.
Approved for public release: distribution is unlimited.

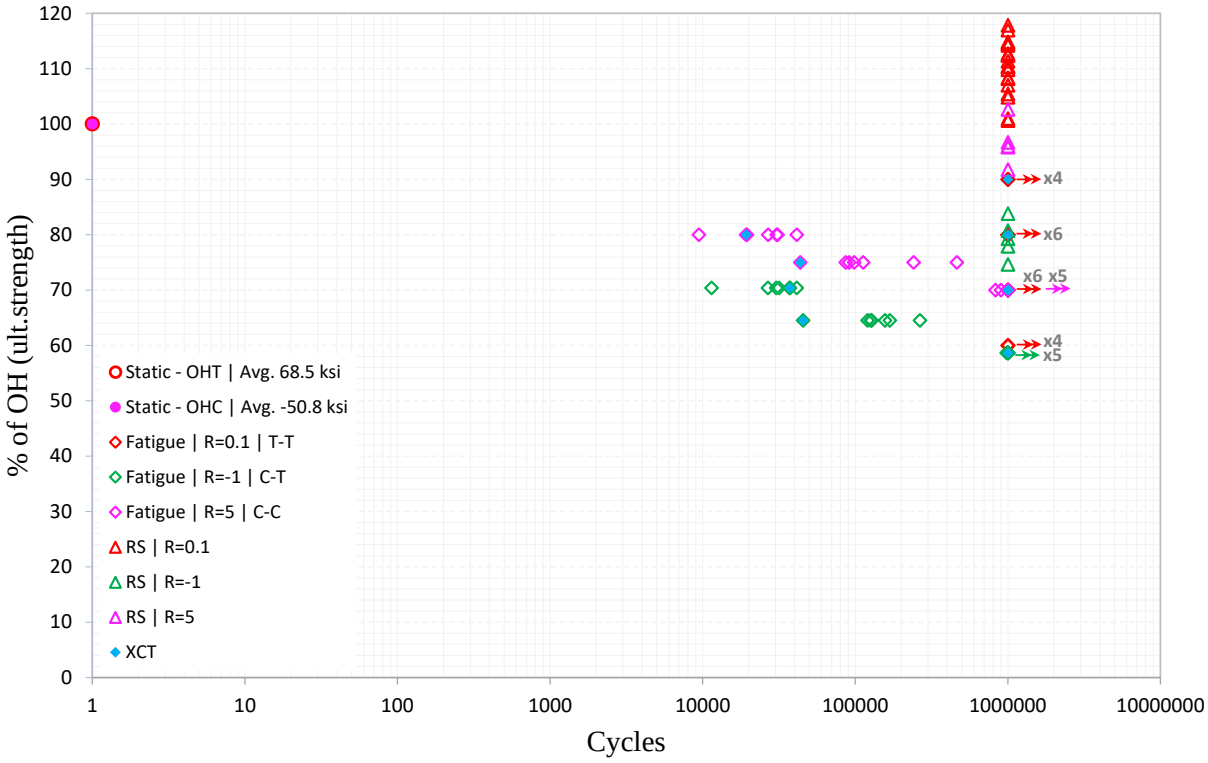


Figure 49. IM7/5320-1 UNI, OH, 25/50/25 fatigue data—normalized.

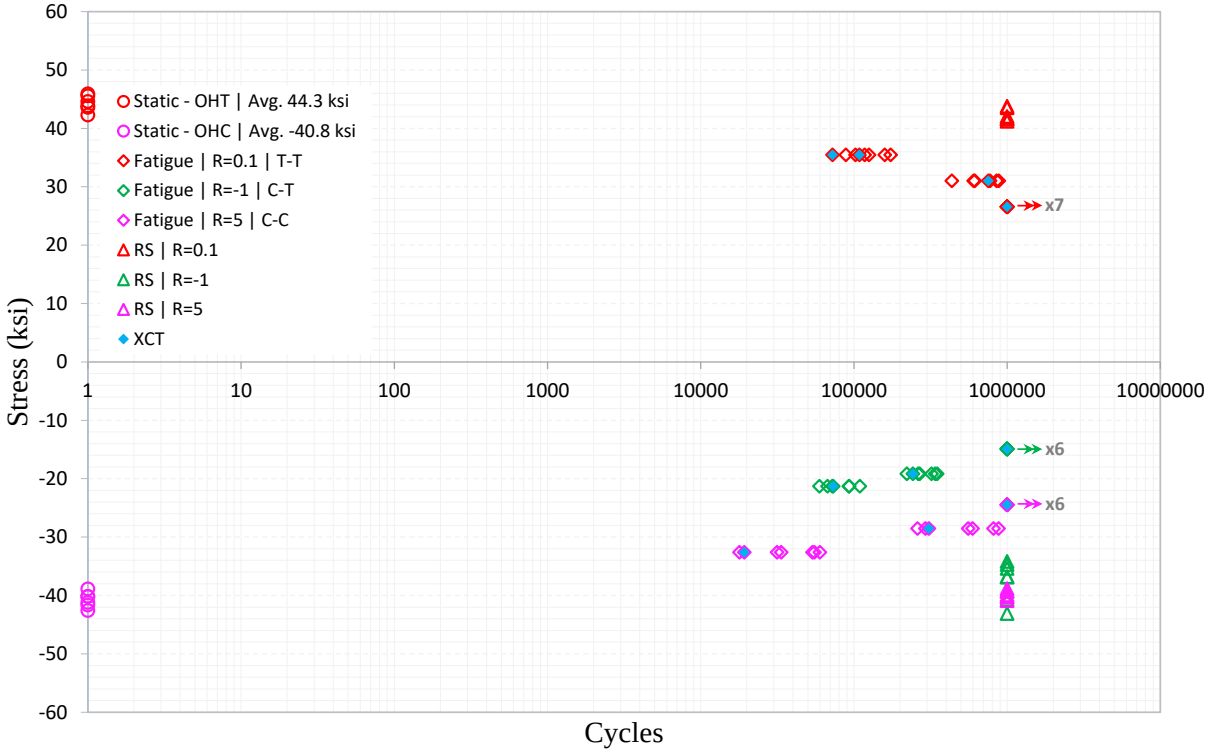


Figure 50. IM7/5320-1 UNI, OH, 10/80/10 fatigue data—measured.

DISTRIBUTION STATEMENT A.
Approved for public release: distribution is unlimited.

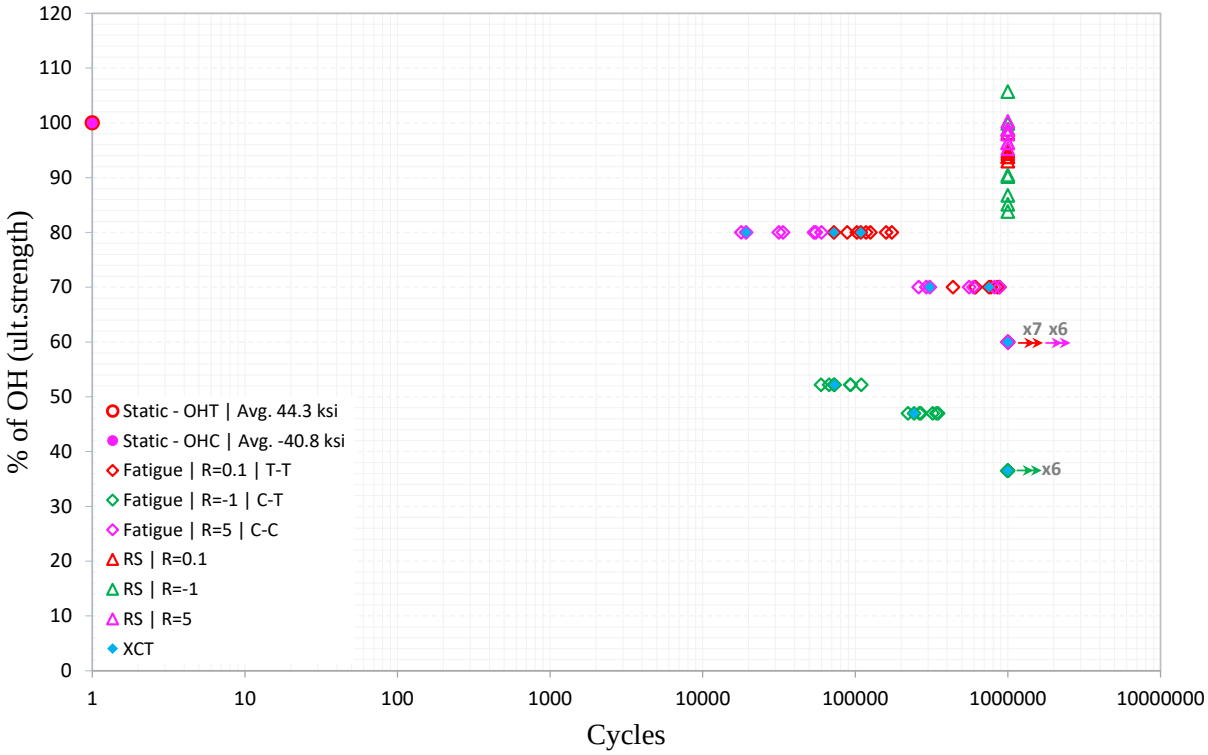


Figure 51. IM7/5320-1 UNI, OH, 10/80/10 fatigue data—normalized.

6.1.2 IM7/5320-1 UNI Double-Notch Shear

A comparison of DNS measured and normalized experimental data, for hard and soft layup configurations, are shown in Figures 52 and 53, respectively. Hard layup indicates a lower fatigue resistance than the soft laminates. Note that DNS soft test layup had majority of ±45° near the mid-plane, while hard layup had the majority of 0° plies near the mid-plane.

At least one specimen per each stress level is considered for high-fidelity XCT inspections for detailed fatigue damage characterization. Typically, the notch geometry, which is challenging to machine consistently across the test panel, contributes to the data scatter. However, the fatigue data for both hard and soft laminates indicate typical data scatter observed for composites. The shape parameters, which are indicators for data scatter, also confirm this by producing higher shape parameters than what is historically observed for composites (1.25).

Unlike in the case of open-hole specimens, fatigue wearout was indicated by the steep SN curves for DNS. This was also reflected in the residual strength of runout specimens that were always lower than the quasi-static strength data.

DISTRIBUTION STATEMENT A.
Approved for public release: distribution is unlimited.

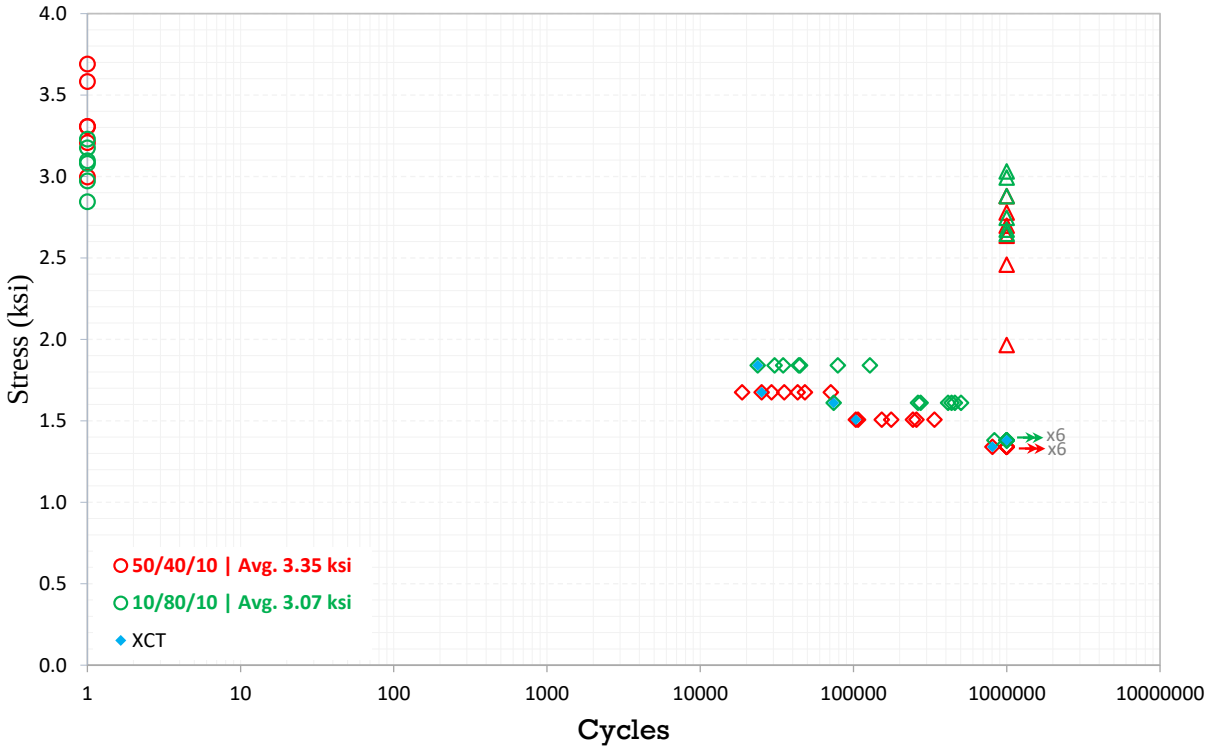


Figure 52. IM7/5320-1 UNI, DNS fatigue data—measured.

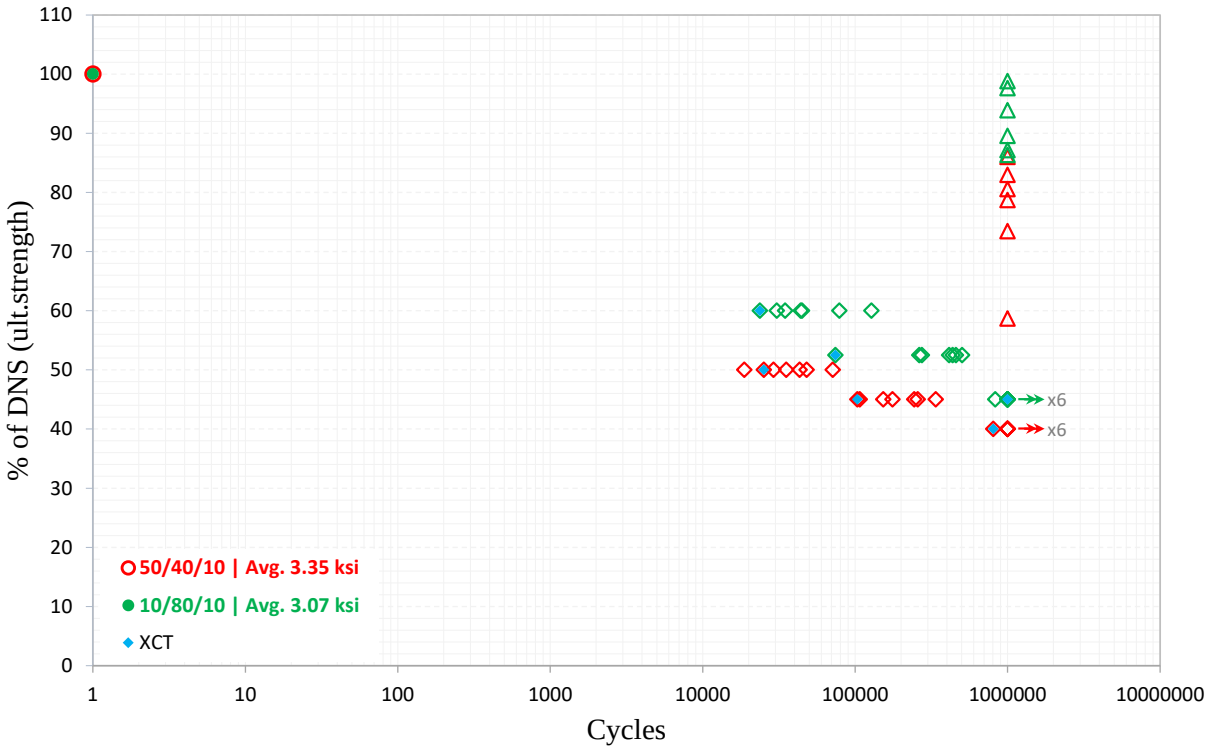


Figure 53. IM7/5320-1 UNI, DNS fatigue data—normalized.

DISTRIBUTION STATEMENT A.
Approved for public release: distribution is unlimited.

6.1.3 IM7/5320-1 UNI Interlaminar Tension

A comparison of interlaminar tension measured and normalized data (with respect to the ultimate static strength) for hard and soft layup configurations are as shown in Figures 54 and 55, respectively. Static data for hard laminates indicated higher data scatter than that for soft laminates. Although hard laminate data indicated somewhat longer fatigue life in general, the ILT SN data for both laminates indicated similar behavior (within the data scatter). This is because ILT is a matrix-dominant property at ply interfaces. In addition to the three major stress levels, fatigue tests were conducted at two additional stress levels for both laminate stacking sequences. Pre-test NDI scans were performed using XCT for the majority of the ILT specimens and compared with the XCT scans obtained at various fatigue intervals as well as after residual strength of runout specimens. This comparison was performed in order to investigate the influence of manufacturing anomalies such as voids, ply waviness, and resin-rich areas on the initiation and propagation of damage that affects the fatigue data scatter of ILT (see section 7.4).

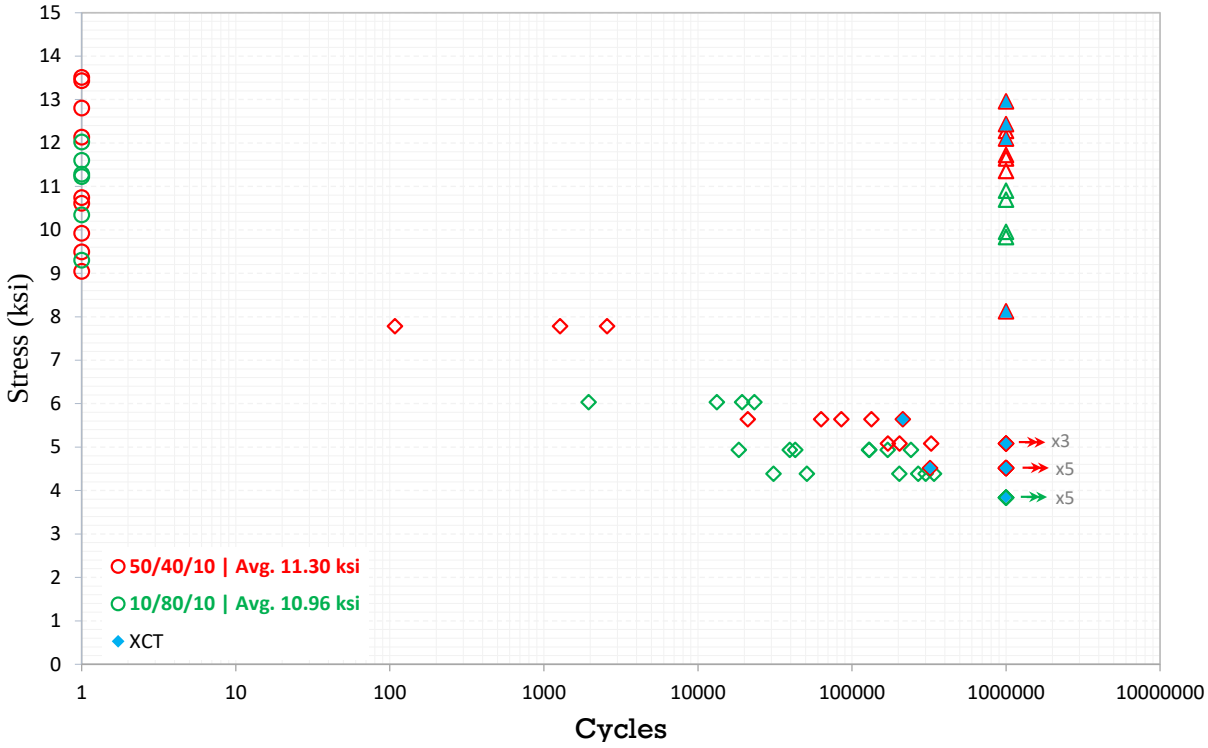


Figure 54. IM7/5320-1 UNI, ILT fatigue data—measured.

DISTRIBUTION STATEMENT A.
Approved for public release: distribution is unlimited.

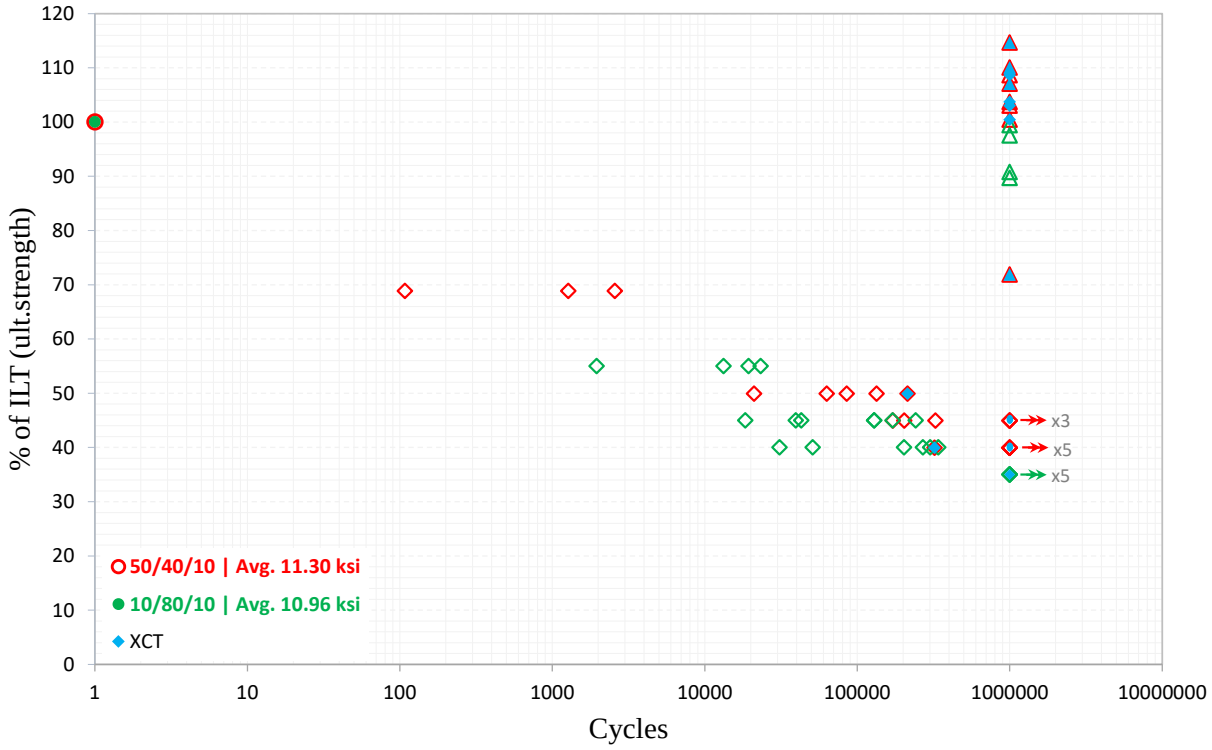


Figure 55. IM7/5320-1 UNI, ILT fatigue data—normalized.

6.1.4 IM7/5320-1 UNI Short Beam Shear

The short-beam shear SN data for 100/0/0 layup configuration is shown in Figure 56. Normalized SBS SN data are compared with normalized DNS SN data (both hard and soft laminates) in Figure 57. Although both of these test methods produce interlaminar failure modes (mode II), the failure mechanics. For example, SBS produces mode II loading between plies as a result of beam bending while DNS produces mode II loading due to in-plane shear. SBS specimens had either single or multiple delaminations as shown in Figure 58. In contrast, DNS specimens had failure near the mid plies, where the highest in-plane shear stress exists (Figure 59). Normalized SBS SN curve compares well with the normalized soft DNS specimen, including the residual strength data.

DISTRIBUTION STATEMENT A.
Approved for public release: distribution is unlimited.

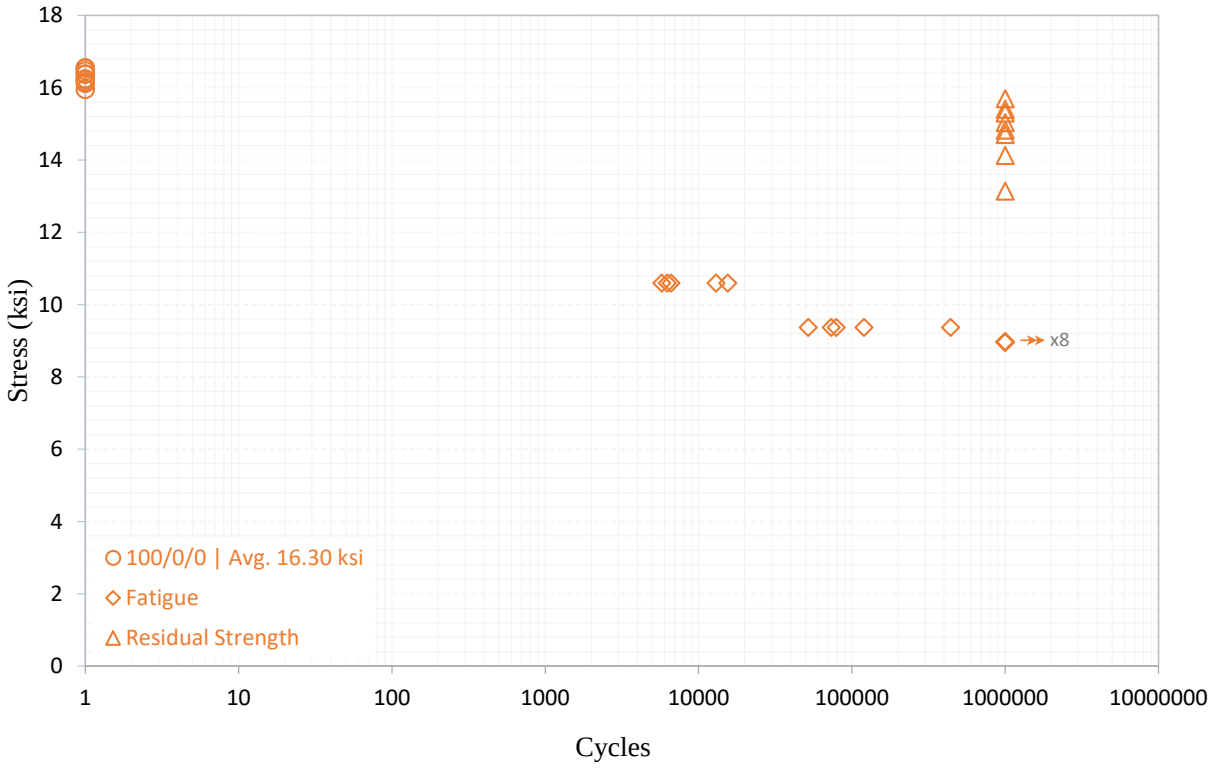


Figure 56. IM7/5320-1 UNI, 100/0/0, SBS, fatigue data.

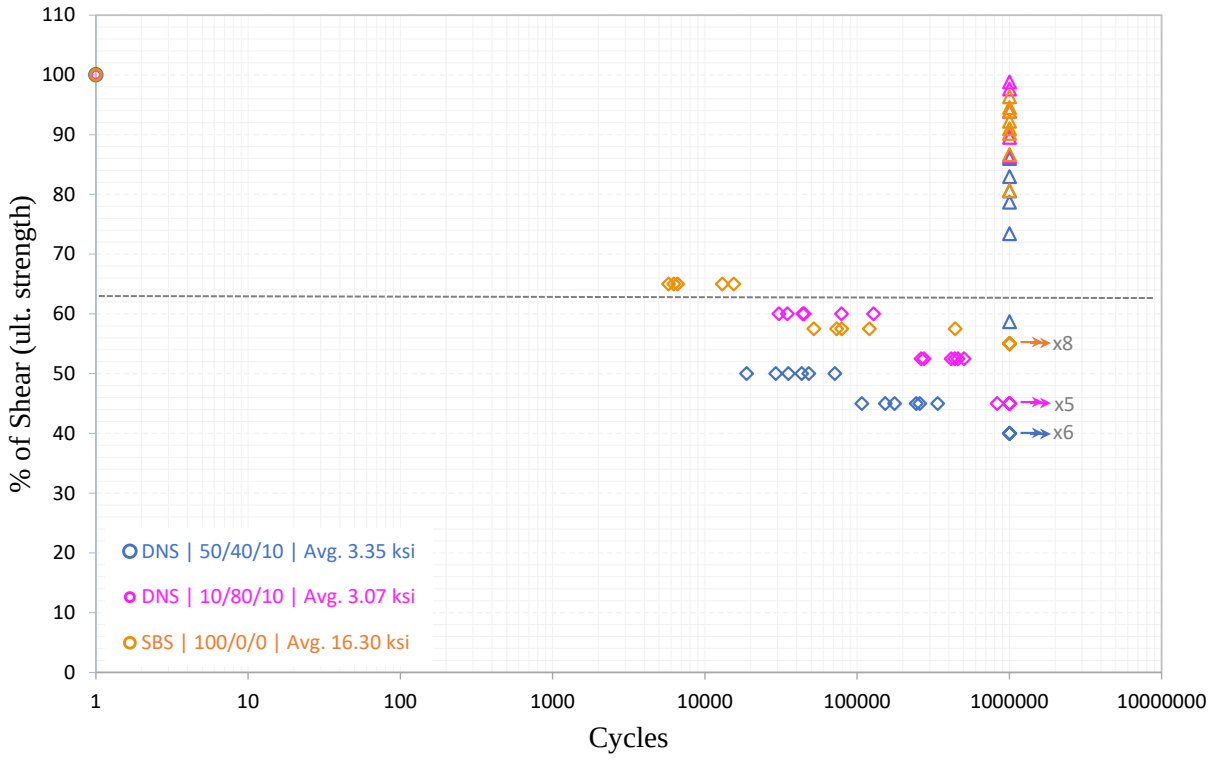


Figure 57. Comparison between DNS and SBS for IM7/5320-1 UNI data—normalized.

DISTRIBUTION STATEMENT A.
Approved for public release: distribution is unlimited.

Compared to SBS, DNS require significant amount of materials as well as several CNC machining steps. DNS failure is sensitive to the notch depth and the quality of machining and prone to high data scatter for poorly machined specimens. Therefore, DNS specimen quality was carefully inspected prior to selecting specimens for testing.

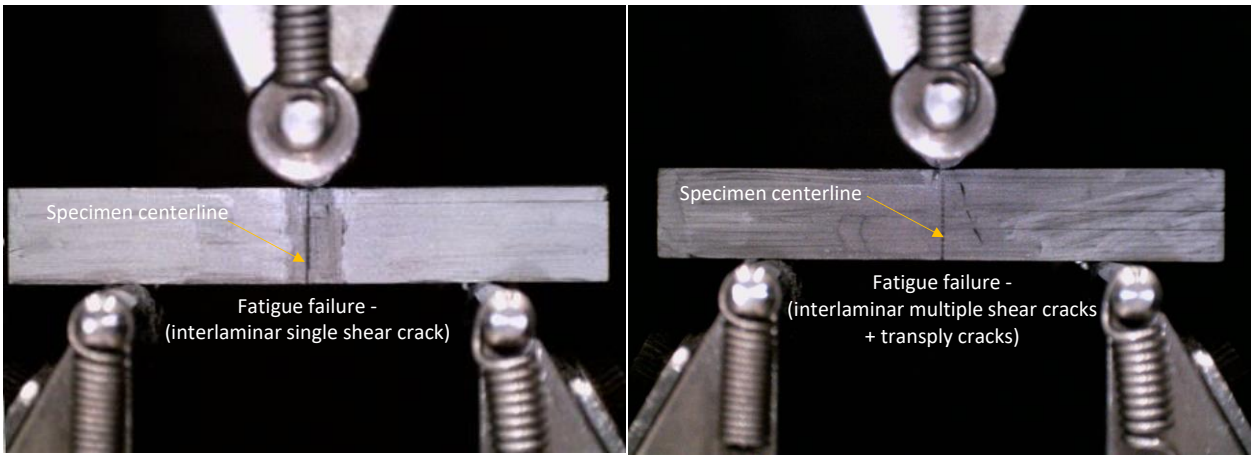


Figure 58. Representative SBS failure modes for IM7/5320-1 UNI, 100/0/0.

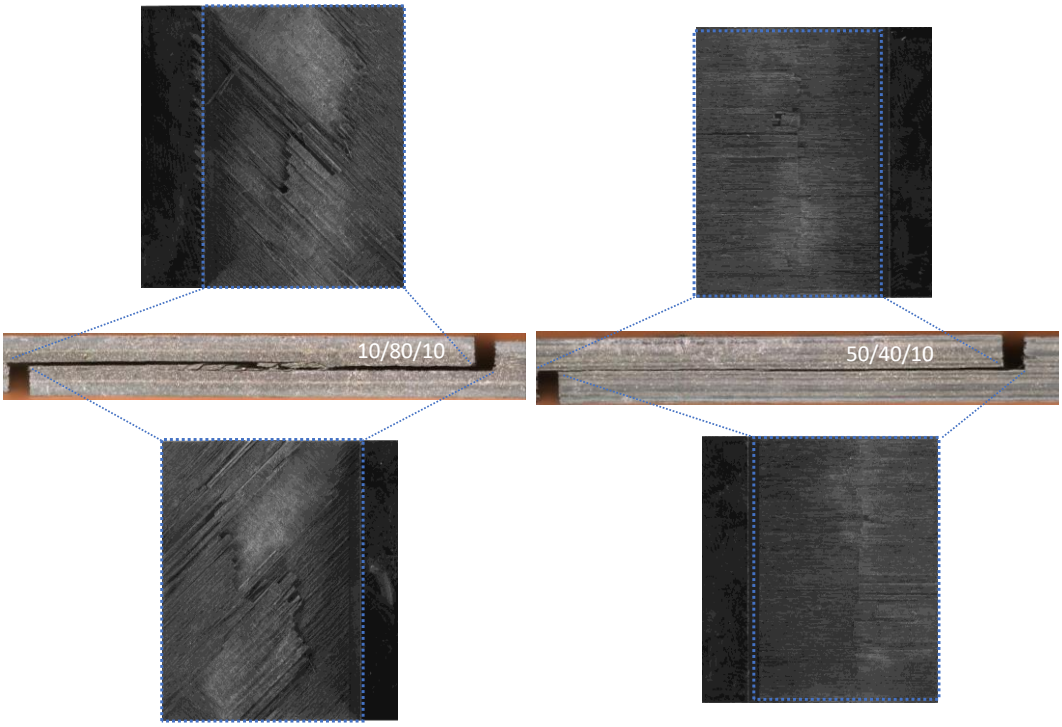


Figure 59. Representative DNS failure modes for IM7/5320-1 UNI, 10/80/10 and 50/40/10.

DISTRIBUTION STATEMENT A.
Approved for public release: distribution is unlimited.

6.2 Solvay 5320-1/ T650 8-Harness Satin fabric

6.2.1 T650/5320-1 8HS Open-Hole Compression/Tension

Fatigue analyses of T650/5320-1 8HS specimens from 11 data sets are included in this section. Each data set contains a minimum of three fatigue stress levels and at least six static strength data points. Once the Sendeckyj fitting parameters C and S are determined, the fitting curve for the SN data is obtained. SN curves with the Sendeckyj fitting parameters for T650/5320-1 8HS are included in Appendix A.

Fatigue life scatter analysis data are summarized in Table 14. The shape parameters corresponding to each SN curve using individual Weibull, joint Weibull, and Sendeckyj scatter analyses are denoted as $\hat{\alpha}_{IW}$, $\hat{\alpha}_{JW}$, and $\hat{\alpha}_{Sendeckyj}$, respectively.

Table 14 – Fatigue life scatter analysis for T650/5320-1 8HS.

Specimen Configuration			Weibull Analysis		Sendeckyj Analysis	
Layup	Test Description	Stress Ratio (R)	$\hat{\alpha}_{IW}$	$\hat{\alpha}_{JW}$	$\hat{\alpha}_{Sendeckyj}$ (w/o static)	$\hat{\alpha}_{Sendeckyj}$ (w/ static)
40/20/40	OHT-T	0.1	All Runouts			
	OHC-C	5	1.335	1.340	1.343	1.153
	OHC-T	–1	4.766	4.793	4.743	3.314
	DNS	0.1	3.445	3.238	3.110	2.731
	ILT	0.1	1.921	1.316	1.256	1.404
25/50/25	OHT-T	0.1	All Runouts			
	OHC-C	5	1.600	1.527	1.498	1.667
	OHC-T	–1	3.835	3.266	3.135	2.909
10/80/10	OHT-T	0.1	2.361	2.031	2.099	1.945
	OHC-C	5	2.289	2.113	1.710	1.798
	OHC-T	–1	7.204	5.744	5.658	4.240
	DNS	0.1	4.861	4.821	5.048	2.932
	ILT	0.1	1.489	1.399	1.408	1.215
100/0/0	SBS	0.1	2.076	2.055	1.929	1.663

Figure 60 shows the summary of a detailed fatigue life scatter analysis conducted on T650/5320-1 8HS using individual Weibull, joint Weibull, and Sendeckyj analyses (with and without static). The Sendeckyj equivalent strength values based on the fatigue data are pooled and compared against the tested static strength data along with their CVs in Table 15 and are also graphically presented in Figure 61.

DISTRIBUTION STATEMENT A.
Approved for public release: distribution is unlimited.

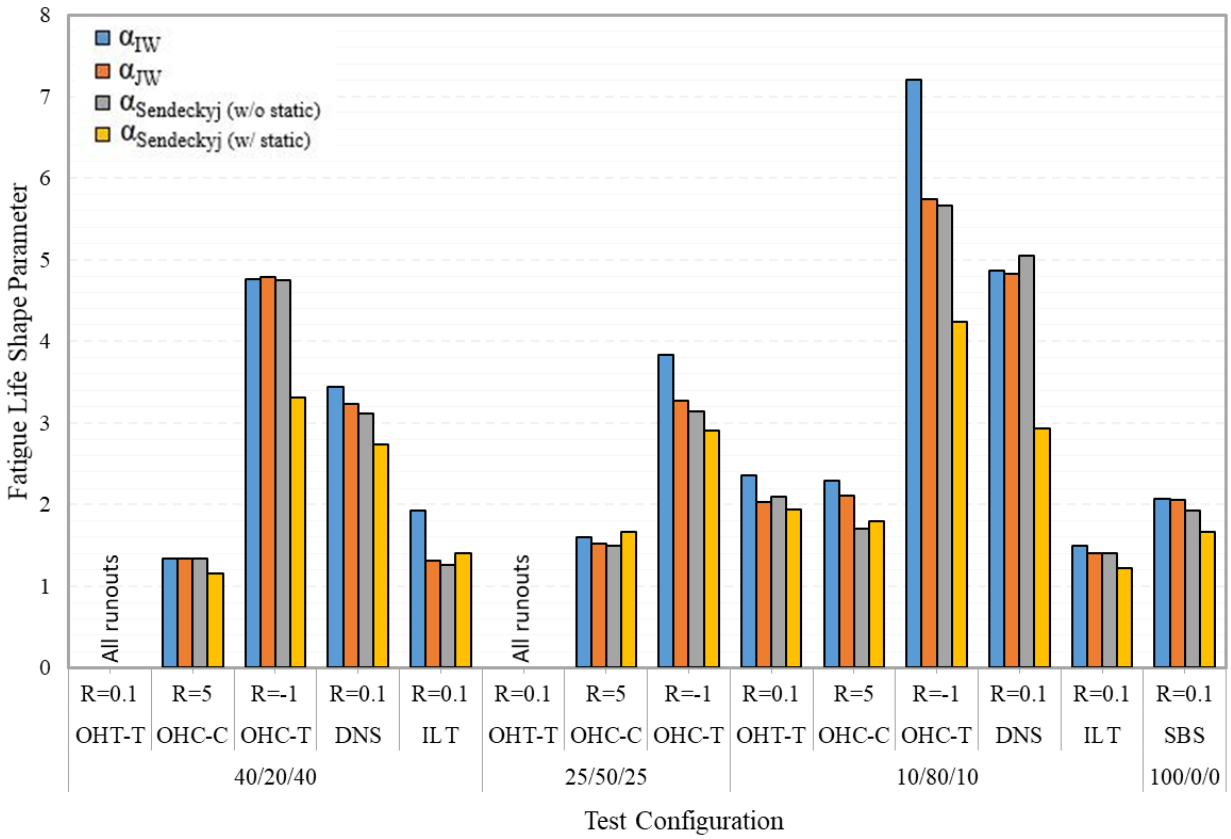


Figure 60. Summary of shape parameters for T650/5320-1 8HS SN data.

Table 15 – Static strength comparison for T650/5320-1 8HS.

Specimen Configuration		Static Test		Pooled Sendeckyj Analysis	
Layup	Test Description	Strength (ksi)	CV (%)	Strength (ksi)	CV (%)
40/20/40	OHT	60.734	6.937	59.486	6.662
	OHC	58.054	4.322	57.498	4.553
	OH	58.054	4.322	56.080	8.885
	DNS	4.206	3.649	4.048	9.899
	ILT	6.794	6.674	6.768	12.113
25/50/25	OHT	48.501	4.533	47.297	5.853
	OHC	49.766	3.020	48.459	4.028
	OH	49.766	3.020	47.272	9.619
10/80/10	OHT	41.485	2.042	40.274	6.339
	OHC	41.116	1.497	40.021	6.197
	OH	41.116	1.497	41.116	4.519
	DNS	4.340	1.006	4.150	7.608
	ILT	6.489	8.621	6.655	6.457
100/0/0	SBS	12.441	2.977	12.312	3.796

DISTRIBUTION STATEMENT A.
Approved for public release: distribution is unlimited.

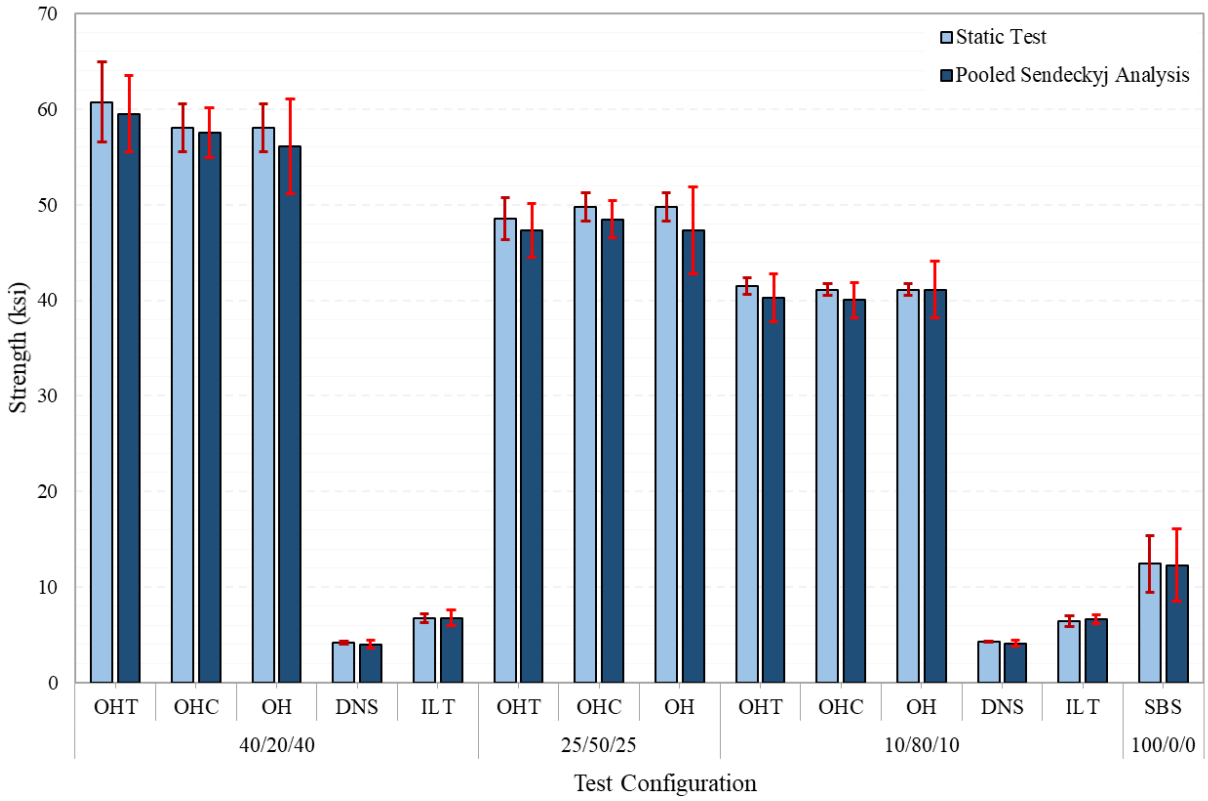


Figure 61. Comparison of quasi-static strength and pooled Sendeckyj equivalent strength for T650/5320-1 8HS.

A comparison of T650/5320-1 8HS OHT (R = 0.1), OHC (R = 5), and OHC/T (R = –1) measured and normalized experimental data for hard, quasi-isotropic, and soft layup configurations are shown in Figures 62 to 67. Similar to the observations for UNI, R = –1 data indicated the least fatigue resistance, especially for soft laminates. Tension-tension (R = 0.1) fatigue of hard and quasi-isotropic laminates had all runouts, even at extremely high stress levels, indicating great fatigue resistance. Therefore, no fatigue analysis was conducted for those cases. The residual strength data for runouts at one million cycles indicated a significant increase in static strength, especially for the hard layup, possibly due to the reduction of local stress concentration caused by microcracks around the hole. At least one specimen per each stress level was considered for high-fidelity XCT inspections for detailed fatigue damage characterization.

DISTRIBUTION STATEMENT A.
Approved for public release: distribution is unlimited.

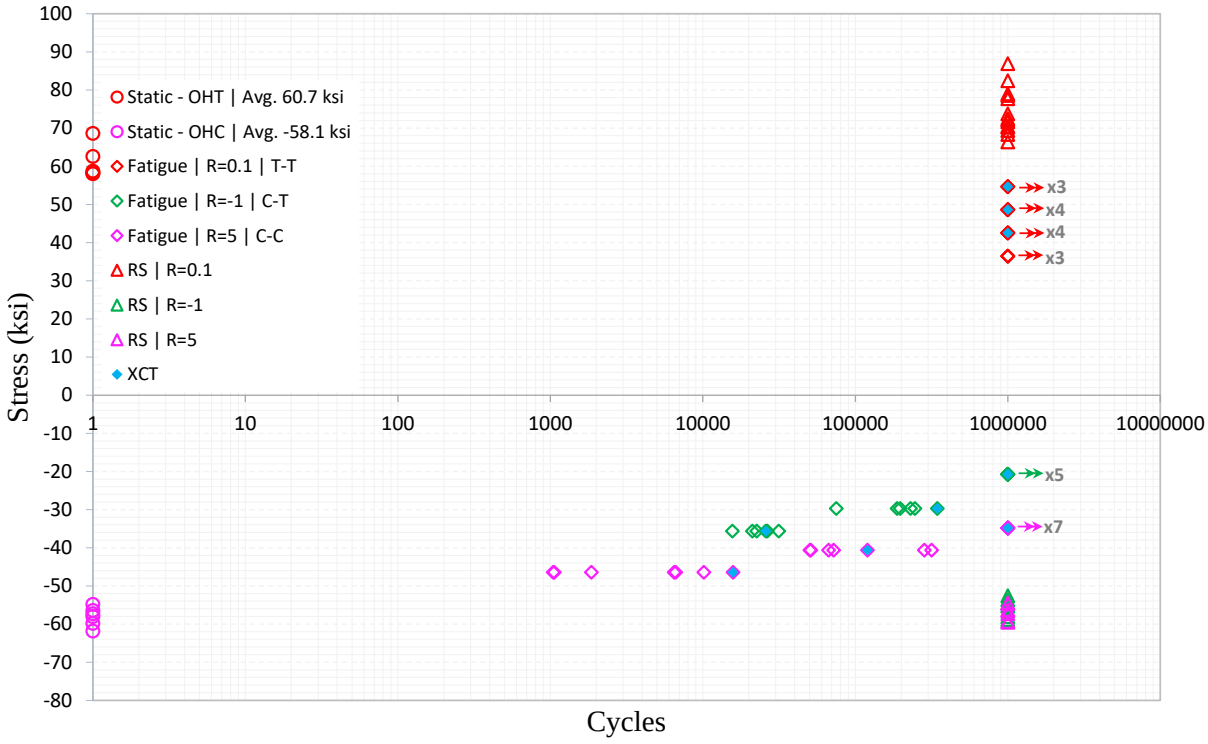


Figure 62. T650/5320-1 8HS, OH, 40/20/40 fatigue data—measured.

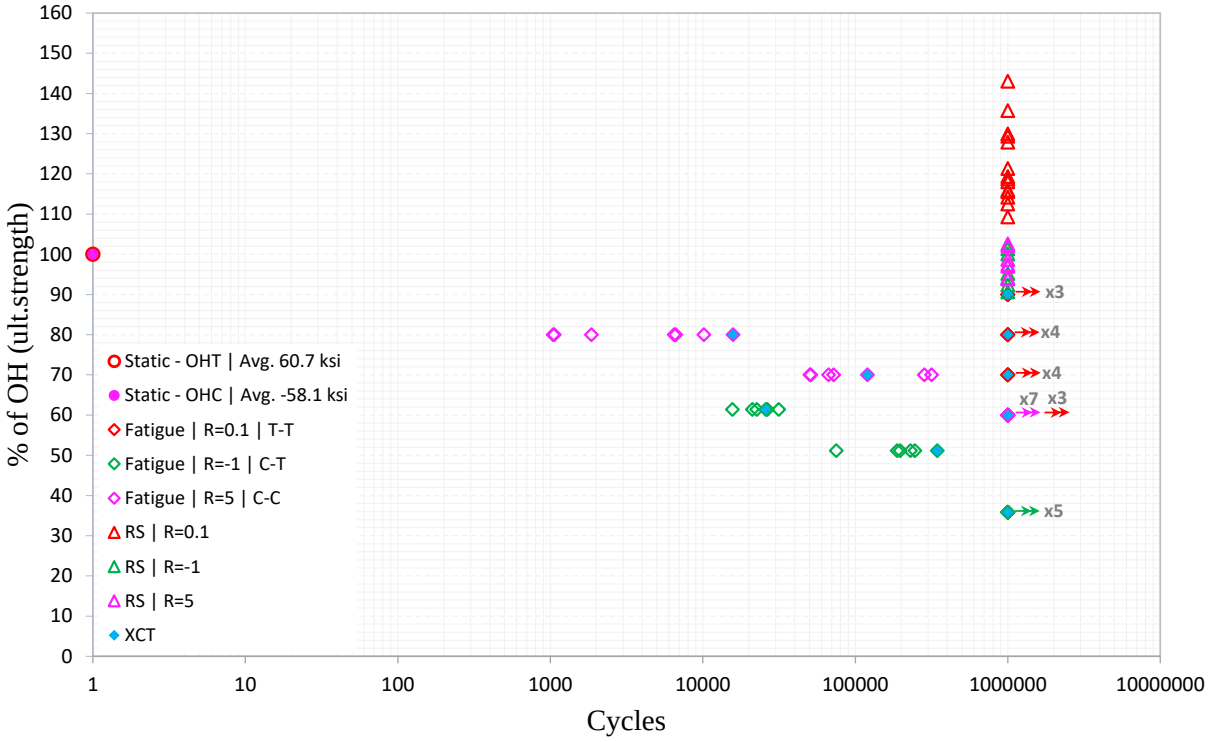


Figure 63. T650/5320-1 8HS, OH, 40/20/40 fatigue data—normalized.

DISTRIBUTION STATEMENT A.
Approved for public release: distribution is unlimited.

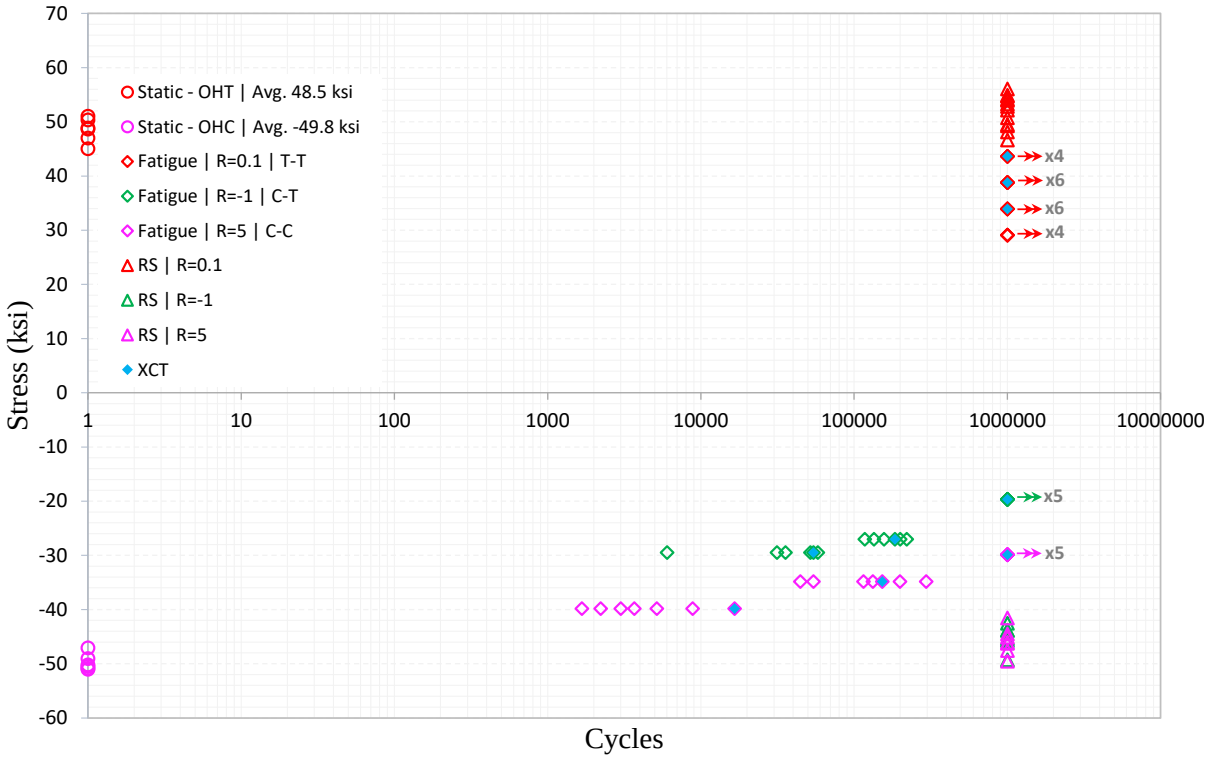


Figure 64. T650/5320-1 8HS, OH, 25/50/25 fatigue data—measured.

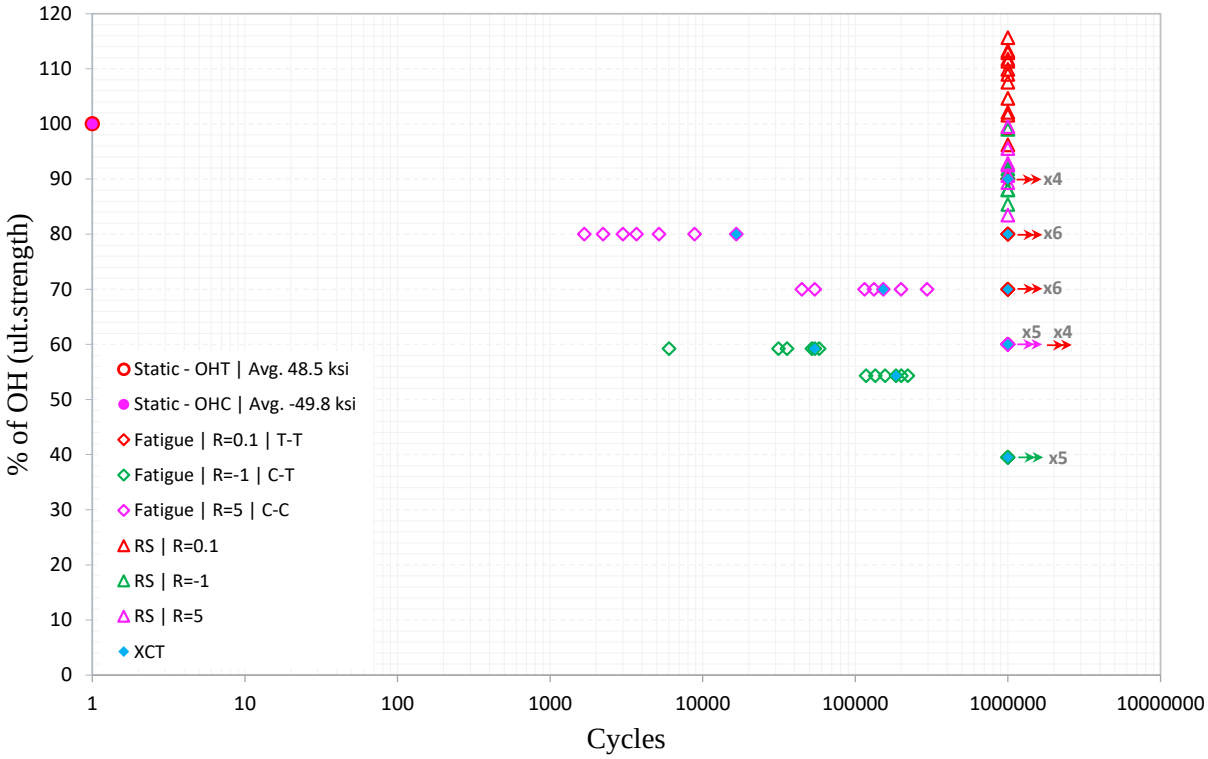


Figure 65. T650/5320-1 8HS, OH, 25/50/25 fatigue data—normalized.

DISTRIBUTION STATEMENT A.
Approved for public release: distribution is unlimited.

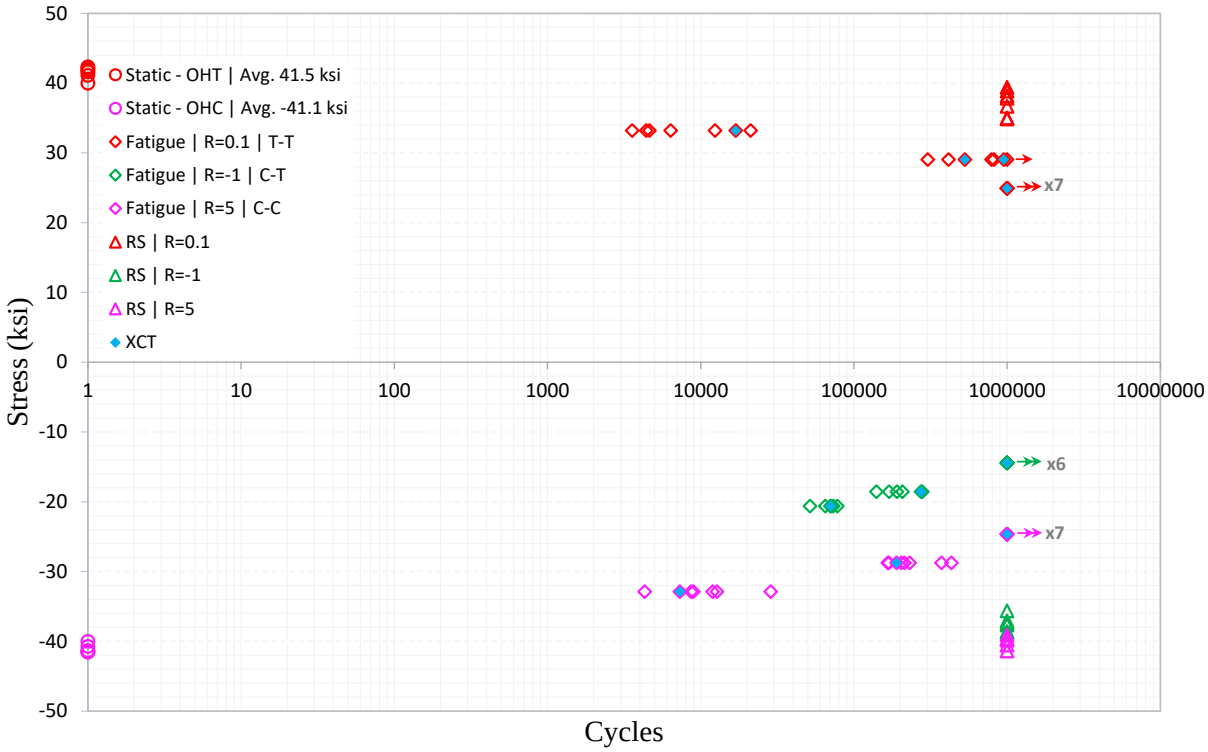


Figure 66. T650/5320-1 8HS, OH, 10/80/10 fatigue data—measured.

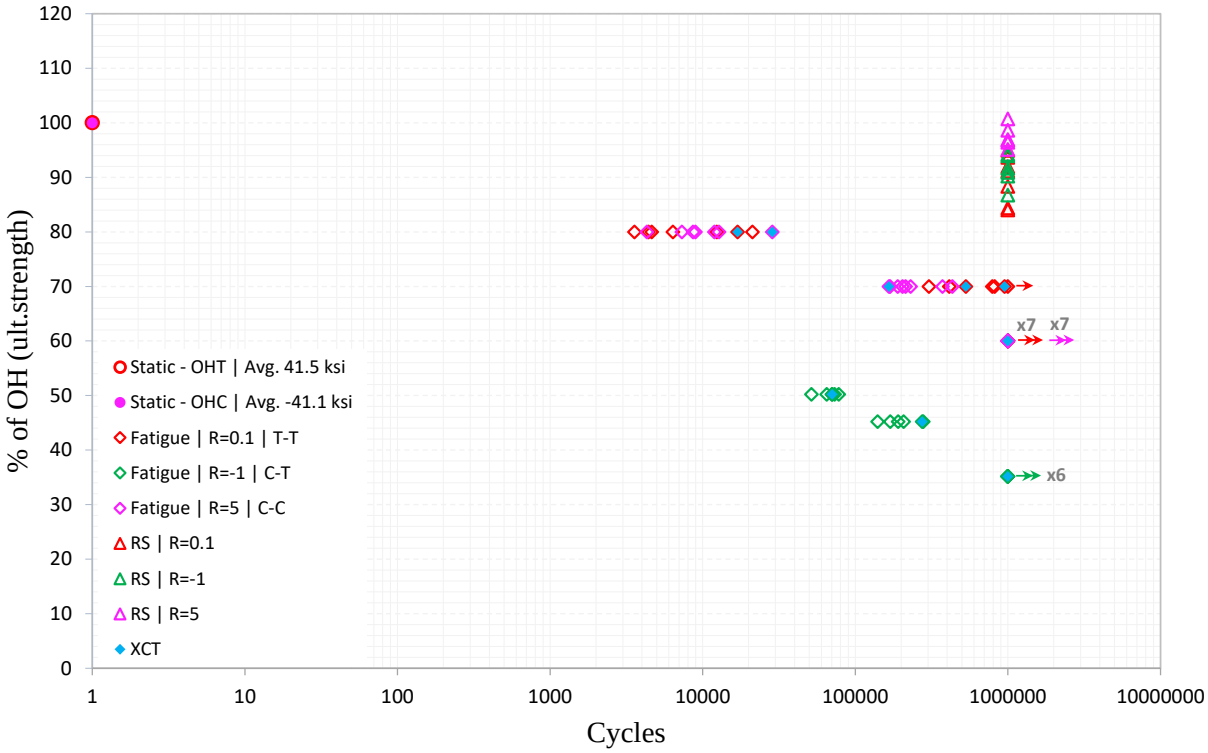


Figure 67. T650/5320-1 8HS, OH, 10/80/10 fatigue data—normalized.

DISTRIBUTION STATEMENT A.
Approved for public release: distribution is unlimited.

6.2.2 T650/5320-1 8HS Double-Notch Shear

A comparison of DNS measured and normalized experimental data for hard and soft layup configurations are shown in Figures 68 and 69, respectively. SN data curves show that both 40/20/40 hard layup with the majority of 0° and ±90° plies and 10/80/10 soft layup with majority of ±45° plies exhibit a very similar fatigue behavior. Similar to UNI, the 8HS hard layup indicated a lower fatigue resistance than the soft laminates. At least one specimen per each stress level was considered for high-fidelity XCT inspections for detailed fatigue damage characterization. Fatigue data for both hard and soft laminates indicate typical data scatter observed for composites. The shape parameters, which are indicators of data scatter, also confirm this by producing higher shape parameters than what is historically observed for composites (1.25).

Unlike the case for open-hole specimens, fatigue wearout was indicated by the steep SN curves for DNS. This was also reflected in the residual strength of runout specimens that were always lower than the quasi-static strength data.

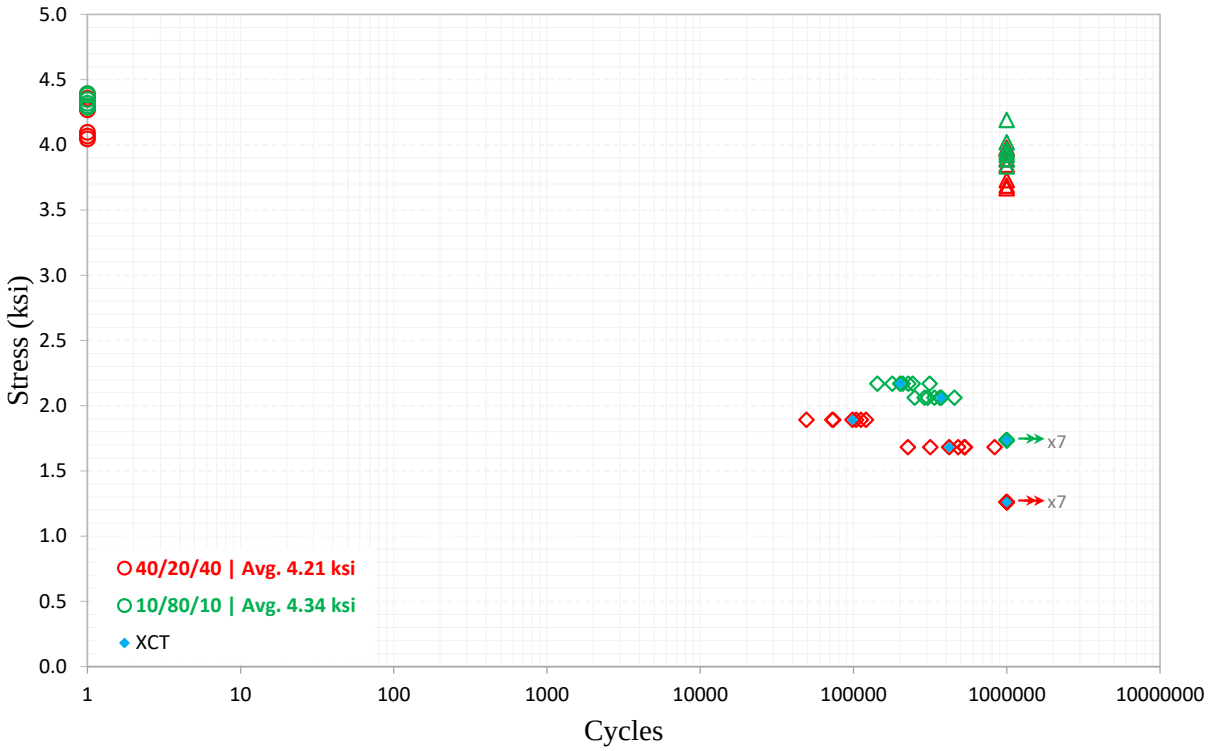


Figure 68. T650/5320-1 8HS, DNS fatigue data—measured.

DISTRIBUTION STATEMENT A.
Approved for public release: distribution is unlimited.

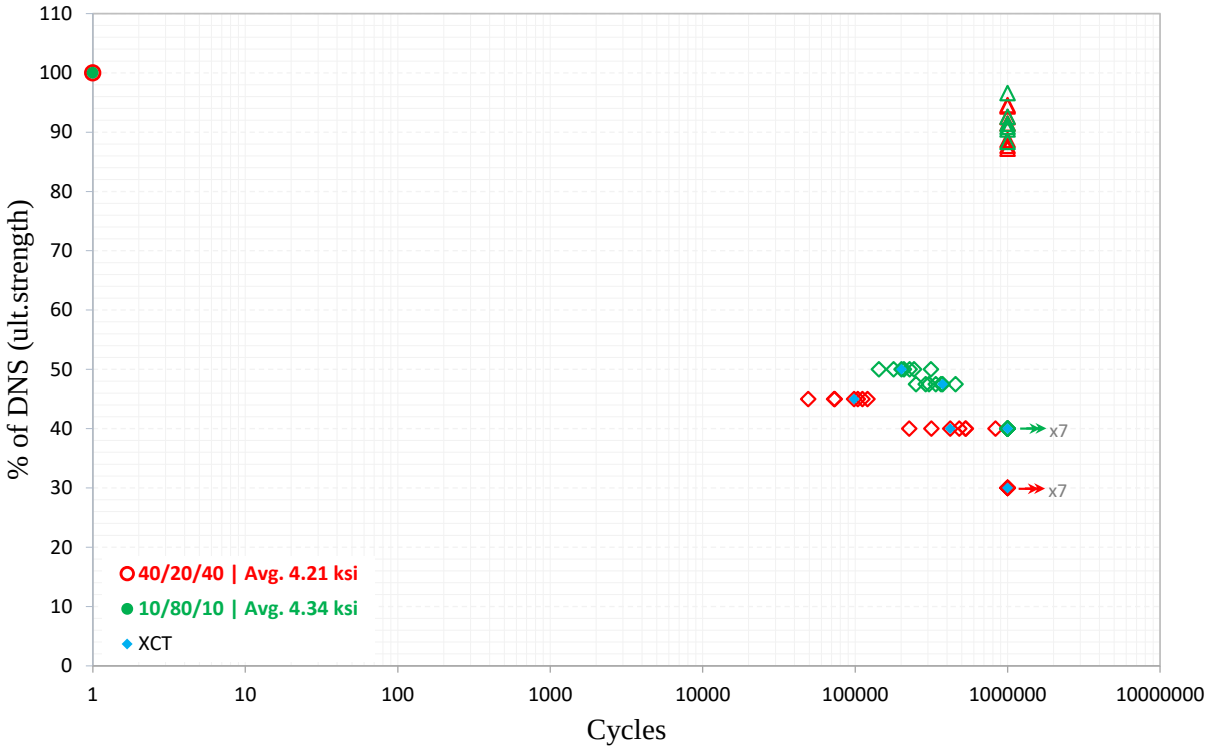


Figure 69. T650/5320-1 8HS, DNS fatigue data—normalized.

6.2.3 T650/5320-1 8HS Interlaminar Tension

A comparison of interlaminar tension measured and normalized data (with respect to the ultimate static strength) for hard and soft layup configurations are as shown in Figures 70 and 71, respectively. SN data for both laminates including residual strength of runouts indicated similar behavior. In addition to the three major stress levels, fatigue tests were conducted at two additional high stress levels for both laminate stacking sequences. Pre-test NDI scans were performed using XCT for the majority of the ILT specimens and compared with the XCT scans obtained at various fatigue intervals as well as after residual strength of runout specimens.

6.2.4 T650/5320-1 8HS Short Beam Shear

The short-beam shear SN data for 100/0/0 layup configuration is shown in Figure 72. Normalized SBS SN data are compared with normalized DNS SN data (both hard and soft laminates) in Figure 73.

DISTRIBUTION STATEMENT A.
Approved for public release: distribution is unlimited.

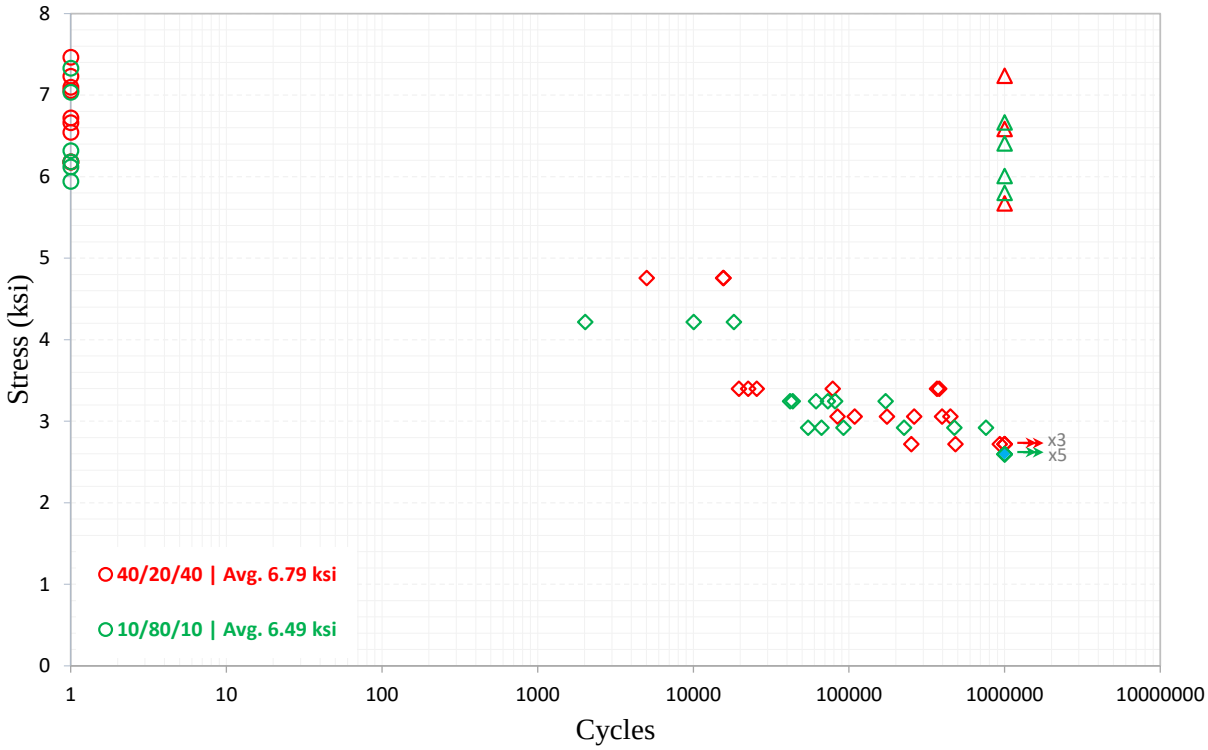


Figure 70. T650/5320-1 8HS, ILT fatigue data—measured.

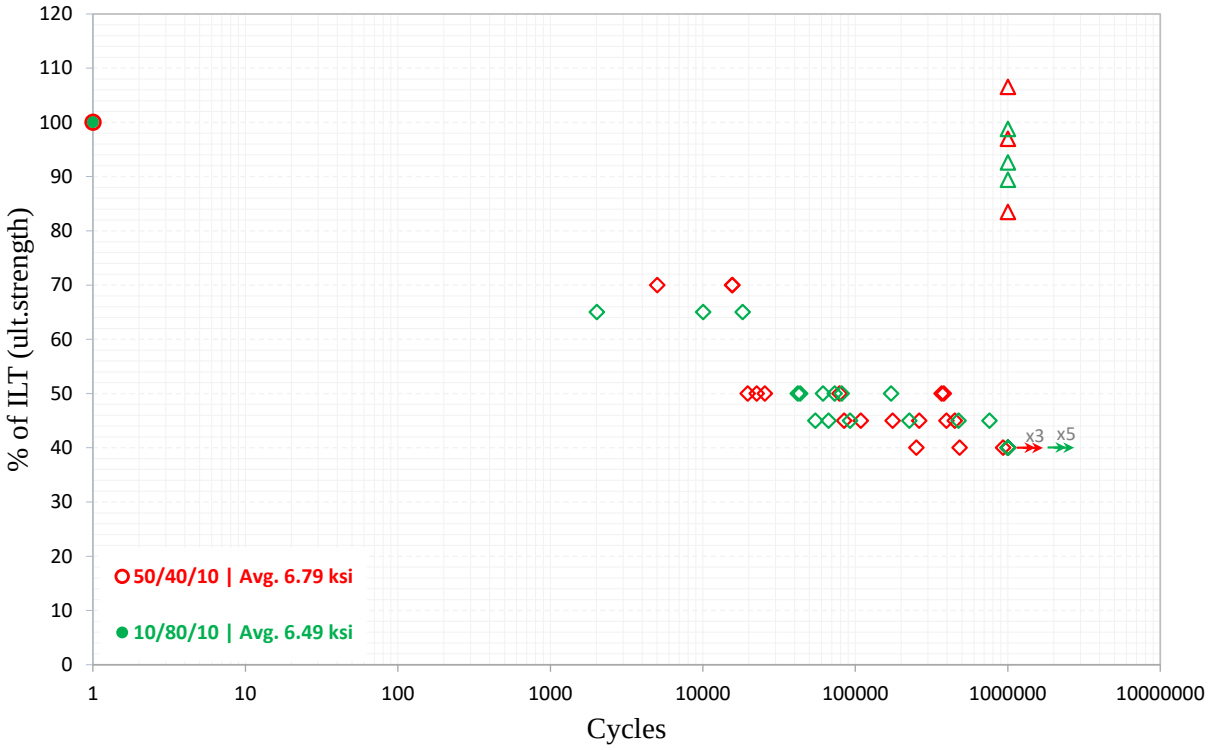


Figure 71. T650/5320-1 8HS, ILT fatigue data—normalized.

DISTRIBUTION STATEMENT A.
Approved for public release: distribution is unlimited.

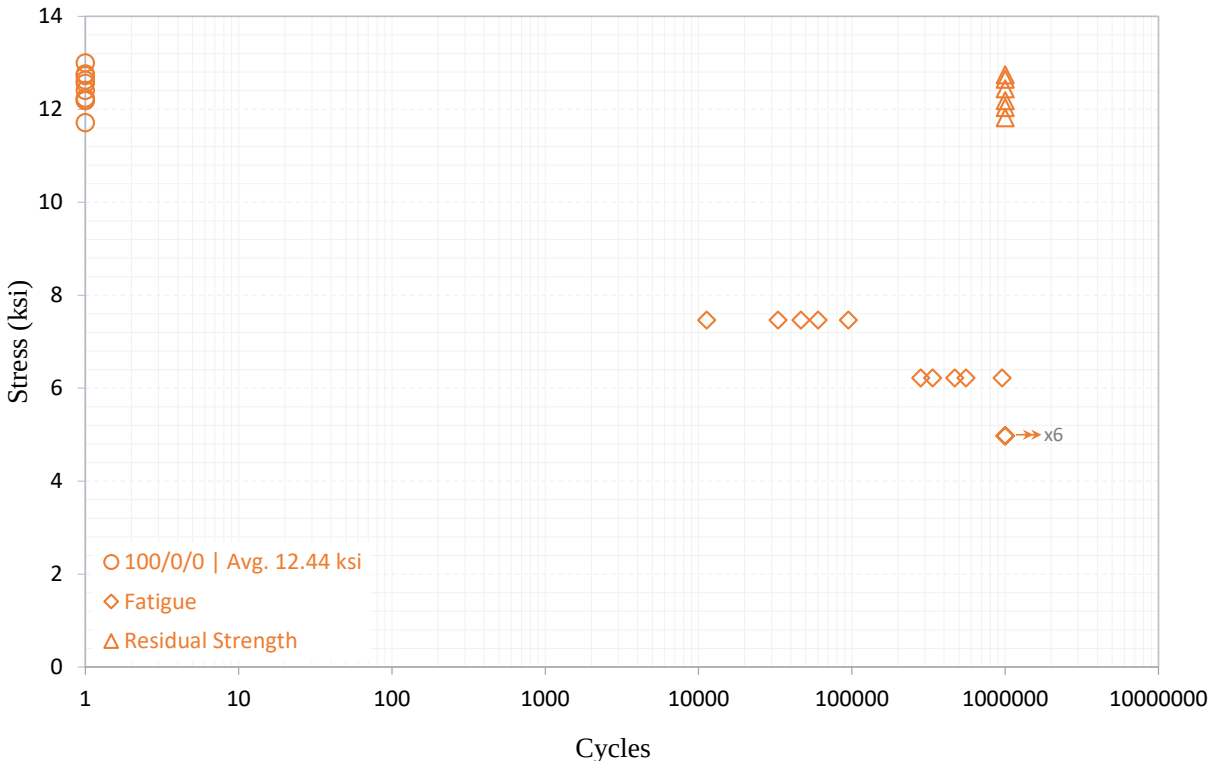


Figure 72. T650/5320-1 8HS, 100/0/0, SBS, fatigue data.

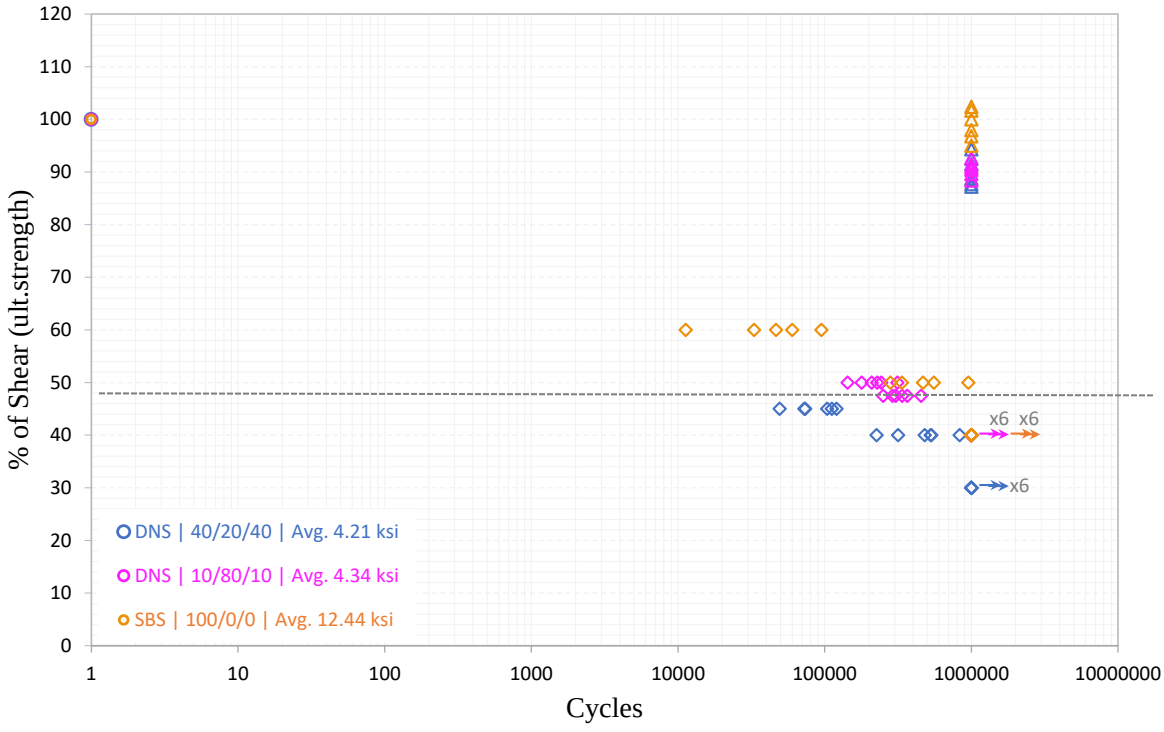


Figure 73. Comparison between DNS and SBS for T650/5320-1 8HS data—normalized.

DISTRIBUTION STATEMENT A.
Approved for public release: distribution is unlimited.

6.3 Solvay 5250-4 (BMI)/ IM7 Unidirectional Tape

6.3.1 IM7/5250-4 UNI Open-Hole Compression/Tension

Similar to the IM7/5320-1 UNI material system, SN curves show that both hard and quasi-isotropic laminates had excellent fatigue resistance. Also, the residual strength data of runouts were higher than the quasi-static strength data, especially for hard laminates. This will be considered for an accurate assessment using XCT. The effects of random flaws that occurred in the laminate during cyclic fatigue may be restricted only for some delaminations of fibers, with the remainder exhibiting the material's ultimate strength along with the stress concentration effects around the specimen gage/hole section.

Fatigue analysis of IM7/5250-4 UNI specimens from 11 data sets is included in this section. Each data set contains a minimum of three fatigue stress levels and at least six static strength data points. SN curves with the Sendeckyj fitting parameters for IM7/5250-4 UNI are included in Appendix A.

Fatigue life scatter analysis data are summarized in Table 16. The shape parameters corresponding to each SN curve using individual Weibull, joint Weibull, and Sendeckyj scatter analyses are denoted as $\hat{\alpha}_{IW}$, $\hat{\alpha}_{JW}$, and $\hat{\alpha}_{Sendeckyj}$, respectively.

Table 16 – Fatigue life scatter analysis for IM7/5250-4 UNI.

Specimen Configuration			Weibull Analysis		Sendeckyj Analysis	
Layup	Test Description	Stress Ratio (R)	$\hat{\alpha}_{IW}$	$\hat{\alpha}_{JW}$	$\hat{\alpha}_{Sendeckyj}$ (w/o static)	$\hat{\alpha}_{Sendeckyj}$ (w/ static)
50/40/10	OHT-T	0.1	All Runouts			
	OHC-C	5	1.646	0.803	0.692	0.515
	OHC-T	–1	1.565	1.536	1.700	0.946
	DNS	0.1	2.246	2.241	2.203	2.300
	ILT	0.1	0.693	0.693		0.382
25/50/25	OHT-T	0.1	5.342	5.341		0.813
	OHC-C	5	3.450	2.738	3.156	1.061
	OHC-T	–1	2.118	2.091	1.748	1.410
10/80/10	OHT-T	0.1	4.175	4.170	4.109	2.928
	OHC-C	5	2.874	2.845	2.330	2.258
	OHC-T	–1	8.843	8.676	8.605	9.302
	DNS	0.1	2.857	2.857	2.795	2.120
	ILT	0.1	1.858	2.116	1.777	1.712
100/0/0	SBS	0.1	1.900	1.900	2.334	2.194

Figure 74 provides a summary of the detailed fatigue life scatter analysis conducted on IM7/5250-4 UNI using individual Weibull, joint Weibull, and Sendeckyj analyses (with and

DISTRIBUTION STATEMENT A.
Approved for public release: distribution is unlimited.

without static). Except for the hard ILT SN curve, the rest of the SN data analysis using individual Weibull analysis indicated shape parameters higher than the historic 1.25 value. However, most of the hard and quasi-isotropic data analyses using Sendeckyj with static data indicated either significantly lower or close shape parameters indicating significant data scatter compared to 5320-1 UNI and 8HS.

The Sendeckyj equivalent strength values based on the fatigue data are pooled and compared against the tested static strength data along with their CVs in Table 17 and also shown in Figure 75.

A comparison of IM7/5250-4 UNI OHT (R = 0.1), OHC (R = 5), and OHC/T (R = –1) measured and normalized experimental data for hard, quasi-isotropic, and soft layup configurations are shown in Figures 76 to 81. Unlike for the case of 5320-1 UNI and 8HS material systems, R = –1 data for the 5250-4 material system were similar to R = 5 fatigue data, except for soft laminates. Tension-tension (R = 0.1) fatigue of the hard laminates all had runouts, even at extremely high stress levels, indicating great fatigue resistance. Therefore, no fatigue analysis was conducted for those cases. The residual strength data for runouts at a million cycles indicate a significant increase in static strength, especially for the hard layup, possibly due to the reduction of local stress concentration caused by microcracks around the hole. At least one specimen per each stress level was considered for high-fidelity XCT inspections for detailed fatigue damage characterization.

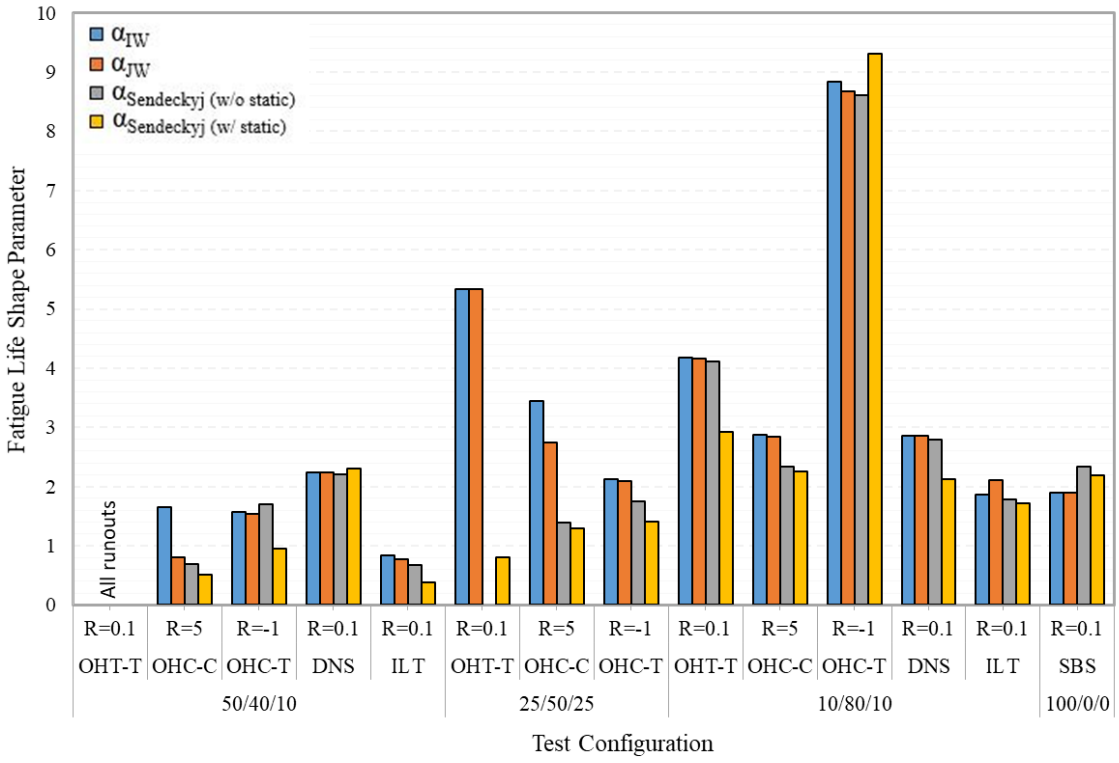


Figure 74. Summary of shape parameters for IM7/5250-4 UNI SN data.

DISTRIBUTION STATEMENT A.
Approved for public release: distribution is unlimited.

Table 17 – Static strength comparison for IM7/5250-4 UNI.

Specimen Configuration		Static Test		Pooled Sendeckyj Analysis	
Layup	Test Description	Strength (ksi)	CV (%)	Strength (ksi)	CV (%)
50/40/10	OHT	127.176	2.625	124.280	5.216
	OHC	69.925	4.845	71.177	3.309
	OH	69.925	4.845	67.825	6.590
	DNS	3.650	2.676	3.575	3.826
	ILT	10.863	9.599	10.953	9.262
25/50/25	OHT	76.483	2.659	75.920	4.394
	OHC	52.646	4.106	52.689	6.317
	OH	52.646	4.106	51.700	7.198
10/80/10	OHT	49.116	2.066	47.635	5.306
	OHC	41.715	1.030	40.678	4.280
	OH	41.715	1.030	40.433	5.740
	DNS	3.204	5.074	3.188	4.591
	ILT	11.655	5.967	11.750	5.896
100/0/0	SBS	16.439	1.805	16.225	3.553

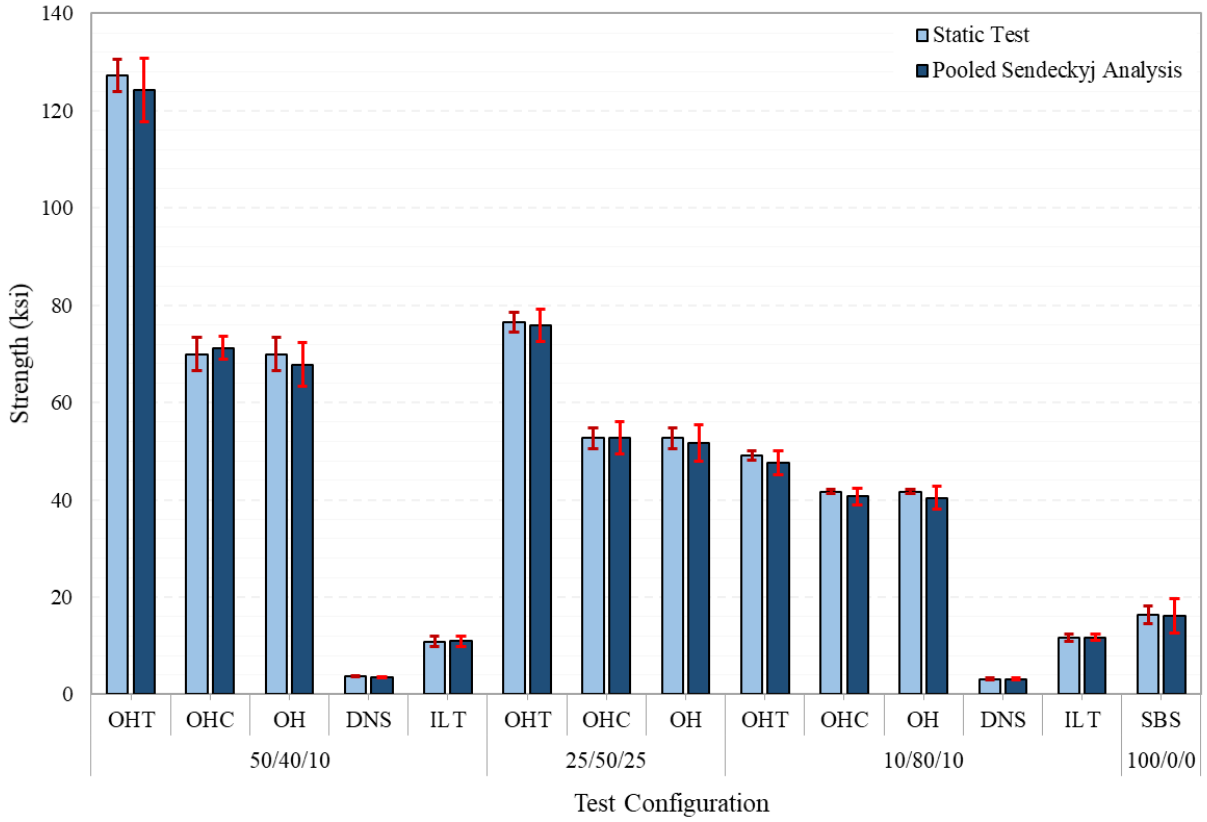


Figure 75. Comparison of quasi-static strength and pooled Sendeckyj equivalent strength for IM7/5250-4 UNI.

DISTRIBUTION STATEMENT A.
Approved for public release: distribution is unlimited.

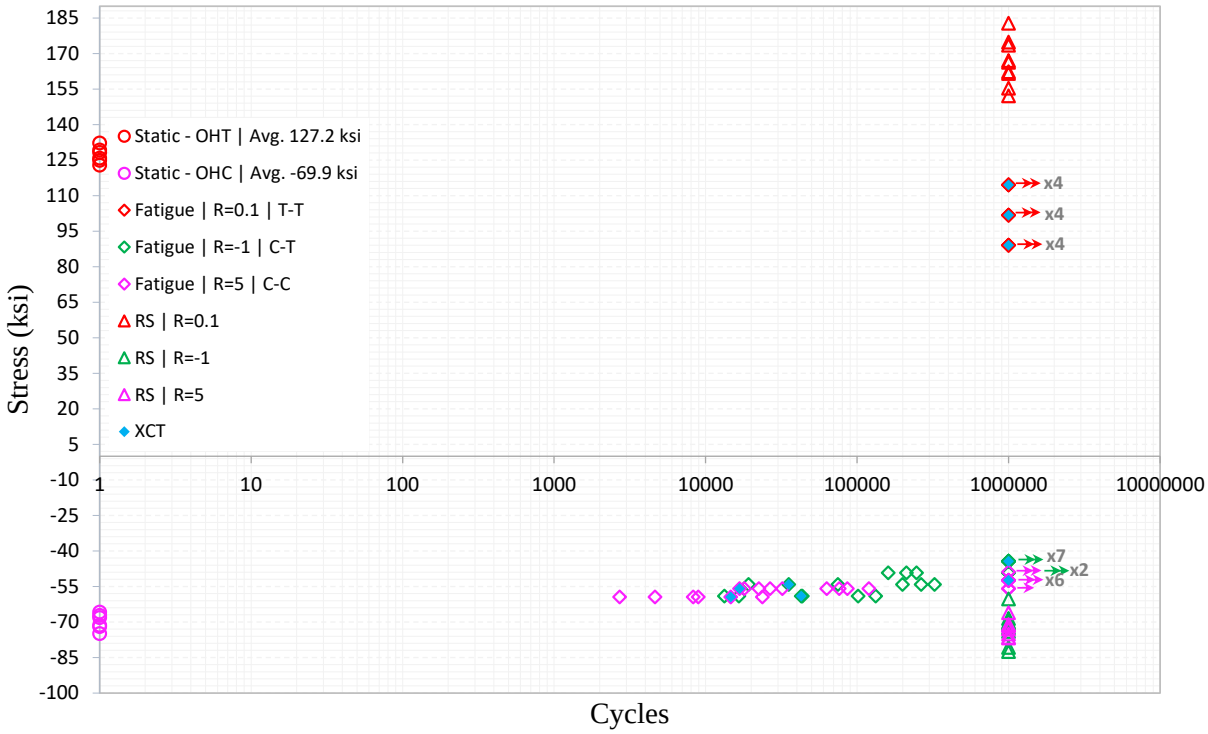


Figure 76. IM7/5250-4 UNI, OH, 50/40/10 fatigue data—measured.

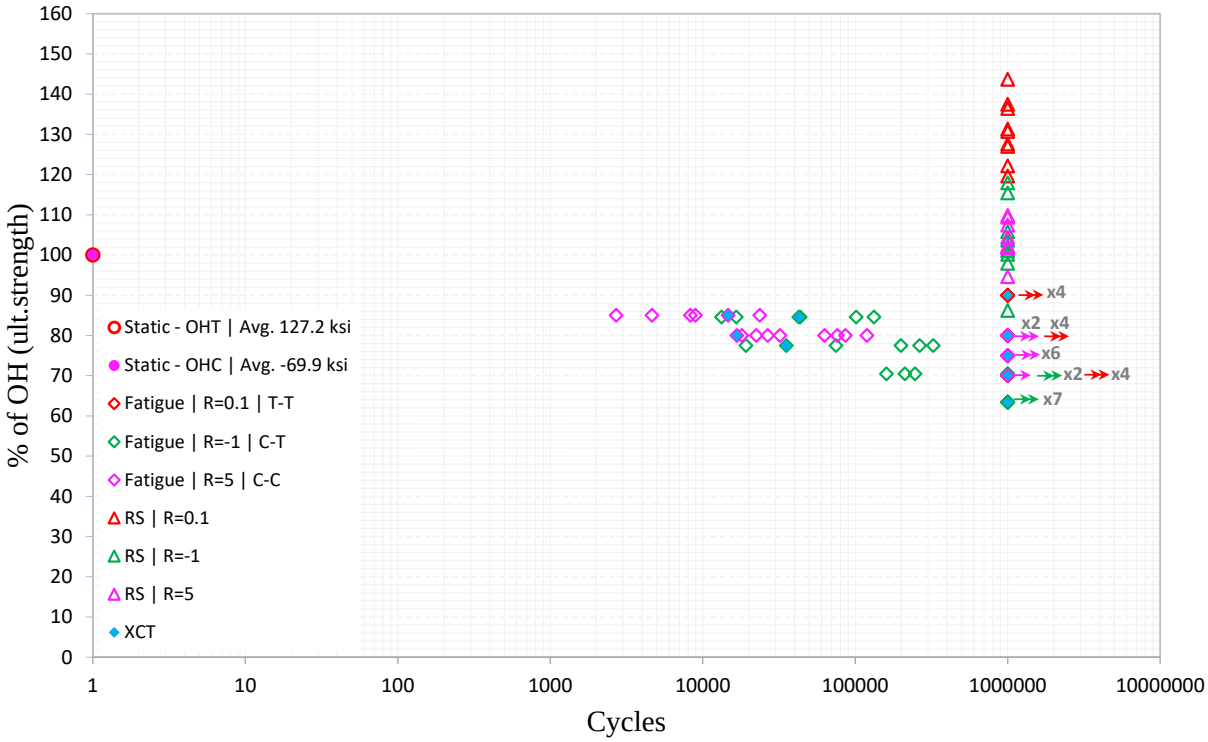


Figure 77. IM7/5250-4 UNI, OH, 50/40/10 fatigue data—normalized.

DISTRIBUTION STATEMENT A.
Approved for public release: distribution is unlimited.

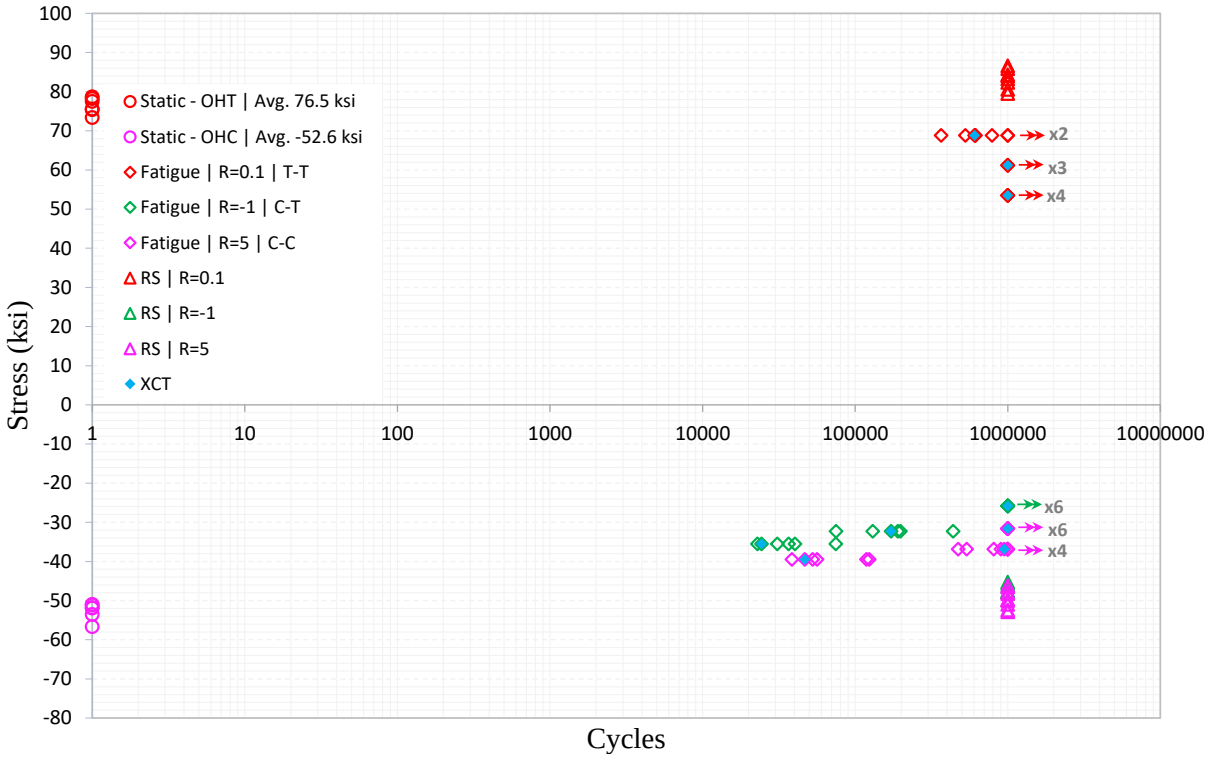


Figure 78. IM7/5250-4 UNI, OH, 25/50/25 fatigue data—measured.

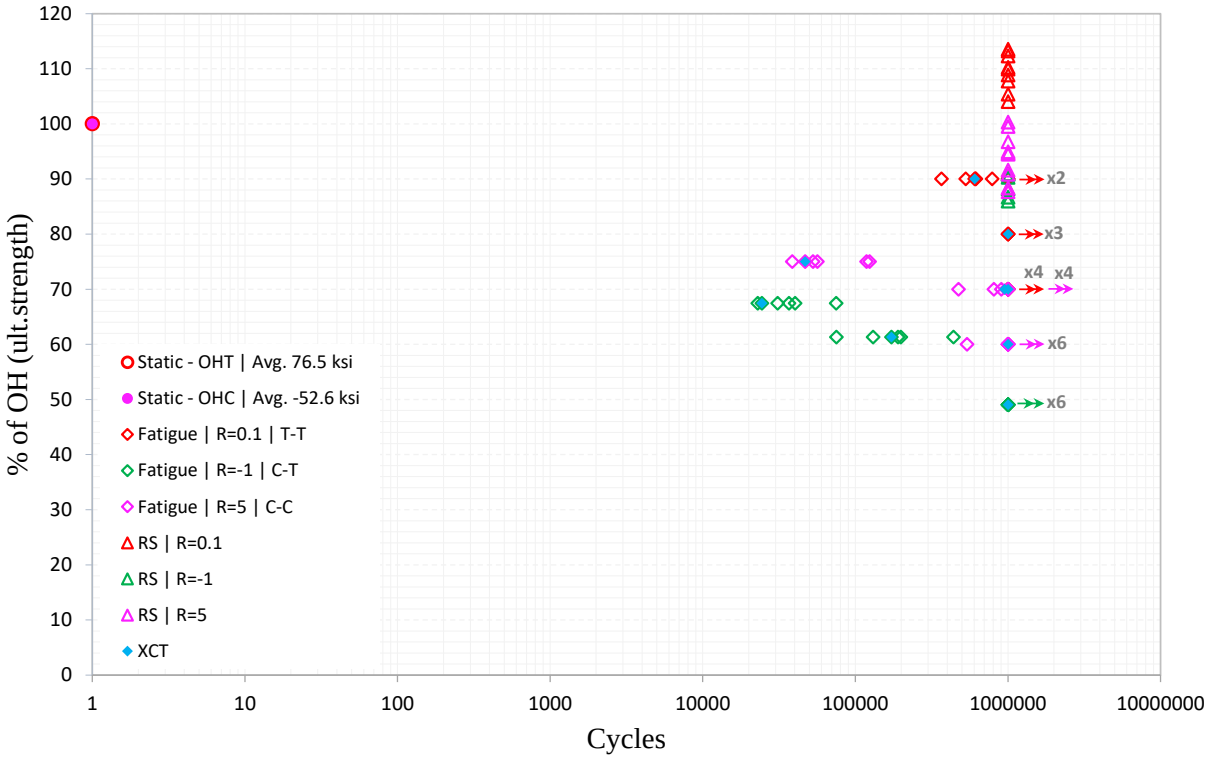


Figure 79. IM7/5250-4 UNI, OH, 25/50/25 fatigue data—normalized.

DISTRIBUTION STATEMENT A.
Approved for public release: distribution is unlimited.

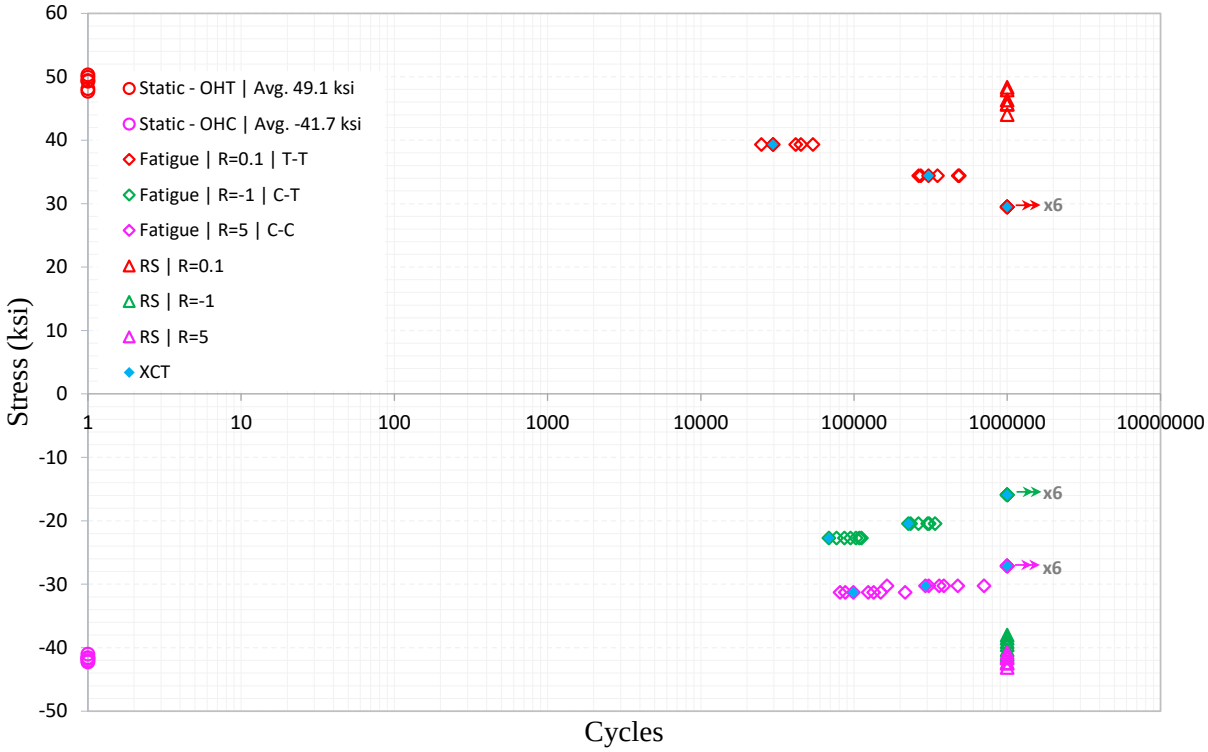


Figure 80. IM7/5250-4 UNI, OH, 10/80/10 fatigue data—measured.

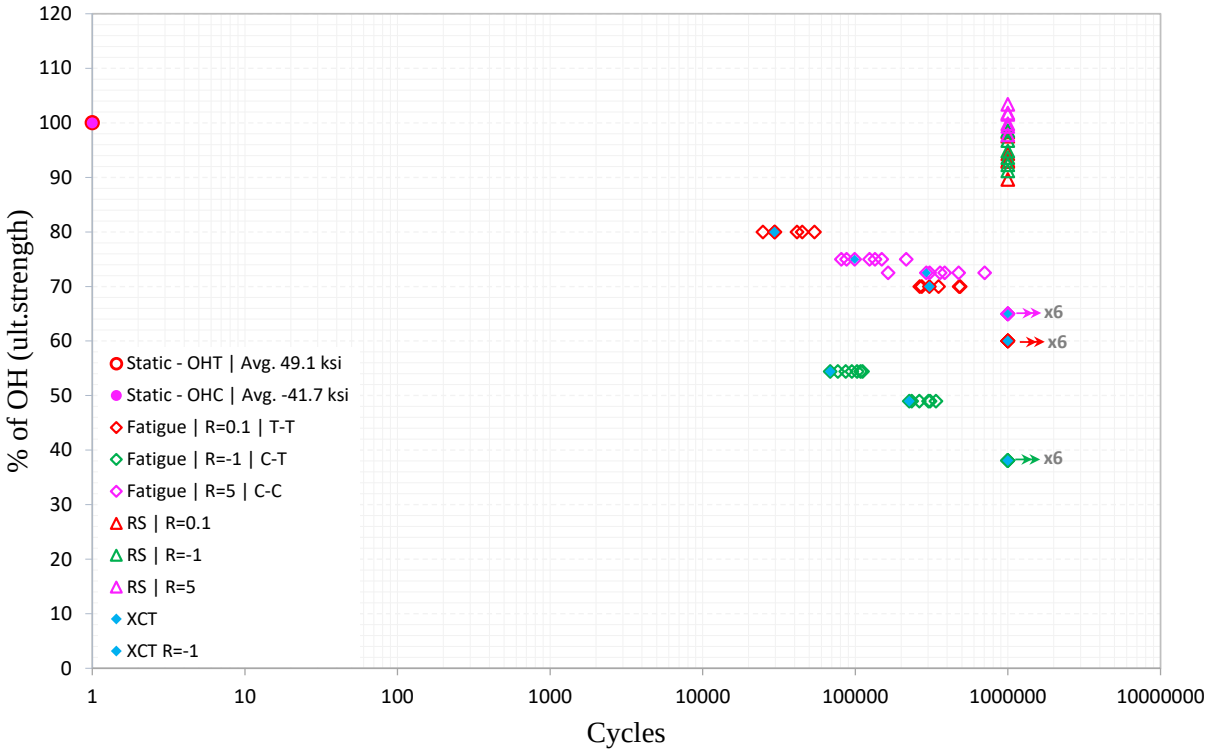


Figure 81. IM7/5250-4 UNI, OH, 10/80/10 fatigue data—normalized.

DISTRIBUTION STATEMENT A.
Approved for public release: distribution is unlimited.

6.3.2 IM7/5250-4 UNI Double-Notch Shear

A comparison of DNS measured and normalized (with respect to the ultimate static strength) experimental data for hard (50/40/10) and soft (10/80/10) layup configurations are shown in Figures 82 and 83. SN data curves show that both 50/40/10 hard layup with the majority of 0° and ±45° plies and 10/80/10 ±45° plies dominant layup exhibit a very similar fatigue behavior. One specimen per each stress level is considered for an accurate assessment using XCT.

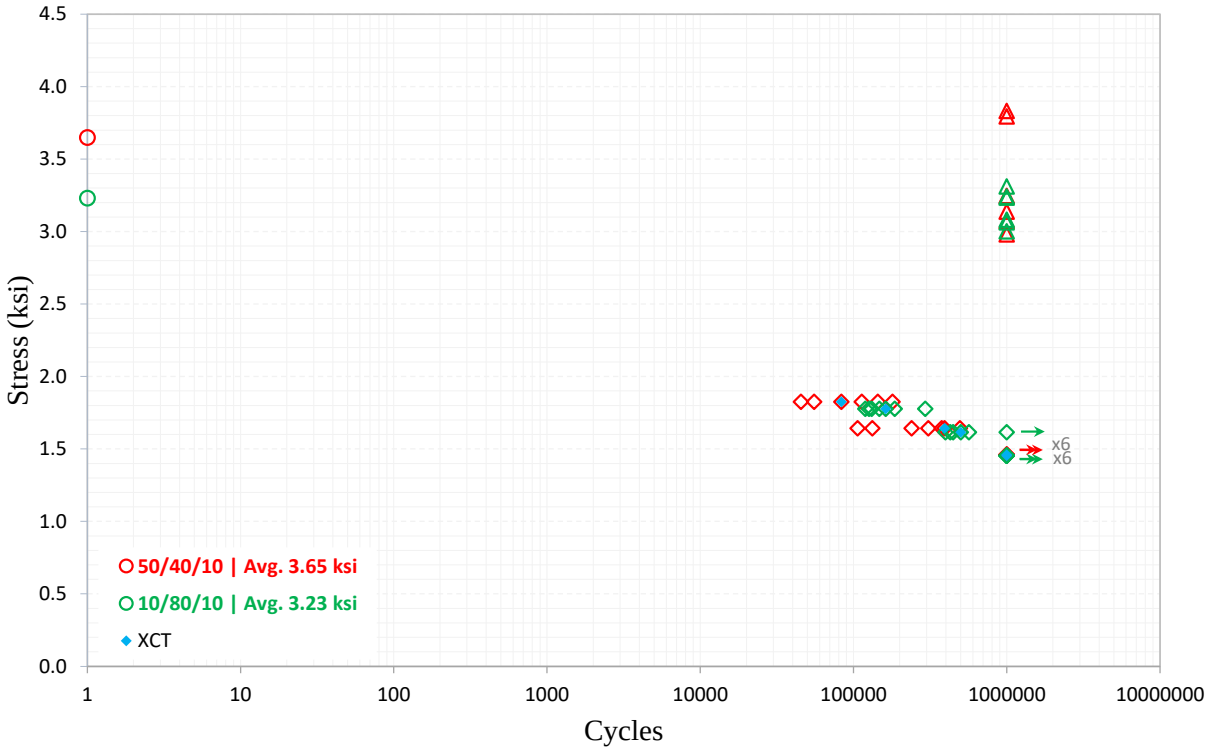


Figure 82. IM7/5250-4 UNI, DNS fatigue data—measured.

DISTRIBUTION STATEMENT A.
Approved for public release: distribution is unlimited.

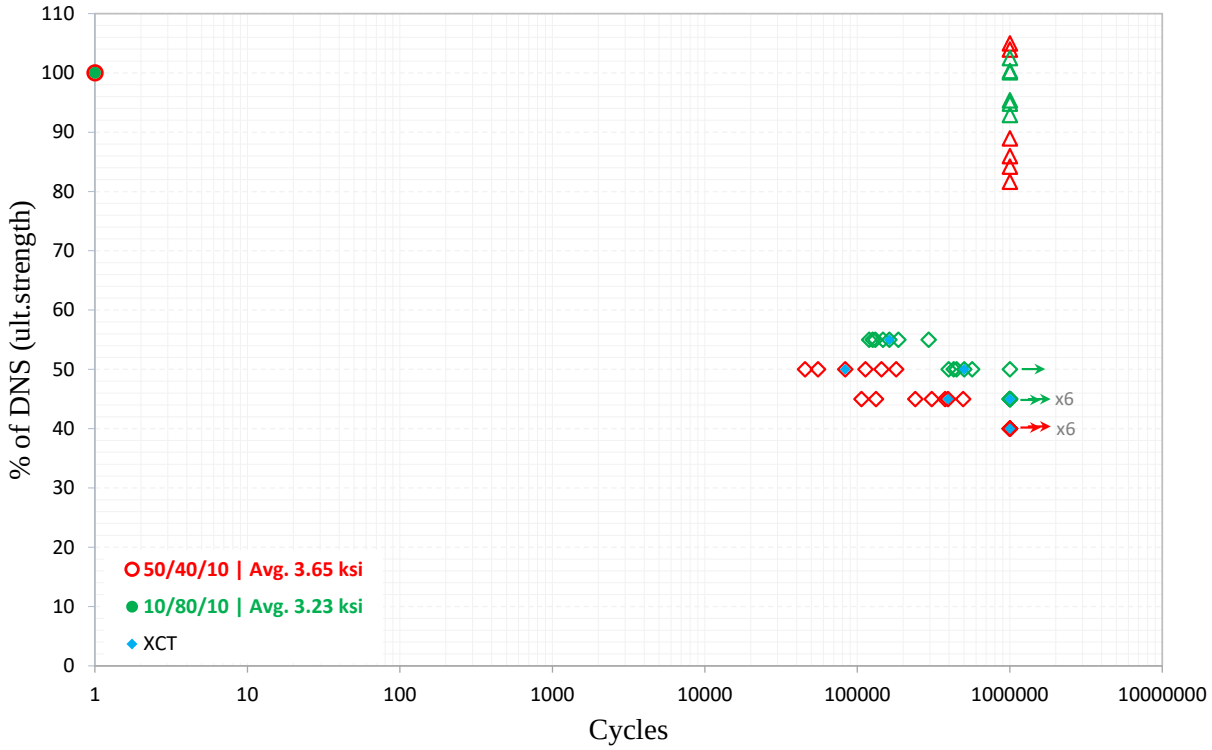


Figure 83. IM7/5250-4 UNI, DNS fatigue data—normalized.

6.3.3 IM7/5250-4 UNI Interlaminar Tension

A comparison of interlaminar tension measured and normalized data (with respect to the ultimate static strength) for hard and soft layup configurations are as shown in Figures 84 and 85, respectively. In addition to the three major stress levels, fatigue tests were conducted at an additional high stress level for both laminate stacking sequences. Unlike for the other two material systems, soft laminate lower fatigue life than that for hard laminates of BMI. Pre-test NDI scans were performed using XCT for the majority of the ILT specimens and compared with the XCT scans obtained at various fatigue intervals as well as after residual strength of runout specimens.

6.3.4 IM7/5250-4 UNI Short Beam Shear

The short-beam shear SN data for 100/0/0 layup configuration is shown in Figure 86. Normalized SBS SN data are compared with normalized DNS (both hard and soft laminates) in Figure 87.

DISTRIBUTION STATEMENT A.
Approved for public release: distribution is unlimited.

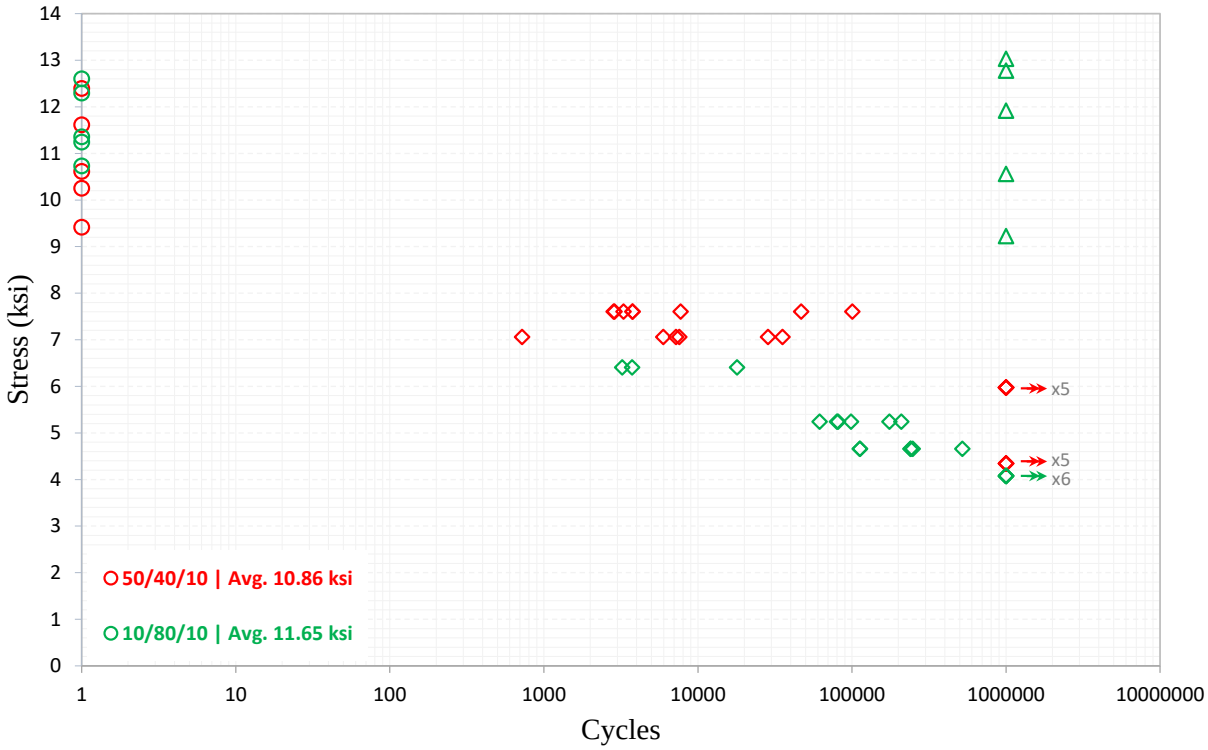


Figure 84. IM7/5250-4 UNI, ILT fatigue data—measured.

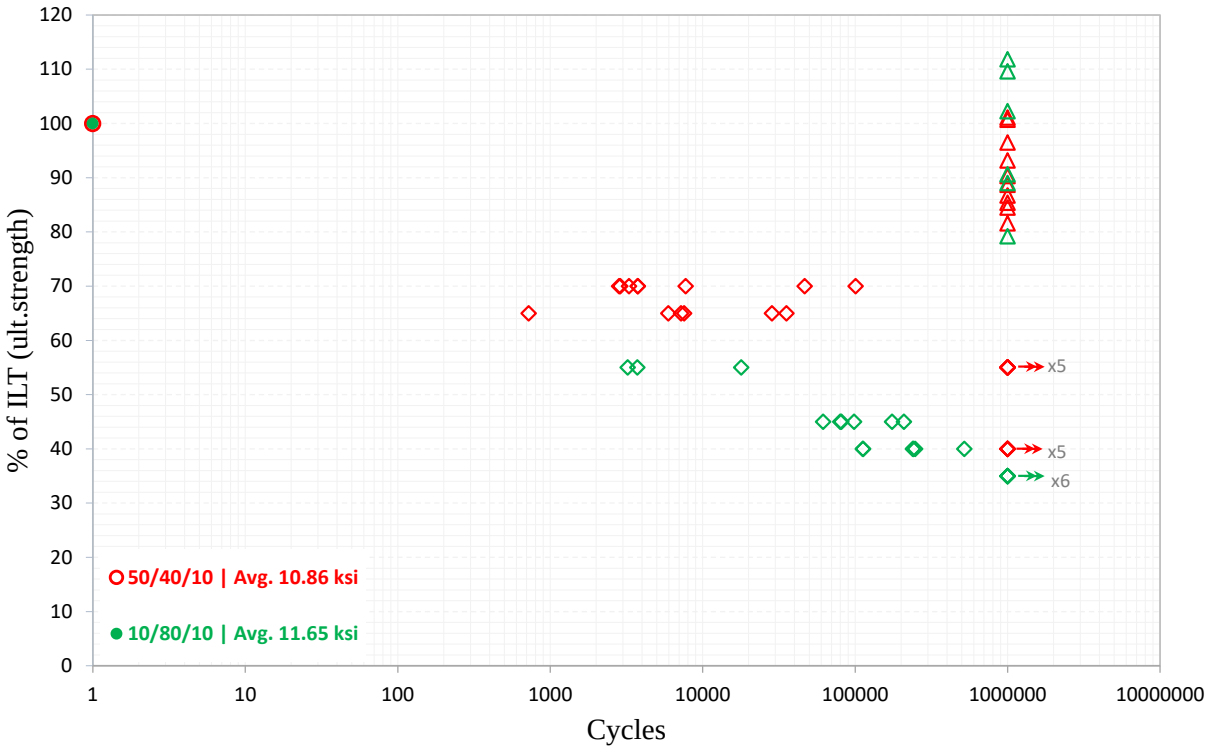


Figure 85. IM7/5250-4 UNI, ILT fatigue data—normalized.

DISTRIBUTION STATEMENT A.
Approved for public release: distribution is unlimited.



Figure 86. IM7/5250-4 UNI, 100/0/0, SBS, fatigue data.

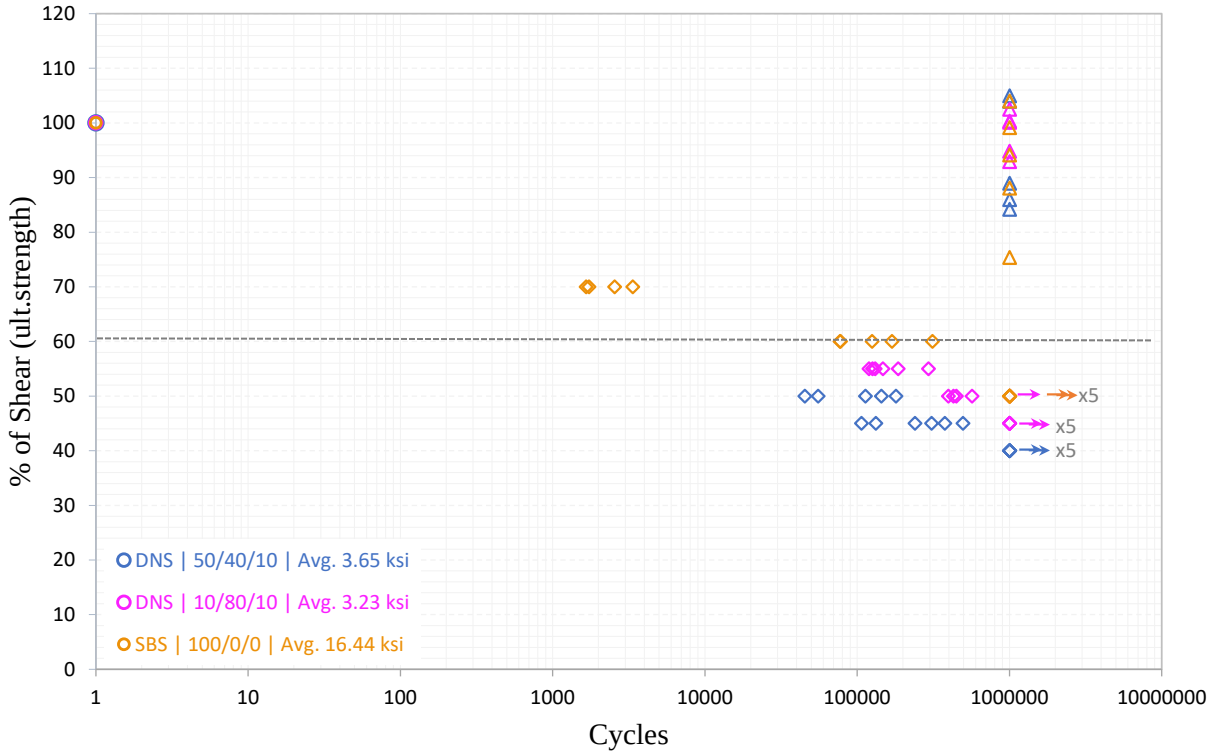


Figure 87. Comparison between DNS and SBS for IM7/5250-4 UNI data—normalized.

DISTRIBUTION STATEMENT A.
Approved for public release: distribution is unlimited.

6.4 Load-Enhancement Factor

Shape parameters calculated for SN curves for each material system were subjected to a Weibull analysis for calculating the modal shape parameter using equation (15). Table 18 shows a summary of Weibull analysis conducted for shape parameters of each material (see the table number below the material name for the shape parameters included in the analysis of each material). Please note that this round of Weibull analysis was conducted for the shape parameters ($\hat{\alpha}$ values) calculated using individual Weibull, joint Weibull, and Sendeckyj (without and with static data) scatter analysis of SN data. Finally, the shape parameters for all SN curves under each of the SN scatter analysis method was subjected to a Weibull analysis (AMCSC) to obtain a representative modal life shape parameter (MLSP) for the collection of data included in this report.

Table 18 – Calculation of MLSP.

Data Set	Weibull Parameters	IW	JW	Sendeckyj (without static)	Sendeckyj (with static)
IM7/5320-1 UNI (Table 12)	α	2.629	2.4599	2.6144	2.6526
	β	3.539	3.2405	3.2363	2.0817
	α Modal	**2.950**	**2.621**	**2.691**	**1.742**
	Number of SN Curves	12	12	12	12
T650/5320-1 8HS (Table 14)	α	1.961	2.0346	1.9549	2.6285
	β	3.521	3.1878	3.1206	2.5394
	α Modal	**2.448**	**2.286**	**2.163**	**2.117**
	Number of SN Curves	12	12	12	12
IM7/5250-4 UNI (Table 16)	α	1.662	1.5722	1.4242	1.1993
	β	3.451	3.2910	2.8138	2.3267
	α Modal	**1.983**	**1.730**	**1.202**	**0.521**
	Number of SN Curves	13	13	12	13
AMCSC (All 3 materials)	α	1.945	1.879	1.809645	1.606288
	β	3.511	3.250	3.072399	2.350619
	α Modal	**2.423**	**2.169**	**1.970**	**1.282**
	Number of SN Curves	37	37	36	37

Table 19 shows a comparison life factor calculated using equation (1) and LEF calculated using equation (5) for the data in this report. The MLSP was calculated using the individual Weibull analysis data of SN curves. These data are compared with historic values in references [1] and [2], designated as Navy and NIAR, respectively. A similar comparison is in

DISTRIBUTION STATEMENT A.
Approved for public release: distribution is unlimited.

Table 20 for the SN data analysis conducted using Sendeckyj analysis.

Table 19 – Comparison of LEF based on individual Weibull analysis of SN data.

MSSP	**20.000**	**26.310**	**25.095**	**22.665**	**24.083**	**30.128**
MLSP	**1.250**	**2.980**	**2.423**	**2.950**	**2.448**	**1.983**
# of Lives (N)	**NAVY**	**NIAR**	**AMCSC**	**IM7/5320-1 UNI**	**T650/5320-1 8HS**	**IM7/5250-4 UNI**
1.00	**1.177**	**1.121**	**1.130**	**1.142**	**1.135**	**1.109**
1.25	**1.161**	**1.093**	**1.105**	**1.109**	**1.110**	**1.093**
2.00	1.127	1.037	1.056	1.044	1.058	1.059
2.50	1.111	1.011	1.034	1.014	1.034	1.044
3.00	**1.099**		**1.016**		**1.015**	**1.031**
3.50	1.088		1.001		0.999	1.021
4.00	1.079					1.012
4.50	1.071					1.004
5.00	1.064					
6.00	1.052					
7.00	1.042					
8.00	1.034					
9.00	1.026					
13.50	1.000					
N_F	**13.6**	**2.7**	**3.5**	**2.8**	**3.5**	**4.8**

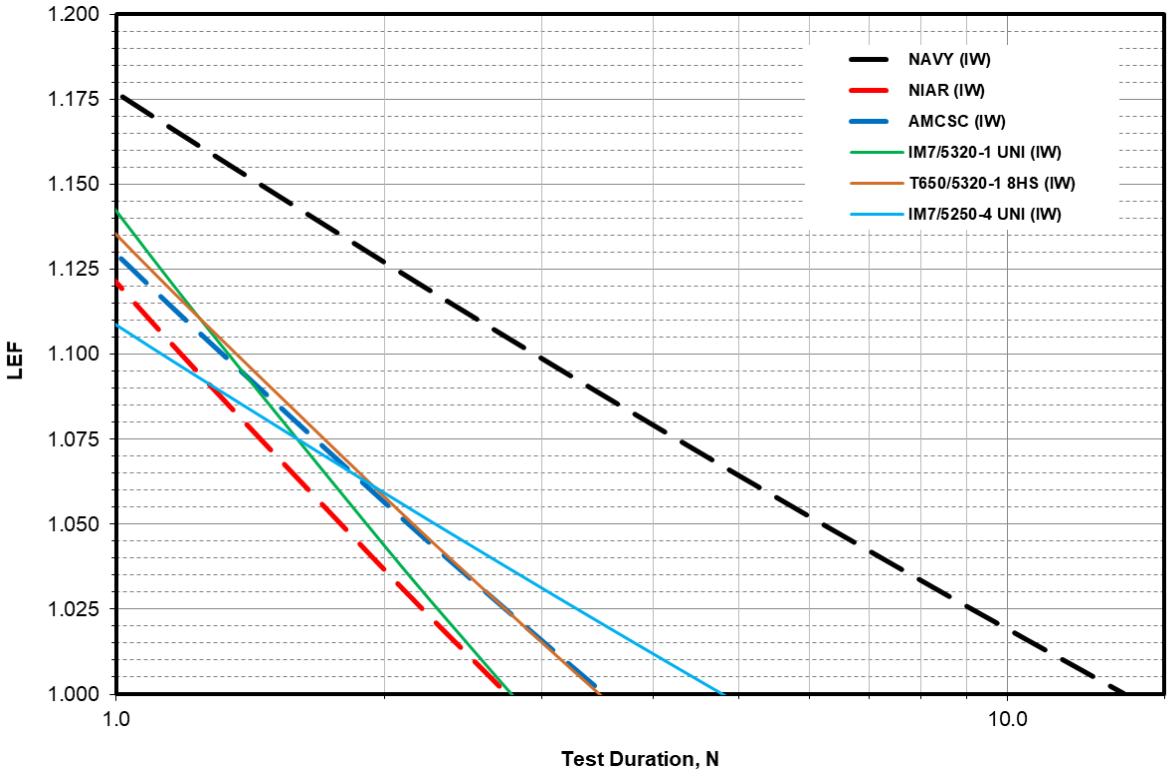
DISTRIBUTION STATEMENT A.
Approved for public release: distribution is unlimited.

Table 20 – Comparison of LEF based on Sendecky analysis (with static) of SN data.

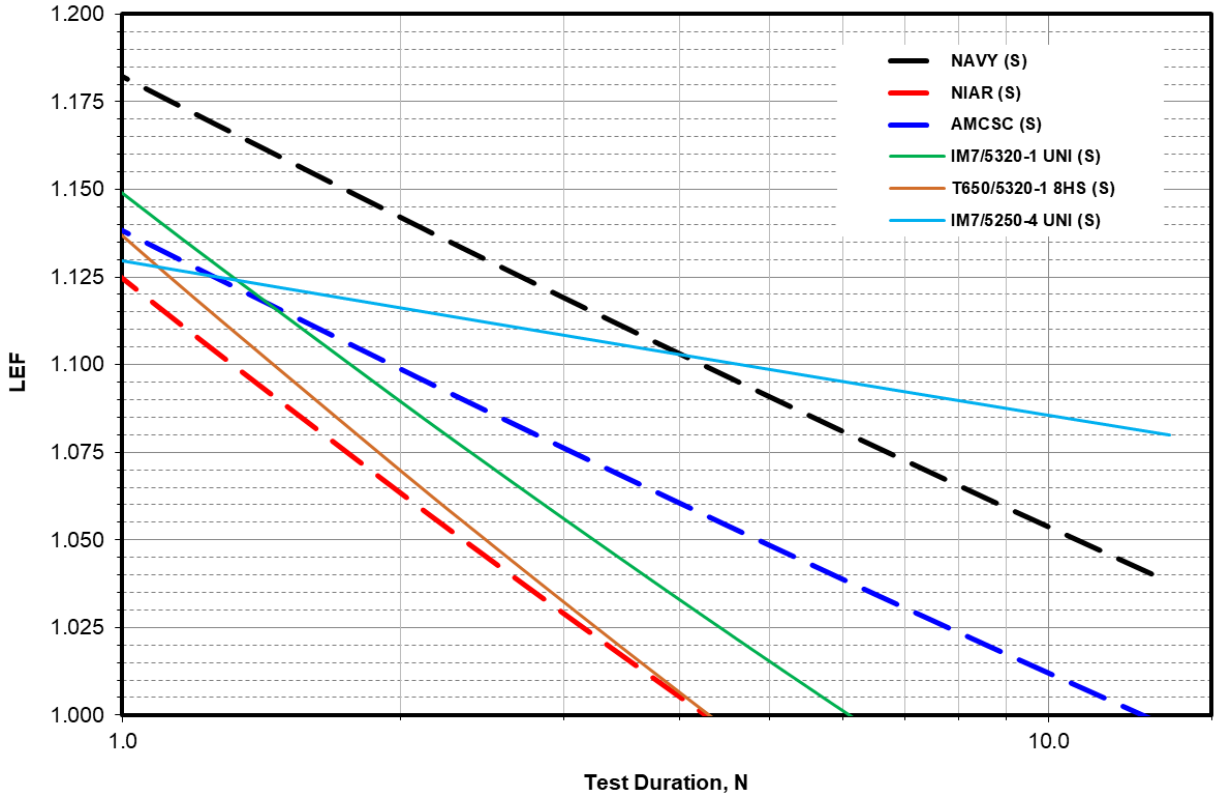
MSSP	**20.000**	**26.310**	**25.095**	**22.665**	**24.083**	**30.128**
MLSP	**1.000**	**2.131**	**1.282**	**1.742**	**2.117**	**0.521**
# of Lives (N)	**NAVY**	**NIAR**	**AMCSC**	**IM7/5320-1 UNI**	**T650/5320-1 8HS**	**IM7/5250-4 UNI**
1.00	1.182	1.125	1.138	1.149	1.137	1.130
1.25	1.169	1.104	1.125	1.129	1.115	1.125
2.00	1.142	1.063	1.099	1.089	1.070	1.116
2.50	1.129	1.044	1.086	1.071	1.049	1.112
3.00	1.119	1.029	1.076	1.056	1.032	1.108
3.50	1.110	1.016	1.068	1.043	1.018	1.105
4.00	1.103	1.005	1.060	1.033	1.007	1.103
4.50	1.097	0.996	1.054	1.024	0.996	1.101
5.00	1.091	0.987	1.048	1.015	0.987	1.099
6.00	1.081	0.973	1.039	1.001	0.971	1.095
7.00	1.073	0.961	1.031	0.989	0.958	1.092
8.00	1.065	0.950	1.024	0.979	0.947	1.090
9.00	1.059	0.941	1.017	0.970	0.937	1.087
13.50	1.038	0.911	0.997	0.941	0.904	1.080
N_F	**28.4**	**4.3**	**12.6**	**6.1**	**4.3**	**1149**

LEF generated using both individual Weibull and Sendeckyj analyses of SN data are also shown in Figure 88. According to the comparison of SN data analysis using individual Weibull data, LEF curves for all 3 material systems represent lower LEF requirements compared to history values in ref. [1] and closer to the values report in ref. [2] for modern composite materials. However, the Sendeckyj analysis of IM7/5250-4 UNI LEF curve shows significantly higher LEF requirements compared to historic values due to high data scatter observed in SN data, which resulted in a low MLSP for this material system. This resulted in an excessively high life factor of 1149. This also significantly impacted AMSCS (S) LEF curve, which is a representative LEF curve for all three material systems included in this report. Although AMCSC (S) LEF curve is higher than NIAR (S) curve, it still lower than Navy (S) curve. The LEF requirements for IM7/5250-4 UNI is below Navy values up to 4 test lives (N=4). Beyond that point, it shows higher LEF requirements than Navy values. Typically, full-scale structural tests are conducted for 2 or 3 test durations (N). Therefore, the use of Navy LEF for BMI materials up to 4 test lifetimes is conservative.

DISTRIBUTION STATEMENT A.
Approved for public release: distribution is unlimited.



(a) Individual Weibull (IW) analysis of SN data



(b) Sendeckyj (S) analysis of SN data

Figure 88. LEF curves for various scatter analysis methods of SN data.

DISTRIBUTION STATEMENT A.
Approved for public release: distribution is unlimited.

7. COMPOSITE DEFECTS AND FAILURE ANALYSIS

This section includes findings for several additional studies conducted to understand the strength and fatigue behavior of composites. Detailed inspections, thermal analyses, and mechanical tests were performed to understand the following:

- Investigation of resin-rich areas noted on XCT images of IM7/53201 UNI and IM7/5250-4 UNI materials.
- Visible excessive fiber gaps noted on IM7/5250-4 UNI.
- Manufacturing defects of interlaminar tension specimen.
- Effects of extended post-cure on IM7/53201 UNI and IM7/5250-4 UNI materials.
- Damage growth of open-hole tension-tension fatigue.

Due to their heterogeneous microstructures, fatigue damage growth mechanics of composites are complex and highly dependent on the type of loading mode and load sequencing. Similarly, the bonded joints, especially with composite adherends, have complex multi-mode failures, but the sequence of failure events is not well understood. Unlike for metals where striation marks can be used for understanding the damage growth rates and mechanics, the final destructive failure mode tends to overshadow damage initiation sites and propagation details in composites. Damage initiation and propagation in composites typically occur from an internal defect/feature or from an area where there is a stress concentration (i.e., fastener hole or impact damage) and are not visible with standard NDI techniques until they are within the inspection threshold of the equipment or the inspection method, which is also a function of materials, geometry, and location of the defect/feature. Although standard NDI techniques such as ultrasonic testing (UT) and pulse thermography are adequate for detecting such defects, in-depth information related to manufacturing defects (including certain manufacturing features that could potentially be failure initiation or nucleation sites) is required to fully understand the structural capability (i.e., strength and durability) of composites. In addition to high-fidelity post-manufacturing inspections, detailed inspections are required to detect damage initiation and monitor damage propagation through the heterogeneous microstructures of composites. Therefore, a high-fidelity 3D inspection technique such as X-ray computed tomography is required to investigate the damage growth mechanics and interaction of multiple failure modes. Such detailed damage characteristics can then be used for development and validation of high-fidelity progressive damage growth analysis (PDA) techniques and life prediction tools. More importantly, the damage accumulation and growth in composites need to be fully characterized to aid in certification as well as establishing damage tolerance testing and analysis protocols.

Computed tomography is a high-fidelity nondestructive inspection technique that reconstructs 3D images of an object, including the internal surfaces and interior details, from numerous micron-level two-dimensional (2D) digital radiographic projections using smart computer algorithms and high-performance computing power. Digital radiographic images are generated by 360° rotation of the object on a motorized stage, which is in between a micro-focus X-ray

DISTRIBUTION STATEMENT A.
Approved for public release: distribution is unlimited.

source and a detector. The real-time evaluation capability of XCT with digital radiography increases productivity and eliminates the cost of consumables that are required during a traditional X-ray. High-performance multi-threaded computing and novel reconstruction techniques enable the production of dynamic volumetric 3D models that include time and motion (4D), which allows for real-time inspections of a moving part by combining time and motion as well as eliminating motion artifacts.

The progressive damage growth of CFRP composites listed previously in Table 3 was studied using various layup sequences, stress ratios, and failure modes. A database of detailed 3D XCT data over fatigue lifetime, referred to as 4D XCT, was developed. Typically, the NDI or full-field displacement/strain measurements are not acquired during a fatigue test, because they are time consuming and may not be economical in some cases. As an alternative, specimen compliance change (or inverse of stiffness) can be calculated by simply outputting data during fatigue testing, without interrupting the fatigue test, and calculating the slope of the load-displacement curve. Thus, it is recommended that specimen compliance, especially for notched specimens, be monitored throughout the fatigue test to better understand the failure mechanism and damage propagation. X-ray computed tomography, digital image correlation, and C-scan data were used to establish guidelines for determining the fatigue failure of specimens that were not obvious, i.e., internal delimitations and fiber/matrix cracks that are not visible in thick composite specimens.

An industrial computed tomography system built by North Star Imaging, Inc® was utilized for the assessment of damage progression in the open-hole and double-notch shear test specimens. Most of the XCT scans for this program were accomplished at 150 kV tube voltage, 200 μA target current at 10.01 frames per second and 8.67x magnification with a 400 x 400-micron pixel pitch detector (binning), resulting in ~22.76 μm scan resolution. XCT data gathered over the fatigue lifetime of a specimen generate a significant amount of information.

Each fatigue stress level had about six fatigue specimens, and at least one of them was selected for detailed XCT analysis. Once several fatigue tests were carried out and the approximate fatigue failure number of cycles were identified, XCT scan intervals were set so that about five XCT scans could be obtained for 4D XCT damage characterization over the fatigue test duration. Since most of the damage progression occurred towards the end of fatigue cycling, XCT inspection intervals were arranged to capture as much of the damage progression towards the final failure. For this, the stiffness degradation data from compliance checks also can be used for determining the XCT scan.

An interactive software was developed to filter and threshold each ply subjectively to capture microcracks and delamination, and then filter out noise. This software ensures that certain features are visible prior to the quantification of damage by allowing the end-user to subjectively filter and threshold each ply to capture only flaws and delamination in the specimen with

DISTRIBUTION STATEMENT A.
Approved for public release: distribution is unlimited.

filtering undue noise. The software tool was developed to examine the XCT data for quantification of damage growth by doing the following:

- Interpreting ply-by-ply fatigue damage progression.
- Interpreting fatigue damage area percent increase.
- Characterizing cross-section damage (where excessive delamination exists before primary failure).

To assess the damaged area percentage increase, the total pixel count of damage increase from the previous cycle was divided by the total pixel count of the corresponding ply scan at the initial scan before starting the fatigue test. The relative damage area increase in pixel count was calculated with respect to the data collected during the previous inspection interval. The difference in the area of damage was considered instead of total damage throughout the fatigue in order to study the progressive damage. Figure 89 shows the ply-by-ply damage information extracted for the IM7/5320-1 UNI quasi-isotropic test specimen using binary scale data analysis.

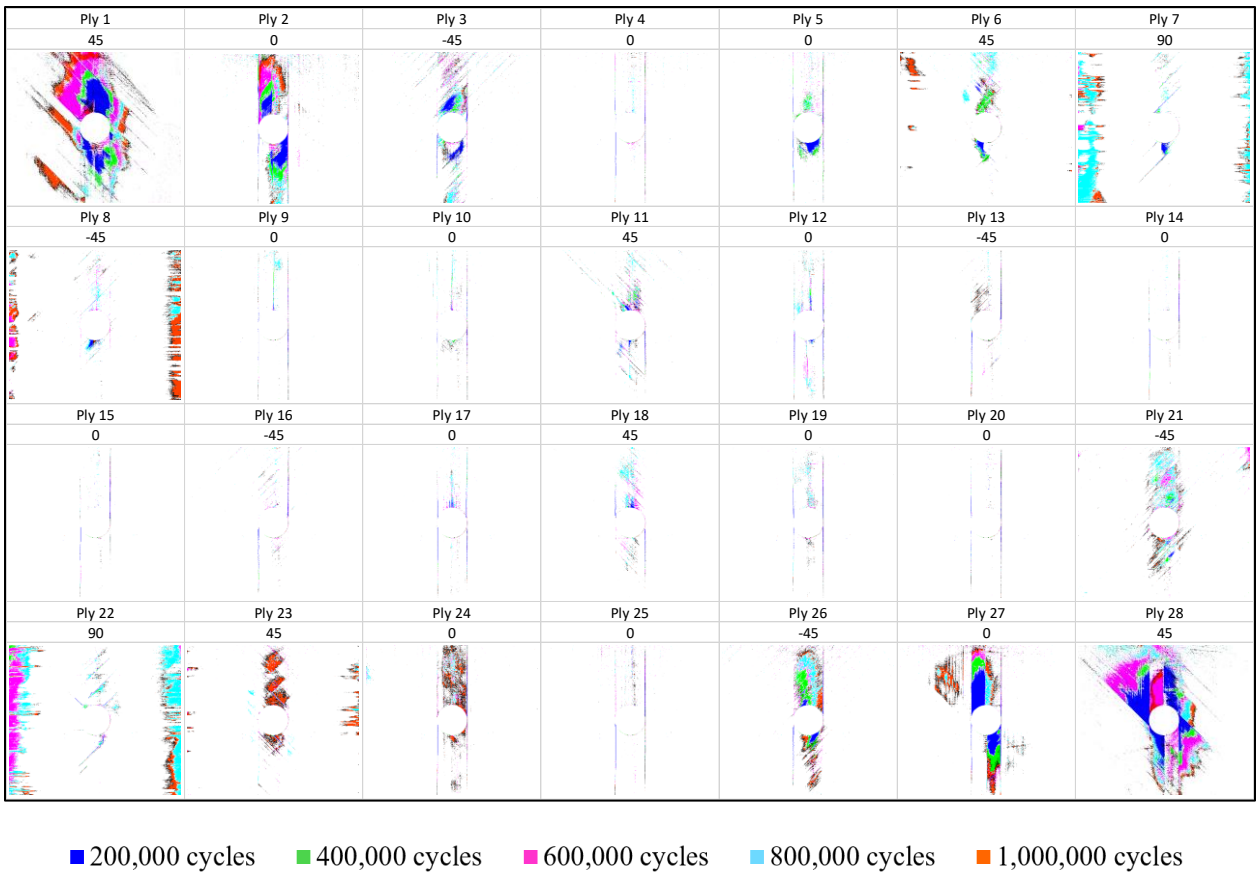


Figure 89. Ply-by-ply XCT damage progression data for IM7/5250-4 UNI, 50/40/10 layup, OHT, R = 0.1.

In order to quantify the progressive damage growth information shown in Figure 89, the interactive software was used for generating the ply-by-ply percent damage growth data shown

DISTRIBUTION STATEMENT A.
Approved for public release: distribution is unlimited.

in Figure 90. As can be seen, there is minimal delamination growth in 0° plies, and most of the delamination growth is on the outermost 45° plies and 90° inner plies. There is 4 to 6 percent damage growth in both of the outermost 45° plies at 200,000 cycle XCT scan (dark blue). The next 200,000 cycles (green) showed less than 1 percent damage growth in these two plies. From 400,000 to 600,000 cycles (pink), additional 6 to 7 percent delamination growth is observed. From 600,000 to 800,000 cycles (light blue), most of the damage (approximately 6 percent) was observed in the inner 90° plies. Finally, from 800,000 to 1,000,000 cycles, approximately 4 percent delamination growth was observed in one of the outermost 45° plies. Although this methodology is not as straight forward as metal crack growth, it provides a means of quantifying the delamination growth across multi-layer composites in a meaningful manner.

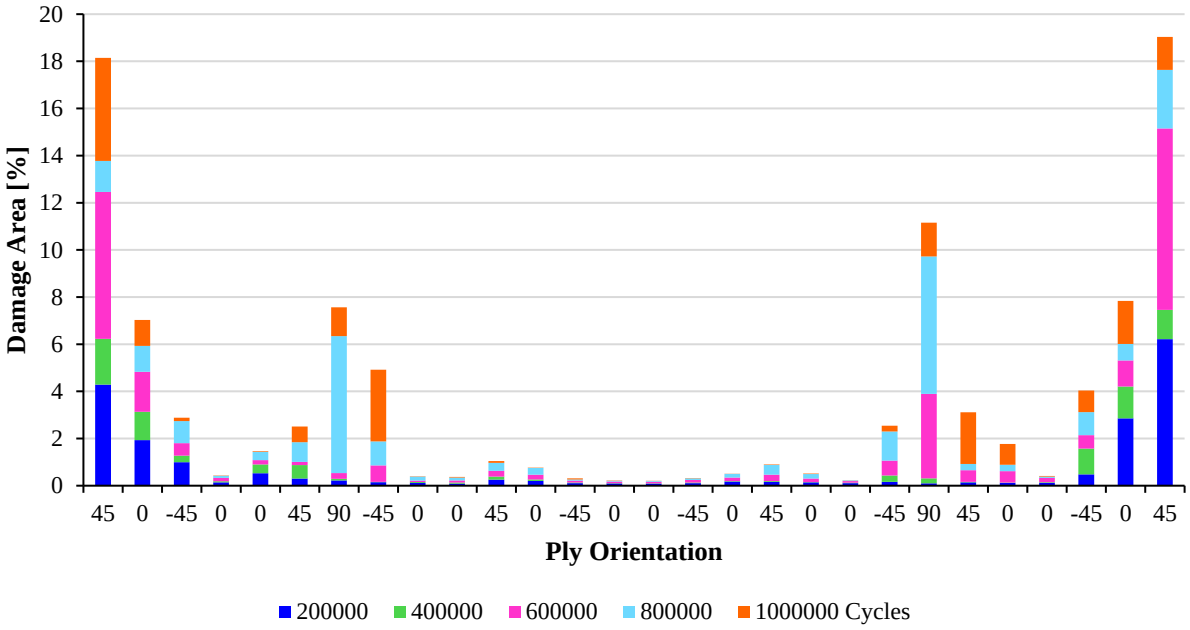


Figure 90. Damage area percent increase for IM7/5250-4 UNI, 50/40/10 layup, OHT, R = 0.1.

The same data that was used for the ply-by-ply binary scale analysis shown in Figure 89 was analyzed using the second technique (grayscale), as shown in Figure 91. There were no significant differences between the scan results of these two data analysis techniques. However, the delamination growth from binary scale data analysis was more clear than that from grayscale data analysis. The XCT inspections performed for the progressive damage characterization are summarized in Appendix B.

DISTRIBUTION STATEMENT A.
Approved for public release: distribution is unlimited.

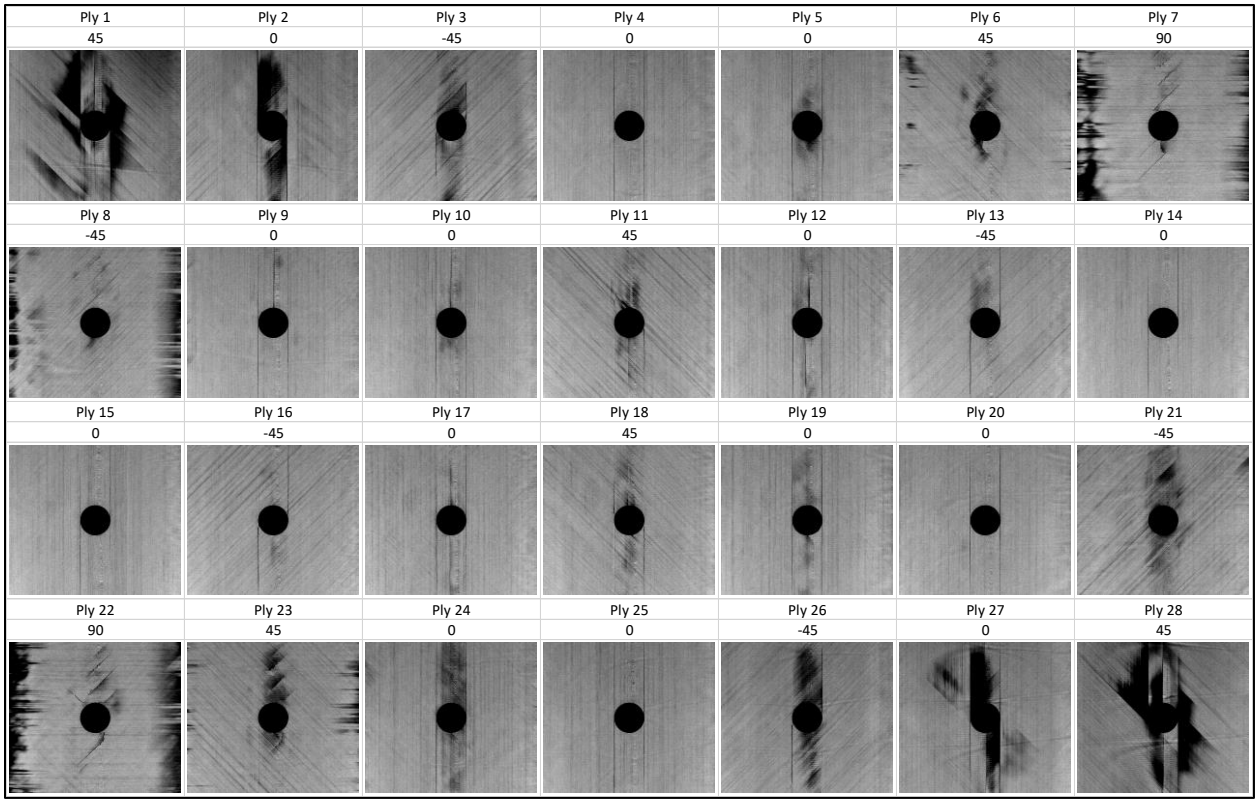


Figure 91. Ply-by-ply scan for IM7/5250-4 UNI, 50/40/10 layup, OHT, R = 0.1.

7.1 Post-Processing of X-ray Computed Tomography Data

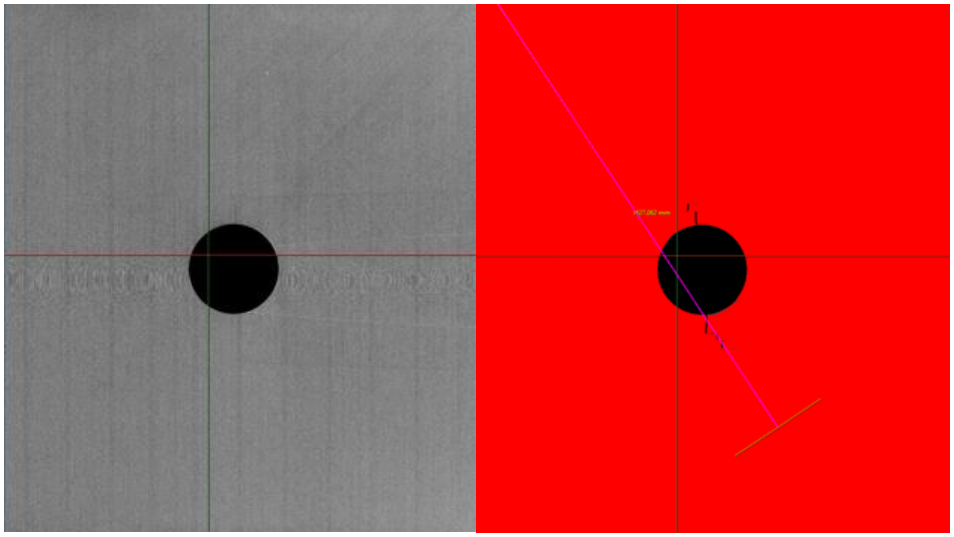
XCT data captured at pre-test, intermediate inspection intervals, fatigue failure, and runout are subjected to additional post-processing in order to extract ply-level progressive damage growth information. Since this requires analysis of large amount of XCT data, a simple and reliable method of viewing/quantifying fatigue damage accumulation is warranted.

Post-XCT imaging and reconstruction of radiographs are performed using a proprietary North Star Imaging (NSI) processing product, efX-CT FULL Computed Tomography Software. Upon 3D reconstruction, efX-CT is used to export slices of the volume in the form of tiff images. The tiff images, commonly containing 200 to 400 slices, are imported into Synopsis Simpleware software. Slice count varies as total volume increases due to formation of large delaminations. Using these imported slices, Simpleware generates a 3D volume for additional processing. First, the histogram is adjusted to ensure optimum contrast between laminate and cracks/damage regions (Figure 92.a). To assist, a line profile covering both undamaged and damaged regions is utilized and the undamaged volume is masked (Figure 92.b).

With the undamaged regions masked, specimen hole center is located to ensure proper alignment for subsequent processing. The cropped volume, which still contains small regions of unmasked area in undamaged regions, is filtered to fill groups containing less than 3 voxels (Figure 93.a). Hiding the mask, all 200 to 400 slices are inspected and the slice number containing the best

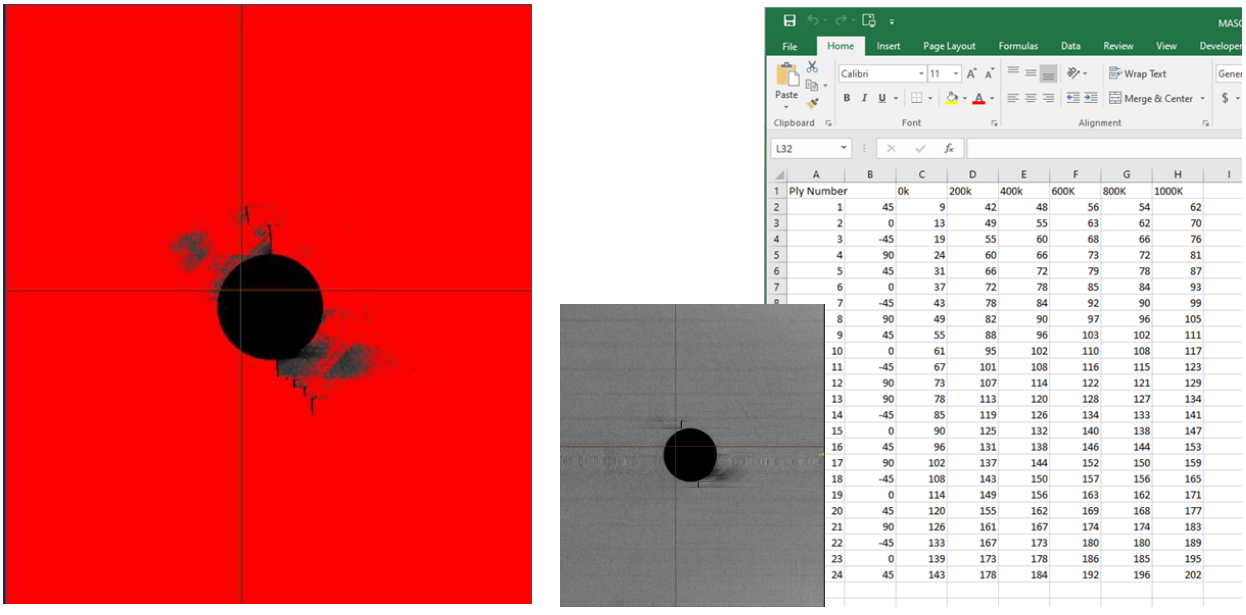
DISTRIBUTION STATEMENT A.
Approved for public release: distribution is unlimited.

representation of a given ply as illustrated in Figure 93.b is used for damage characterization and 4D XCT.



(a) (b)

Figure 92. (a) Histogram adjustment and (b) line profile evaluation for thresholding.



Ply Number	0k	200k	400k	600K	800K	1000K
1	45	9	42	48	56	54	62
2	0	13	49	55	63	62	70
3	-45	19	55	60	68	66	76
4	90	24	60	66	73	72	81
5	45	31	66	72	79	78	87
6	0	37	72	78	85	84	93
7	-45	43	78	84	92	90	99
8	90	49	82	90	97	96	105
9	45	55	88	96	103	102	111
10	0	61	95	102	110	108	117
11	-45	67	101	108	116	115	123
12	90	73	107	114	122	121	129
13	90	78	113	120	128	127	134
14	-45	85	119	126	134	133	141
15	0	90	125	132	140	138	147
16	45	96	131	138	146	144	153
17	90	102	137	144	152	150	159
18	-45	108	143	150	157	156	165
19	0	114	149	156	163	162	171
20	45	120	155	162	169	168	177
21	90	126	161	167	174	174	183
22	-45	133	167	173	180	180	189
23	0	139	173	178	186	185	195
24	45	143	178	184	192	196	202

(a) (b)

Figure 93. a) Cropped volume with filtering applied and (b) demonstration of Microsoft Excel spreadsheet documenting slice-to-ply correlations for each inspection interval.

Upon documentation of slice numbers corresponding to ply numbers in Microsoft Excel, a script is executed to export all slices with the aforementioned mask applied. This process is performed for each inspection interval and data is stored within each respective cycle count folder. Upon completion of exporting slices for all intervals, an in-house program uses the spreadsheet,

DISTRIBUTION STATEMENT A.
Approved for public release: distribution is unlimited.

containing representative slice numbers, to import and process the data. This processing consists of applying a color mask to damaged regions, varying for each interval number, and performing a subtraction of interval N-1 from N, where N is the inspection interval number. This subtraction allows only damage progression from the previous inspection interval to be documented. For each interval, percentage of total area is computed for monitoring and displaying damage accumulation for each ply as shown in Figure 94. Damage area data can then be shown graphically. Additionally, exported ply images can be combined for generation of 4D XCT videos.

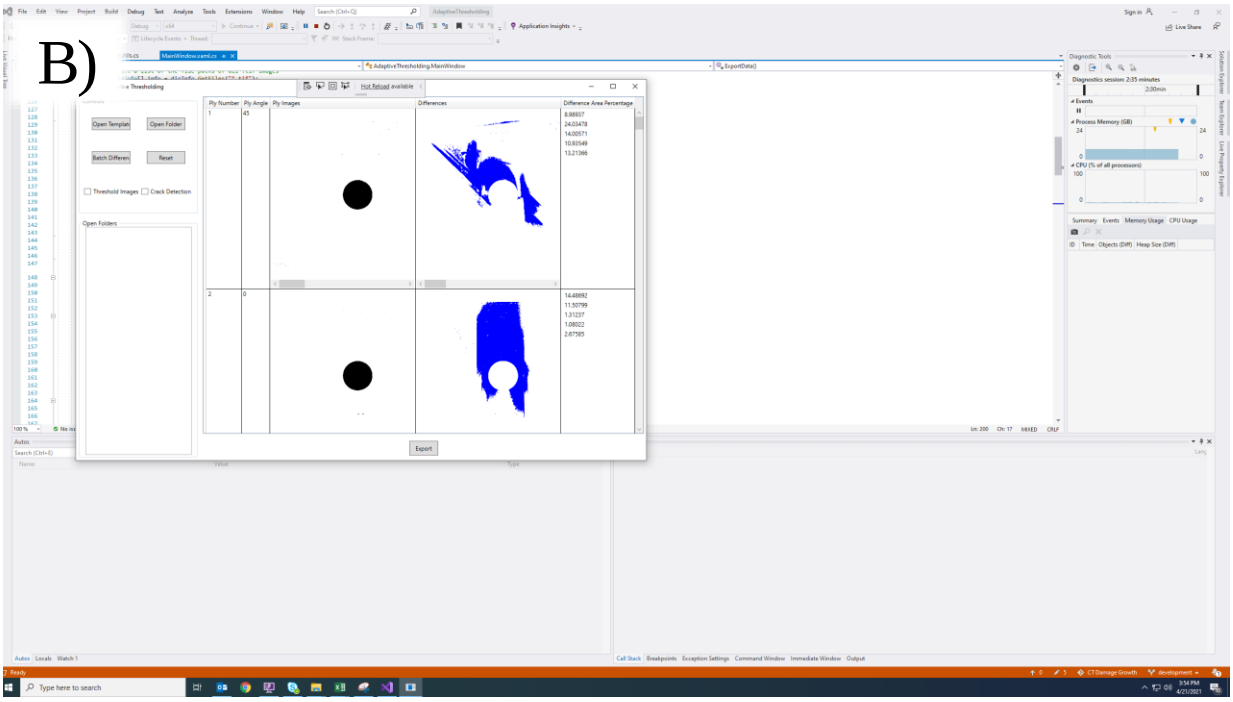


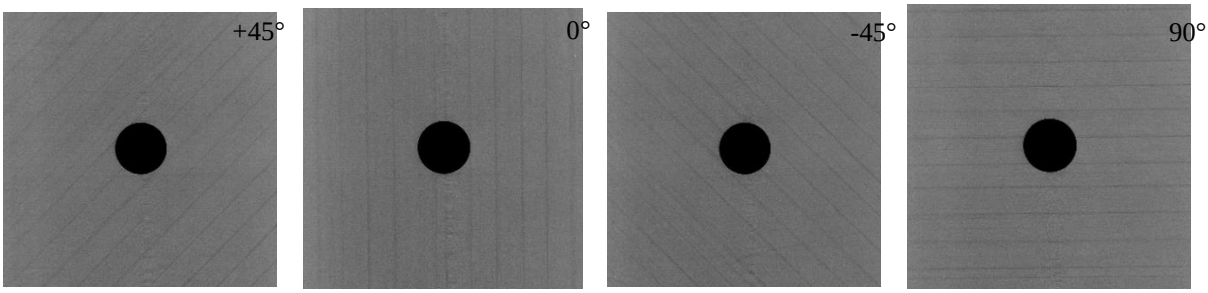
Figure 94 – Interface for viewing processed data through in-house software.

7.2 Investigation of Resin-Rich Areas

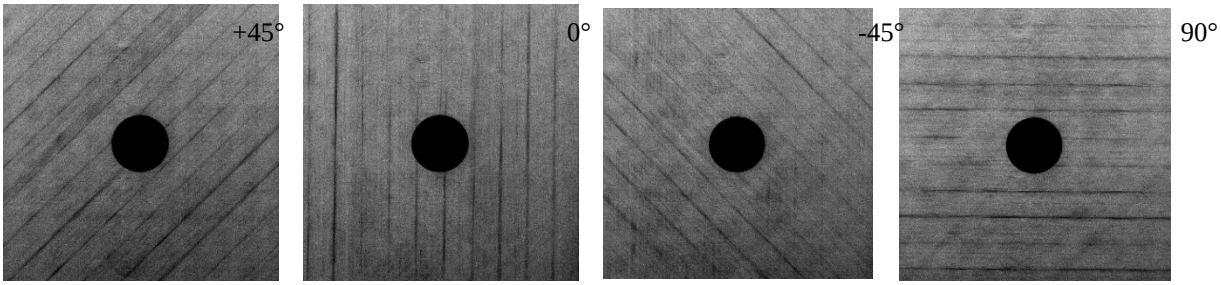
XCT images of test specimens manufactured from IM7/5320-1 and IM7/5250-4 unidirectional tape material systems indicated resin-rich lines equally spaced running parallel to the fiber direction throughout each ply (Figure 95). These lines were not visible to the naked eye on IM7/5320-1 UNI. The photomicrographs of IM7/5320-1 UNI specimens shown in Figure 96 indicate that the spacing of the resin-rich areas is approximately 0.12 inch, which matches the width of a carbon fiber tow after flattening during the prepreg manufacturing process. The locations of the dark lines (resin-rich areas) were first identified using an Olympus BX51M optical microscope at lower magnification, and then they were closely inspected using a Keyence laser microscope at higher magnification. The red dashed line in Figure 96 indicates the typical width of a tow, and the photomicrograph confirmed the resin-rich area where the two tows meet.

DISTRIBUTION STATEMENT A.
Approved for public release: distribution is unlimited.

IM7/5320-1 UNI panels manufactured by Boeing and Spirit AeroSystems using different material batches were inspected, and the same resin-rich areas were observed.



(a) IM7/5320-1 UNI



(b) IM7/5250-4 UNI

Figure 95. Resin-rich areas observed in XCT scans of OH UNI specimens.

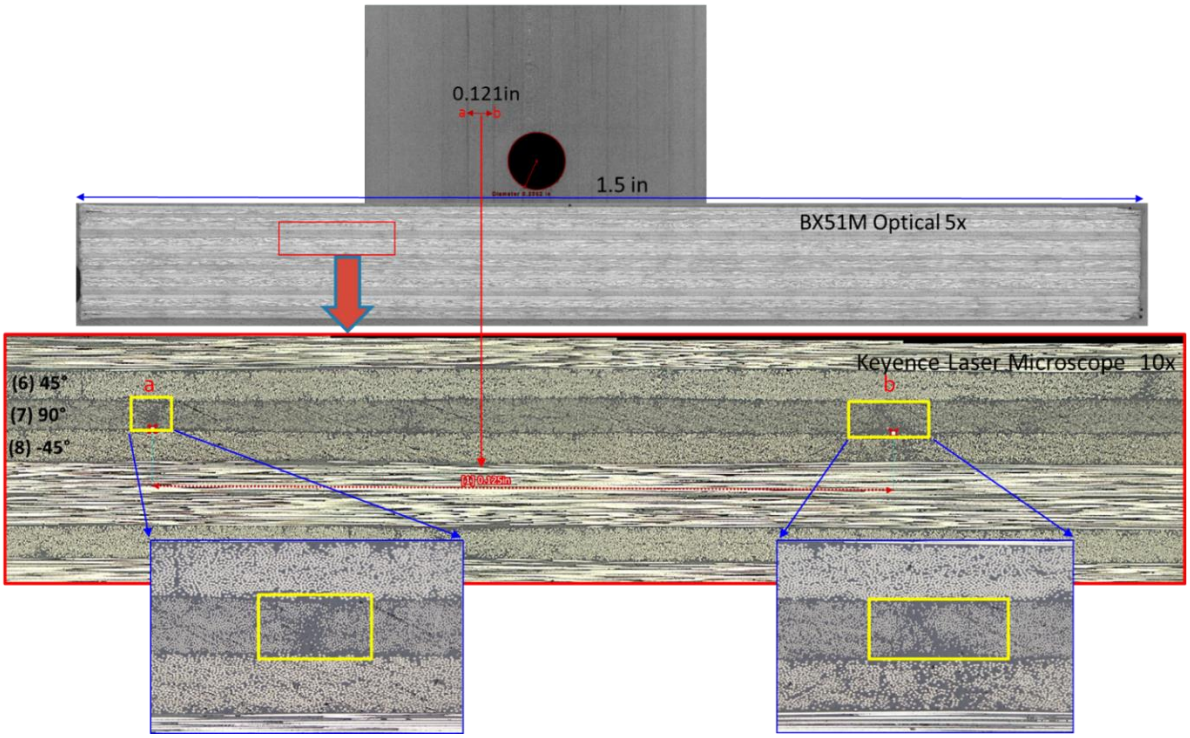


Figure 96. Photomicrographs of resin-rich areas in IM7/5320-1 UNI.

DISTRIBUTION STATEMENT A.
Approved for public release: distribution is unlimited.

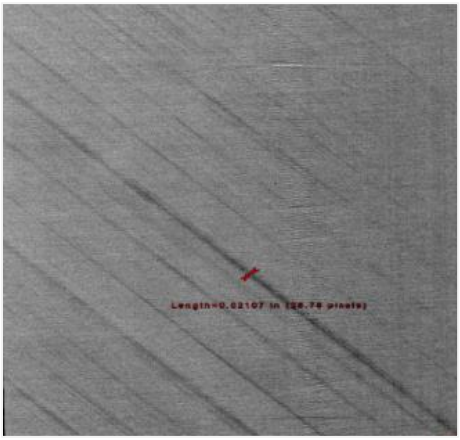
7.3 Visible Fiber Gaps

During the initial handling (cutting and layup) of the material, visible fiber gaps were noticed in the prepreg plies of the IM7/5250-4 material system. These gaps coincided with the locations where one tow connected to the other. Figure 97 shows these fiber gaps, which are visible to the naked eye. The measurements of the fiber gaps were as high as 0.016 inch. However, they were less than the typical aircraft material specification (gaps less than 0.03 inch) for this type of material system. Therefore, the test panels were manufactured using this material system. Although XCT scans of manufactured panels indicted the resin-rich regions, they were as obvious as for IM7/5320-1 UNI using photomicrographs.

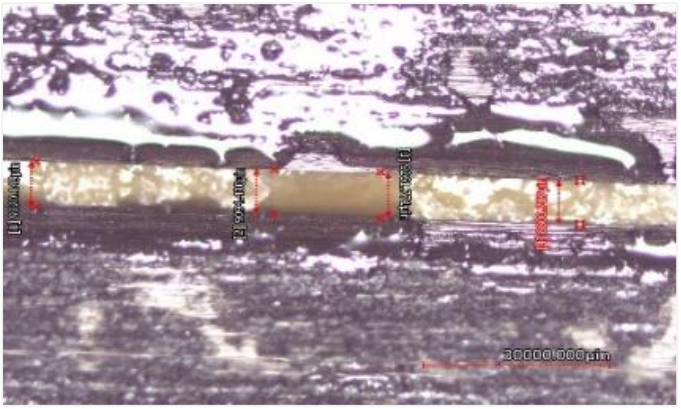
Detailed progressive damage growth inspections carried out using XCT indicated that these resin-rich areas can influence the localized damage growth but are not significant enough to change the failure mode or cause significant data scatter.



(a) Visual Inspection



(b) XCT Inspection



(c) Laser Microscopic Inspection



(d) Photomicrograph

Figure 97. Inspections of gaps in IM7/5250-4 UNI.

DISTRIBUTION STATEMENT A.
Approved for public release: distribution is unlimited.

7.4 Interlaminar-Tension Specimen Quality

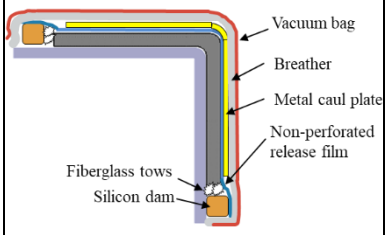
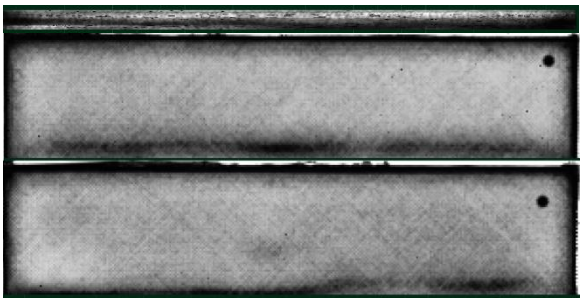
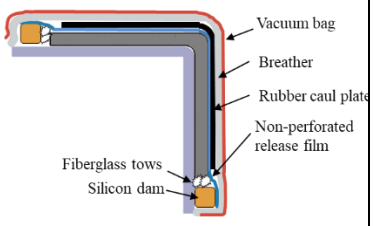
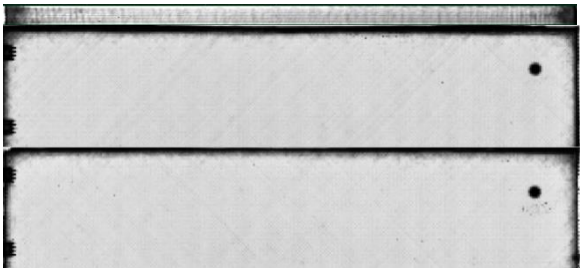
The manufacturing quality of the interlaminar tension specimen was sensitive to ILT strength and fatigue life as well as data scatter [34]. Typical manufacturing defects include voids/porosity, fiber waviness, resin-rich areas, and thickness variation. Previous findings have shown that these manufacturing defects are more prominent in concave tools than in convex tools [35]. Therefore, all ILT panels were fabricated with convex tooling. Although convex tooling has less porosity, fiber waviness and resin-rich areas in the curved region, care must be taken to ensure that the thickness is consistent. Therefore, each material system requires a series of process improvement trials prior to manufacturing test panels.

The manufacturing quality of curved-beam ILT specimens was improved by performing a series of preliminary manufacturing trials and inspections. Table 21 shows changes made to the standard panel manufacturing method of IM7/5320-1 UNI material in order to improve the panel quality by significantly reducing porosity levels. Three of the major changes include the following:

- Increase the room temperature of the final assembly debulking from 8 to 16 hours.
- Change the metal caul plate to a rubber caul plate.
- Increase the number of vacuum ports from one to two.

The TTU C-scans shown in Table 21 reveal the impact of these changes on reducing the porosity levels in the curved portion as well as on two flat areas of the material system.

Table 21 – Manufacturing improvements with IM7/5320-1 material system.

Bagging Configuration	Bagging Schematic	Panel Quality (TTU C-scans)
<u>Initial:</u> 8-hour room temperature debulk of final assembly, metal caul plate, one vacuum source		
<u>Final:</u> 16-hour room temperature debulk of final assembly, rubber caul plate, two vacuum sources		

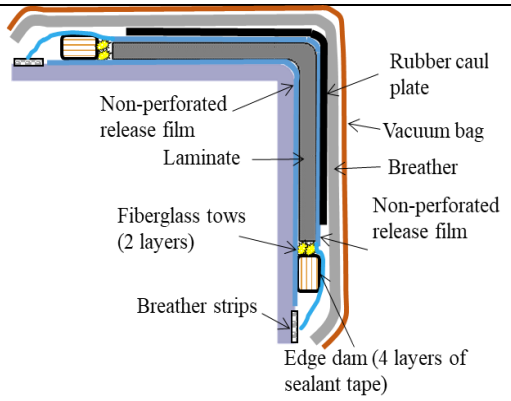
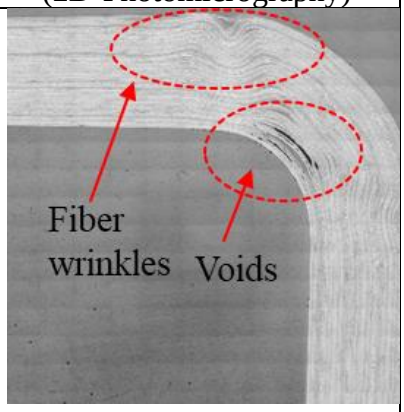
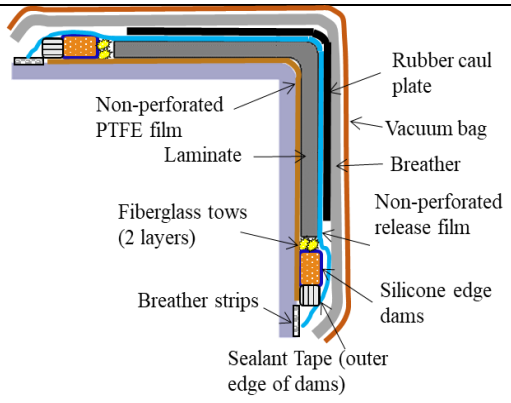
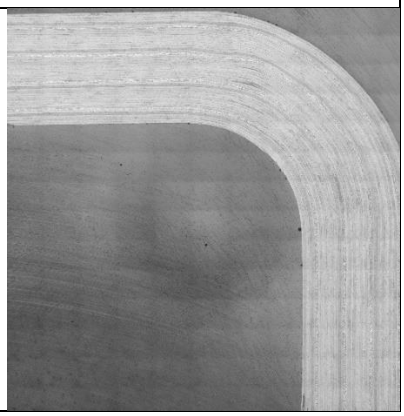
DISTRIBUTION STATEMENT A.
Approved for public release: distribution is unlimited.

Table 22 shows changes made to the standard panel manufacturing method of IM7/5250-4 UNI material in order to improve the panel quality by significantly reducing porosity levels and fiber waviness. Several of the major changes include the following:

- Use PTFE film on the tool side instead of non-perforated film on the tool side.
- Debulk every 2 plies instead of every 4 plies.
- Change the metal caul plate to a rubber caul plate.
- Increase the number of vacuum ports from one to two during debulking and final assembly.
- Use sealant tape instead of silicon for the edge dams.
- Increase the room temperature of the final assembly debulking from 2 to 4 hours.

TTU C-scans obtained for process trials as well as the photomicrographs shown in Table 22 indicate the impact of these changes on reducing porosity levels, long voids/delaminations, fiber waviness, and resin-rich areas.

Table 22 – Manufacturing improvements with IM7/5250-4 material system.

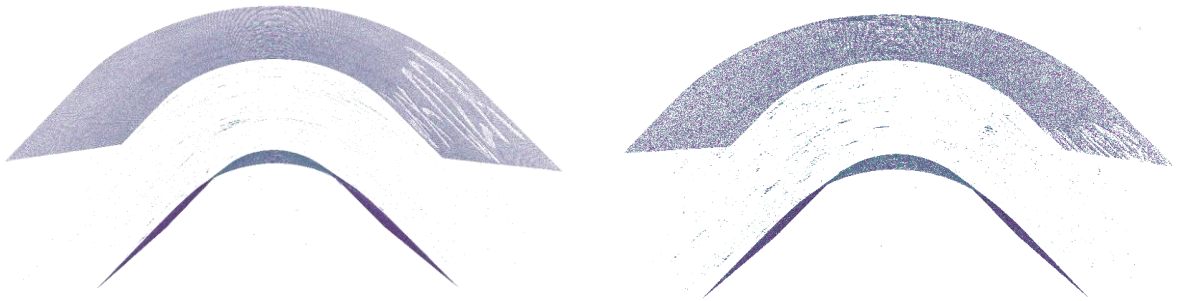
Bagging Configuration	Bagging Schematic	Panel Quality (2D-Photomicrography)
Initial: Non-perforated release film on tool side, debulking every 4 plies, one vacuum source during debulking, sealant tape edge dams, 2-hour room temperature debulking of final assembly, two vacuum sources during cure		
Final: PTFE film on tool side, debulking every 2 plies, two vacuum sources during debulking, sealant tape edge dams, 4-hour room temperature debulking of final assembly, two vacuum sources during cure		

Every ILT test panel was carefully inspected using TTU C-scans in order to avoid using areas

DISTRIBUTION STATEMENT A.
Approved for public release: distribution is unlimited.

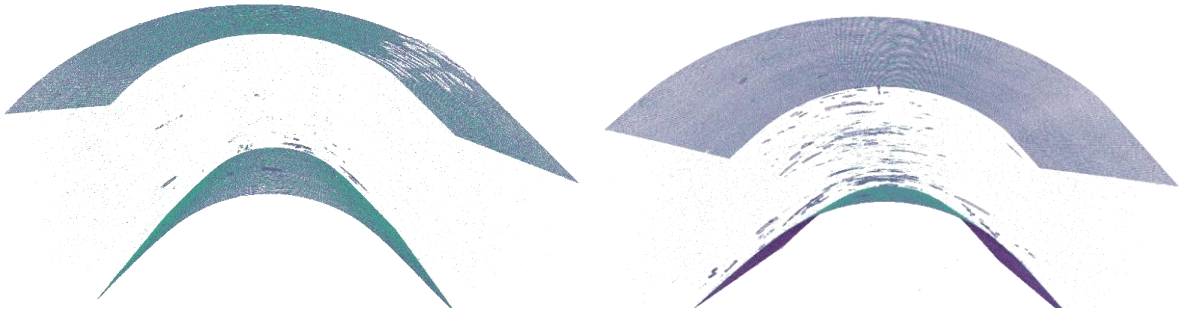
with high-porosity levels. Once specimens were manufactured, every ILT fatigue specimen was subjected to XCT scans prior to testing so that the post-failure XCT scan could be used for investigating the influence of manufacturing defects on the damage initiation and propagation. Figure 98 to 101 illustrate representative XCT images with various levels of porosity (low to high) of ILT specimens observed for each material system. Furthermore, the measurements were captured into a 3D model and their contribution was carefully quantified to the scatter in the test data. This method was useful for determining reliable interlaminar material property with the amount of present manufacturing defects.

2D radiographs of ILT carved regions were obtained using either NSI X7000 or Xradia Versa 520 XCT system, at different angular positions while rotating the specimen 360°. The X7000 scans were performed at 90 kV voltage and 200 µA current at 1.5 frames per second to achieve image resolutions of 20 µm. The Xradia scans were obtained at 40 kV voltage and 75 µA current at 0.1 frames per second to achieve image resolutions of 34 µm. The 2-D radiographic images (projections) were reconstructed using the efX-CT software (NSI) to obtain the 3D volume of the specimen. The void visualization, quantification, and locations were performed using the VGSTUDIO MAX3.4 software (Volume Graphics®).



(a) Typical (b) Areas with significant porosity

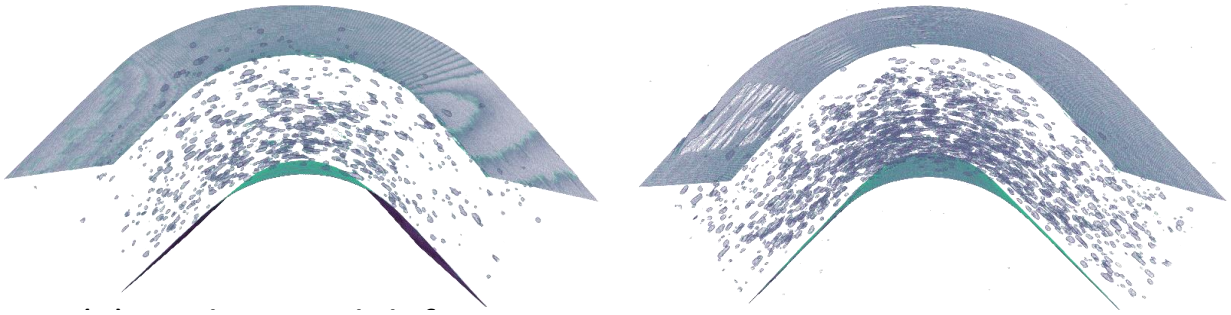
Figure 98. Representative porosity levels in IM7/5250-4 UNI.



(a) Typical (b) Areas with significant porosity

Figure 99. Representative porosity levels in IM7/5320-1 UNI.

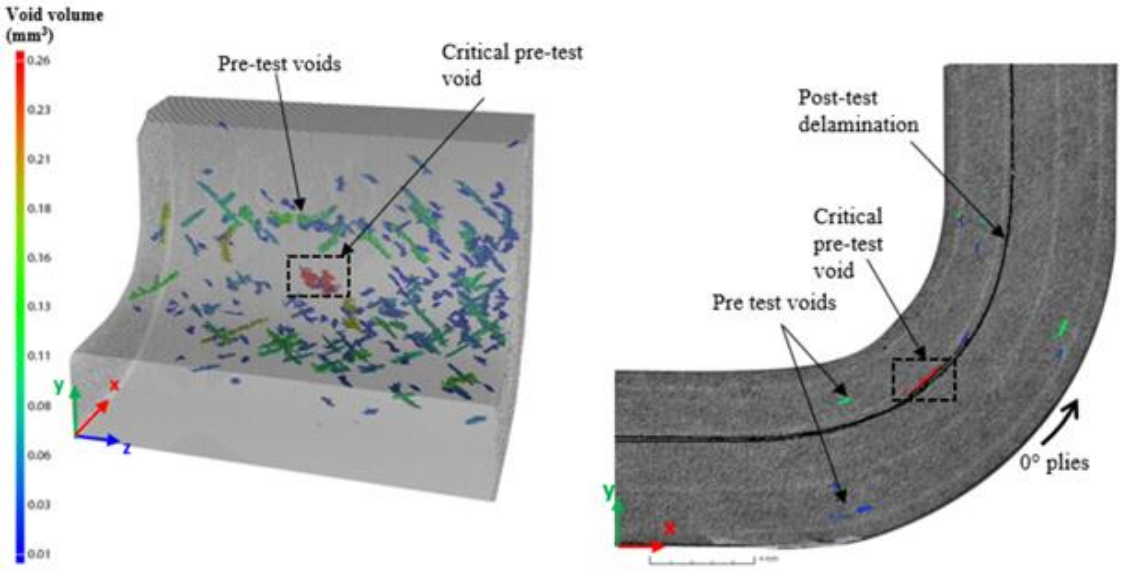
DISTRIBUTION STATEMENT A.
Approved for public release: distribution is unlimited.



(a) Typical (b) Areas with significant porosity

Figure 100. Representative porosity levels in T650/5320-1 8HS.

In order to investigate the influence of manufacturing defects such as porosity/voids, fiber waviness, and resin-rich areas on the final failure, pre-and post-test 3D volumes were merged using VGSTUDIO MAX feature-based registration method. This helps visualizing the influence of manufacturing defects in pre-test scans on the failure mode(s) observed in post-test scans. As shown in Figure 101(a), manufacturing defects are quantified to determine any areas that has manufacturing defects above acceptance levels. The volume of a void was calculated by determining the total number of voxels within the void. In addition to the volume, the location (hoop and radial directions) of critical voids were determined as shown in Figure 102. The hoop location was measured from the apex of the curved section of the ILT specimen. The reference axis was defined from where the tangent lines (orange dotted lines) intersected from both inner and outer radii. The radial location was defined as a percentage thickness with respect to the total specimen thickness.



(a) (b)

Figure 101. (a) pre-test manufacturing defects and (b) post-test damage overlay along critical void locations.

DISTRIBUTION STATEMENT A.
Approved for public release: distribution is unlimited.

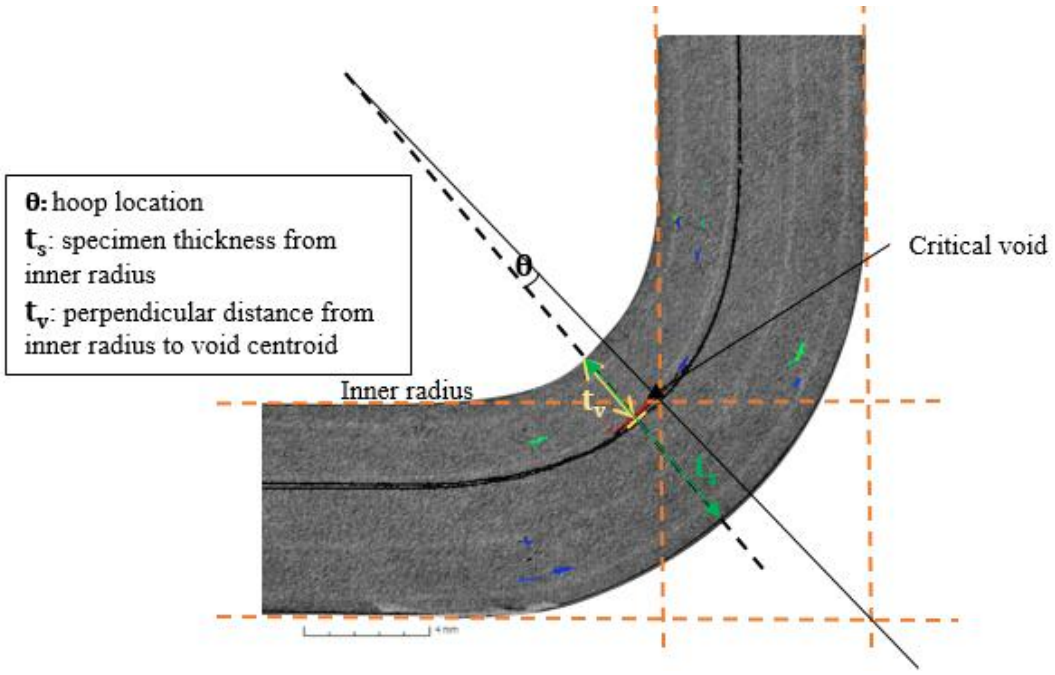


Figure 102. Example of quantifying of critical void location(s).

Comparison of pre-test and post-failure XCT scans were used to investigate the root cause of the data scatter observed on ILT fatigues specimens. Figure 103 shows an example of data scatter in IM7/5320-1 UNI ILT (hard laminate) quasi-static, fatigue and residual strength data. Batch 2 produced significantly lower quasi-static strength and fatigue performance than the other two material batches. Batch 1 and 3 average quasi-static strength values are 13.47 ksi and 11.44 ksi, respectively, while batch 2 has an average value of 9.83 ksi. In addition, most of the fatigue specimens from Batch 1 and 2 survived lower stress levels, while Batch 2 specimens had failures. XCT inspection data obtained for specimens manufactured using Batch 2 materials indicated higher levels of porosity than that for the specimens manufactured using the other two material batches. High level of porosity in Batch 2 specimens resulted in lower fatigue lives and residual strength.

Table 23 presents the findings such as pre-test void volume (total), critical void volume (potential void present near delaminations), and hoop and radial location of critical void(s). The following conclusions can be drawn based on the summary of results obtained.

1. Cycles to failure has a direct relationship with the specimen void content.
2. The critical void closer to either 50% of the specimen thickness or to the apex of the curved region has a higher tendency to influence failure initiation.
3. The smaller voids have less influence on the failure initiation regardless of the stress level and void location.

DISTRIBUTION STATEMENT A.
Approved for public release: distribution is unlimited.

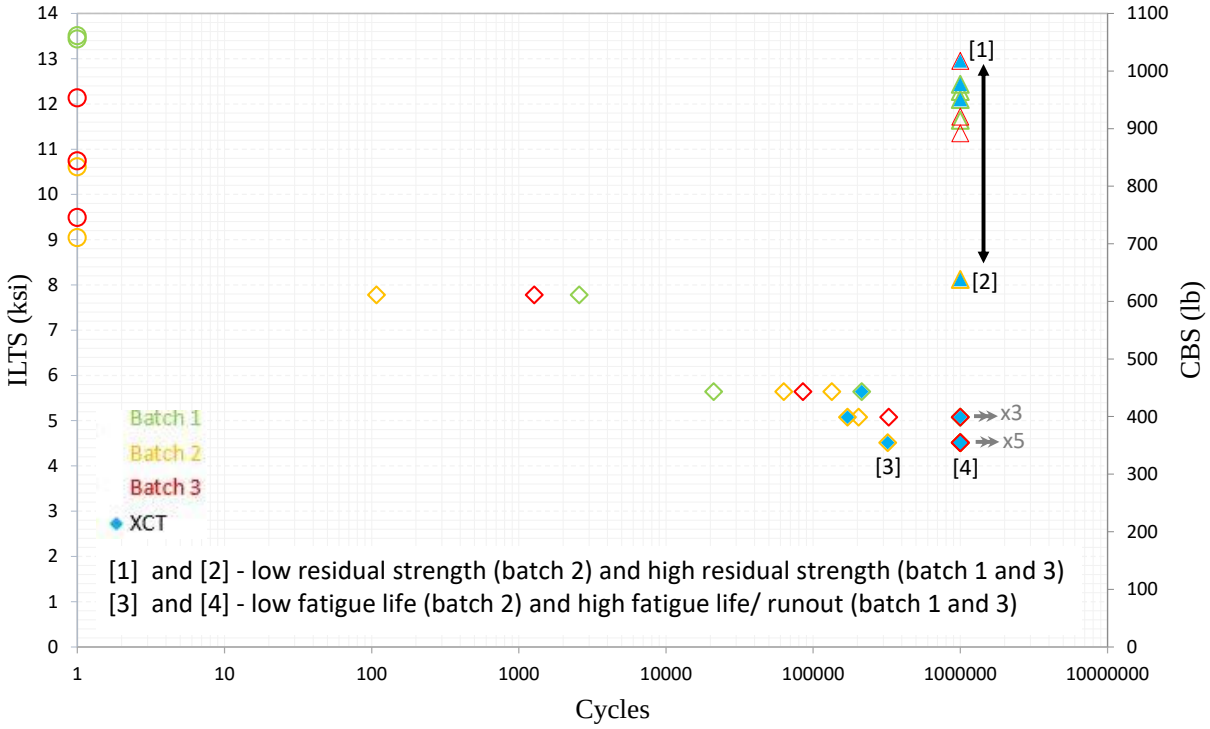


Figure 103. IM7/5320-1 UNI, 50/40/10, ILT fatigue data with XCT.

Table 23 – Summary of porosity assessment and damage characterization for IM7/5320-1 UNI, 50/40/10.

Stress Level	No. cycles	Residual strength (ksi)	Pre-test void volume (mm^3)	Critical void volume (mm^3)	Hoop location of critical void, θ, (degrees)	Radial location of critical void, % thickness (t_v/t_s)
SL1	1000000[1]	12.10	0.08	0.02	11.82	12.10
	1000000[1]	12.96	0.17	0.02	31.66	41.90
	1000000[1]	8.12	0.38	0.07	25.57	18.59
	321595	–	1.79	0.12	24.56	48.90
SL2	1000000[1]	12.43	0.02	X	X	X
	171113	–	7.22	0.09	2.15	33.10
SL3	213867	–	0.34	0.15	14.67	10.20

1 - Runout
X - No evidence of pre-test void near delaminations

DISTRIBUTION STATEMENT A.
Approved for public release: distribution is unlimited.

7.5 Effects of Extended Post-Cure

Often composite parts undergo a post-manufacturing secondary rework process that subjects the materials into an extended post-cure (EPC) of heat cycles beyond what is recommended for the original (baseline) cure cycle. Such additional heat or post-cure cycles may change the material characteristics and must be considered during design. Several static and fatigue test specimens were added to the original SN curves in order to investigate the EPC on the mechanical performance of both 5320-1 and 5250-4 resin systems. In addition, several thermal analysis specimens were added to determine the effects of EPC on the thermal characteristics of each resin system. Thermal analyses were performed using both dynamic mechanical analysis (DMA) [32] and differential scanning calorimetry (DSC) [33].

Since the EPC could primarily affect the resin properties, a soft (10/80/10) layup configuration was selected for this investigation. Also, a 100-hour EPC was considered the maximum, and several intermediate EPC hours were investigated. Also, batch 3 from each material was selected for the investigation, and comparisons were made with respect to the baseline test data from the same material batch to avoid any contribution from material batch-to-batch variability. For the EPC panels, the standard cure time as specified per material manufacturer processing parameters, 2 hours for 5320-1 and 6 hours for 5250-4, was used, followed by an additional free-standing cure cycle up to 100 hours in a circulating air oven shown in Figures 105 and 106 respectively. The only difference between the flat and curved panels was in the initial room temperature debulking, where curved panels had double the debulking time over flat panels.

EPC tests were carried out for open-hole (R = 5 and R = –1), interlaminar tension (R = 0.1), and double-notch shear (R = 0.1) test specimens manufactured using soft laminates of material batch 3. The test matrix for the 20-, 30-, 50-, and 100-hour EPCs is shown in Table 24. Testing initially began with open-hole specimens with a 20-, 30-, and 50-hour EPC. Two specimens (out of six) from each EPC category were tested as quasi-static loading, while the remaining four specimens were tested at two different fatigue stress levels (two each). These fatigue stress levels were selected to match the stress levels used for baseline SN curves for comparison purposes.

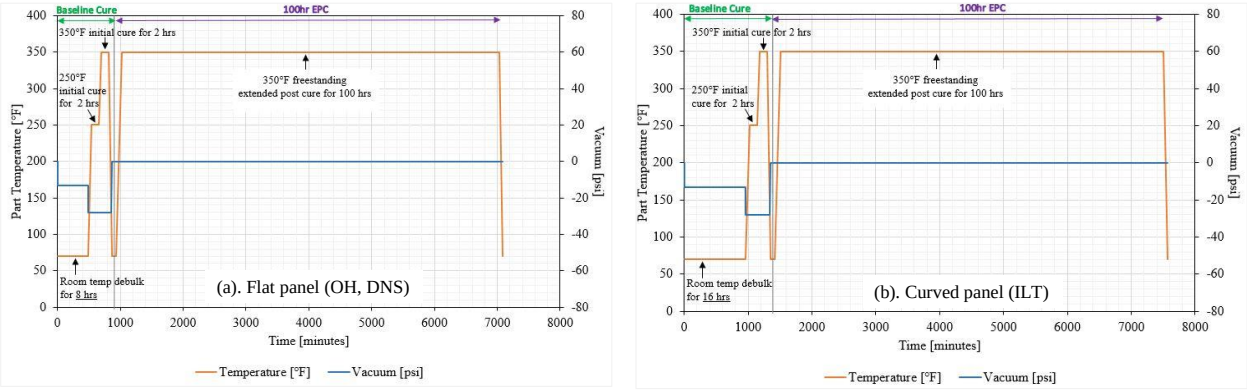


Figure 104. IM7/5320-1 UNI 100-hour EPC for (a) flat panels and (b) curved panels.

DISTRIBUTION STATEMENT A.
Approved for public release: distribution is unlimited.

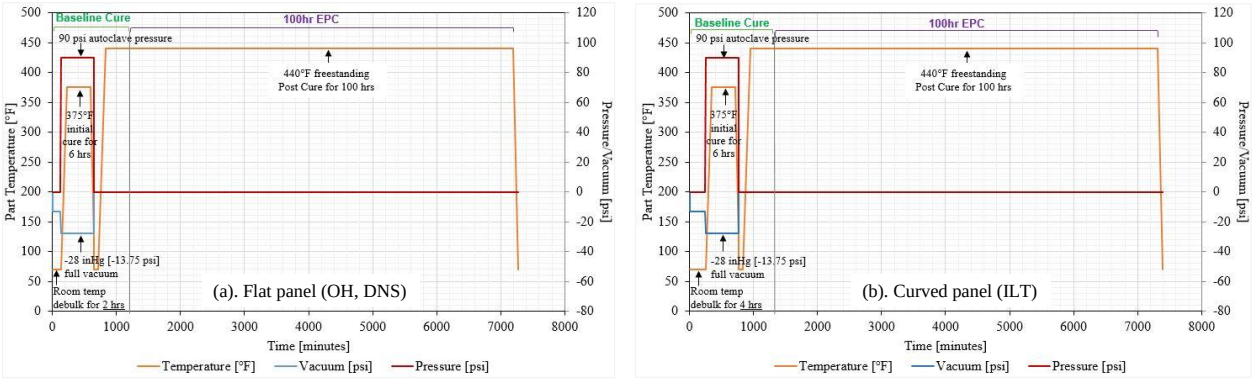


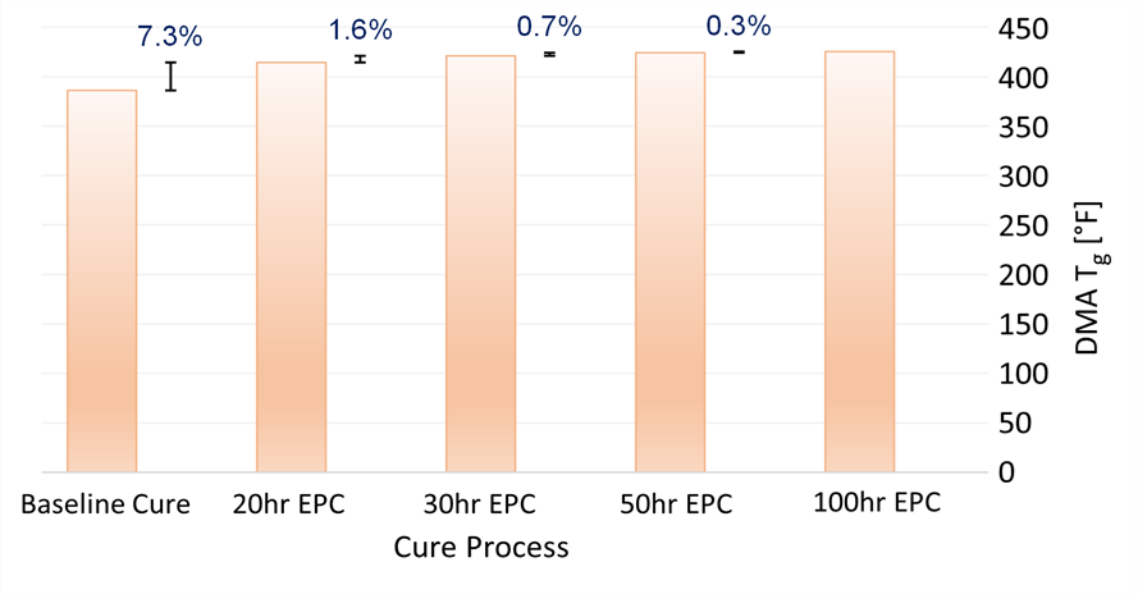
Figure 105. IM7/5250-4 UNI 100-hour EPC for (a) flat panels and (b) curved panels.

Table 24 – Number of EPC test specimens.

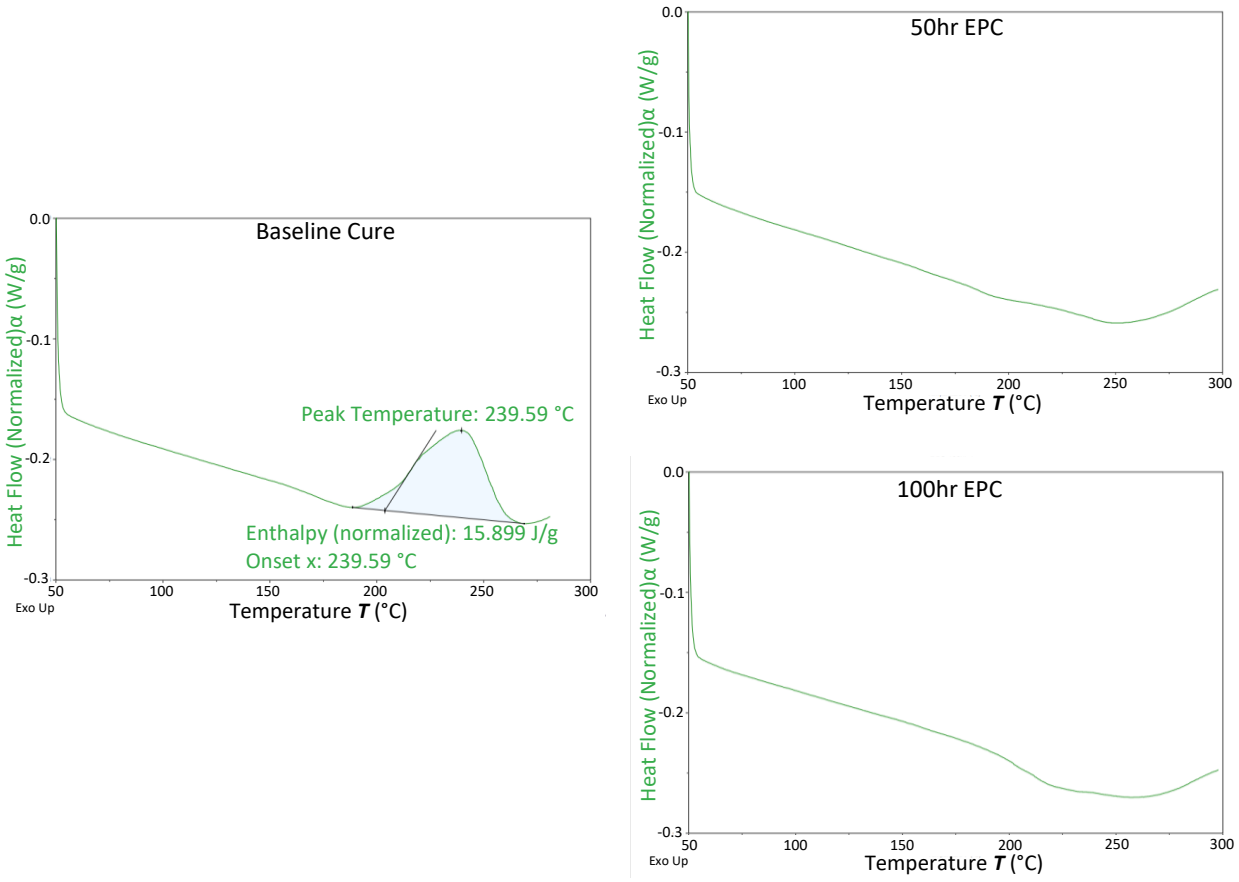
Material	Test Method	Stress Ratio (R)	Extended Post-Cure (hours)			
			(20)	(30)	(50)	(100)
IM7/5320-1 Uni	OHC-C	5	6	6	6	6
	OHC-T	–1				6
	ILT	0.1				6
	DNS	0.1				6
IM7/5250-4 Uni	OHC-C	5			6	6
	OHC-T	–1				6
	ILT	0.1				6
	DNS	0.1				6

After preliminary studies, it was found that the effect of 20- to 50-hour EPC was minimal, so the remaining EPC study focused on a 100-hour study to demonstrate the effects of the extreme case of EPC to produce more notable results. Figure 106 shows the effects of EPC on thermal characteristics of IM7/5320-1 from two different thermal techniques. The glass-transition temperature was increased up to a 50-hour EPC and stabilized, indicating that the material had achieved full cure around 50 hours of post-cure. An exothermic heat of reaction (area under curve in j/g) observed in DSC results for baseline cure indicates that the material was not fully cured. No exothermic heat of reaction was noticed for the 50-hour and 100-hour (EPC, confirming the observation noted in Tg results that indicated full cure by a 50-hour EPC. After the initial open-hole EPC mechanical tests and thermal analyses data, it was determined that only the 100-hour EPC would be tested for interlaminar tension and double-notch shear.

DISTRIBUTION STATEMENT A.
Approved for public release: distribution is unlimited.



(a) Glass-Transition Temperature from DMA



(b) Exothermic Reaction from DSC

Figure 106. Thermal analysis of EPC for IM7/5320-1 UNI.

DISTRIBUTION STATEMENT A.
Approved for public release: distribution is unlimited.

In general, a small increase in the mechanical properties can be observed in the CFRP because the extended post-cure reactivates the molecular mobility of partially cured polymeric chains, thereby causing an increase in cross-link density in the material structure and consequently increasing the glass-transition temperature, as previously seen in Figure 106. Further application of heat after attaining full cure could decrease the mechanical properties due to matrix deterioration followed by weakening of the fiber-matrix interface.

Table 25 shows an overall comparison between the baseline and 100-hour EPC for quasi-static and residual strength data. Every case indicated a decrease in strength due to the 100-hour EPC, especially for ILT specimens.

Table 25 – Comparison of Baseline and EPC for strength data.

Material	Test Method	Stress Ratio	Baseline	100hr EPC	Change (ksi)	Change (%)
IM7/5320-1 UNI	OHC - Static Strength	—	42.09	39.33	2.76	–6.6
	OHC-C - Residual Strength	5	40.28	38.18	2.10	–5.2
	OHC-T - Residual Strength	–1	38.75	35.85	2.90	–7.5
	ILT - Static Strength	—	11.81	8.42	3.39	–28.7
	ILT - Residual Strength	0.1	10.26	7.99	2.28	–22.2
	DNS - Static Strength	—	3.16	2.99	0.17	–5.5
	DNS - Residual Strength	0.1	2.87	2.56	0.31	–10.8
IM7/5250-4 UNI	OHC - Static Strength	—	41.53	40.20	1.33	–3.21
	OHC-C - Residual Strength	5	42.38	38.86	3.52	–8.31
	OHC-T Residual Strength	–1	38.55	35.99	2.56	–6.64
	ILT - Static Strength	—	10.99	8.83	2.16	–19.69
	ILT - Residual Strength	0.1	9.90	8.38	1.52	–15.34
	DNS - Static Strength	—	3.35	3.16	0.20	–5.87
	DNS - Residual Strength	0.1	3.16	3.02	0.14	–4.29

Figure 107 compares quasi-static, fatigue (R = 5), and residual strength test data collected at multiple EPC cycles with batch 3 baseline cure data for IM7/5320-1 open-hole specimens. The OHC quasi-static and residual strength data showed a small decrease in strength with increasing EPC duration (less than 10 percent even for a 100-hour EPC). Although the highest stress level and residual strength data indicated a small degradation as the EPC is increased, overall fatigue results were within the scatter band of baseline specimens. Figure 108 extends the comparison for stress ratios of R = 5 and R = –1 data along with residual strength data points. Similar to R = 5 data, R = –1 residual stregth data indicated wearout as the EPC is increased, but overall EPC fatigue data are within the scatter band of the baseline fatigue data.

DISTRIBUTION STATEMENT A.
Approved for public release: distribution is unlimited.



Figure 107. Baseline and EPC SN data for IM7/5320-1 UNI, R = 5, OHC-C.

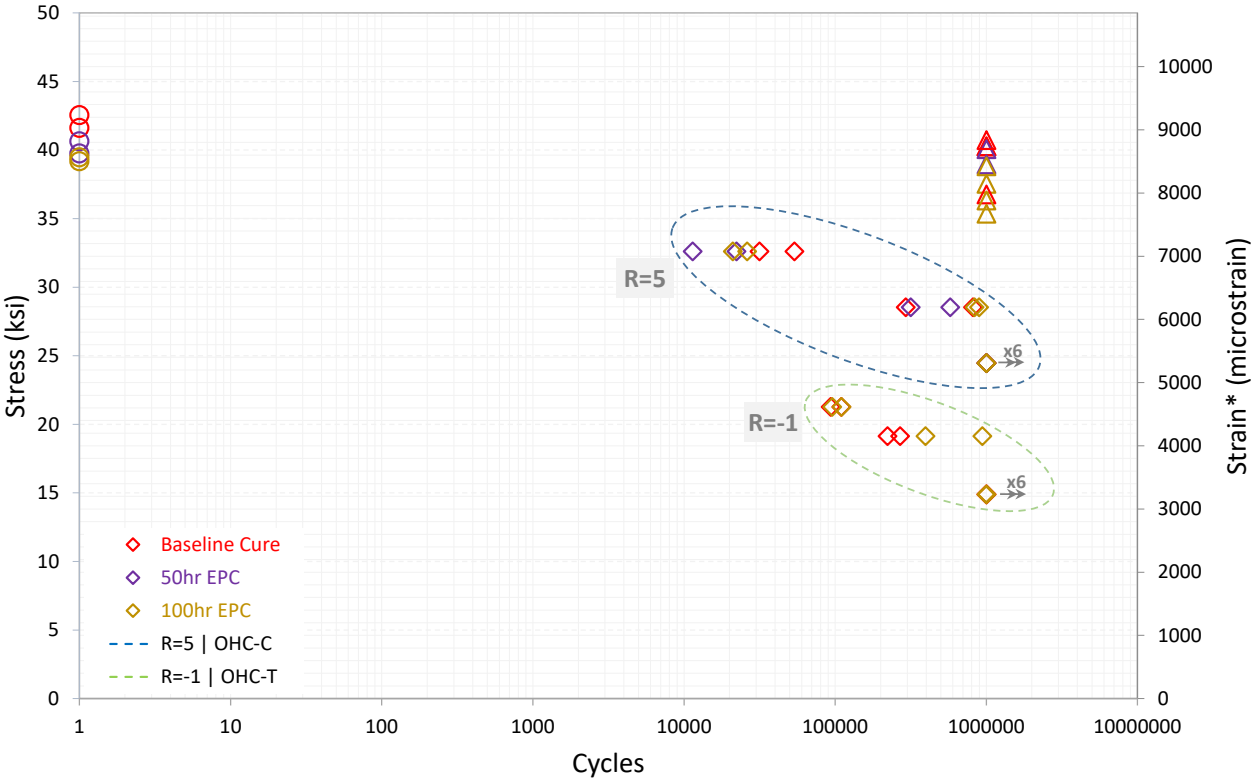


Figure 108. Baseline and EPC SN data for IM7/5320-1 UNI OH.

DISTRIBUTION STATEMENT A.
Approved for public release: distribution is unlimited.

Figure 109 shows baseline and EPC SN data for IM7/5250-4 open-hole test specimens. This comparison includes both R = 5 and R = –1 stress ratios. Similar to the observations for IM7/5320-1 OH specimens, the quasi-static strength and residual strength indicate a small decrease as the EPC is increased, but fatigue data are within the scatter band of baseline test data.

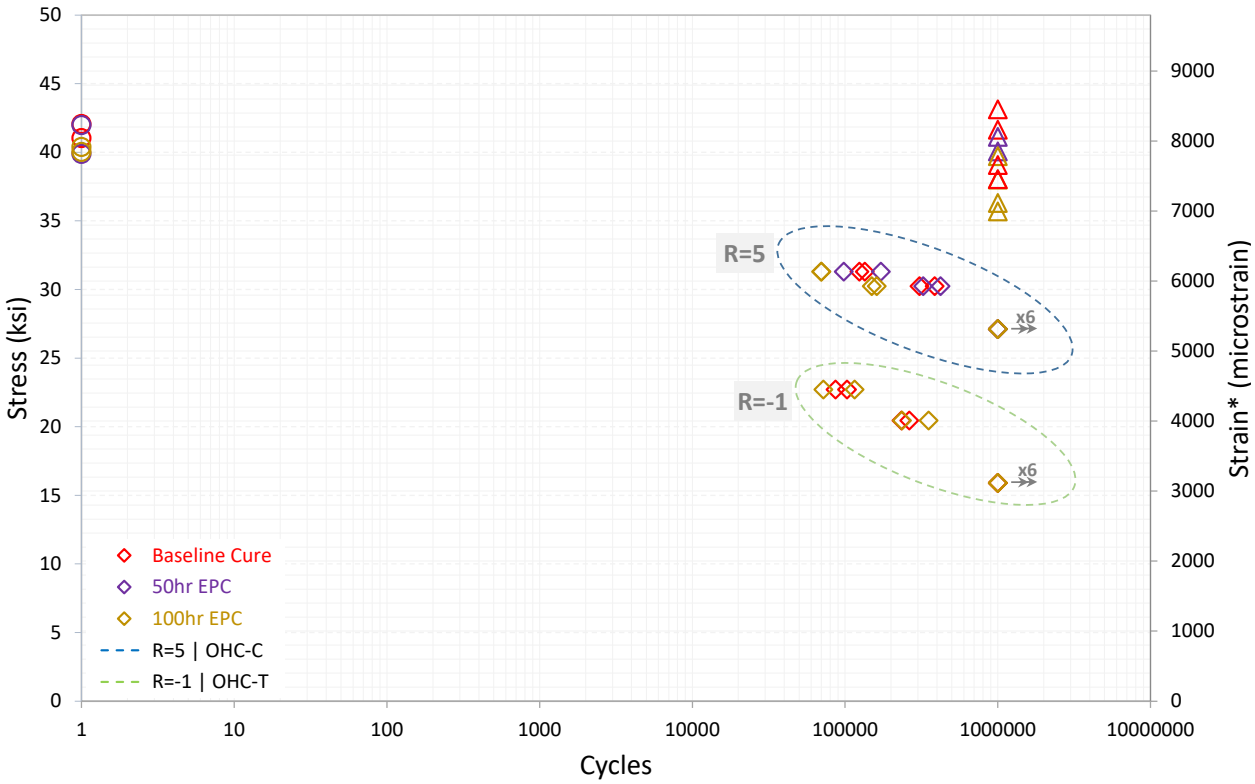


Figure 109. Baseline and EPC SN data for IM7/5250-4 UNI OHC.

Figures 111 and 112 show comparisons of baseline and EPC for IM7/5320-1 and IM7/5250-4 UNI double-notch specimens, respectively. Similar to the OH specimens, quasi-static and residual strength indicated a minor decrease, but fatigue data indicated no significant effects due to the EPC. Therefore, the in-plane failure modes (OH and DNS) had no significant effects due to the EPC.

Unlike OH or DNS specimens, the interlaminar tension failure mode for both IM7/5320-1 and IM7/5250-4 material systems indicated a significant reduction in strength and fatigue life due to the EPC. IM7/5320-1 quasi-static strength after the 100-hour EPC was decreased by about 30 percent (Figure 112), while this was about 20 percent for IM7/5250-4 (Figure 113). Fatigue life for most cases, except for an intermediate stress level of IM7/5250-4, was significantly decreased. Residual strength data for both material systems indicated 15 to 20 percent reduction due to the EPC. These observations indicate that ILT strength, which is a matrix-dominant out-of-plane failure mode, is clearly affected by the EPC.

DISTRIBUTION STATEMENT A.
Approved for public release: distribution is unlimited.

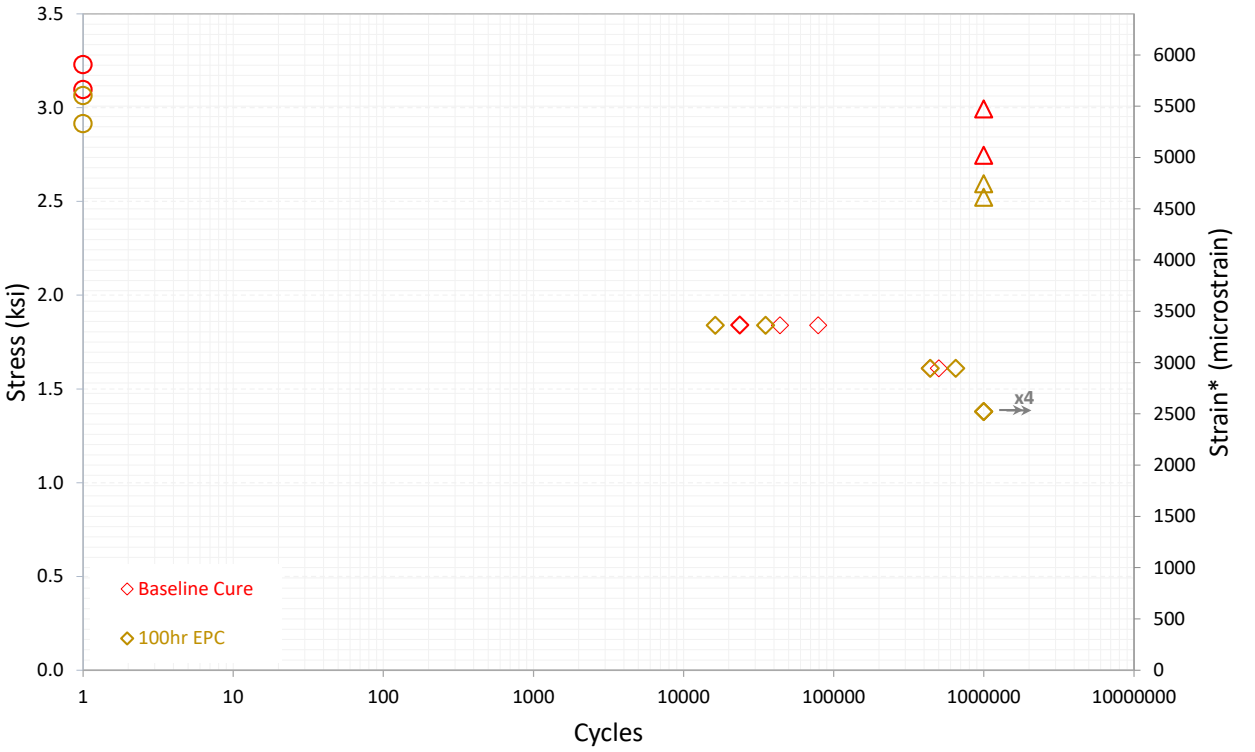


Figure 110. Baseline and EPC SN data for IM7/5320-1 UNI DNS.

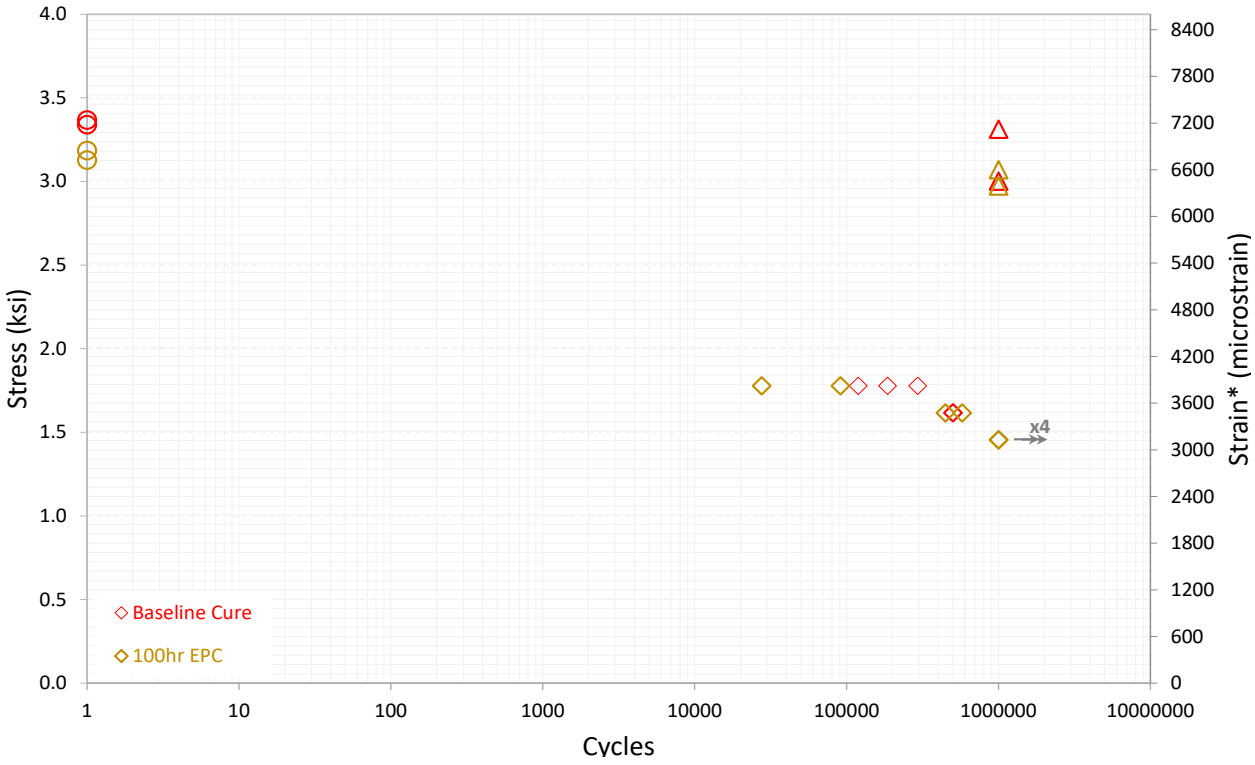


Figure 111. Baseline and EPC SN data for IM7/5250-4 UNI DNS.

DISTRIBUTION STATEMENT A.
Approved for public release: distribution is unlimited.

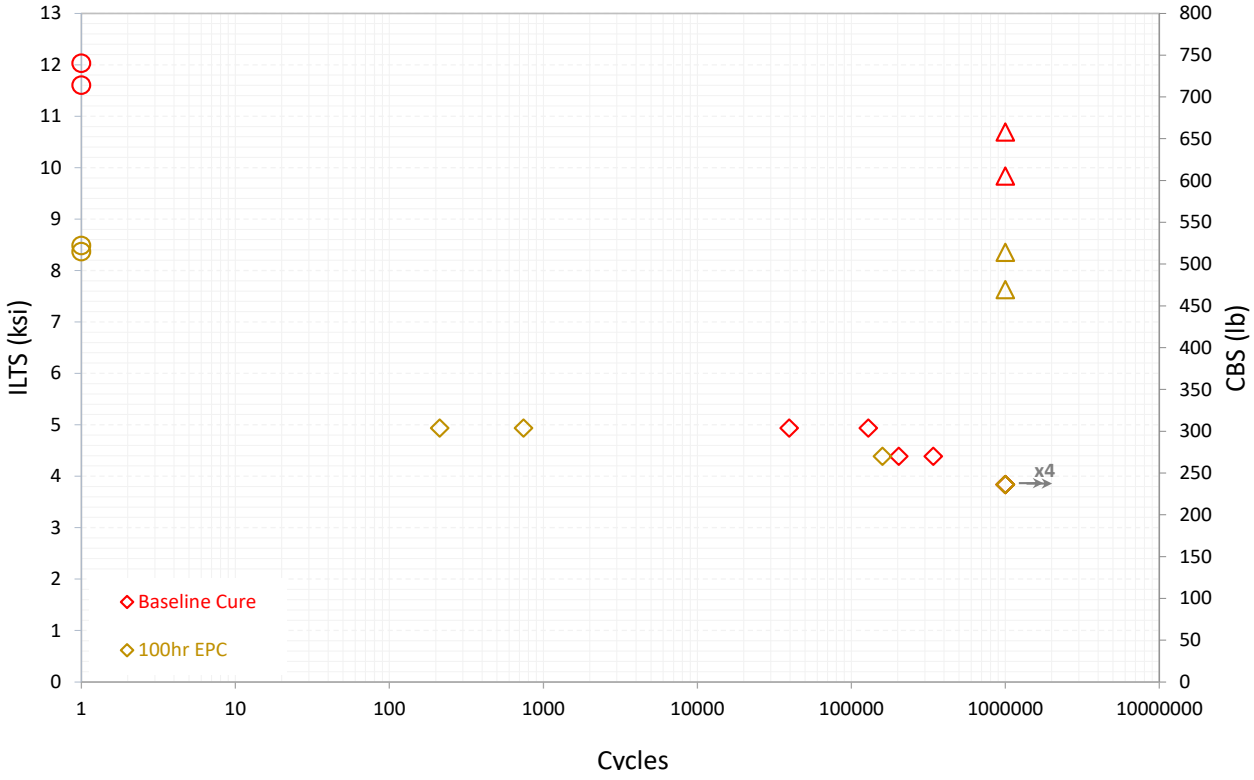


Figure 112. Baseline and EPC SN data for IM7/5320-1 UNI ILT.

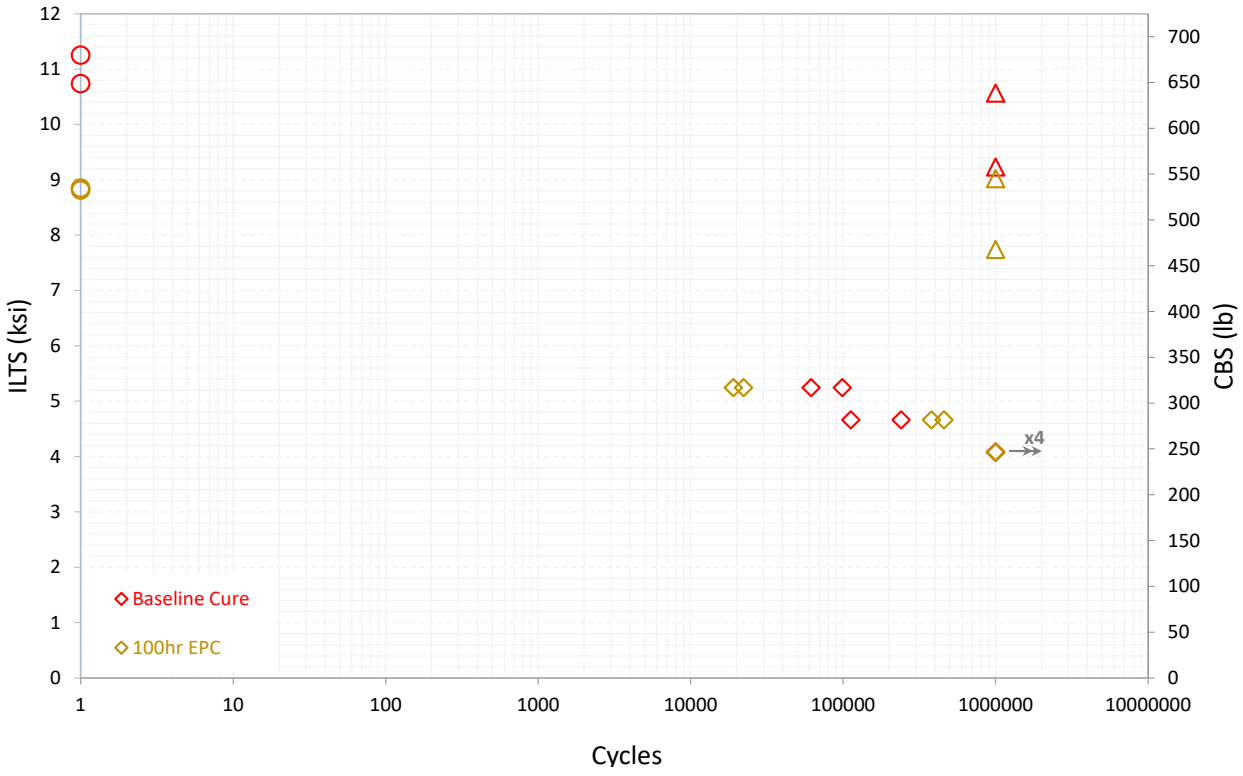


Figure 113. Baseline and extended post-cure SN data for IM7/5250-4 UNI ILT.

DISTRIBUTION STATEMENT A.
Approved for public release: distribution is unlimited.

7.6 Damage Growth under Open-Hole Tension-Tension Fatigue

Tension-tension fatigue specimens (R = 0.1) for hard and quasi-isotropic laminates survived a million cycles (runout condition) at stress levels as high as 90 percent of the quasi-static average value. Although these specimens did not indicate two-part failures, apparent stiffness degradation monitored using the slope of the load-displacement curve throughout the fatigue testing indicated a gradual fatigue wearout, especially at high stress levels. Nevertheless, the residual strength values for all cases were significantly higher than the corresponding quasi-static strength value. Quasi-static strength of pristine composite is notch sensitive.

In addition to apparent stiffness degradation, XCT high-fidelity inspections were performed at several fatigue intervals in order to monitor the progressive damage growth. XCT showed microcracks around the hole at low stress levels and significant delaminations at high stress levels.

7.6.1 IM7/5320-1 UNI OHT-T

Figure 114 shows the tension-tension fatigue tests conducted at 60, 70, 80, and 90 percent of quasi-static average strength for IM7/5320-1 UNI. Results indicated no apparent (two-part) fatigue failures, with an average increase in strength of 26 percent.

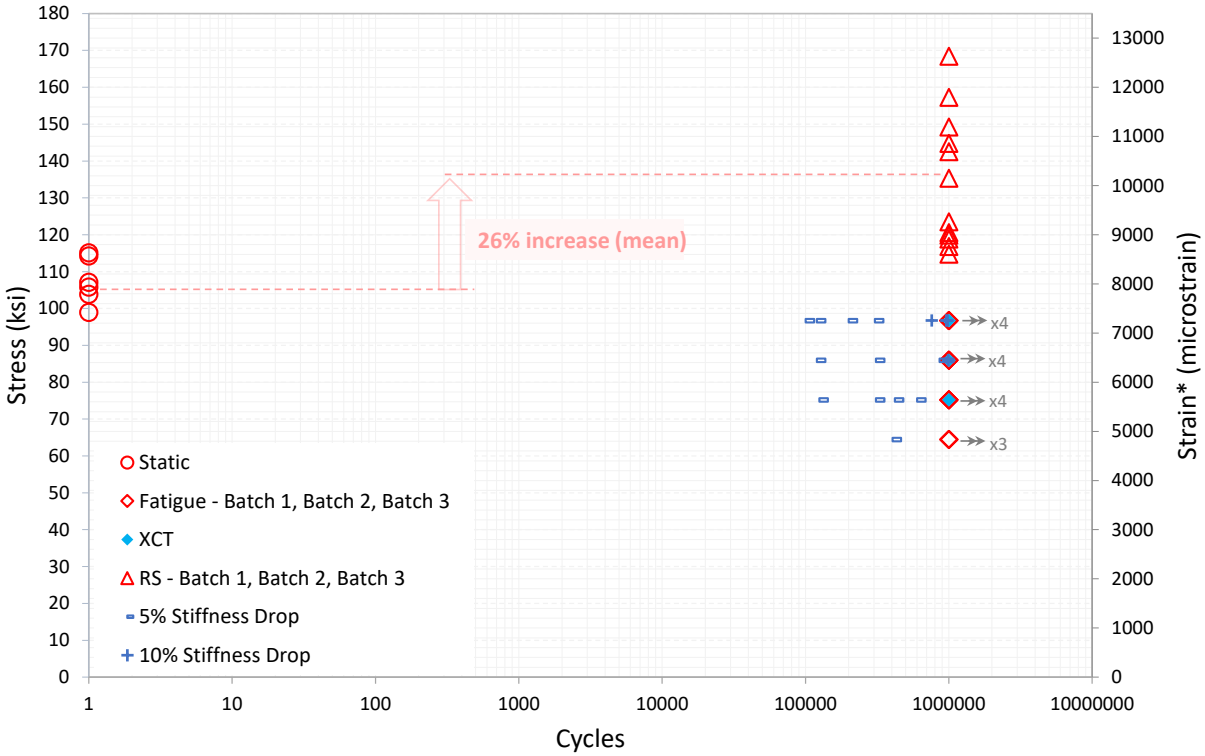


Figure 114. OHT-T SN data for IM7/5320-1 UNI, 50/40/10.

Figure 115 shows the apparent stiffness degradation of a representative IM7/5320-1 UNI fatigue test specimen for 60, 70, 80, and 90 percent fatigue stress levels. Specimens from the lower

DISTRIBUTION STATEMENT A.
Approved for public release: distribution is unlimited.

stress level (SL1 60% of quasi-static strength) showed less than a 5 percent stiffness drop at one million cycles, except for one specimen that had a 5 percent stiffness drop as early as 405,000 cycles. These SL1 specimens also showed almost no delamination as well as the smallest increase in residual strength after runout, an average increase of 9.2 percent. SL2 (70%) specimens showed a stiffness drop of 5 to 10 percent; a 5 percent decrease was noted as early as 125,000 cycles and as late as 600,000 cycles. At this stress level, small delaminations in the vicinity of hole could be observed. The resulting residual strength increase for SL2 was an average of 12.5 percent, with minimal damage at runout. SL3 (80%) began to show 10 percent stiffness degradation by 990,000 cycles as well as a moderate amount of delamination, resulting in an average residual strength increase of 38.4 percent. Finally, SL4 (90%) specimens showed 5 percent stiffness degradation as early as 120,000 cycles and 10 percent degradation as early as 760,000 cycles.

Although the stiffness degradation data indicated fatigue wearout, Figure 116 shows an increase in residual strength after one million cycles, which is as much as 42 percent for some cases, and it is proportional to the fatigue stress level. The microcrack formation at low stress levels can reduce the stress concentration near the hole, which may increase the residual strength of OH specimens after fatigue. The large delaminations at higher stress levels should significantly reduce the residual strength, but the observations shown in Figure 116 are counterintuitive. In order to investigate the reason for the increase in residual strength as a function of the fatigue stress level, a thorough failure analysis was conducted using high-fidelity inspections.

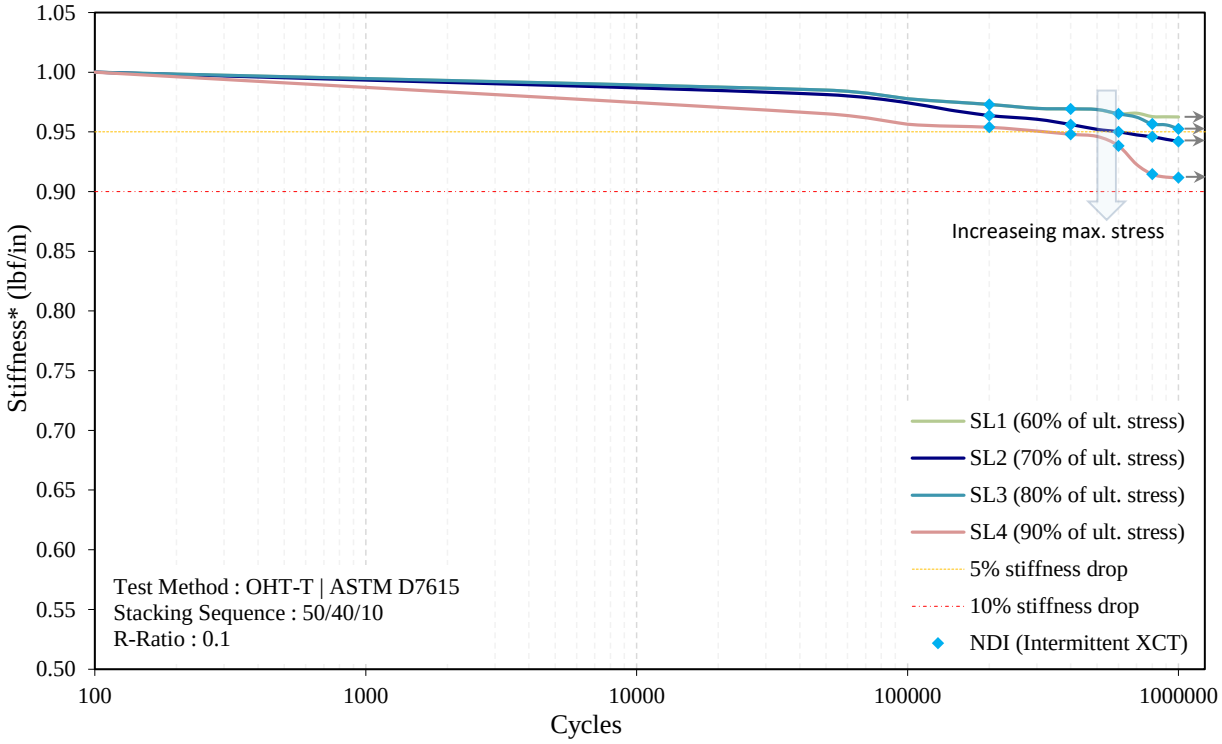


Figure 115. OHT-T stiffness degradation (normalized) for IM7/5320-1 UNI, 50/40/10.

DISTRIBUTION STATEMENT A.
Approved for public release: distribution is unlimited.

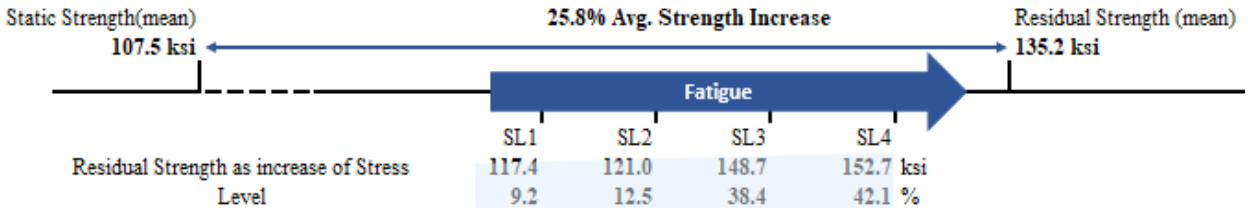
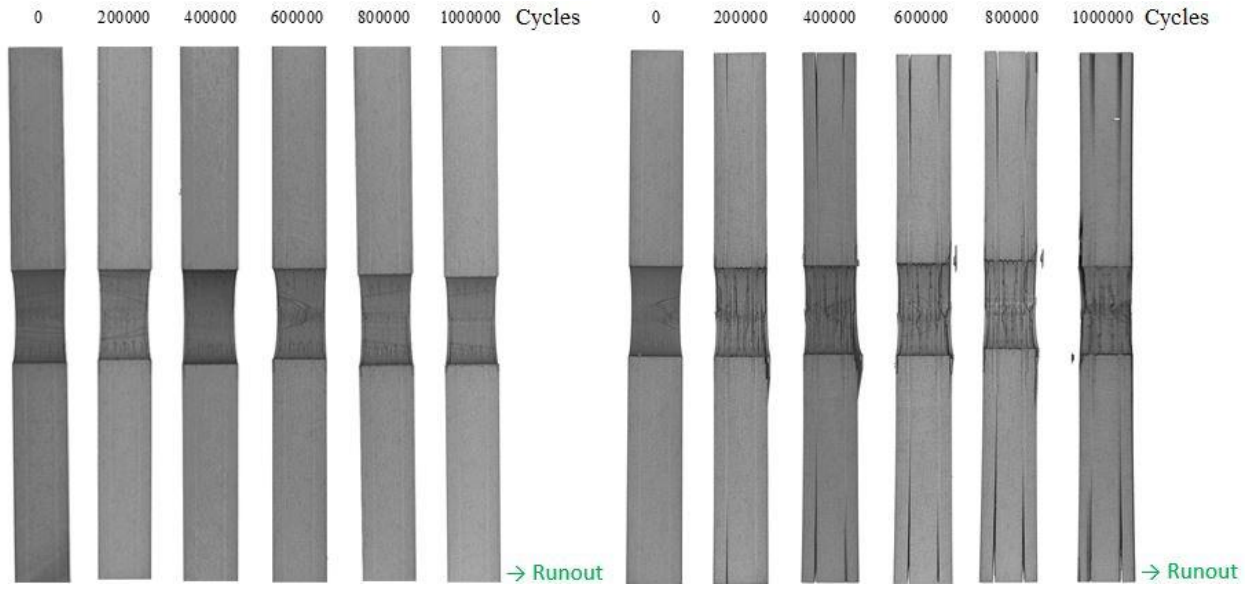


Figure 116. OHT-T residual strength increase for IM7/5320-1 UNI, 50/40/10.

Figure 117 shows that the SL2 specimen virtually had no damage (only localized microcracks around the hole), while the SL4 specimen had significant delaminations as the fatigue cycles progressed. Figure 118 shows a detailed failure analysis of XCT images, indicating that initial delaminations were observed in interfaces of the outermost plies (mostly off-axes).



(a) SL2 (70%) (b) SL4 (90%)

Figure 117. XCT damage indications near hole for IM7/5320-1 UNI, 50/40/10.

At around 400,000 cycles, the inner off-axes plies started developing significant microcracks, followed by delaminations that resulted in separating the specimen into three parts, which were still held by off-axes plies. Further examination of ply-by-ply XCT data indicates that fiber splitting in the 0° plies sections them into columns that run parallel to the fiber direction, thus making them independent of each other. This fiber splitting typically starts tangential to the hole and propagates toward the end of the test specimen, as shown in Figure 119(a), separating the middle column that includes the hole from the rest of the specimen. Column 1, which includes the hole, has no continuous fibers. However, columns 1 and 3 have continuous fibers, dividing the remainder of the 0° ply into two unnotched specimens. Typically, at this stage, off-axes plies (45° and 90°) also have developed fiber splitting, resulting in no continuous fibers in those plies. At high stress levels where delaminations are prominent, the specimen also separates into layers,

DISTRIBUTION STATEMENT A.
Approved for public release: distribution is unlimited.

as shown in Figure 119(b), across off-axes plies since they have significant microcracks and intralaminar cracks.

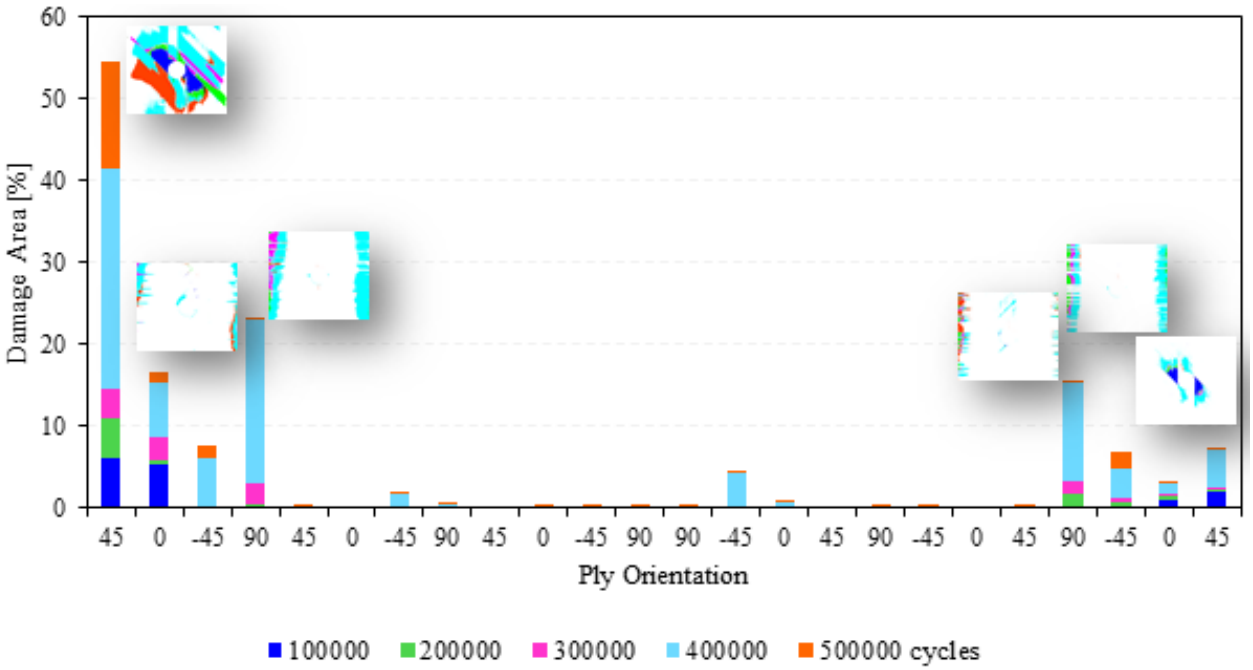
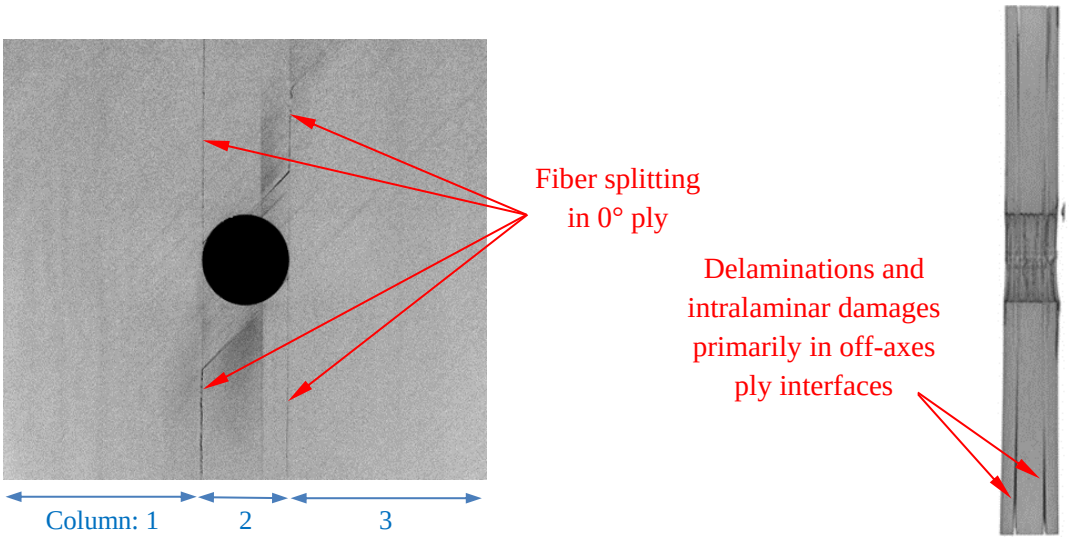


Figure 118. OHT-T fatigue damage increase for IM7/5320-1 UNI, 50/40/10, SL4.



(a) In-Plane Fiber Splitting (b) Delaminations

Figure 119. Fiber splitting in 0° ply and delaminations near off-axes plies.

The stress concentration factor (K_t), which is the ratio of maximum stress near a circular hole to the far-field applied stress, for an anisotropic material is given by

DISTRIBUTION STATEMENT A.
Approved for public release: distribution is unlimited.

$$K_t = \frac{\sigma_{max}}{\sigma_{app}} = 1 + \sqrt{2 \cdot \left[\sqrt{\frac{E_X}{E_y}} - \nu_{xy}\right] + \frac{E_x}{G_{xy}}} \quad (16)$$

Where E_x and E_y are the Young's moduli in the longitudinal and transverse directions, respectively, ν_{xy} is the Poisson's ratio in the x–y plane, and G_{xy} is the in-plane shear modulus. When microcracks are formed near the hole under fatigue loading, the localized softening redistributes the stress around the hole away from it. Analogous to the plastic zone created near holes in metals, this reduces the stress concentration around the hole, in turn greatly reducing the notch sensitivity. This is also evident in the diminishing fatigue notch sensitivity, as shown previously in Figure 14. Since fibers carry the majority of loads, the reduced stress concentration prolongs the failure of tension-tension fatigue loading. In addition, the residual strength of runout specimens is increased for hard and quasi-isotropic laminates, but not for soft laminates. The increase in residual strength was proportional to the percentage of 0^o plies.

Intermittent XCT inspections of low stress levels that only had microcracks indicated about 12 percent increase in residual strength, which can be attributed to the localized softening due to microcracks around the hole. However, this does not explain the continued increase of the residual strength at higher stress levels, which exhibited large delaminations after a million cycles.

Since the off-axes plies have significant damage, their load-carrying capacity at this stage is minimal or negligible. Therefore, these failure mechanics make the fibers in columns 1 and 3 of 0° plies the primary load-carrying members for tension loads. However, since hole presence is no longer influencing the stress concentration, the remainder of the 0° plies (columns 1 and 3) function as unnotched specimens. As shown previously in Figure 14, the unnotched quasi-static strength can be as much as twice the notched strength for composites. Therefore, the failure strength of the net section assuming that only 0° has a load-carrying capacity and there is uniform stress distribution across the net section (columns 1 and 3) due to the diminished notched sensitivity, the strength of the load-carrying portion of the 0° can be expressed as:

$$\sigma_{Net} = \left[\sigma^{tu} \cdot \left(1 - \frac{D}{W}\right)\right] \cdot P \quad (17)$$

where σ^{tu} is the ultimate 0° tensile strength of the material, D is the hole diameter (=0.25 inch), W is the specimen width (=1.5 inch), and P is the percentage of 0° plies in the laminate (P = 0.5). For IM7/5320-1 UNI, the ultimate tensile strength is 315.91 ksi [36]. This results in a strength value of 131.63 ksi, which is about 22 percent higher than the quasi-static strength. Assuming the contribution from off-axes fibers and using the sizing chart shown in Figure 120, the factor P corresponding to 50/40/10 is 0.6. This results in a net strength of 157.96 ksi, which is closer to the average residual strength of SL4 after a million cycles (152.7 ksi). Figure 117 shows that these plies are still intact near the hole for SL4 (90%); therefore, this assumption is justified. The 3 percent difference between σ_{Net} and residual strength of SL4 specimen after million cycles

DISTRIBUTION STATEMENT A.
Approved for public release: distribution is unlimited.

may be due to the presence of microcracks in the runout specimens. These observations indicate that the increase in residual strength is primarily due to the diminished notch effects caused by fiber splitting tangential to the hole edges, primarily in the 0° plies.

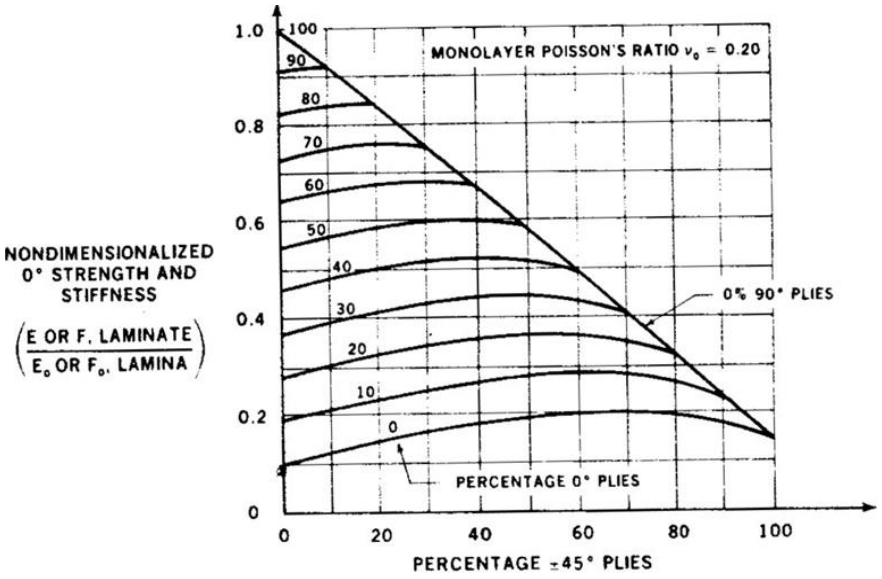


Figure 120. Simple laminate sizing chart [37].

A similar trend was observed for IM7/5320-1 UNI, 25/50/25 residual strength specimens, although the increase in strength as the stress level was increased was less than what was observed for the hard laminate (Figure 121).

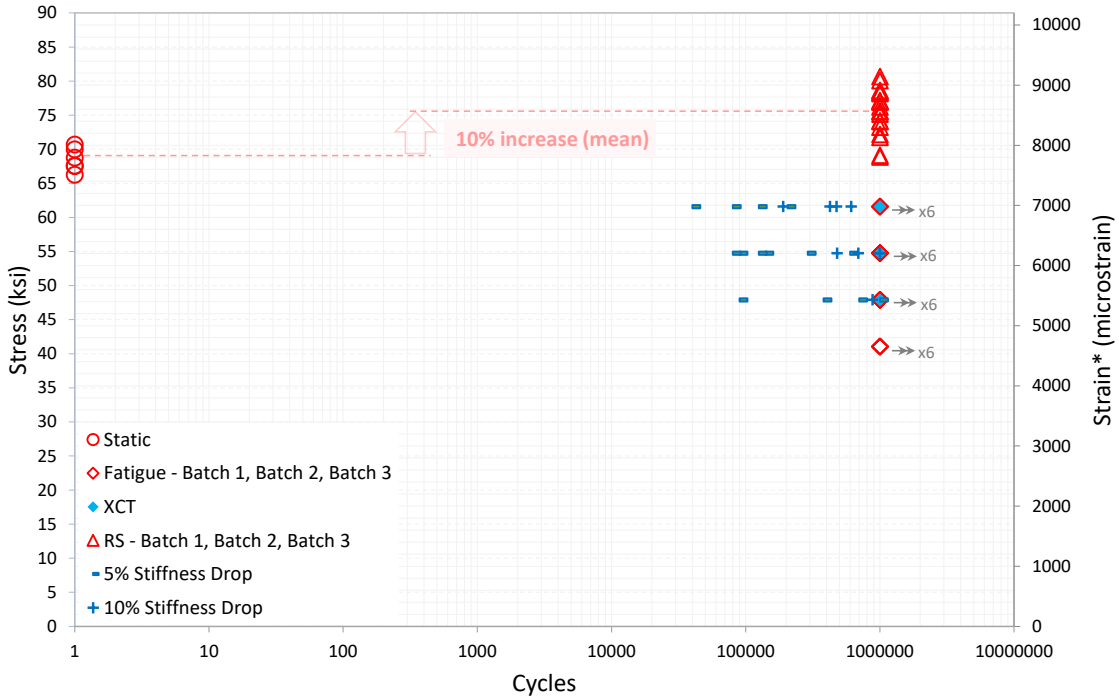


Figure 121. OHT-T SN data for IM7/5320-1 UNI, 25/50/25.

DISTRIBUTION STATEMENT A.
Approved for public release: distribution is unlimited.

Figure 122 shows the stiffness degradation of representative specimens from each stress level. SL1 (60%) specimens showed less than a 5 percent stiffness drop at one million cycles and indicated only microcracks near the hole, with an approximate residual strength increase of 7.2 percent (Figure 123). SL2 (70%) specimens showed a total stiffness drop of 5 to 10 percent (5 percent decrease as early as 90,000 cycles and as late as one million cycles, as well as one specimen that had a 10 percent drop at 880,000 cycles). At this stress level, minor delaminations, especially on the outermost 45° ply interface with 0° ply as early as 200,000 cycles, were observed in XCT inspections (Figure 124). The resulting residual strength increase for SL2 was about 11 percent. SL3 (80%) began to show 5 percent stiffness degradation around 90,000 cycles followed by a 10 percent drop as early as 480,000 cycles. Also, a moderate amount of delamination was observed. The resulting residual strength increase for SL3 was about 13.4 percent. Finally, SL4 (90%) specimens showed 5 percent stiffness degradation as early as 40,000 cycles and 10 percent as early as 190,000 cycles. Specimens in this stress level resulted in significant stiffness degradation and about 17.8 percent increase in residual strength, as shown in Figure 123. The detailed PDA techniques of XCT data for this stress level also show that the delaminations were primarily concentration around the four outermost plies on each side, starting first on the interface between the outermost 45° and 0° plies (Figure 125).

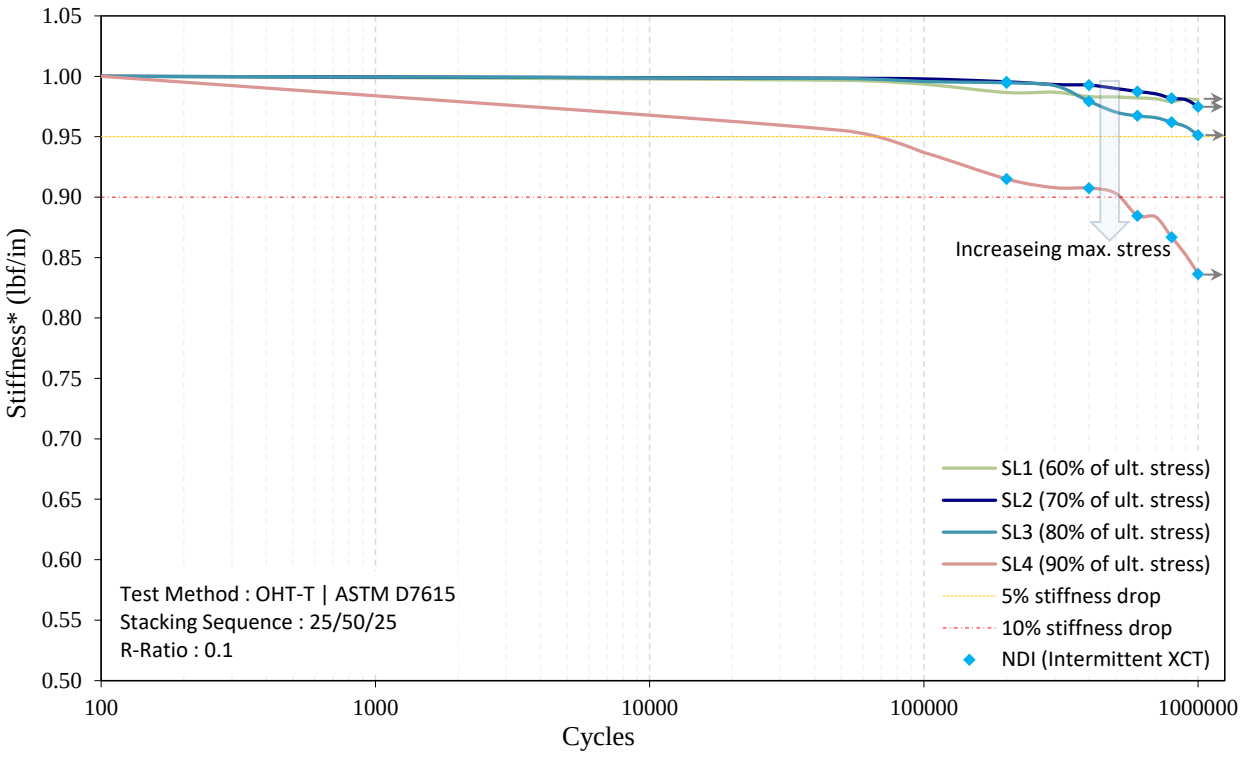


Figure 122. OHT-T stiffness degradation (normalized) for IM7/5320-1 uni, 25/50/25.

DISTRIBUTION STATEMENT A.
Approved for public release: distribution is unlimited.

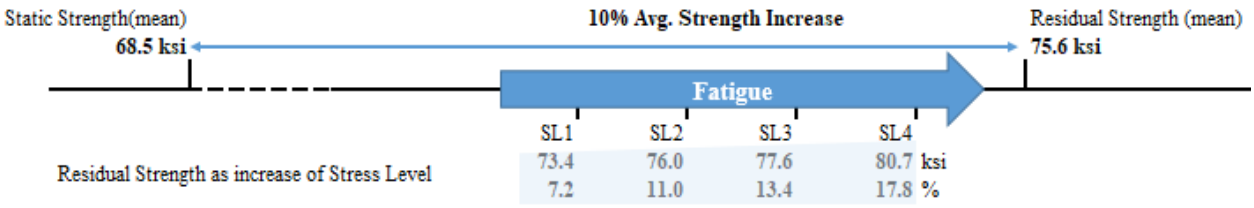
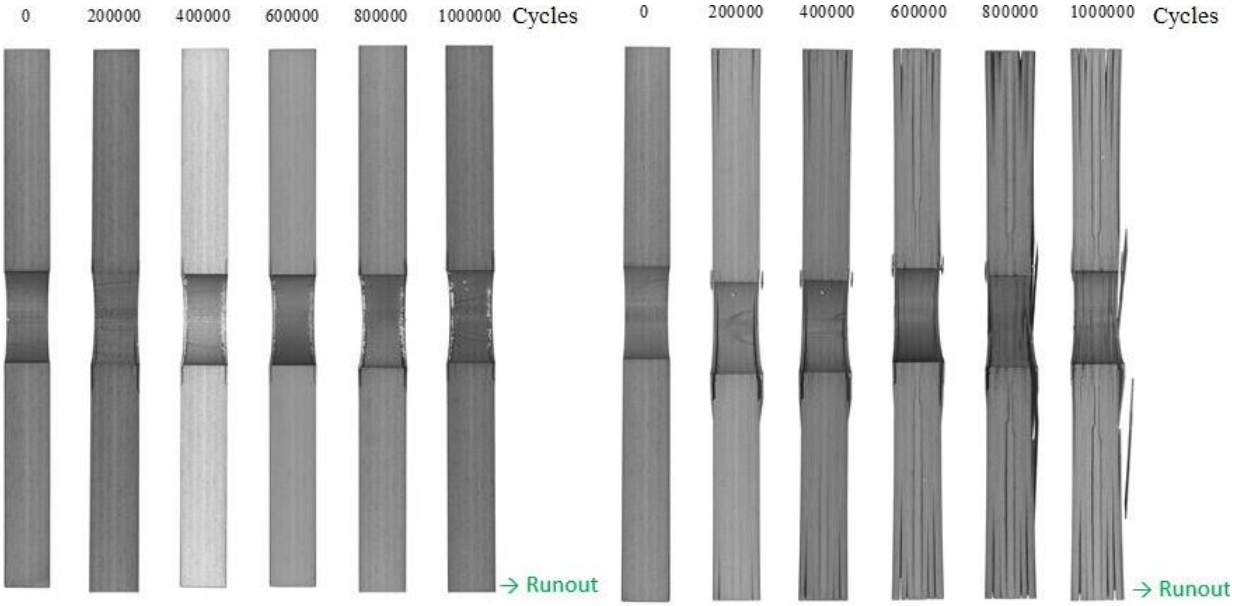


Figure 123. OHT-T residual strength increase for IM7/5320-1 uni, 25/50/25.



(a) SL2 (70%) (b) SL4 (90%)

Figure 124. XCT damage indications near hole for IM7/5320-1 UNI, 25/50/25 OHT-T.

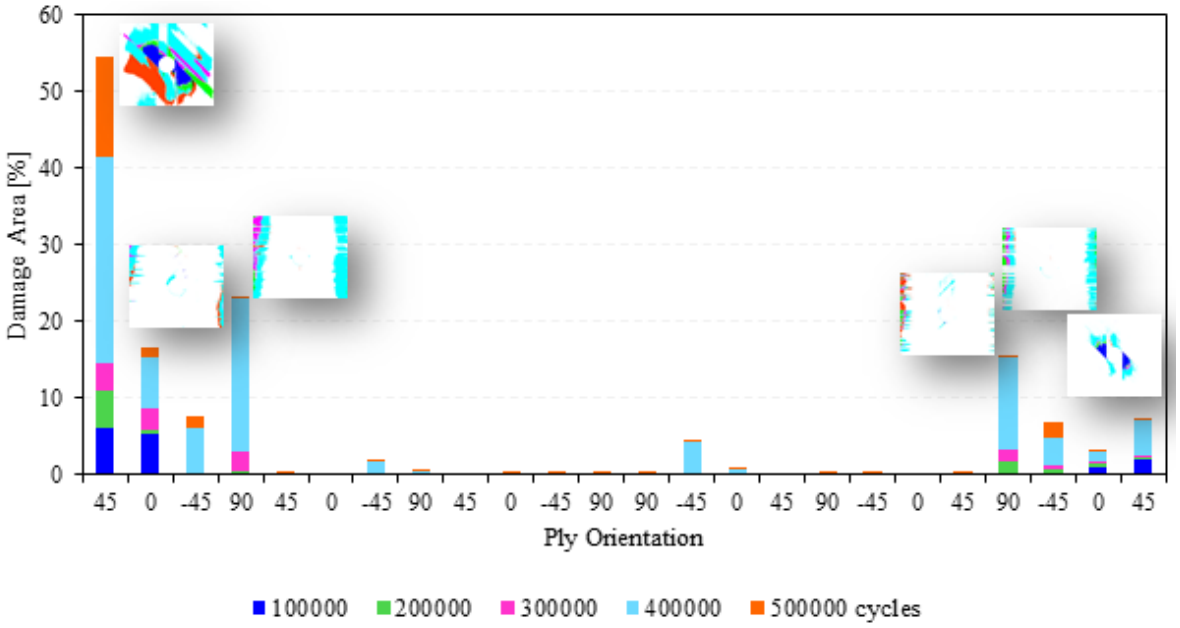


Figure 125. OHT-T fatigue damage increase for IM7/5320-1 UNI, 25/50/25, SL4.

DISTRIBUTION STATEMENT A.
Approved for public release: distribution is unlimited.

Calculation of effective strength based on equation (17) considering the contribution only from 0° plies (P = 0.25) and then considering all plies (Figure 117 ➔ P = 0.4) indicated the residual strength values for the net section without notch effects to be 65.8 and 105.3 ksi, respectively. The average residual strength of IM7/5320-1 UNI quasi-isotropic runouts was 80.7 ksi, which is in between the range.

7.6.2 IM7/5250-4 OHT-T

As shown in Figure 126, IM7/5250-4 UNI indicated an increase in residual strength of runouts, and the magnitude increased as the fatigue stress level increased (same trend as for IM7/53201 UNI). Figure 127 shows the stiffness degradation of representative specimens from each stress level. Figure 128 shows that the residual strength increased about 22.9, 32.1, and 36. 9 percent of quasi-static strength for SL1 (70%), SL2 (80%), and SL3 (90%), respectively.

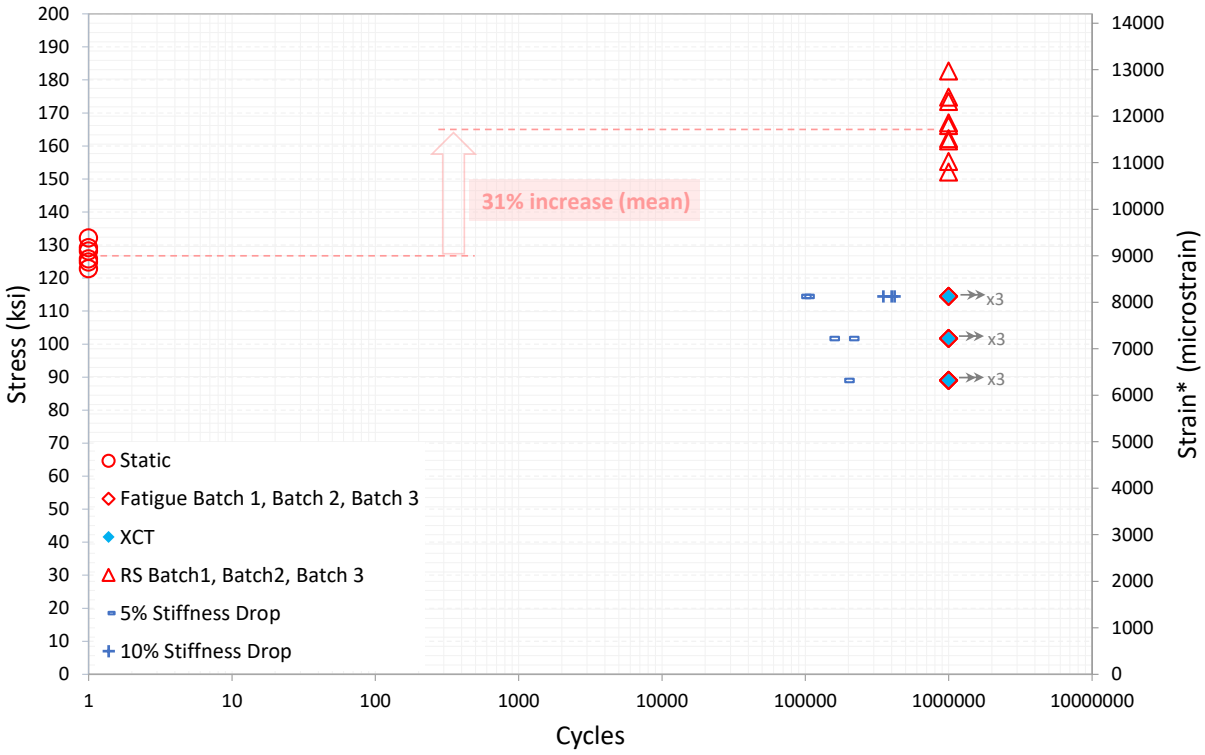


Figure 126. OHT-T SN data for IM7/5250-4 UNI, 50/40/10.

DISTRIBUTION STATEMENT A.
Approved for public release: distribution is unlimited.

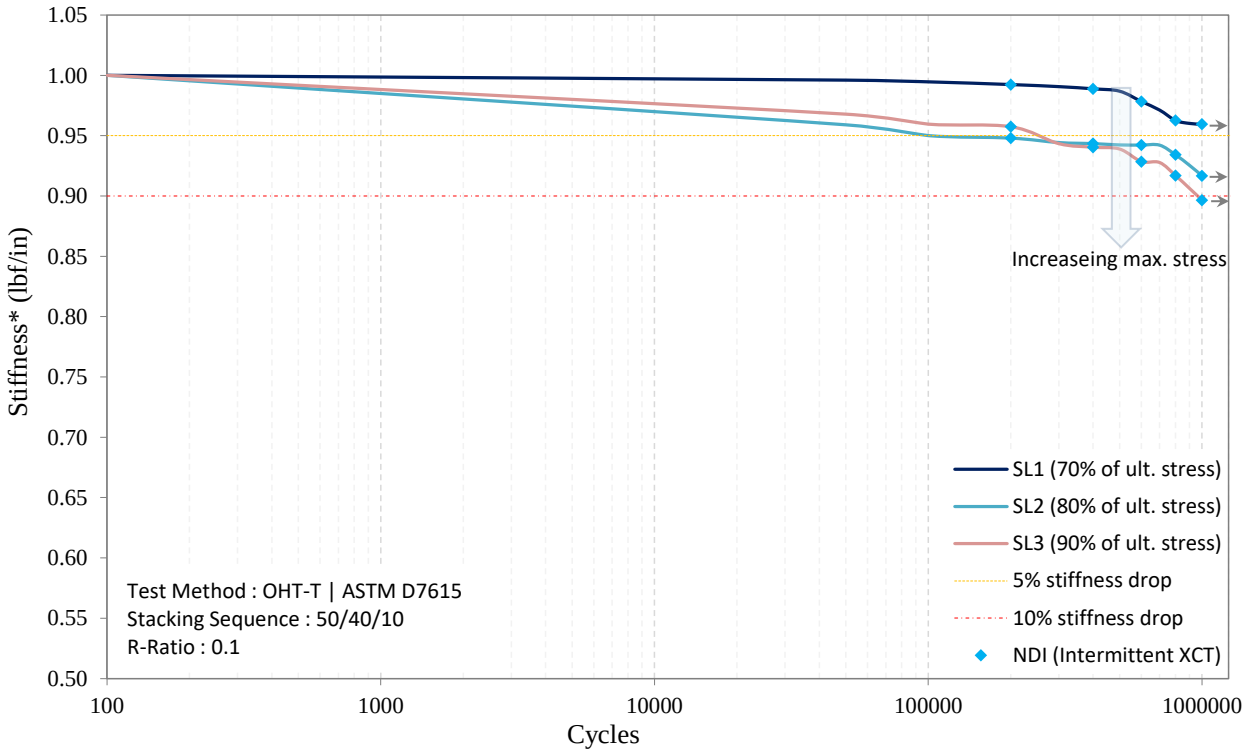


Figure 127. OHT-T stiffness degradation (normalized) for IM7/5250-4 UNI, 50/40/10.

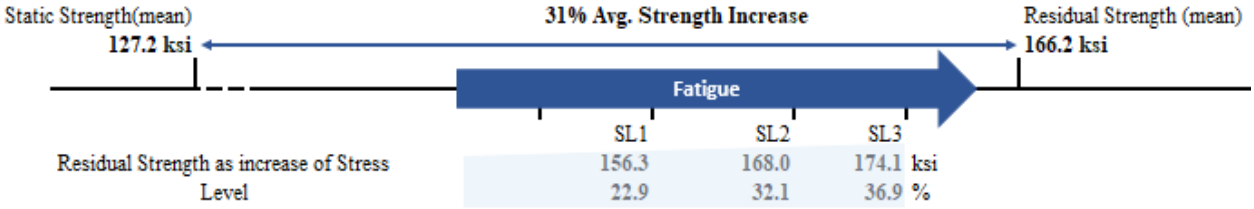
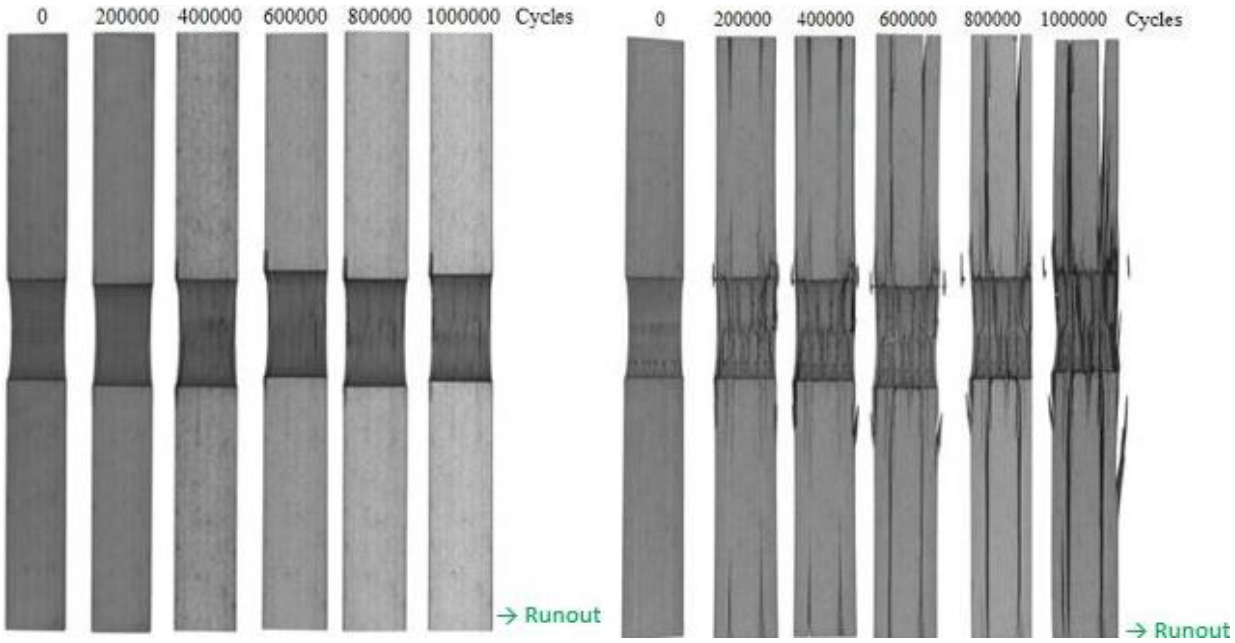


Figure 128. OHT-T residual strength increase for IM7/5250-4 UNI, 50/40/10.

SL1 (70%) specimens showed less than a 5 percent stiffness drop at one million cycles and indicated only microcracks and minor delaminations (outermost ply) near the hole as seen in Figure 129(a). These specimens also resulted in an average residual strength increase of 22.9 percent. SL3 (90%) showed a stiffness drop of 5 percent as early as 100,000 cycles and had large amounts of delaminations, as shown in Figure 129(b). SL3 (90%) specimens also showed the highest increase in residual strength, which is about 36.9 percent for runouts.

DISTRIBUTION STATEMENT A.
Approved for public release: distribution is unlimited.



(a) SL1 (70%) (b) SL3 (90%)

Figure 129. XCT damage indications near hole for IM7/5250-4 UNI, 50/40/10 OHT-T.

The detailed analysis of XCT data shown in Figure 130 indicates that the delaminations started near the outermost 45° interface around 200,000 cycles. As the fatigue cycles progressed towards 600,000 cycles, the interior 45° and 90° interfaces developed delaminations. The microcracks and intralaminar cracks in these off-axes plies coalesced and propagated towards the interfaces and initiated delaminations. Fiber splitting is also evident in these off-axes plies in some cases terminated at the 0° fiber splits, indicating a crack-arrest mechanism.

Calculation of effective strength based on equation (17) with ultimate tensile strength of 308 ksi [38] considering the contribution only from 0° plies (P = 0.5) and then considering all plies (Figure 117 ➔ P = 0.6) indicates residual strength values for the net section without notch effects to be 128.3 and 154.0 ksi, respectively. The average residual strength of IM7/5250-4 UNI quasi-isotropic runouts was 174.1 ksi, which is higher than both values obtained using equation (17).

DISTRIBUTION STATEMENT A.
Approved for public release: distribution is unlimited.

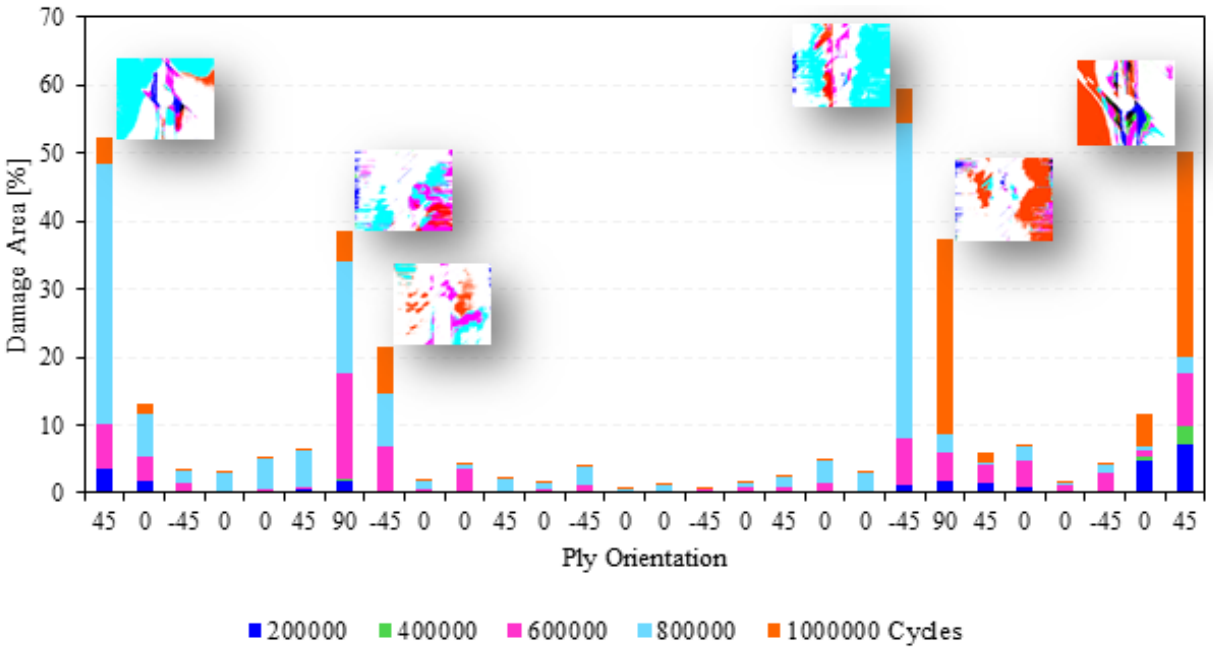


Figure 130. OHT-T fatigue damage increase for IM7/5250-4 UNI, 50/40/10, SL3.

A similar trend of increased residual strength was also observed for quasi-isotropic layup tension-tension OH fatigue specimens (Figure 131). Similar to the case for IM7/5320-1 UNI, the increase in residual strength was less than the increase for hard layup, as shown in Figure 126. Quasi-isotropic specimens had less delaminations than that observed for hard laminate runouts. Thus, notch sensitivity was still present and causing a reduction in residual strength compared to hard laminates, but still higher than the quasi-static strength.

Figure 132 shows the aparent stiffness degradation of a representative specimen from each stress level. SL1 (70%) specimens had a stiffness drop of approximately 5 percent and localized microcracks around the hole, while SL2 (80%) had a stiffness drop of about 10 percent as early as 100,000 cycles with delaminations compared to SL1. SL3 (90%) specimens had a combination of failure and runout. The SL3 runout specimens had more delamination and stiffness degradation than any other specimens, and an approximately 5 percent stiffnesss drop was noted as early as 38,000 cycles and a 10 percent drop around 160,000 cycles.

Figure 133 shows that the highest increase in residual strength (10.3 percent) was for SL2. Overall this increase was less than what was observed for IM7/5250-4 UNI hard laminates. A large amount of delamination observed in SL3 specimens (Figure 134) may have resulted the smallest increase in residual strength. Unlike 50/40/10 specimens, 25/50/25 specimens saw a larger amount of lateral crack development, especially for SL3 (90%). These cracks likely contributed to the failure of several specimens at SL3 and the significant decrease in residual strength compared to runouts from the other two stress levels. Detailed analysis of XCT data shows that delamination was predominantly on the outermost off-axes plies, similar to the observation in IM7/5320-1 UNI (Figure 135).

DISTRIBUTION STATEMENT A.
Approved for public release: distribution is unlimited.

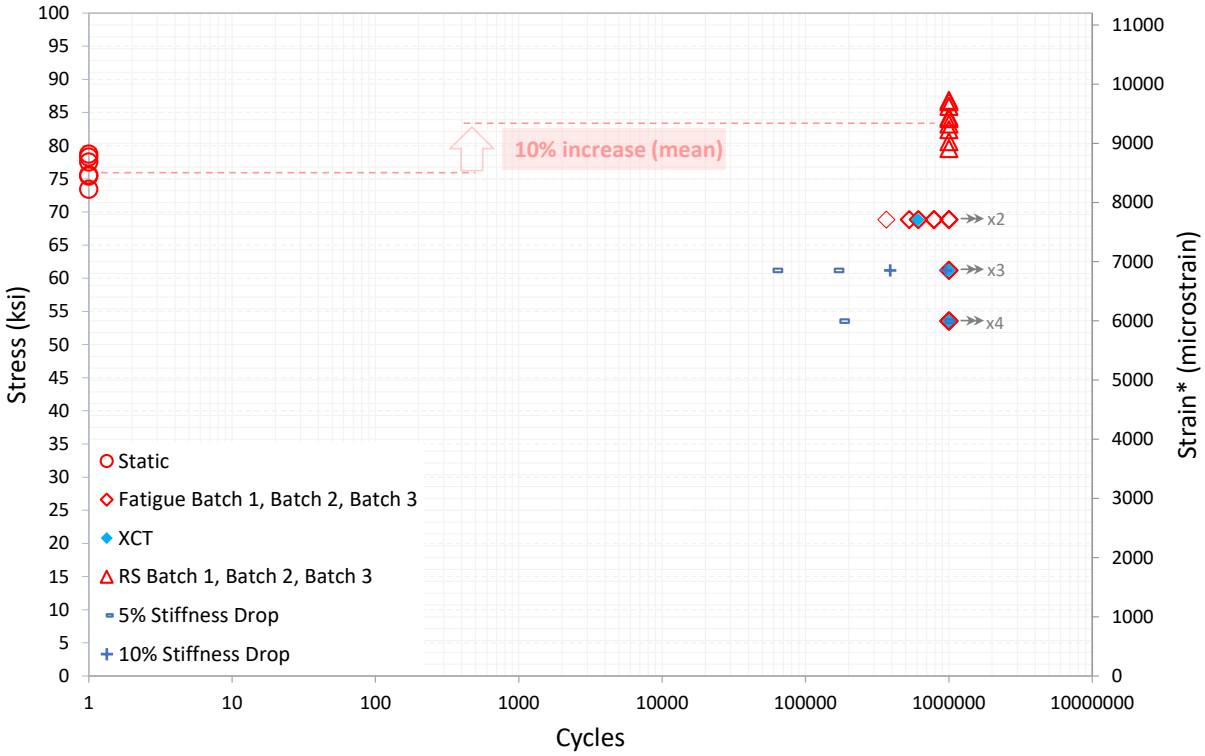


Figure 131. OHT-T SN data for IM7/5250-4 UNI, 25/50/25.

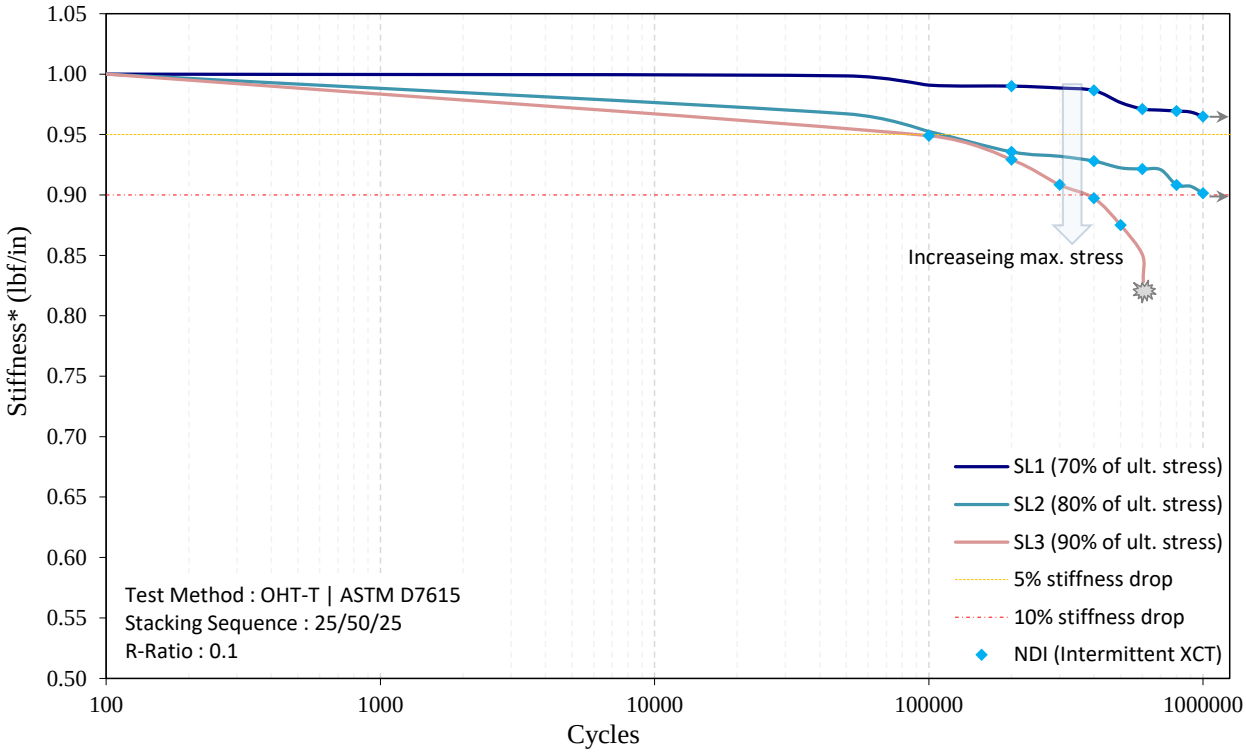


Figure 132. OHT-T stiffness degradation (normalized) for IM7/5250-4 UNI, 25/50/25.

DISTRIBUTION STATEMENT A.
Approved for public release: distribution is unlimited.

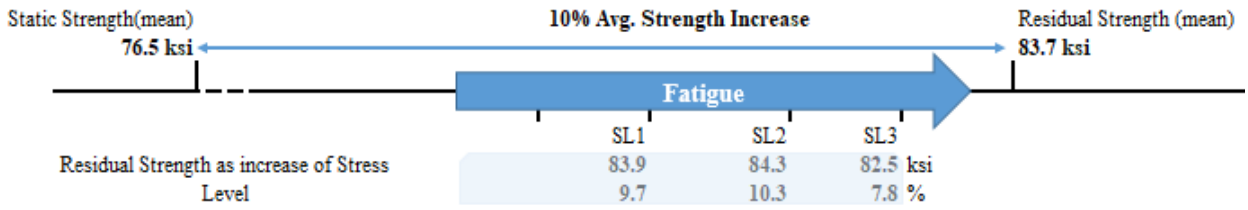
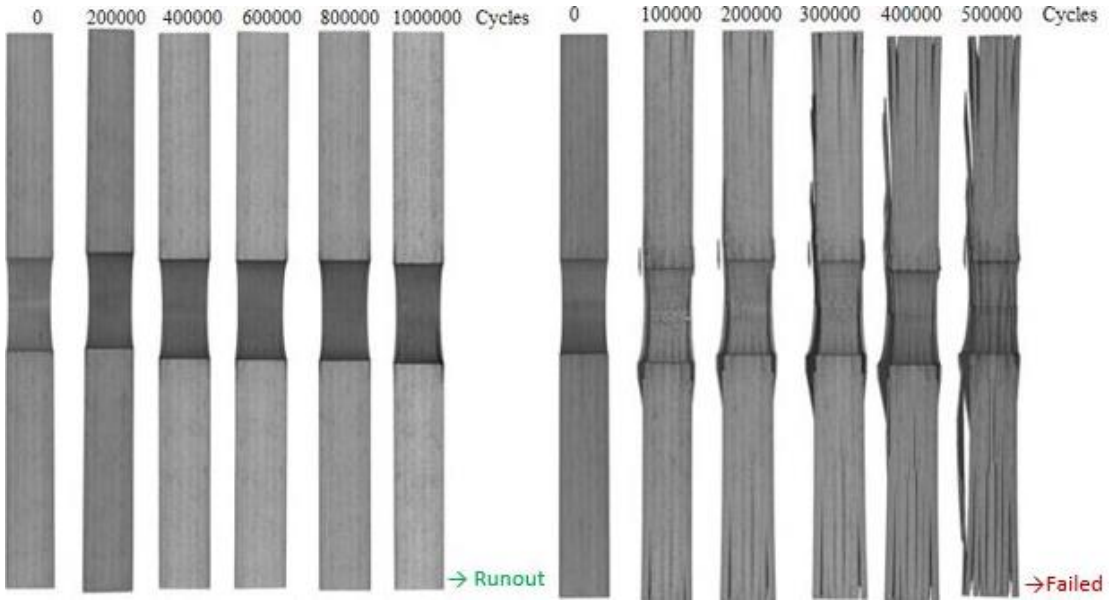


Figure 133. OHT-T residual strength increase for IM7/5250-4 uni, 25/50/25.



(a) SL1 (70%) (b) SL3 (90%)

Figure 134. XCT damage indications near hole for IM7/5320-1 UNI, 25/50/25 OHT-T.

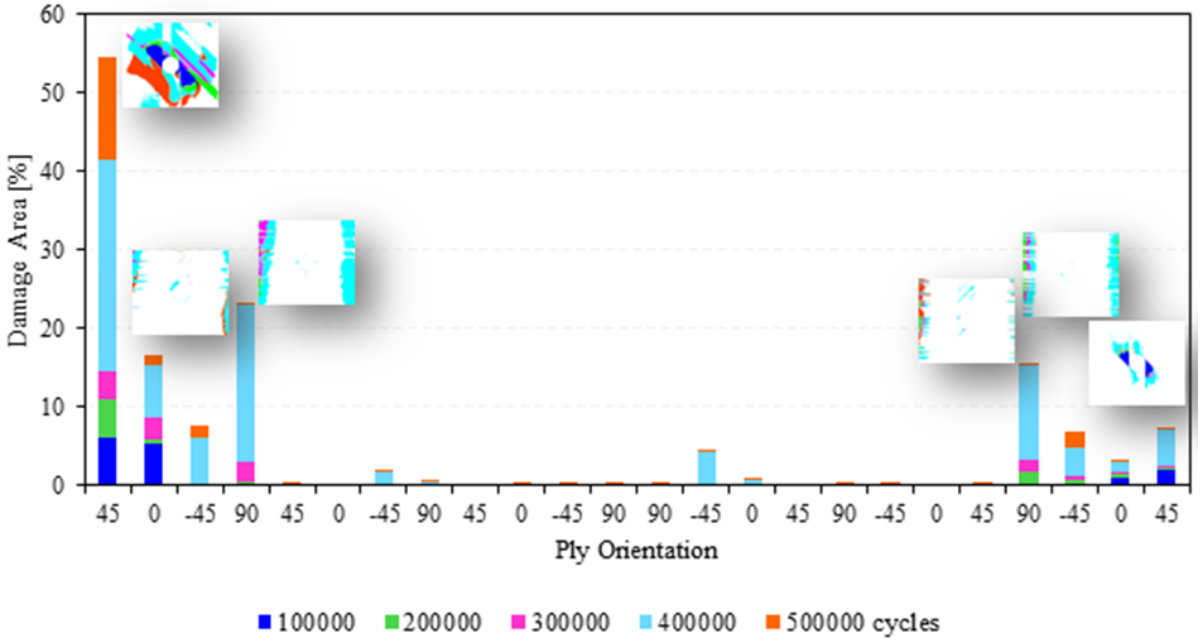


Figure 135. OHT-T fatigue damage increase for IM7/5250-4 UNI, 25/50/25, SL3.

DISTRIBUTION STATEMENT A.
Approved for public release: distribution is unlimited.

The calculation of effective strength based on equation (17) considering the contribution only from 0° plies (P = 0.25) and then considering all plies (Figure 117 ➔ P = 0.4) indicated residual strength values for the net section without notch effects to be 64.17 and 102.67 ksi, respectively. The average residual strength of IM7/5320-1 UNI quasi-isotropic runouts was 82.5 ksi, which was in between the range.

7.6.3 T650/5320-1 OHT-T

Figure 136 shows the increase in residual strength of T650/5320-1 8HS fabric hard (40/20/40) laminate specimens. Unlike both IM7/5320-1 and IM7/5250-4 unidirectional specimens, T650/5320-1 8HS fabric specimens did not show significant ply delaminations.

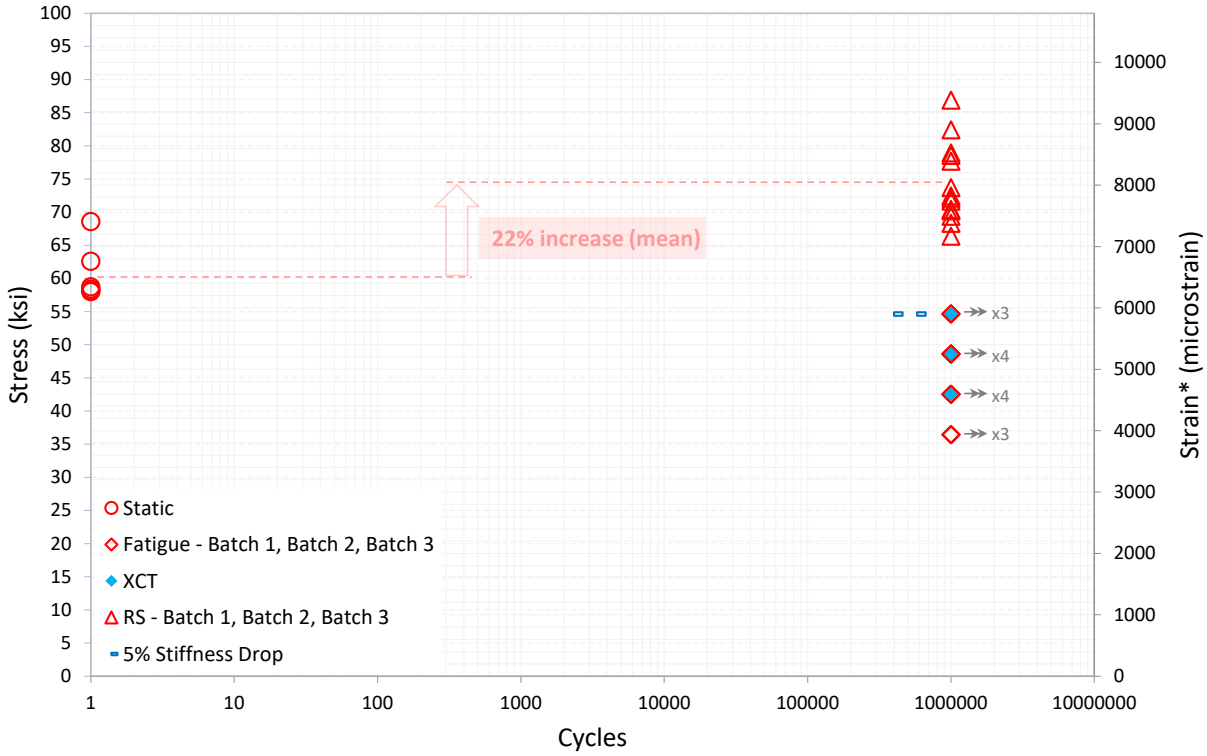


Figure 136. OHT-T SN data for T650/5320-1 8HS, 40/20/40.

Figure 137 shows the stiffness degradation of a representative test specimen from each stress level. SL1 (60%) and SL2 (70%) specimens showed less than 5 percent stiffness degradation at runout. SL1 specimens also showed no delamination and the smallest increase in residual strength at runout (19.9 percent as shown in Figure 138). SL3 (80%) showed minor damage but less than 5 percent stiffness degradation and an average residual strength increase of 18.5 percent. SL4 (90%) specimens showed approximately 5 percent stiffness degradation around 400,000 cycles for one specimen. Most specimens in this stress level had less than a 5 percent stiffness drop and minor localized damage around the hole, as can be seen in Figure 139. These specimens had an average increase in residual strength of 30.8 percent compared to quasi-static strength.

DISTRIBUTION STATEMENT A.
Approved for public release: distribution is unlimited.

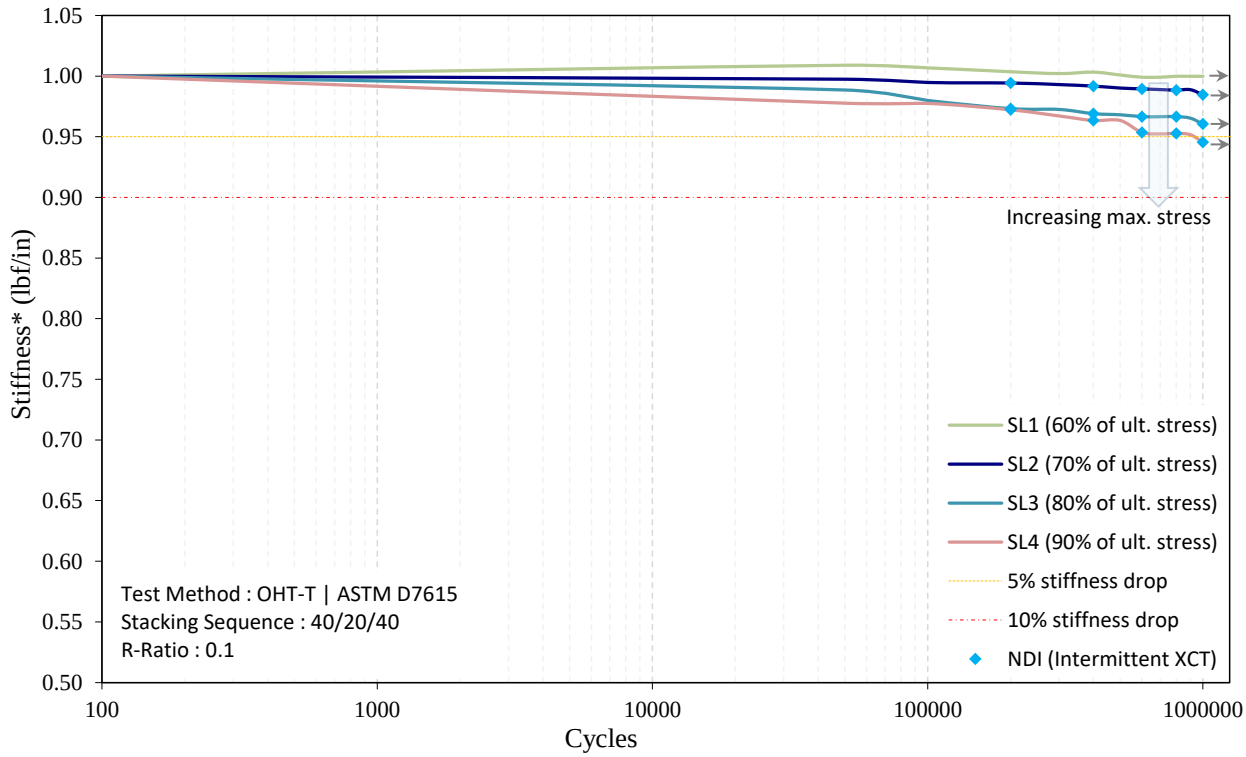


Figure 137. OHT-T stiffness degradation (normalized) for T650/5320-1 8HS, 40/20/40.

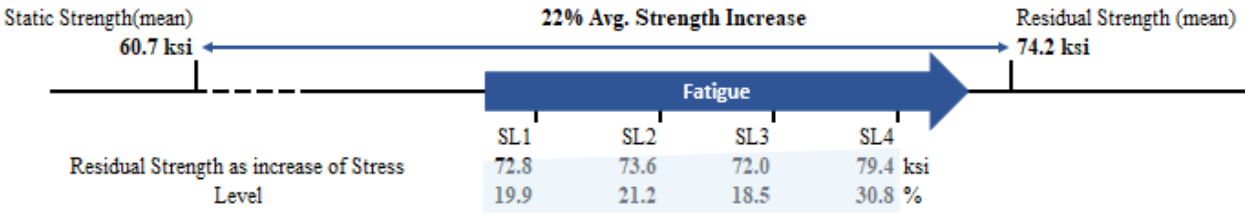


Figure 138. OHT-T residual strength increase for T650/5320-1 8HS, 40/20/40.

DISTRIBUTION STATEMENT A.
Approved for public release: distribution is unlimited.

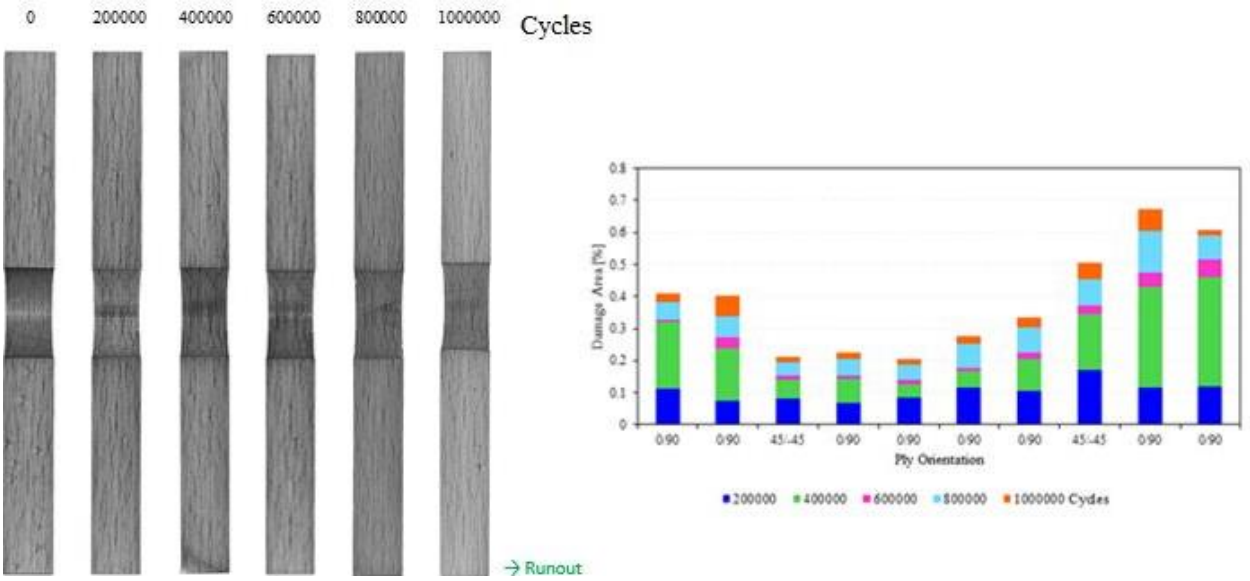


Figure 139. XCT damage indications near hole for T650/5320-1 8HS, 40/20/40 OHT-T.

Figure 140 shows an increase in residual strength of T650/5320-1 8HS quasi-isotropic specimens. Similar to both IM7/5320-1 and IM7/5250-4 UNI specimens, this increase in residual strength of quasi-isotropic specimens was significantly less than that for hard laminates.

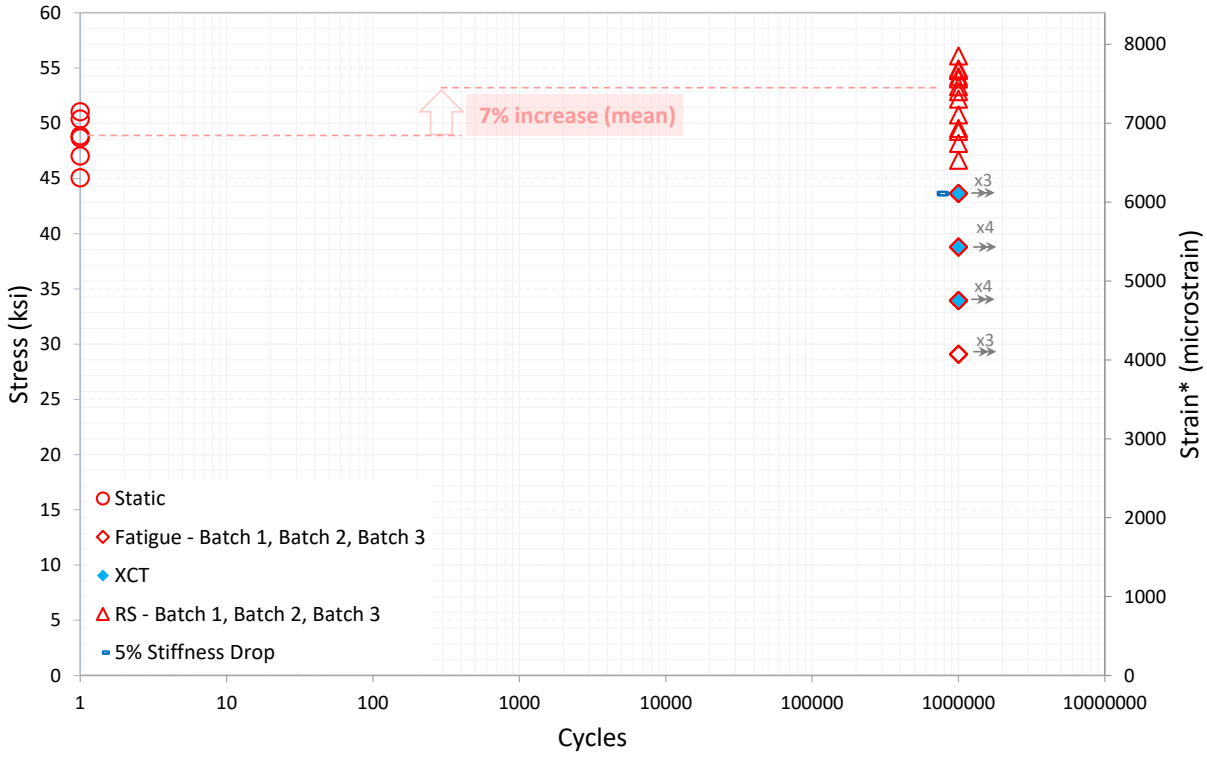


Figure 140. OHT-T SN data for T650/5320-1 8HS, 25/50/25.

DISTRIBUTION STATEMENT A.
Approved for public release: distribution is unlimited.

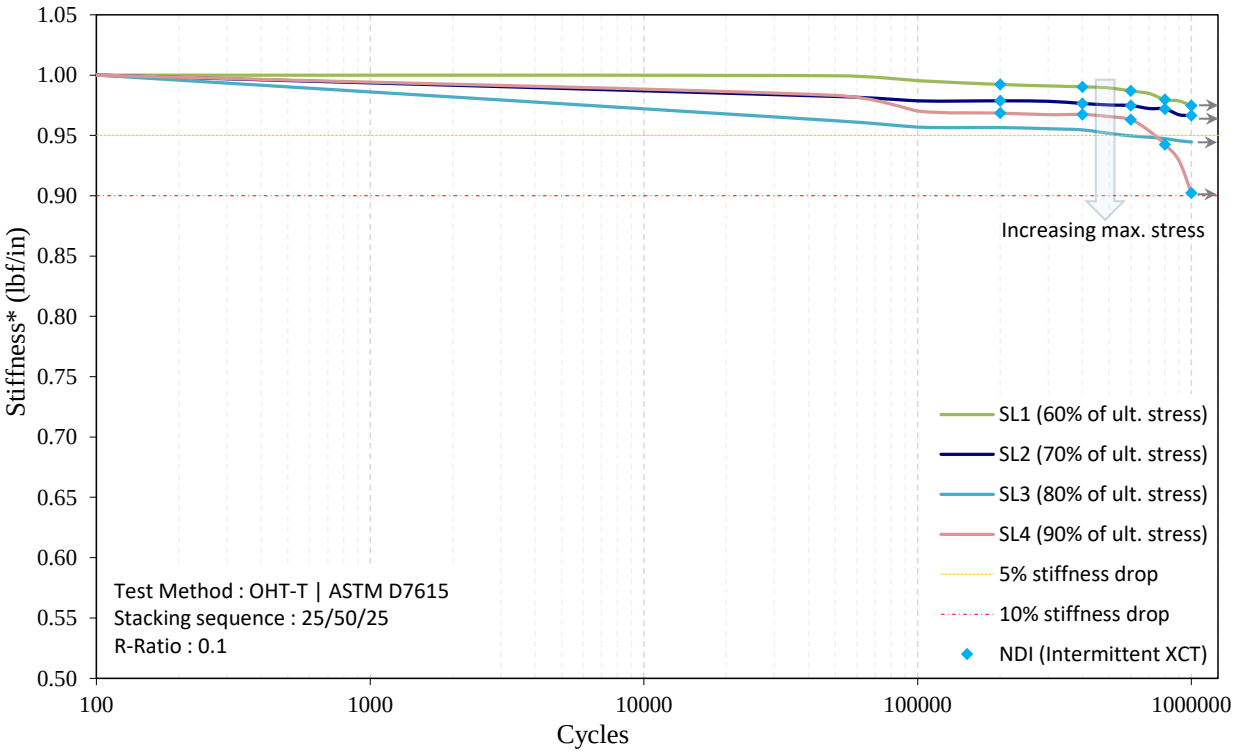


Figure 141. OHT-T stiffness degradation (normalized) for T650/5320-1 8HS, 25/50/25.

Figure 141 shows the apparent stiffness degradation of one representative specimen from each stress level. SL1 (60%) and SL2 (70%) specimens showed mostly less than a 5 percent stiffness drop at runout and no delaminations. Figure 142 shows that the increase in residual strength for SL1 and SL2 were 7.3 and 5.1 percent, respectively. SL3 (80%) indicated minor damage and a stiffness degradation of 5 percent or more. The average residual strength increase at runout for these specimens was approximately 6 percent. SL4 (90%) specimens showed 5 percent stiffness degradation around 740,000 cycles for one specimen, but none of them reached a 10 percent stiffness drop; most specimens in this stress level had less than a 5 percent stiffness drop. SL4 had an average increase in residual strength of 12 percent.

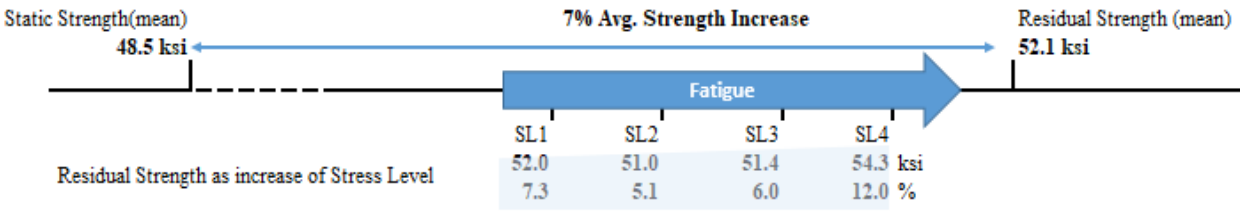


Figure 142. OHT-T residual strength increase for T650/5320-1 8HS, 25/50/25.

Unlike 40/20/40, these specimens showed minor damage within the notch area (Figure 143). However, the damage observed in these specimens was significantly less than what was observed in the unidirectional specimens.

DISTRIBUTION STATEMENT A.
Approved for public release: distribution is unlimited.

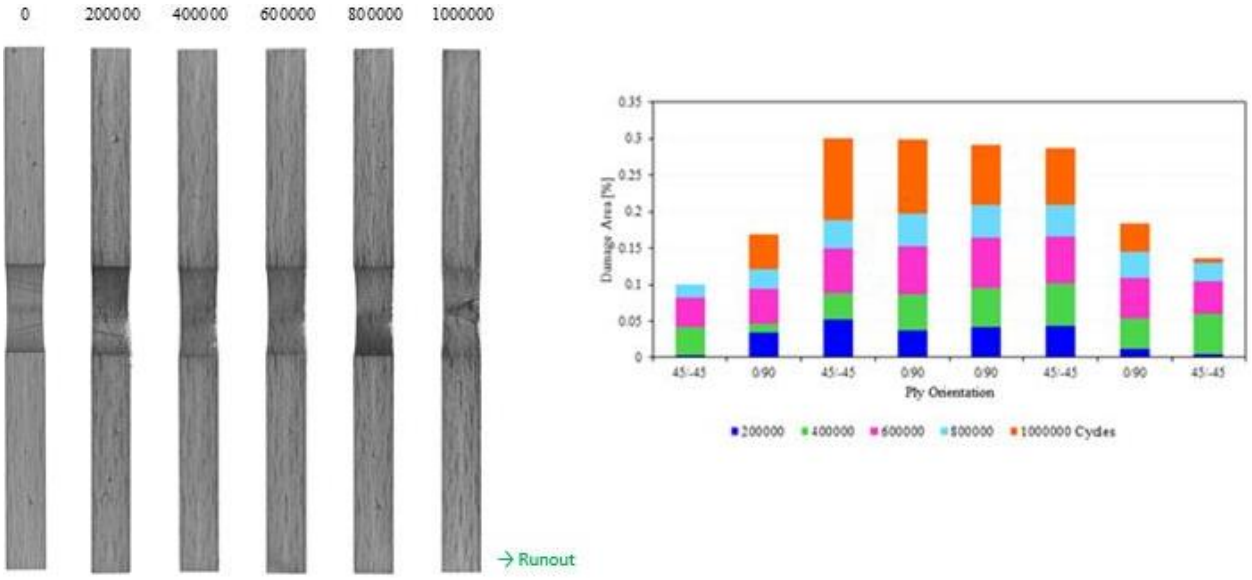


Figure 143. XCT damage indications near hole for T650/5320-1 8HS, 25/50/25 OHT-T.

DISTRIBUTION STATEMENT A.
Approved for public release: distribution is unlimited.

8. CONCLUSIONS

This report contains a fatigue evaluation and details of progressive damage growth data for IM7/5302-1 UNI, IM7/5250-4 UNI, and T650/5320-1 8HS fabric material systems. Three distinct material batches from each material were selected to evaluate batch variability. Test specimens were fabricated using three different laminate configurations (hard, quasi-isotropic, and soft) and tested under three different fatigue stress ratios (R = 0.1, 5, and –1). Open-hole, interlaminar (curved-beam) shear, double-notch shear, and short-beam shear failure modes were selected for the test program. High-fidelity XCT inspections were conducted for at least one specimen from each stress level at predetermined fatigue intervals (4D XCT). In addition, the apparent stiffness degradation was monitored using the slope of the load vs. displacement curve. All tests were carried out at room-temperature ambient conditions. One million fatigue cycles were considered the runout condition, and residual strength was evaluated for runouts.

Tension-tension (R = 0.1) OH fatigue specimens indicated all runouts, even at stress levels as high as 90 percent of quasi-static strength. Although these specimens indicated significant amounts of delamination at these high stress levels, minimal damage was noted (microcracks around the hole) for stress levels less than or equal to 80 percent stress level. Typical operational conditions for aircraft are significantly less than these stress levels. Therefore, the OH failure mode, which is the in-plane loading mode, is not a fatigue concern. For all three material systems, fatigue wearout behavior was observed for 80 percent stress level and above, but the residual strength of hard and quasi-isotropic runouts indicated higher values than quasi-static strength. In addition, the increase in residual strength was proportional to the fatigue stress level, which is counterintuitive, because the specimens from higher stress levels indicated significant damage for UNI and some minor damage for 8HS. Runouts for 8HS with low stress levels indicated only localized microcracks around the hole. Typically, microcracks around the hole that develop during fatigue cycles tend to reduce the stress concentration (analogous to metal plastic zone development that results in crack growth retardation) and increase the OH tensile strength. At low stress levels, XCT scans of runouts indicated localized microcracks that may have contributed to the increase in residual strength. However, the runouts at higher stress levels, especially for unidirectional specimens, indicated significant delamination and fiber splitting. Therefore, the increase in residual strength of runout specimens was believed to be due to the diminishing notch effects as a result of fiber splitting and delamination near the interfaces of off-axes plies. XCT data showed that most of the damage in UNI specimens were on the outermost plies, especially on off-axes plies. When interior damage was noted, it was primarily in off-axes plies. Fiber splitting in 0° plies tends to diminish the notch effects and also cause crack arrest, even in off-axes plies.

OH fatigue tests conducted for various stress ratios indicated that load reversal (R = –1) is the most damaging and fatigue-critical stress ratio. This stress ratio had the least data scatter as well, which is in line with the general observation that the longer the fatigue, the higher the scatter.

DISTRIBUTION STATEMENT A.
Approved for public release: distribution is unlimited.

DNS fatigue tests indicated that the fatigue life of hard laminates is less than for soft laminates, which is opposite the observations for OH specimens.

Out of 39 cases of fatigue SN curves included in this report, only the IM7/5250-4 UNI hard laminate ILT case had a shape parameter of less than 1.25, which is the historic modal life shape parameter reported for composite fatigue data (this statement is only applicable for individual Weibull data, since historic values were generated using individual Weibull analysis). The ILT failure mode for all three material systems indicated relatively low values of shape parameters, indicating a higher data scatter than the other failure modes investigated in this study. This is primarily due to the sensitivity of this failure mode to manufacturing defects such as porosity, resin-rich areas, and fiber waviness in the curved portion of the test specimens. Preliminary manufacturing trials with detailed inspections were performed in order to optimize the process to reduce manufacturing defects and improve the specimen quality. ILT specimens were subjected to pre-test XCT in order to investigate the effects of any defects in the curved region on the final failure mode. The improvement in material stability and controls placed in process specifications for modern composites have significantly reduced the data scatter. This is reflected in high shape parameters (note that the higher the shape parameters, the less the scatter) calculated for these three material systems.

In addition to conducting fatigue testing for three distinct material batches, additional tests were included with a set of soft specimens from batch 3 that had an extended post-cure up to 100 hours. The OHC quasi-static and residual strength data showed a small decrease in strength with increasing extended post-cure duration (less than 10 percent, even for a 100-hour EPC). Although the highest stress level and residual strength data indicated a small degradation as the EPC was increased, overall fatigue results were within the scatter band of baseline specimens. Both $R = 5$ and $R = -1$ residual strength data indicated wearout as the EPC was increased, but overall EPC fatigue data are within the scatter band of the baseline fatigue data.

In general, all failure modes that had fatigue failures indicated no significant scatter, which is historically seen on composite data. Furthermore, none of the failure modes indicated material batch variability. Scatter analysis of SN data was conducted using individual Weibull, joint Weibull, and Sendeckyj wearout models. Since tension-tension ($R = 0.1$) fatigue specimens of 5320-1 UNI and 8HS hard and quasi-isotropic laminates as well as the IM7/5250-4 UNI hard laminate only had runouts, no scatter analysis was conducted for those cases. Individual Weibull analysis indicated higher shape parameters than for joint Weibull and Sendeckyj analyses. The Sendeckyj analysis including static data yields the most conservative shape parameters to be used for generating life factors and load-enhancement factor curves.

When applying the load-enhancement factor for hybrid structural test substantiation, care must be taken to ensure that the metal parts do not exceed their clipping levels or high loads that result in crack growth retardation. Both multi-LEF and deferred severity spectrum approaches can be used to safely accomplish this for composite-dominant structures. The multi-LEF approach, if

DISTRIBUTION STATEMENT A.
Approved for public release: distribution is unlimited.

applicable, requires the least amount of additional work and can be applied to the composite-metal hybrid test spectrum with some additional fracture mechanics analysis of the metallic structure and minor modifications to the test spectrum. If the multi-LEF approach is not able to maintain all high loads in the composite spectrum below clipping levels for metals, then a two-phase deferred severity spectrum can be applied in conjunction with the multi-LEF. In order to substantiate the spectrum modifications, especially for the case of DSS, several coupon/element-level tests are required to ensure that the modified spectrum does not significantly alter the damage growth behavior or result in an unexpected failure mode. Both of these approaches provide cost-effective certification test solutions and reduce certification time significantly, compared to current practices for hybrid test substantiation.

DISTRIBUTION STATEMENT A.
Approved for public release: distribution is unlimited.

9. REFERENCES

1. Whitehead, R. S., Kan, H. P., Cordero, R., and Seather, E. S., Certification Testing Methodology for Composite Structures, Report No. NADC-87042-60, Volumes I and II, October 1986.
2. Tomblin, J. S., and Seneviratne, W. P., "Determining the Fatigue Life of Composite Aircraft Structures Using Life and Load-Enhancement Factors," DOT/FAA/AR-10/6, 2011.
3. Seneviratne, W., "Certification Challenges for Composite Structures," Keynote Speech: Digimat Users' Meeting, Liege, Belgium, 2013.
4. Seneviratne, W., and Tomblin, J., "Accelerating Composite Material Qualification Using Statistically-Significant Multi-Scale Progressive Damage Models," CAMX, Anaheim, CA, 2016.
5. Shyprykevich, P., Tomblin, J. S., and Vangel, M. G., "The Development and Use of a Common Database for Composite Materials," *Testing, Design and Acceptance Criteria,* ASTM STP 1416, A. Zureick and A. T. Nettles, eds., American Society for Testing and Materials, West Conshohocken, PA, 2002, pp. 99-115.
6. Advanced General Aviation Transport Experiments, www.niar.wichita.edu/agate.
7. National Center for Advanced Materials Performance, www.niar.wichita.edu/coe/ncamp.asp.
8. Tomblin, J., and Seneviratne, W., "Laminate Statistical Allowable Generation for Fiber-Reinforced Composite Materials: Lamina Variability Method," DOT/FAA/AR-06/53, January 2009.
9. Yang, C., Sun, C., Seneviratne, W., and Shashidhar, A., "Thermally Induced Loads of Fastened Hybrid Composite/Aluminum Structures due to Large CTE Differences," *AIAA Journal of Aircraft,* Vol. 45, No. 2, March-April 2008.
10. Seneviratne, W. P., and Tomblin, J. S., "Certification of Composite-Metal Hybrid Structures using Load-Enhancement Factors," FAA Joint Advanced Materials and Structures (JAMS)/Aircraft Airworthiness and Sustainment (AA&S), Baltimore, MD, 2012.
11. Seneviratne, W., Tomblin, J., and Kittur, M., "Durability and Residual Strength of Adhesively Bonded Composite Joints: The Case of F/A-18 A-D Wing Root Stepped-Lap Joint," in *Fatigue and Fracture of Adhesively-Bonded Composite Joints*, Cambridge, UK: Elsevier 2015.
12. Seneviratne, W., Tomblin, J., Kittur, M., and Rahman, A., "Aging Evaluation of F/A-18 A-D Wing-Root Stepped-Lap Joint," NATO AVT-266 Research Specialist Meeting, Torino, Italy, April 2018.
13. Seneviratne, W., and Tomblin, J., "Deferred Severity Spectrum for Durability and Damage Tolerance Certification Testing of Hybrid Structures," CAMX, Anaheim, CA, 2016.
14. Seneviratne, W., and Tomblin, J., "Life of Composites under Variable Amplitude Fatigue using ST Method," AIAA SciTech Forum, 2021.
15. Sanger, K. B., "Certification Testing Methodology for Composite Structures," Report No. NADC-86132-60, January 1986.

DISTRIBUTION STATEMENT A.
Approved for public release: distribution is unlimited.

16. Lameris, J., “The Use of Load Enhancement Factors in the Certification of Composite Aircraft Structures,” NLR Report: NLR TP 90068 U, February 1990.

17. Seneviratne, W., “Fatigue-Life Determination of Damage-Tolerant Composite Airframe,” Wichita State University, December 2008.

18. Seneviratne, W. P., and Tomblin, J. S., “Certification of Composite-Metal Hybrid Structures Using Load-Enhancement Factors,” FAA Joint Advanced Materials and Structures (JAMS)/Aircraft Airworthiness and Sustainment (AA&S), Baltimore, MD, 2012.

19. Seneviratne, W., “Durability and Damage Tolerance Certification Test Procedure for Composite-Metal Hybrid Structures with the Use of Single Full-Scale Test Article,” 11th International Fatigue Congress, Melbourne, Australia, March 2014.

20. Seneviratne, W. P., and Tomblin, J. S., “Load Sequencing Effects and Damage Growth Retardation of Composites,” FAA Joint Advanced Materials and Structures (JAMS), Grapevine, TX, March 2016.

21. Tomblin, J. S., and Seneviratne, W. P., “Durability and Damage Tolerance Testing of a Beechcraft Starship Forward-Wing with Large Damages,” DOT/FAA/TC-13/26, 2017.

22. Badaliance, R., and Dill, H. D., “Compression Fatigue Life Prediction Methodology for Composite Structures,” NADC-83060-60, Volumes I and II, September, 1982.

23. Sendeckyj, G. P., “Fitting Models to Composite Materials Fitting Data,” Test methods and Design Allowables for Fibrous Composites, ASTM STP 734, in C. C. Chamis, ed., American Society for Testing and Materials, 1981, pp. 245-260.

24. Life Data Analysis Reference, ReliaSoft Corporation, Tucson, AZ.

25. CYCOM 5320-1 IM7 Unidirectional and T650 8HS Fabric, MASC Process Specification Rev. A. NIAR, WSU, June 2020.

26. CYCOM 5250-4 IM7G Unidirectional, MASC Process Specification Rev. A. NIAR, WSU, June 2020.

27. Seneviratne, W., and Tomblin, J., “In-Situ Material State Monitoring Using Embedded Sensors and Cure Kinetics for Process Optimization of Polymer Composites,” SAMPE, Longbeach, CA, May 2018.

28. ASTM D6484/D6484M – 14, Standard Test Method for Open-Hole Compressive Strength of Polymer Matrix Composite Laminates, 2014.

29. ASTM D3846-08, Standard Test Method for In-Plane Shear Strength of Reinforced Plastics, 2008.

30. ASTM D6415/D6415M − 06a, Standard Test Method for Measuring the Curved Beam Strength of a Fiber-Reinforced Polymer-Matrix Composite, 2006.

31. ASTM D2344/D2344M – 16, Standard Test Method for Short-Beam Strength of Polymer Matrix Composite Materials and Their Laminates, 2016.

32. ASTM D7028 – 07, Standard Test Method for Glass Transition Temperature (DMA Tg) of Polymer Matrix Composites by Dynamic Mechanical Analysis (DMA)), 2007.

DISTRIBUTION STATEMENT A.
Approved for public release: distribution is unlimited.

33. ASTM D3418 – 12, Standard Test Method for Transition Temperatures and Enthalpies of Fusion and Crystallization of Polymer by Differential Scanning Calorimetry, 2012.
34. Schaefer J., Justusson B., Patel Devin., Pike M., and Liguore S., "High Fidelity Database and Validation Protocols for Structural Failure Mode Characterization," ONR, Volumes I and II, June, 2017.
35. Seneviratne, W., Tomblin, J., Liyanage, S., and Shah, H., "Process Simulation Models and Noninvasive In-Situ Material State Monitoring for Detection of Process-Induced Damages in Polymer Composites," WSU/NIAR Report CAM-RP-2018-009 N/C (submitted to Office of Naval Research), March 2019.
36. CYCOM® 5320-1 IM7 12K 145 gsm 33%RW Unidirectional Tape Qualification Test Plan, Results & Material Property Data Report, Cytec Document No. 5320-12, December 2014.
37. Hart-Smith L.J. , A New Approach to Fibrous Composite Laminate Strength Prediction, Douglas Paper 8366, presented to MIL-HDBK-17 Committee Meeting, Singer Island, Palm Beach, Florida, 1989.
38. CYCOM® 5250-4 prepreg System, Technical Data Sheet, March 2011.

DISTRIBUTION STATEMENT A.
Approved for public release: distribution is unlimited.

APPENDIX A - S/N DATA AND SENDECKYJ ANALYSIS

This section contains individual data summaries along with their SN curves that were used for the fatigue life scatter analysis. Sendeckyj model analysis was conducted on the SN data; the fitting curves are displayed for a graphical confirmation that the fitting parameters are reasonable. Data for the three material batches presented in SN curves are separated by unique colors to distinguish the material batch variability. Test specimens that were subjected to detailed XCT are indicated with dark blue filling.

In tables included in this appendix, n, σ_A, σ_R and σ_e are the number of cycles survived (n=1 indicates static failure), the fatigue stress level (or static failure stress value), the residual strength after surviving the corresponding number of cycles, and the equivalent static strength (pooled), respectively.

A.1 SN Data and Sendeckyj Fitting Models for IM7/5320-1 Unidirectional Tape

Table A.1 – SN data for IM7/5320-1, 50/40/10, R=0.1, OHT-T.

Specimen	Batch	σ_A	n	σ_R	σ_e
MASC1-B1DO11-0X3	1	107.036	1		
MASC1-B2DO11-0X4	2	115.059	1		
MASC1-B2DO11-0X3	2	114.193	1		
MASC1-B3DO11-0X4	3	105.781	1		
MASC1-B1DO11-0X4	1	103.763	1		
MASC1-B3DO11-0X3	3	98.896	1		
MASC1-B1DO11-3K2	1	96.709	1000000	149.226	
MASC1-B2DO11-3K2	2	96.709	1000000	157.224	
MASC1-B3DO11-3K2	3	96.709	1000000	144.778	
MASC1-B3DO11-XX2	3	96.709	1000000	159.604	
MASC1-B1DO11-3K1	1	85.964	1000000	168.409	
MASC1-B2DO11-3K1	2	85.964	1000000	142.534	
MASC1-B3DO11-3K1	3	85.964	1000000	135.295	
MASC1-B1DO11-2K1	1	75.218	1000000	119.900	
MASC1-B1DO11-2K2	1	75.218	1000000	121.634	
MASC1-B2DO11-2K1	2	75.218	1000000	123.509	
MASC1-B3DO11-2K1	3	75.218	1000000	118.834	
MASC1-B1DO11-1K1	1	64.473	1000000	116.773	
MASC1-B2DO11-1K1	2	64.473	1000000	120.581	
MASC1-B3DO11-1K1	3	64.473	1000000	114.726	

Sendeckyj wearout analysis prediction and equivalent static strength data for IM7/5320-1 unidirectional tape, 50/40/10, R=0.1 OH, are not included as all fatigue specimens were runouts (Table A.1).

DISTRIBUTION STATEMENT A.
Approved for public release: distribution is unlimited.

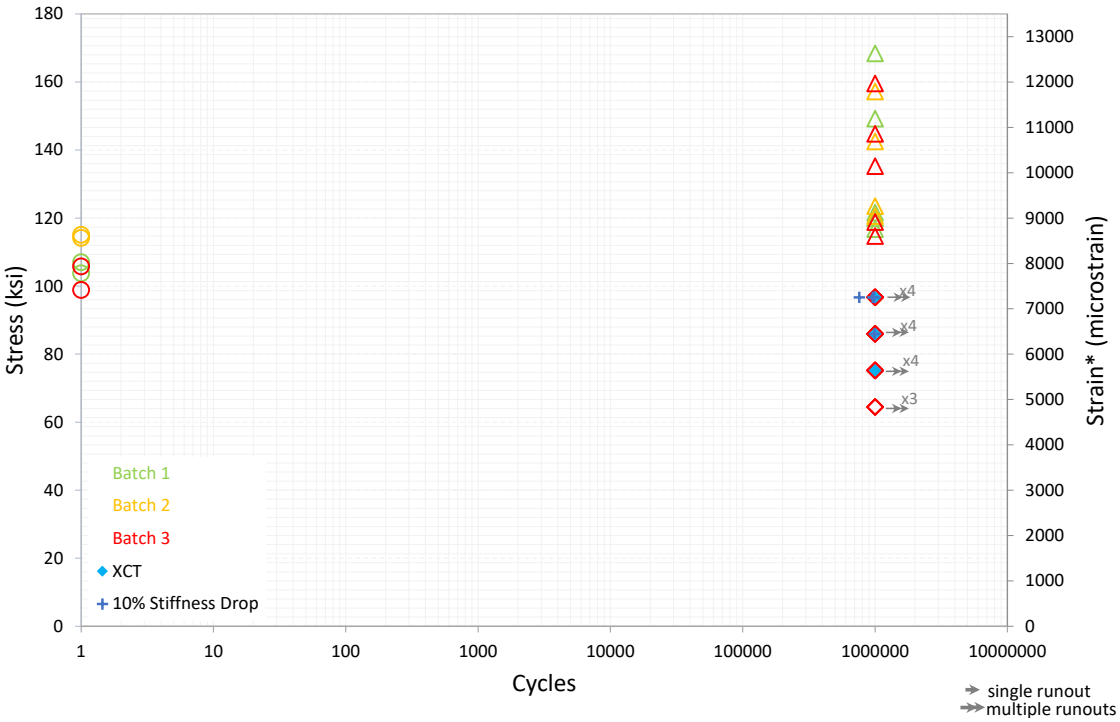


Figure A.1 – SN data for IM7/5320-1, 50/40/10, R=0.1, OHT-T.

DISTRIBUTION STATEMENT A.
Approved for public release: distribution is unlimited.

Table A.2 – SN data for IM7/5320-1, 50/40/10, R=5, OHC-C.

Specimen	Batch	σ_A	n	σ_R	σ_e
MASC1-B1DO11-0X1	1	66.256	1		
MASC1-B3DO11-0X1	3	72.642	1		
MASC1-B1DO11-0X2	1	71.488	1		
MASC1-B2DO11-0X2	2	71.243	1		
MASC1-B2DO11-0X1	2	69.702	1		
MASC1-B3DO11-0X2	3	68.296	1		
MASC1-B1DO11-3L1	1	55.950	2887		68.645
MASC1-B1DO11-XX6	1	55.950	6165		69.552
MASC1-B2DO11-3L2	2	55.950	10905		70.242
MASC1-B3DO11-3L1	3	55.950	6677		69.648
MASC1-B3DO11-3L2	3	55.950	10122		70.151
MASC1-B3DO11-XX7	3	55.950	17487		70.818
MASC1-B1DO11-1L1	1	52.453	1000000	73.339	73.552
MASC1-B1DO11-1L2	1	52.453	1000000	68.019	71.292
MASC1-B1DO11-XX8	1	52.453	1000000	74.473	74.566
MASC1-B2DO11-1L1	2	52.453	628817		70.639
MASC1-B2DO11-1L2	2	52.453	1000000	70.524	71.768
MASC1-B3DO11-1L1	3	52.453	1000000	72.307	72.741
MASC1-B3DO11-1L2	3	52.453	1000000	75.403	75.450
MASC1-B1DO11-3L2	1	52.453	689254		70.751
MASC1-B1DO11-2L1	1	48.956	1000000	72.949	72.955
MASC1-B1DO11-XX7	1	48.956	1000000	71.369	71.389
MASC1-B2DO11-2L1	2	48.956	1000000	69.537	69.622
MASC1-B3DO11-2L1	3	48.956	1000000	69.806	69.875
MASC1-B3DO11-2L2	3	48.956	1000000	72.099	72.110

DISTRIBUTION STATEMENT A.
Approved for public release: distribution is unlimited.

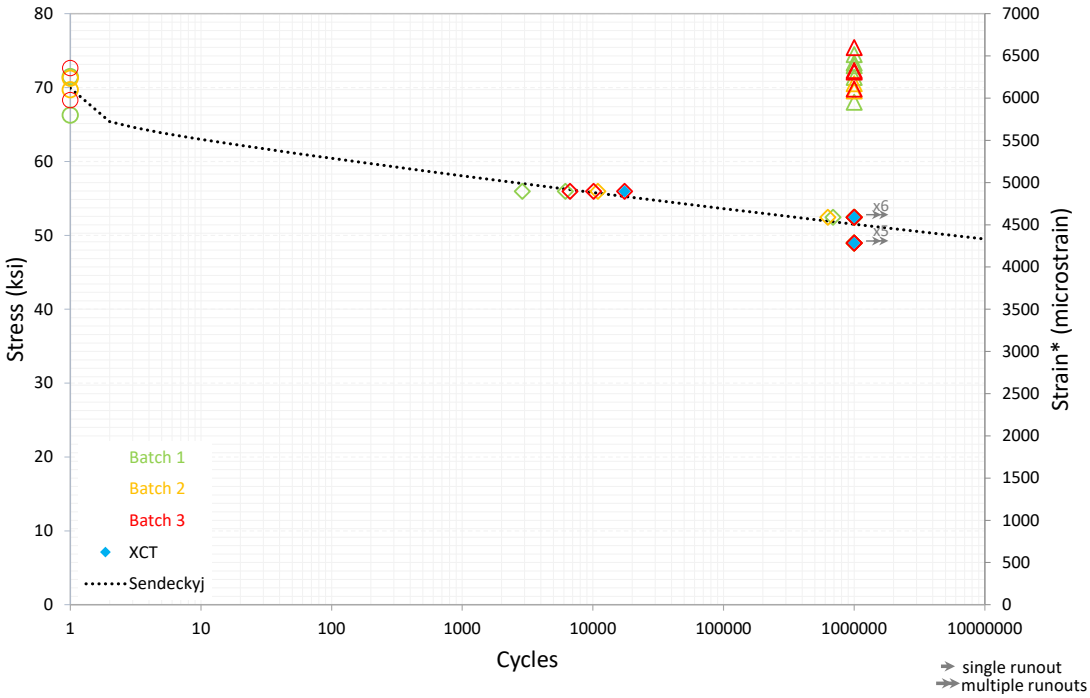


Figure A.2 – SN data with Sendeckyj fitting model for IM7/5320-1, 50/40/10, R=5, OHC-C.

DISTRIBUTION STATEMENT A.
Approved for public release: distribution is unlimited.

Table A.3 – SN data for IM7/5320-1, 50/40/10, R=-1, OHC-T.

Specimen	Batch	σ_A	n	σ_R	σ_e
MASC1-B1DO11-0X1	1	66.256	1	'	'
MASC1-B3DO11-0X1	3	72.642	1	'	'
MASC1-B1DO11-0X2	1	71.488	1	'	'
MASC1-B2DO11-0X2	2	71.243	1	'	'
MASC1-B2DO11-0X1	2	69.702	1	'	'
MASC1-B3DO11-0X2	3	68.296	1	'	'
MASC1-B1DO11-3M1	1	62.087	16041	'	75.265
MASC1-B1DO11-3M2	1	62.087	8795	'	73.099
MASC1-B2DO11-XX5	2	62.087	3063	'	69.581
MASC1-B2DO11-3M2	2	62.087	5812	'	71.669
MASC1-B3DO11-3M1	3	62.087	16054	'	75.268
MASC1-B3DO11-3M2	3	62.087	10690	'	73.791
MASC1-B1DO11-2M1	1	53.218	116161	'	71.165
MASC1-B1DO11-2M2	1	53.218	174608	'	72.628
MASC1-B2DO11-XX4	2	53.218	225003	'	73.553
MASC1-B2DO11-2M2	2	53.218	174281	'	72.621
MASC1-B3DO11-2M1	3	53.218	151246	'	72.109
MASC1-B3DO11-2M2	3	53.218	215856	'	73.401
MASC1-B1DO11-XX3	1	48.783	581075	'	70.698
MASC1-B1DO11-XX2	1	48.783	600942	'	70.817
MASC1-B2DO11-XX8	2	48.783	720334	'	71.462
MASC1-B2DO11-XX7	2	48.783	614997	'	70.899
MASC1-B3DO11-XX5	3	48.783	325759	'	68.682
MASC1-B3DO11-XX6	3	48.783	562172	'	70.581
MASC1-B1DO11-1M1	1	44.348	1000000	82.500	82.548
MASC1-B1DO11-1M2	1	44.348	1000000	66.402	68.562
MASC1-B2DO11-XX3	2	44.348	926010	'	65.786
MASC1-B2DO11-1M2	2	44.348	1000000	81.425	81.487
MASC1-B3DO11-1M1	3	44.348	1000000	83.660	83.697
MASC1-B3DO11-1M2	3	44.348	1000000	77.294	77.457

DISTRIBUTION STATEMENT A.
Approved for public release: distribution is unlimited.

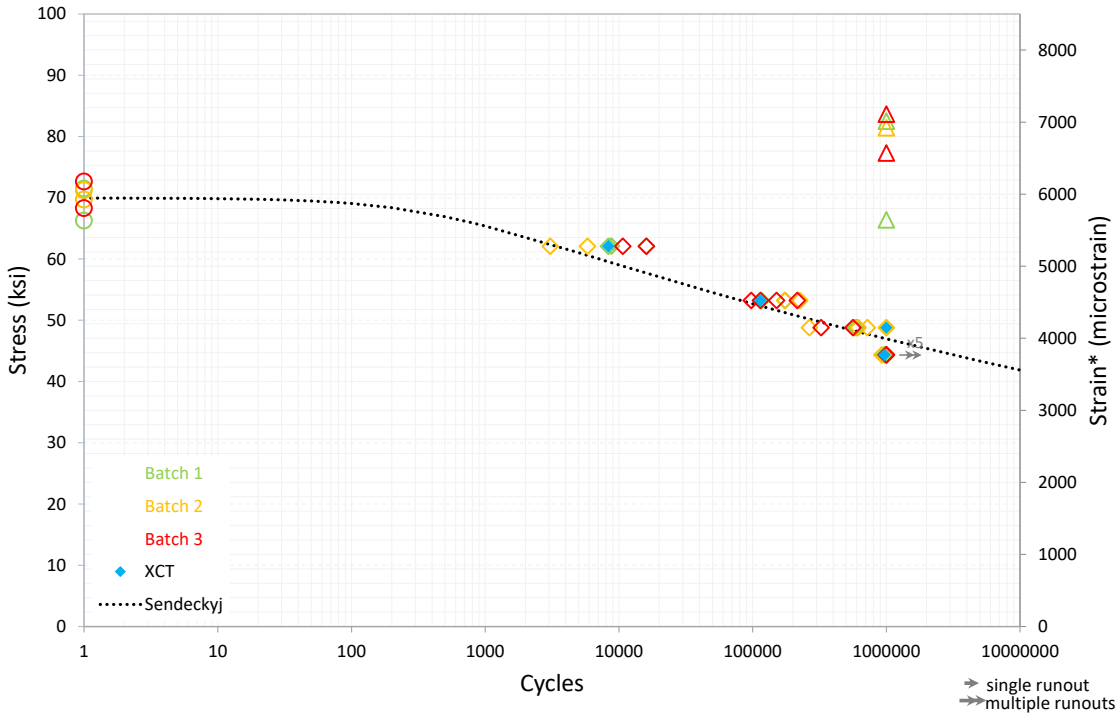


Figure A.3 – SN data with Sendeckyj fitting model for IM7/5320-1, 50/40/10, R=-1, OHC-T.

DISTRIBUTION STATEMENT A.
Approved for public release: distribution is unlimited.

Table A.4 – SN Data for IM7/5320-1, 25/50/25, R=0.1, OHT-T.

Specimen	Batch	σ_A	n	σ_R	σ_e
MASC1-B1EO11-0X3	1	67.570	1		
MASC1-B3EO11-0X3	3	70.683	1		
MASC1-B3EO11-0X4	3	69.976	1		
MASC1-B2EO11-0X4	2	68.769	1		
MASC1-B1EO11-0X4	1	67.518	1		
MASC1-B2EO11-0X3	2	66.247	1		
MASC1-B1EO11-1K2	1	61.614	1000000	69.146	
MASC1-B3EO11-1K2	3	61.614	1000000	68.890	
MASC1-B3EO11-2K2	3	61.614	1000000		
MASC1-B3EO11-XX1	3	61.614	1000000	80.677	
MASC1-B2EO11-XX1	2	54.768	1000000	80.078	
MASC1-B1EO11-3K1	1	54.768	1000000	74.075	
MASC1-B1EO11-3K2	1	54.768	1000000	78.191	
MASC1-B2EO11-3K1	2	54.768	1000000	76.982	
MASC1-B2EO11-3K2	2	54.768	1000000	77.157	
MASC1-B3EO11-3K1	3	54.768	1000000	78.633	
MASC1-B3EO11-3K2	3	54.768	1000000	78.350	
MASC1-B1EO11-XX1	1	47.922	1000000	76.942	
MASC1-B1EO11-2K1	1	47.922	1000000	75.172	
MASC1-B1EO11-2K2	1	47.922	1000000	74.177	
MASC1-B2EO11-2K1	2	47.922	1000000	75.610	
MASC1-B2EO11-2K2	2	47.922	1000000	75.518	
MASC1-B3EO11-2K1	3	47.922	1000000	78.532	
MASC1-B1EO11-1K1	1	41.076	1000000	72.187	
MASC1-B2EO11-1K1	2	41.076	1000000	71.767	
MASC1-B2EO11-1K2	2	41.076	1000000	73.257	
MASC1-B3EO11-1K1	3	41.076	1000000	76.221	

DISTRIBUTION STATEMENT A.
Approved for public release: distribution is unlimited.

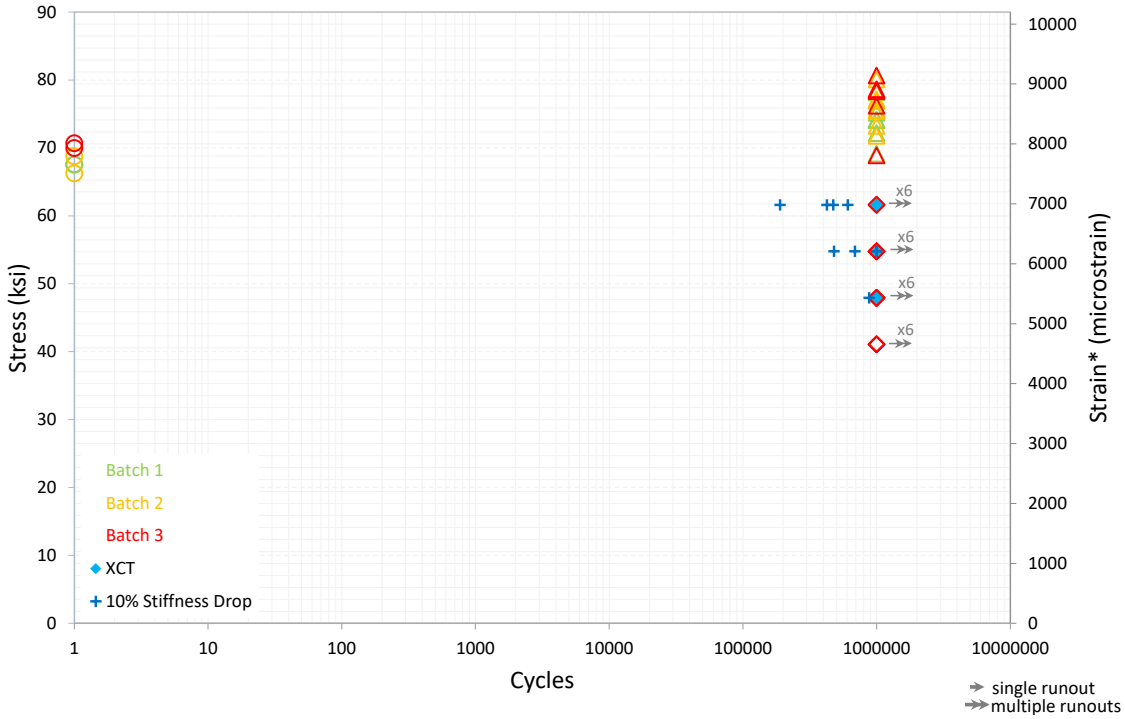


Figure A.4 – SN data for IM7/5320-1, 25/50/25, R=0.1, OHT-T.

Sendeckyj wearout analysis prediction and equivalent static strength data for IM7/5320-1 unidirectional tape, 25/50/25, R=0.1 OH, are not included as all fatigue specimens were runouts (Table A.4).

DISTRIBUTION STATEMENT A.
Approved for public release: distribution is unlimited.

Table A.5 – SN data for IM7/5320-1, 25/50/25, R=5, OHC-C.

Specimen	Batch	σ_A	n	σ_R	σ_e
MASC1-B1EO11-0X1	1	50.186	1	"	"
MASC1-B2EO11-0X1	2	51.855	1	"	"
MASC1-B3EO11-0X1	3	51.384	1	"	"
MASC1-B3EO11-0X2	3	51.221	1	"	"
MASC1-B1EO11-0X2	1	50.834	1	"	"
MASC1-B2EO11-0X2	2	49.497	1	"	"
MASC1-B1EO11-3L1	1	40.664	30925	"	51.606
MASC1-B1EO11-3L2	1	40.664	9452	"	49.997
MASC1-B2EO11-3L1	2	40.664	19514	"	50.975
MASC1-B2EO11-3L2	2	40.664	41348	"	52.008
MASC1-B3EO11-3L1	3	40.664	30572	"	51.590
MASC1-B3EO11-3L2	3	40.664	26823	"	51.410
MASC1-B3EO11-XX2	3	40.664	19249	"	50.956
MASC1-B1EO11-1L1	1	38.122	91062	"	49.796
MASC1-B1EO11-1L2	1	38.122	112704	"	50.081
MASC1-B2EO11-1L1	2	38.122	241077	"	51.108
MASC1-B2EO11-1L2	2	38.122	86457	"	49.727
MASC1-B2EO11-XX3	2	38.122	43628	"	48.827
MASC1-B3EO11-1L1	3	38.122	98478	"	49.900
MASC1-B3EO11-1L2	3	38.122	463054	"	52.008
MASC1-B1EO11-2L1	1	35.581	900109	"	49.411
MASC1-B1EO11-2L2	1	35.581	828938	"	49.302
MASC1-B1EO11-XX3	1	35.581	1000000	49.156	50.290
MASC1-B2EO11-2L1	2	35.581	1000000	48.783	50.140
MASC1-B2EO11-2L2	2	35.581	1000000	46.649	49.682
MASC1-B3EO11-2L1	3	35.581	1000000	52.161	52.352
MASC1-B3EO11-2L2	3	35.581	1000000	48.707	50.113

DISTRIBUTION STATEMENT A.
Approved for public release: distribution is unlimited.

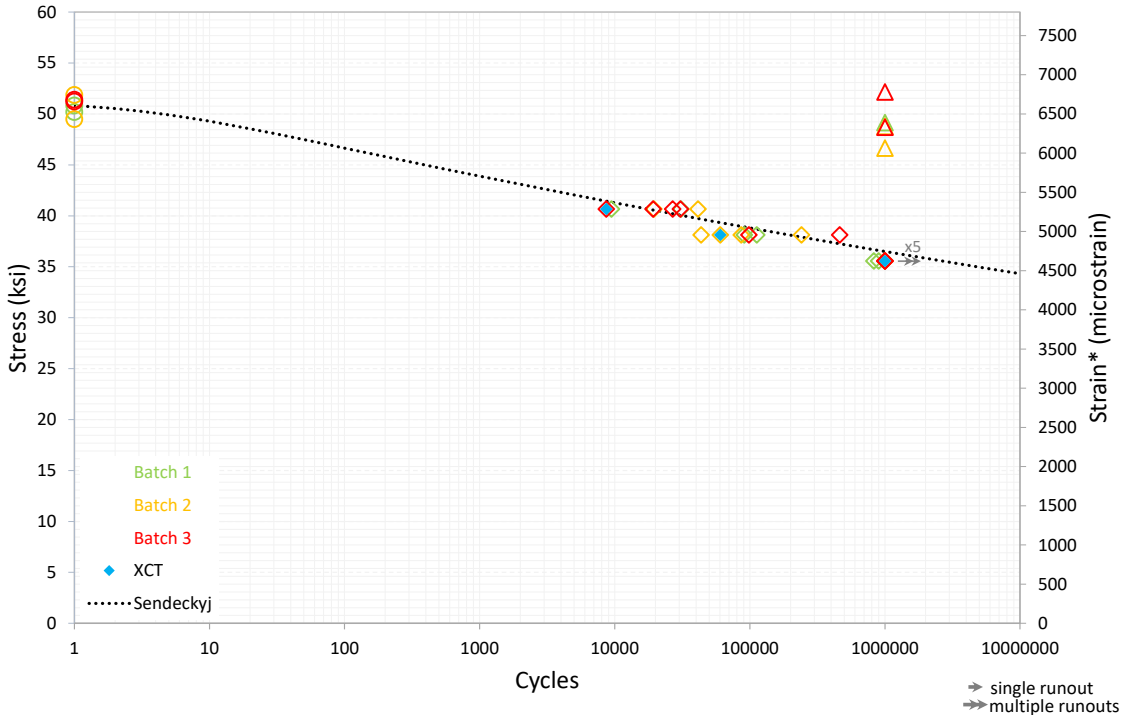


Figure A.5 – SN data with Sendeckyj fitting model for IM7/5320-1, 25/50/25, R=5, OHC-C.

DISTRIBUTION STATEMENT A.
Approved for public release: distribution is unlimited.

Table A.6 – SN data for IM7/5320-1, 25/50/25, R=-1, OHC-T.

Specimen	Batch	σ_A	n	σ_R	σ_e
MASC1-B1EO11-0X1	1	50.186	1	℅	℅
MASC1-B2EO11-0X1	2	51.855	1	℅	℅
MASC1-B3EO11-0X1	3	51.384	1	℅	℅
MASC1-B3EO11-0X2	3	51.221	1	℅	℅
MASC1-B1EO11-0X2	1	50.834	1	℅	℅
MASC1-B2EO11-0X2	2	49.497	1	℅	℅
MASC1-B1EO11-2M1	1	35.787	26732	℅	51.354
MASC1-B1EO11-2M2	1	35.787	37066	℅	52.102
MASC1-B2EO11-2M1	2	35.787	11434	℅	49.461
MASC1-B2EO11-2M2	2	35.787	31647	℅	51.739
MASC1-B3EO11-2M1	3	35.787	30360	℅	51.644
MASC1-B3EO11-2M2	3	35.787	41394	℅	52.357
MASC1-B1EO11-3M2	1	32.805	168119	℅	51.063
MASC1-B1EO11-XX5	1	32.805	264951	℅	52.101
MASC1-B2EO11-3M1	2	32.805	156777	℅	50.906
MASC1-B2EO11-3M2	2	32.805	128027	℅	50.452
MASC1-B3EO11-3M1	3	32.805	120265	℅	50.312
MASC1-B3EO11-3M2	3	32.805	125827	℅	50.413
MASC1-B1EO11-XX2	1	29.823	1000000	42.609	50.285
MASC1-B1EO11-1M2	1	29.823	1000000	39.605	50.242
MASC1-B1EO11-XX7	1	29.823	1000000	41.804	50.266
MASC1-B2EO11-1M1	2	29.823	981370	℅	50.190
MASC1-B2EO11-1M2	2	29.823	1000000	37.946	50.235
MASC1-B3EO11-1M1	3	29.823	1000000	41.036	50.254
MASC1-B3EO11-1M2	3	29.823	1000000	40.299	50.247

DISTRIBUTION STATEMENT A.
Approved for public release: distribution is unlimited.

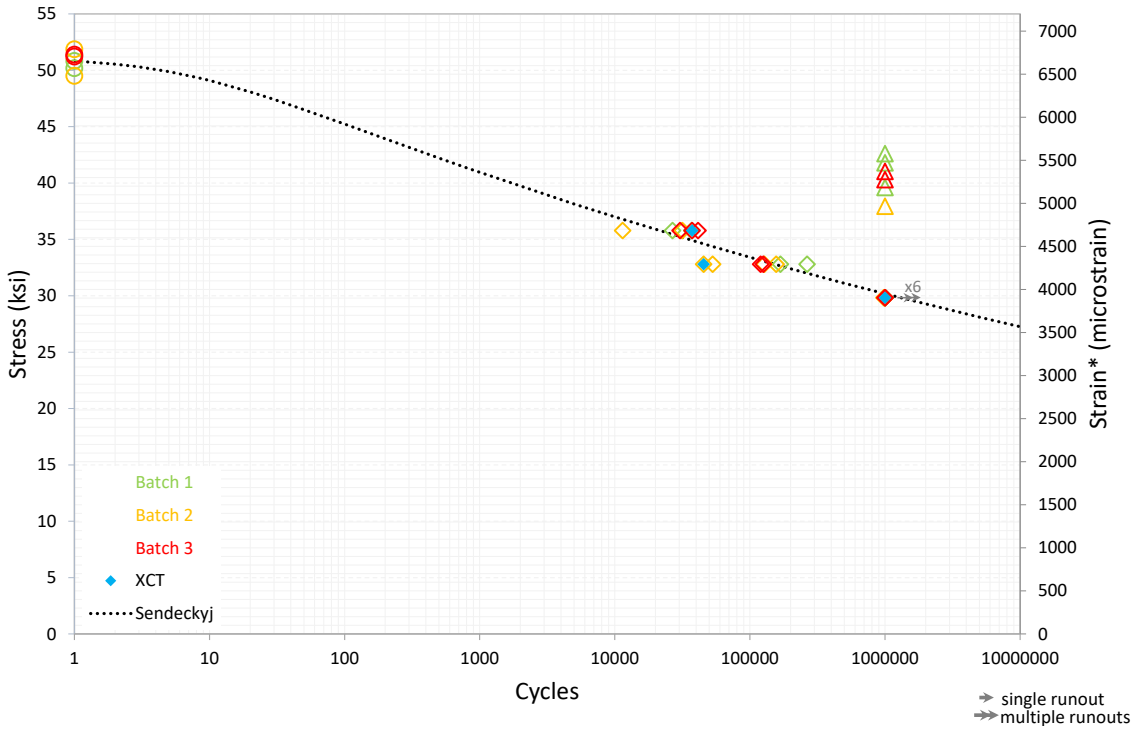


Figure A.6 – SN data with Sendeckyj fitting model for IM7/5320-1, 25/50/25, R=-1, OHC-T.

DISTRIBUTION STATEMENT A.
Approved for public release: distribution is unlimited.

Table A.7 – SN data for IM7/5320-1, 10/80/10, R=0.1, OHT-T.

Specimen	Batch	σ_A	n	σ_R	σ_e
MASC1-B1FO11-0X3	1	42.301	1	৩	৩
MASC1-B2FO11-0X4	2	45.937	1	৩	৩
MASC1-B3FO11-0X4	3	45.597	1	৩	৩
MASC1-B3FO11-0X3	3	44.595	1	৩	৩
MASC1-B2FO11-0X3	2	43.868	1	৩	৩
MASC1-B1FO11-0X4	1	43.622	1	৩	৩
MASC1-B1FO11-3K1	1	35.456	117524	৩	48.173
MASC1-B1FO11-3K2	1	35.456	125653	৩	48.345
MASC1-B2FO11-3K1	2	35.456	159218	৩	48.959
MASC1-B2FO11-3K2	2	35.456	173547	৩	49.185
MASC1-B3FO11-3K1	3	35.456	102390	৩	47.820
MASC1-B3FO11-3K2	3	35.456	88544	৩	47.452
MASC1-B3FO11-XX1	3	35.456	72552	৩	46.951
MASC1-B3FO11-XX2	3	35.456	108651	৩	47.972
MASC1-B1FO11-2K1	1	31.024	614246	৩	46.042
MASC1-B1FO11-2K2	1	31.024	436235	৩	45.208
MASC1-B2FO11-2K1	2	31.024	881537	৩	46.939
MASC1-B2FO11-2K2	2	31.024	774783	৩	46.617
MASC1-B2FO11-XX1	2	31.024	753140	৩	46.546
MASC1-B3FO11-2K1	3	31.024	604467	৩	46.002
MASC1-B3FO11-2K2	3	31.024	854330	৩	46.861
MASC1-B1FO11-1K1	1	26.592	1000000	41.217	42.432
MASC1-B1FO11-1K2	1	26.592	1000000	42.027	42.951
MASC1-B1FO11-XX1	1	26.592	1000000	41.578	42.655
MASC1-B2FO11-1K1	2	26.592	1000000	41.827	42.816
MASC1-B2FO11-1K2	2	26.592	1000000	43.522	44.065
MASC1-B3FO11-1K1	3	26.592	1000000	41.571	42.650

DISTRIBUTION STATEMENT A.
Approved for public release: distribution is unlimited.



Figure A.7 – SN data with Sendeckyj fitting model for IM7/5320-1, 10/80/10, R=0.1, OHT-T.

DISTRIBUTION STATEMENT A.
Approved for public release: distribution is unlimited.

Table A.8 – SN data for IM7/5320-1, 10/80/10, R=5, OHC-C.

Specimen	Batch	σ_A	n	σ_R	σ_e
MASC1-B1FO11-0X1	1	40.191	1		
MASC1-B3FO11-0X2	3	42.556	1		
MASC1-B3FO11-0X1	3	41.621	1		
MASC1-B2FO11-0X1	2	41.198	1		
MASC1-B2FO11-0X2	2	40.149	1		
MASC1-B1FO11-0X2	1	38.876	1		
MASC1-B1FO11-3L1	1	32.612	33584		41.340
MASC1-B1FO11-3L2	1	32.612	17895		40.126
MASC1-B2FO11-3L1	2	32.612	60072		42.498
MASC1-B2FO11-3L2	2	32.612	55195		42.327
MASC1-B3FO11-3L1	3	32.612	53642		42.270
MASC1-B3FO11-3L2	3	32.612	31566		41.218
MASC1-B3FO11-XX5	3	32.612	19286		40.268
MASC1-B1FO11-2L1	1	28.536	260381		39.881
MASC1-B1FO11-2L2	1	28.536	558263		41.360
MASC1-B2FO11-2L1	2	28.536	595604		41.488
MASC1-B2FO11-2L2	2	28.536	881197		42.272
MASC1-B2FO11-XX2	2	28.536	308285		40.203
MASC1-B3FO11-2L1	3	28.536	816227		42.117
MASC1-B3FO11-2L2	3	28.536	292522		40.103
MASC1-B1FO11-1L1	1	24.459	1000000	39.279	39.637
MASC1-B1FO11-1L2	1	24.459	1000000	40.877	41.047
MASC1-B1FO11-XX2	1	24.459	1000000	39.933	40.198
MASC1-B2FO11-1L1	2	24.459	1000000	39.288	39.645
MASC1-B2FO11-1L2	2	24.459	1000000	38.846	39.283
MASC1-B3FO11-1L1	3	24.459	1000000	40.280	40.505
MASC1-B3FO11-1L2	3	24.459	1000000	40.274	40.500

DISTRIBUTION STATEMENT A.
Approved for public release: distribution is unlimited.

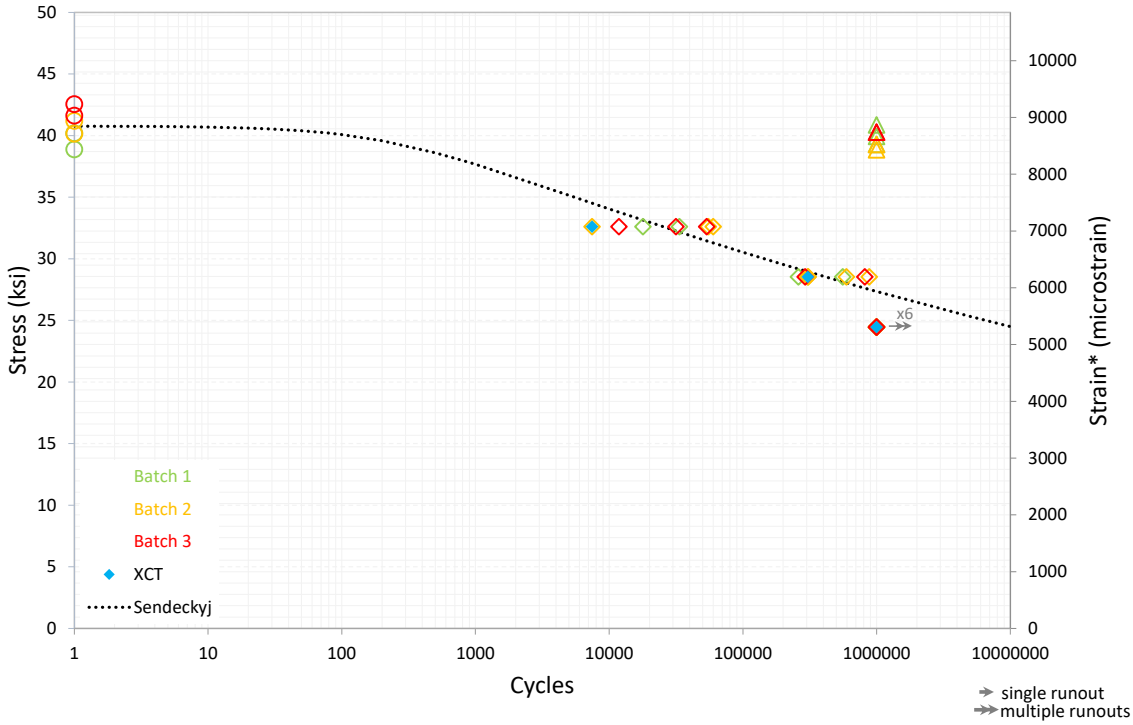


Figure A.8 – SN data with Sendeckyj fitting model for IM7/5320-1, 10/80/10, R=5, OHC-C.

DISTRIBUTION STATEMENT A.
Approved for public release: distribution is unlimited.

Table A.9 – SN data for IM7/5320-1, 10/80/10, R=-1, OHC-T.

Specimen	Batch	σ_A	n	σ_R	σ_e
MASC1-B1FO11-0X1	1	40.191	1	"	"
MASC1-B3FO11-0X2	3	42.556	1	"	"
MASC1-B3FO11-0X1	3	41.621	1	"	"
MASC1-B2FO11-0X1	2	41.198	1	"	"
MASC1-B2FO11-0X2	2	40.149	1	"	"
MASC1-B1FO11-0X2	1	38.876	1	"	"
MASC1-B1FO11-3M1	1	21.271	59608	"	41.009
MASC1-B1FO11-3M2	1	21.271	67318	"	41.330
MASC1-B2FO11-3M1	2	21.271	92686	"	42.184
MASC1-B2FO11-3M2	2	21.271	72449	"	41.524
MASC1-B3FO11-3M1	3	21.271	93147	"	42.197
MASC1-B3FO11-3M2	3	21.271	109461	"	42.635
MASC1-B3FO11-XX7	3	21.271	73237	"	41.553
MASC1-B1FO11-2M1	1	19.144	349412	"	41.330
MASC1-B1FO11-2M2	1	19.144	262983	"	40.585
MASC1-B2FO11-2M1	2	19.144	339859	"	41.256
MASC1-B2FO11-XX3	2	19.144	321167	"	41.107
MASC1-B2FO11-XX4	2	19.144	180735	"	39.623
MASC1-B3FO11-XX6	3	19.144	221399	"	40.141
MASC1-B3FO11-2M2	3	19.144	268696	"	40.641
MASC1-B1FO11-XX3	1	14.890	1000000	34.706	36.116
MASC1-B1FO11-1M2	1	14.890	1000000	35.366	36.508
MASC1-B1FO11-XX4	1	14.890	1000000	34.174	35.835
MASC1-B2FO11-1M1	2	14.890	1000000	43.091	43.171
MASC1-B2FO11-1M2	2	14.890	1000000	36.875	37.563
MASC1-B3FO11-1M1	3	14.890	1000000	36.767	37.481
MASC1-B3FO11-1M2	3	14.890	1000000	40.731	40.910

DISTRIBUTION STATEMENT A.
Approved for public release: distribution is unlimited.

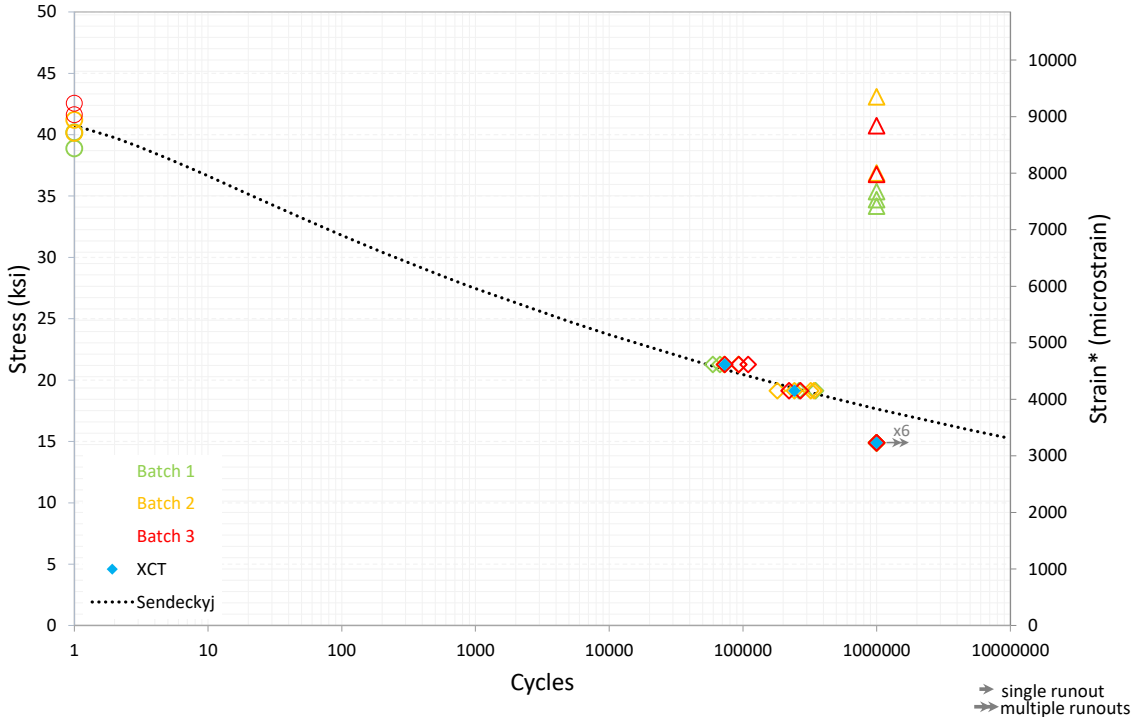


Figure A.9 – SN data with Sendeckyj fitting model for IM7/5320-1, 10/80/10, R=-1, OHC-T.

DISTRIBUTION STATEMENT A.
Approved for public release: distribution is unlimited.

Table A.10 – SN data for IM7/5320-1, 50/40/10, R=0.1, DNS.

Specimen	Batch	σ_A	n	σ_R	σ_e
MASC1-B1DD11-XX4	1	3.690	1		
MASC1-B1DD11-XX5	1	3.582	1		
MASC1-B3DD11-XX4	3	3.307	1		
MASC1-B2DD11-XX4	2	3.306	1		
MASC1-B3DD11-XX3	3	3.208	1		
MASC1-B2DD11-XX3	2	2.997	1		
MASC1-B2DD11-XXB	2	1.842	15512		3.646
MASC1-B2DD11-XXD	2	1.842	16507		3.661
MASC1-B3DD11-XX9	3	1.842	8900		3.515
MASC1-B1DD11-XXA	1	1.674	48118		3.570
MASC1-B1DD11-XXB	1	1.674	18754		3.355
MASC1-B2DD11-3K2	2	1.674	71216		3.664
MASC1-B2DD11-XX6	2	1.674	35285		3.498
MASC1-B3DD11-3K2	3	1.674	29169		3.454
MASC1-B3DD11-XX5	3	1.674	43224		3.545
MASC1-B3DD11-XX8	3	1.674	25192		3.421
MASC1-B1DD11-XX8	1	1.507	337470		3.654
MASC1-B1DD11-XXD	1	1.507	107106		3.388
MASC1-B2DD11-2K2	2	1.507	152848		3.468
MASC1-B2DD11-XX7	2	1.507	257780		3.590
MASC1-B2DD11-XX9	2	1.507	103482		3.380
MASC1-B3DD11-2K1	3	1.507	175873		3.500
MASC1-B3DD11-2K2	3	1.507	243881		3.577
MASC1-B1DD11-XXF	1	1.339	1000000	1.965	3.487
MASC1-B1DD11-XXG	1	1.339	1000000	2.635	3.490
MASC1-B1DD11-XXK	1	1.339	805478		3.438
MASC1-B2DD11-1K2	2	1.339	1000000	2.459	3.488
MASC1-B2DD11-XX8	2	1.339	1000000	2.698	3.492
MASC1-B3DD11-XXA	3	1.339	1000000	2.778	3.494
MASC1-B3DD11-1K2	3	1.339	1000000	2.879	3.499

DISTRIBUTION STATEMENT A.
Approved for public release: distribution is unlimited.

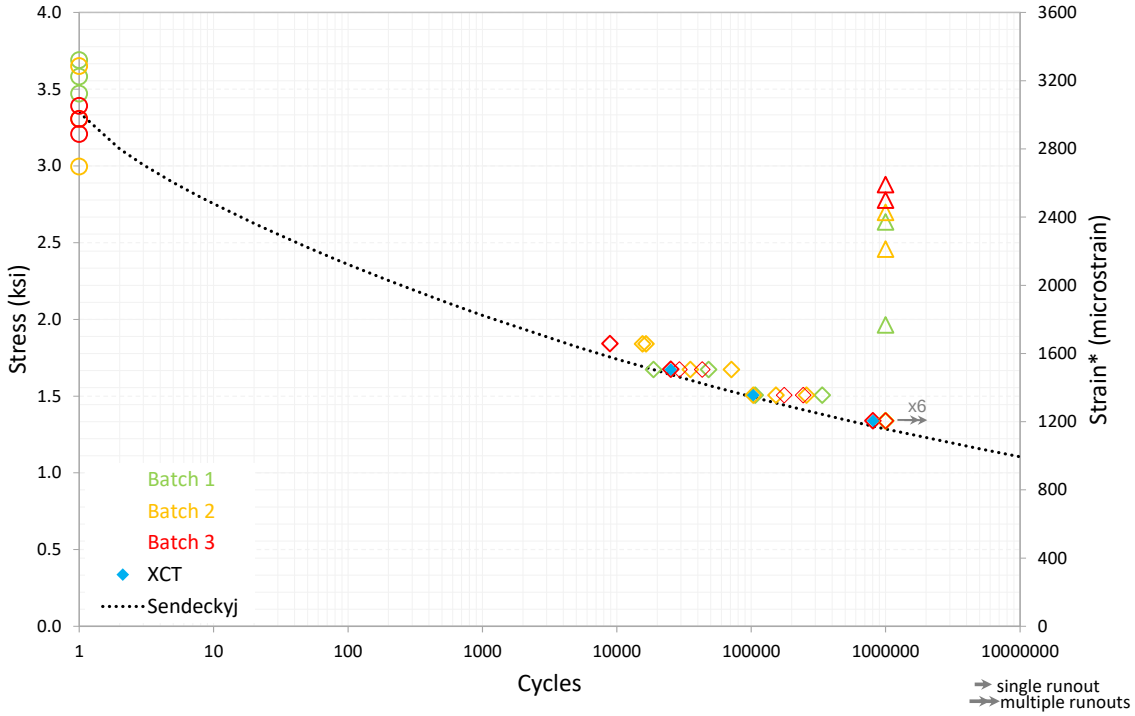


Figure A.10 – SN data with Sendeckyj fitting model for IM7/5320-1, 50/40/10, R=0.1, DNS.

DISTRIBUTION STATEMENT A.
Approved for public release: distribution is unlimited.

Table A.11 – SN data for IM7/5320-1, 10/80/10, R=0.1, DNS.

Specimen	Batch	σ_A	n	σ_R	σ_e
MASC1-B3FD11-XX4	3	3.229	1		
MASC1-B1FD11-XX5	1	3.175	1		
MASC1-B3FD11-XX3	3	3.097	1		
MASC1-B1FD11-XX6	1	3.080	1		
MASC1-B2FD11-XX3	2	2.972	1		
MASC1-B2FD11-XX4	2	2.845	1		
MASC1-B1FD11-XX8	1	1.840	44784		3.114
MASC1-B2FD11-3K1	2	1.840	30596		3.049
MASC1-B2FD11-3K2	2	1.840	34745		3.070
MASC1-B3FD11-3K1	3	1.840	78890		3.213
MASC1-B3FD11-3K2	3	1.840	43900		3.110
MASC1-B3FD11-XXK	3	1.840	23709		3.006
MASC1-B1FD11-XX9	1	1.610	413892		3.081
MASC1-B1FD11-1K2	1	1.610	458888		3.098
MASC1-B1FD11-XXC	1	1.610	74309		2.802
MASC1-B2FD11-XX5	2	1.610	274476		3.011
MASC1-B2FD11-XX7	2	1.610	263262		3.004
MASC1-B3FD11-XX5	3	1.610	436578		3.090
MASC1-B3FD11-1K2	3	1.610	502218		3.114
MASC1-B1FD11-2K2	1	1.380	1000000	2.879	2.945
MASC1-B1FD11-XXD	1	1.380	1000000	3.030	3.061
MASC1-B2FD11-XX8	2	1.380	1000000	2.647	2.828
MASC1-B2FD11-XXB	2	1.380	830834		2.744
MASC1-B2FD11-XXD	2	1.380	1000000	2.746	2.867
MASC1-B3FD11-XXA	3	1.380	1000000	2.993	3.030
MASC1-B3FD11-XXB	3	1.380	1000000	2.673	2.837

DISTRIBUTION STATEMENT A.
Approved for public release: distribution is unlimited.

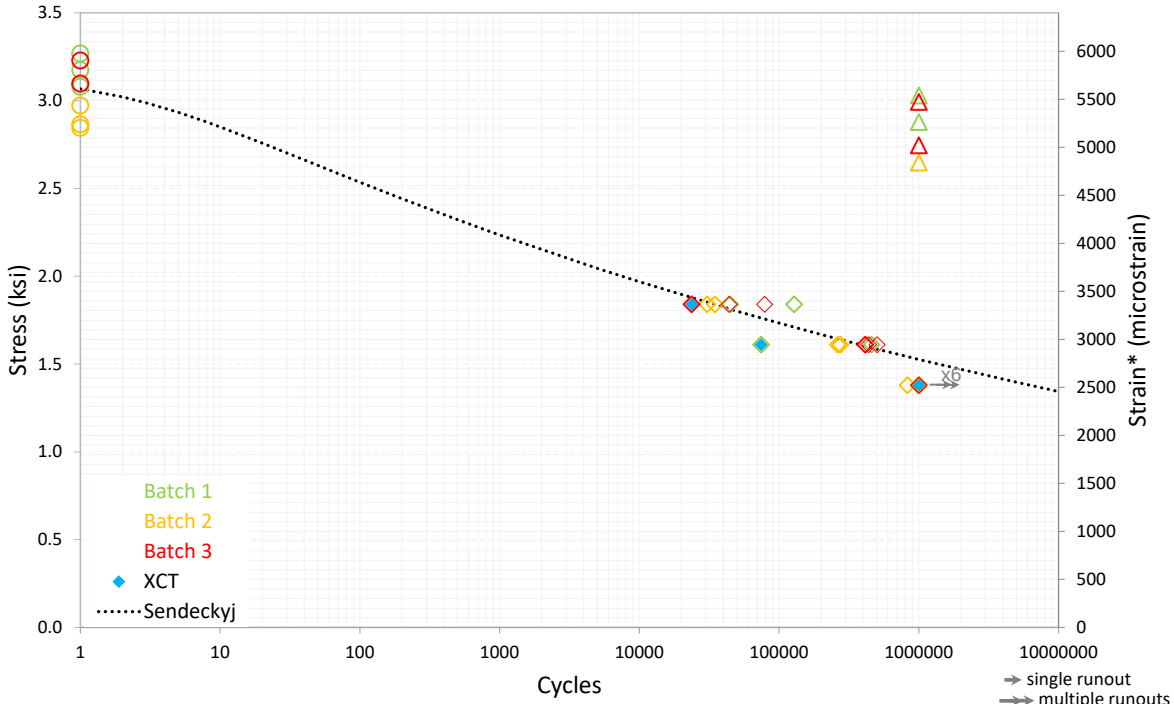


Figure A.11 – SN data with Sendeckyj fitting model for IM7/5320-1, 10/80/10, R=0.1, DNS.

DISTRIBUTION STATEMENT A.
Approved for public release: distribution is unlimited.

Table A.12 – SN data for IM7/5320-1, 50/40/10, R=0.1, ILT.

Specimen	Batch	σ_A	n	σ_R	σ_e
MASC1-B1DI11-0X2	1	13.510	1	৩	৩
MASC1-B1DI11-0X1	1	13.437	1	৩	৩
MASC1-B1DI11-XX7	1	12.807	1	৩	৩
MASC1-B3DI11-0X2	3	12.138	1	৩	৩
MASC1-B3DI11-XX1	3	10.745	1	৩	৩
MASC1-B2DI11-0X2	2	10.613	1	৩	৩
MASC1-B2DI11-XX5	2	9.922	1	৩	৩
MASC1-B3DI11-0X1	3	9.492	1	৩	৩
MASC1-B2DI11-0X1	2	9.045	1	৩	৩
MASC1-B1DI11-XX8	1	7.224	2574	৩	13.508
MASC1-B2DI11-XX5	2	7.224	108	৩	11.502
MASC1-B3DI11-XX6	3	7.224	1274	৩	13.036
MASC1-B1DI11-XX4	1	5.641	213867	৩	13.190
MASC1-B1DI11-XX5	1	5.641	21065	৩	11.731
MASC1-B2DI11-XX3	2	5.641	63115	৩	12.400
MASC1-B2DI11-XX4	2	5.641	133848	৩	12.881
MASC1-B3DI11-3K2	3	5.641	85268	৩	12.590
MASC1-B1DI11-XX2	1	5.077	1000000	12.275	13.061
MASC1-B1DI11-XX3	1	5.077	1000000	12.434	13.115
MASC1-B2DI11-2K2	2	5.077	171113	৩	11.738
MASC1-B2DI11-XX2	2	5.077	203737	৩	11.842
MASC1-B3DI11-XX3	3	5.077	326301	৩	12.127
MASC1-B3DI11-XX4	3	5.077	1000000	11.721	12.934
MASC1-B1DI11-4K1	1	4.513	1000000	11.641	11.947
MASC1-B1DI11-4K2	1	4.513	1000000	12.099	12.266
MASC1-B2DI11-4K1	2	4.513	321595	৩	10.772
MASC1-B2DI11-4K2	2	4.513	1000000	8.124	11.409
MASC1-B3DI11-1K1	3	4.513	1000000	12.955	13.006
MASC1-B3DI11-1K2	3	4.513	1000000	11.352	11.786

DISTRIBUTION STATEMENT A.
Approved for public release: distribution is unlimited.

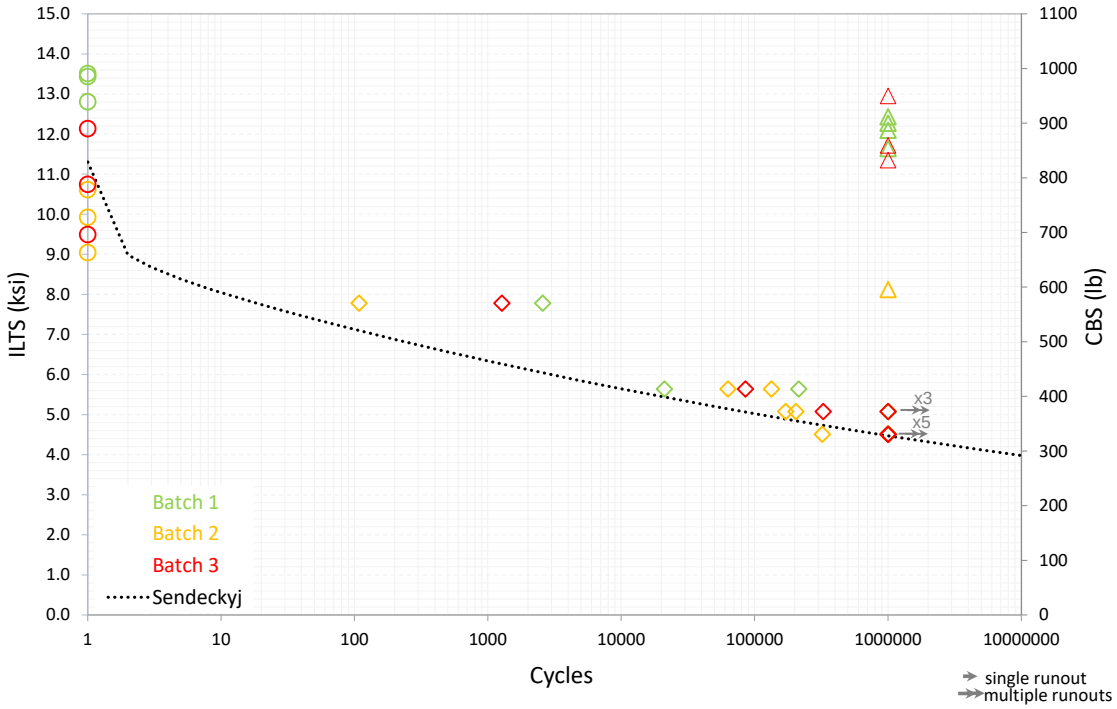


Figure A.12 – SN data with Sendeckyj fitting model for IM7/5320-1, 50/40/10, R=0.1, ILT.

DISTRIBUTION STATEMENT A.
Approved for public release: distribution is unlimited.

Table A.13 – SN data for IM7/5320-1, 10/80/10, R=0.1, ILT.

Specimen	Batch	σ_A	n	σ_R	σ_e
MASC1-B3FI11-0X1	3	12.027	1		
MASC1-B3FI11-0X2	3	11.601	1		
MASC1-B2FI31-XX2	2	11.283	1		
MASC1-B1FI31-XX2	1	11.226	1		
MASC1-B1FI31-XX1	1	10.344	1		
MASC1-B2FI31-0X2	2	9.303	1		
MASC1-B1FI31-XX5	1	6.030	1954		10.182
MASC1-B1FI31-XX6	1	6.030	13295		11.803
MASC1-B3FI21-3K2	3	6.030	19395		12.152
MASC1-B1FI31-1K2	1	4.934	18431		9.904
MASC1-B1FI31-XX3	1	4.934	129344		11.509
MASC1-B2FI31-3K1	2	4.934	170582		11.757
MASC1-B2FI31-XX7	2	4.934	241381		12.076
MASC1-B2FI31-4K2	2	4.934	42899		10.571
MASC1-B3FI11-XX5	3	4.934	39484		10.503
MASC1-B3FI11-3K2	3	4.934	129055		11.507
MASC1-B1FI31-2K1	1	4.386	51021		9.523
MASC1-B1FI31-2K2	1	4.386	30974		9.164
MASC1-B2FI31-2K1	2	4.386	269346		10.826
MASC1-B2FI31-XX6	2	4.386	301070		10.919
MASC1-B3FI11-4K1	3	4.386	203044		10.593
MASC1-B1FI31-XX4	1	3.837	1000000	9.951	10.817
MASC1-B2FI31-XX4	2	3.837	1000000	10.900	11.302
MASC1-B2FI31-1K2	2	3.837	1000000		
MASC1-B3FI11-4K2	3	3.837	1000000	10.693	11.173
MASC1-B3FI11-1K2	3	3.837	1000000	9.834	10.776

DISTRIBUTION STATEMENT A.
Approved for public release: distribution is unlimited.

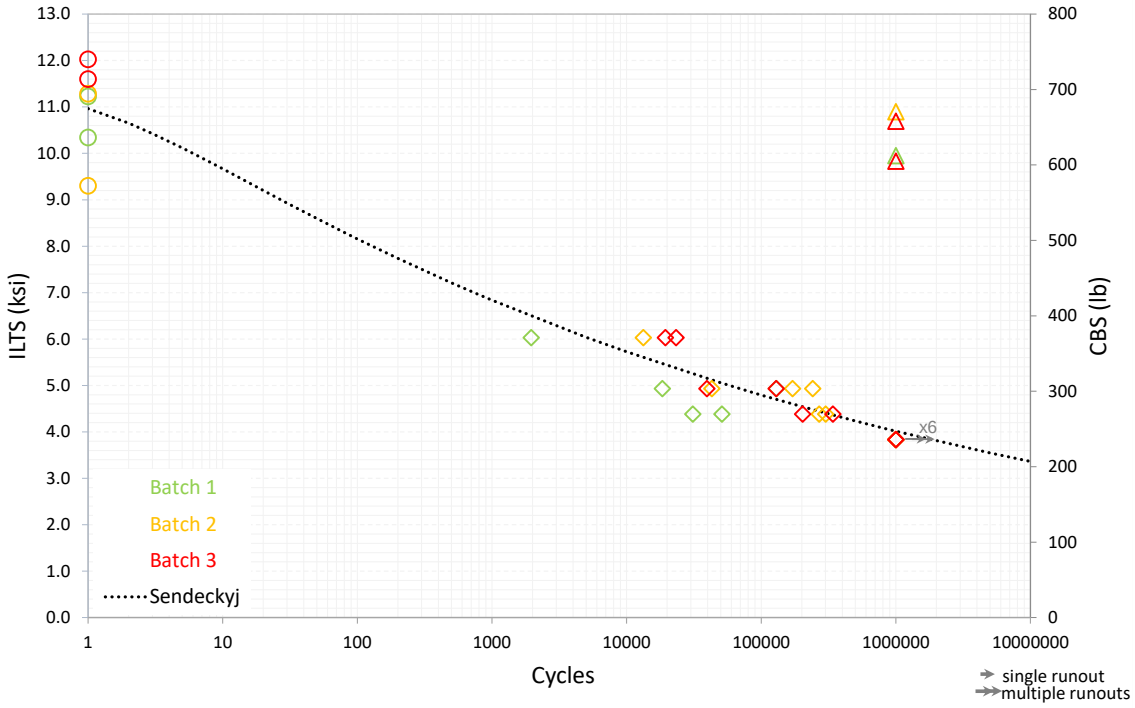


Figure A.13 – SN data with Sendeckyj fitting model for IM7/5320-1, 10/80/10, R=0.1, ILT.

DISTRIBUTION STATEMENT A.
Approved for public release: distribution is unlimited.

Table A.14 – SN data for IM7/5320-1, 100/0/0, R=0.1, SBS.

Specimen	Batch	σ_A	n	σ_R	σ_e
MASC1-B3AS11-0X1	3	16.548	1		
MASC1-B3AS11-0X3	3	16.539	1		
MASC1-B2AS11-0X3	2	16.461	1		
MASC1-B2AS11-0X4	2	16.380	1		
MASC1-B3AS11-0X2	3	16.371	1		
MASC1-B2AS11-1K2	2	16.245	1		
MASC1-B2AS11-1K1	2	16.223	1		
MASC1-B1AS11-0X1	1	16.167	1		
MASC1-B1AS11-0X2	1	16.118	1		
MASC1-B1AS11-0X3	1	15.949	1		
MASC1-B1AS11-3K1	1	10.595	6250		16.070
MASC1-B2AS11-1K1	2	10.595	6613		16.100
MASC1-B2AS11-1K2	2	10.595	5763		16.027
MASC1-B3AS11-1K1	3	10.595	13020		16.468
MASC1-B3AS11-1K2	3	10.595	15491		16.563
MASC1-B1AS11-XX1	1	9.373	51901		15.255
MASC1-B1AS11-3K2	1	9.373	79010		15.469
MASC1-B2AS11-3K1	2	9.373	440127		16.380
MASC1-B2AS11-3K2	2	9.373	119987		15.686
MASC1-B3AS11-3K1	3	9.373	73362		15.431
MASC1-B1AS11-2K1	1	8.965	1000000	13.144	16.102
MASC1-B1AS11-XX4	2	8.965	1000000	14.706	16.135
MASC1-B2AS11-2K1	2	8.965	1000000	14.829	16.144
MASC1-B2AS11-XX3	2	8.965	1000000	15.034	16.165
MASC1-B3AS11-2K1	3	8.965	1000000	15.303	16.206
MASC1-B3AS11-2K2	3	8.965	1000000	15.699	16.308
MASC1-B3AS11-XX1	3	8.965	1000000	15.407	16.228
MASC1-B3AS11-XX2	3	8.965	1000000	14.128	16.111

DISTRIBUTION STATEMENT A.
Approved for public release: distribution is unlimited.

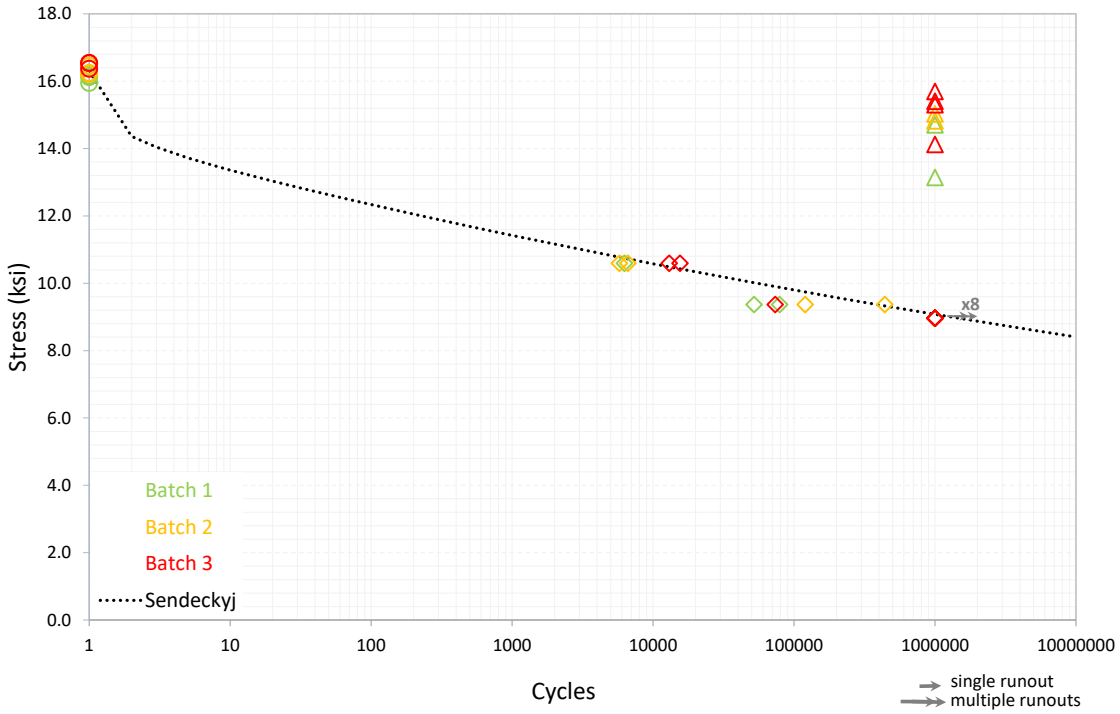


Figure A.14 – SN data with Sendeckyj fitting model for IM7/5320-1, 100/0/0, R=0.1, SBS.

DISTRIBUTION STATEMENT A.
Approved for public release: distribution is unlimited.

A.2 SN Data and Sendeckyj Fitting Models for T650/5320-1 8 Harness Satin Fabric

SN data and Sendeckyj fitting model to fatigue data analysis for the T650/5320-1 8HS tests are displayed and are also found in the MASC database. In these tables, n, σ_A, σ_R and σ_e are the number of cycles survived (n=1 indicates static failure), the fatigue stress level (or static failure stress value), the residual strength after surviving the corresponding number of cycles, and the equivalent static strength (pooled), respectively.

Table A.15 – SN data for T650/5320-1, 40/20/40, R=0.1, OHT-T.

Specimen	Batch	σ_A	n	σ_R	σ_e
MASC1-C1GO11-0X3	1	68.579	1	"	"
MASC1-C1GO11-0X4	1	62.581	1	"	"
MASC1-C2GO11-0X3	2	58.737	1	"	"
MASC1-C2GO11-0X4	2	58.371	1	"	"
MASC1-C3GO11-0X3	3	58.138	1	"	"
MASC1-C3GO11-0X4	3	57.999	1	"	"
MASC1-C1GO11-3K2	1	54.661	1000000	73.692	
MASC1-C2GO11-3K2	2	54.661	1000000	77.678	
MASC1-C3GO11-XX1	3	54.661	1000000	86.884	
MASC1-C2GO11-XX2	2	48.587	1000000	70.409	
MASC1-C1GO11-3K1	1	48.587	1000000	72.093	
MASC1-C2GO11-3K1	2	48.587	1000000	66.381	
MASC1-C3GO11-3K1	3	48.587	1000000	78.926	
MASC1-C1GO11-XX1	1	42.514	1000000	70.178	
MASC1-C1GO11-2K2	1	42.514	1000000	72.454	
MASC1-C2GO11-2K1	2	42.514	1000000	69.365	
MASC1-C3GO11-2K1	3	42.514	1000000	82.417	
MASC1-C1GO11-1K1	1	36.440	1000000	68.319	
MASC1-C2GO11-1K1	2	36.440	1000000	71.664	
MASC1-C3GO11-1K1	3	36.440	1000000	78.544	

DISTRIBUTION STATEMENT A.
Approved for public release: distribution is unlimited.



Figure A.15 – SN data for T650/5320-1, 40/20/40, R=0.1, OHT-T.

Sendeckyj wearout analysis prediction and equivalent static strength data for T650/5320-1 8 harness satin fabric, 40/20/40, R=0.1 OH, are not included as all fatigue specimens were runouts (Table A.15).

DISTRIBUTION STATEMENT A.
Approved for public release: distribution is unlimited.

Table A.16 – SN data for T650/5320-1, 40/20/40, R=5, OHC-C.

Specimen	Batch	σ_A	n	σ_R	σ_e
MASC1-C1GO11-0X1	1	61.862	1		
MASC1-C1GO11-0X2	1	59.854	1		
MASC1-C2GO11-0X1	2	58.081	1		
MASC1-C2GO11-0X2	2	57.284	1		
MASC1-C3GO11-0X1	3	56.431	1		
MASC1-C3GO11-0X2	3	54.813	1		
MASC1-C1GO11-3L1	1	46.443	1044		57.151
MASC1-C1GO11-3L2	1	46.443	1857		58.295
MASC1-C2GO11-3L1	2	46.443	1060		57.181
MASC1-C2GO11-3L2	2	46.443	10162		61.809
MASC1-C3GO11-3L1	3	46.443	6655		60.915
MASC1-C3GO11-3L2	3	46.443	6488		60.861
MASC1-C1GO11-2L1	1	40.638	51027		57.175
MASC1-C1GO11-2L2	1	40.638	50343		57.148
MASC1-C2GO11-XX1	2	40.638	283777		60.657
MASC1-C2GO11-2L2	2	40.638	72105		57.860
MASC1-C2GO11-XX3	2	40.638	120356		58.890
MASC1-C3GO11-2L1	3	40.638	66826		57.709
MASC1-C3GO11-2L2	3	40.638	317039		60.889
MASC1-C1GO11-1L1	1	34.832	1000000	54.489	55.709
MASC1-C1GO11-1L2	1	34.832	1000000	57.299	57.676
MASC1-C1GO11-XX2	1	34.832	1000000	59.308	59.460
MASC1-C2GO11-1L1	2	34.832	1000000	56.309	56.891
MASC1-C2GO11-1L2	2	34.832	1000000	54.671	55.809
MASC1-C3GO11-1L1	3	34.832	1000000	56.581	57.098
MASC1-C3GO11-1L2	3	34.832	1000000	59.539	59.676

DISTRIBUTION STATEMENT A.
Approved for public release: distribution is unlimited.

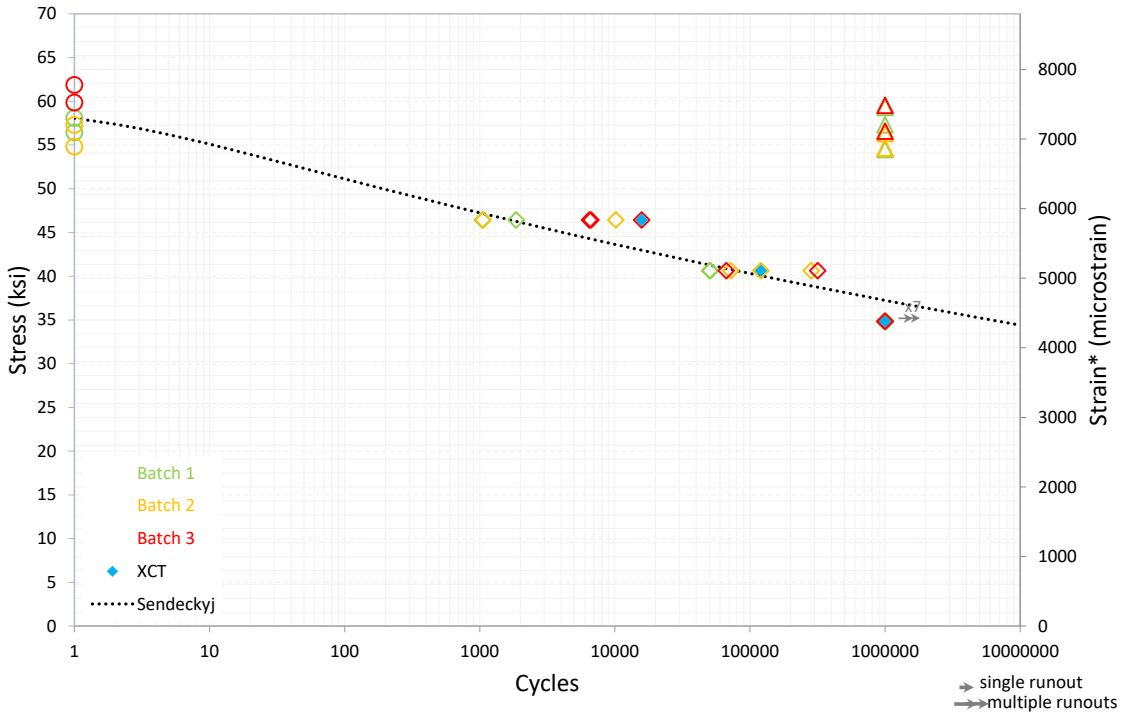


Figure A.16 – SN data with Sendeckyj fitting model for T650/5320-1, 40/20/40, R=5, OHC-C.

DISTRIBUTION STATEMENT A.
Approved for public release: distribution is unlimited.

Table A.17 – SN data for T650/5320-1, 40/20/40, R=-1, OHC-T.

Specimen	Batch	σ_A	n	σ_R	σ_e
MASC1-C1GO11-0X1	1	61.862	1	-	-
MASC1-C1GO11-0X2	1	59.854	1	-	-
MASC1-C2GO11-0X1	2	58.081	1	-	-
MASC1-C2GO11-0X2	2	57.284	1	-	-
MASC1-C3GO11-0X1	3	56.431	1	-	-
MASC1-C3GO11-0X2	3	54.813	1	-	-
MASC1-C1GO11-2M1	1	35.636	22599	-	58.085
MASC1-C1GO11-2M2	1	35.636	26464	-	58.878
MASC1-C2GO11-2M1	2	35.636	21137	-	57.753
MASC1-C2GO11-2M2	2	35.636	25918	-	58.772
MASC1-C3GO11-2M1	3	35.636	15611	-	56.272
MASC1-C3GO11-2M2	3	35.636	31504	-	59.766
MASC1-C1GO11-3M1	1	29.697	196837	-	58.305
MASC1-C1GO11-3M2	1	29.697	246102	-	59.436
MASC1-C2GO11-3M1	2	29.697	75111	-	53.667
MASC1-C2GO11-3M2	2	29.697	187839	-	58.070
MASC1-C3GO11-3M1	3	29.697	230130	-	59.094
MASC1-C3GO11-3M2	3	29.697	345114	-	61.191
MASC1-C1GO11-1M1	1	20.788	1000000	58.845	59.200
MASC1-C1GO11-1M2	1	20.788	1000000	58.104	58.508
MASC1-C2GO11-1M1	2	20.788	1000000	55.284	55.951
MASC1-C2GO11-1M2	2	20.788	1000000	53.624	54.523
MASC1-C3GO11-1M1	3	20.788	1000000	54.592	55.348
MASC1-C3GO11-1M2	3	20.788	1000000	52.603	53.684

DISTRIBUTION STATEMENT A.
Approved for public release: distribution is unlimited.

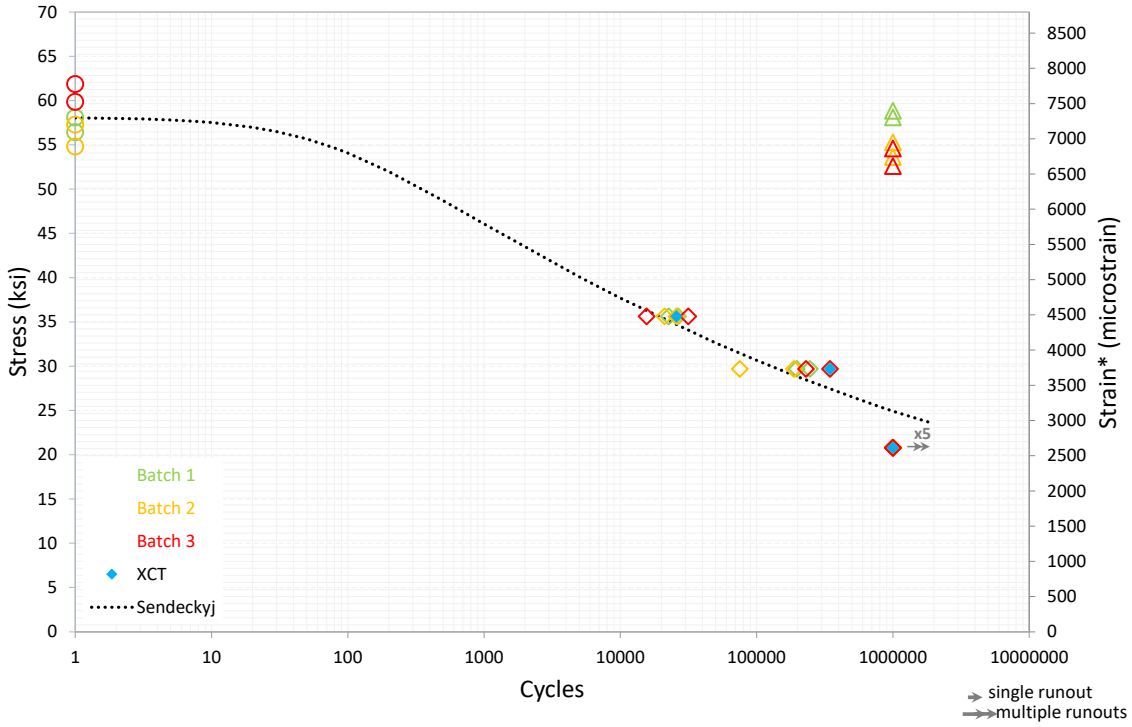


Figure A.17 – SN data with Sendeckyj fitting model for T650/5320-1, 40/20/40, R=-1, OHC-T.

DISTRIBUTION STATEMENT A.
Approved for public release: distribution is unlimited.

Table A.18 – SN data for T650/5320-1, 25/50/25, R=0.1, OHT-T.

Specimen	Batch	σ_A	n	σ_R	σ_e
MASC1-C1EO11-0X3	1	51.033	1		
MASC1-C1EO11-0X4	1	50.370	1		
MASC1-C2EO21-0X4	2	48.861	1		
MASC1-C2EO21-0X3	2	48.672	1		
MASC1-C3EO11-0X3	3	47.022	1		
MASC1-C3EO11-0X4	3	45.049	1		
MASC1-C2EO21-3K2	2	43.651	1000000	52.175	
MASC1-C3EO11-3K2	3	43.651	1000000	54.757	
MASC1-C3EO11-XX1	3	43.651	1000000	56.083	
MASC1-C2EO21-2K2	2	38.801	1000000	49.275	
MASC1-C1EO11-3K1	1	38.801	1000000	49.524	
MASC1-C2EO21-3K1	2	38.801	1000000	52.857	
MASC1-C3EO11-3K1	3	38.801	1000000	54.009	
MASC1-C1EO11-1K2	1	33.951	1000000	48.170	
MASC1-C1EO11-2K1	1	33.951	1000000	46.658	
MASC1-C2EO21-2K1	2	33.951	1000000	54.208	
MASC1-C3EO11-2K1	3	33.951	1000000	54.923	
MASC1-C1EO11-1K1	1	29.101	1000000	50.752	
MASC1-C2EO21-1K1	2	29.101	1000000	53.303	
MASC1-C3EO11-1K1	3	29.101	1000000		

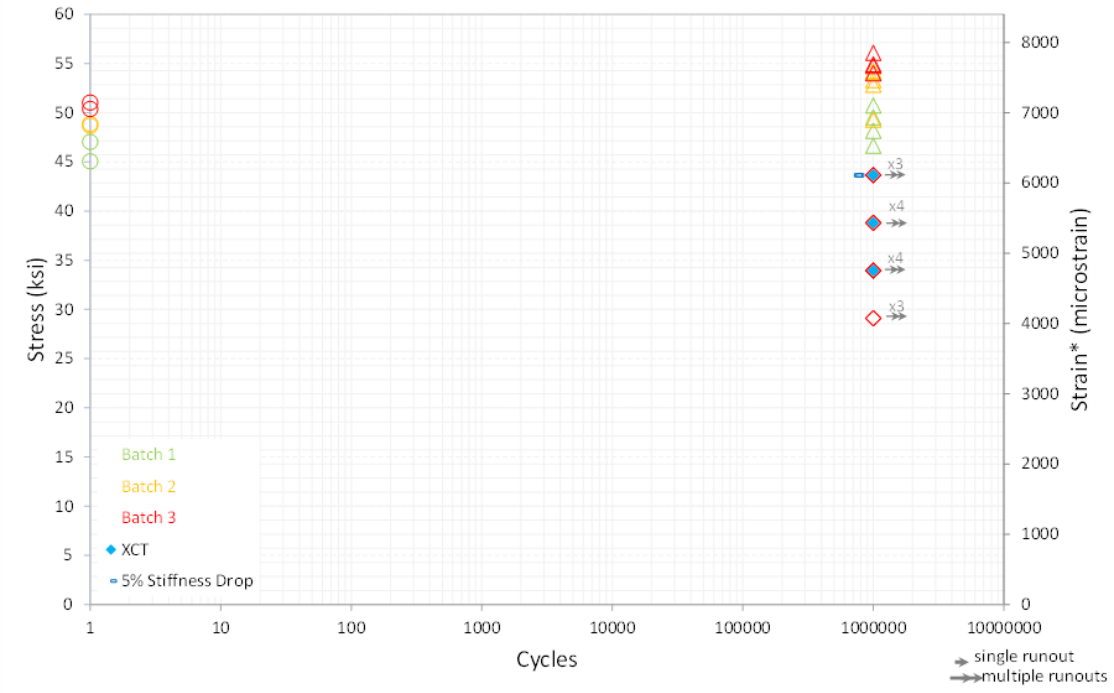


Figure A.18 – SN data for T650/5320-1, 25/50/25, R=0.1, OHT-T.

DISTRIBUTION STATEMENT A.
Approved for public release: distribution is unlimited.

Sendeckyj wearout analysis prediction and equivalent static strength data for T650/5320-1 8 harness satin fabric, 25/50/25, R=0.1 OH, are not included as all fatigue specimens were runouts (Table).

Table A.18 – SN data for T650/5320-1, 25/50/25, R=5, OHC-C.

Specimen¤	Batch¤	σ_A¤	n¤	σ_R¤	σ_e¤	¤
MASC1-C3EO11-0X3¤	3¤	50.987¤	1¤	¶¤	¶¤	¤
MASC1-C3EO11-0X2¤	3¤	50.857¤	1¤	¶¤	¶¤	¤
MASC1-C1EO11-0X1¤	1¤	50.483¤	1¤	¶¤	¶¤	¤
MASC1-C2EO21-0X1¤	2¤	50.190¤	1¤	¶¤	¶¤	¤
MASC1-C2EO21-0X2¤	2¤	49.029¤	1¤	¶¤	¶¤	¤
MASC1-C1EO11-0X1¤	1¤	47.050¤	1¤	¶¤	¶¤	¤
MASC1-C1EO11-3L1¤	1¤	39.813¤	2218¤	¶¤	47.794¤	¤
MASC1-C1EO11-3L2¤	1¤	39.813¤	1674¤	¶¤	47.257¤	¤
MASC1-C2EO21-3L1¤	2¤	39.813¤	8841¤	¶¤	50.543¤	¤
MASC1-C2EO21-XX1¤	2¤	39.813¤	5161¤	¶¤	49.452¤	¤
MASC1-C3EO11-XX2¤	3¤	39.813¤	2994¤	¶¤	48.376¤	¤
MASC1-C3EO11-3L1¤	3¤	39.813¤	3681¤	¶¤	48.781¤	¤
MASC1-C3EO11-3L2¤	3¤	39.813¤	16574¤	¶¤	51.849¤	¤
MASC1-C1EO11-XX1¤	1¤	34.836¤	44611¤	¶¤	47.230¤	¤
MASC1-C1EO11-2L2¤	1¤	34.836¤	54224¤	¶¤	47.607¤	¤
MASC1-C2EO21-XX2¤	2¤	34.836¤	114900¤	¶¤	49.083¤	¤
MASC1-C2EO21-2L1¤	2¤	34.836¤	199375¤	¶¤	50.196¤	¤
MASC1-C2EO21-2L2¤	2¤	34.836¤	152692¤	¶¤	49.654¤	¤
MASC1-C3EO11-2L1¤	3¤	34.836¤	132370¤	¶¤	49.366¤	¤
MASC1-C3EO11-2L2¤	3¤	34.836¤	294839¤	¶¤	51.001¤	¤
MASC1-C1EO11-1L1¤	1¤	29.860¤	1000000¤	44.461¤	46.638¤	¤
MASC1-C1EO11-1L2¤	1¤	29.860¤	1000000¤	46.202¤	47.394¤	¤
MASC1-C1EO11-XX2¤	1¤	29.860¤	1000000¤	41.530¤	46.093¤	¤
MASC1-C2EO21-1L1¤	2¤	29.860¤	1000000¤	45.092¤	46.867¤	¤
MASC1-C2EO21-1L2¤	2¤	29.860¤	1000000¤	46.059¤	47.317¤	¤
MASC1-C3EO11-1L1¤	3¤	29.860¤	1000000¤	47.545¤	48.243¤	¤
MASC1-C3EO11-1L2¤	3¤	29.860¤	1000000¤	49.520¤	49.817¤	¤

DISTRIBUTION STATEMENT A.
Approved for public release: distribution is unlimited.

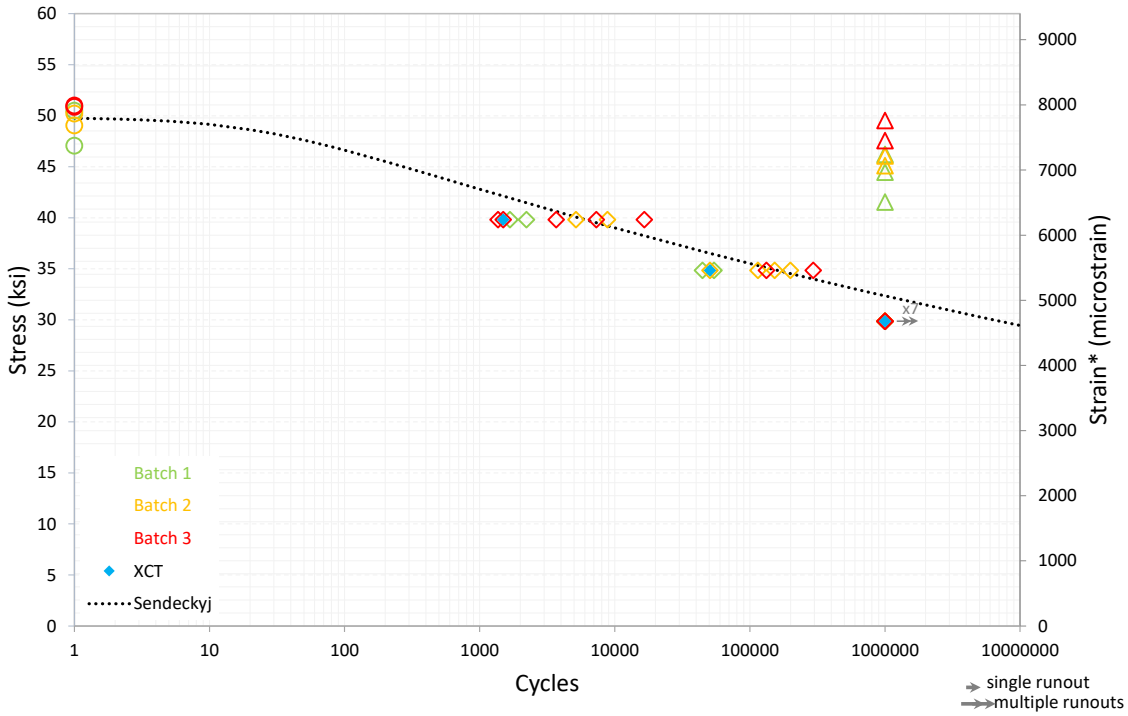


Figure A.19 – SN data with Sendeckyj fitting model for T650/5320-1, 25/50/25, R=5, OHC-C.

DISTRIBUTION STATEMENT A.
Approved for public release: distribution is unlimited.

Table A.19 – SN data for T650/5320-1, 25/50/25, R=-1, OHC-T.

Specimen	Batch	σ_A	n	σ_R	σ_e
MASC1-C3EO11-0X3	3	50.987	1		
MASC1-C3EO11-0X2	3	50.857	1		
MASC1-C1EO11-0X1	1	50.483	1		
MASC1-C2EO21-0X1	2	50.190	1		
MASC1-C2EO21-0X2	2	49.029	1		
MASC1-C1EO11-0X1	1	47.050	1		
MASC1-C1EO11-2M1	1	29.480	51832		50.962
MASC1-C1EO11-2M2	1	29.480	23717		45.352
MASC1-C2EO21-2M1	2	29.480	31364		49.595
MASC1-C2EO21-2M2	2	29.480	54218		51.086
MASC1-C3EO11-XX4	3	29.480	35689		49.943
MASC1-C3EO11-2M2	3	29.480	57962		51.271
MASC1-C1EO11-3M1	1	27.023	156468		49.594
MASC1-C1EO11-3M2	1	27.023	220369		50.523
MASC1-C2EO21-3M1	2	27.023	117468		48.831
MASC1-C2EO21-3M2	2	27.023	134840		49.197
MASC1-C3EO11-3M1	3	27.023	199643		50.253
MASC1-C3EO11-3M2	3	27.023	184473		50.039
MASC1-C1EO11-1M1	1	19.653	1000000	42.497	43.121
MASC1-C1EO11-1M2	1	19.653	1000000	49.276	49.329
MASC1-C2EO21-1M1	2	19.653	1000000	45.701	45.894
MASC1-C2EO21-1M2	2	19.653	1000000	43.826	44.210
MASC1-C3EO11-1M1	3	19.653	1000000	43.789	44.179
MASC1-C3EO11-1M2	3	19.653	1000000	45.331	45.552

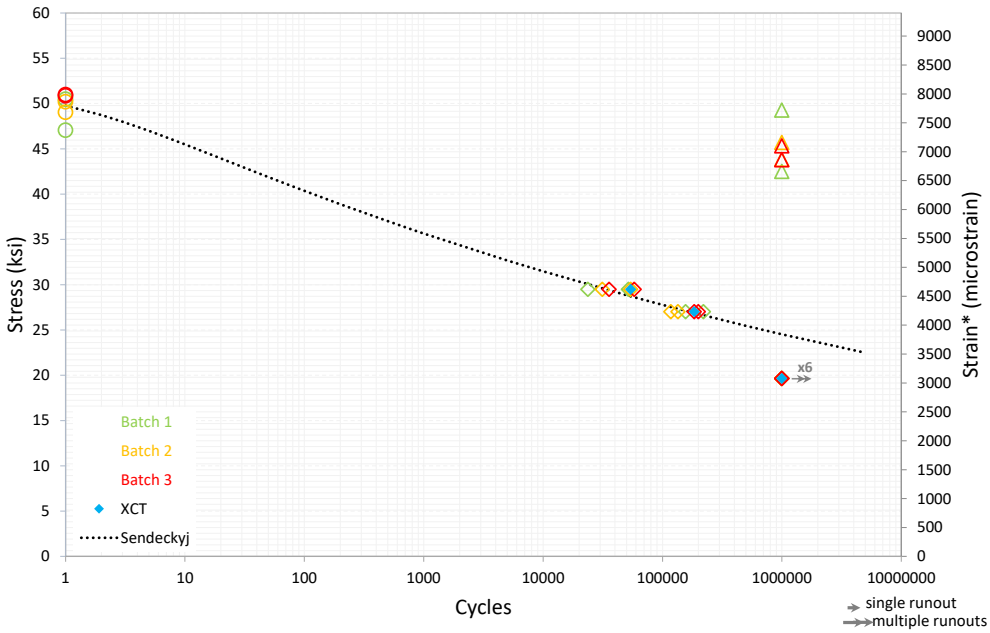


Figure A.20 – SN data with Sendeckyj fitting model for T650/5320-1, 25/50/25, R=-1, OHC-T.

DISTRIBUTION STATEMENT A.
Approved for public release: distribution is unlimited.

Table A.20 – SN data for T650/5320-1, 10/80/10, R=0.1, OHT-T.

Specimen	Batch	σ_A	n	σ_R	σ_e
MASC1-C1FO11-0X4	1	42.324	1		
MASC1-C1FO11-0X3	1	42.072	1		
MASC1-C3FO11-0X3	3	41.821	1		
MASC1-C2FO11-0X3	2	41.618	1		
MASC1-C3FO11-0X4	3	41.089	1		
MASC1-C2FO11-0X4	2	39.984	1		
MASC1-C1FO11-3K1	1	33.188	3575		40.751
MASC1-C1FO11-XX1	1	33.188	21167		43.015
MASC1-C2FO11-3K1	2	33.188	4406		41.011
MASC1-C2FO11-3K2	2	33.188	4632		41.073
MASC1-C3FO11-3K1	3	33.188	6375		41.474
MASC1-C3FO11-3K2	3	33.188	12392		42.320
MASC1-C3FO11-XX1	3	33.188	16958		42.726
MASC1-C1FO11-2K1	1	29.039	530171		41.511
MASC1-C1FO11-2K2	1	29.039	303803		40.814
MASC1-C2FO11-2K1	2	29.039	820266		42.066
MASC1-C2FO11-2K2	2	29.039	413735		41.199
MASC1-C2FO11-XX1	2	29.039	1000000		42.320
MASC1-C3FO11-2K1	3	29.039	951241		42.256
MASC1-C3FO11-2K2	3	29.039	791750		42.021
MASC1-C1FO11-1K1	1	24.891	1000000	39.392	39.469
MASC1-C1FO11-1K2	1	24.891	1000000	38.149	38.352
MASC1-C1FO11-XX2	1	24.891	1000000	38.864	38.981
MASC1-C2FO11-1K1	2	24.891	1000000	36.657	37.259
MASC1-C2FO11-1K2	2	24.891	1000000	35.015	36.577
MASC1-C3FO11-1K1	3	24.891	1000000	37.820	38.081
MASC1-C3FO11-1K2	3	24.891	1000000	34.856	36.539

DISTRIBUTION STATEMENT A.
Approved for public release: distribution is unlimited.

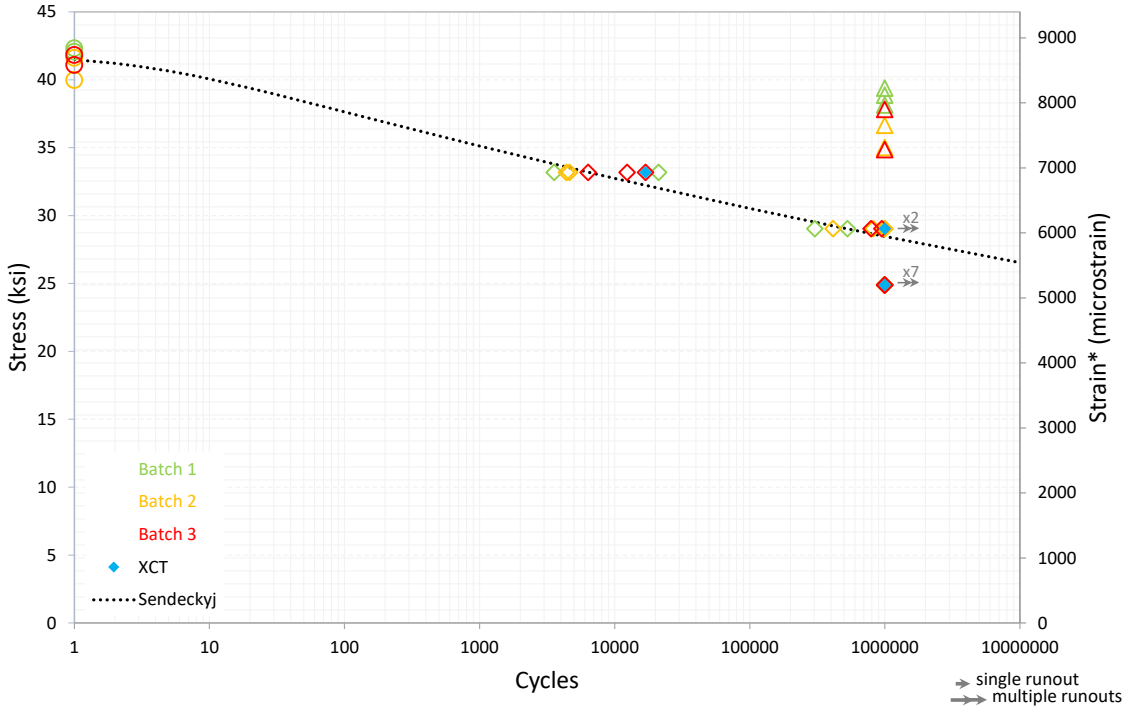


Figure A.21 – SN data with Sendeckyj fitting model for T650/5320-1, 10/80/10, R=0.1, OHT-T.

DISTRIBUTION STATEMENT A.
Approved for public release: distribution is unlimited.

Table A.21 – SN data for T650/5320-1, 10/80/10, R=5, OHC-C.

Specimen	Batch	σ_A	n	σ_R	σ_e
MASC1-C2FO11-0X2	2	41.553	1		
MASC1-C2FO11-0X1	2	41.532	1		
MASC1-C1FO11-0X2	1	41.510	1		
MASC1-C1FO11-0X1	1	41.337	1		
MASC1-C3FO11-0X2	3	40.734	1		
MASC1-C3FO11-0X1	3	40.029	1		
MASC1-C1FO11-3L1	1	32.893	8630		40.591
MASC1-C1FO11-3L2	1	32.893	4308		39.458
MASC1-C2FO11-3L1	2	32.893	12780		41.248
MASC1-C2FO11-3L2	2	32.893	11960		41.136
MASC1-C3FO11-XX2	3	32.893	7301		40.315
MASC1-C3FO11-3L1	3	32.893	8955		40.652
MASC1-C3FO11-3L2	3	32.893	28644		42.635
MASC1-C1FO11-2L1	1	28.781	213748		40.515
MASC1-C1FO11-2L2	1	28.781	168997		40.126
MASC1-C2FO11-2L1	2	28.781	203961		40.437
MASC1-C2FO11-2L2	2	28.781	373247		41.453
MASC1-C2FO11-XX3	2	28.781	166306		40.099
MASC1-C3FO11-2L1	3	28.781	230849		40.643
MASC1-C3FO11-2L2	3	28.781	432282		41.704
MASC1-C1FO11-1L1	1	24.669	1000000		36.999
MASC1-C1FO11-1L2	1	24.669	1000000	39.107	39.480
MASC1-C1FO11-XX3	1	24.669	1000000	39.794	40.052
MASC1-C2FO11-1L1	2	24.669	1000000	40.551	40.721
MASC1-C2FO11-1L2	2	24.669	1000000	41.408	41.515
MASC1-C3FO11-1L1	3	24.669	1000000	39.648	39.927
MASC1-C3FO11-1L2	3	24.669	1000000	39.845	40.096

DISTRIBUTION STATEMENT A.
Approved for public release: distribution is unlimited.

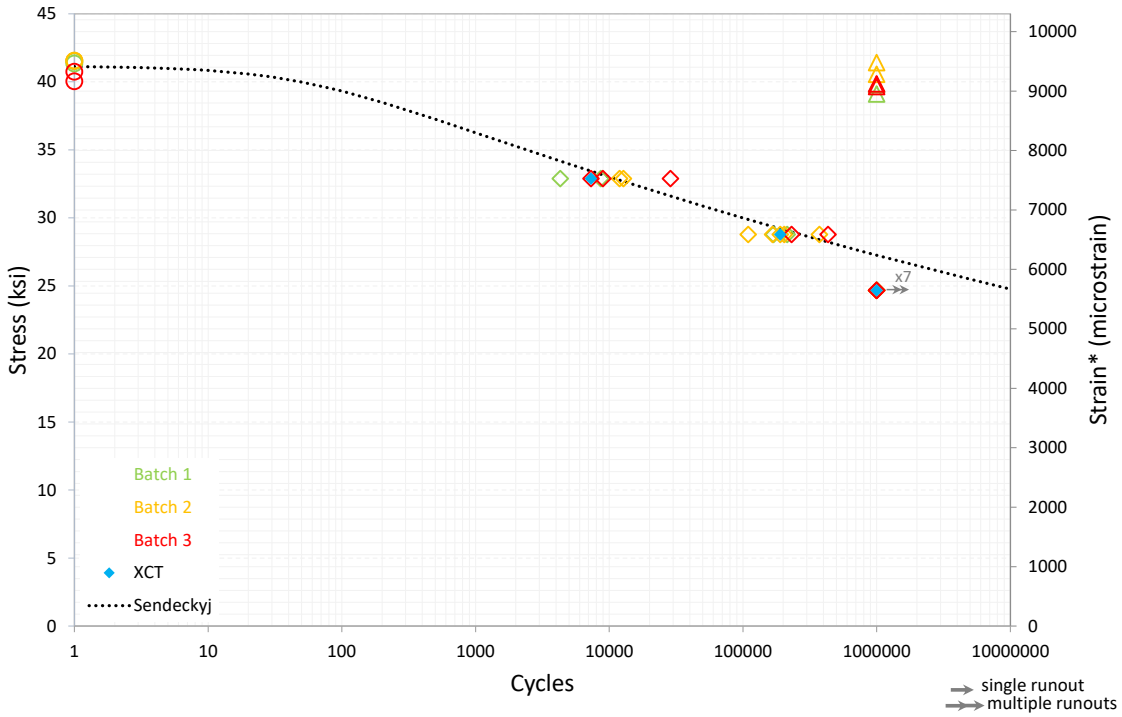


Figure A.22 – SN data with Sendeckyj fitting model for T650/5320-1, 10/80/10, R=5, OHC-C.

DISTRIBUTION STATEMENT A.
Approved for public release: distribution is unlimited.

Table A.22 – SN data for T650/5320-1, 10/80/10, R=-1, OHC-T.

Specimen	Batch	σ_A	n	σ_R	σ_e
MASC1-C2FO11-0X2	1	41.553	1		
MASC1-C2FO11-0X1	1	41.532	1		
MASC1-C1FO11-0X2	2	41.510	1		
MASC1-C1FO11-0X1	2	41.337	1		
MASC1-C3FO11-0X2	3	40.734	1		
MASC1-C3FO11-0X1	3	40.029	1		
MASC1-C1FO11-3M1	1	20.650	64991		41.413
MASC1-C1FO11-3M2	1	20.650	51659		40.806
MASC1-C2FO11-3M1	2	20.650	70348		41.624
MASC1-C2FO11-3M2	2	20.650	73171		41.729
MASC1-C3FO11-3M1	3	20.650	77962		41.900
MASC1-C3FO11-3M2	3	20.650			41.634
MASC1-C1FO11-2M1	1	18.585	140047		39.156
MASC1-C1FO11-2M2	1	18.585	190871		39.943
MASC1-C2FO11-2M1	2	18.585	279084		40.930
MASC1-C2FO11-2M2	2	18.585	274246		40.884
MASC1-C3FO11-XX4	3	18.585	169518		39.640
MASC1-C3FO11-XX5	3	18.585	207592		40.159
MASC1-C1FO11-1M1	1	14.455	1000000	35.664	36.775
MASC1-C1FO11-XX4	1	14.455	1000000	37.687	38.249
MASC1-C2FO11-1M1	2	14.455	1000000	38.623	39.029
MASC1-C2FO11-1M2	2	14.455	1000000	38.740	39.130
MASC1-C3FO11-1M1	3	14.455	1000000	37.092	37.782
MASC1-C3FO11-1M2	3	14.455	1000000	37.373	37.999

DISTRIBUTION STATEMENT A.
Approved for public release: distribution is unlimited.

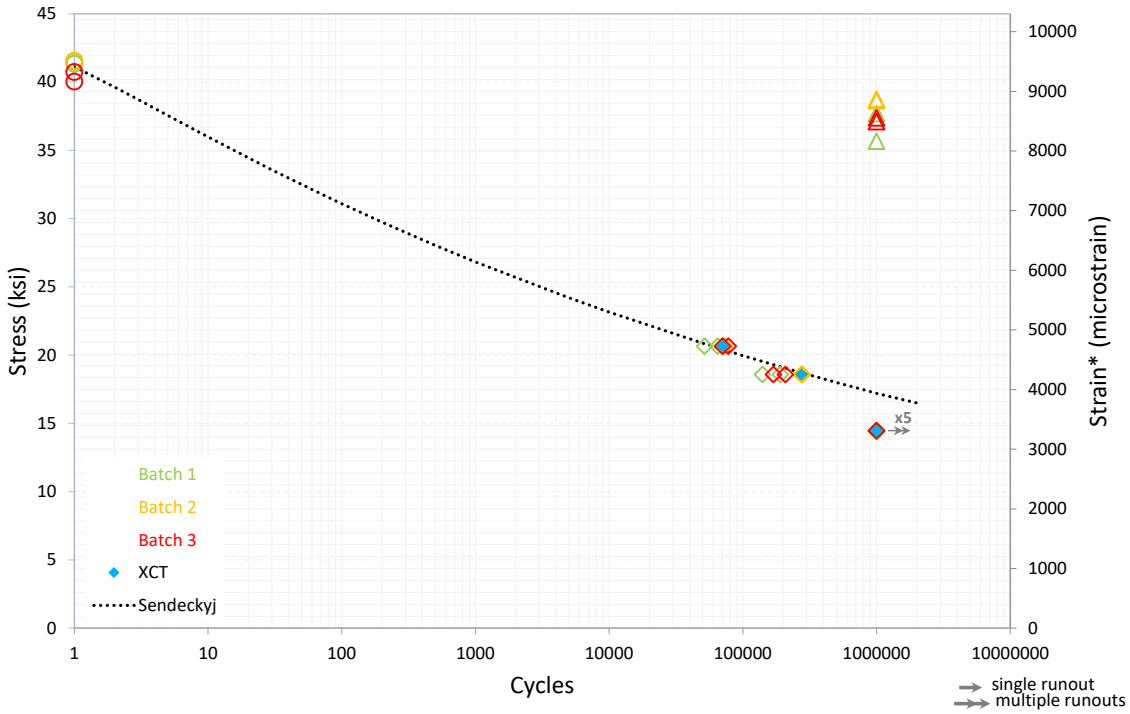


Figure A.23 – SN data and Sendeckyj fitting model for T650/5320-1, 10/80/10, R=-1, OHC-T.

DISTRIBUTION STATEMENT A.
Approved for public release: distribution is unlimited.

Table A.23 – SN data for T650/5320-1, 40/20/40, R=0.1, DNS.

Specimen	Batch	σ_A	n	σ_R	σ_e
MASC1-C3GD11-XX4	3	4.391	1		
MASC1-C3GD11-XX3	3	4.360	1		
MASC1-C2GD11-XX4	2	4.270	1		
MASC1-C1GD11-XX4	1	4.097	1		
MASC1-C2GD11-XX3	2	4.069	1		
MASC1-C1GD11-XX3	1	4.048	1		
MASC1-C1GD11-XX8	1	2.103	43326		4.342
MASC1-C2GD11-XX8	2	2.103	43001		4.339
MASC1-C3GD11-XX9	3	2.103	54610		4.425
MASC1-C1GD11-2K1	1	1.893	111860		4.224
MASC1-C1GD11-2K2	1	1.893	104023		4.199
MASC1-C2GD11-2K1	2	1.893	73620		4.081
MASC1-C2GD11-2K2	2	1.893	49255		3.949
MASC1-C2GD11-XX7	2	1.893	98487		4.180
MASC1-C3GD11-2K1	3	1.893	120612		4.250
MASC1-C3GD11-2K2	3	1.893	72722		4.077
MASC1-C1GD11-1K1	1	1.682	316846		4.089
MASC1-C1GD11-1K2	1	1.682	532883		4.267
MASC1-C1GD11-XX7	1	1.682	420485		4.185
MASC1-C2GD11-1K1	2	1.682	481863		4.232
MASC1-C2GD11-XX5	2	1.682	832027		4.425
MASC1-C3GD11-1K2	3	1.682	226154		3.977
MASC1-C1GD11-XX5	3	1.682	528989		4.264
MASC1-C1GD11-3K2	1	1.262	1000000	3.731	3.809
MASC1-C2GD11-3K1	1	1.262	1000000	3.847	3.904
MASC1-C2GD11-3K2	2	1.262	1000000	3.669	3.761
MASC1-C3GD11-3K1	2	1.262	1000000	3.688	3.776
MASC1-C3GD11-3K2	3	1.262	1000000	3.967	4.009
MASC1-C3GD11-XX6	3	1.262	1000000	3.891	3.942
MASC1-C3GD11-XX4	3	1.262	1000000	3.978	4.019

DISTRIBUTION STATEMENT A.
Approved for public release: distribution is unlimited.

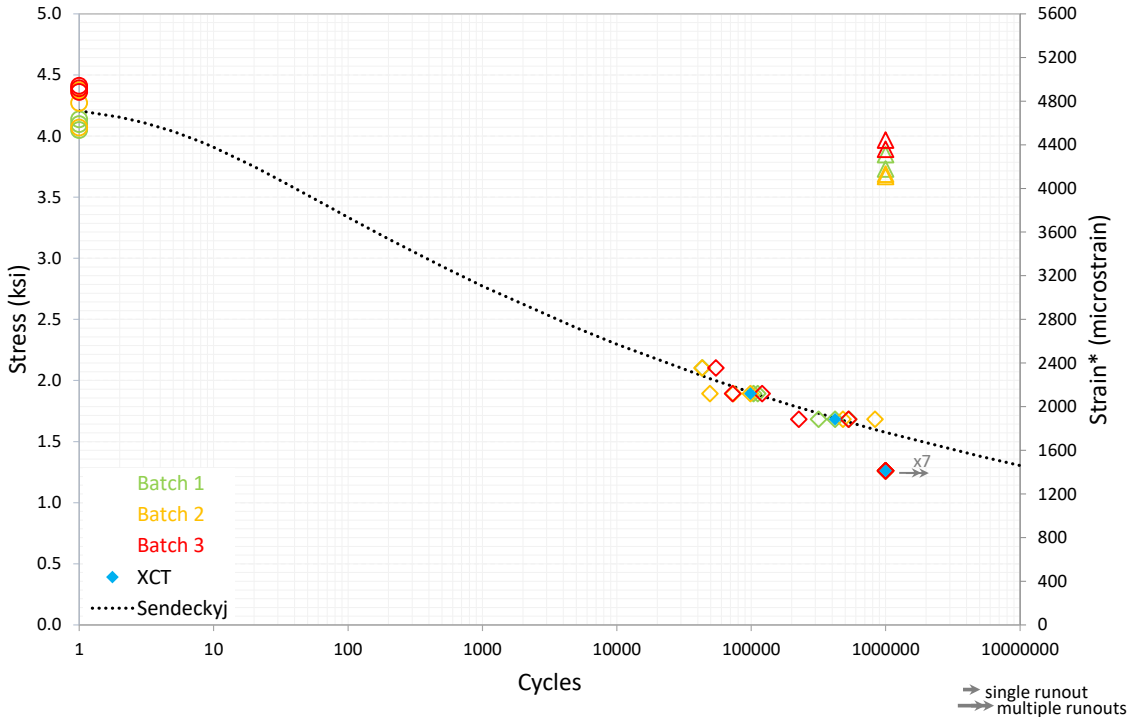


Figure A.24 – SN data with Sendeckyj fitting model for T650/5320-1, 40/20/40, R=0.1, DNS.

DISTRIBUTION STATEMENT A.
Approved for public release: distribution is unlimited.

Table A.24 – SN data for T650/5320-1, 10/50/10, R=0.1, DNS.

Specimen	Batch	σ_A	n	σ_R	σ_e
MASC1-C2FD11-XX5	2	4.394	1		
MASC1-C3FD11-XX3	3	4.384	1		
MASC1-C2FD11-XX4	2	4.350	1		
MASC1-C1FD11-XX4	1	4.320	1		
MASC1-C3FD11-XX4	3	4.301	1		
MASC1-C1FD11-XX3	1	4.289	1		
MASC1-C2FD11-XX8	2	2.387	50681		4.337
MASC1-C2FD11-XX9	2	2.387	57136		4.372
MASC1-C3FD11-XX6	3	2.387	48819		4.326
MASC1-C1FD11-2K1	1	2.170	227996		4.360
MASC1-C2FD11-2K1	1	2.170	313874		4.454
MASC1-C2FD11-2K2	2	2.170	178957		4.290
MASC1-C2FD11-XX7	2	2.170	243263		4.379
MASC1-C3FD11-2K1	2	2.170	201556		4.324
MASC1-C3FD11-2K2	3	2.170	143316		4.227
MASC1-C1FD11-4K1	3	2.170	209083		4.335
MASC1-C1FD11-XX7	1	2.061	251029		4.168
MASC1-C2FD11-4K1	1	2.061	290726		4.209
MASC1-C2FD11-4K2	2	2.061	455137		4.337
MASC1-C3FD11-4K1	2	2.061	365889		4.274
MASC1-C3FD11-4K2	3	2.061	304827		4.223
MASC1-C3FD11-XX5	3	2.061	337593		4.251
MASC1-C1FD11-XX5	3	2.061	374237		4.281
MASC1-C1FD11-1K2	1	1.736	1000000	3.945	4.086
MASC1-C1FD11-XX8	1	1.736	1000000	3.967	4.100
MASC1-C2FD11-1K1	1	1.736	1000000	3.925	4.074
MASC1-C2FD11-1K2	2	1.736	1000000	3.890	4.054
MASC1-C3FD11-1K1	2	1.736	1000000	3.835	4.024
MASC1-C3FD11-1K2	3	1.736	1000000	4.020	4.134
MASC1-C2FD11-XX5	3	1.736	1000000	4.192	4.261

DISTRIBUTION STATEMENT A.
Approved for public release: distribution is unlimited.

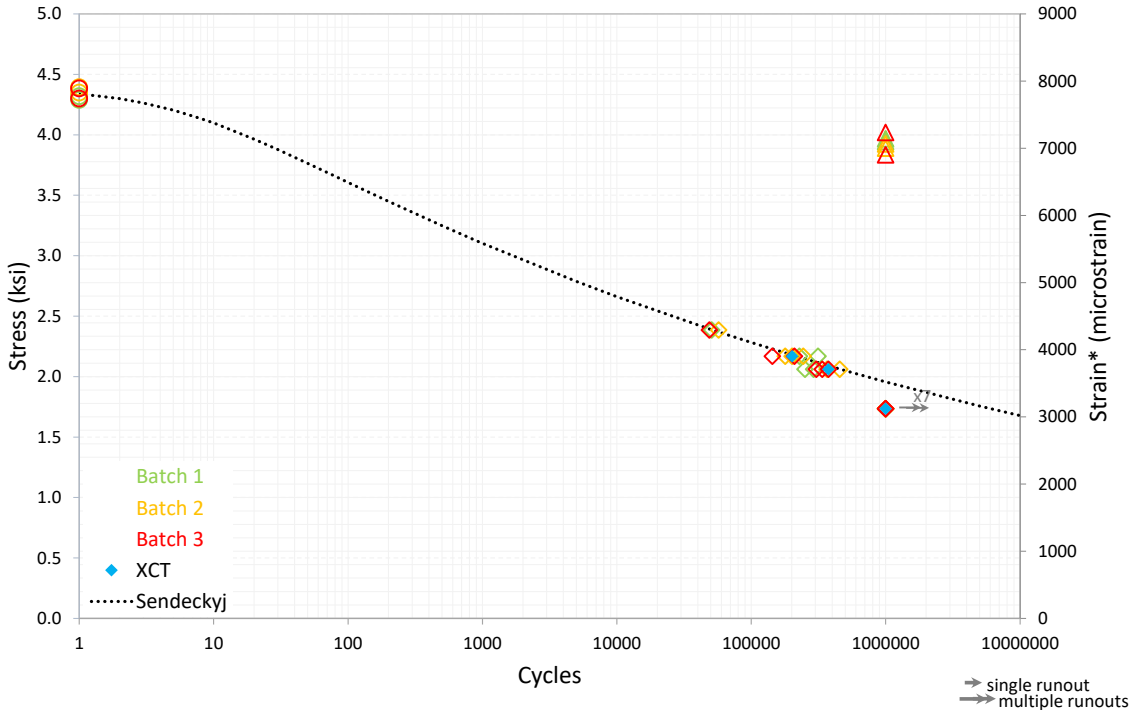


Figure A.25 – SN data with Sendeckyj fitting model for T650/5320-1, 10/80/10, R=0.1, DNS.

DISTRIBUTION STATEMENT A.
Approved for public release: distribution is unlimited.

Table A.25 – SN data for T650/5320-1, 40/20/40, R=0.1, ILT.

Specimen	Batch	σ_A	n	σ_R	σ_e
MASC1-C2GI11-XX1	2	7.467	1		
MASC1-C2GI11-0X1	2	7.231	1		
MASC1-C1GI11-XX1	1	7.098	1		
MASC1-C2GI11-0X2	2	7.059	1		
MASC1-C3GI11-0X1	3	6.720	1		
MASC1-C1GI11-0X2	1	6.662	1		
MASC1-C3GI11-XX1	3	6.544	1		
MASC1-C1GI11-0X1	1	6.183	1		
MASC1-C3GI11-0X2	3	6.178	1		
MASC1-C1GI11-XX2	1	4.755	15620		7.549
MASC1-C1GI11-XX7	1	4.755	15543		7.545
MASC1-C3GI11-XX3	3	4.755	5018		6.697
MASC1-C1GI11-3K1	1	3.397	25485		5.683
MASC1-C1GI11-3K2	1	3.397	78595		6.416
MASC1-C2GI11-3K1	2	3.397	367568		7.580
MASC1-C2GI11-3K2	2	3.397	379704		7.607
MASC1-C3GI11-3K1	3	3.397	22512		5.608
MASC1-C3GI11-3K2	3	3.397	19650		5.527
MASC1-C1GI11-2K1	1	3.057	262038		6.576
MASC1-C1GI11-2K2	1	3.057	448208		6.969
MASC1-C2GI11-2K1	2	3.057	395715		6.876
MASC1-C3GI11-2K1	3	3.057	84429		5.819
MASC1-C3GI11-2K2	3	3.057	108520		5.979
MASC1-C3GI11-XX5	3	3.057	175423		6.297
MASC1-C1GI11-1K1	1	2.717	1000000	5.671	6.889
MASC1-C1GI11-1K2	1	2.717	930047		6.703
MASC1-C2GI11-XX3	2	2.717	1000000	6.586	9.029
MASC1-C2GI11-XX4	2	2.717	1000000	7.237	8.479
MASC1-C3GI11-1K1	3	2.717	250953		5.818
MASC1-C3GI11-4K2	3	2.717	483121		6.245

DISTRIBUTION STATEMENT A.
Approved for public release: distribution is unlimited.

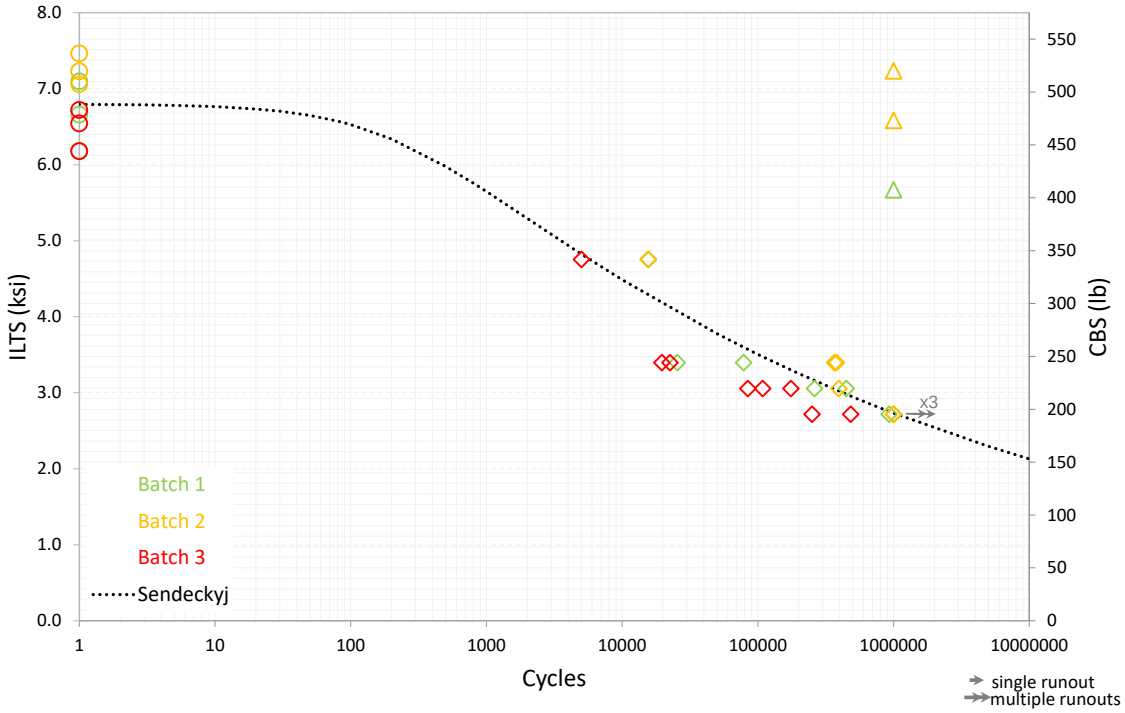


Figure A.26 – SN data with Sendeckyj fitting model for T650/5320-1, 40/20/40, R=0.1, ILT.

DISTRIBUTION STATEMENT A.
Approved for public release: distribution is unlimited.

Table A.26 – SN data for T650/5320-1, 10/80/10, R=0.1, ILT.

Specimen	Batch	σ_A	n	σ_R	σ_e
MASC1-C2FI11-0X2	2	7.331	1		
MASC1-C2FI11-0X1	2	7.036	1		
MASC1-C3FI11-0X1	3	6.319	1		
MASC1-C1FI11-0X1	1	6.182	1		
MASC1-C3FI11-0X2	3	6.120	1		
MASC1-C1FI11-0X2	1	5.944	1		
MASC1-C1FI11-4K2	1	3.893	10054		7.085
MASC1-C2FI11-4K2	2	3.893	18234		7.388
MASC1-C3FI11-4K2	3	3.893	2017		6.328
MASC1-C1FI11-3K1	1	3.244	73230		6.789
MASC1-C1FI11-3K2	1	3.244	81366		6.839
MASC1-C2FI11-3K1	2	3.244	171580		7.208
MASC1-C2FI11-3K2	2	3.244	61327		6.705
MASC1-C3FI11-3K1	3	3.244	41857		6.527
MASC1-C3FI11-3K2	3	3.244	43507		6.545
MASC1-C1FI11-2K1	1	2.920	474343		6.969
MASC1-C1FI11-2K2	1	2.920	757818		7.202
MASC1-C2FI11-2K1	2	2.920	54668		5.986
MASC1-C2FI11-2K2	2	2.920	92179		6.211
MASC1-C3FI11-2K1	3	2.920	225813		6.615
MASC1-C3FI11-2K2	3	2.920	66628		6.070
MASC1-C1FI11-1K2	1	2.595	1000000		
MASC1-C2FI11-1K1	2	2.595	1000000	6.664	6.930
MASC1-C2FI11-1K2	2	2.595	1000000	5.801	6.606
MASC1-C3FI11-1K1	3	2.595	1000000	6.008	6.651
MASC1-C3FI11-1K2	3	2.595	1000000	6.408	6.794

DISTRIBUTION STATEMENT A.
Approved for public release: distribution is unlimited.

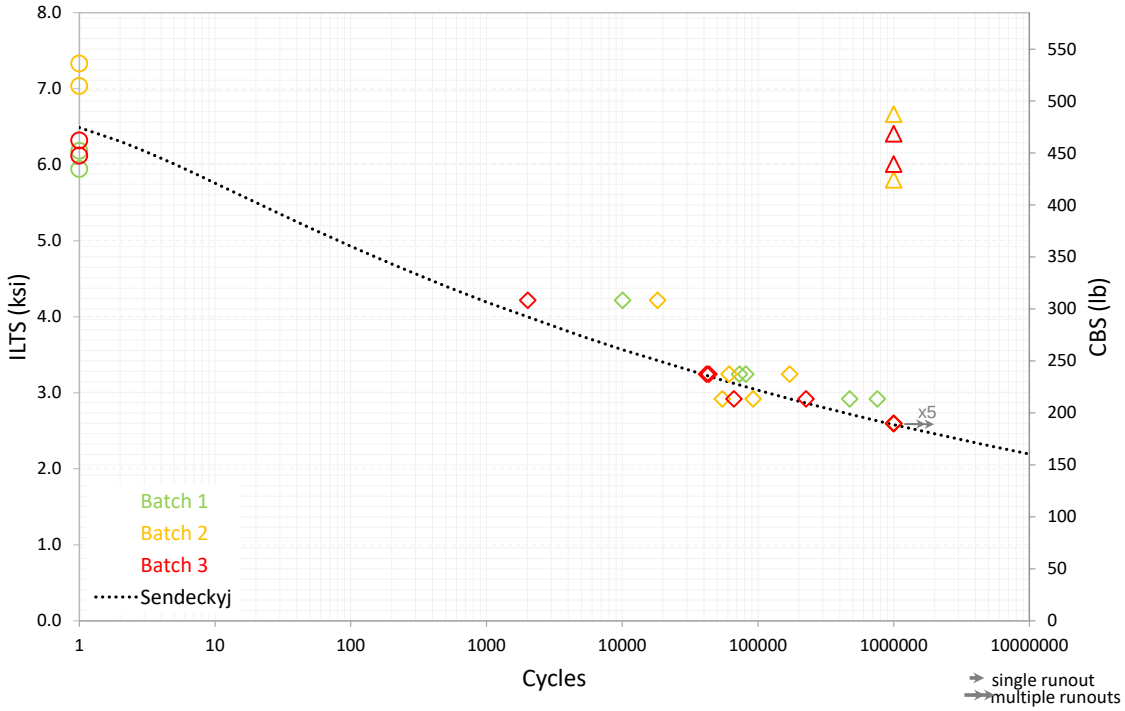


Figure A.27 – SN data with Sendeckyj fitting model for T650/5320-1, 10/80/10, R=0.1, ILT.

DISTRIBUTION STATEMENT A.
Approved for public release: distribution is unlimited.

Table A.28 – SN data for T650/5320-1, 100/0/0, R=0.1, SBS.

Specimen	Batch	σ_A	n	σ_R	σ_e
MASC1-C2AS11-0X1	2	12.999	1		
MASC1-C2AS11-0X3	2	12.758	1		
MASC1-C2AS11-0X2	2	12.725	1		
MASC1-C1AS11-0X4	1	12.624	1		
MASC1-C1AS11-0X1	1	12.559	1		
MASC1-C1AS11-0X2	1	12.406	1		
MASC1-C3AS11-0X2	3	12.241	1		
MASC1-C3AS11-0X1	3	12.196	1		
MASC1-C3AS11-0X3	3	12.186	1		
MASC1-C1AS11-0X3	1	11.714	1		
MASC1-C1AS11-3K1	1	7.465	33000		11.860
MASC1-C1AS11-3K2	1	7.465	46574		12.185
MASC1-C2AS11-3K1	2	7.465	94893		12.885
MASC1-C2AS11-3K2	2	7.465	60093		12.431
MASC1-C3AS11-3K1	3	7.465	11298		10.906
MASC1-C1AS11-2K1	1	6.220	954186		12.872
MASC1-C1AS11-2K2	1	6.220	555750		12.336
MASC1-C2AS11-2K1	2	6.220	468489		12.172
MASC1-C3AS11-2K1	3	6.220	280914		11.692
MASC1-C3AS11-2K2	3	6.220	336030		11.858
MASC1-C1AS11-1K1	1	4.976	1000000	11.820	11.976
MASC1-C1AS11-1K4	1	4.976	1000000	12.039	12.167
MASC1-C2AS11-1K1	2	4.976	1000000	12.649	12.723
MASC1-C2AS11-1K2	2	4.976	1000000	12.742	12.810
MASC1-C3AS11-1K1	3	4.976	1000000	12.440	12.529
MASC1-C3AS11-1K2	3	4.976	1000000	12.186	12.298

DISTRIBUTION STATEMENT A.
Approved for public release: distribution is unlimited.

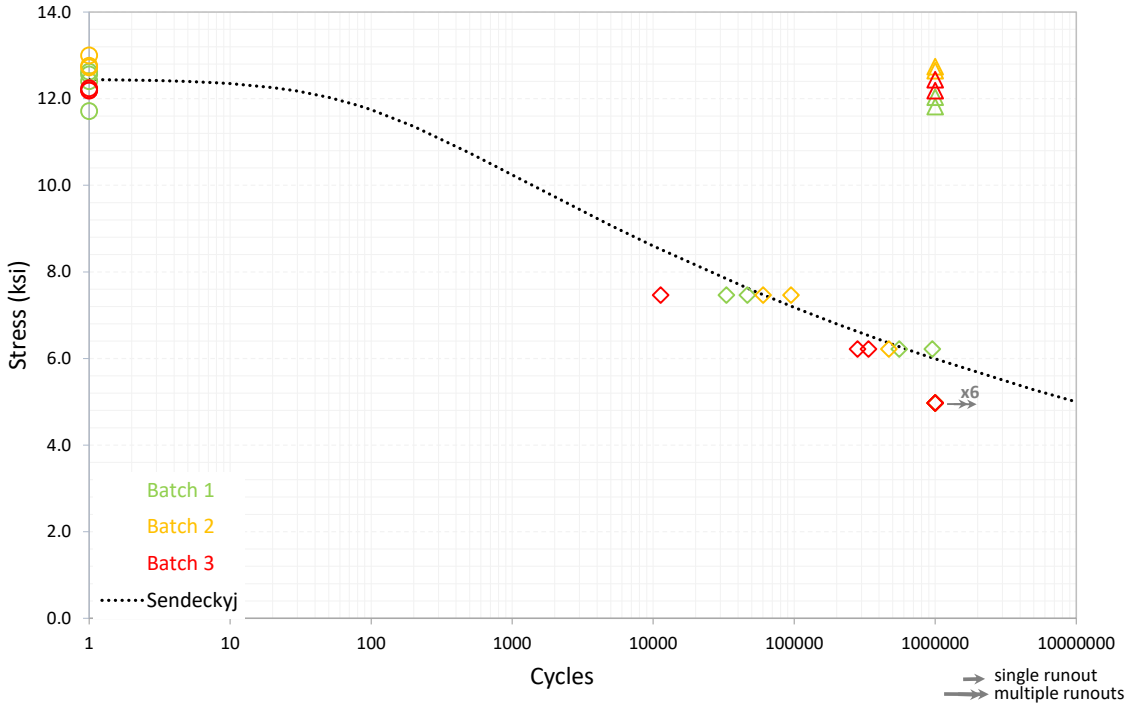


Figure A.28 – SN data with Sendeckyj fitting model for T650/5320-1, 100/0/0, R=0.1, SBS.

A.3 SN Data and Sendeckyj Fitting Models for IM7/5250-4 Unidirectional Tape

SN data and Sendeckyj fitting model to fatigue data analysis for the IM7/5250-4 unidirectional tape tests are displayed, and are also found in the MASC database. In these tables, n, σ_A, σ_R and σ_e are the number of cycles survived (n=1 indicates static failure), the fatigue stress level (or static failure stress value), the residual strength after surviving the corresponding number of cycles, and the equivalent static strength (pooled), respectively.

DISTRIBUTION STATEMENT A.
Approved for public release: distribution is unlimited.

Table A.27 – SN data for IM7/5250-4, 50/40/10, R=0.1, OHT-T.

Specimen¤	Batch¤	σ_A¤	n¤	σ_R¤	σ_e¤	¤
MASC1-A1DO11-0X3¤	1¤	132.143¤	1¤	¶¤	¶¤	¤
MASC1-A1DO11-0X4¤	1¤	129.221¤	1¤	¶¤	¶¤	¤
MASC1-A2DO11-0X3¤	2¤	128.167¤	1¤	¶¤	¶¤	¤
MASC1-A2DO11-0X4¤	2¤	125.814¤	1¤	¶¤	¶¤	¤
MASC1-A3DO11-0X3¤	3¤	124.859¤	1¤	¶¤	¶¤	¤
MASC1-A3DO11-0X4¤	3¤	122.855¤	1¤	¶¤	¶¤	¤
MASC1-A1DO11-3K1¤	1¤	114.459¤	1000000¤	182.712¤	¤	¤
MASC1-A2DO11-3K1¤	2¤	114.459¤	1000000¤	173.497¤	¤	¤
MASC1-A3DO11-3K1¤	3¤	114.459¤	1000000¤	166.210¤	¤	¤
MASC1-A1DO11-2K1¤	1¤	101.741¤	1000000¤	167.015¤	¤	¤
MASC1-A2DO11-2K1¤	2¤	101.741¤	1000000¤	174.799¤	¤	¤
MASC1-A3DO11-2K1¤	3¤	101.741¤	1000000¤	162.270¤	¤	¤
MASC1-A3DO11-XX5¤	3¤	89.023¤	1000000¤	¤	¤	¤
MASC1-A2DO11-1K1¤	2¤	89.023¤	1000000¤	155.343¤	¤	¤
MASC1-A3DO11-1K1¤	3¤	89.023¤	1000000¤	152.127¤	¤	¤

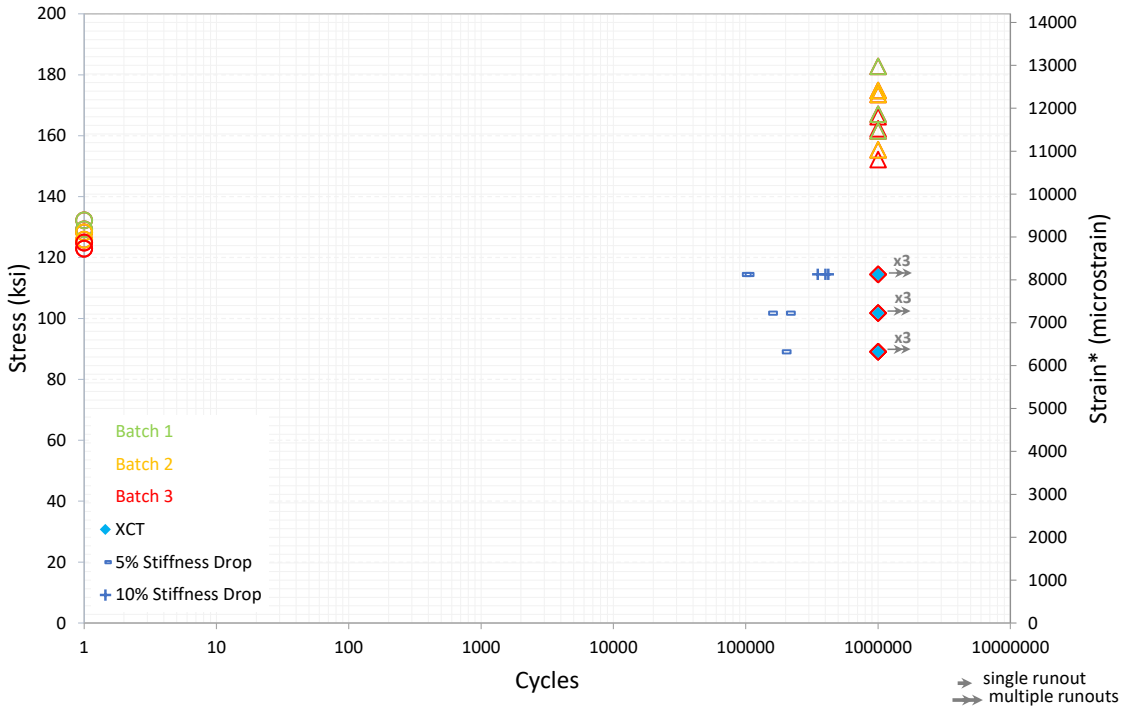


Figure A.29 – SN data for IM7/5250-4, 50/40/10, R=0.1, OHT-T.

Sendeckyj wearout analysis prediction and equivalent static strength data for IM7/5250-4 unidirectional tape, 50/40/10, R=0.1 OH, are not included as all fatigue specimens were runouts (Table A.27).

DISTRIBUTION STATEMENT A.
Approved for public release: distribution is unlimited.

Table A.28 – SN data for IM7/5250-4, 50/40/10, R=5, OHC-C.

Specimen	Batch	σ_A	n	σ_R	σ_e
MASC1-A1DO11-0X1	1	74.906	1		
MASC1-A1DO11-0X2	1	71.921	1		
MASC1-A2DO11-0X1	2	71.395	1		
MASC1-A2DO11-0X2	2	68.160	1		
MASC1-A3DO11-0X1	3	67.281	1		
MASC1-A3DO11-0X2	3	65.886	1		
MASC1-A1DO11-XX3	1	59.436	23676		73.998
MASC1-A1DO11-3L2	1	59.436	4639		72.540
MASC1-A2DO11-3L1	2	59.436	8959		73.125
MASC1-A2DO11-3L2	2	59.436	2708		72.065
MASC1-A3DO11-3L1	3	59.436	14657		73.566
MASC1-A3DO11-3L2	3	59.436	8298		73.057
MASC1-A1DO11-XX8	1	55.940	22449		69.600
MASC1-A1DO11-1K2	1	55.940	32086		69.904
MASC1-A1DO11-1L2	1	55.940	26668		69.746
MASC1-A2DO11-1L1	2	55.940	18016		69.413
MASC1-A2DO11-XX3	2	55.940	62927		70.481
MASC1-A2DO11-XX4	2	55.940	76251		70.646
MASC1-A3DO11-1L2	3	55.940	86135		70.752
MASC1-A3DO11-XX3	3	55.940	119537		71.035
MASC1-A3DO11-1L1	3	55.940	1000000	76.509	76.527
MASC1-A1DO11-3L1	1	55.940	1000000	76.800	76.813
MASC1-A1DO11-2L1	1	52.444	1000000		
MASC1-A1DO11-2L2	1	52.444	1000000	71.551	71.571
MASC1-A2DO11-2L1	2	52.444	1000000	71.125	71.157
MASC1-A2DO11-2L2	2	52.444	1000000	66.140	68.400
MASC1-A3DO11-2L1	3	52.444	1000000	72.994	72.998
MASC1-A3DO11-2L2	3	52.444	1000000	71.339	71.365

DISTRIBUTION STATEMENT A.
Approved for public release: distribution is unlimited.

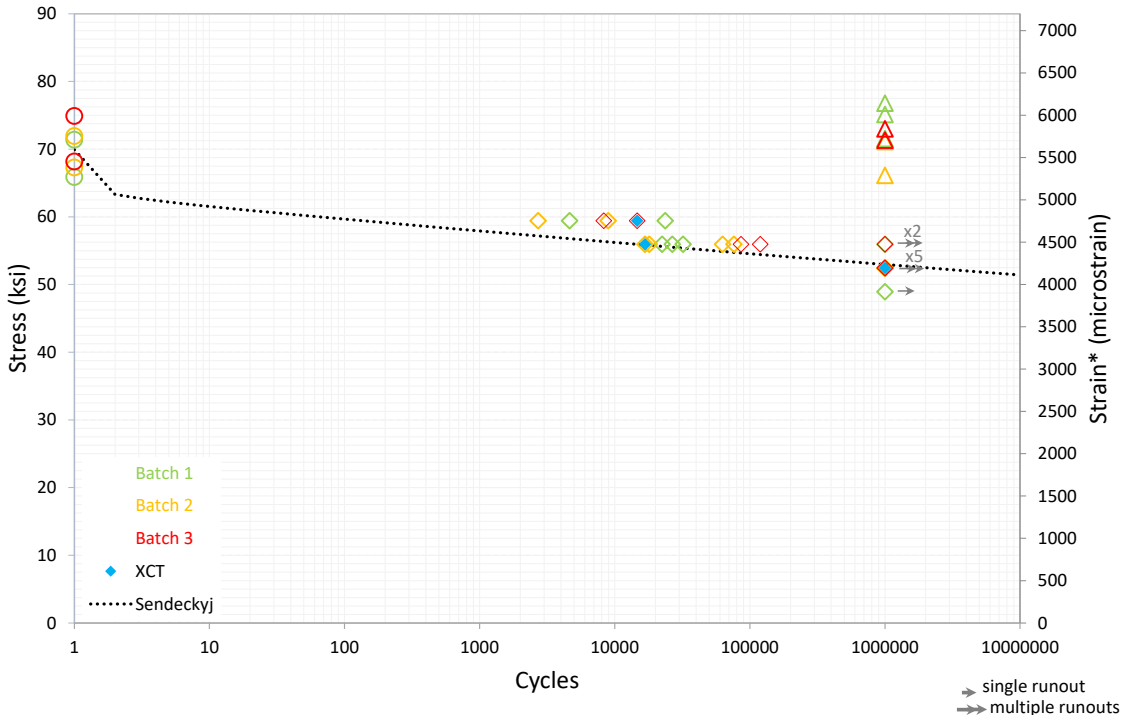


Figure A.30 – SN data with Sendeckyj fitting model for IM7/5250-4, 50/40/10, R=5, OHC-C.

DISTRIBUTION STATEMENT A.
Approved for public release: distribution is unlimited.

Table A.29 – SN data for IM7/5250-4, 50/40/10, R=-1, OHC-T.

Specimen	Batch	σ_A	n	σ_R	σ_e
MASC1-A1DO11-0X1	1	74.906	1		
MASC1-A1DO11-0X2	1	71.921	1		
MASC1-A2DO11-0X1	2	71.395	1		
MASC1-A2DO11-0X2	2	68.160	1		
MASC1-A3DO11-0X1	3	67.281	1		
MASC1-A3DO11-0X2	3	65.886	1		
MASC1-A1DO11-XX6	1	59.130	19234		71.048
MASC1-A1DO11-XX7	1	59.130	16608		70.668
MASC1-A1DO11-2K2	1	59.130	42762		73.154
MASC1-A2DO11-XX2	2	59.130	13290		70.097
MASC1-A3DO11-XX1	3	59.130	101485		75.509
MASC1-A3DO11-XX2	3	59.130	43502		73.200
MASC1-A1DO11-2M1	1	54.203	132559		69.899
MASC1-A1DO11-2M2	1	54.203	199517		70.956
MASC1-A2DO11-2M1	2	54.203	35325		66.591
MASC1-A2DO11-2M2	2	54.203	74674		68.443
MASC1-A3DO11-2M1	3	54.203	264746		71.697
MASC1-A3DO11-2M2	3	54.203	324921		72.238
MASC1-A1DO11-1M2	1	49.275	212012		64.649
MASC1-A2DO11-1M1	2	49.275	160338		63.989
MASC1-A2DO11-1M2	2	49.275	246897		65.012
MASC1-A3DO11-1M1	3	49.275	1000000	72.496	73.002
MASC1-A3DO11-1M2	3	49.275	1000000	70.037	71.146
MASC1-A1DO11-3M1	1	44.348	1000000	73.958	73.977
MASC1-A1DO11-XX5	1	44.348	1000000	82.479	82.480
MASC1-A1DO11-XX4	1	44.348	1000000	80.732	80.734
MASC1-A2DO11-3M2	2	44.348	1000000	70.655	70.716
MASC1-A2DO11-XX1	2	44.348	1000000	60.273	62.601
MASC1-A3DO11-3M1	3	44.348	1000000	68.491	68.627
MASC1-A3DO11-3M2	3	44.348	1000000	71.209	71.259

DISTRIBUTION STATEMENT A.
Approved for public release: distribution is unlimited.

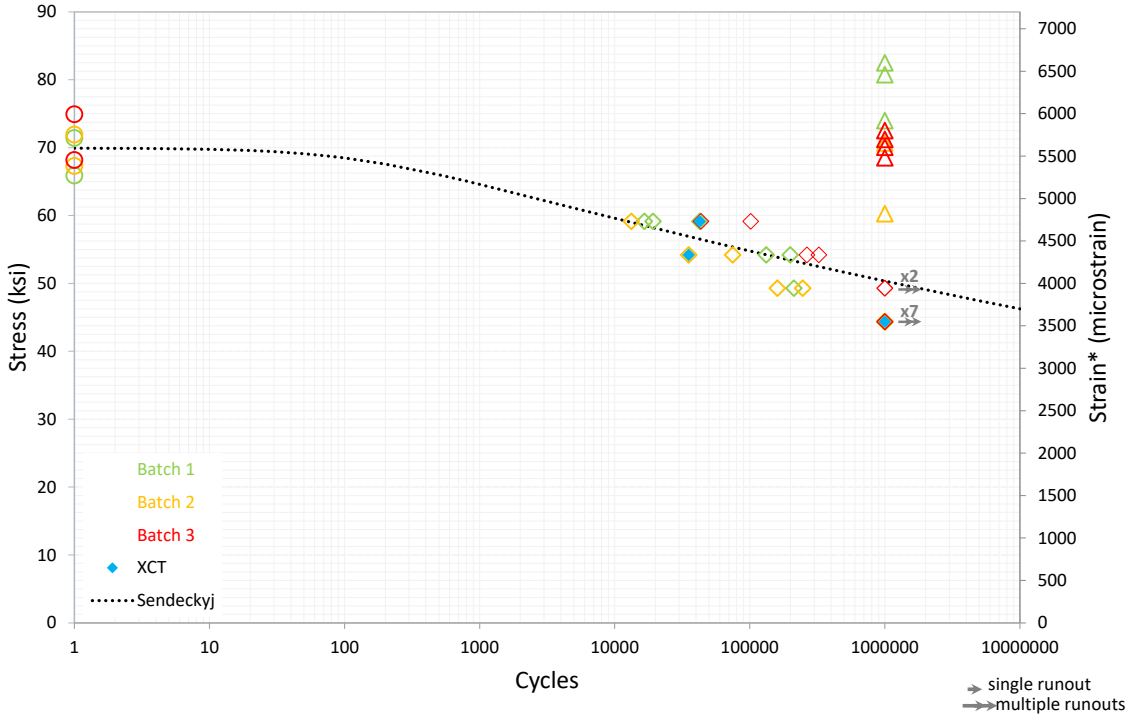


Figure A.31 – SN data with Sendeckyj fitting model for IM7/5250-4, 50/40/10, R=-1, OHC-T.

DISTRIBUTION STATEMENT A.
Approved for public release: distribution is unlimited.

Table A.30 – SN data for IM7/5250-4, 25/50/25, R=0.1, OHT-T.

Specimen	Batch	σ_A	n	σ_R	σ_e
MASC1-A1EO11-0X4	1	78.707	1		
MASC1-A2EO11-0X3	2	78.285	1		
MASC1-A1EO11-0X3	1	77.512	1		
MASC1-A2EO11-0X4	2	75.575	1		
MASC1-A3EO11-0X3	3	75.410	1		
MASC1-A3EO11-0X4	3	73.409	1		
MASC1-A1EO11-3K1	1	68.835	788097		78.019
MASC1-A1EO11-3K2	1	68.835	1000000	84.322	84.322
MASC1-A1EO11-XX1	1	68.835	614610		77.847
MASC1-A2EO11-3K1	2	68.835	612316		77.844
MASC1-A2EO11-3K2	2	68.835	1000000	80.587	80.611
MASC1-A2EO11-XX2	2	68.835	528503		77.742
MASC1-A3EO11-3K1	3	68.835	605661		77.837
MASC1-A3EO11-3K2	3	68.835	366391		77.489
MASC1-A1EO11-2K1	1	61.186	1000000	86.833	
MASC1-A2EO11-2K1	2	61.186	1000000	86.605	
MASC1-A3EO11-2K1	3	61.186	1000000	79.569	
MASC1-A1EO11-1K1	1	53.538	1000000	82.403	
MASC1-A1EO11-1K2	1	53.538	1000000		
MASC1-A2EO11-1K1	2	53.538	1000000	84.073	
MASC1-A3EO11-1K1	3	53.538	1000000	83.255	

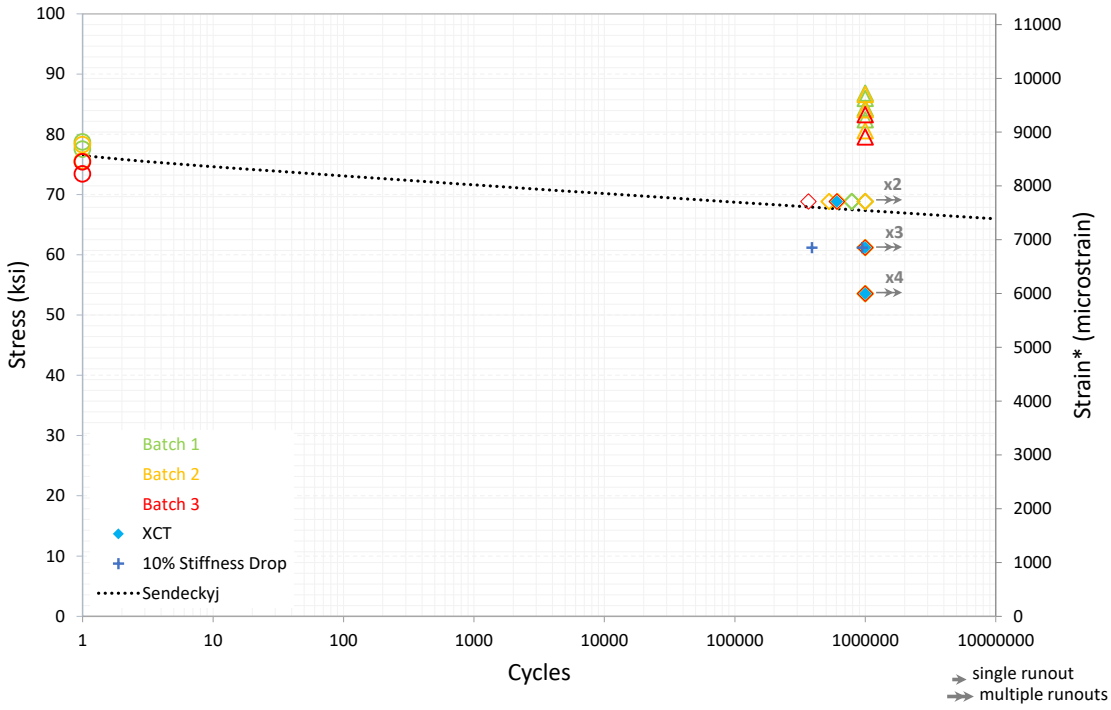


Figure A.32 – SN data with Sendeckyj fitting model for IM7/5250-4, 25/50/25, R=0.1, OHT-T.

DISTRIBUTION STATEMENT A.
Approved for public release: distribution is unlimited.

Sendeckyj equivalent static strength data for IM7/5250-4 unidirectional tape, 25/50/25, R=0.1 OH, is not included for stress level 1 and 2 as all fatigue specimens within those two stress levels were only runouts (Table A.30).

Table A.31 – SN data for IM7/5250-4, 25/50/25, R=5, OHC-C.

Specimen	Batch	σ_A	n	σ_R	σ_e
MASC1-A1EO11-0X1	1	56.647	1		
MASC1-A3EO11-0X2	3	53.510	1		
MASC1-A1EO11-0X2	1	51.904	1		
MASC1-A2EO11-0X2	2	51.774	1		
MASC1-A3EO11-0X1	3	51.109	1		
MASC1-A2EO11-0X1	2	50.932	1		
MASC1-A1EO11-2L1	1	39.485	56348		55.018
MASC1-A1EO11-2L2	1	39.485	38571		54.525
MASC1-A2EO11-2L1	2	39.485	46829		54.777
MASC1-A2EO11-2L2	2	39.485	123878		56.059
MASC1-A3EO11-2L1	3	39.485	52782		54.933
MASC1-A3EO11-2L2	3	39.485	118377		55.999
MASC1-A1EO11-1L1	1	36.852	949923		54.918
MASC1-A1EO11-1L2	1	36.852	1000000	46.161	54.986
MASC1-A1EO11-XX2	1	36.852	1000000	47.838	54.989
MASC1-A1EO11-XX3	1	36.852	1000000	49.966	55.009
MASC1-A2EO11-1L1	2	36.852	473470		54.016
MASC1-A2EO11-1L2	2	36.852	904544		54.854
MASC1-A3EO11-1L1	3	36.852	809486		54.710
MASC1-A3EO11-1L2	3	36.852	1000000	46.506	54.987
MASC1-A3EO11-XX1	3	36.852	539156		54.184
MASC1-A1EO11-3L1	1	31.588	1000000	52.820	52.830
MASC1-A1EO11-3L2	1	31.588	1000000	49.832	49.941
MASC1-A2EO11-3L1	2	31.588	1000000	52.394	52.408
MASC1-A2EO11-3L2	2	31.588	1000000	48.235	48.604
MASC1-A3EO11-XX2	3	31.588	1000000	50.930	50.976
MASC1-A3EO11-3L2	3	31.588	1000000	49.750	49.866

DISTRIBUTION STATEMENT A.
Approved for public release: distribution is unlimited.

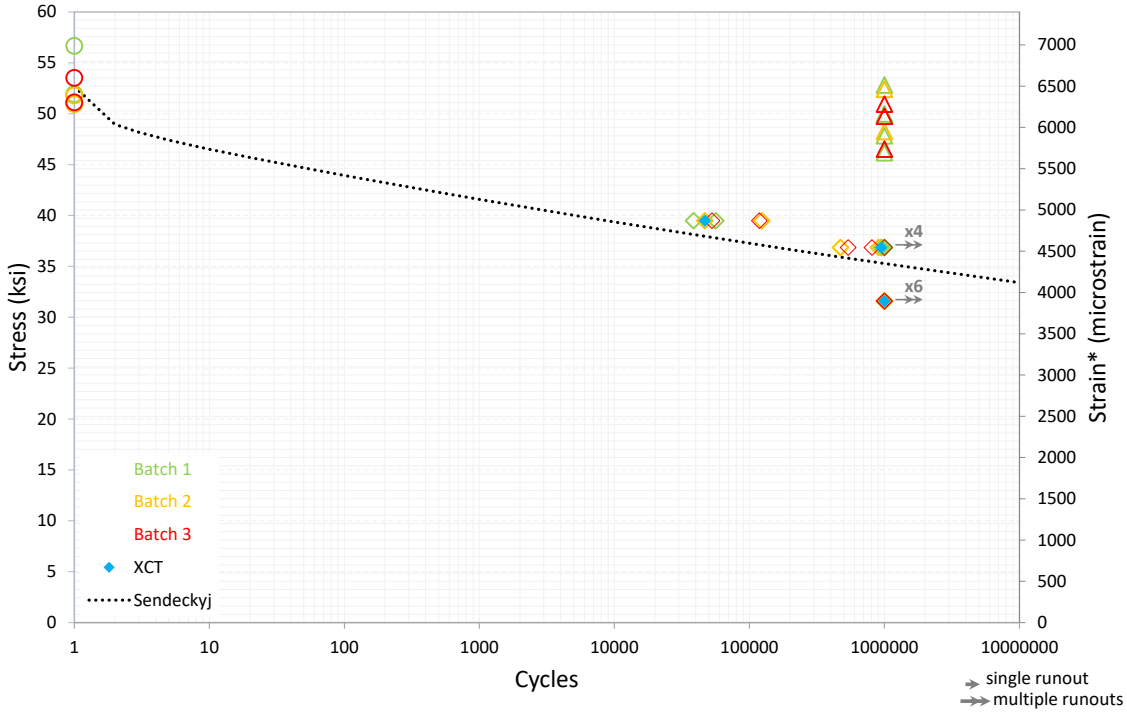


Figure A.33 – SN data with Sendeckyj fitting model for IM7/5250-4, 25/50/25, R=5, OHC-C.

DISTRIBUTION STATEMENT A.
Approved for public release: distribution is unlimited.

Table A.32 – SN data for IM7/5250-4, 25/50/25, R=-1, OHC-T.

Specimen	Batch	σ_A	n	σ_R	σ_e
MASC1-A1EO11-0X1	1	56.647	1		
MASC1-A3EO11-0X2	3	53.510	1		
MASC1-A1EO11-0X2	1	51.904	1		
MASC1-A2EO11-0X2	2	51.774	1		
MASC1-A3EO11-0X1	3	51.109	1		
MASC1-A2EO11-0X1	2	50.932	1		
MASC1-A1EO11-2M1	1	35.510	74799		56.625
MASC1-A1EO11-2M2	1	35.510	40324		55.172
MASC1-A2EO11-2M1	2	35.510	24404		54.018
MASC1-A2EO11-2M2	2	35.510	30885		54.556
MASC1-A3EO11-2M1	3	35.510	22913		53.875
MASC1-A3EO11-2M2	3	35.510	36717		54.955
MASC1-A1EO11-1M1	1	32.282	172295		53.318
MASC1-A1EO11-1M2	1	32.282	130559		52.699
MASC1-A2EO11-1M1	2	32.282	190344		53.542
MASC1-A2EO11-1M2	2	32.282	198289		53.634
MASC1-A3EO11-1M1	3	32.282	439446		55.460
MASC1-A3EO11-1M2	3	32.282	75015		51.484
MASC1-A1EO11-3M1	1	25.826	1000000	47.827	48.483
MASC1-A1EO11-3M2	1	25.826	1000000	46.437	47.567
MASC1-A2EO11-3M1	2	25.826	1000000	47.853	48.502
MASC1-A2EO11-3M2	2	25.826	1000000	45.255	46.972
MASC1-A3EO11-3M1	3	25.826	1000000	45.637	47.145
MASC1-A3EO11-3M2	3	25.826	1000000	47.542	48.278

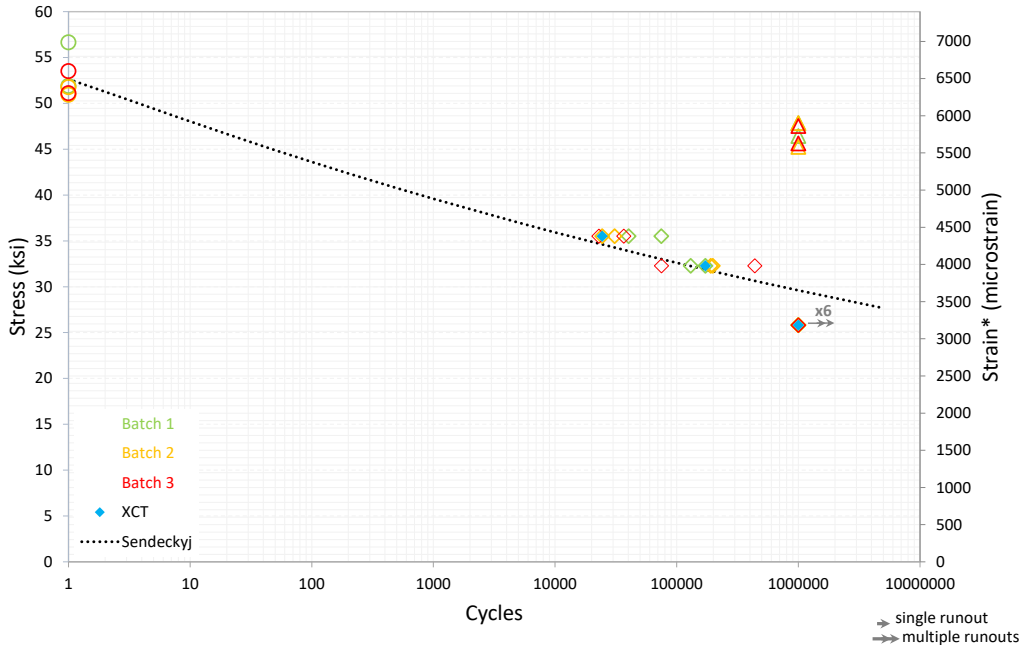


Figure A.34 – SN data with Sendeckyj fitting model for IM7/5250-4, 25/50/25, R=-1, OHC-T.

DISTRIBUTION STATEMENT A.
Approved for public release: distribution is unlimited.

Table A.33 – SN data for IM7/5250-4, 10/80/10, R=0.1, OHT-T.

Specimen	Batch	σ_A	n	σ_R	σ_e
MASC1-A2FO11-0X4	2	50.289	1		
MASC1-A2FO11-0X3	2	49.921	1		
MASC1-A1FO11-0X3	1	49.390	1		
MASC1-A3FO11-0X3	3	49.287	1		
MASC1-A1FO11-0X4	1	48.103	1		
MASC1-A3FO11-0X4	3	47.704	1		
MASC1-A1FO11-3K1	1	39.293	41560		49.869
MASC1-A1FO11-3K2	1	39.293	45000		50.059
MASC1-A2FO11-3K1	2	39.293	29721		49.079
MASC1-A2FO11-3K2	2	39.293	53991		50.496
MASC1-A3FO11-3K1	3	39.293	29600		49.070
MASC1-A3FO11-3K2	3	39.293	24836		48.662
MASC1-A1FO11-2K1	1	34.381	478948		49.058
MASC1-A1FO11-2K2	1	34.381	487271		49.098
MASC1-A2FO11-2K1	2	34.381	305951		48.013
MASC1-A2FO11-2K2	2	34.381	351004		48.331
MASC1-A3FO11-2K1	3	34.381	272808		47.750
MASC1-A3FO11-2K2	3	34.381	264513		47.679
MASC1-A1FO11-1K1	1	29.469	1000000	47.917	48.215
MASC1-A1FO11-1K2	1	29.469	1000000	46.331	46.879
MASC1-A2FO11-1K1	2	29.469	1000000	48.309	48.565
MASC1-A2FO11-1K2	2	29.469	1000000	45.624	46.338
MASC1-A3FO11-1K1	3	29.469	1000000	45.717	46.407
MASC1-A3FO11-1K2	3	29.469	1000000	44.027	45.290

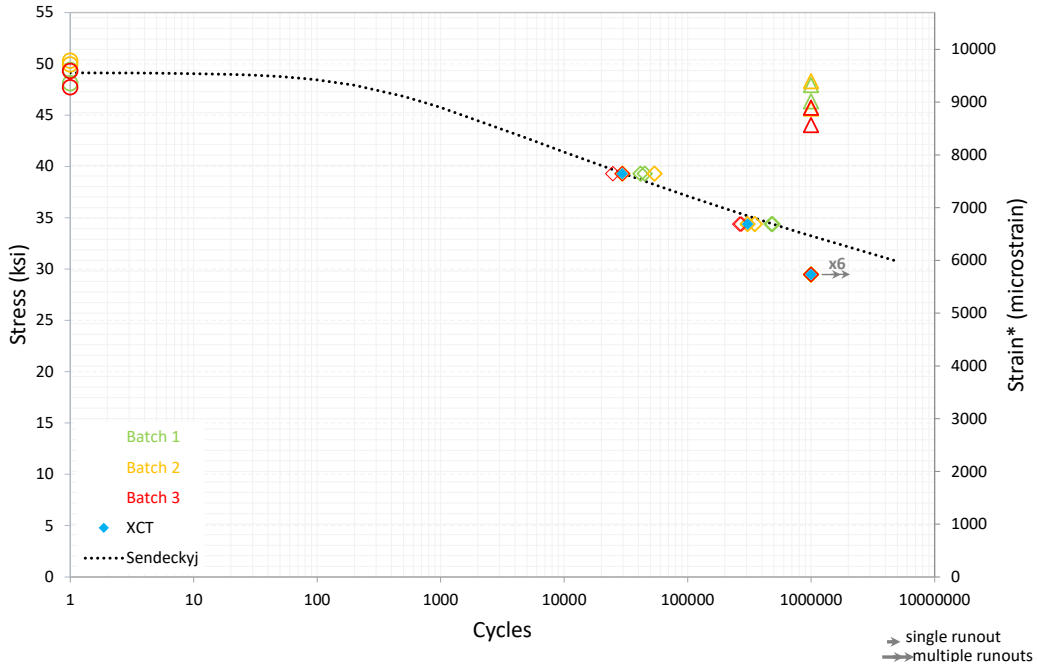


Figure A.35 – SN data with Sendeckyj fitting model for IM7/5250-4, 10/80/10, R=0.1, OHT-T.

DISTRIBUTION STATEMENT A.
Approved for public release: distribution is unlimited.

Table A.34 – SN data for IM7/5250-4, 10/80/10, R=5, OHC-C.

Specimen	Batch	σ_A	n	σ_R	σ_e
MASC1-A1FO11-0X1	1	42.274	1		
MASC1-A3FO11-0X2	3	42.044	1		
MASC1-A1FO11-0X2	1	41.688	1		
MASC1-A2FO11-0X2	2	41.668	1		
MASC1-A2FO11-0X1	2	41.595	1		
MASC1-A3FO11-0X1	3	41.018	1		
MASC1-A1FO11-2L1	1	31.286	149398		42.018
MASC1-A1FO11-2L2	1	31.286	87789		41.585
MASC1-A2FO11-2L1	2	31.286	81061		41.520
MASC1-A2FO11-2L2	2	31.286	215852		42.321
MASC1-A3FO11-2L1	3	31.286	123905		41.865
MASC1-A3FO11-2L2	3	31.286	134551		41.933
MASC1-A1FO11-1L1	1	30.243	164162		40.692
MASC1-A1FO11-XX1	1	30.243	475868		41.546
MASC1-A2FO11-1L1	2	30.243	704679		41.865
MASC1-A2FO11-1L2	2	30.243	360063		41.320
MASC1-A3FO11-1L1	3	30.243	307039		41.192
MASC1-A3FO11-1L2	3	30.243	386043		41.377
MASC1-A1FO11-3L1	1	27.114	1000000	42.358	42.360
MASC1-A1FO11-3L2	1	27.114	1000000	42.461	42.463
MASC1-A2FO11-3L1	2	27.114	1000000	41.450	41.457
MASC1-A2FO11-3L2	2	27.114	1000000	41.641	41.647
MASC1-A3FO11-3L1	3	27.114	1000000	40.783	40.799
MASC1-A3FO11-3L2	3	27.114	1000000	43.128	43.129

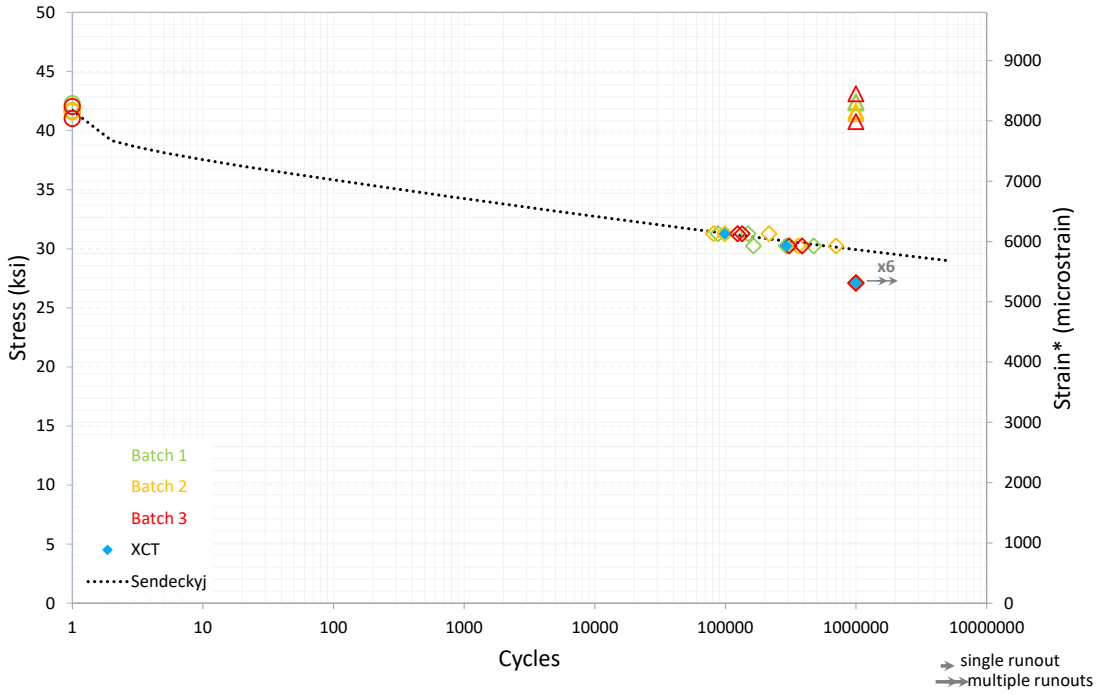


Figure A.36 – SN data with Sendeckyj fitting model for IM7/5250-4, 10/80/10, R=5, OHC-C.

DISTRIBUTION STATEMENT A.
Approved for public release: distribution is unlimited.

Table A.35 – SN data for IM7/5250-4, 10/80/10, R=-1, OHC-T.

Specimen	Batch	σ_A	n	σ_R	σ_e
MASC1-A1FO11-0X1	1	42.274	1		
MASC1-A3FO11-0X2	3	42.044	1		
MASC1-A1FO11-0X2	1	41.688	1		
MASC1-A2FO11-0X2	2	41.668	1		
MASC1-A2FO11-0X1	2	41.595	1		
MASC1-A3FO11-0X1	3	41.018	1		
MASC1-A1FO11-3M1	1	22.708	111653		42.427
MASC1-A1FO11-3M2	1	22.708	108349		42.306
MASC1-A2FO11-3M1	2	22.708	95024		41.783
MASC1-A2FO11-3M2	2	22.708	102922		42.100
MASC1-A3FO11-3M1	3	22.708	76885		40.951
MASC1-A3FO11-3M2	3	22.708	86523		41.413
MASC1-A1FO11-2M1	1	20.437	338340		42.423
MASC1-A1FO11-2M2	1	20.437	309445		42.065
MASC1-A2FO11-2M1	2	20.437	226324		40.834
MASC1-A2FO11-XX3	2	20.437	301981		41.968
MASC1-A3FO11-XX3	3	20.437	262989		41.420
MASC1-A3FO11-2M2	3	20.437	234164		40.966
MASC1-A1FO11-1M1	1	15.895	1000000	41.104	42.119
MASC1-A1FO11-1M2	1	15.895	1000000	39.561	40.950
MASC1-A2FO11-1M1	2	15.895	1000000	38.511	40.224
MASC1-A2FO11-1M2	2	15.895	1000000	40.354	41.537
MASC1-A3FO11-1M1	3	15.895	1000000	38.042	39.921
MASC1-A3FO11-1M2	3	15.895	1000000	39.061	40.597

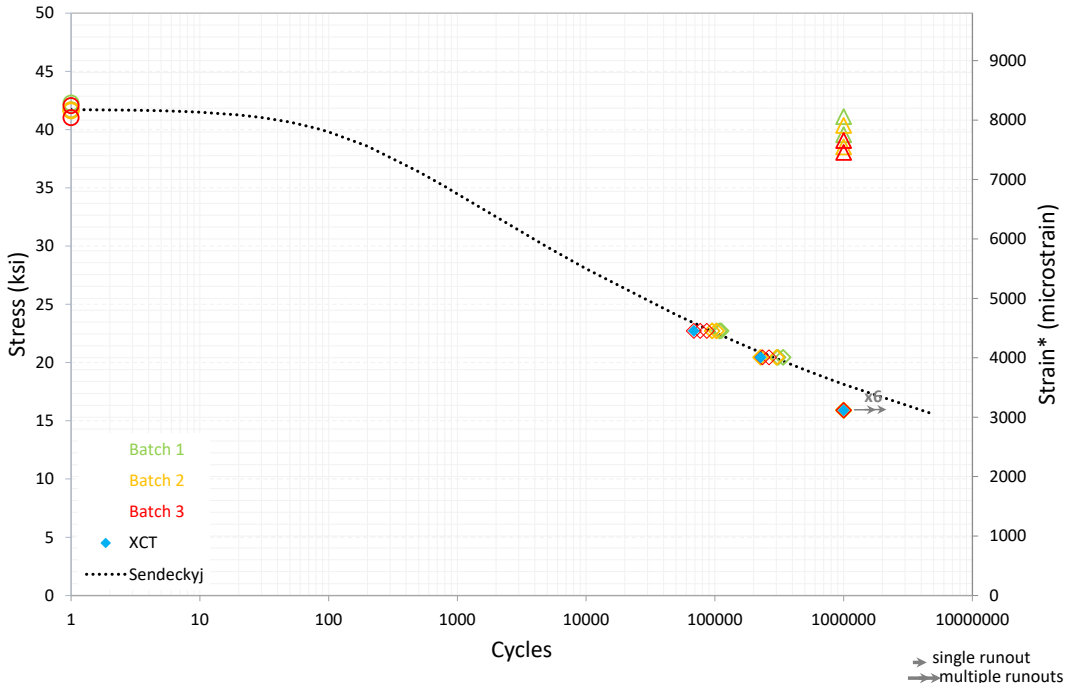


Figure A.37 – SN data with Sendeckyj fitting model for IM7/5250-4, 10/80/10, R=-1, OHC-T.

DISTRIBUTION STATEMENT A.
Approved for public release: distribution is unlimited.

Table A.36 – SN data for IM7/5250-4, 50/40/10, R=0.1, DNS.

Specimen	Batch	σ_A	n	σ_R	σ_e
MASC1-A1DD11-0X1	1	3.787	1		
MASC1-A2DD11-0X2	2	3.684	1		
MASC1-A3DD11-0X1	3	3.668	1		
MASC1-A1DD11-0X2	1	3.642	1		
MASC1-A3DD11-0X2	3	3.632	1		
MASC1-A2DD11-0X1	2	3.486	1		
MASC1-A1DD11-XX4	1	2.190	14683		3.840
MASC1-A2DD11-XX5	2	2190	5679		3.586
MASC1-A3DD11-XX5	3	2190	5942		3.597
MASC1-A1DD11-3K1	1	1.825	179785		3.833
MASC1-A1DD11-3K2	1	1.825	113129		3.707
MASC1-A2DD11-3K1	2	1.825	45326		3.470
MASC1-A2DD11-3K2	2	1.825	55245		3.520
MASC1-A3DD11-3K1	3	1.825	143851		3.772
MASC1-A3DD11-3K2	3	1.825	83260		3.626
MASC1-A1DD11-XX2	1	1.642	494093		3.710
MASC1-A1DD11-2K2	1	1.642	307620		3.586
MASC1-A2DD11-2K1	2	1.642	132537		3.375
MASC1-A2DD11-XX3	2	1.642	106498		3.322
MASC1-A2DD11-2K2	2	1.642	392877		3.650
MASC1-A3DD11-XX3	3	1.642	376432		3.638
MASC1-A3DD11-XX1	3	1.642	239682		3.522
MASC1-A1DD11-XX1	1	1.460	1000000	3.794	3.864
MASC1-A1DD11-1K2	1	1.460	1000000	2.980	3.499
MASC1-A2DD11-1K1	2	1.460	1000000	3.832	3.895
MASC1-A1DD11-0X1	2	1.460	1000000	3.137	3.526
MASC1-A2DD11-0X2	3	1.460	1000000	3.072	3.513
MASC1-A3DD11-0X1	3	1.460	1000000	3.246	3.555

DISTRIBUTION STATEMENT A.
Approved for public release: distribution is unlimited.

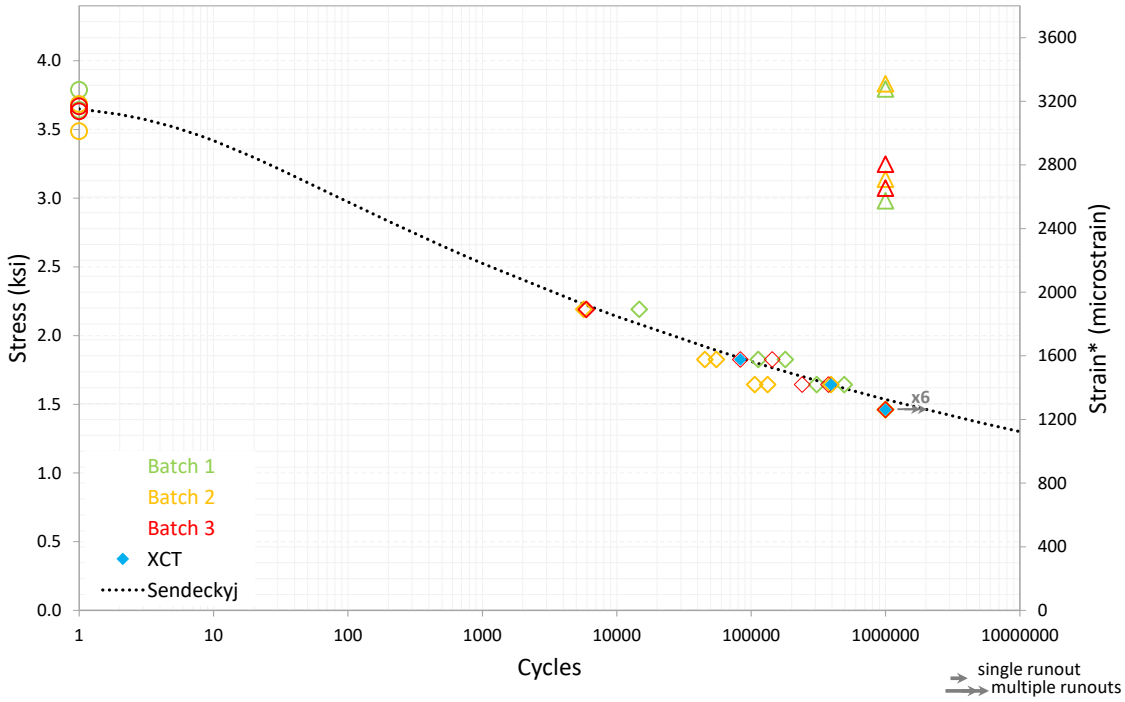


Figure A.38 – SN data with Sendeckyj fitting model for IM7/5250-4, 50/40/10, R=0.1, DNS.

DISTRIBUTION STATEMENT A.
Approved for public release: distribution is unlimited.

Table A.37 – SN data for IM7/5250-4, 10/80/10, R=0.1, DNS.

Specimen	Batch	σ_A	n	σ_R	σ_e
MASC1-A3FD11-0X2	3	3.366	1		
MASC1-A3FD11-XX1	3	3.339	1		
MASC1-A2FD11-0X2	2	3.264	1		
MASC1-A1FD11-0X2	1	3.257	1		
MASC1-A1FD11-0X1	1	3.239	1		
MASC1-A2FD11-0X1	2	2.921	1		
MASC1-A1FD11-XX1	1	1.939	39242		3.302
MASC1-A2FD11-XX1	2	1.939	65105		3.404
MASC1-A3FD11-XX2	3	1.939	28003		3.236
MASC1-A1FD11-2K1	1	1.777	147342		3.277
MASC1-A1FD11-2K2	1	1.777	131282		3.255
MASC1-A2FD11-2K1	2	1.777	126065		3.247
MASC1-A2FD11-2K2	2	1.777	162259		3.296
MASC1-A3FD11-2K1	3	1.777	119357		3.236
MASC1-A3FD11-2K2	3	1.777	293338		3.415
MASC1-A3FD11-XX1	3	1.777	185714		3.323
MASC1-A1FD11-3K1	1	1.615	428494		3.176
MASC1-A1FD11-3K2	1	1.615	397246		3.162
MASC1-A2FD11-XX2	2	1.615	566865		3.230
MASC1-A3FD11-3K1	3	1.615	447209		3.185
MASC1-A3FD11-3K2	3	1.615	501674		3.207
MASC1-A1FD11-1K1	1	1.454	1000000	3063.386	3.166
MASC1-A1FD11-1K2	1	1.454	1000000	3081.962	3.178
MASC1-A2FD11-1K1	2	1.454	1000000	3234.470	3.285
MASC1-A2FD11-1K2	2	1.454	1000000	3241.178	3.291
MASC1-A3FD11-1K1	3	1.454	1000000	3001.494	3.132
MASC1-A3FD11-1K2	3	1.454	1000000	3311.184	3.348

DISTRIBUTION STATEMENT A.
Approved for public release: distribution is unlimited.

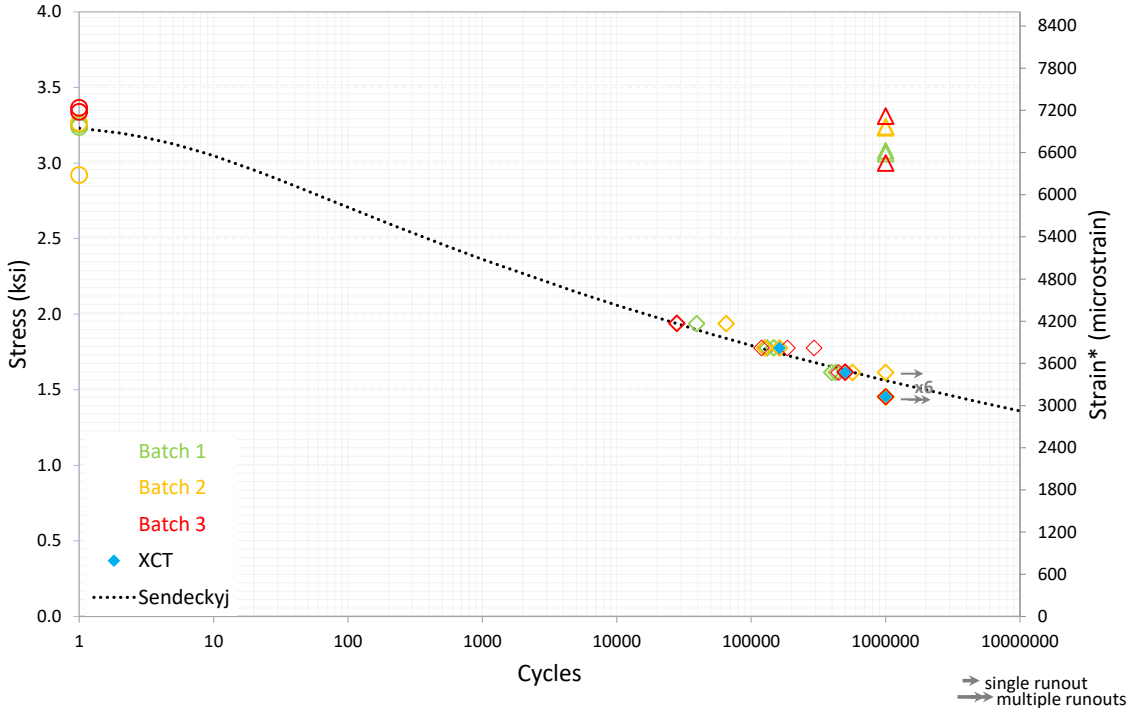


Figure A.39 – SN data with Sendeckyj fitting model for IM7/5250-4, 10/80/10, R=0.1, DNS.

DISTRIBUTION STATEMENT A.
Approved for public release: distribution is unlimited.

Table A.38 – SN data for IM7/5250-4, 50/40/10, R=0.1, ILT.Specimen

Specimen	Batch	σ_A	n	σ_R	σ_e
MASC1-A3DI11-0X2	3	12.397	1		
MASC1-A2DI21-XX2	2	11.618	1		
MASC1-A2DI21-XX1	2	10.869	1		
MASC1-A1DI21-0X1	1	10.619	1		
MASC1-A3DI11-0X1	3	10.254	1		
MASC1-A1DI21-0X2	1	9.420	1		
MASC1-A1DI21-2K2	1	7.604	3763		11.790
MASC1-A1DI21-XX2	1	7.604	3290		11.758
MASC1-A1DI31-XX1	1	7.604	2879		11.727
MASC1-A1DI21-2K2	1	7.604	3763		11.790
MASC1-A1DI31-XX5	1	7.604	7729		11.960
MASC1-A2DI21-4K1	2	7.604	100747		12.588
MASC1-A3DI11-XX1	3	7.604	2836		11.724
MASC1-A3DI11-2K2	3	7.604	46764		12.397
MASC1-A1DI21-3K2	1	5.975	1000000	8.862	10.354
MASC1-A2DI21-3K1	2	5.975	1000000	10.983	10.994
MASC1-A2DI21-3K2	2	5.975	1000000	9.420	10.356
MASC1-A3DI11-3K1	3	5.975	1000000	10.482	10.572
MASC1-A3DI11-3K2	3	5.975	1000000	9.636	10.359
MASC1-A1DI21-1K2	1	4.345	1000000	9.180	9.180
MASC1-A2DI21-1K1	2	4.345	1000000	9.274	9.274
MASC1-A2DI21-1K2	2	4.345	1000000	9.811	9.811
MASC1-A3DI11-1K1	3	4.345	1000000	10.124	10.124
MASC1-A3DI11-1K2	3	4.345	1000000	10.940	10.940

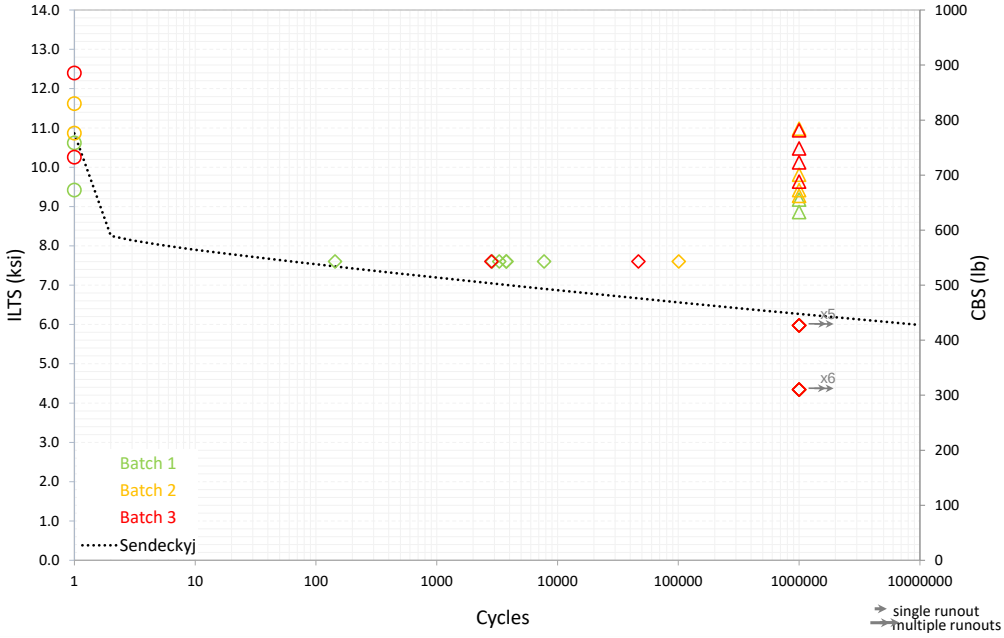


Figure A.40 – SN data with Sendeckyj fitting model for IM7/5250-4, 50/40/10, R=0.1, ILT.

DISTRIBUTION STATEMENT A.
Approved for public release: distribution is unlimited.

Table A.39 – SN data for IM7/5250-4, 10/80/10, R=0.1, ILT.

Specimen	Batch	σ_A	n	σ_R	σ_e
MASC1-A1FI21-0X1	1	12.607	1		
MASC1-A1FI21-0X2	1	12.298	1		
MASC1-A2FI21-0X1	2	11.680	1		
MASC1-A2FI21-0X2	2	11.358	1		
MASC1-A3FI21-0X1	3	11.249	1		
MASC1-A3FI21-0X2	3	10.736	1		
MASC1-A1FI21-4K1	1	6.410	3738		11.186
MASC1-A2FI21-4K1	2	6.410	17939		12.694
MASC1-A3FI21-4K1	3	6.410	3222		11.053
MASC1-A1FI21-3K1	1	5.245	174980		12.482
MASC1-A1FI21-3K2	1	5.245	79967		11.718
MASC1-A2FI21-3K1	2	5.245	81346		11.734
MASC1-A2FI21-3K2	2	5.245	208921		12.661
MASC1-A3FI21-XX1	3	5.245	61630		11.474
MASC1-A3FI21-3K2	3	5.245	98655		11.918
MASC1-A1FI21-2K1	1	4.662	247904		11.410
MASC1-A1FI21-1K1	1	4.662	112912		10.709
MASC1-A2FI21-XX1	2	4.662	241133		11.385
MASC1-A2FI21-XX3	2	4.662	520623		12.114
MASC1-A3FI21-2K1	3	4.662	112297		10.704
MASC1-A3FI21-2K2	3	4.662	239736		11.380
MASC1-A1FI21-XX4	1	4.079	1000000	12.778	12.960
MASC1-A1FI21-XX5	1	4.079	1000000	13.032	13.176
MASC1-A2FI21-1K1	2	4.079	1000000	10.375	11.478
MASC1-A2FI21-1K2	2	4.079	1000000	11.919	12.281
MASC1-A3FI21-1K1	3	4.079	1000000	9.229	11.253
MASC1-A3FI21-1K2	3	4.079	1000000	10.564	11.542

DISTRIBUTION STATEMENT A.
Approved for public release: distribution is unlimited.

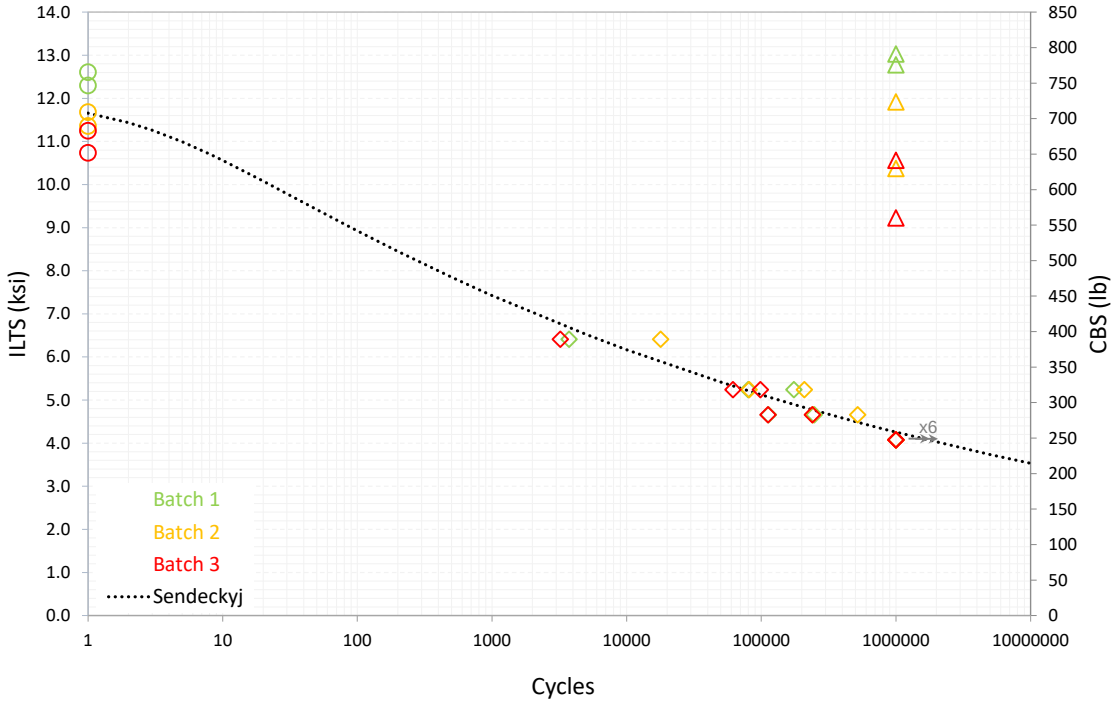


Figure A.41 – SN data with Sendeckyj fitting model for IM7/5250-4, 10/80/10, R=0.1, ILT.

DISTRIBUTION STATEMENT A.
Approved for public release: distribution is unlimited.

Table 40 – SN data for IM7/5250-4, 100/0/0, R=0.1, SBS.

Specimen	Batch	σ_A	n	σ_R	σ_e
MASC1-A1AS11-0X1	1	16.691	1		
MASC1-A1AS11-0X2	1	16.464	1		
MASC1-A1AS11-0X3	1	16.630	1		
MASC1-A2AS11-0X1	2	16.611	1		
MASC1-A2AS11-0X2	2	16.826	1		
MASC1-A2AS11-0X3	2	16.481	1		
MASC1-A3AS11-0X1	3	16.166	1		
MASC1-A3AS11-0X2	3	15.913	1		
MASC1-A3AS11-4K1	3	16.172	1		
MASC1-A1AS11-3K1	1	11.508	2551		16.415
MASC1-A1AS11-3K3	1	11.508	1728		16.181
MASC1-A2AS11-3K2	2	11.508	1659		16.157
MASC1-A3AS11-3K1	3	11.508	3356		16.581
MASC1-A1AS11-2K1	1	9.864	77550		15.952
MASC1-A1AS11-XX1	1	9.864	77041		15.948
MASC1-A2AS11-XX1	2	9.864	168782		16.415
MASC1-A3AS11-2K1	3	9.864	312014		16.790
MASC1-A3AS11-2K2	3	9.864	125210		16.235
MASC1-A1AS11-1K1	1	8.220	1000000	12.388	14.610
MASC1-A2AS11-1K1	2	8.220	1000000	15.471	15.579
MASC1-A2AS11-1K2	2	8.220	1000000	17.096	17.105
MASC1-A3AS11-1K1	3	8.220	1000000	16.299	16.329
MASC1-A3AS11-1K2	3	8.220	1000000	14.476	14.919

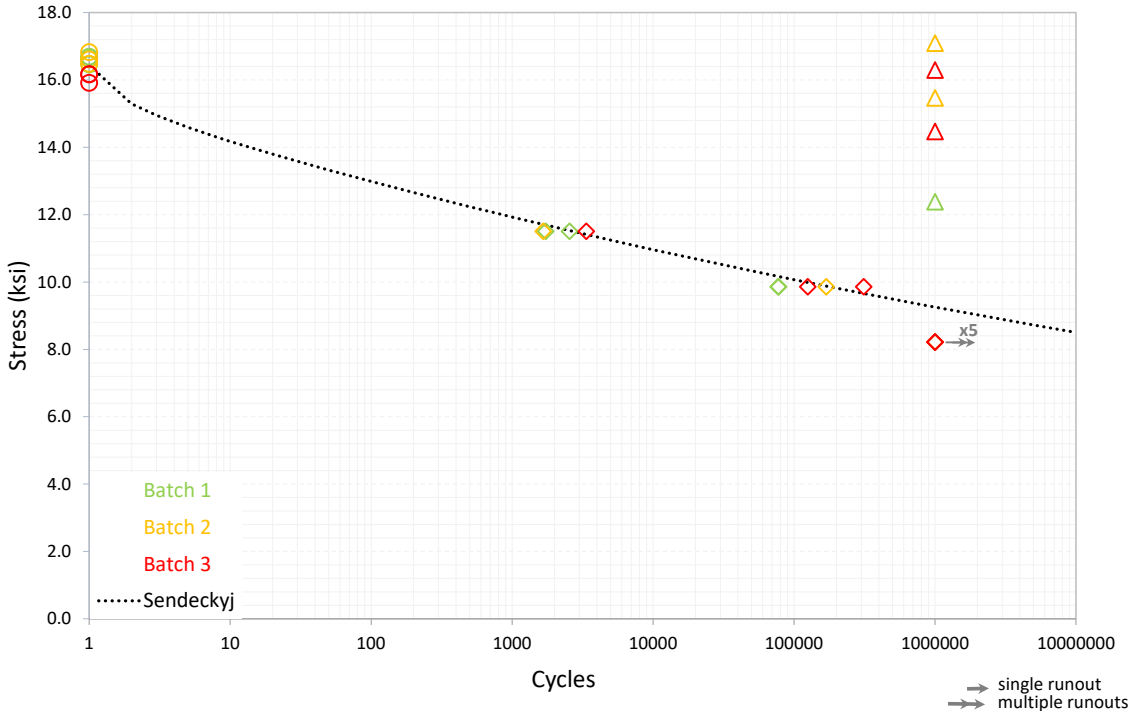


Figure A.42 – SN data with Sendeckyj fitting model for IM7/5250-4, 100/0/0, R=0.1, SBS.

DISTRIBUTION STATEMENT A.
Approved for public release: distribution is unlimited.

APPENDIX B - PROGRESSIVE DAMAGE GROWTH

A.4 Progressive Damage Growth for IM7/5320-1 UNI

The progressive damage growth of fiber-reinforced laminated composite materials is typically start internally and propagate as the fatigue loading is continued. Local damage may be initiated at an early life in notched specimens and may propagate as the fatigue life increases. Thus, the progressive failure analysis of such notched components is essential to predict their accurate mechanical behavior under various loading conditions. This section includes IM7/5320-1 unidirectional laminate subjected to uniaxial tensile loading, considering three different layups, hard (50/40/10), quasi (25/50/25), and soft (10/80/10). The laminate stacking sequences (CPT 0.0054") include 28 plies for hard layup and 24 plies for quasi and soft layups with stacking sequences [45/0/-45/02/45/90/-45/02/45/0/-45/0]s, [45/0/-45/90]3s and [45/-45/45/-45/90/-45/0/45/-45/45/-45/45]s, respectively.

50/40/10 Open-Hole Test

R=0.1, OHT-T → Specimens: SL-1 (60%), SL-2 (70%), SL-3 (80%), and SL-4 (90%)
R=5.0, OHC-C → Specimens: SL-1 (70%), SL-2 (75%), and SL-3 (80%)
R=-1, OHT-C → Specimens: SL-1 (50%), SL-2 (55%), SL-3 (60%) and SL-4 (70%)

Specimens were fatigued until failure or one-million cycles (runout) was achieved. A minimum of three stress levels were used, but in some instances a fourth stress level was added to achieve more failures and add extra reliability to the data analysis.

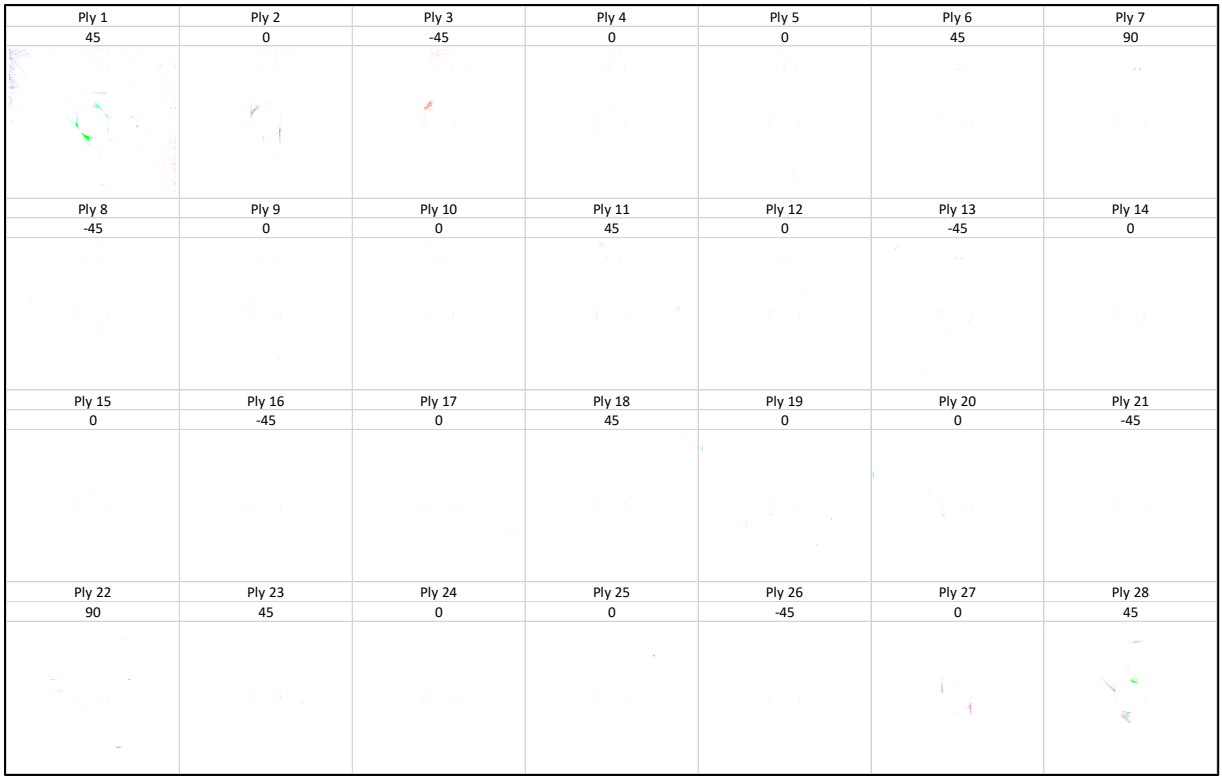
For R=0.1, all specimens survived in fatigue at four stress levels and developed an apparent increase in residual strength. This was due to the stress relief that occurred when the outer plies and the regions above and below the hole were delaminated (Figure B.1). These specimens experienced extensive delamination on the outermost plies (respective to stress). SL-1 and SL-2 specimens exhibited minor delamination near the hole that was restricted to their outermost plies (Figure Figure B.2). Edge delamination was significant at SL-3 although that did not lead to a catastrophic specimen failure. In addition, SL-3 displayed major delamination throughout plies directly above and below the hole in the 0° direction. However, it exhibited delamination propagating from the outer edges within its 90° and adjacent 45° plies (Figure B.3).

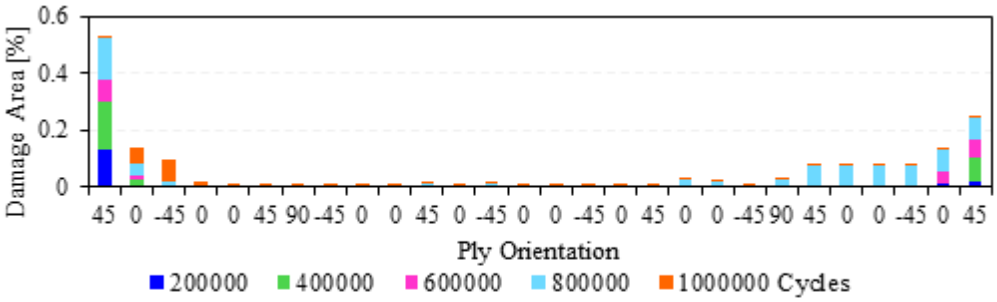
For R=5.0, SL-1 and SL-2 specimens survived fatigue with minor damage at the end of fatigue and developed a slight increase in residual strength (Figure B.5 and Figure B.6) while SL-3 failed early (17,487 cycles) and exhibited significant damage with some fiber failure. Surface matrix crack propagation started at the outermost plies and then saturated to innermost plies within the region around the hole (Figure B.7). Failure behavior in this group ultimately leads to an accelerated failure of the specimen.

DISTRIBUTION STATEMENT A.
Approved for public release: distribution is unlimited.

For R= -1, SL-2 survived while SL-1 and SL-3 specimens failed. This peculiar outcome may be due to the resin-rich areas within the plies noted in this material (Figure B.9). Starting at 200,000 cycles, delamination and matrix cracks developed at the edges of the gage area and also inside of the specimen. As a result of the present gaps these flaws may tended to grow with major out-of-plane deformation. In addition, load reversal was the most critical fatigue stress ratio across all fatigue cases. Fiber splitting or matrix crack along the fiber direction was observed on several plies. SL-1 and SL-2 uniquely displayed significant delamination propagating from their outer edges in their final scan (Figure B.9 and Figure B.10). Note that the delamination grew in the direction of the load forming a triangle between the 45° and 0° direction (Figure B.11).

DISTRIBUTION STATEMENT A.
Approved for public release: distribution is unlimited.





Specimen ID	MASC1-B1DO11-2K2
Test Method	OHT-T
Material System	IM7 5320-1
Ply Layup	50/40/10
Number of Plies	28
Stress Ratio	0.1
% Stress	70% of Ultimate Stress
Final Cycles	1,000,000 (runout)
1) Separation between the fibers of a 0° ply.	
2) Delamination of a layer, vertically extending from the hole in the 0° direction.	

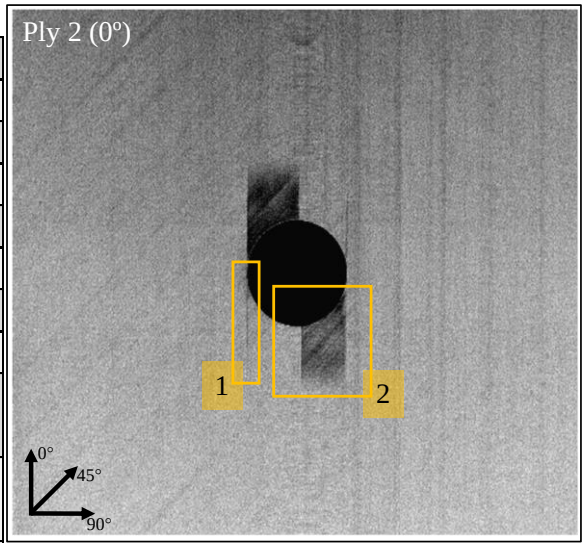
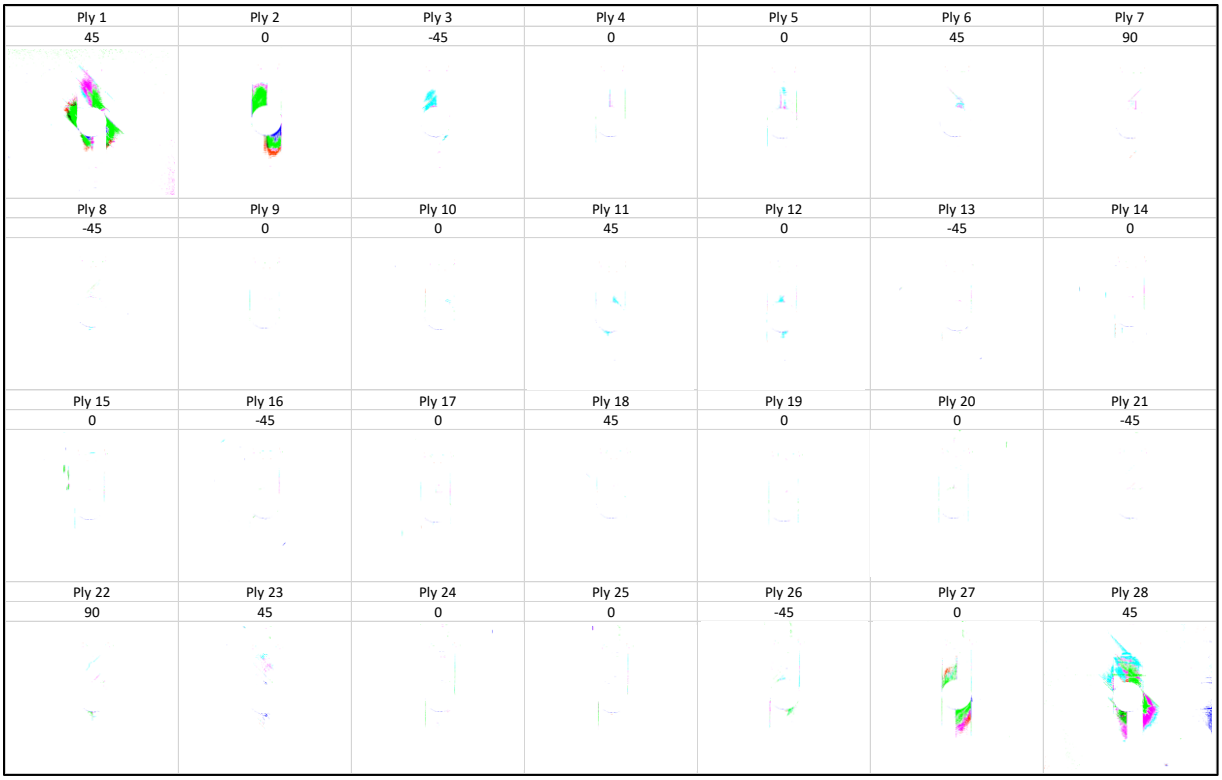
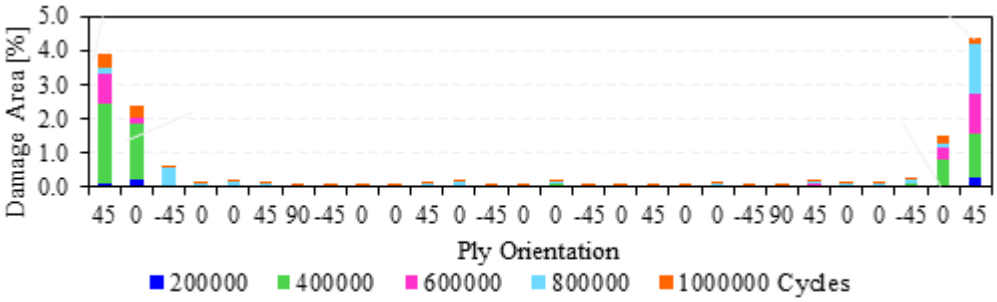


Figure B.1 – Ply-by-ply damage growth and area increase for IM7/5320-1, 50/40/10, R=0.1, SL1.

DISTRIBUTION STATEMENT A.
Approved for public release: distribution is unlimited.





Specimen ID	MASC1-B2DO11-XX2
Test Method	OHT-T
Material System	IM7 5320-1
Ply Layup	50/40/10
Number of Plies	28
Stress Ratio	0.1
% Stress	80% of Ultimate Stress
Final Cycles	1,000,000 (runout)
1) Separation between the fibers of a 0° ply.	
2) Delamination of a layer, vertically extending from the hole in the 0° direction.	

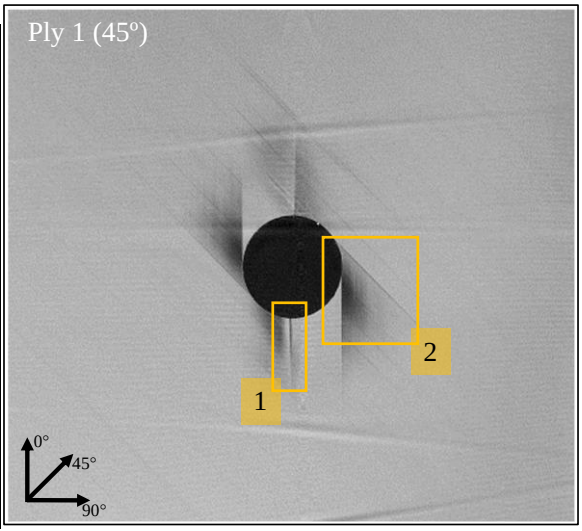


Figure B.2 – Ply-by-ply damage growth and area increase for IM7/5320-1, 50/40/10, R=0.1, SL2.

DISTRIBUTION STATEMENT A.
Approved for public release: distribution is unlimited.

Continued…	MASC1-B2DO11-XX2
Test Method	OHT-T
Material System	IM7 5320-1
Ply Layup	50/40/10
Number of Plies	28
Stress Ratio	0.1
% Stress	80% of Ultimate Stress
Final Cycles	1,000,000 (runout)
1) Fiber failure vertically extending from the hole in the 0° direction.	
2) Fiber failure near the hole (not formed from the hole) in the 45° direction.	

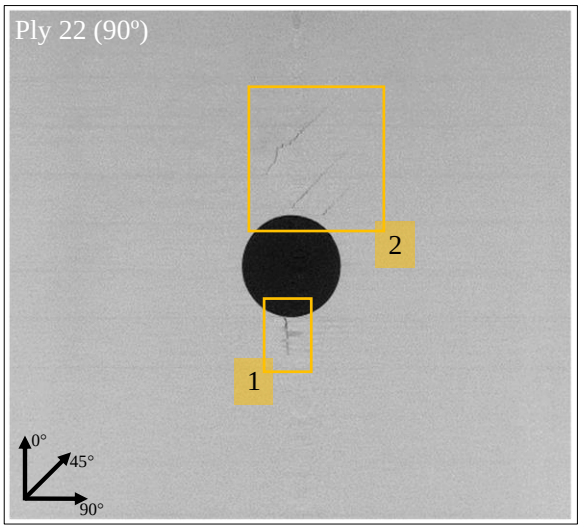
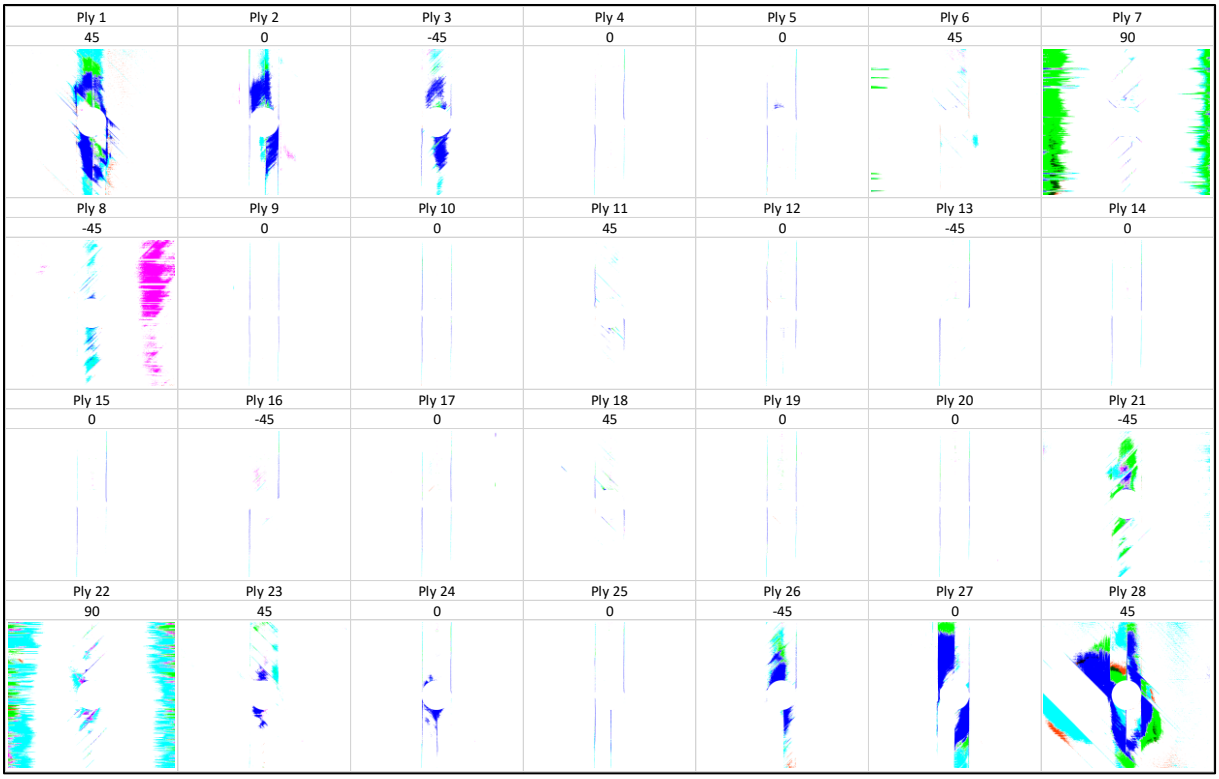
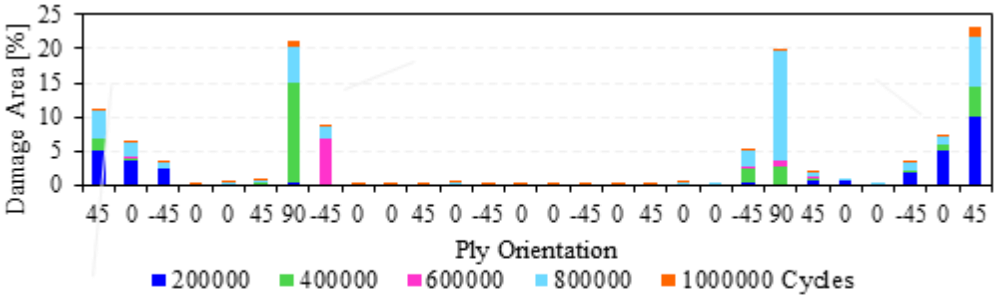


Figure B.2 – Ply-by-ply damage growth and area increase for IM7/5320-1, 50/40/10, R=0.1, SL2 (cont.).

DISTRIBUTION STATEMENT A.
Approved for public release: distribution is unlimited.





Specimen ID	MASC1-B3DO11-XX2
Test Method	OHT-T
Material System	IM7 5320-1
Ply Layup	50/40/10
Number of Plies	28
Stress Ratio	0.1
% Stress	90% of Ultimate Stress
Final Cycles	1,000,000 (runout)
1) Delamination from the outer edge extending to the center along the 90° direction.	
Delamination of a layer, vertically extending from the hole in the 0° direction.	

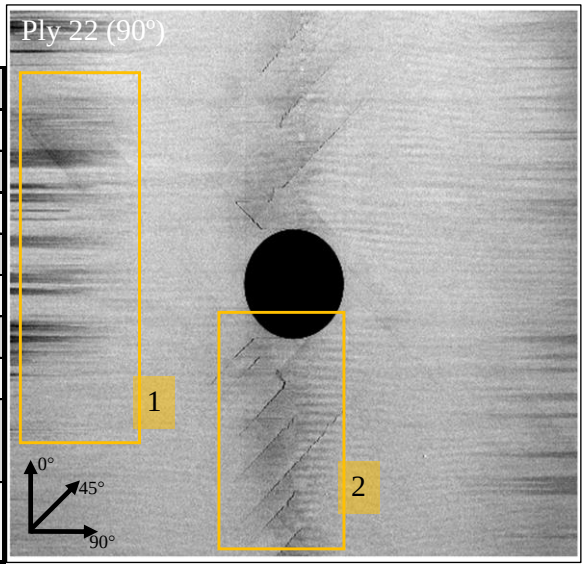


Figure B.3 – Ply-by-ply damage growth and area increase for IM7/5320-1, 50/40/10, R=0.1, SL3.

DISTRIBUTION STATEMENT A.
Approved for public release: distribution is unlimited.

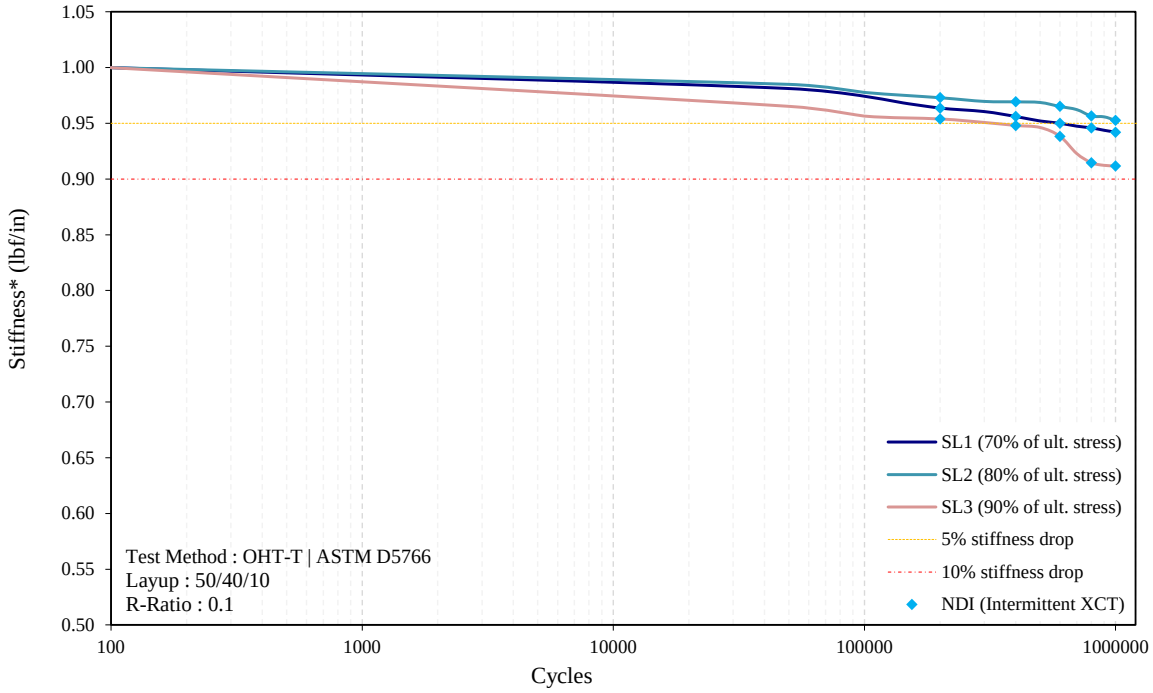
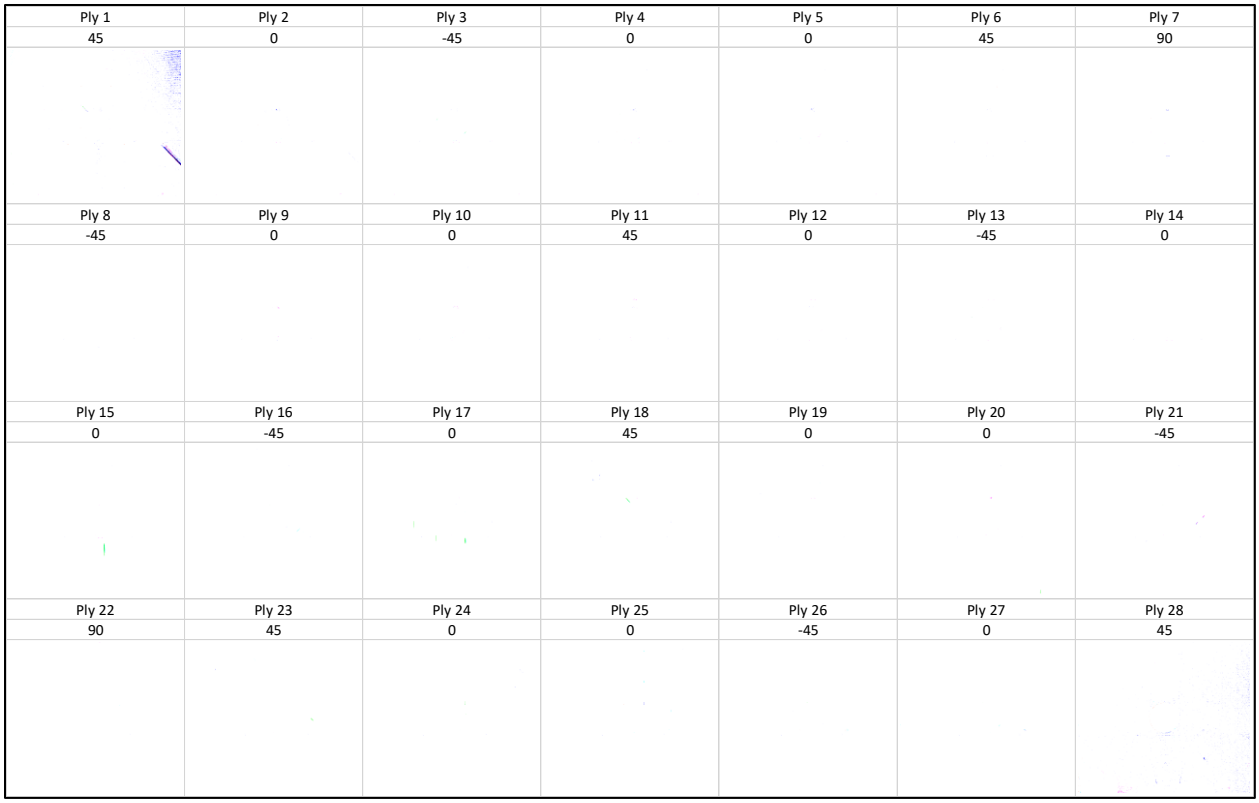
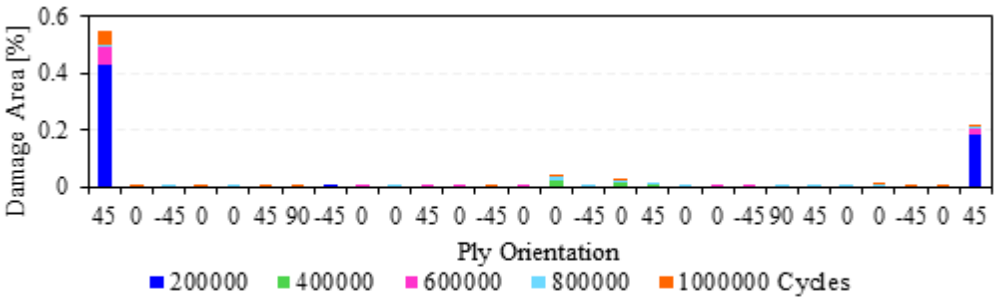


Figure B.4 – Apparent stiffness change during fatigue (normalized by initial compliance) for IM7/5320-1 UNI, 50/40/10 layup, OHT-T, R=0.1.

DISTRIBUTION STATEMENT A.
Approved for public release: distribution is unlimited.





Specimen ID	MASC1-B1DO11-XX7
Test Method	OHC-C
Material System	IM7 5320-1
Ply Layup	50/40/10
Number of Plies	28
Stress Ratio	5.0
% Stress	70% of Ultimate Stress
Final Cycles	1,000,000 (runout)
1) Damaged carbon fiber due to machining process, minor elongation after fatigue.	
Comment) No significant damage after fatigue.	

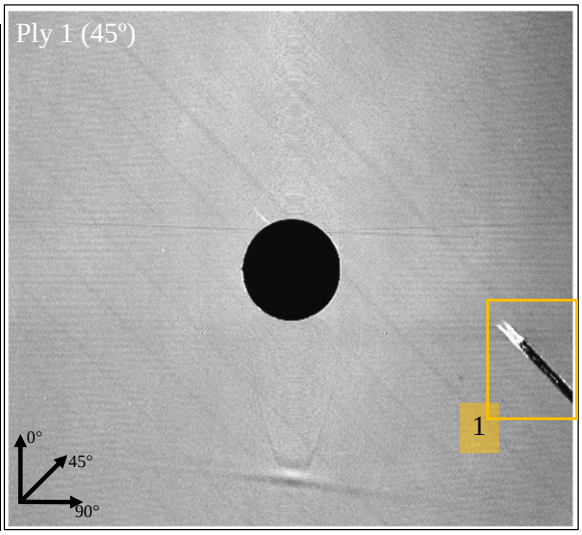
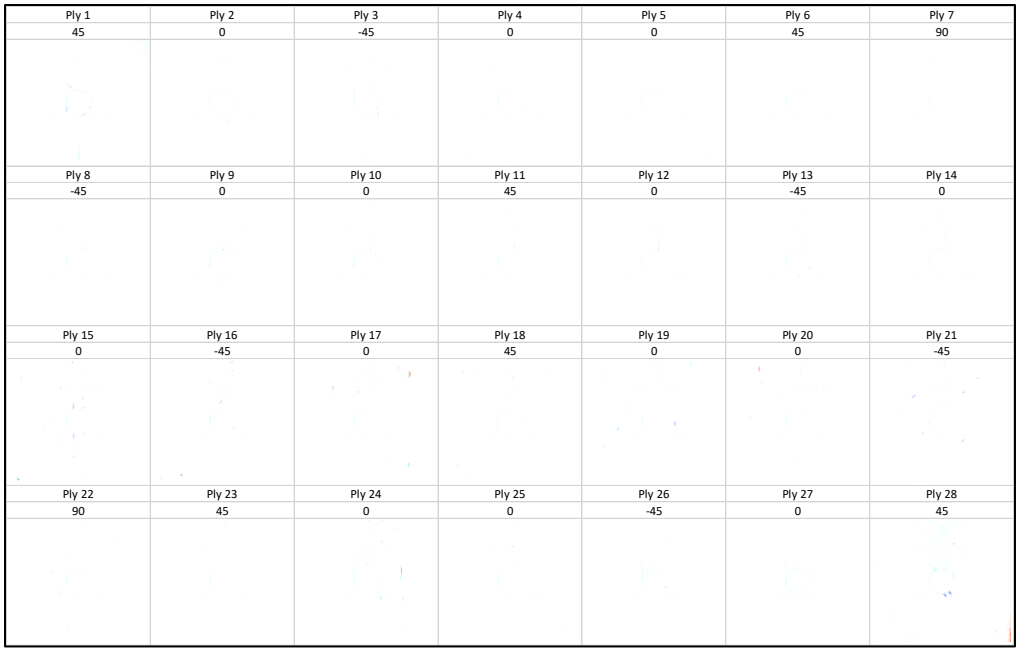
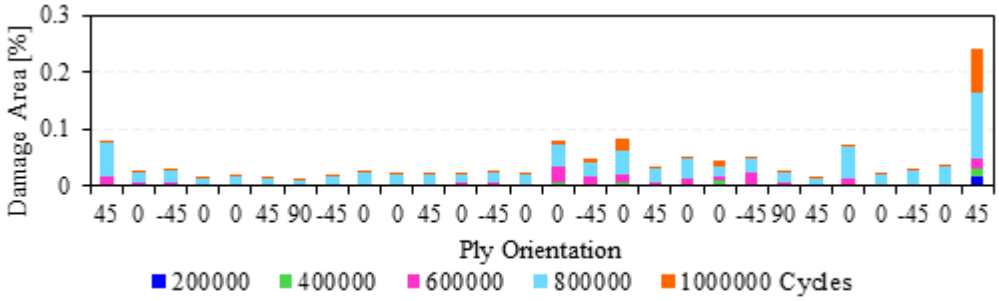


Figure B.5 – Ply-by-ply damage growth and area increase for IM7/5320-1, 50/40/10, R=5, SL1.

DISTRIBUTION STATEMENT A.
Approved for public release: distribution is unlimited.





Specimen ID	MASC1-B1DO11-XX8
Test Method	OHC-C
Material System	IM7 5320-1
Ply Layup	50/40/10
Number of Plies	28
Stress Ratio	5.0
% Stress	75% of Ultimate Stress
Final Cycles	1,000,000 (runout)
1) Delamination of a layer, vertically extending from the hole in the 0° direction.	
Comment) No significant damage after fatigue.	

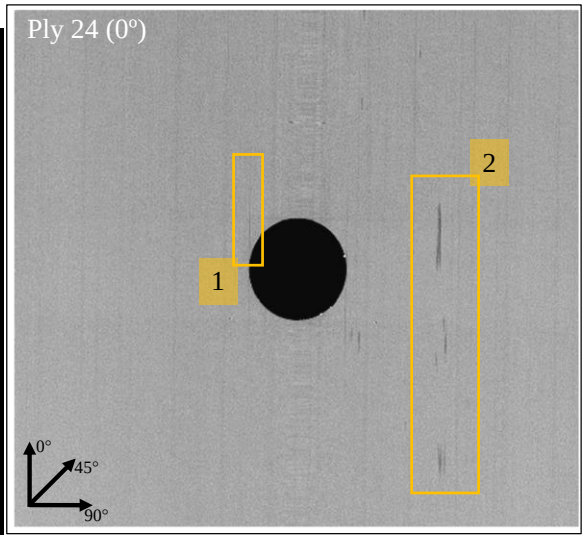
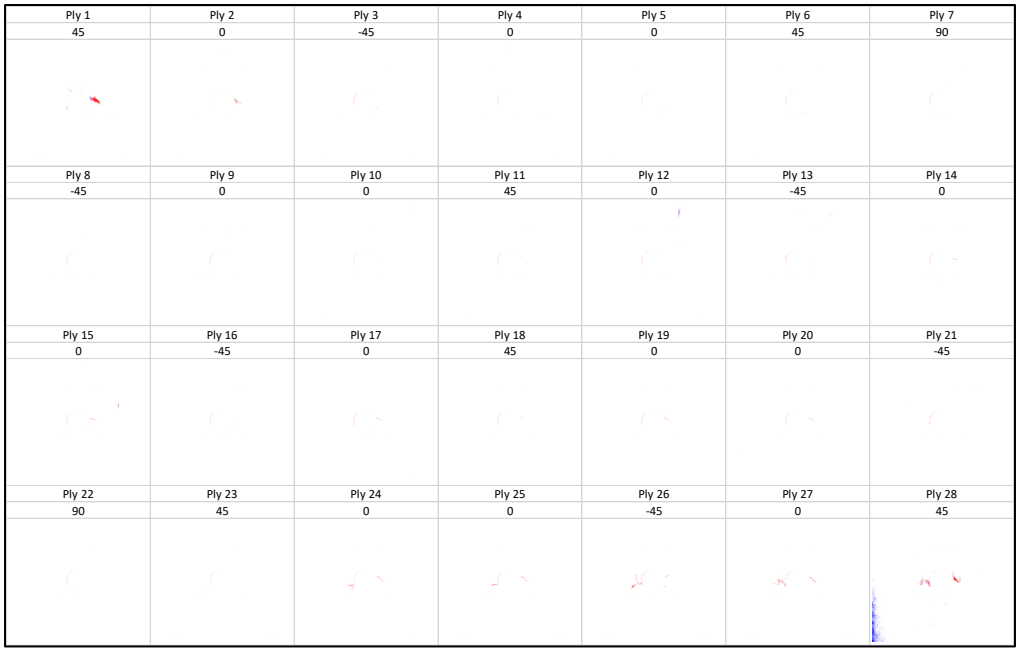
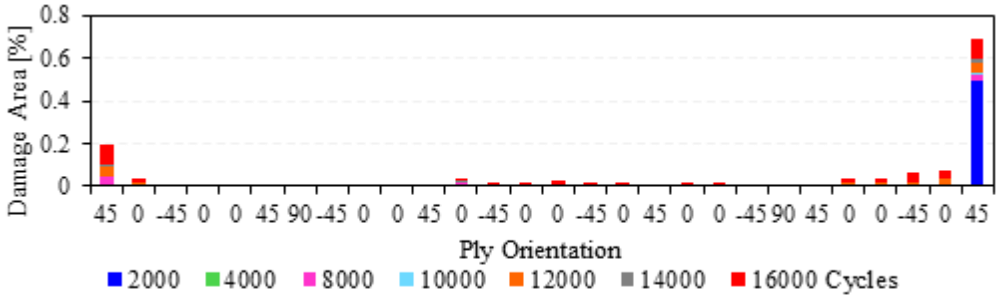


Figure B.6 – Ply-by-ply damage growth and area increase for IM7/5320-1, 50/40/10, R=5, SL2.

DISTRIBUTION STATEMENT A.
Approved for public release: distribution is unlimited.





Specimen ID	MASC1-B3DO11-XX7
Test Method	OHC-C
Material System	IM7 5320-1
Ply Layup	50/40/10
Number of Plies	28
Stress Ratio	5.0
% Stress	80% of Ultimate Stress
Final Cycles	17,487
1) Fiber failure extending radially from the hole failing perpendicular to the 45° ply.	

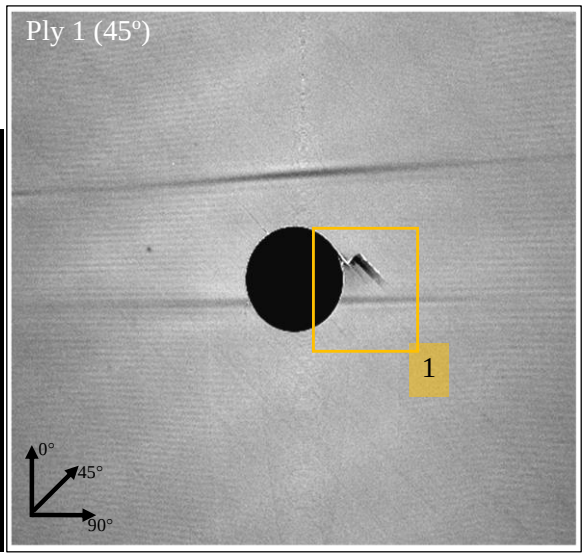


Figure B.7 – Ply-by-ply damage growth and area increase for IM7/5320-1, 50/40/10, R=5, SL3.

DISTRIBUTION STATEMENT A.
Approved for public release: distribution is unlimited.

Continued…	MASC1-B3DO11-XX7
Test Method	OHC-C
Material System	IM7 5320-1
Ply Layup	50/40/10
Number of Plies	28
Stress Ratio	5.0
% Stress	80% of Ultimate Stress
Final Cycles	17,487
1) Fiber failure extending radially from the hole failing across the 0° ply in the 45° direction.	

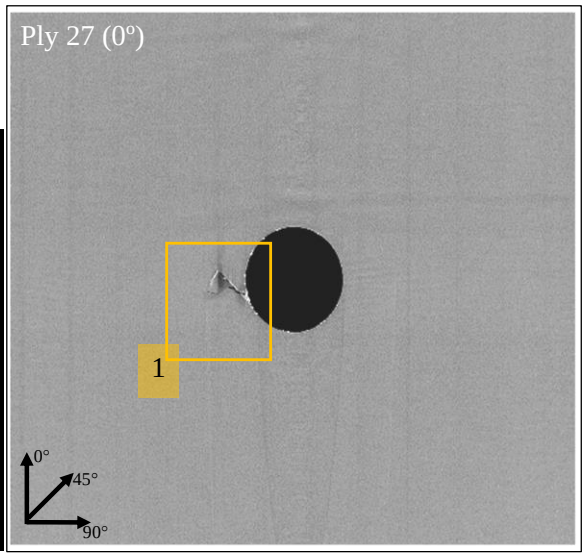


Figure B.7 – Ply-by-ply damage growth and area increase for IM7/5320-1, 50/40/10, R=5, SL3 (cont.).

DISTRIBUTION STATEMENT A.
Approved for public release: distribution is unlimited.

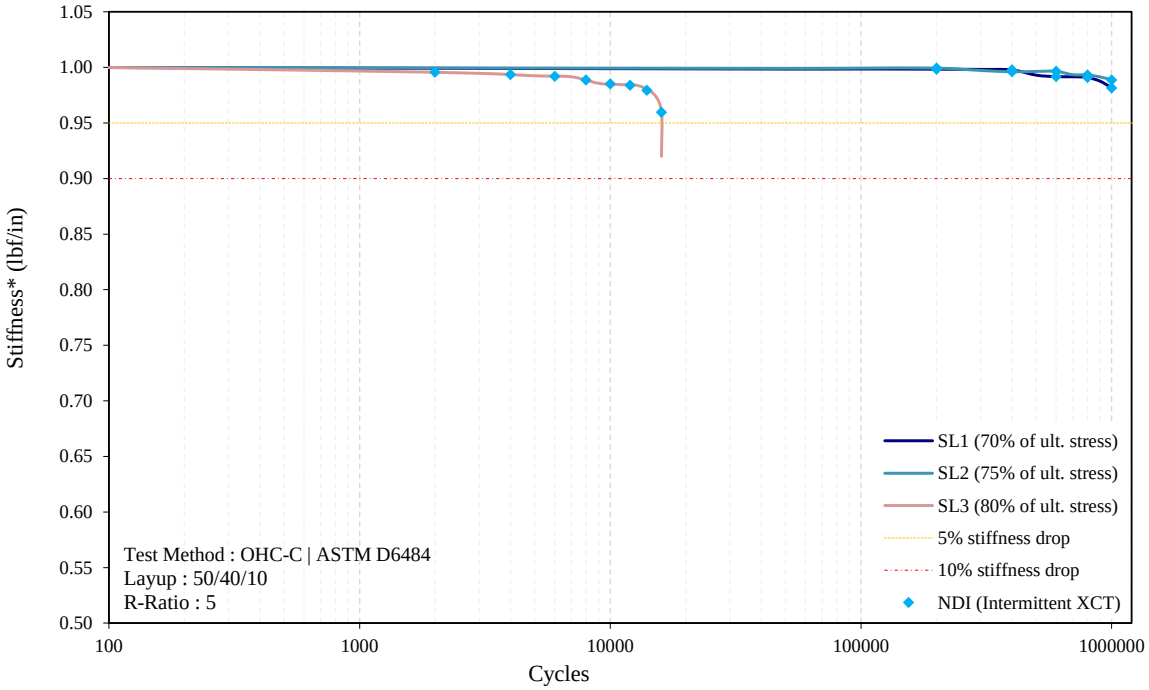
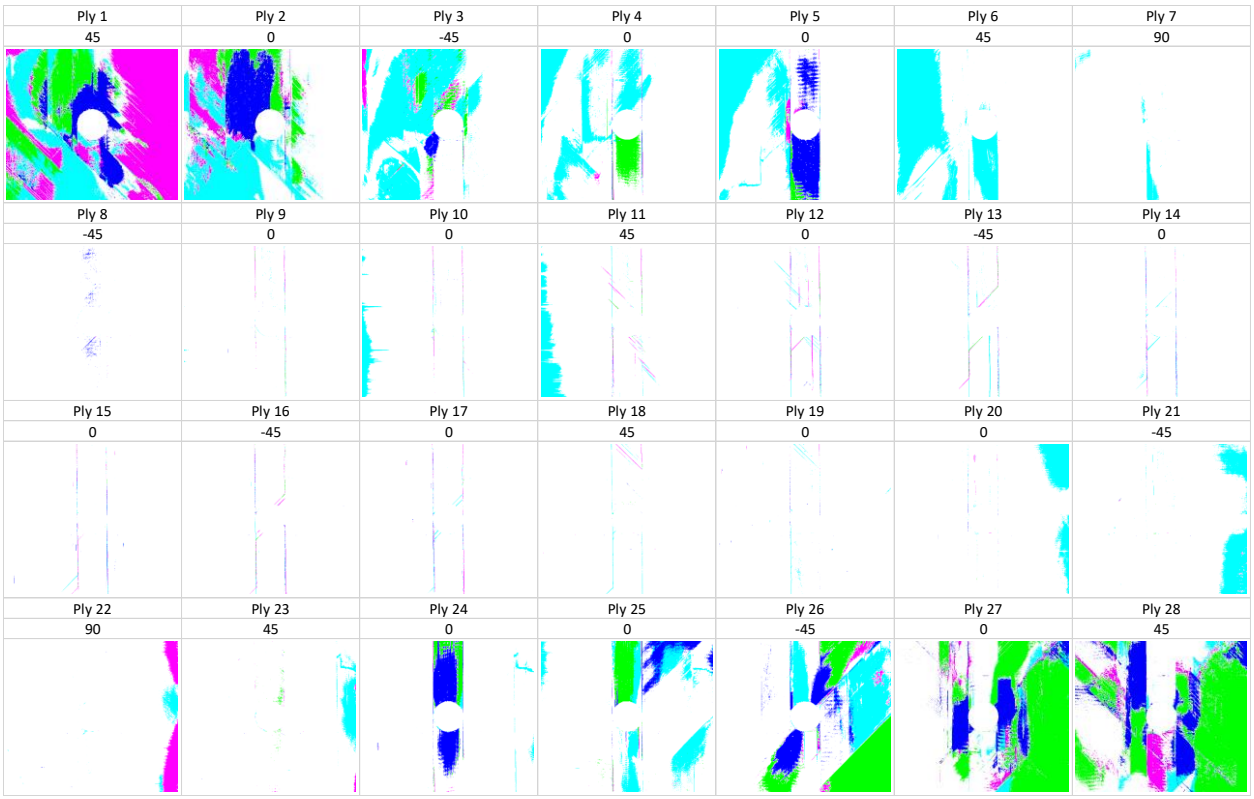
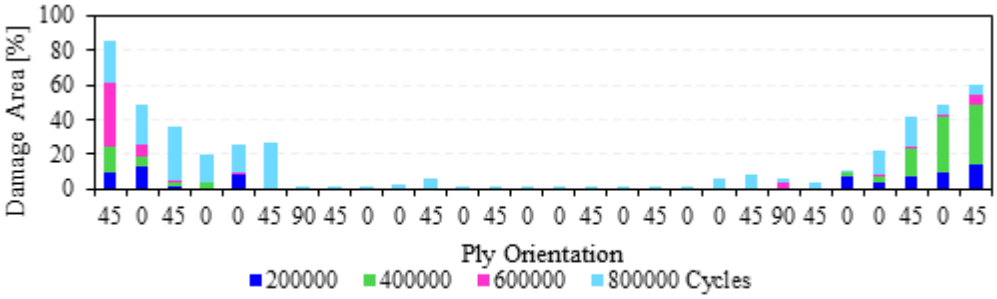


Figure B.8 – Apparent stiffness change during fatigue (normalized by initial compliance) for IM7/5320-1 UNI, 50/40/10 layup, OHC-C, R=5.

DISTRIBUTION STATEMENT A.
Approved for public release: distribution is unlimited.





Specimen ID	MASC1-B1DO11-1K2
Test Method	OHC-T
Material System	IM7 5320-1
Ply Layup	50/40/10
Number of Plies	28
Stress Ratio	-1.0
% Stress	50% of Ultimate Stress
Final Cycles	968,885
1) Fiber failure propagating vertically and tangent from hole in the 0° direction	
2) Large amount of fiber failure and separation of the 45° ply.	
3) Complete delamination of the 45° ply.	

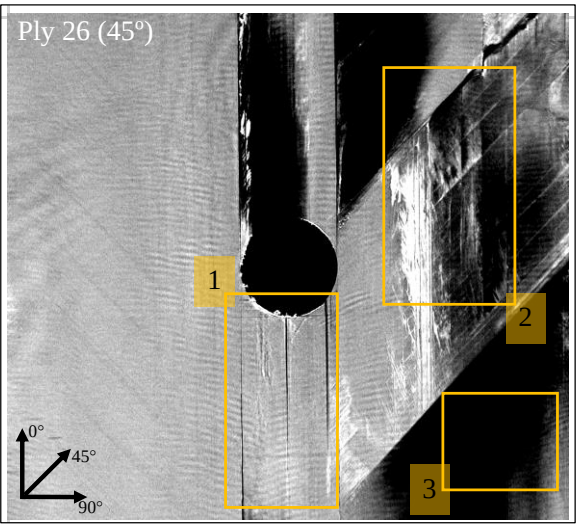
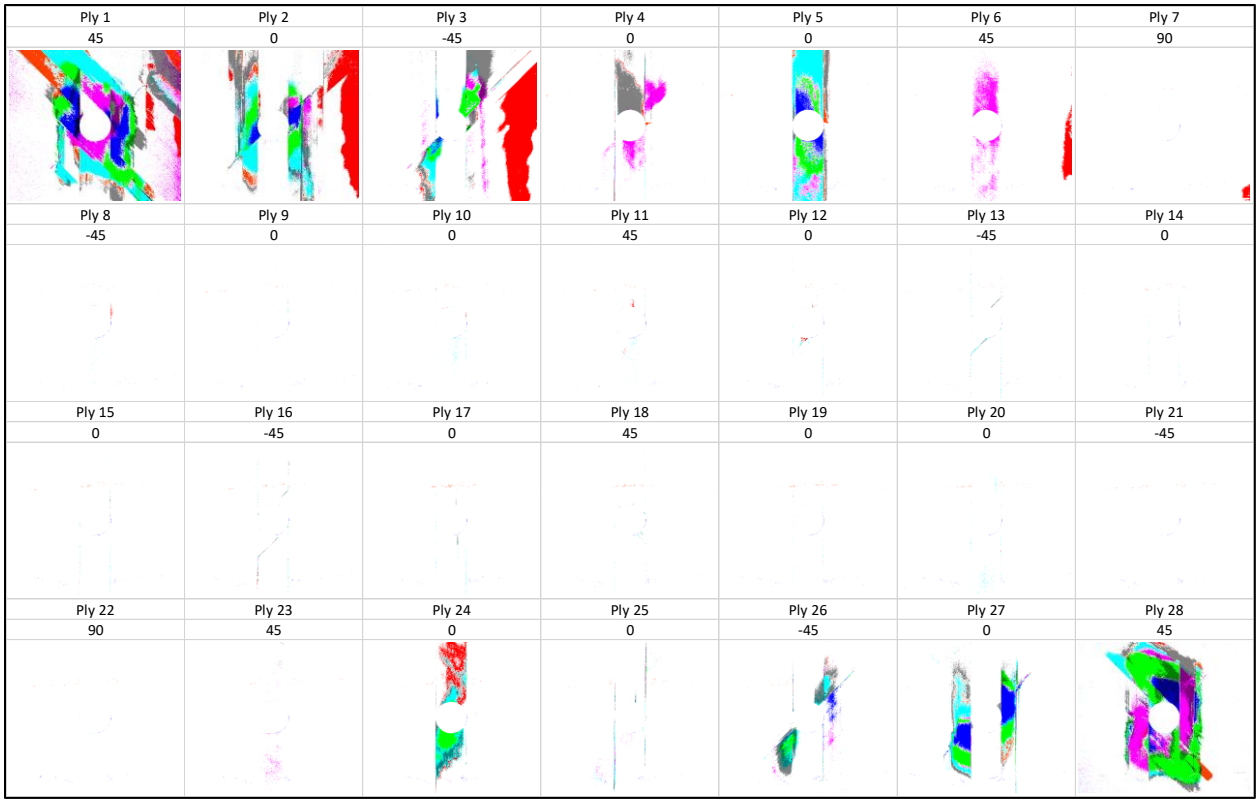
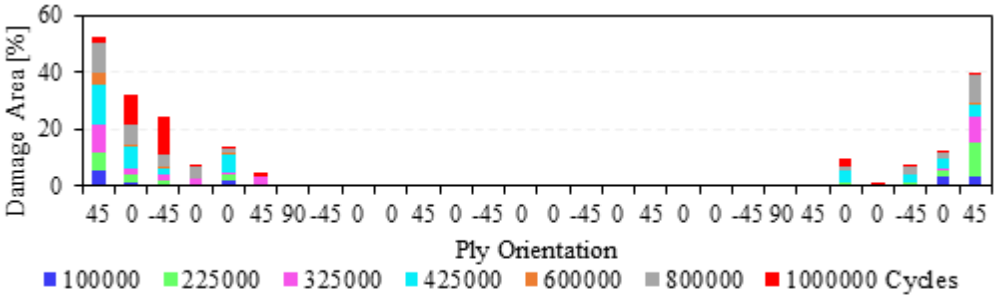


Figure B.9 – Ply-by-ply damage growth and area increase for IM7/5320-1, 50/40/10, R=-1, SL1.

DISTRIBUTION STATEMENT A.
Approved for public release: distribution is unlimited.





Specimen ID	MASC1-B2DO11-2K2
Test Method	OHC-T
Material System	IM7 5320-1
Ply Layup	50/40/10
Number of Plies	28
Stress Ratio	-1.0
% Stress	55% of Ultimate Stress
Final Cycles	1,000,000 (runout)
1) Fiber failure propagating vertically and tangent from hole in the 0° direction	
2) Large amount of fiber failure in the 45° direction.	
3) Delamination of the 0° ply along one side of the specimen.	

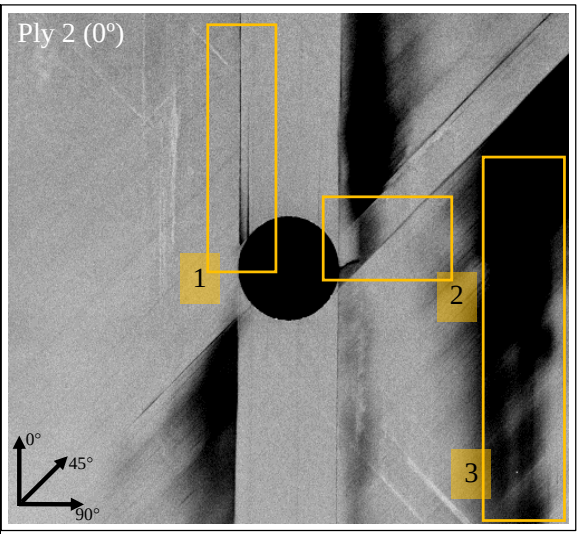
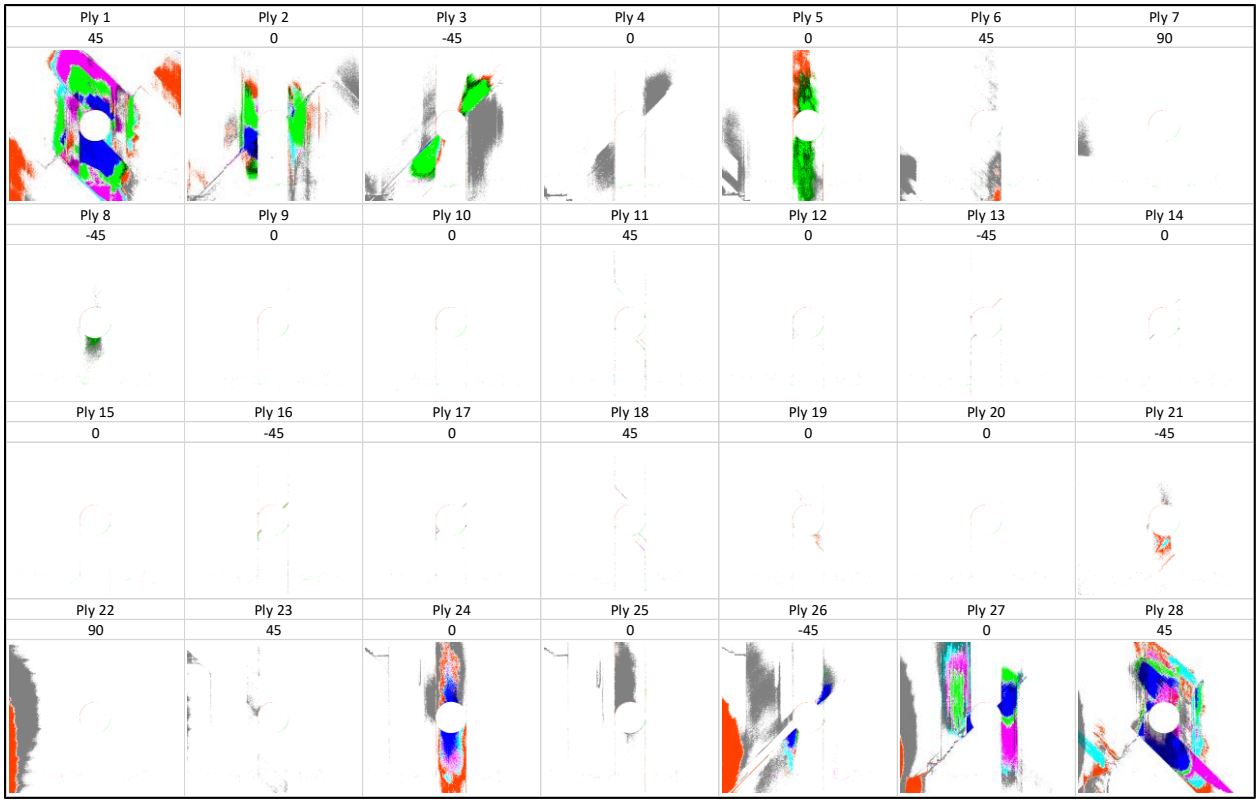
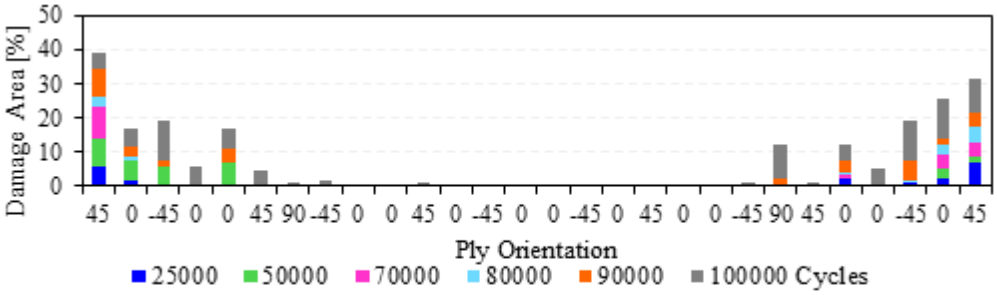


Figure B.10 – Ply-by-ply damage growth and area increase for IM7/5320-1, 50/40/10, R=-1, SL2.

DISTRIBUTION STATEMENT A.
Approved for public release: distribution is unlimited.





Specimen ID	MASC1-B3DO11-2K2
Test Method	OHC-T
Material System	IM7 5320-1
Ply Layup	50/40/10
Number of Plies	28
Stress Ratio	-1.0
% Stress	60% of Ultimate Stress
Final Cycles	114,591
1) Fiber failure across the 0° fibers that have been separated internally.	
2) Large amount of fiber failure in the 45° direction.	
1) Fiber failure extending radially from the hole failing perpendicular to the 45° ply.	

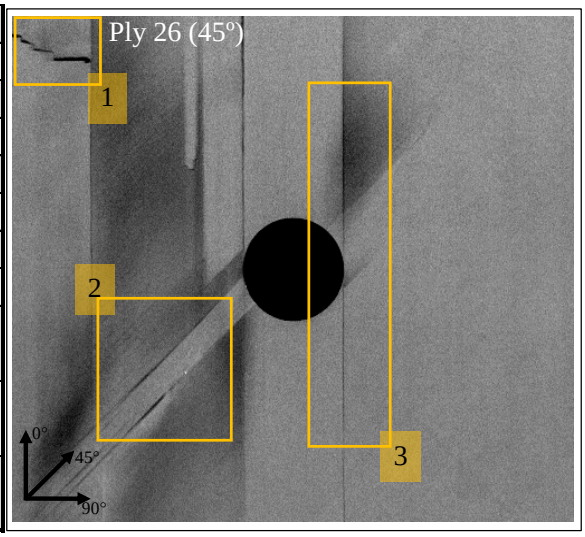


Figure B.11 – Ply-by-ply damage growth and area increase for IM7/5320-1, 50/40/10, R=-1, SL3.

DISTRIBUTION STATEMENT A.
Approved for public release: distribution is unlimited.

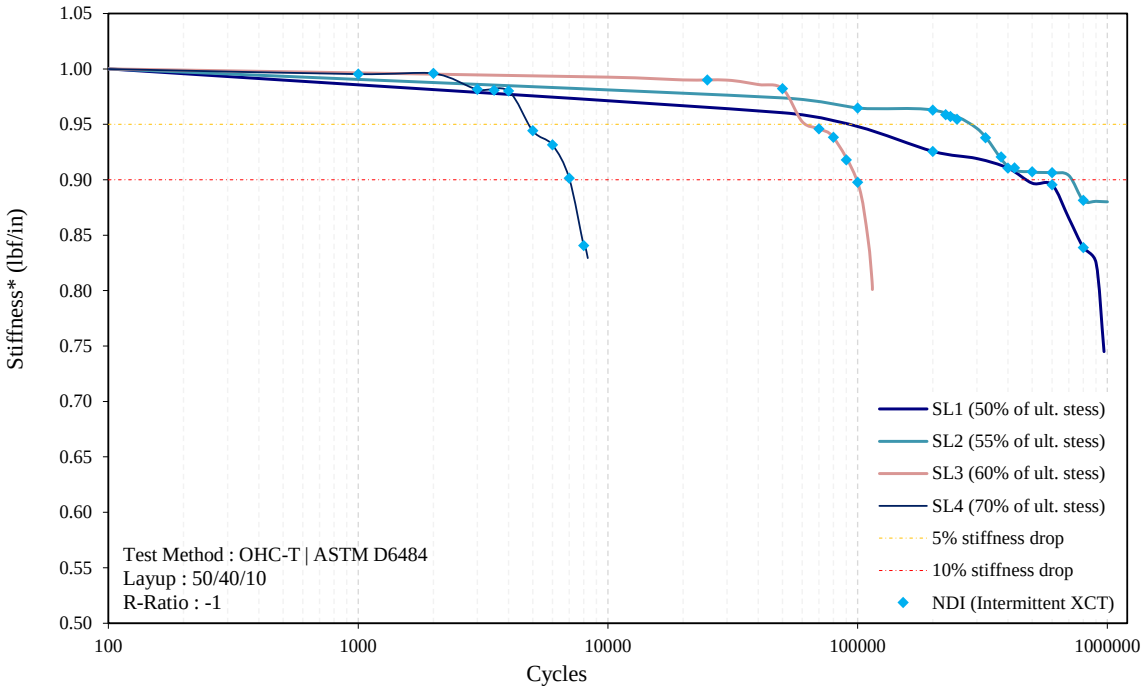


Figure B.12 – Apparent stiffness change during the tension fatigue (normalized by initial compliance) for IM7/5320-1 UNI, 50/40/10 layup, OHC-T, R=-1.

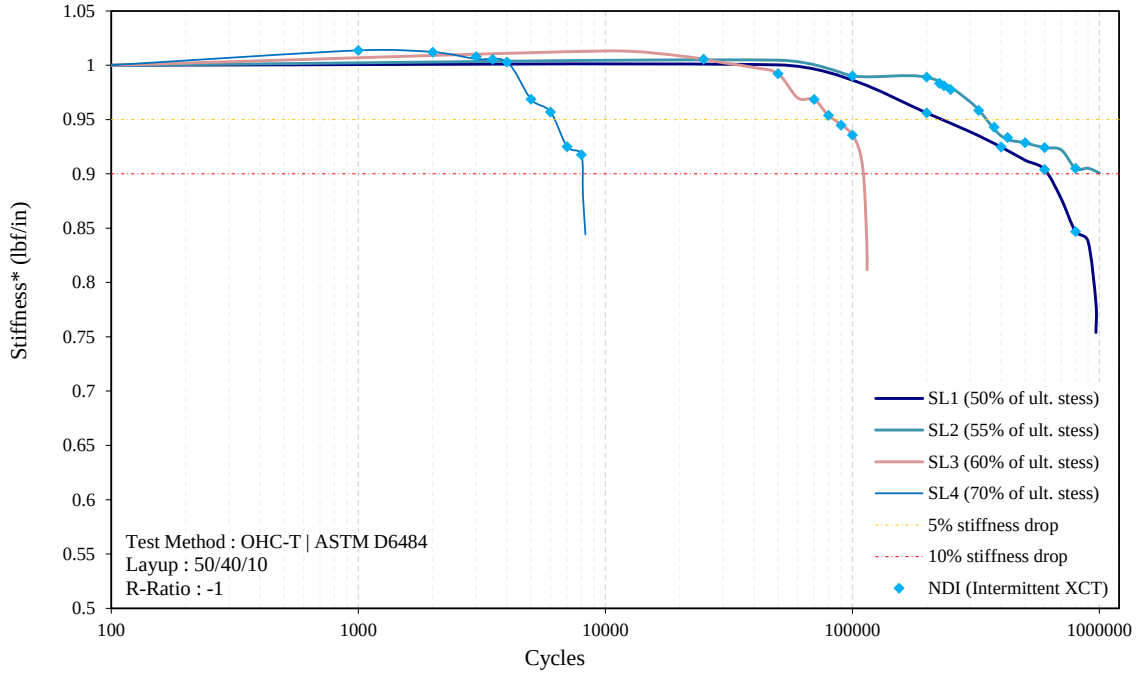


Figure B.13 – Apparent stiffness change during the compression fatigue (normalized by initial compliance) for IM7/5320-1 UNI, 50/40/10 layup, OHC-T, R=-1.

DISTRIBUTION STATEMENT A.
Approved for public release: distribution is unlimited.

25/50/25 Open-Hole Test

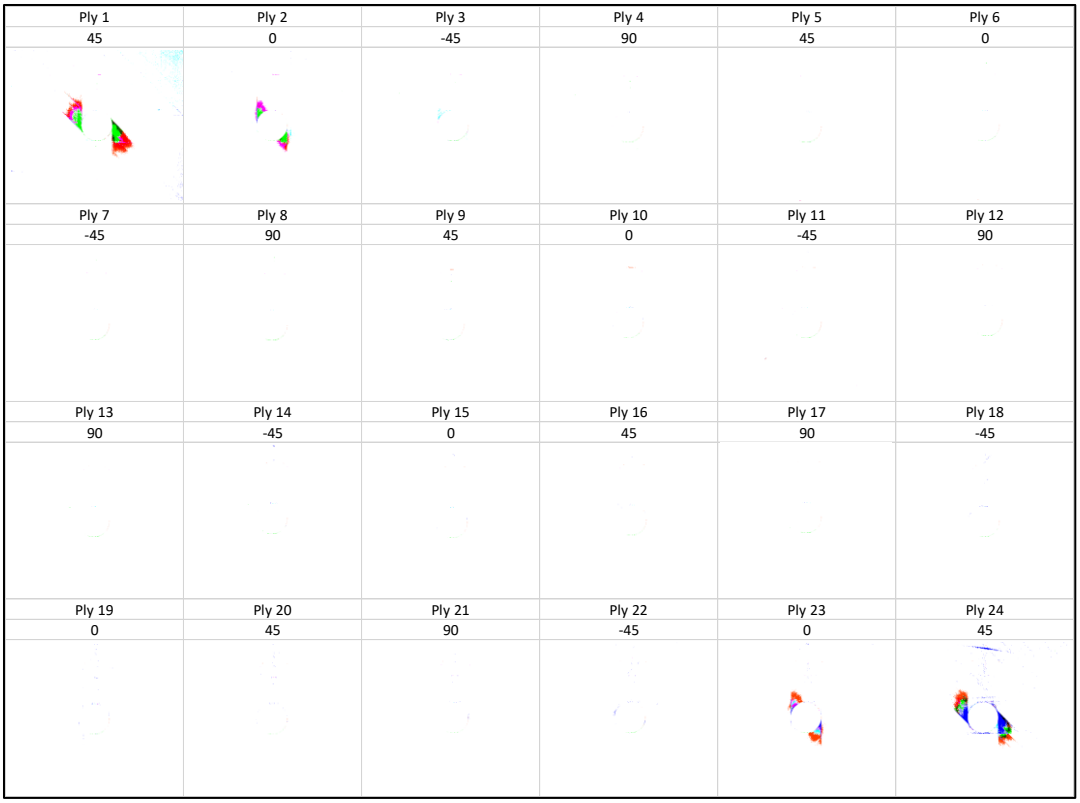
R=0.1, OHT-T → Specimens: SL-1 (70%), SL-2 (80%), and SL-3 (90%)
R=5.0, OHC-C → Specimens: SL-1 (70%), SL-2 (75%), and SL-3 (80%)
R=-1 OHT-C → Specimens: SL-1 (50%), SL-2 (55%), and SL-3 (60%)

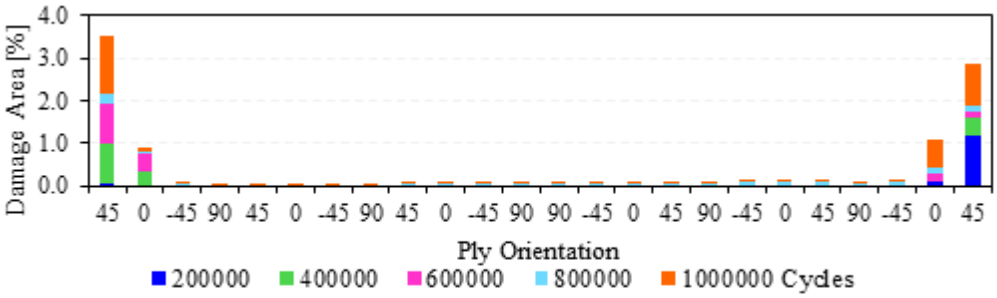
In the observance of progressive damage growth, three specimens were tested for each r-ratio at varying stress levels. Specimens were fatigued until failure or one-million cycles (runout) were achieved. For R=0.1, all 3 specimens survived fatigue and developed an average of 16% increased residual strength. This was due to the stress relief that occurred when the outer plies and the regions above and below the hole that became delaminated. The majority of the damage for SL-1 and SL-2 occurred on the outermost plies near the hole (Figure Figure B.14). SL-2 and SL-3 displayed another region of delamination propagating from the edges growing towards the center of the specimen (Figure B.15). This pattern of delamination is more prominent in SL-3 which is also the only specimen in the group to display fiber failure above and below the hole (Figure B.16).

For R=5.0 only SL-1 survived fatigue and developed a 3% decrease in residual strength. All specimens in this group revealed minor delamination and primarily experienced fiber failure through the hole in the 90° ply direction. This damage is present in all specimens beginning at the outer plies and increasing towards the center plies as the stress level increases (Figure Figure B**.18**). In SL-2 many plies exhibited fiber failure (Figure B.19). This group as a whole demonstrated no signs of significant delamination but specimens in this group that had fiber failure near the hole failed at an accelerated rate (Figure B.20).

For R=-1 only SL 1 survived fatigue and had a 30% decrease in strength after fatigue, which was likely due to the amount of delamination that occurred on the outer plies (Figure B.22). SL-2 and SL-3 exhibited large amounts of fiber failure through the hole on a majority of their plies with the innermost plies experiencing the fewest fiber failures (Figure B.23 and Figure B.24).

DISTRIBUTION STATEMENT A.
Approved for public release: distribution is unlimited.





Specimen ID	MASC1-B1EO11-XX1
Test Method	OHT-T
Material System	IM7 5320-1
Ply Layup	25/50/25
Number of Plies	24
Stress Ratio	0.1
% Stress	70% of Ultimate Stress
Final Cycles	1,000,000 (runout)
1) Delamination of the 45° layer extending from the hole radially outwards along the 45°.	
2) Fiber failure of the 45° extending tangentially from the hole in the 0° direction.	

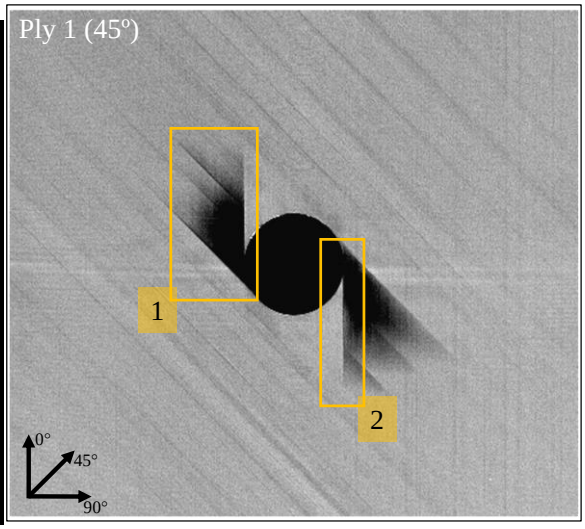
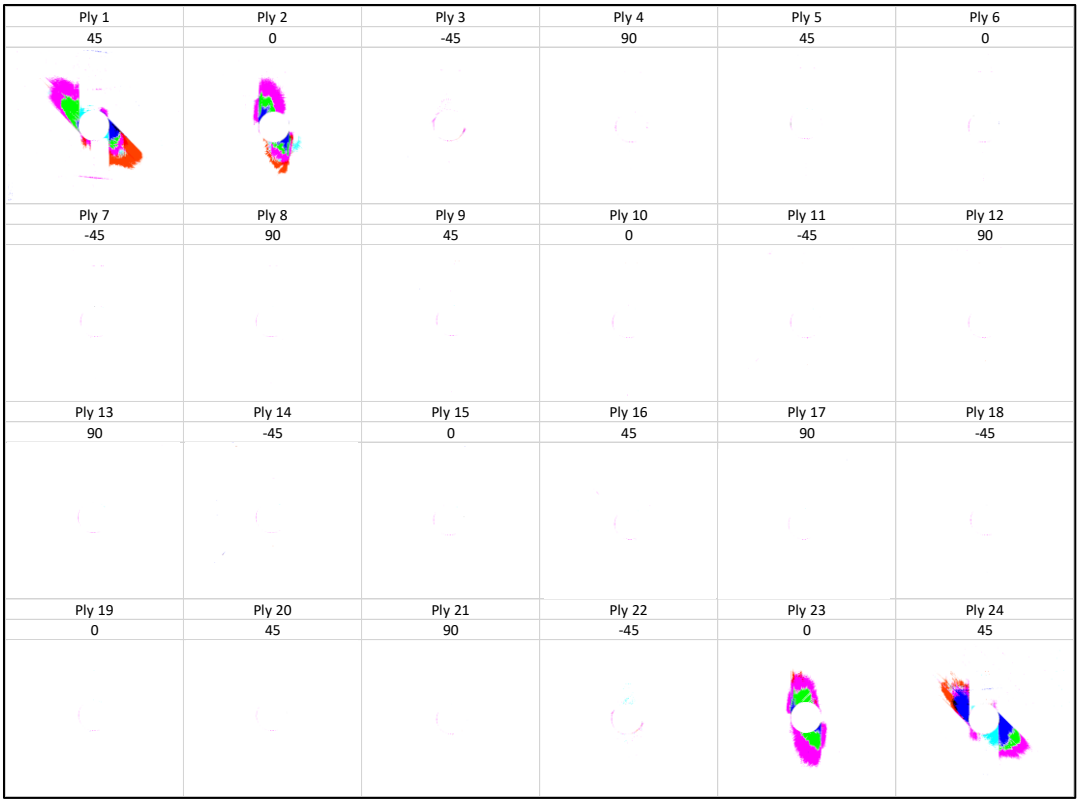
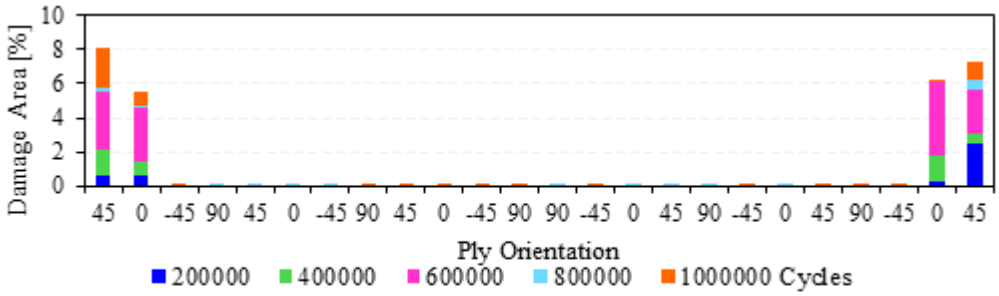


Figure B.14 – Ply-by-ply damage growth and area increase for IM7/5320-1, 25/50/25, R=0.1, SL1.

DISTRIBUTION STATEMENT A.
Approved for public release: distribution is unlimited.





Specimen ID	MASC1-B2EO11-XX1
Test Method	OHT-T
Material System	IM7 5320-1
Ply Layup	25/50/25
Number of Plies	24
Stress Ratio	0.1
% Stress	70% of Ultimate Stress
Final Cycles	1,000,000 (runout)
1) Delamination of the 45° layer extending from the hole radially outwards along the 45°.	
2) Fiber failure of the 45° extending tangentially from the hole in the 0° direction.	
3) Separation between the fibers of a 45° ply extending from the hole.	

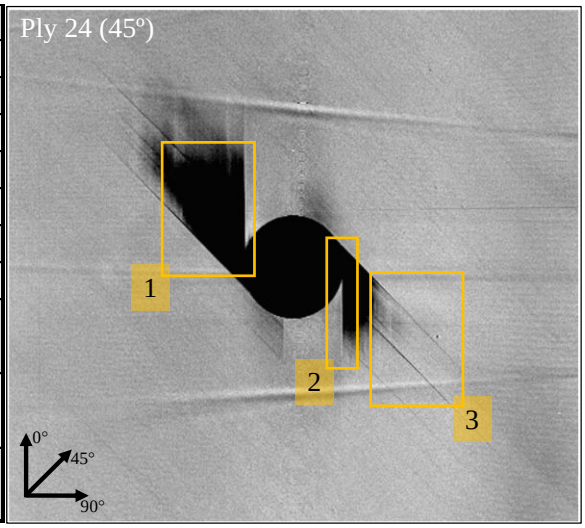
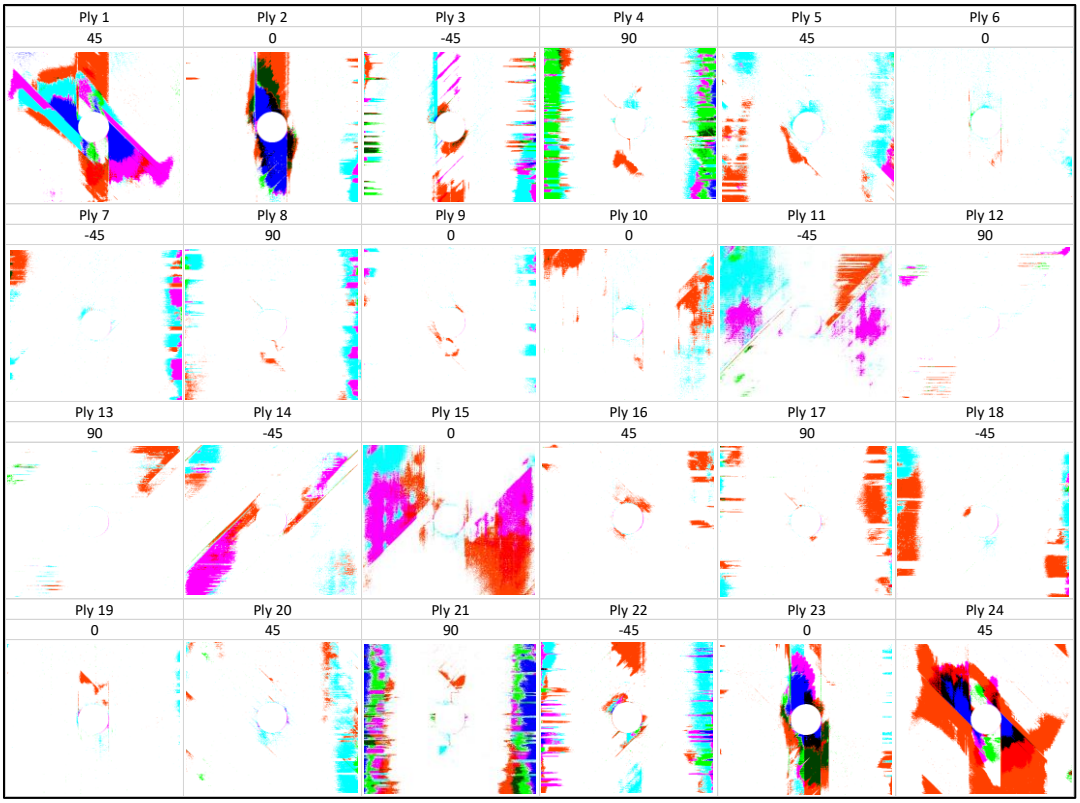
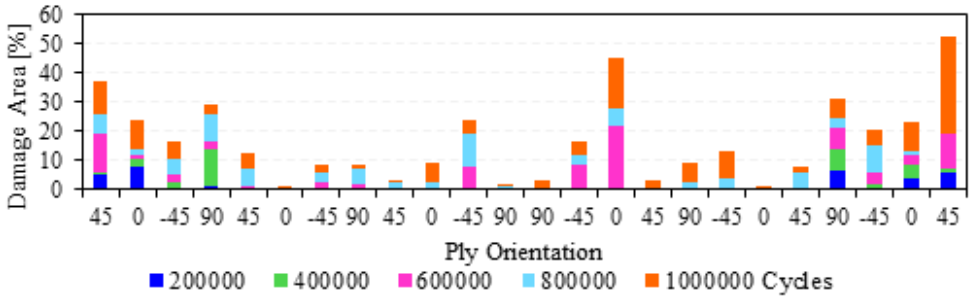


Figure B.15 – Ply-by-ply damage growth and area increase for IM7/5320-1, 25/50/25, R=0.1, SL2.

DISTRIBUTION STATEMENT A.
Approved for public release: distribution is unlimited.





Specimen ID	MASC1-B3EO11-XX1
Test Method	OHT-T
Material System	IM7 5320-1
Ply Layup	25/50/25
Number of Plies	28
Stress Ratio	0.1
% Stress	80% of Ultimate Stress
Final Cycles	1,000,000 (runout)
1) Delamination from the outer edge extending to the center along the 90° direction.	
2) Fiber failure vertically extending from the hole on both sides in the 0° direction.	
3) Fiber failure near the hole (not formed from the hole) in the 45° direction.	

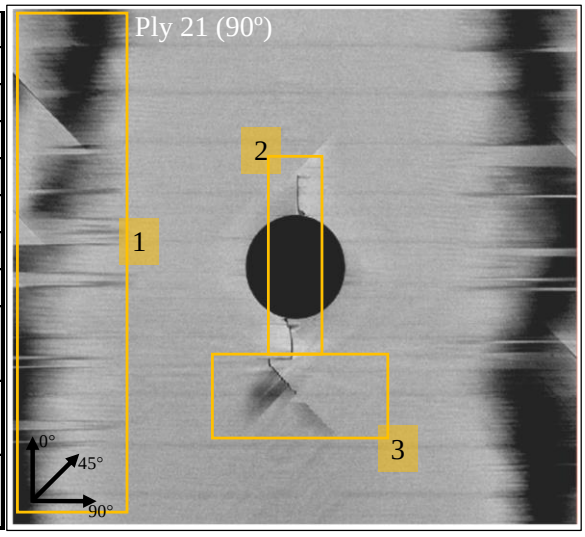


Figure B.16 – Ply-by-ply damage growth and area increase for IM7/5320-1, 25/50/25, R=0.1, SL3.

DISTRIBUTION STATEMENT A.
Approved for public release: distribution is unlimited.

Continued…	MASC1-B3EO11-XX1
Test Method	OHT-T
Material System	IM7 5320-1
Ply Layup	25/50/25
Number of Plies	28
Stress Ratio	0.1
% Stress	90% of Ultimate Stress
Final Cycles	1,000,000 (runout)
1) Delamination from the outer edge extending to the center along the 90° direction.	
2) Separation between the fibers of a 0° ply.	
3) Vertical region of delamination directly above and below the hole.	

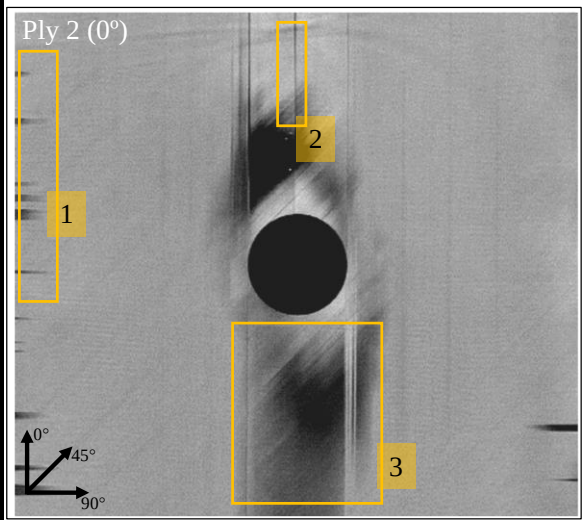


Figure B.16 – Ply-by-ply damage growth and area increase for IM7/5320-1, 25/50/25, R=0.1, SL3 (cont.).

DISTRIBUTION STATEMENT A.
Approved for public release: distribution is unlimited.

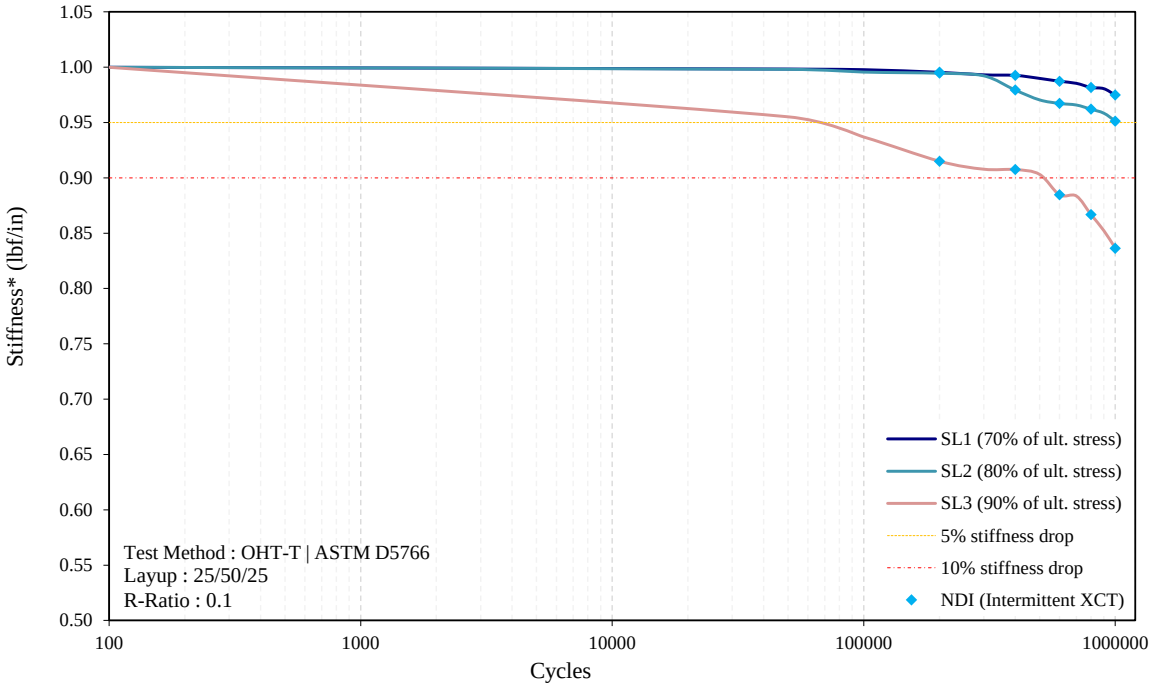
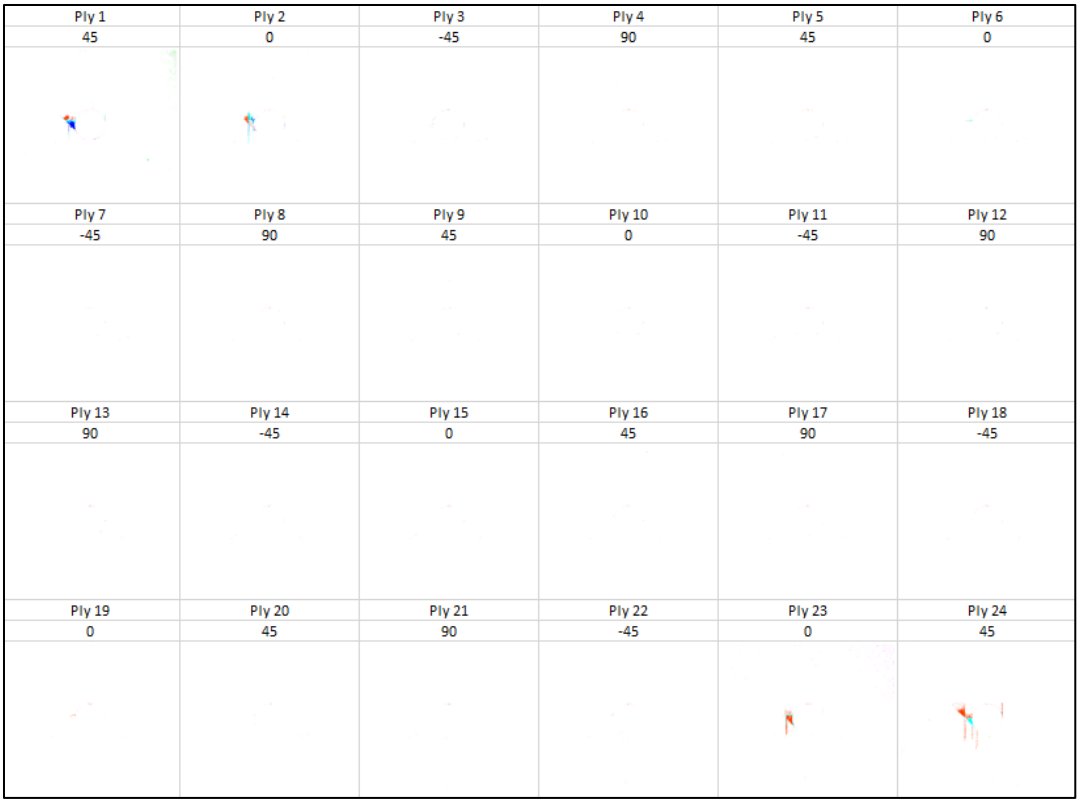
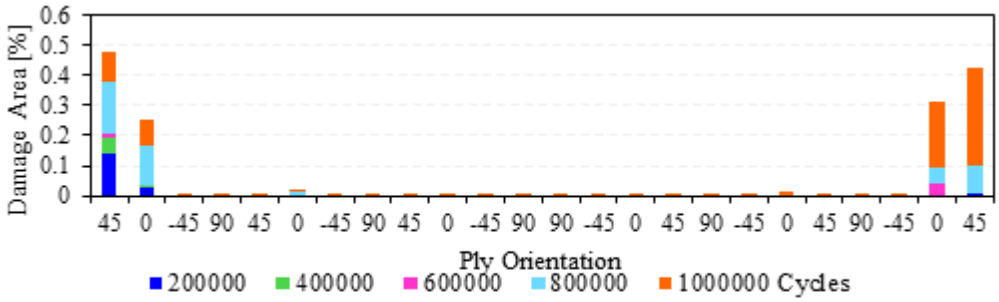


Figure B.17 – Apparent stiffness change during fatigue (normalized by initial compliance) for IM7/5320-1 UNI, 25/50/25 layup, OHT-T, R=0.1.

DISTRIBUTION STATEMENT A.
Approved for public release: distribution is unlimited.





Specimen ID	MASC1-B1EO11-XX3
Test Method	OHC-C
Material System	IM7 5320-1
Ply Layup	25/50/25
Number of Plies	24
Stress Ratio	5.0
% Stress	70% of Ultimate Stress
Final Cycles	1,000,000 (runout)
1) Delamination of the 45° layer extending from the hole radially along the 45°.	
2) The shaded region is an artifact from scanning processes.	

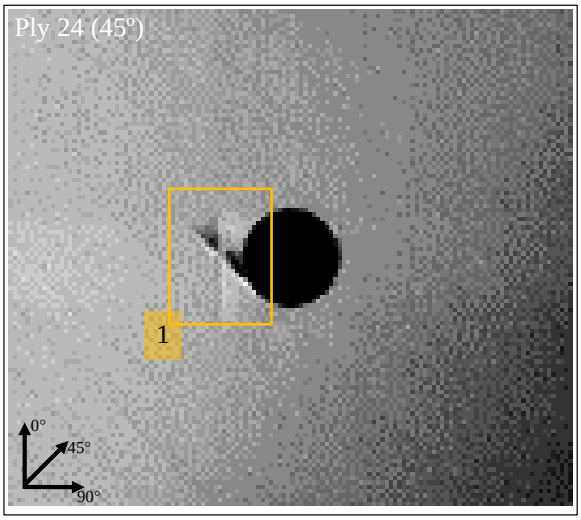
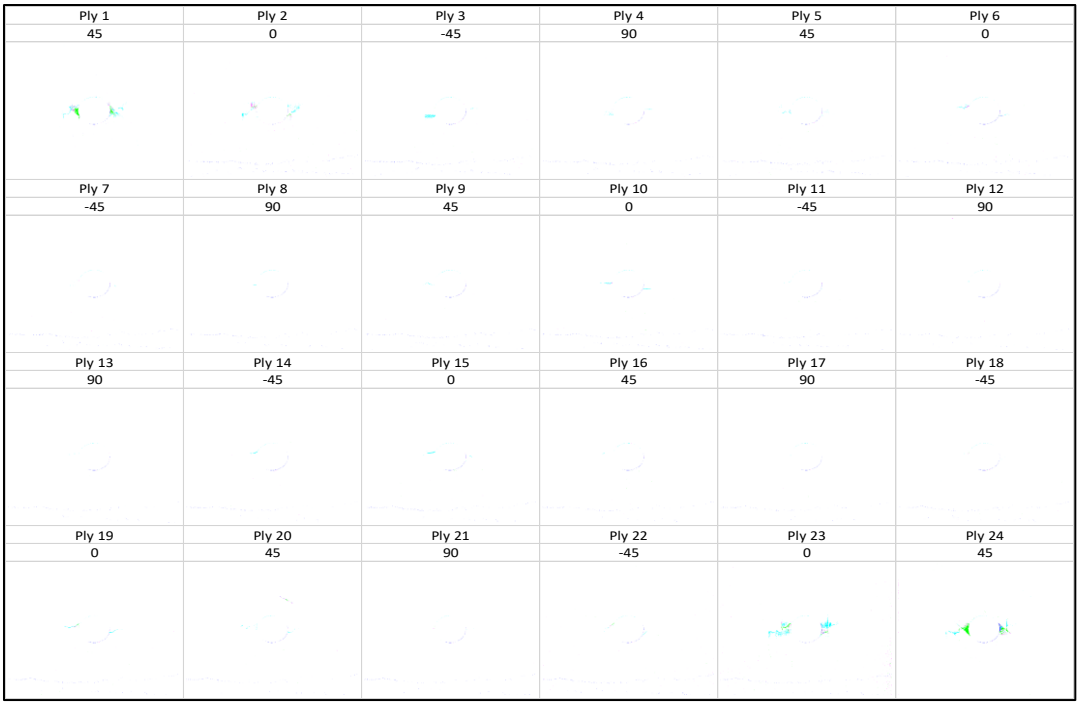
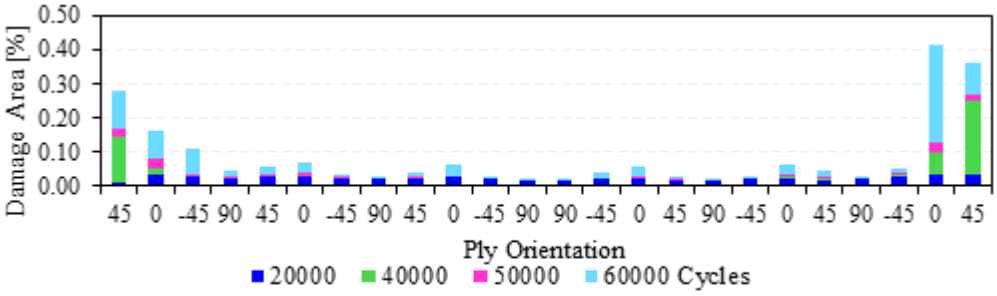


Figure B.18 – Ply-by-ply damage growth and area increase for IM7/5320-1, 25/50/25, R=5, SL1.

DISTRIBUTION STATEMENT A.
Approved for public release: distribution is unlimited.





Specimen ID	MASC1-B2EO11-XX5
Test Method	OHC-C
Material System	IM7 5320-1
Ply Layup	25/50/25
Number of Plies	24
Stress Ratio	5.0
% Stress	75% of Ultimate Stress
Final Cycles	60,494
1) Fiber failure horizontally through the hole perpendicular the 0° plies.	
Comment) This horizontal fiber failure can be seen through all plies of this specimen.	

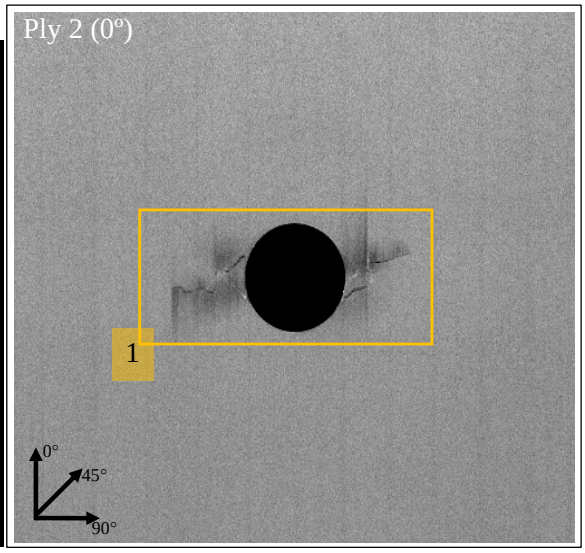
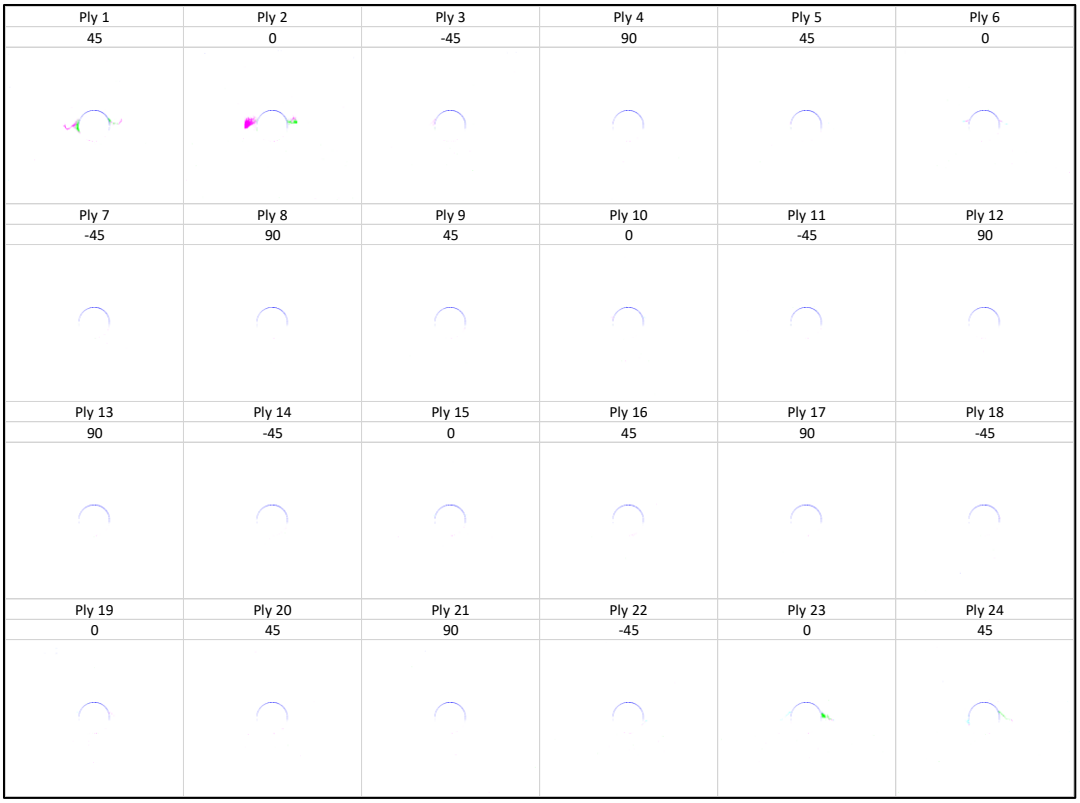
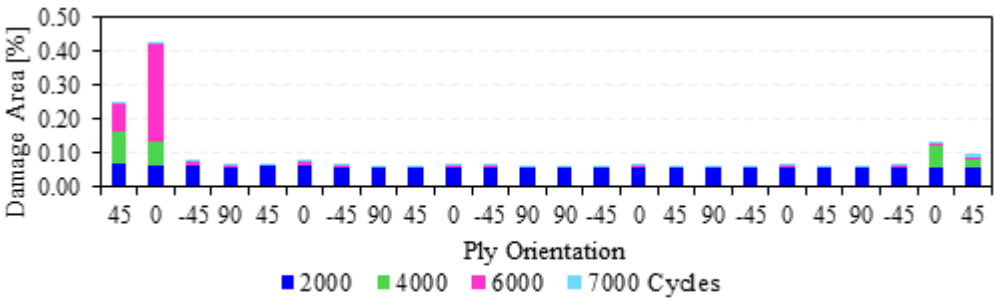


Figure B.19 – Ply-by-ply damage growth and area increase for IM7/5320-1, 25/50/25, R=5, SL2.

DISTRIBUTION STATEMENT A.
Approved for public release: distribution is unlimited.





Specimen ID	MASC1-B3EO11-XX4
Test Method	OHC-C
Material System	IM7 5320-1
Ply Layup	25/50/25
Number of Plies	24
Stress Ratio	5.0
% Stress	80% of Ultimate Stress
Final Cycles	8,673
1) Fiber failure horizontally through the hole perpendicular the 0° plies.	

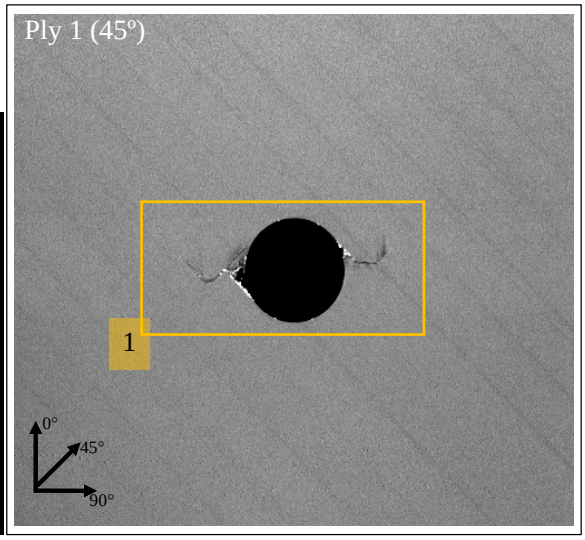


Figure B.20 – Ply-by-ply damage growth and area increase for IM7/5320-1, 25/50/25, R=5, SL3.

DISTRIBUTION STATEMENT A.
Approved for public release: distribution is unlimited.

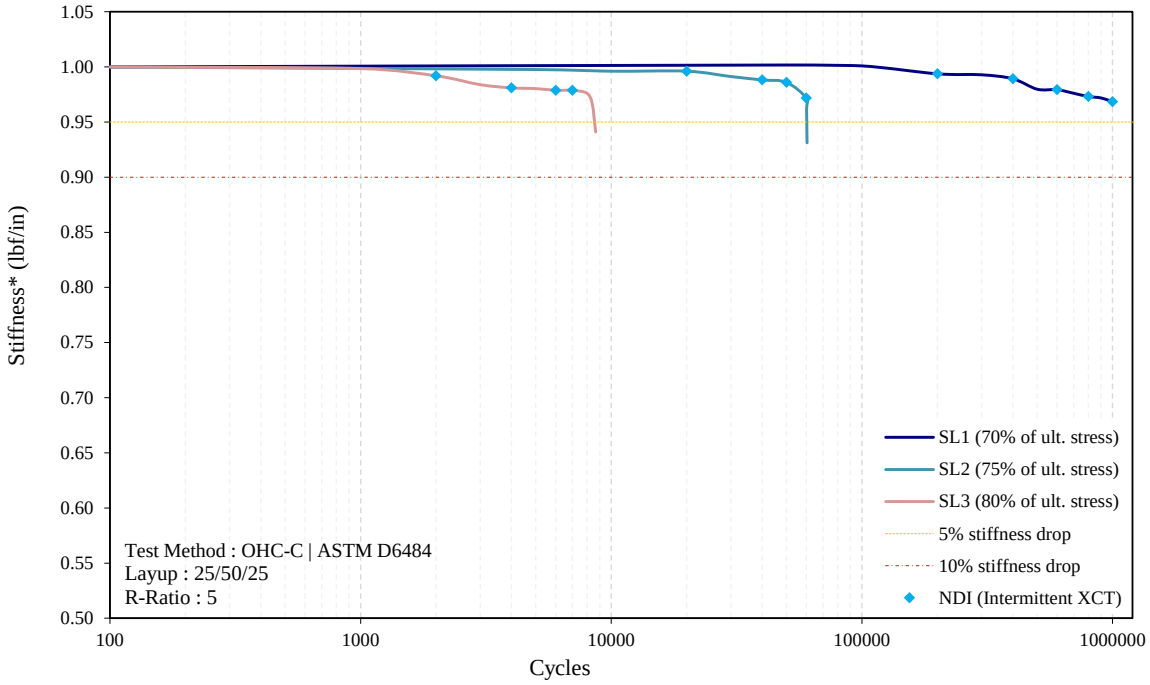
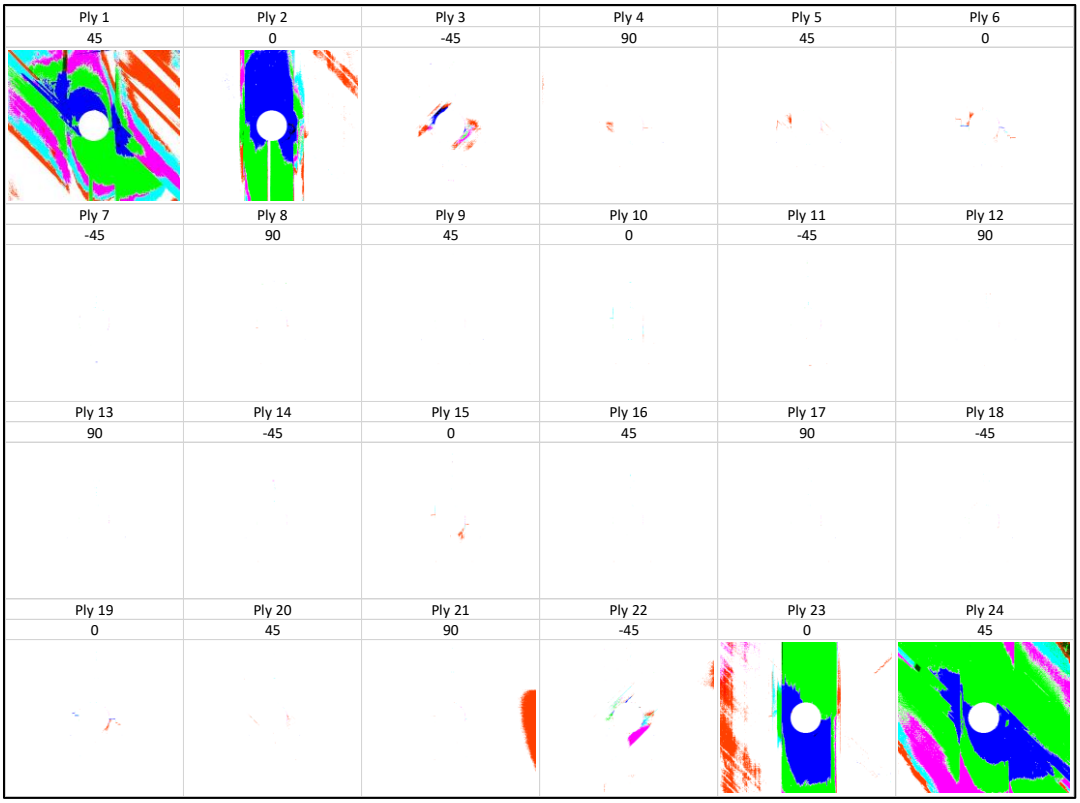
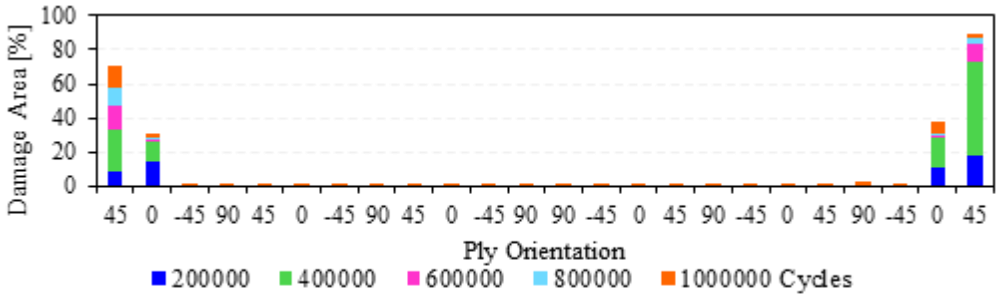


Figure B.21 – Apparent stiffness change during fatigue (normalized by initial compliance) for IM7/5320-1 UNI, 25/50/25 layup, OHC-C, R=5.

DISTRIBUTION STATEMENT A.
Approved for public release: distribution is unlimited.





Specimen ID	MASC1-B1EO11-XX7
Test Method	OHC-T
Material System	IM7 5320-1
Ply Layup	25/50/25
Number of Plies	24
Stress Ratio	-1.0
% Stress	50% of Ultimate Stress
Final Cycles	1,000,000 (runout)
1) Delamination of the 45° layer extending from the hole radially along the 45°.	

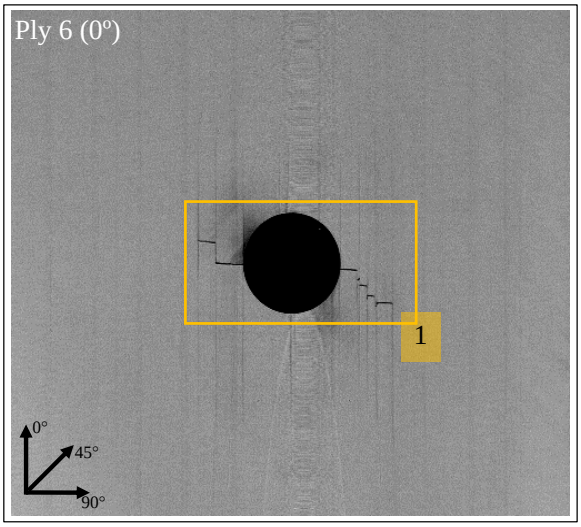
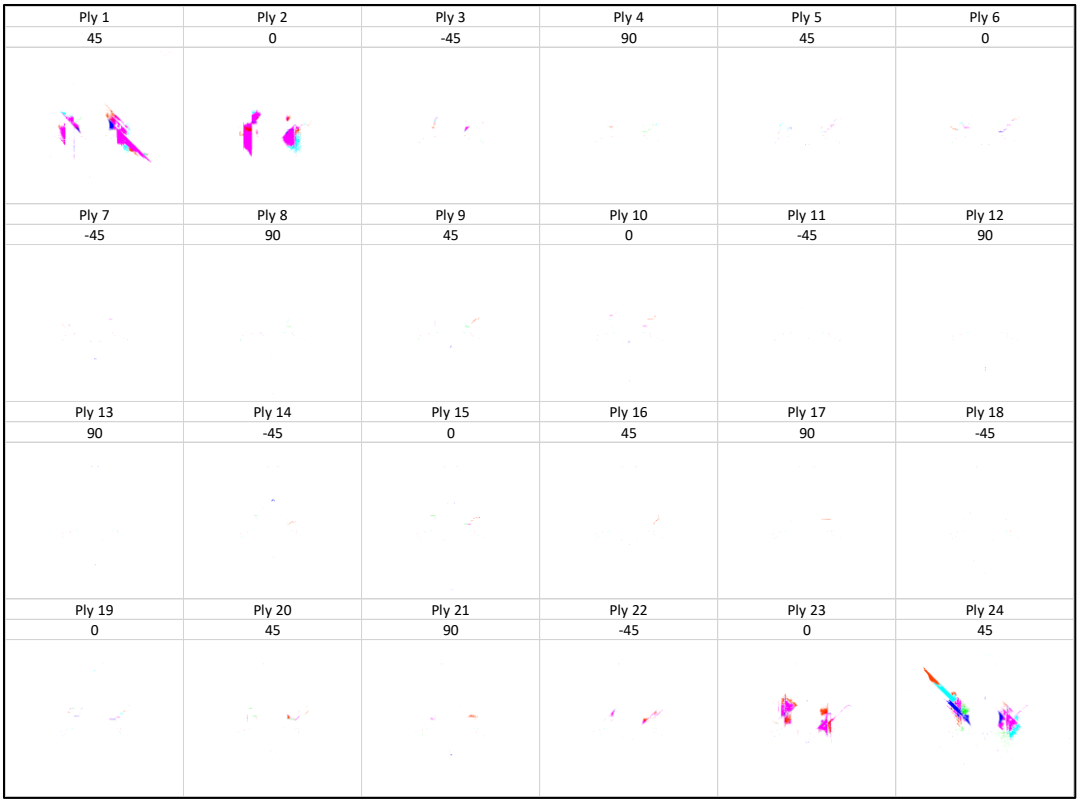
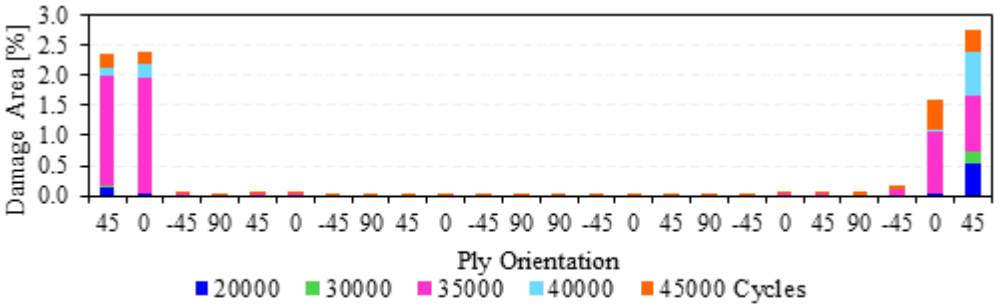


Figure B.22 – Ply-by-ply damage growth and area increase for IM7/5320-1, 25/50/25, R=-1, SL1.

DISTRIBUTION STATEMENT A.
Approved for public release: distribution is unlimited.





Specimen ID	MASC1-B2EO11-XX8
Test Method	OHC-T
Material System	IM7 5320-1
Ply Layup	25/50/25
Number of Plies	24
Stress Ratio	-1.0
% Stress	55% of Ultimate Stress
Final Cycles	45,468
1) Delamination of the 45° layer extending from the hole radially along the 45°.	

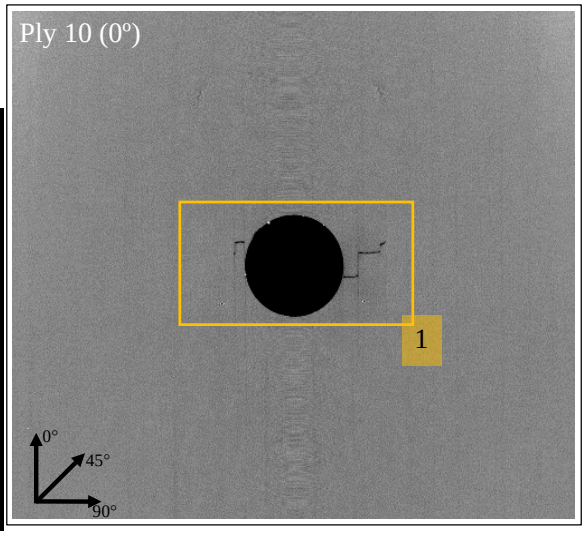
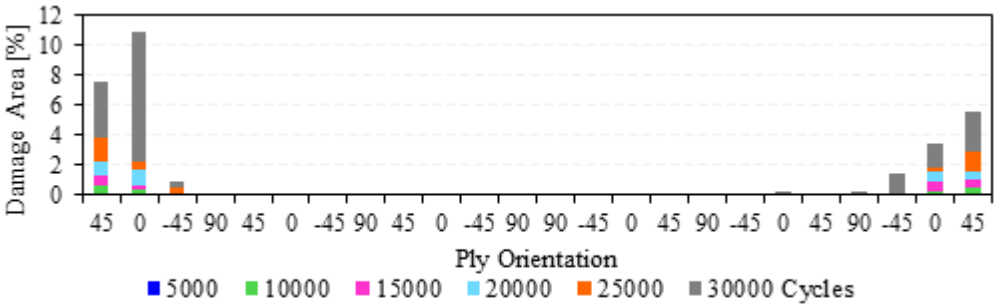


Figure B.23 – Ply-by-ply damage growth and area increase for IM7/5320-1, 25/50/25, R=-1, SL2.

DISTRIBUTION STATEMENT A.
Approved for public release: distribution is unlimited.





Specimen ID	MASC1-B3EO11-XX3
Test Method	OHC-T
Material System	IM7 5320-1
Ply Layup	25/50/25
Number of Plies	24
Stress Ratio	-1.0
% Stress	60% of Ultimate Stress
Final Cycles	37,365
1) Fiber failure horizontally through the hole perpendicular the 0° plies.	

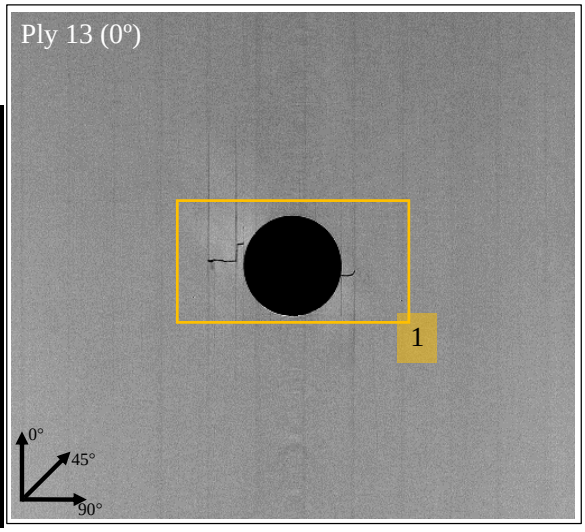


Figure B.24 – Ply-by-ply damage growth and area increase for IM7/5320-1, 25/50/25, R=-1, SL3.

DISTRIBUTION STATEMENT A.
Approved for public release: distribution is unlimited.

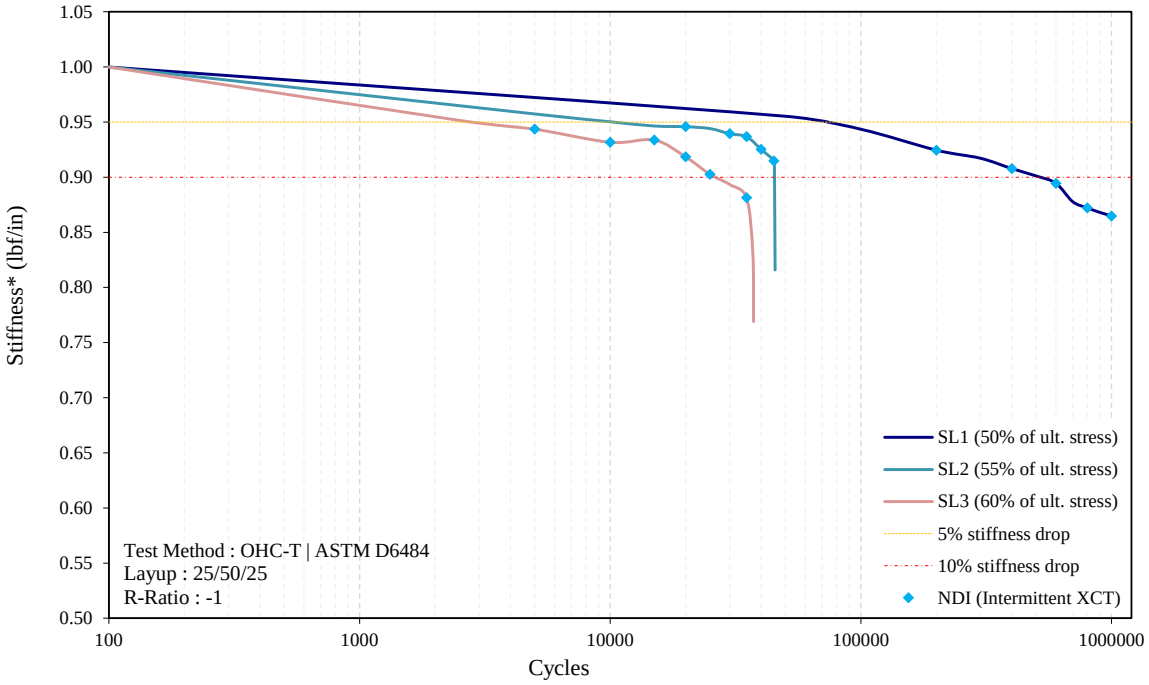


Figure B.25 – Apparent stiffness change during the tension fatigue (normalized by initial compliance) for IM7/5320-1 UNI, 25/50/25 layup, OHC-T, R= -1.

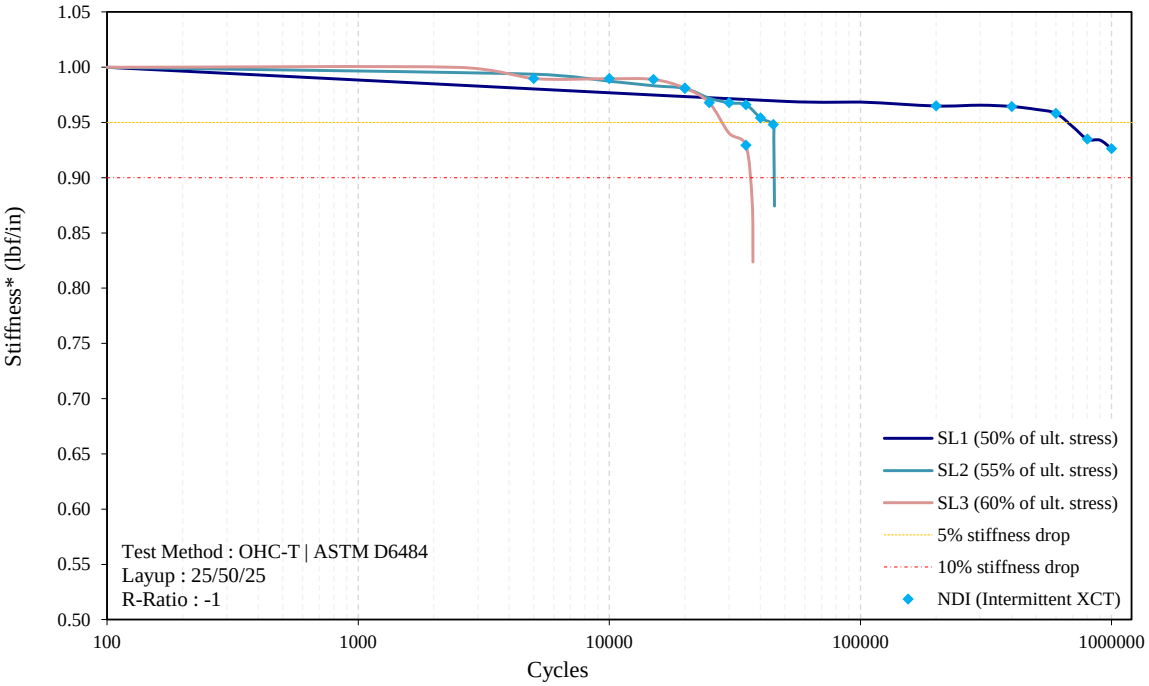


Figure B.26 – Apparent stiffness change during the compression fatigue (normalized by initial compliance) for IM7/5320-1 UNI, 25/50/25 layup, OHC-T, R= -1.

DISTRIBUTION STATEMENT A.
Approved for public release: distribution is unlimited.

10/80/10 Open-Hole Test

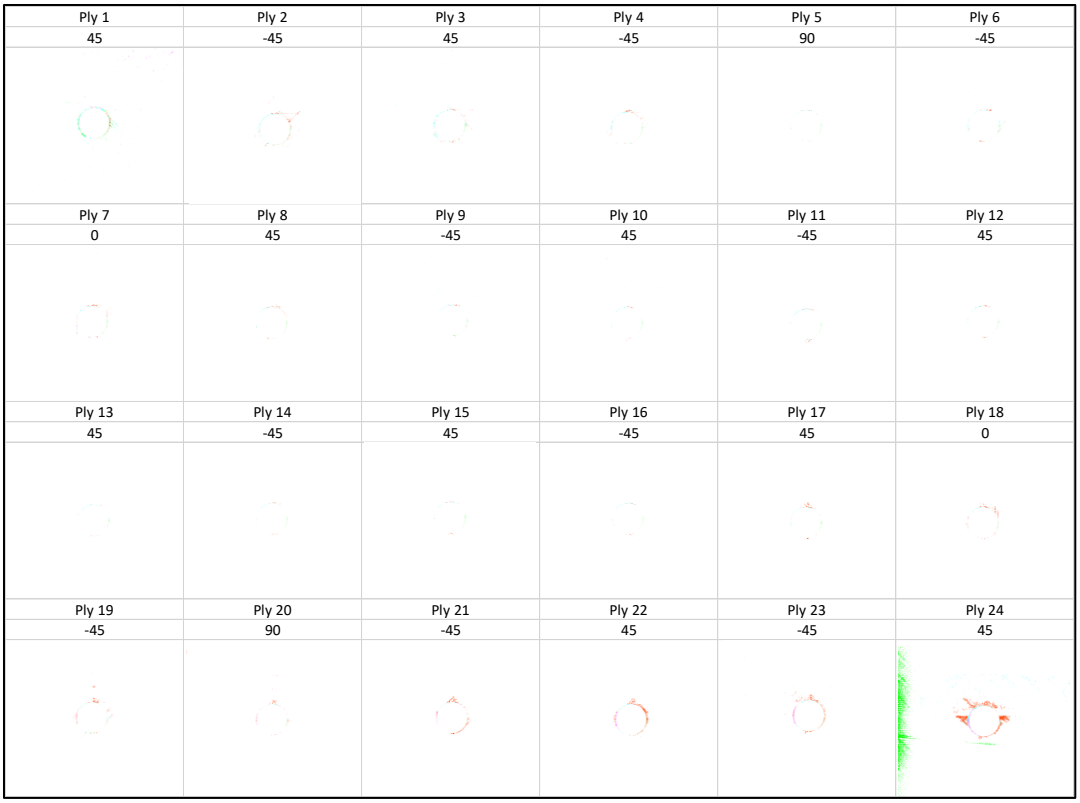
R=0.1, OHT-T → Specimens: SL-1 (60%), SL-2 (70%), and SL-3 (80%)
R=5.0, OHC-C → Specimens: SL-1 (60%), SL-2 (70%), and SL-3 (80%)
R=-1, OHT-C → Specimens: SL-1 (35%), SL-2 (45%), and SL-3 (50%)

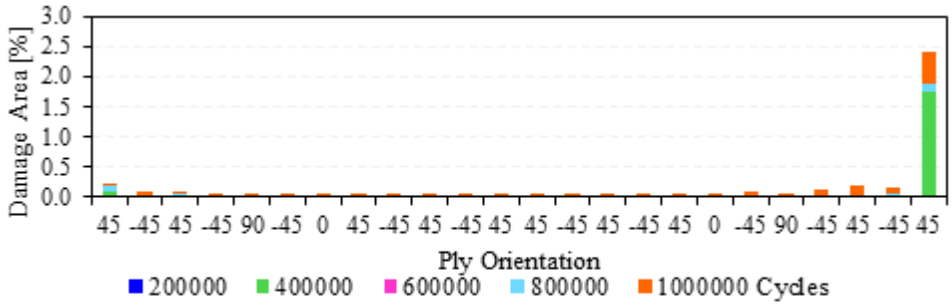
In the observance of progressive damage growth, three specimens were tested for each r-ratio at varying stress levels. Specimens were fatigued until failure or one-million cycles (runout) was achieved. For R=0.1 only SL-1 survived fatigue and developed a 6% decrease in residual strength. No significant delamination near the hole occurred in SL-1 therefore, there was no stress relief when the specimen was tested for residual strength (Figure B.27). SL-2 and SL-3 exhibited the majority of their damage on the 90° and adjacent plies and displayed a region of delamination propagating from the edges growing towards the center of the specimen (Figure B.28). SL-2 and SL-3 display the fibers of individual plies tearing apart during fatigue (Figure B.29) that caused an accelerated failure of the specimens.

For R=5.0 only SL-1 survived fatigue and had a 2% decreased residual strength. SL-1 displayed negligible damage after fatigue (Figure B.31) while SL-2 and SL-3 displayed large amounts of fiber failure through the majority of their plies, excluding innermost plies (Figure Figure B.32). Specimens in this group displayed an overall negligible amount of delamination and fiber failure in this group was the primary cause of accelerated failure (Figure Figure B.33).

For R=-1 only SL-1 survived fatigue and developed an average of 20% decreased residual strength (Figure B.35). No damage is visible throughout the specimens in this group due to the rapid failure these specimens experience after only a few fiber failures (Figure B.36).

DISTRIBUTION STATEMENT A.
Approved for public release: distribution is unlimited.





Specimen ID	MASC1-B1FO11-XX1
Test Method	OHT-T
Material System	IM7 5320-1
Ply Layup	10/80/10
Number of Plies	24
Stress Ratio	0.1
% Stress	60% of Ultimate Stress
Final Cycles	1,000,000 (runout)
1) Separation between the fibers of a 45° ply.	
2) Minor fiber failure perpendicular to the 45° ply.	

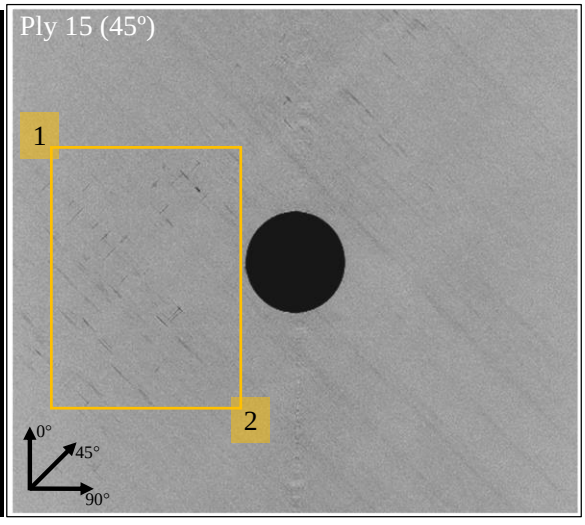
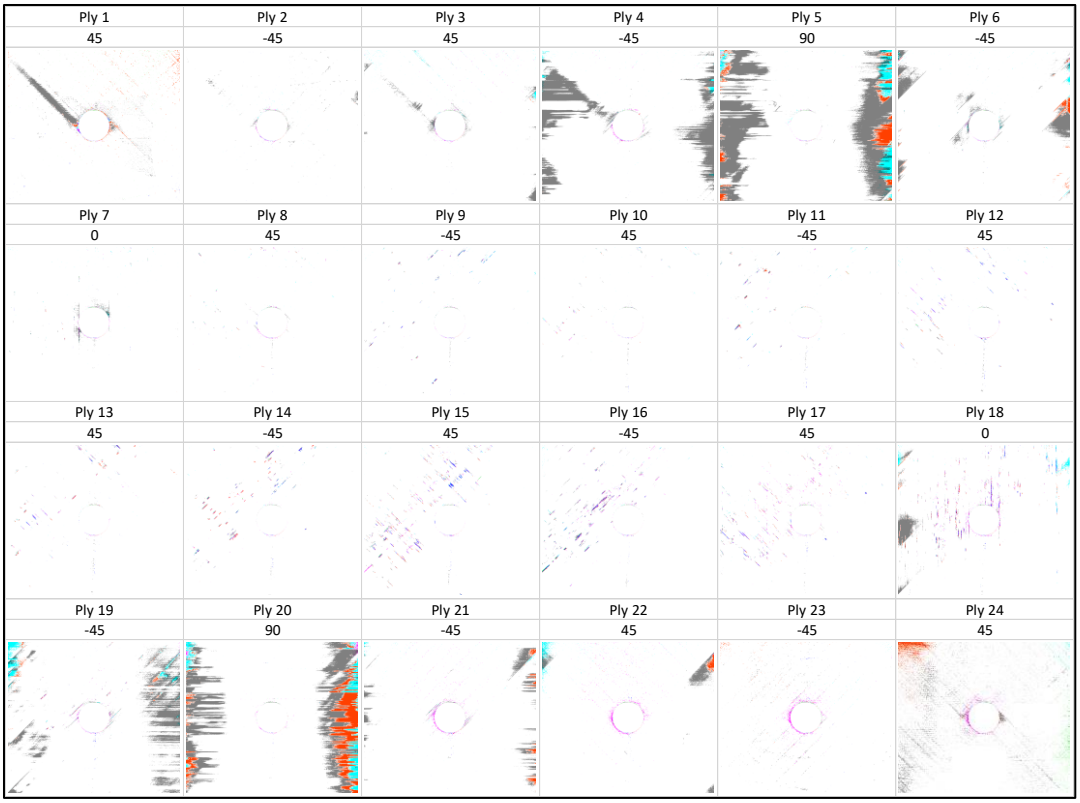
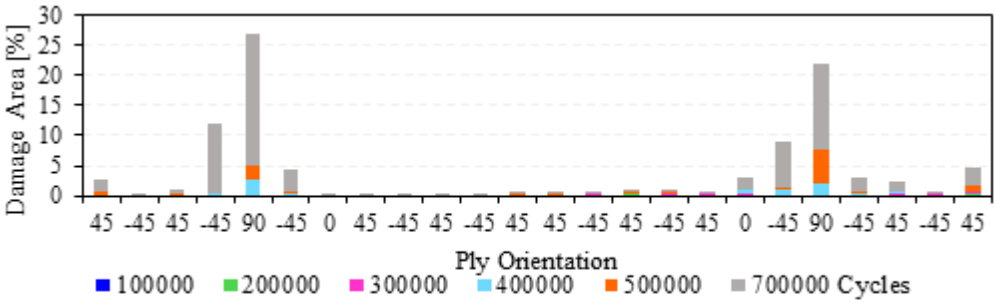


Figure B.27 – Ply-by-ply damage growth and area increase for IM7/5320-1, 10/80/10, R=0.1, SL1.

DISTRIBUTION STATEMENT A.
Approved for public release: distribution is unlimited.





Specimen ID	MASC1-B2FO11-XX1
Test Method	OHT-T
Material System	IM7 5320-1
Ply Layup	10/80/10
Number of Plies	24
Stress Ratio	0.1
% Stress	70% of Ultimate Stress
Final Cycles	753,140
1) Delamination from the outer edge extending to the center along the 90° direction.	

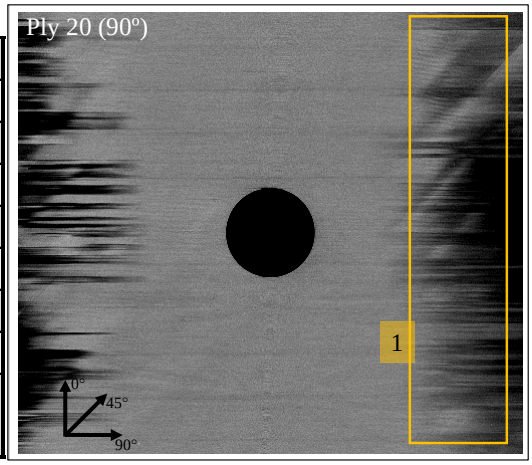
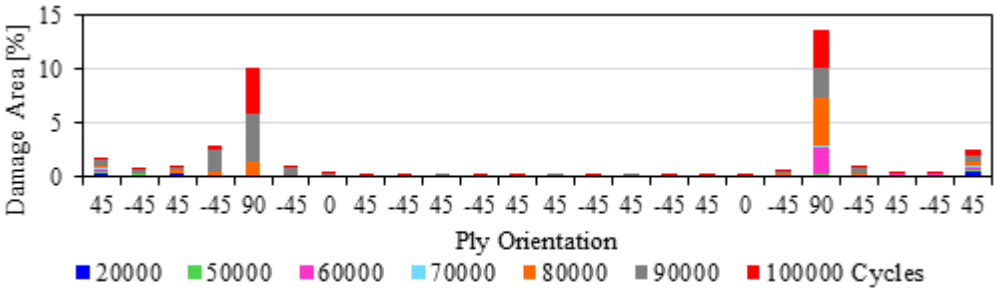


Figure B.28 – Ply-by-ply damage growth and area increase for IM7/5320-1, 10/80/10, R=0.1, SL2.

DISTRIBUTION STATEMENT A.
Approved for public release: distribution is unlimited.





Specimen ID	MASC1-B3FO11-XX2
Test Method	OHT-T
Material System	IM7 5320-1
Ply Layup	10/80/10
Number of Plies	24
Stress Ratio	0.1
% Stress	80% of Ultimate Stress
Final Cycles	108,651
1) Delamination of the 45° layer extending from the hole radially outwards along the 45°.	
2) Fiber failure of the 45° extending tangentially from the hole in the 0° direction.	

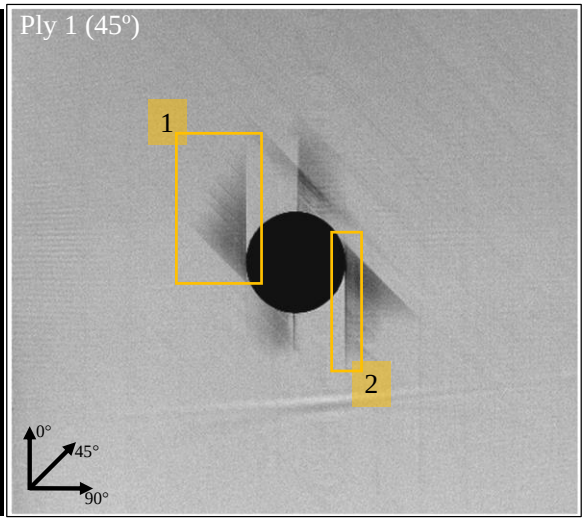


Figure B.29 – Ply-by-ply damage growth and area increase for IM7/5320-1, 10/80/10, R=0.1, SL3.

DISTRIBUTION STATEMENT A.
Approved for public release: distribution is unlimited.

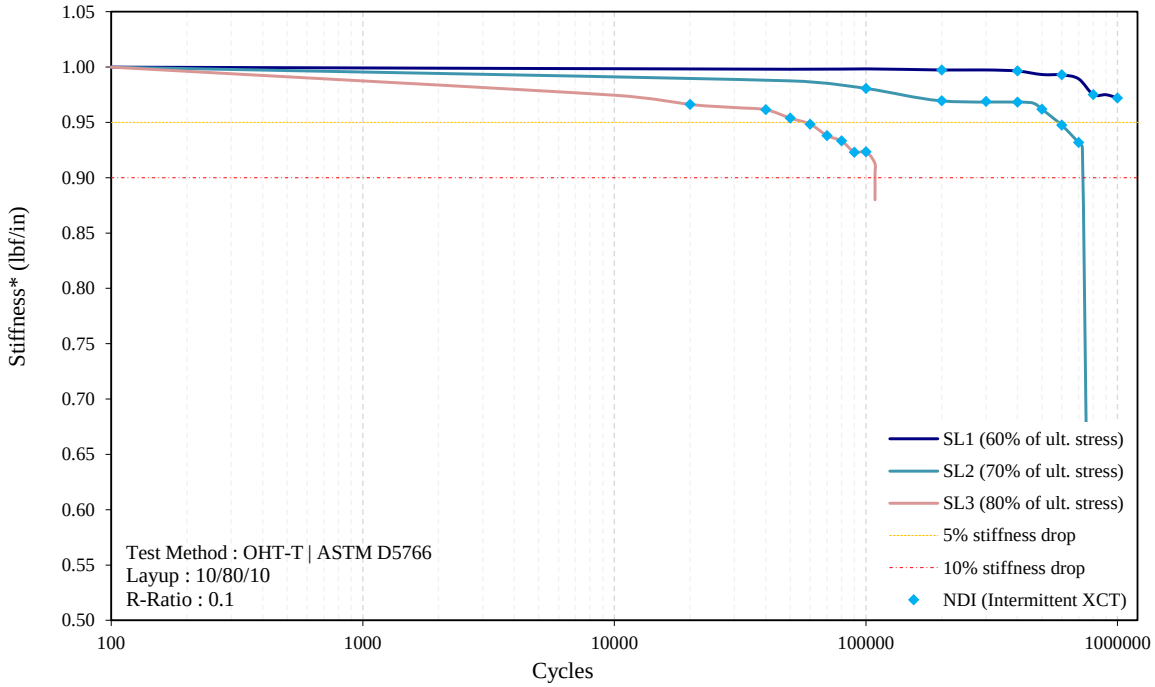
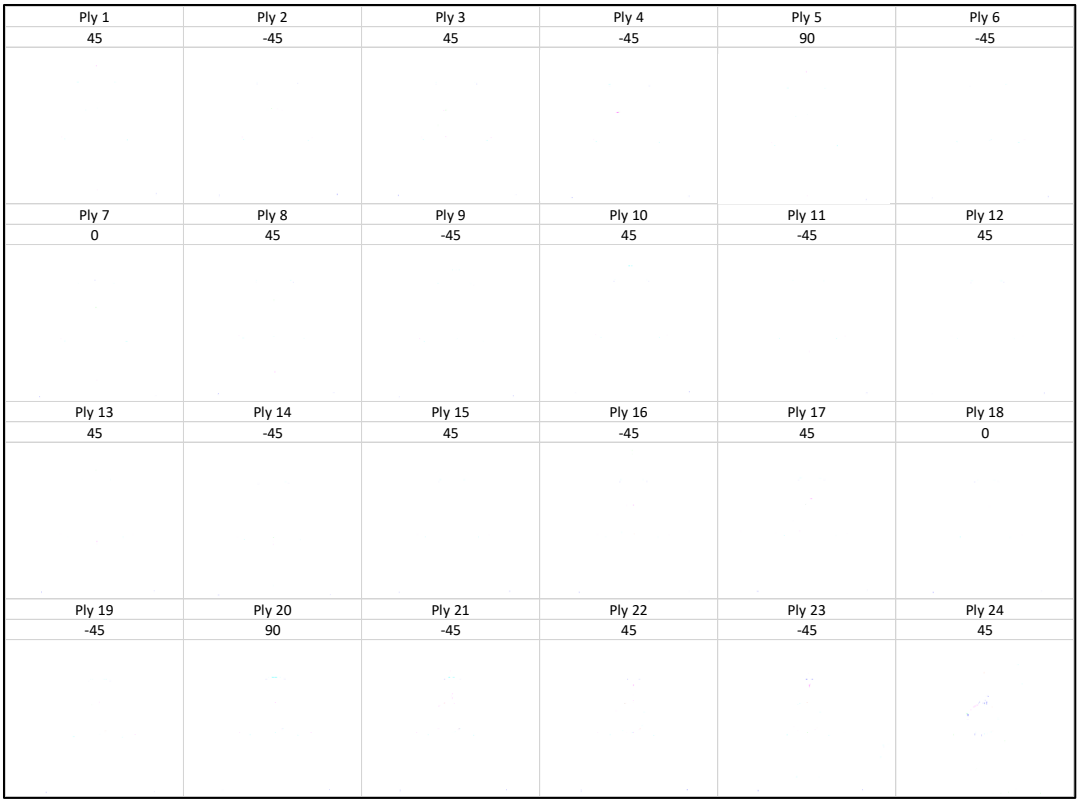
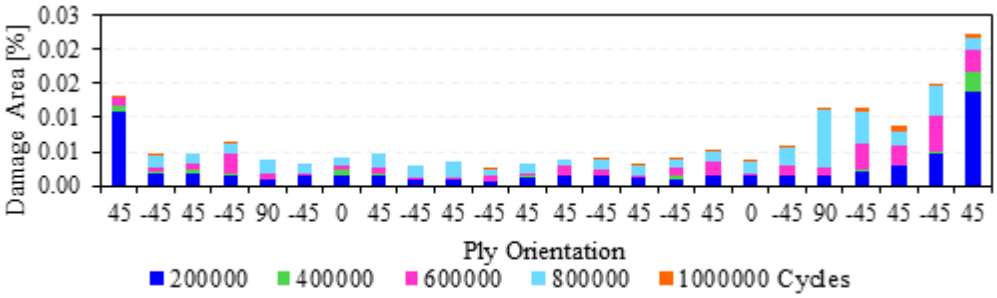


Figure B.30 – Apparent stiffness change during fatigue (normalized by initial compliance) for IM7/5320-1 UNI, 10/80/10 layup, OHT-T, R=0.1.

DISTRIBUTION STATEMENT A.
Approved for public release: distribution is unlimited.





Specimen ID	MASC1-B1FO11-XX2
Test Method	OHC-C
Material System	IM7 5320-1
Ply Layup	10/80/10
Number of Plies	24
Stress Ratio	5.0
% Stress	60% of Ultimate Stress
Final Cycles	1,000,000 (runout)
Comment) No significant damage after fatigue.	

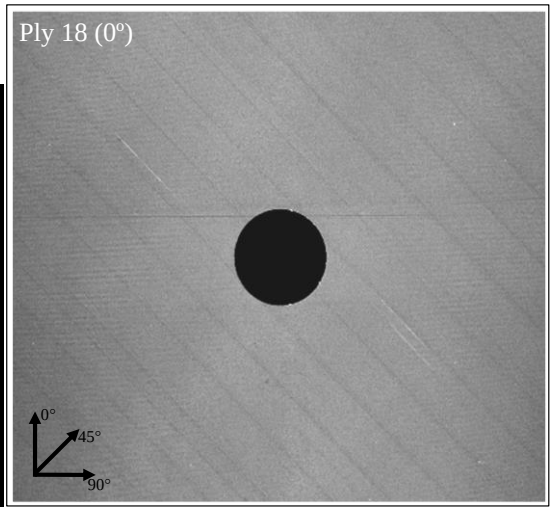
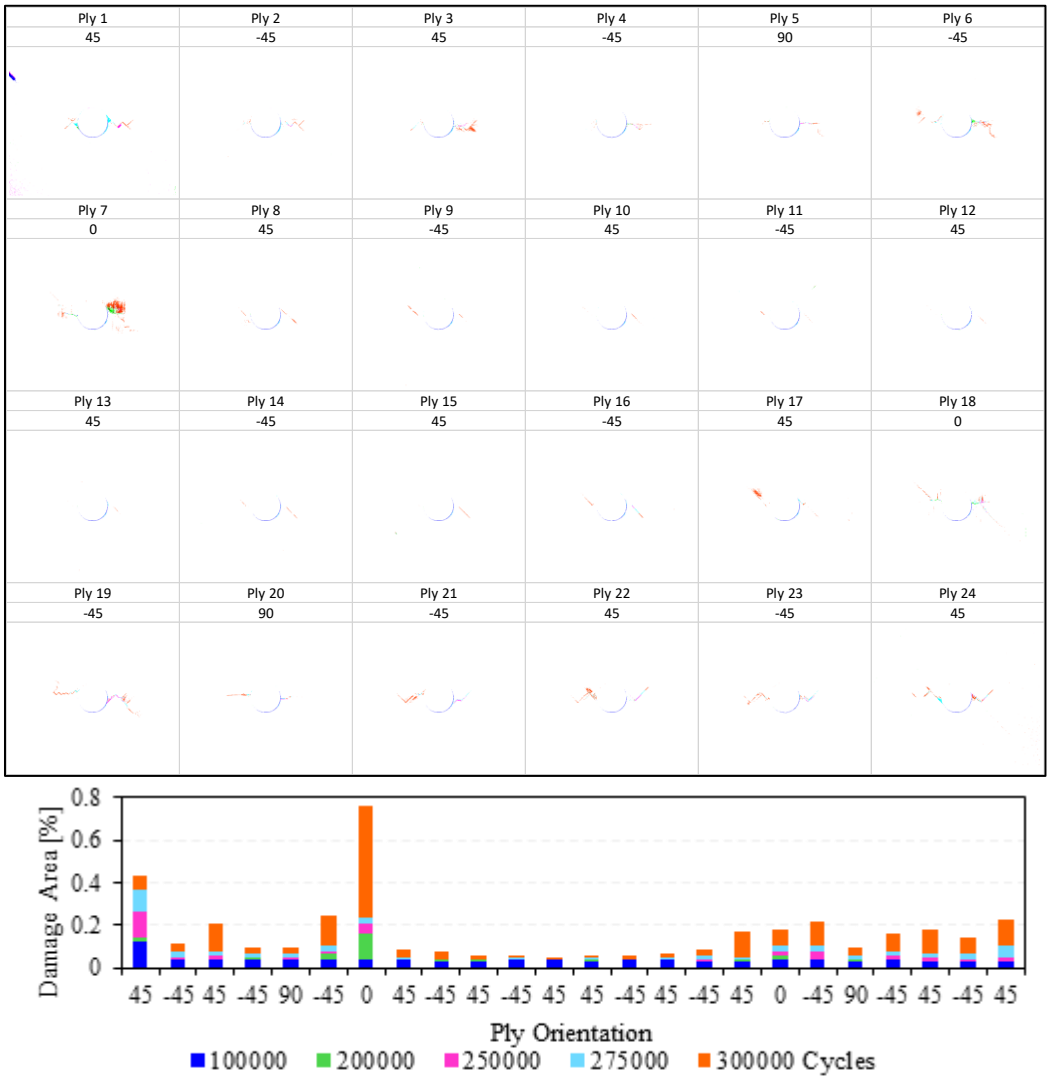


Figure B.31 – Ply-by-ply damage growth and area increase for IM7/5320-1, 10/80/10, R=5, SL1.

DISTRIBUTION STATEMENT A.
Approved for public release: distribution is unlimited.



Specimen ID	MASC1-B2FO11-XX5
Test Method	OHC-C
Material System	IM7 5320-1
Ply Layup	10/80/10
Number of Plies	24
Stress Ratio	5.0
% Stress	70% of Ultimate Stress
Final Cycles	306,213
1) Fiber failure extending radially from the hole failing perpendicular to the 0° ply.	
2) Fiber failure extending along the 45° from the initial crack.	

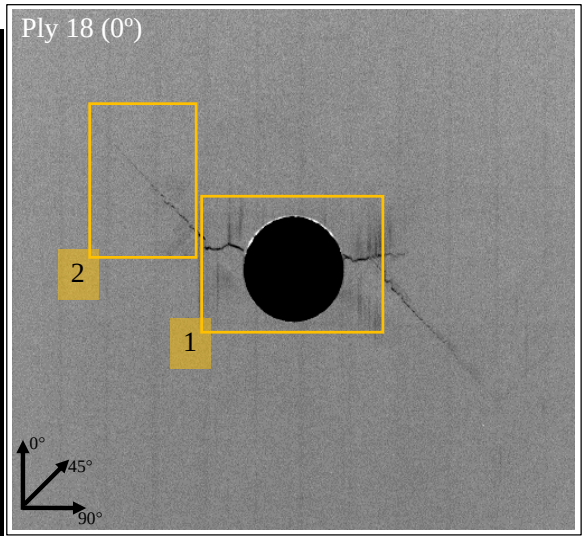
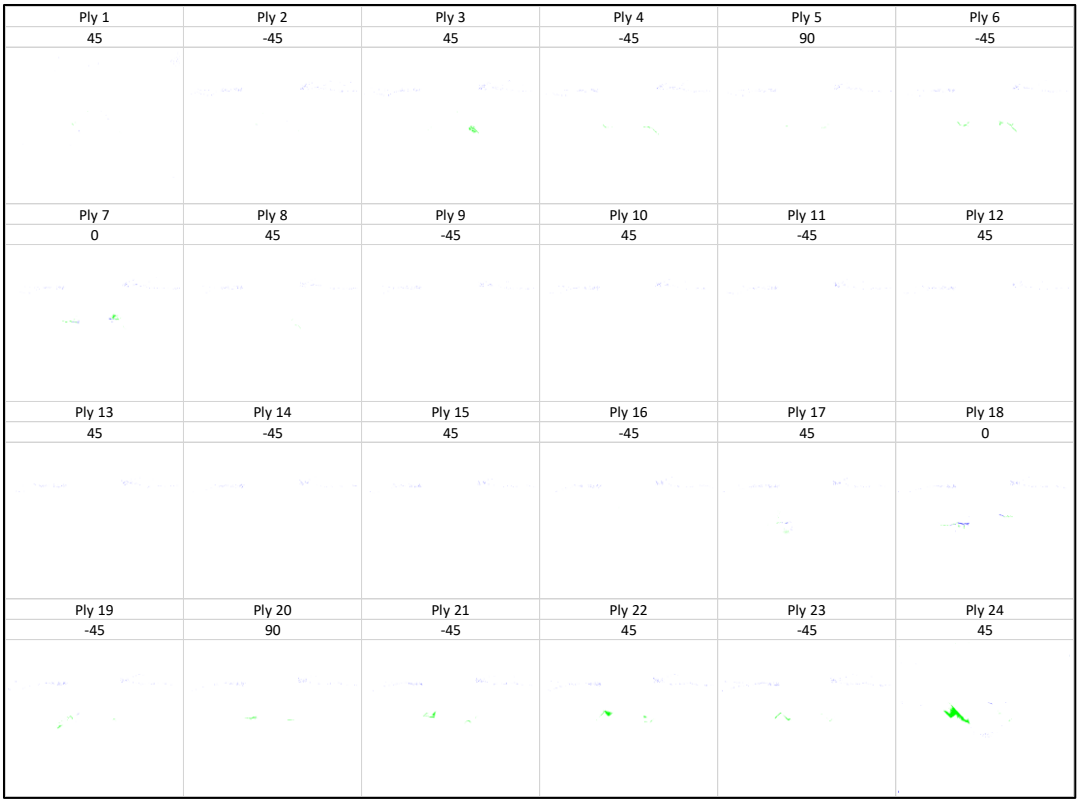
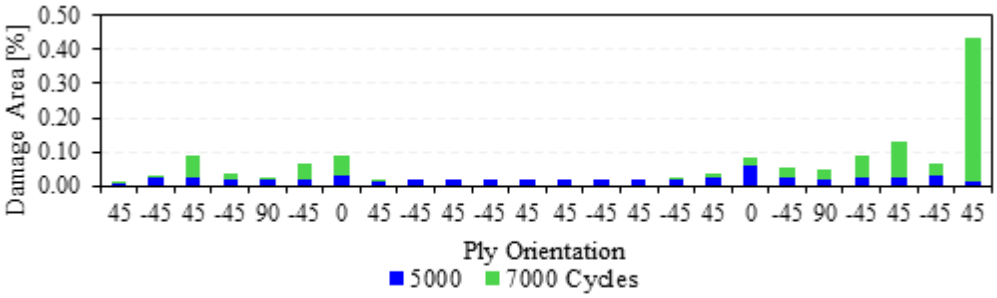


Figure B.32 – Ply-by-ply damage growth and area increase for IM7/5320-1, 10/80/10, R=5, SL2.

DISTRIBUTION STATEMENT A.
Approved for public release: distribution is unlimited.





Specimen ID	MASC1-B2FO11-XX8
Test Method	OHC-C
Material System	IM7 5320-1
Ply Layup	10/80/10
Number of Plies	24
Stress Ratio	5.0
% Stress	80% of Ultimate Stress
Final Cycles	7,440
1) Fiber failure extending radially from the hole failing perpendicular to the 45° ply.	
Comment) This horizontal fiber failure can be seen through all plies of this specimen.	

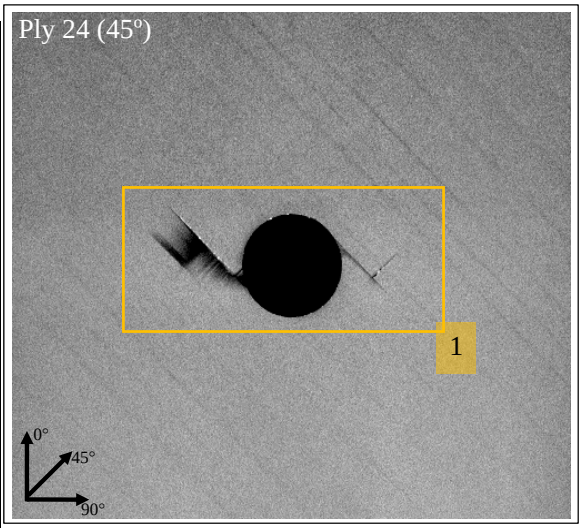


Figure B.33 – Ply-by-ply damage growth and area increase for IM7/5320-1, 10/80/10, R=5, SL3.

DISTRIBUTION STATEMENT A.
Approved for public release: distribution is unlimited.

Continued…	MASC1-B2FO11-XX8
Test Method	OHC-C
Material System	IM7 5320-1
Ply Layup	10/80/10
Number of Plies	24
Stress Ratio	5.0
% Stress	80% of Ultimate Stress
Final Cycles	7,440
1) Fiber failure horizontally through the hole perpendicular the 0° plies.	

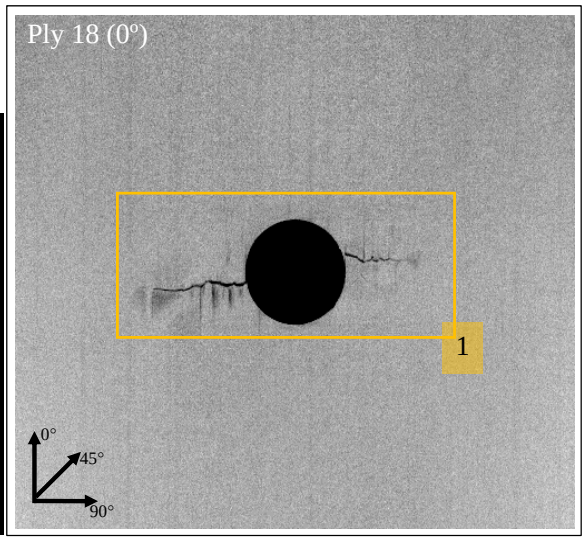


Figure B.33 – Ply-by-ply damage growth and area increase for IM7/5320-1, 10/80/10, R=5, SL3 (cont.).

DISTRIBUTION STATEMENT A.
Approved for public release: distribution is unlimited.

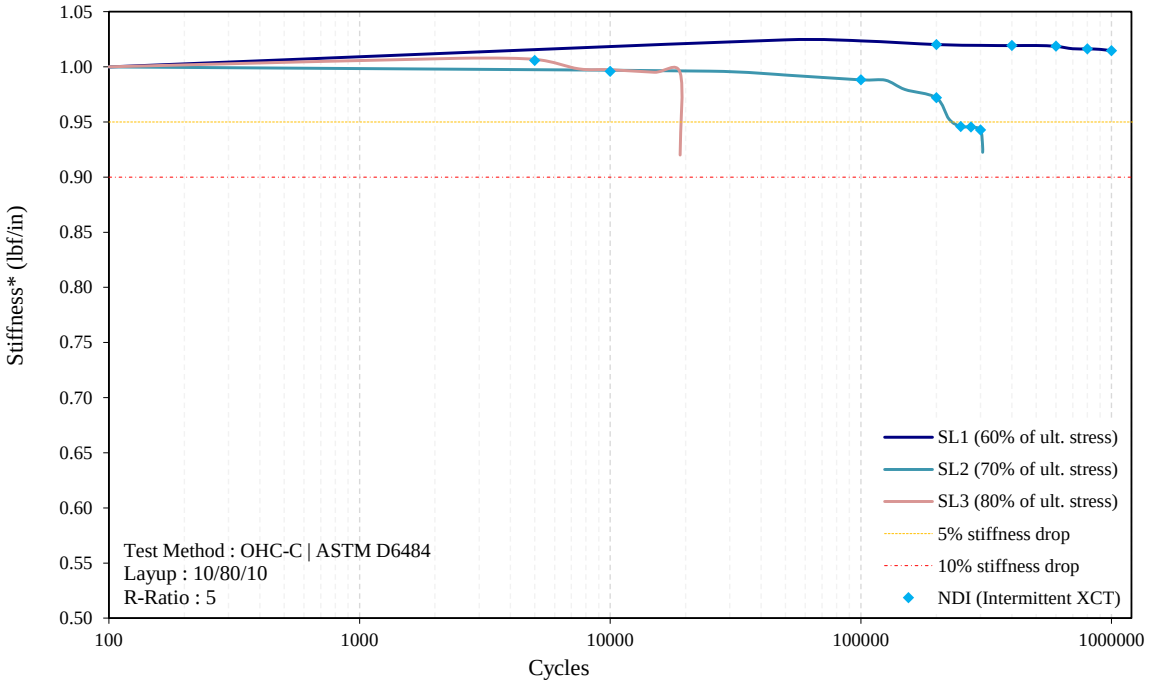
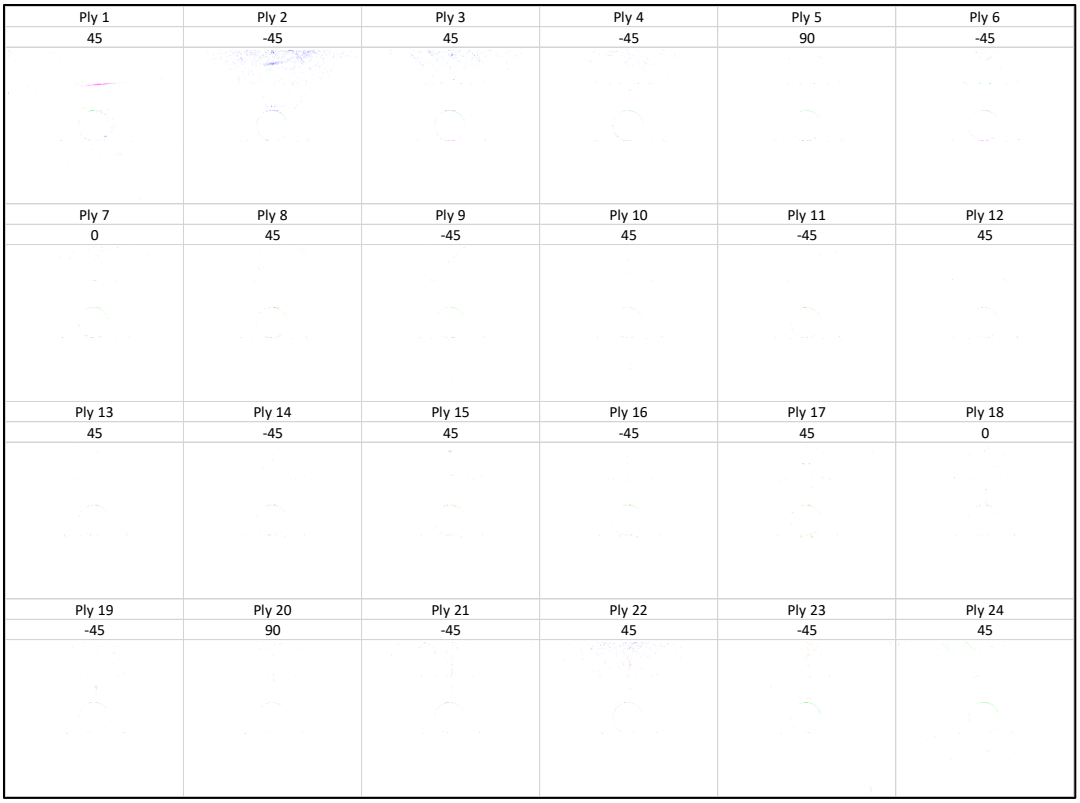
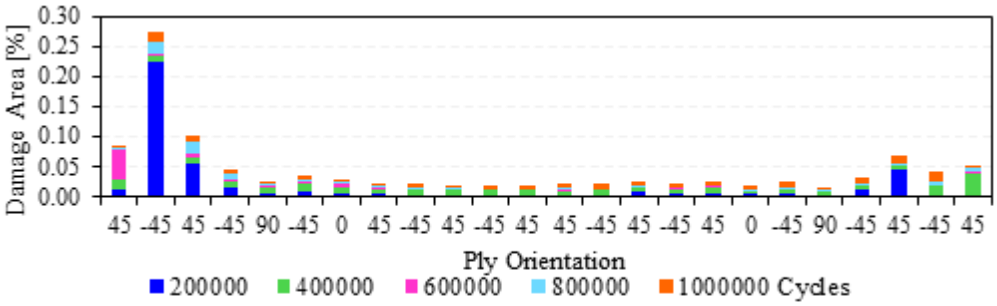


Figure B.34 – Apparent stiffness change during fatigue (normalized by initial compliance) for IM7/5320-1 UNI, 10/80/10 layup, OHC-C, R=5.

DISTRIBUTION STATEMENT A.
Approved for public release: distribution is unlimited.





Specimen ID	MASC1-B1FO11-XX4
Test Method	OHC-T
Material System	IM7 5320-1
Ply Layup	10/80/10
Number of Plies	24
Stress Ratio	-1.0
% Stress	35% of Ultimate Stress
Final Cycles	1,000,000 (runout)
Comment) No significant damage after fatigue.	

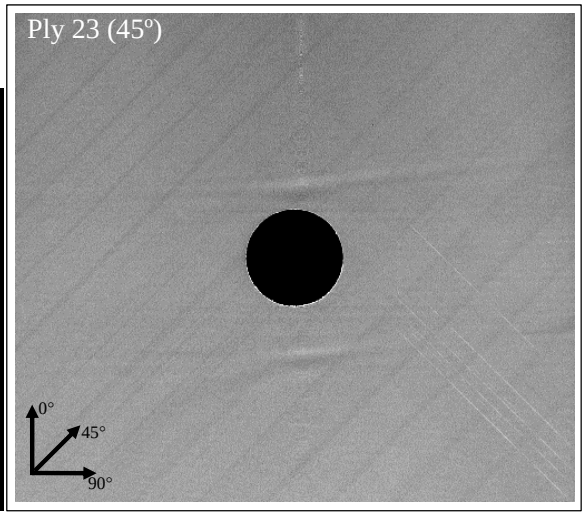
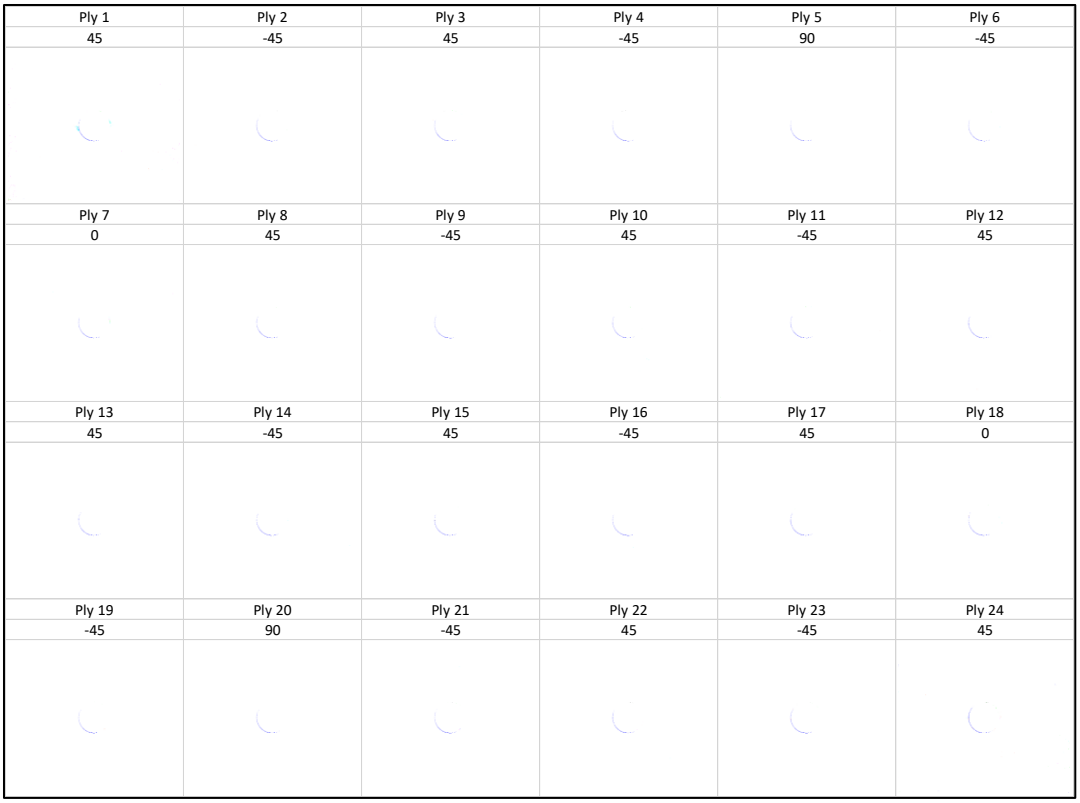
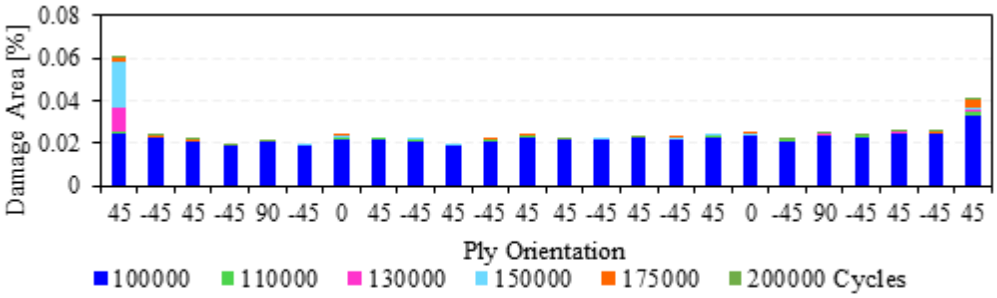


Figure B.35 – Ply-by-ply damage growth and area increase for IM7/5320-1, 10/80/10, R=-1, SL1.

DISTRIBUTION STATEMENT A.
Approved for public release: distribution is unlimited.





Specimen ID	MASC1-B2FO11-XX6
Test Method	OHC-T
Material System	IM7 5320-1
Ply Layup	10/80/10
Number of Plies	24
Stress Ratio	-1.0
% Stress	45% of Ultimate Stress
Final Cycles	242,794
1) Fiber failure perpendicular to the fibers, otherwise insignificant visible damage.	

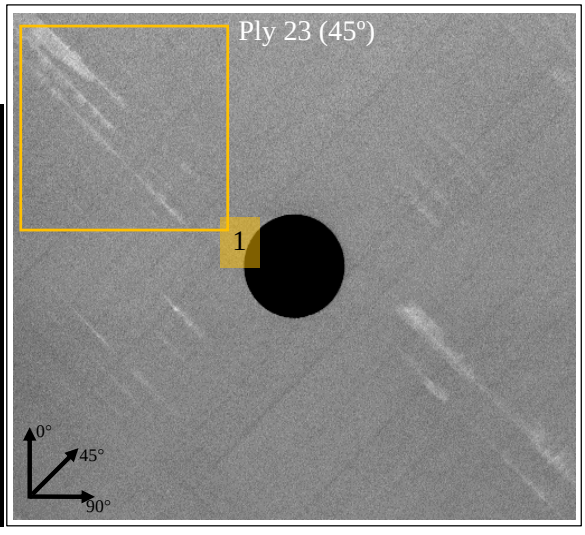
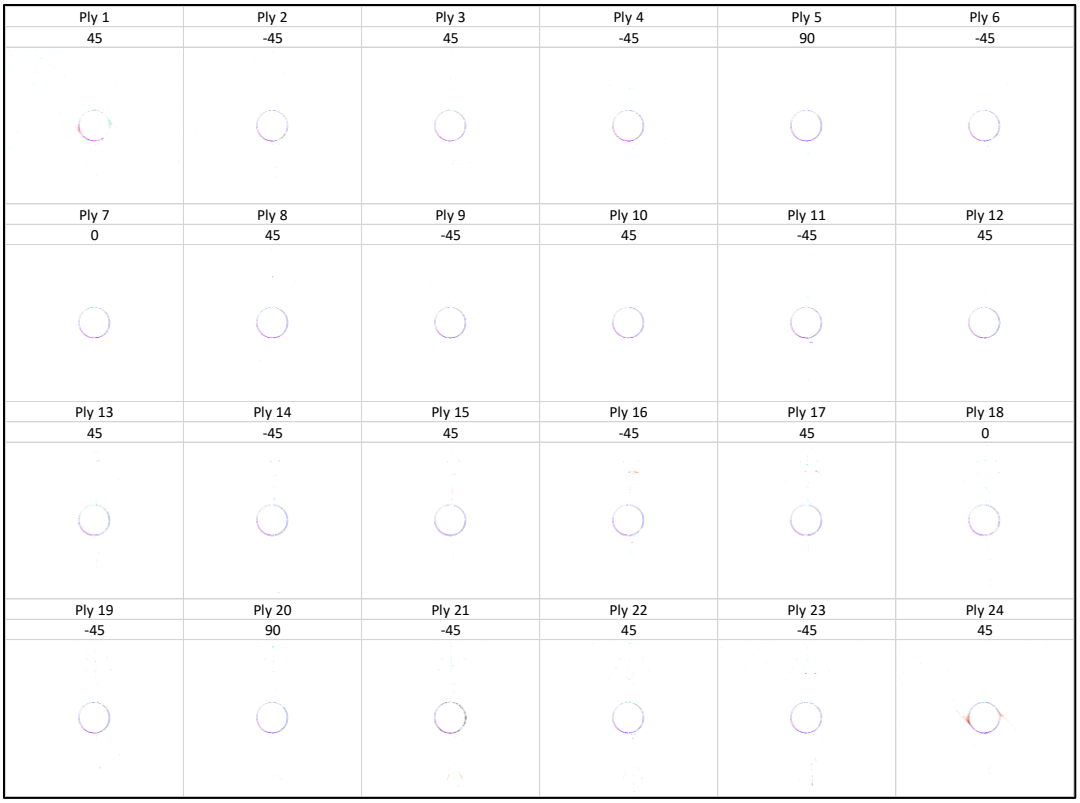
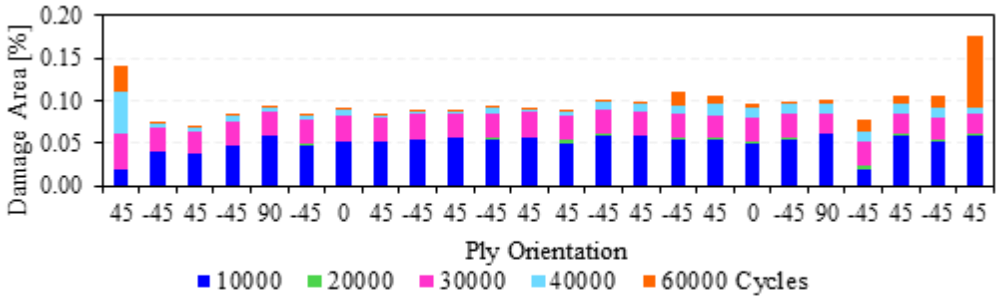


Figure B.36 – Ply-by-ply damage growth and area increase for IM7/5320-1, 10/80/10, R=-1, SL2.

DISTRIBUTION STATEMENT A.
Approved for public release: distribution is unlimited.





Specimen ID	MASC1-B3FO11-XX7
Test Method	OHC-T
Material System	IM7 5320-1
Ply Layup	10/80/10
Number of Plies	24
Stress Ratio	-1.0
% Stress	50% of Ultimate Stress
Final Cycles	73,237
Comment) No significant damage visible.	

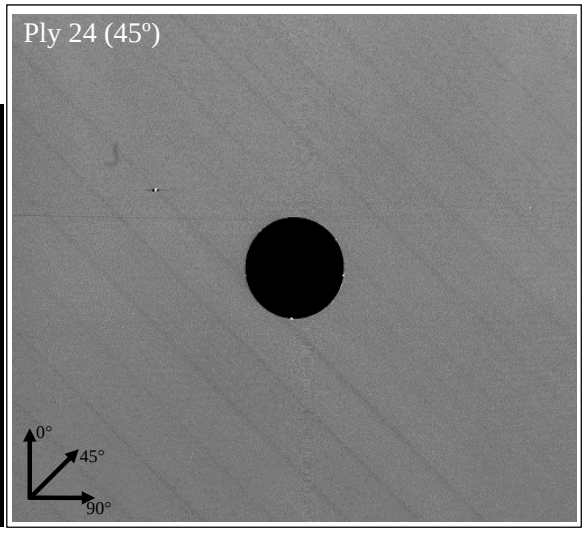


Figure B.37 – Ply-by-ply damage growth and area increase for IM7/5320-1, 10/80/10, R=-1, SL3.

DISTRIBUTION STATEMENT A.
Approved for public release: distribution is unlimited.

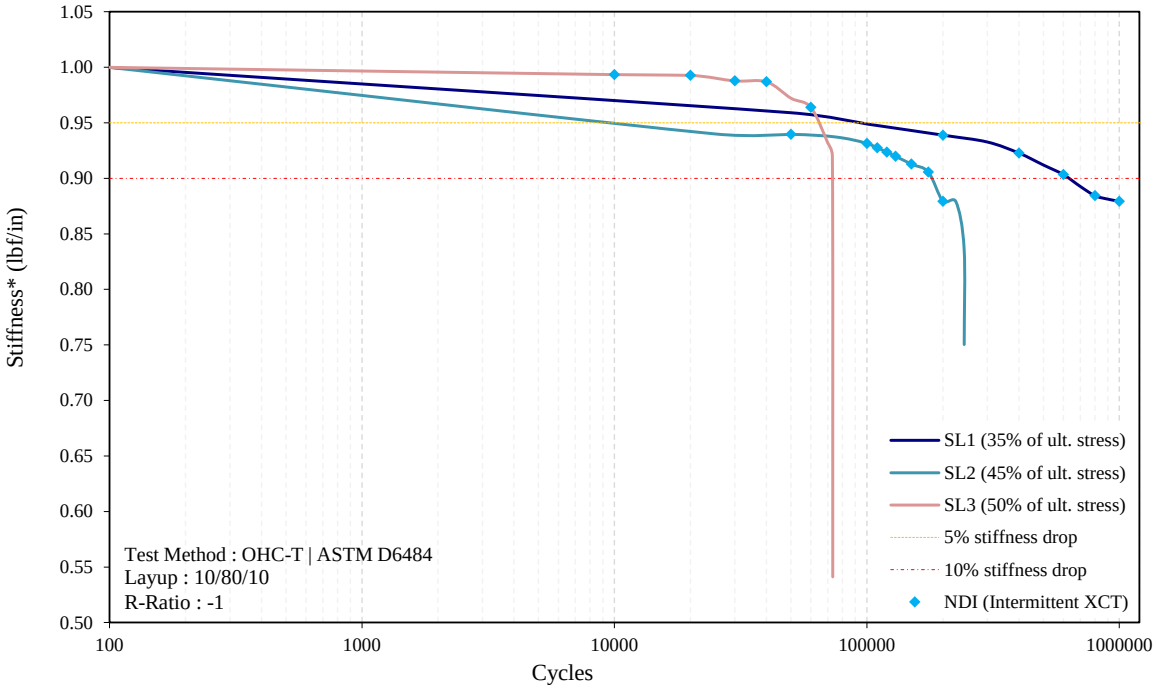


Figure B.38 – Apparent stiffness change during the tension fatigue (normalized by initial compliance) for IM7/5320-1 UNI, 10/80/10 layup, OHC-T, R= -1.

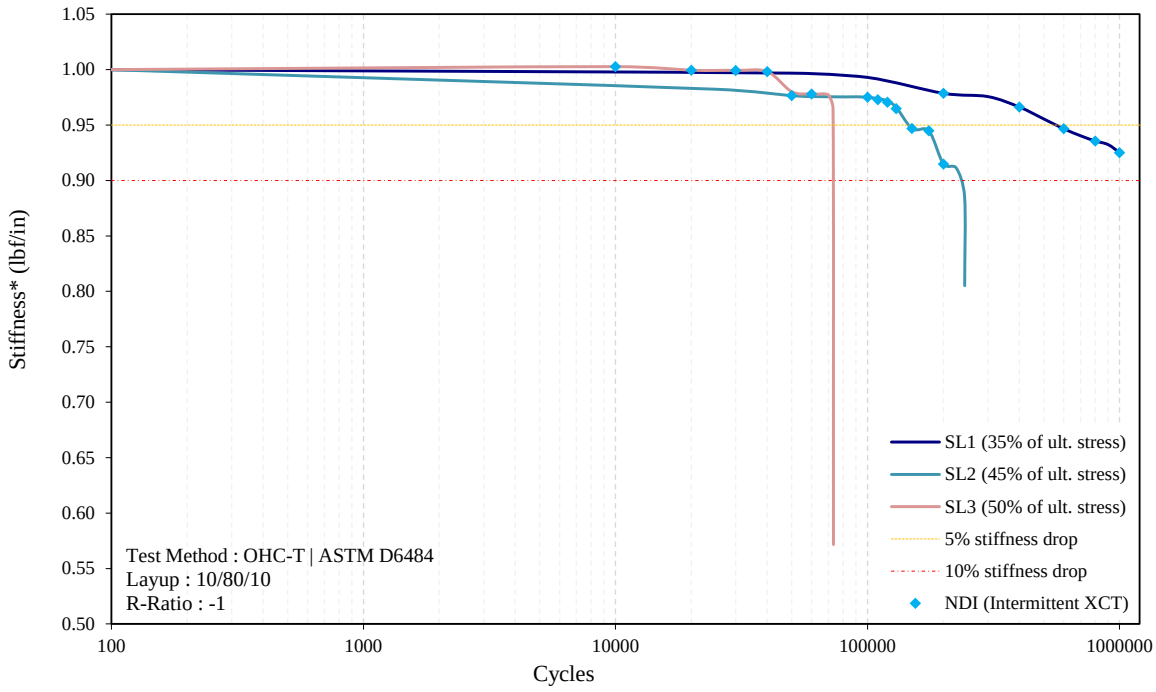


Figure B.39 – Apparent stiffness change during the compression fatigue (normalized by initial compliance) for IM7/5320-1 UNI, 10/80/10 layup, OHC-T, R= -1.

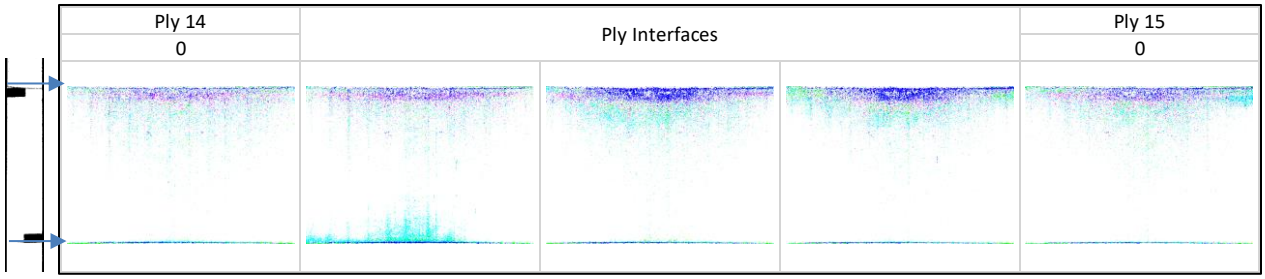
DISTRIBUTION STATEMENT A.
Approved for public release: distribution is unlimited.

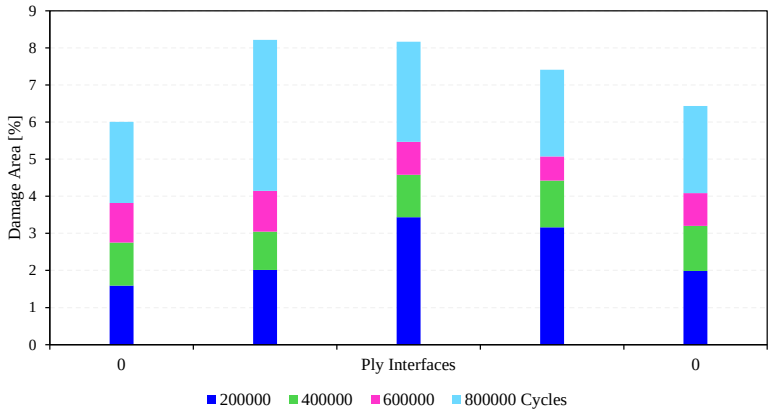
50/40/10 Double Notch Shear

R=0.1, DNS → Specimens: SL-1 (40%), SL-2 (45%), and SL-3 (50%)

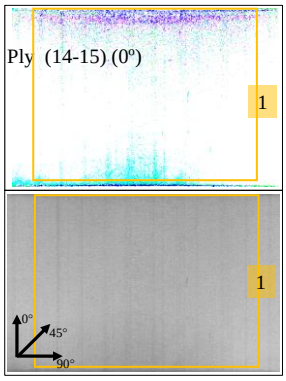
In the observance of progressive damage growth, three specimens were tested in R=0.1 at varying stress levels. Specimens were fatigued until failure or one-million cycles (runout) was achieved. Only SL-1 survived fatigue except for the one tested with intermittent X-ray CT which failed at 805,478 cycles. Specimens from this test method developed an average of 23% decreased residual strength. SL-1 displayed a large sheared area between the 14^{th} and 15^{th} plies with an uneven concentration opposite to the overcut notch (Figure B.40). SL-2 displayed a similar amount of sheared area, however, did not have any overcut notches (Figure B.41). Delamination initiated from both notches relatively even. SL-3 was cut evenly and the majority of delamination measured in the gauge area extended from only one notch (Figure B.42).

DISTRIBUTION STATEMENT A.
Approved for public release: distribution is unlimited.





Specimen ID	MASC1-B1DD11-XXK
Test Method	DNS
Material System	IM7 5320-1 UNI
Ply Layup	50/40/10
Number of Plies	28
Stress Ratio	0.1
% Stress	40% of Ultimate Stress
Final Cycles	805,478
Failure Mode	SHEAR
1) Signs of shearing initiated from both notches extending inwards.	
2) The notch was overcut, stress was not concentrated in the designed shear plane.	



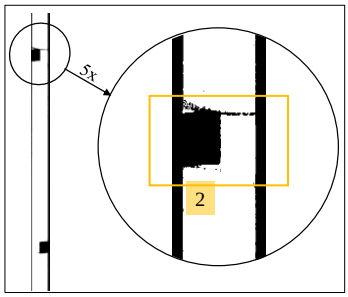
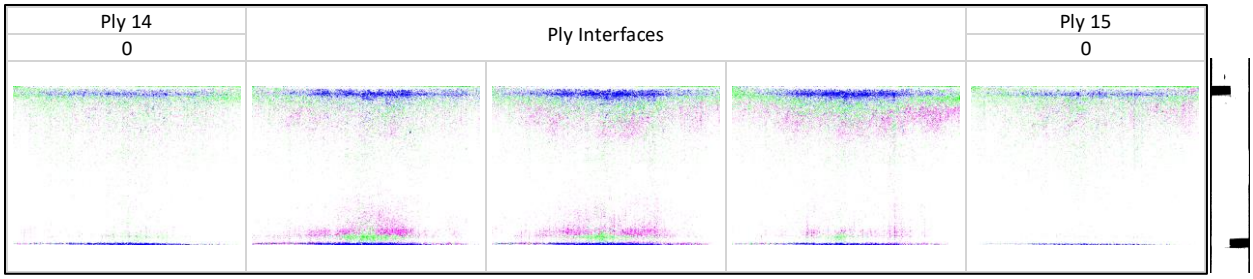
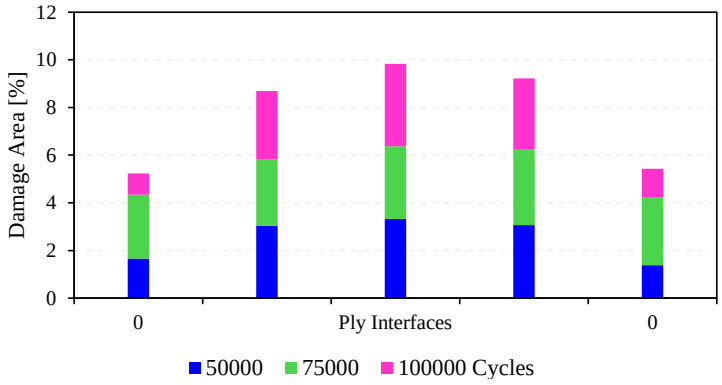


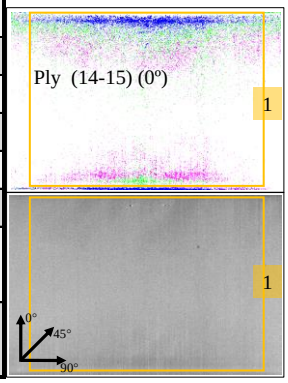
Figure B.40 – Shear gauge damage growth and area increase for IM7/5320-1, 50/40/10, R=0.1, SL1.

DISTRIBUTION STATEMENT A.
Approved for public release: distribution is unlimited.





Specimen ID	MASC1-B2DD11-XX9
Test Method	DNS
Material System	IM7 5320-1 UNI
Ply Layup	50/40/10
Number of Plies	28
Stress Ratio	0.1
% Stress	45% of Ultimate Stress
Final Cycles	103,482
Failure Mode	SHEAR
1) Shear area in this region was uneven, most likely due to the overcut notch.	
2) The notches were cut adequately.	



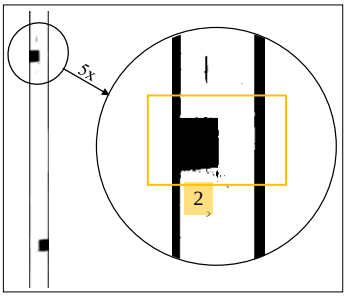
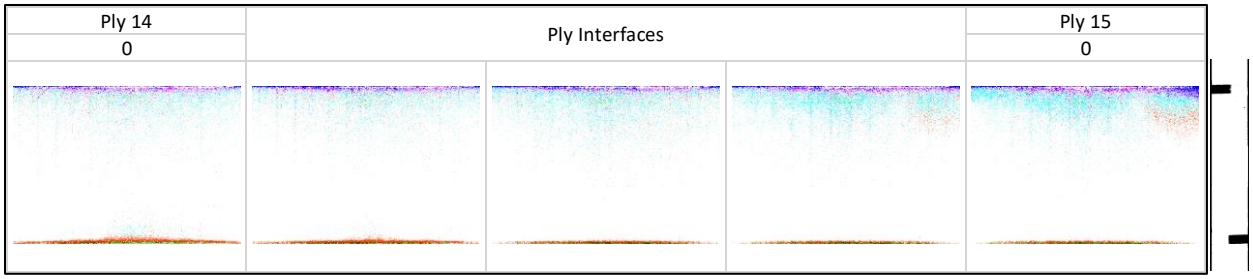
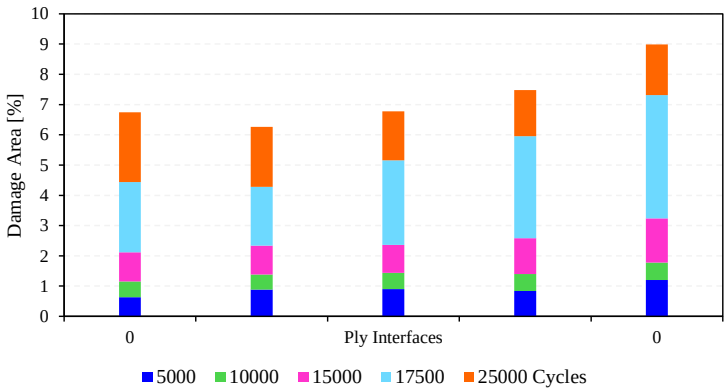


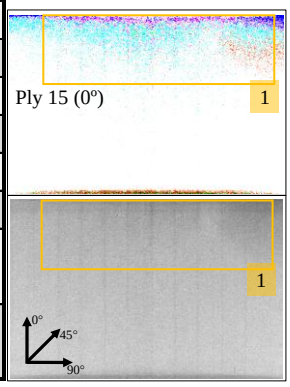
Figure B.41 – Shear gauge damage growth and area increase for IM7/5320-1, 50/40/10, R=0.1, SL2.

DISTRIBUTION STATEMENT A.
Approved for public release: distribution is unlimited.





Specimen ID	MASC1-B3DD11-XX8
Test Method	DNS
Material System	IM7 5320-1 UNI
Ply Layup	50/40/10
Number of Plies	28
Stress Ratio	0.1
% Stress	50% of Ultimate Stress
Final Cycles	25,192
Failure Mode	SHEAR
1) Majority of sheared area initiated from only one notch.	
2) The notches were cut adequately.	



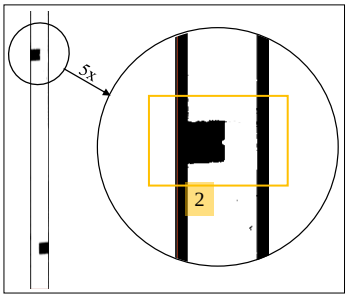


Figure B.42 – Shear gauge damage growth and area increase for IM7/5320-1, 50/40/10, R=0.1, SL3.

DISTRIBUTION STATEMENT A.
Approved for public release: distribution is unlimited.

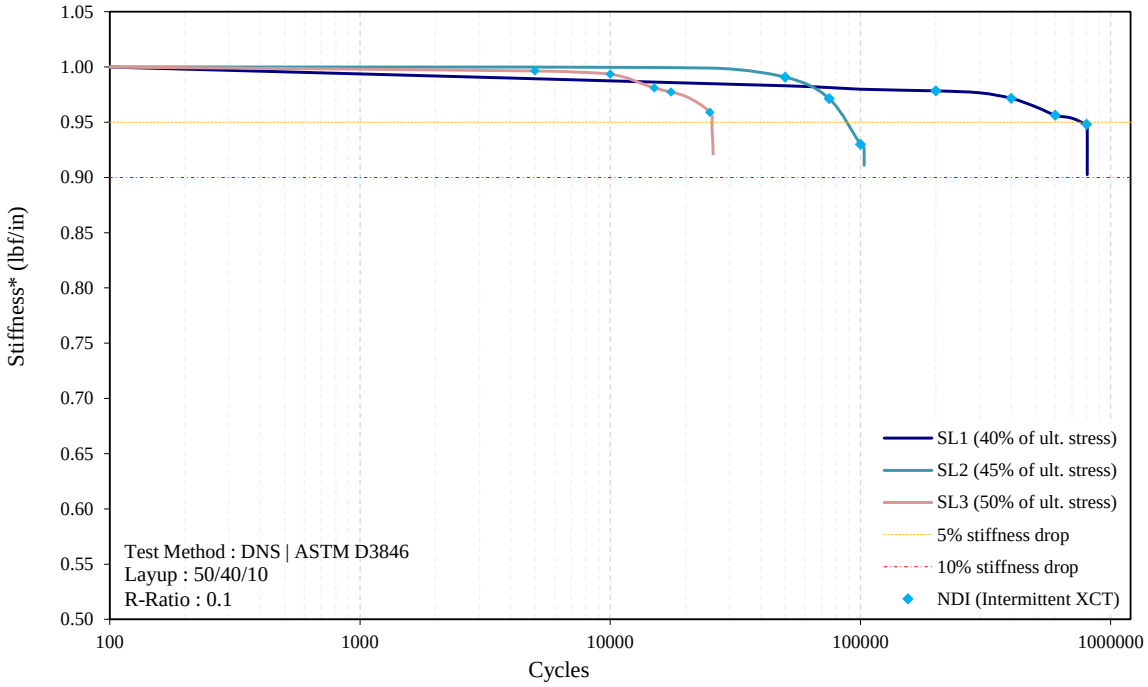


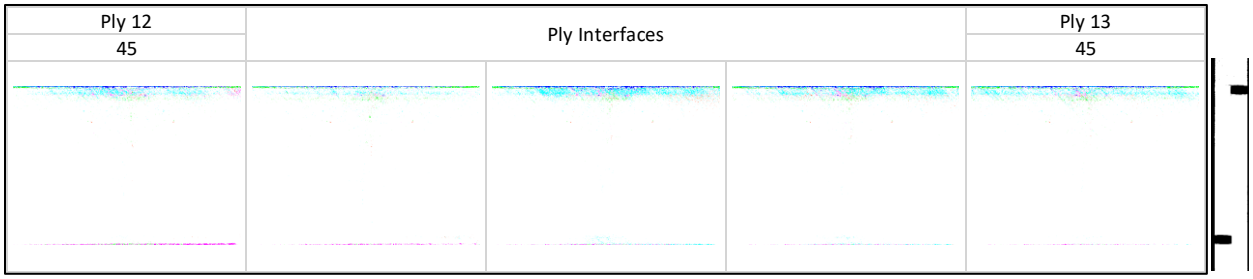
Figure B.43 – Apparent stiffness change during fatigue (normalized by initial compliance) for IM7/5320-1 UNI, 50/40/10 layup, DNS, R=0.1.

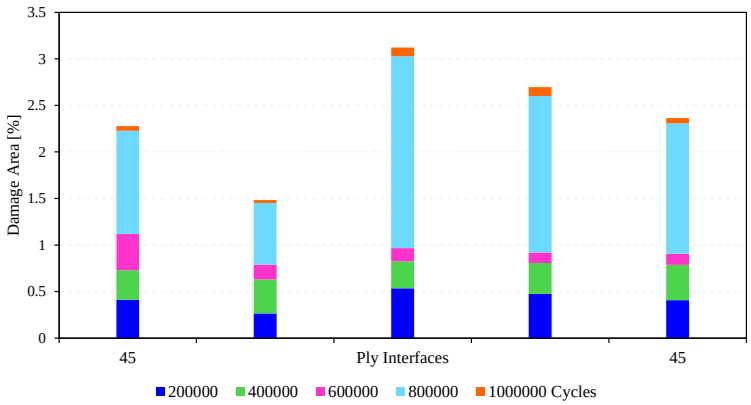
10/80/10 Double Notch Shear

R=0.1, OHT-T → Specimens: SL-1 (60%), SL-2 (70%), and SL-3 (80%)

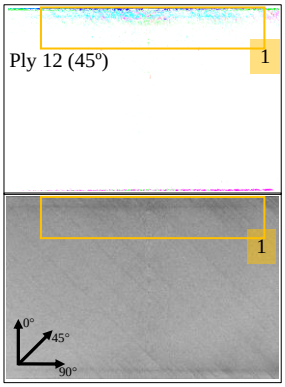
In the observance of progressive damage growth, three specimens were tested in R=0.1 at varying stress levels. Specimens were fatigued until failure or one-million cycles (runout) was achieved. For 10-80-10 only SL-1 survived fatigue and developed a decrease of 8% in residual strength. SL-1 exhibited the majority of its delamination propagating from only one notch (Figure B.44). SL-2 displayed the majority of its sheared area closest to the notch that exhibits signs of being overcut (Figure B.45). SL-3 did not demonstrate signs of being overcut, the majority of its delamination extended from only one notch (Figure B.46).

DISTRIBUTION STATEMENT A.
Approved for public release: distribution is unlimited.





Specimen ID	MASC1-B2FD11-XXD
Test Method	DNS
Material System	IM7 5320-1 UNI
Ply Layup	10/80/10
Number of Plies	24
Stress Ratio	0.1
% Stress	45% of Ultimate Stress
Final Cycles	1,000,000 (runout)
Failure Mode	SHEAR
1) Minor damage throughout specimen, majority of damage from upper notch.	
2) The notches were cut adequately.	



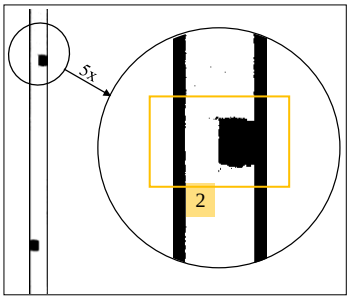
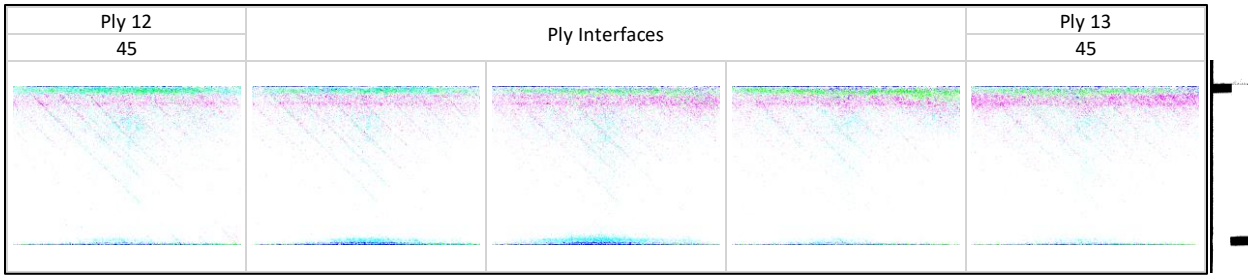
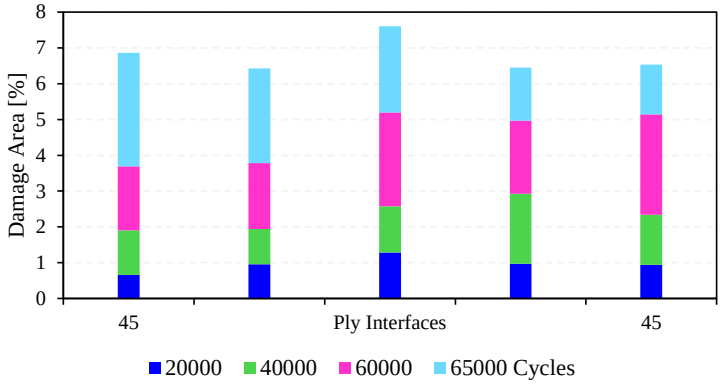


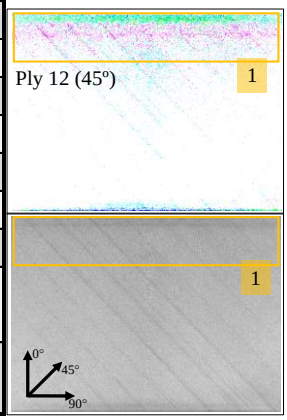
Figure B.44 – Shear gauge damage growth and area increase for IM7/5320-1, 10/80/10, R=0.1, SL1.

DISTRIBUTION STATEMENT A.
Approved for public release: distribution is unlimited.





Specimen ID	MASC1-B1FD11-XXC
Test Method	DNS
Material System	IM7 5320-1 UNI
Ply Layup	10/80/10
Number of Plies	24
Stress Ratio	0.1
% Stress	52.5% of Ultimate Stress
Final Cycles	74,309
Failure Mode	SHEAR
1) Shear concentration in the 45° ply near the notch on one side.	
2) The notch was overcut, stress was not concentrated in the designed shear plane.	



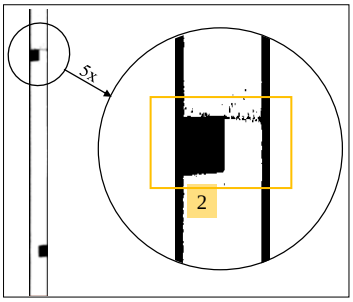
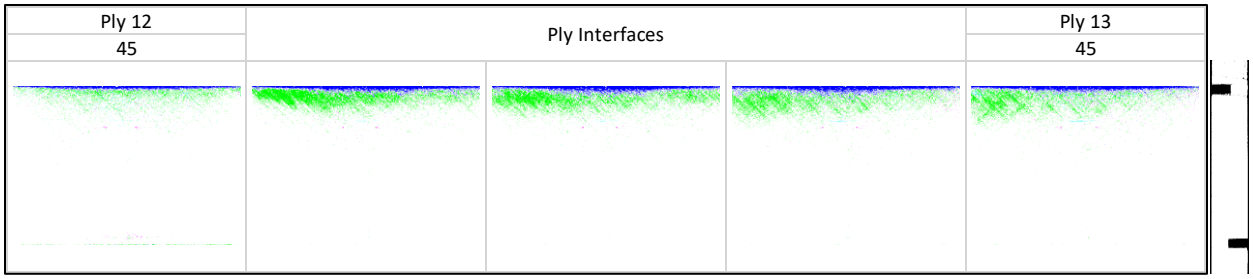
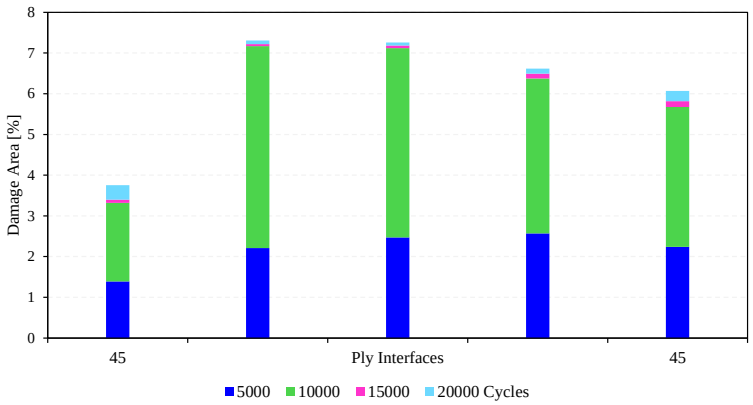


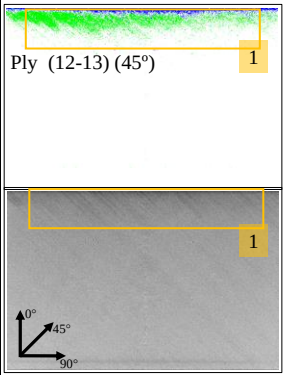
Figure B.45 – Shear gauge damage growth and area increase for IM7/5320-1, 10/80/10, R=0.1, SL2.

DISTRIBUTION STATEMENT A.
Approved for public release: distribution is unlimited.





Specimen ID	MASC1-B3FD11-XXK
Test Method	DNS
Material System	IM7 5320-1 UNI
Ply Layup	10/80/10
Number of Plies	24
Stress Ratio	0.1
% Stress	60% of Ultimate Stress
Final Cycles	23,709
Failure Mode	SHEAR
1) Majority of damage initiates from the upper notch.	
2) The notches were cut adequately.	



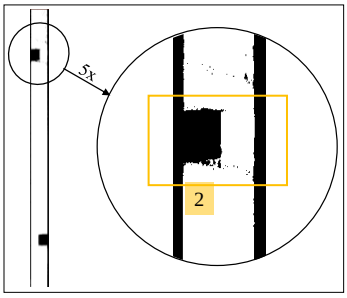


Figure B.46 – Shear gauge damage growth and area increase for IM7/5320-1, 10/80/10, R=0.1, SL3.

DISTRIBUTION STATEMENT A.
Approved for public release: distribution is unlimited.

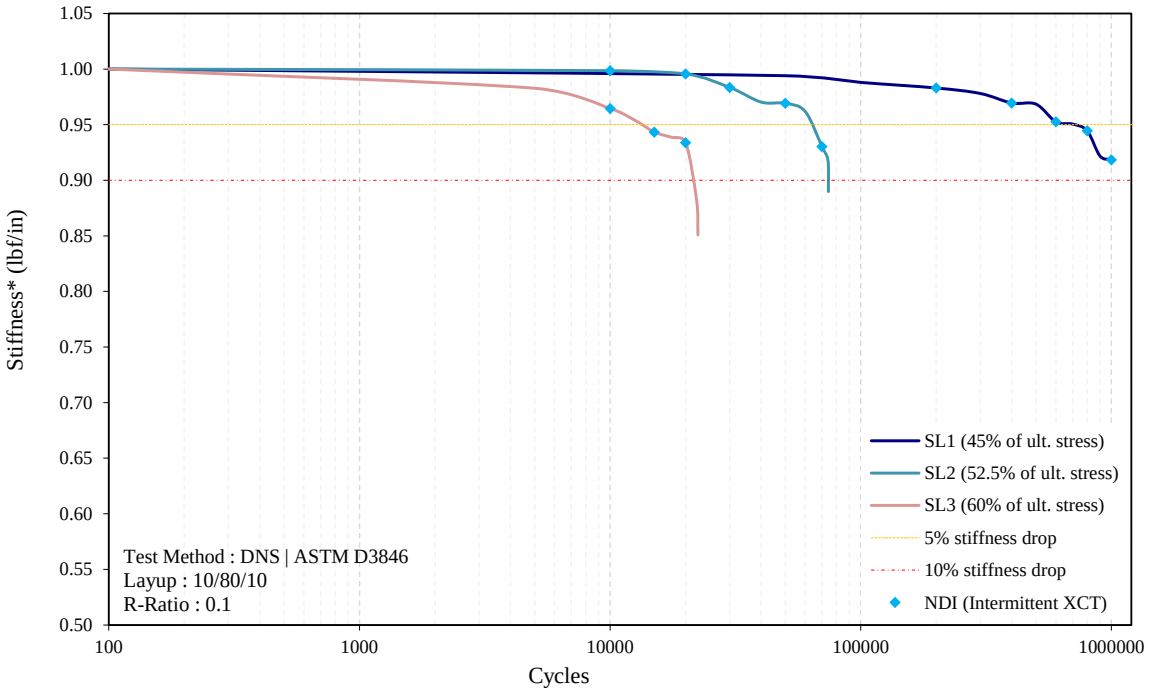


Figure B.47 – Apparent stiffness change during fatigue (normalized by initial compliance) for IM7/5320-1 UNI, 10/80/10 layup, DNS, R=0.1.

DISTRIBUTION STATEMENT A.
Approved for public release: distribution is unlimited.

A.5 Progressive Damage Growth for T650 5320-1 8HS

This section includes T650/5320-1 weave laminates subjected to uniaxial tensile loading, considering three different layups, hard (40/20/40), quasi (25/50/25) and soft (10/80/10). The laminates are composed of equal thickness lamina (CPT 0.0148") 10 plies for hard layup and 8 plies for quasi layup and 10 plies for soft layup with stacking sequences $[0/90/45/0/90]_s$, $[45/0/-45/90]_s$ and $[45/-45/0/45/-45]_s$ respectively.

40/20/40 Open-Hole Test

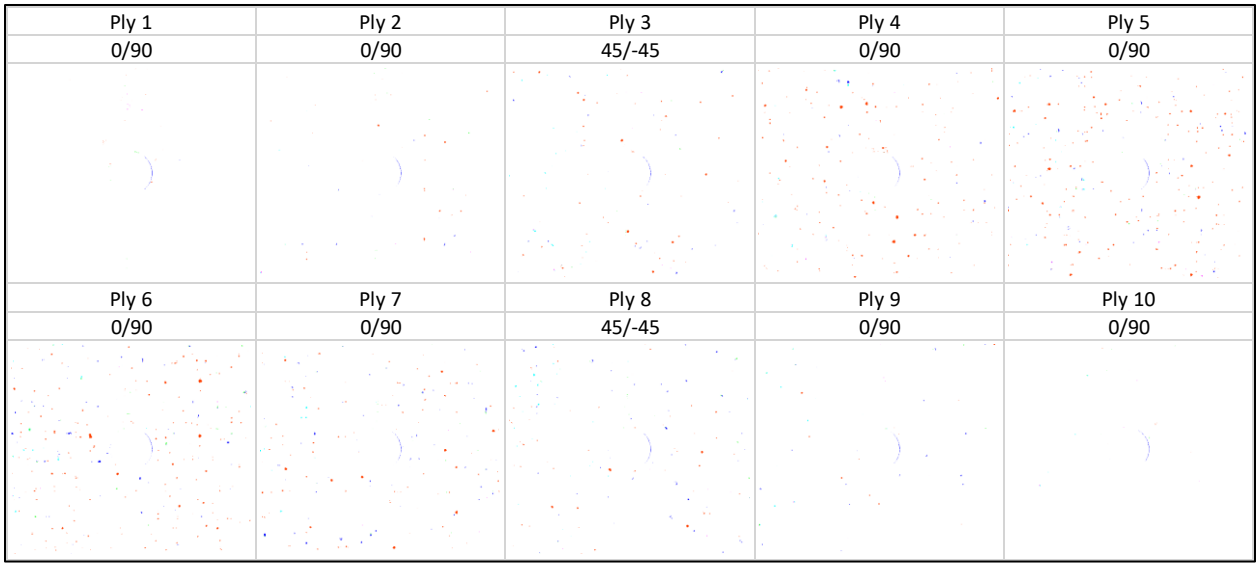
R=0.1, OHT-T → Specimens: SL-1 (70%), SL-2 (80%), and SL-3 (90%)
R=5.0, OHC-C → Specimens: SL-1 (70%), SL-2 (80%), and SL-3 (90%)
R=-1, OHC-T → Specimens: SL-1 (35%), SL-2 (50%), and SL-3 (60%)

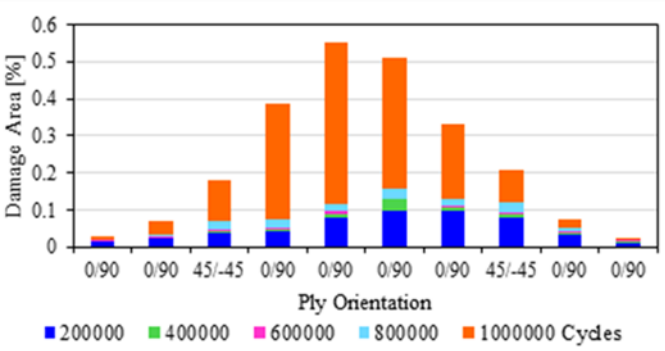
In the observance of progressive damage growth, three specimens were tested for each r-ratio at varying stress levels. Specimens were fatigued until failure or one-million cycles (runout) was achieved. In R=0.1 all 3 specimens survived fatigue and developed an average of 15% decreased residual strength. There was an insignificant amount of delamination near the hole (Figure Figure B.48) for this group in general so the specimens did not develop any stress relief. This group displayed no fiber failure and only SL-3 displayed minor delamination (Figure Figure B.50), instead the majority of damage that propagated in these specimens was directly related to the initial porosity within the woven fibers of this material system (Figure B.49).

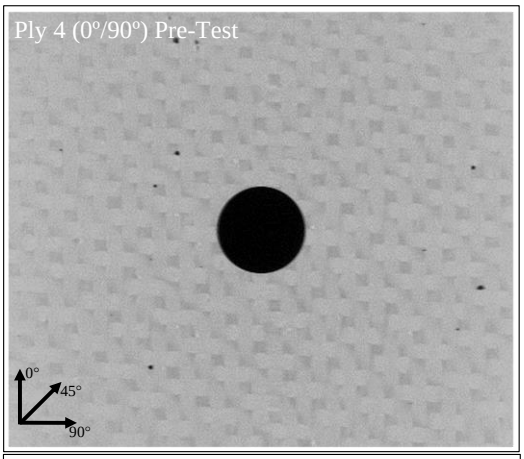
In R=5.0 only SL-1 survived fatigue and developed a 1% increase in residual strength. SL-2 and SL-3 both displayed fiber failure that began on their outermost plies and ultimately lead to failure soon after (Figure Figure B.53). While increased porosity was the significant form of damage, it contributed very little to crack propagation and fiber failure in this group (Figure Figure B.54) but fiber failure in this group appears to lead to an accelerated failure of the specimen.

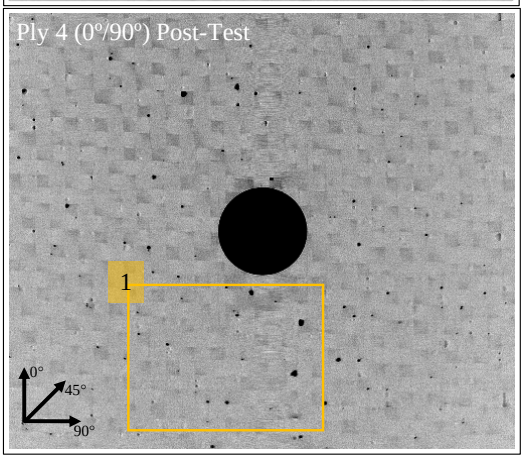
In R=-1 only SL-1 survived fatigue and a 3% decreased residual strength and displayed insignificant damage after fatigue (Figure B.56). SL-2 and SL-3 displayed large fiber failure primarily on their outer plies. The primary reason that SL-3 failed earlier than SL-2 was due to the greater volume of delamination in SL-2 near the hole (Figure B.57) that provided stress relief to the specimen, despite exhibiting a greater number of fiber failures. Fiber failure in this group ultimately lead to an accelerated failure of the specimen.

DISTRIBUTION STATEMENT A.
Approved for public release: distribution is unlimited.





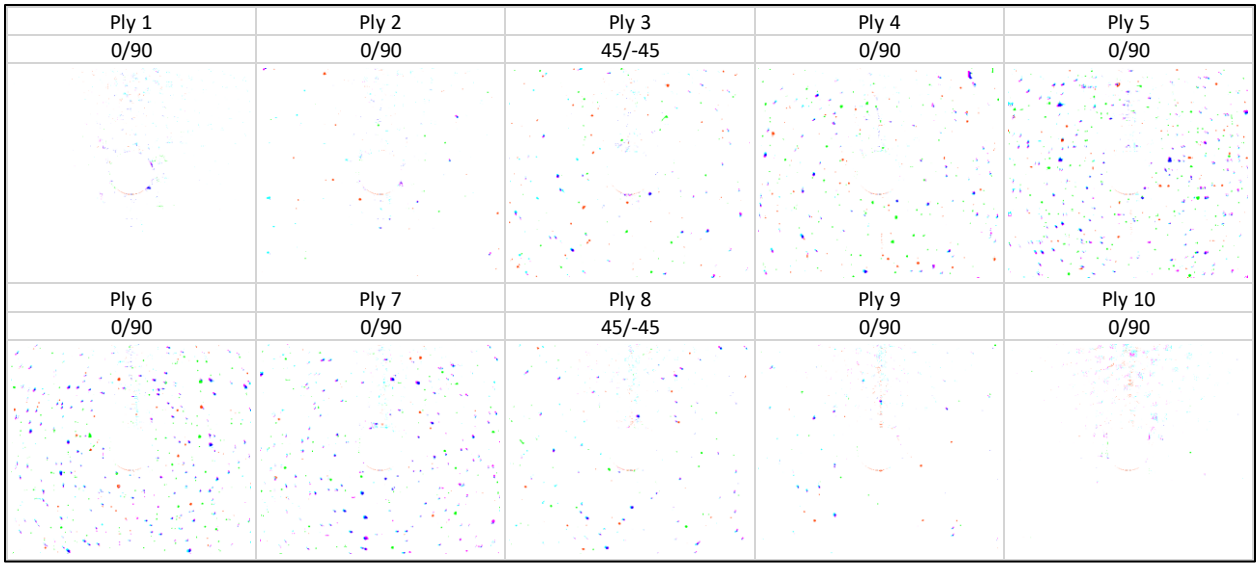


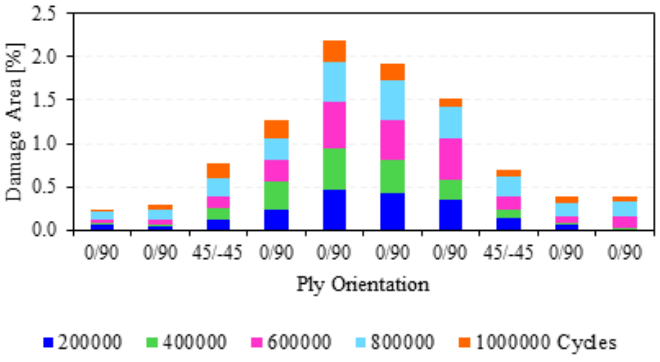


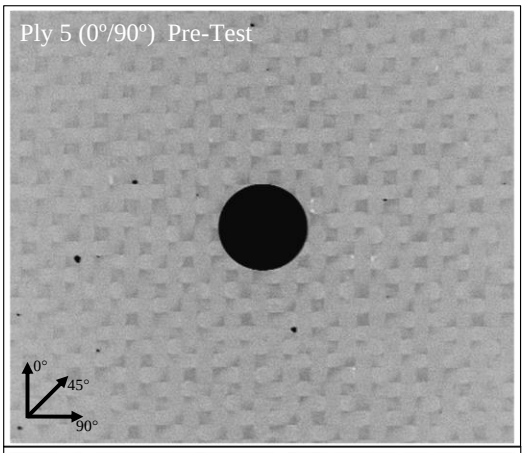
Specimen ID	MASC1-C1GO11-XX1
Test Method	OHT-T
Material System	T650 5320-1 8HS
Ply Layup	40/20/40
Number of Plies	10
Stress Ratio	0.1
% Stress	70% of Ultimate Stress
Final Cycles	1,000,000 (runout)
1) Increased frequency and size of porosities throughout the specimen.	

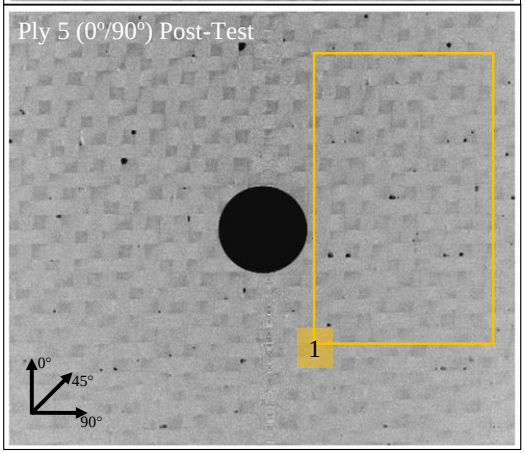
Figure B.48 – Ply-by-ply damage growth and area increase for T650/5320-1, 40/20/40, R=0.1, SL1.

DISTRIBUTION STATEMENT A.
Approved for public release: distribution is unlimited.





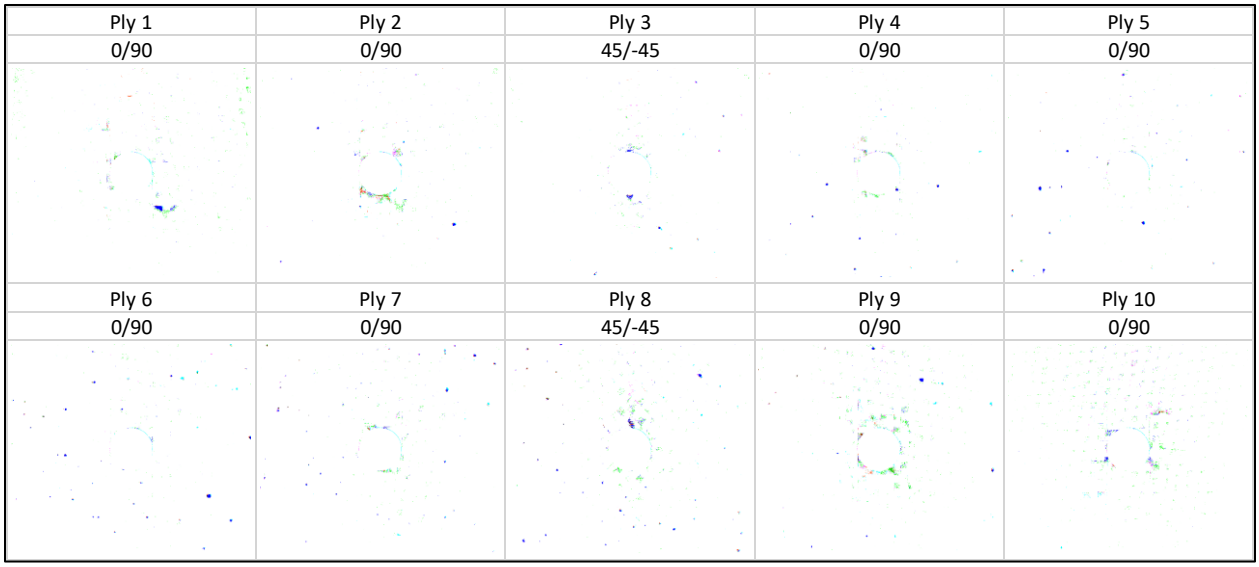


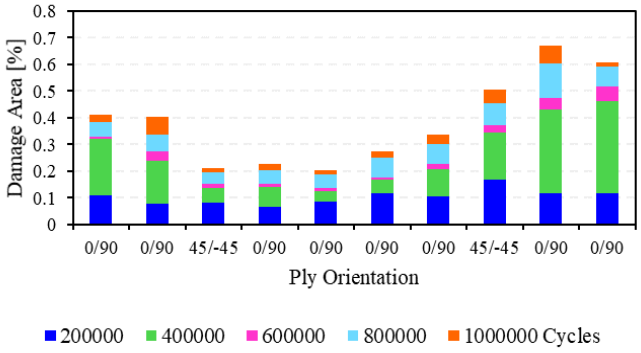


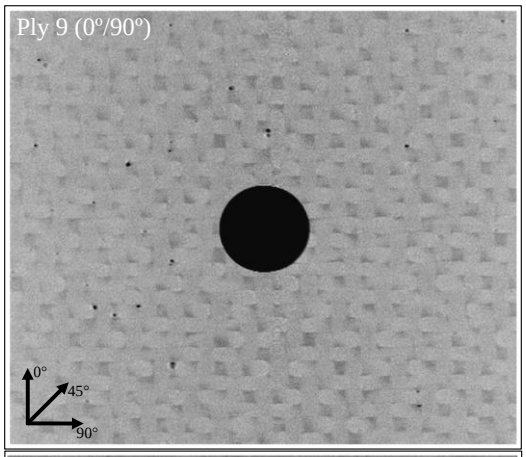
Specimen ID	MASC1-C2GO11-XX2
Test Method	OHT-T
Material System	T650 5320-1 8HS
Ply Layup	40/20/40
Number of Plies	10
Stress Ratio	0.1
% Stress	80% of Ultimate Stress
Final Cycles	1,000,000 (runout)
1) Increased frequency and size of porosities throughout the specimen.	

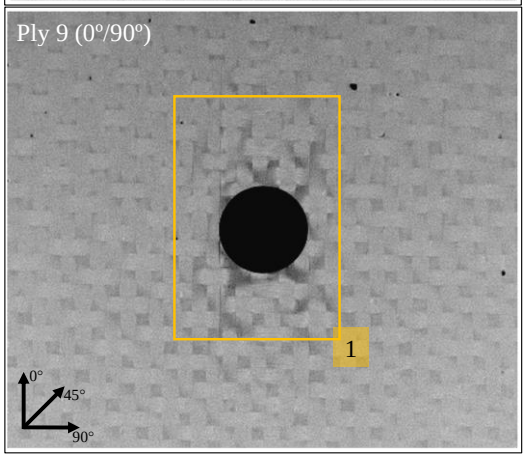
Figure B.49 – Ply-by-ply damage growth and area increase for T650/5320-1, 40/20/40, R=0.1, SL2.

DISTRIBUTION STATEMENT A.
Approved for public release: distribution is unlimited.









Specimen ID	MASC1-C3GO11-XX1
Test Method	OHT-T
Material System	T650 5320-1 8HS
Ply Layup	40/20/40
Number of Plies	10
Stress Ratio	0.1
% Stress	90% of Ultimate Stress
Final Cycles	1,000,000 (runout)
1) Delamination extending radially from the hole in all directions.	

Figure B.50 – Ply-by-ply damage growth and area increase for T650/5320-1, 40/20/40, R=0.1, SL3.

DISTRIBUTION STATEMENT A.
Approved for public release: distribution is unlimited.

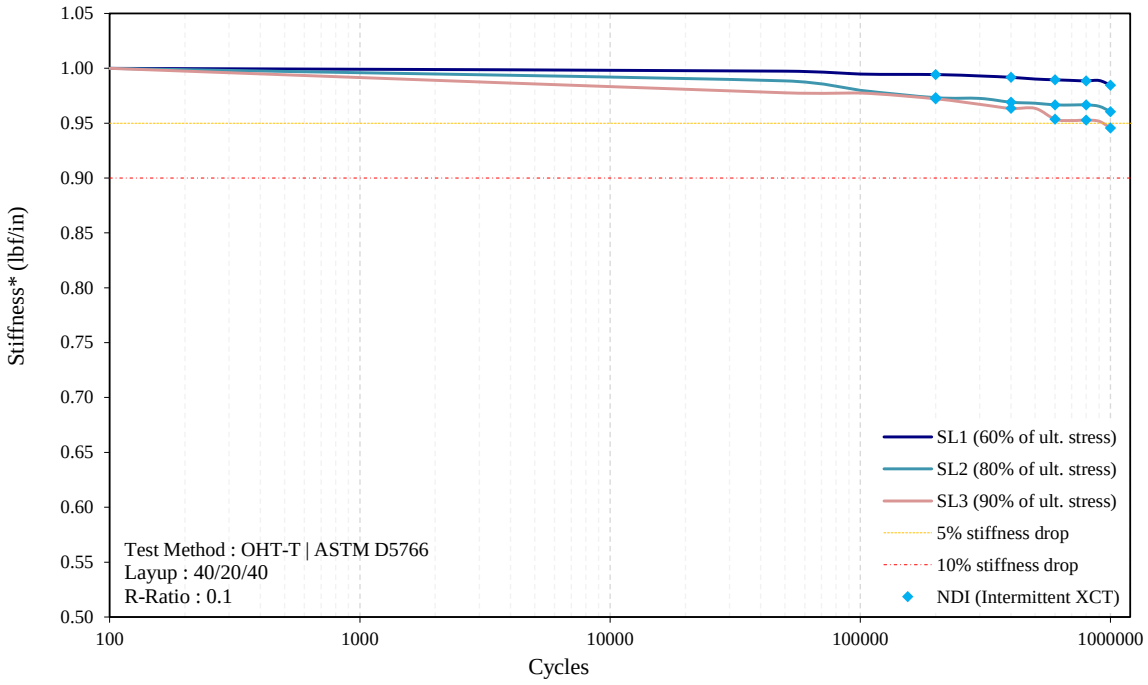
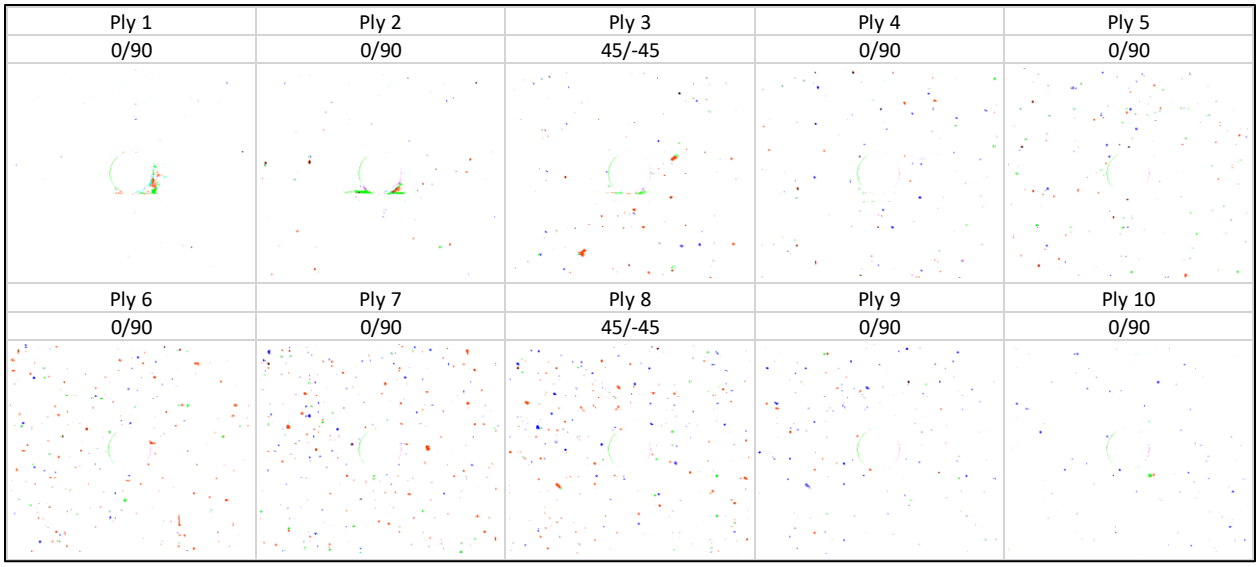
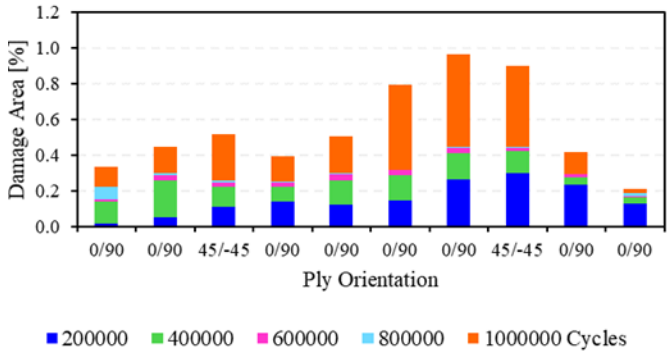
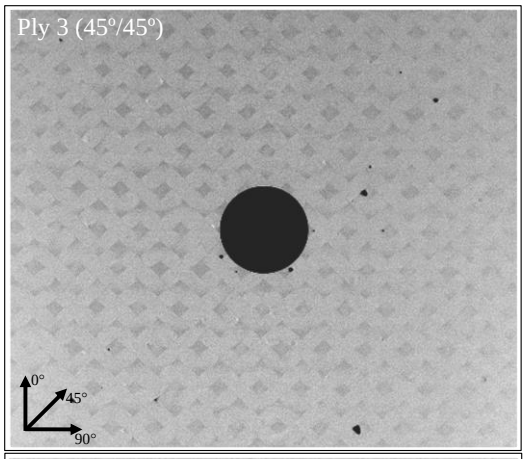


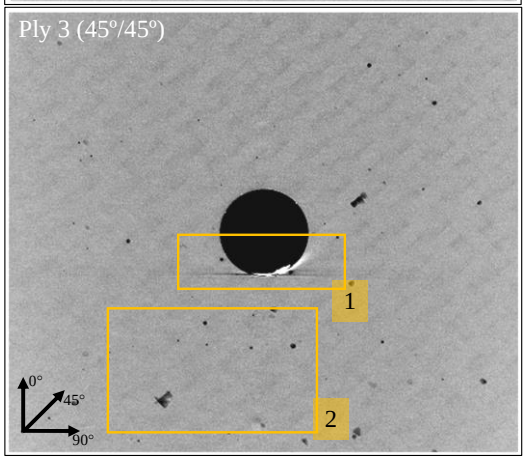
Figure B.51 – Apparent stiffness change during fatigue (normalized by initial compliance) for T650/5320-1 8HS, 40/20/40 layup, OHT-T, R=0.1.

DISTRIBUTION STATEMENT A.
Approved for public release: distribution is unlimited.





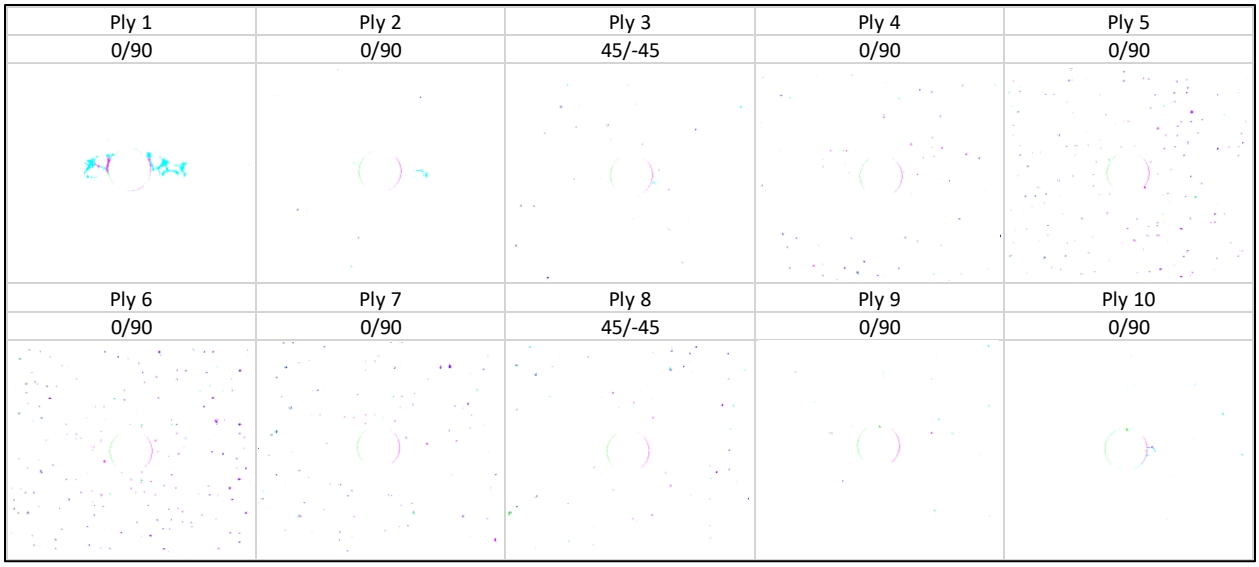


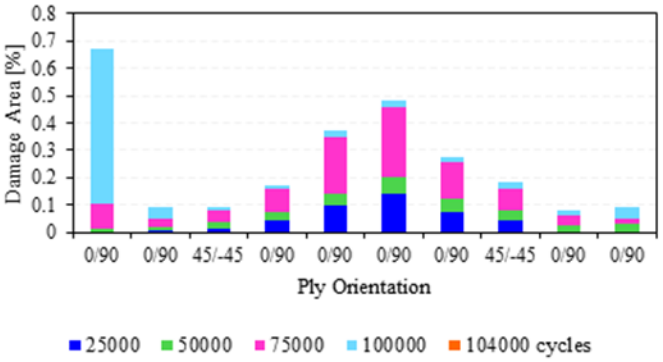


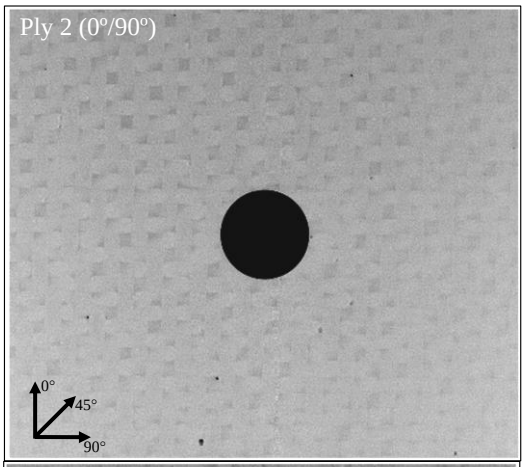
Specimen ID	MASC1-C1GO11-XX2
Test Method	OHC-C
Material System	T650 5320-1 8HS
Ply Layup	40/20/40
Number of Plies	10
Stress Ratio	5.0
% Stress	60% of Ultimate Stress
Final Cycles	1,000,000 (runout)
1) Fiber failure and delamination extending tangentially along the 90° direction.	
2) Increased frequency and size of porosities throughout the specimen.	

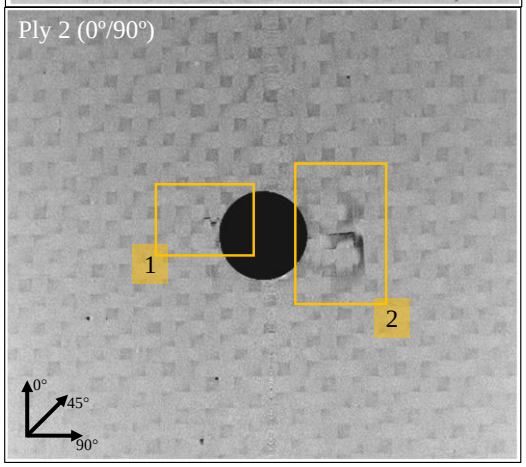
Figure B.52 – Ply-by-ply damage growth and area increase for T650/5320-1, 40/20/40, R=5, SL1.

DISTRIBUTION STATEMENT A.
Approved for public release: distribution is unlimited.





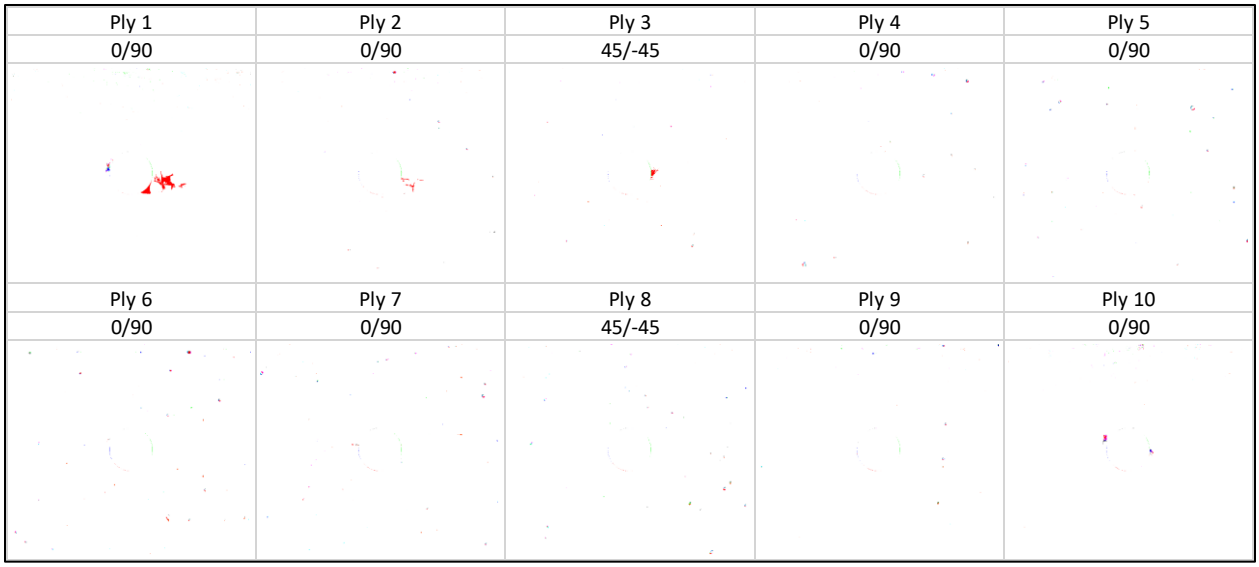


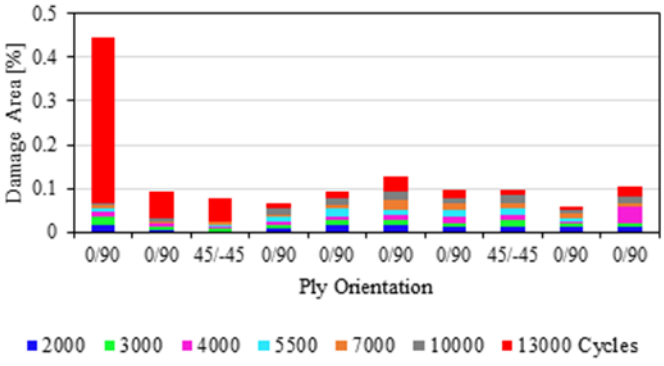


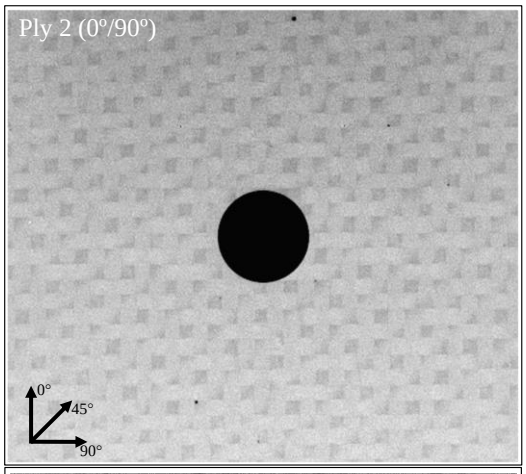
Specimen ID	MASC1-C2GO11-XX3
Test Method	OHC-C
Material System	T650 5320-1 8HS
Ply Layup	40/20/40
Number of Plies	10
Stress Ratio	5.0
% Stress	70% of Ultimate Stress
Final Cycles	120,356
1)Fiber failure extending from the hole in the 90° direction.	
2)Fiber failure and delamination extending from the hole in the 90° direction.	

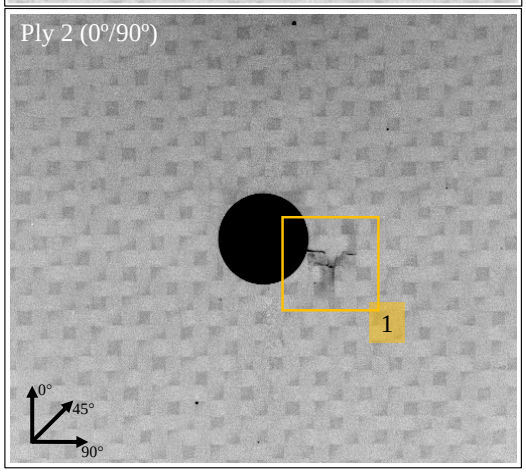
Figure B.53 – Ply-by-ply damage growth and area increase for T650/5320-1, 40/20/40, R=5, SL2.

DISTRIBUTION STATEMENT A.
Approved for public release: distribution is unlimited.









Specimen ID	MASC1-C3GO11-XX5
Test Method	OHC-C
Material System	T650 5320-1 8HS
Ply Layup	40/20/40
Number of Plies	10
Stress Ratio	5.0
% Stress	80% of Ultimate Stress
Final Cycles	15,799
1) Fiber failure extending from the hole in the 90° direction,	

Figure B.54 – Ply-by-ply damage growth and area increase for T650/5320-1, 40/20/40, R=5, SL3.

DISTRIBUTION STATEMENT A.
Approved for public release: distribution is unlimited.

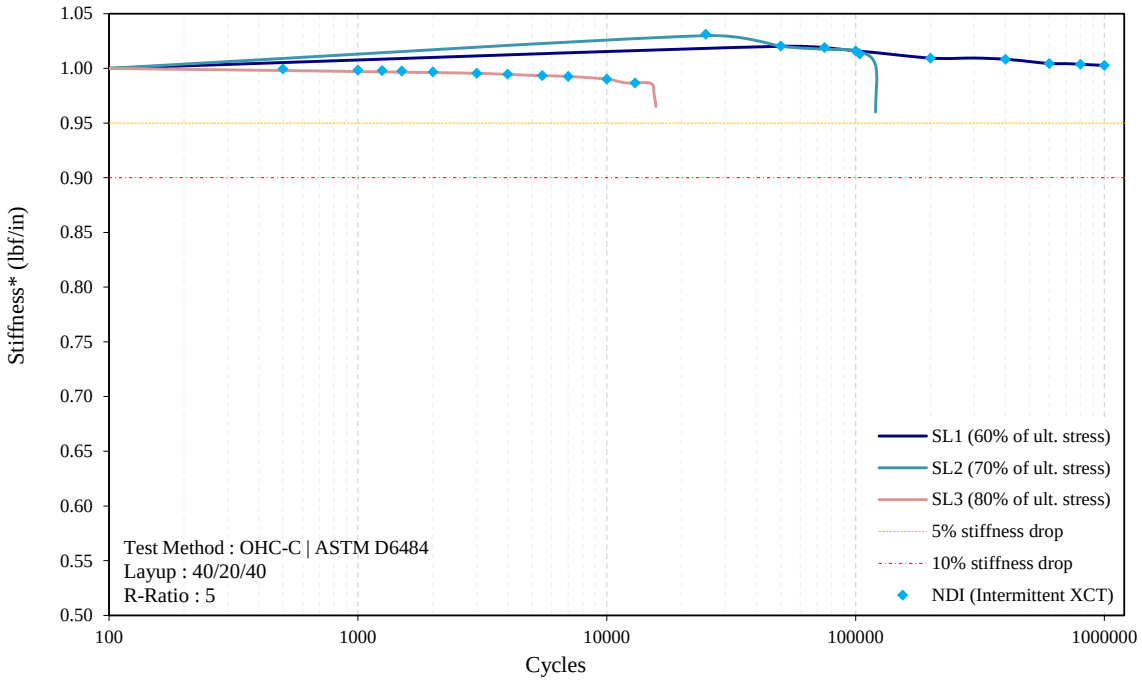
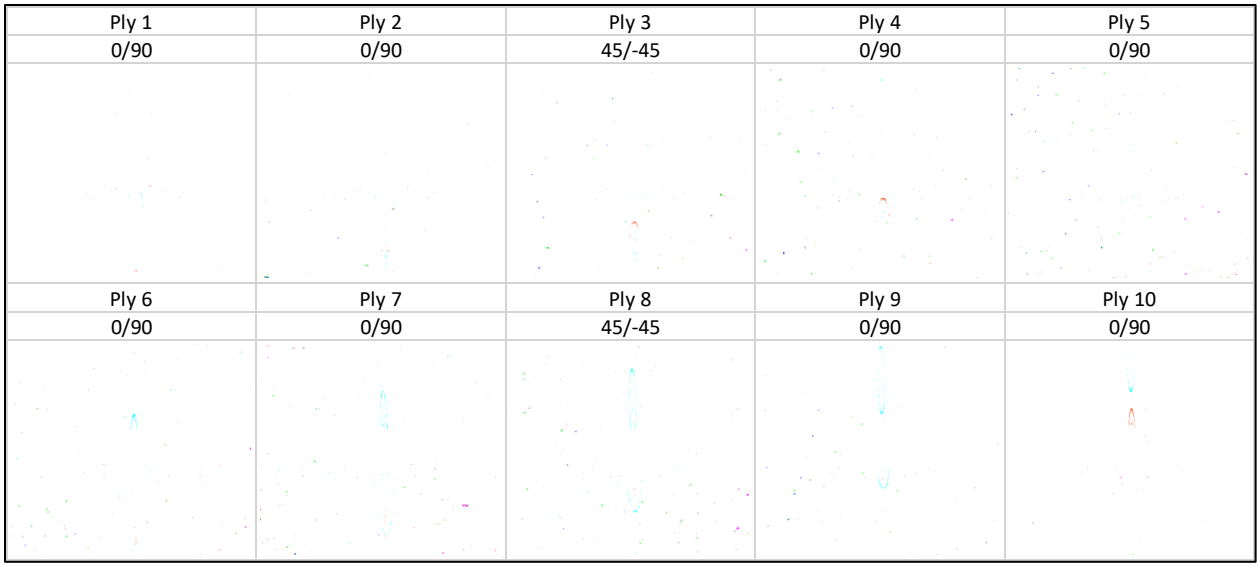
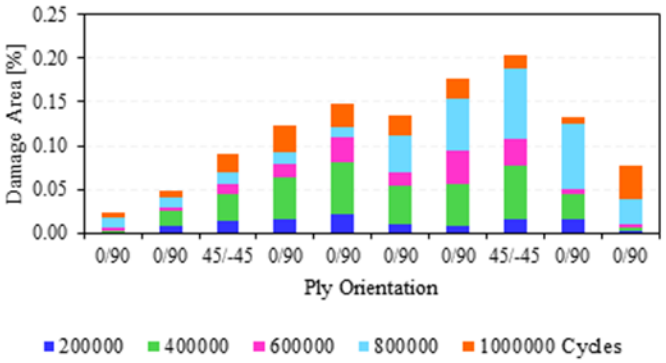
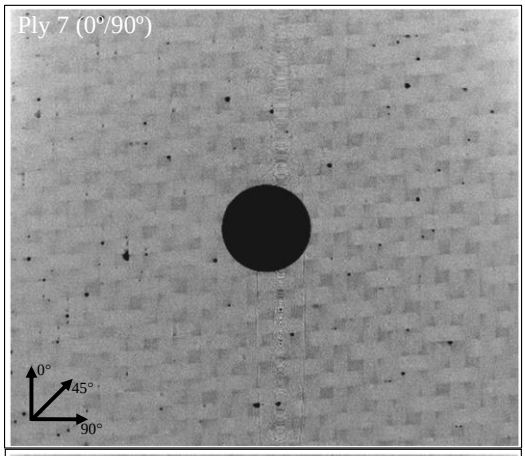


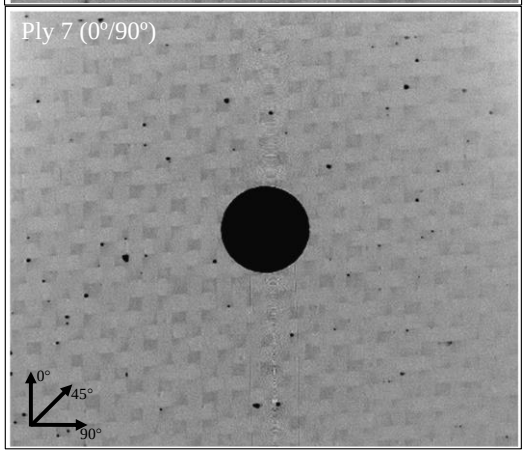
Figure B.55 – Apparent stiffness change during fatigue (normalized by initial compliance) for T650/5320-1 8HS, 40/20/40 layup, OHC-C, R=5.

DISTRIBUTION STATEMENT A.
Approved for public release: distribution is unlimited.





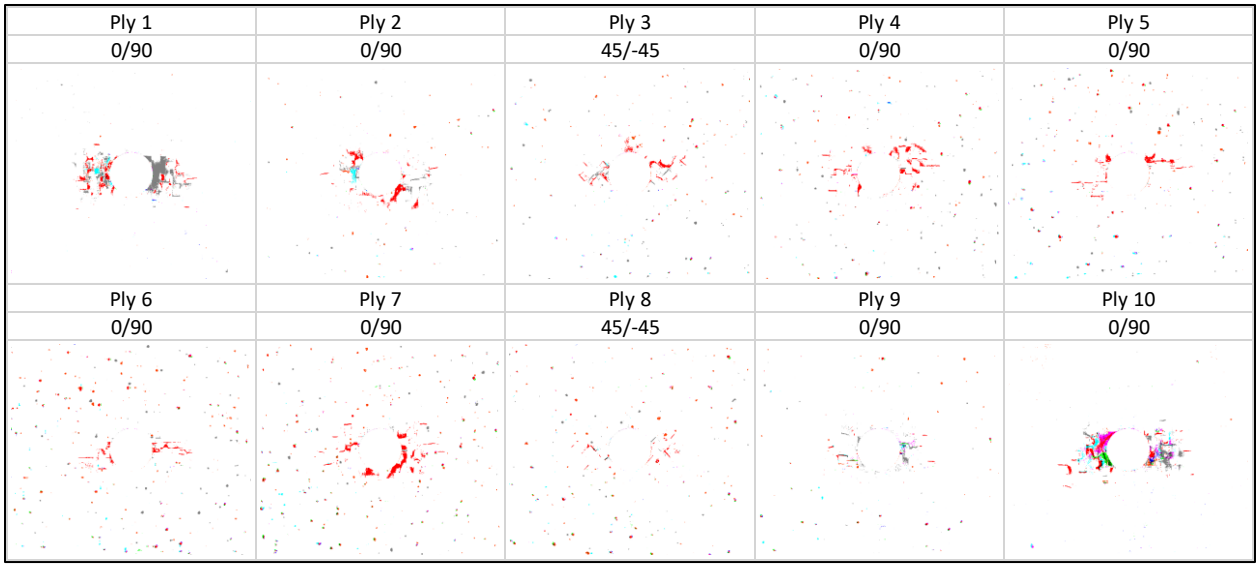


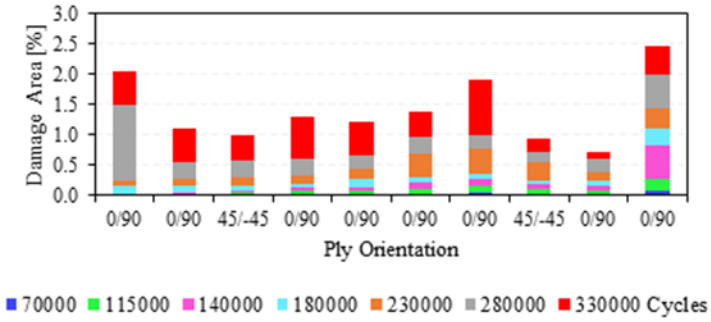


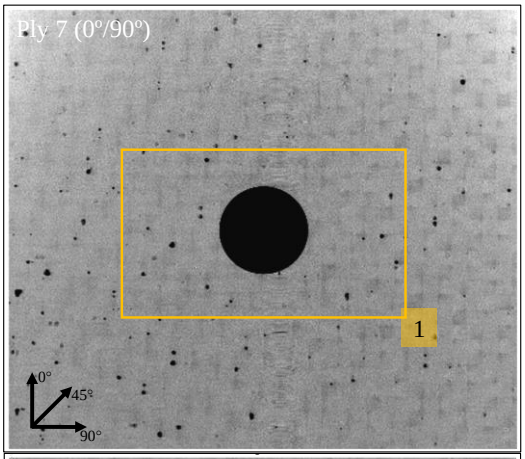
Specimen ID	MASC1-C1GO11-1M2
Test Method	OHC-T
Material System	T650 5320-1 8HS
Ply Layup	40/20/40
Number of Plies	10
Stress Ratio	-1.0
% Stress	35% of Ultimate Stress
Final Cycles	1,000,000 (runout)
Comments) Minor changes to porosities throughout the specimen.	

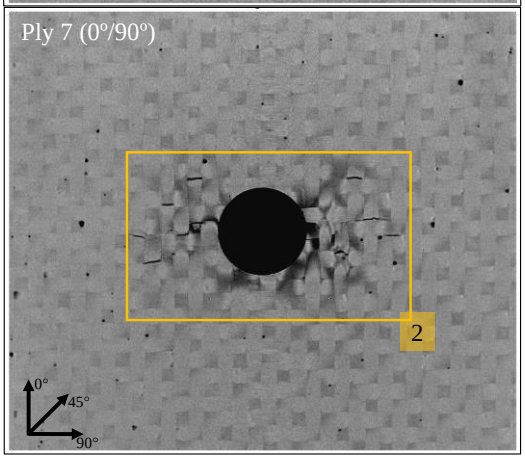
Figure B.56 – Ply-by-ply damage growth and area increase for T650/5320-1, 40/20/40, R=-1, SL1.

DISTRIBUTION STATEMENT A.
Approved for public release: distribution is unlimited.





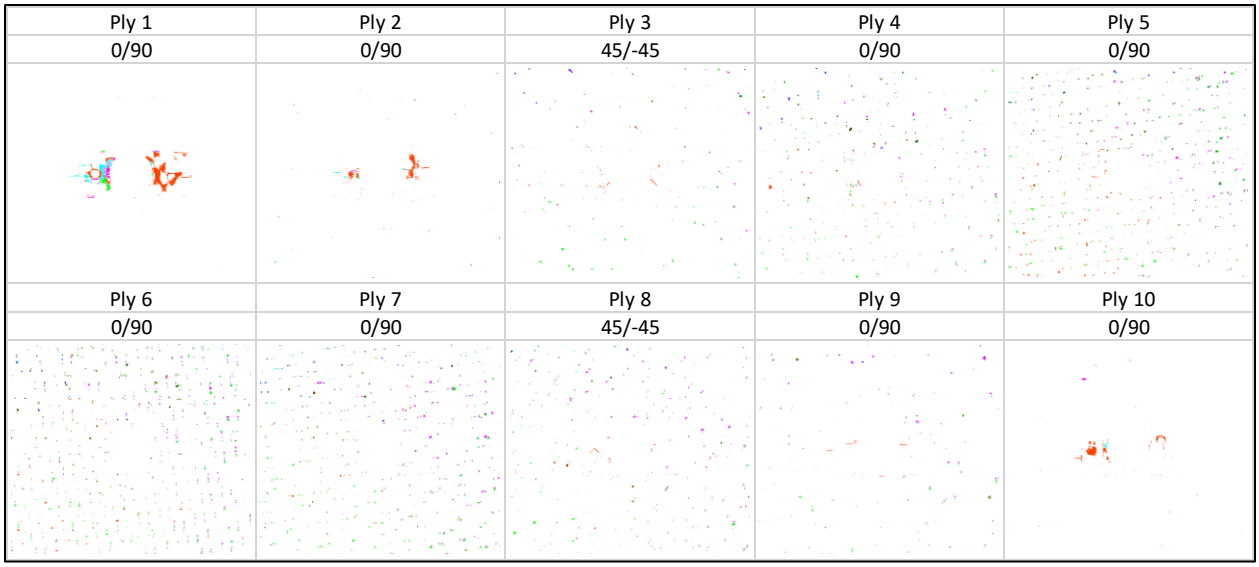


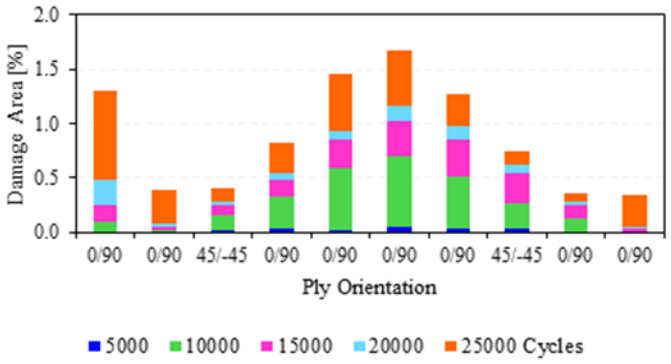


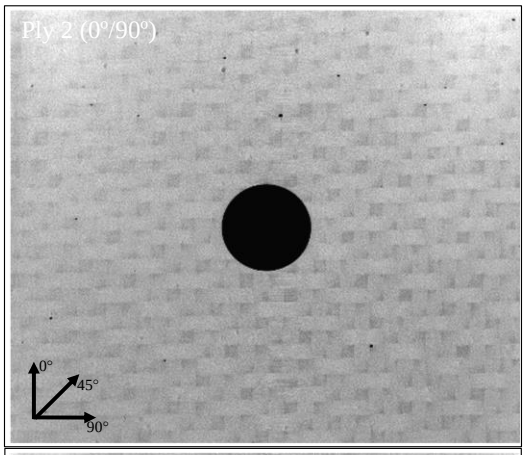
Specimen ID	MASC1-C3GO11-3M2
Test Method	OHC-T
Material System	T650 5320-1 8HS
Ply Layup	40/20/40
Number of Plies	10
Stress Ratio	-1.0
% Stress	50% of Ultimate Stress
Final Cycles	345,114
1) Multiple large porosities near the hole, cracks will propagate from and to these.	
2)Fiber failure and delamination around the hole in the 90° direction.	

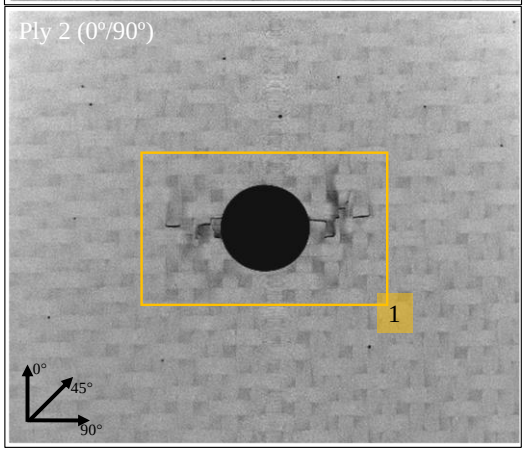
Figure B.57 – Ply-by-ply damage growth and area increase for T650/5320-1, 40/20/40, R=-1, SL2.

DISTRIBUTION STATEMENT A.
Approved for public release: distribution is unlimited.









Specimen ID	MASC1-C2GO11-2M2
Test Method	OHC-T
Material System	T650 5320-1 8HS
Ply Layup	40/20/40
Number of Plies	10
Stress Ratio	-1.0
% Stress	60% of Ultimate Stress
Final Cycles	25,918
1)Fiber failure extending from the hole in both directions along the 90° direction.	

Figure B.58 – Ply-by-ply damage growth and area increase for T650/5320-1, 40/20/40, R=-1, SL3.

DISTRIBUTION STATEMENT A.
Approved for public release: distribution is unlimited.

Continued…	MASC1-C2GO11-2M2
Test Method	OHC-T
Material System	T650 5320-1 8HS
Ply Layup	40-20-40
Number of Plies	10
Stress Ratio	-1.0
% Stress	60% of Ultimate Stress
Final Cycles	25,918
1)Small fiber failure extending from the along the 90º direction.	
Comments) Increased frequency and size of porosities throughout specimen.	

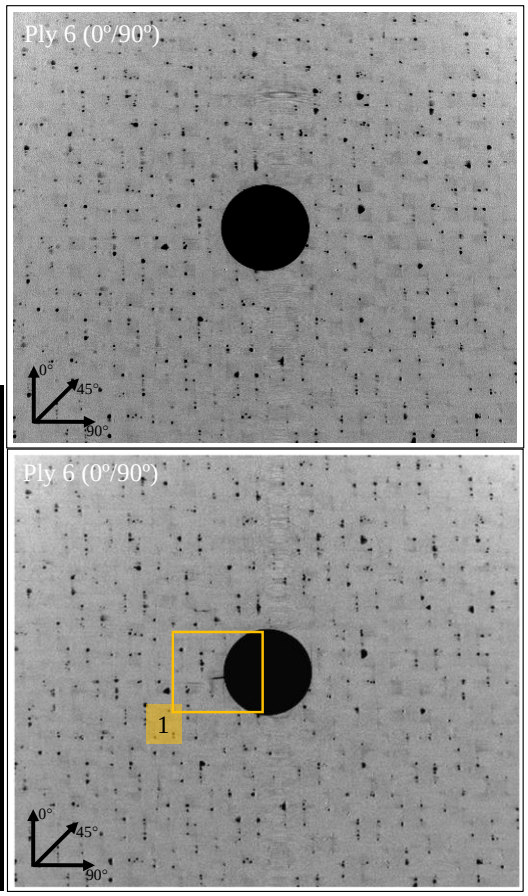


Figure B.58 – Ply-by-ply damage growth and area increase for T650/5320-1, 40/20/40, R=-1, SL3 (cont.).

DISTRIBUTION STATEMENT A.
Approved for public release: distribution is unlimited.

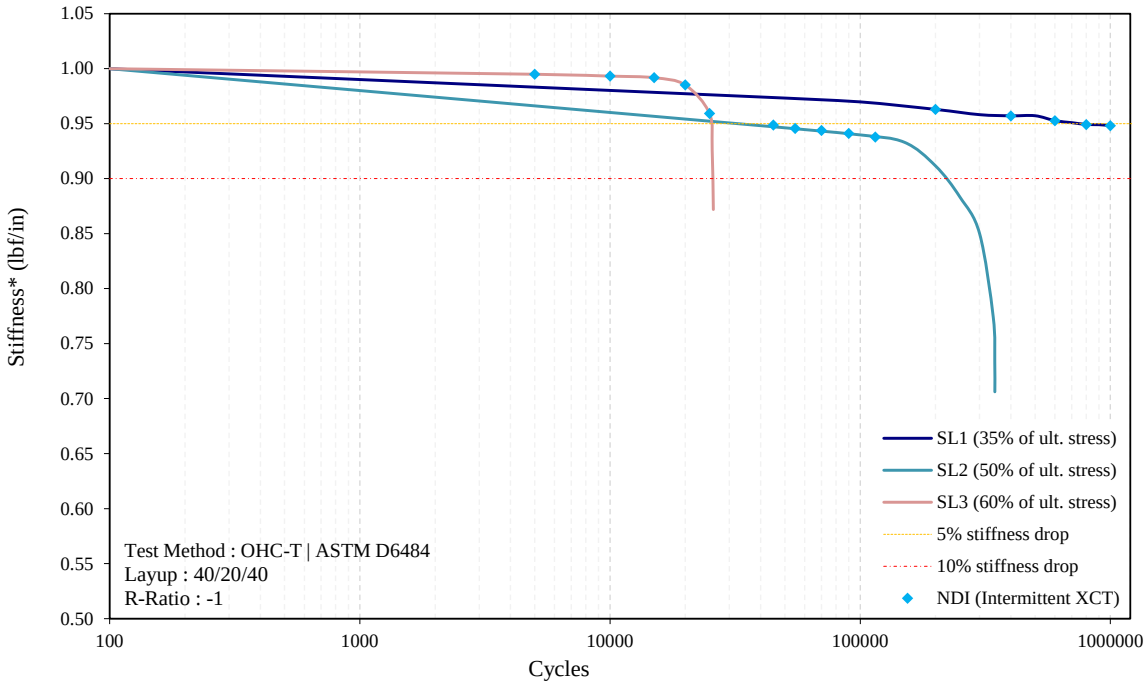


Figure B.59 – Apparent stiffness change during the tension fatigue (normalized by initial compliance) for T650/5320-1 8HS, 40/20/40 layup, OHC-T, R=-1

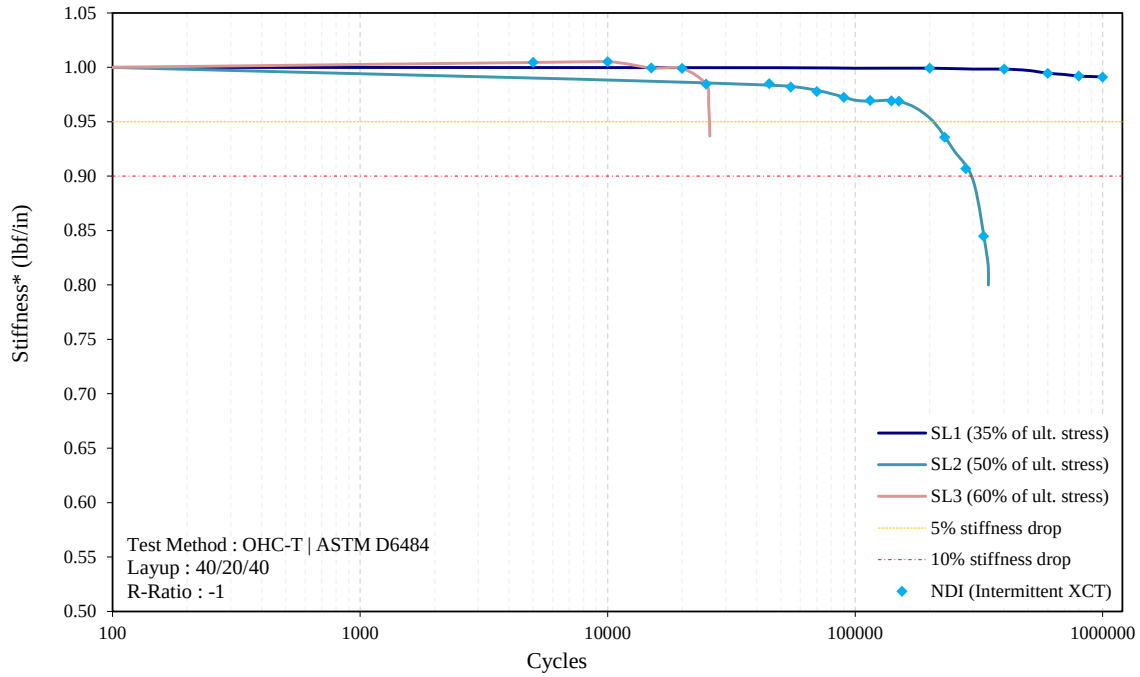


Figure B.60 – Apparent stiffness change during the compression fatigue (normalized by initial compliance) for T650/5320-1 8HS, 40/20/40 layup, OHC-T, R=-1.

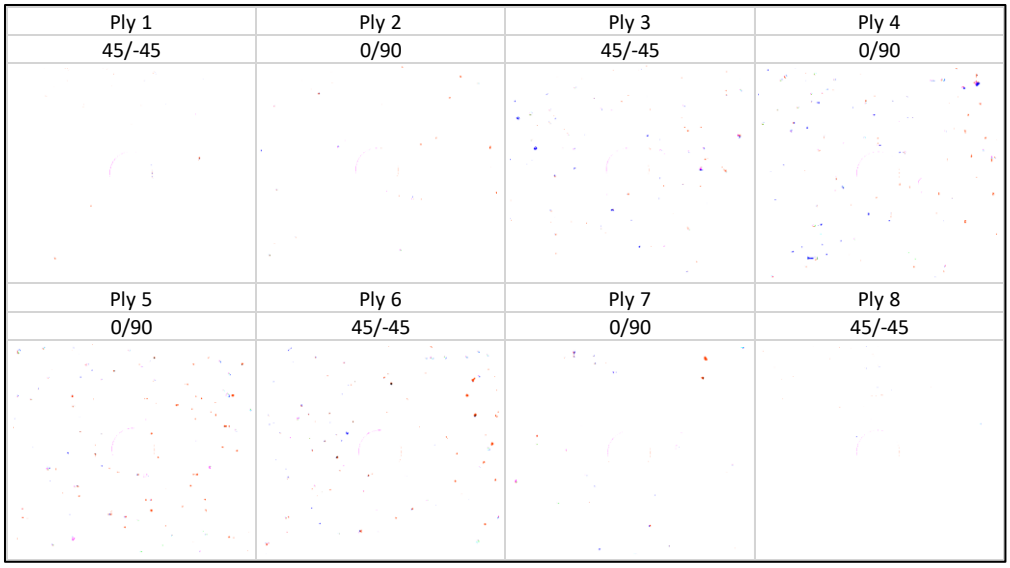
DISTRIBUTION STATEMENT A.
Approved for public release: distribution is unlimited.

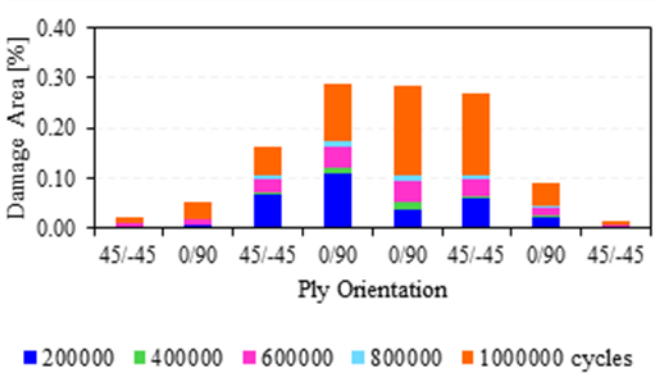
25/50/25 Open-Hole Test

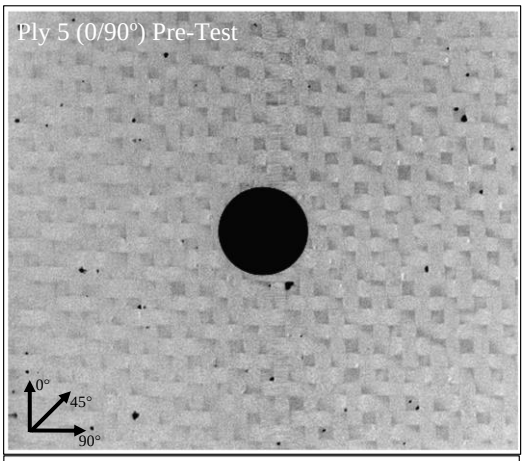
R=0.1, OHT-T → Specimens: SL-1 (70%), SL-2 (80%), and SL-3 (90%)
R=5.0, OHC-C → Specimens: SL-1 (70%), SL-2 (80%), and SL-3 (90%)
R=-1, OHT-C → Specimens: SL-1 (35%), SL-2(50%), and SL-3 (60%)

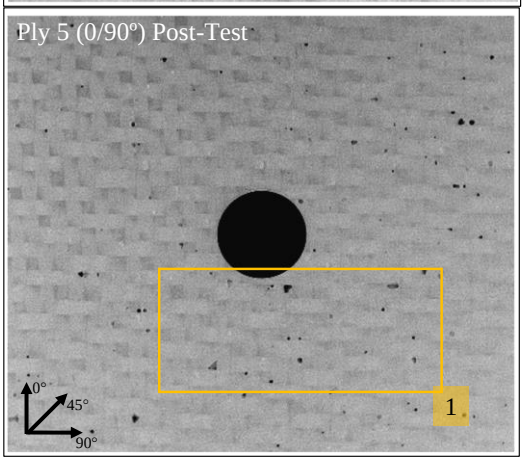
In the observance of progressive damage growth, three specimens were tested for each r-ratio at varying stress levels and specimens were fatigued until failure or one-million cycles (runout) was achieved. In R=0.1 all 3 specimens survived fatigue and developed an average of 6% increased residual strength. This group displayed little fatigue induced damage (Figure Figure B.61) with the primary damage in this group being the enlargement of pre-existent spaces between fibers of each ply (Figure B.62 and Figure Figure B.63).
In R=5.0 only SL-1 survived fatigue and demonstrated a 17% decrease in residual strength. This large drop in strength was due to the fiber failures that formed during fatigue (Figure Figure B.65). SL-2 experienced large quantities of fiber failure and in this group the majority of fiber failure initiates at the innermost 0°/90° ply. The cracks then form through the hole in the 0° direction (Figure B.66). SL-3 failed very soon after cracks began to form around the hole leading to an accelerated failure. Due to this, the image before failure for SL-3 do not represent the true amount of fiber failure and damages that likely would have formed (Figure B.67). While the group had fiber failure, it displayed insignificant amounts of delamination, only forming near fiber failures.
In R=-1 only SL-1 survived fatigue and did not develop any significant change in residual strength or demonstrate damage due to fatigue (Figure B.69). SL-2 and SL-3 in this group displayed an increase in spaces between fibers as well as fiber failures near the hole (Figure Figure B.70). There are fiber failures throughout all plies in SL-2, while SL-3 exhibits only 3 instances of minor fiber failure near the hole primarily on 0°/90° plies (Figure B.71).

DISTRIBUTION STATEMENT A.
Approved for public release: distribution is unlimited.





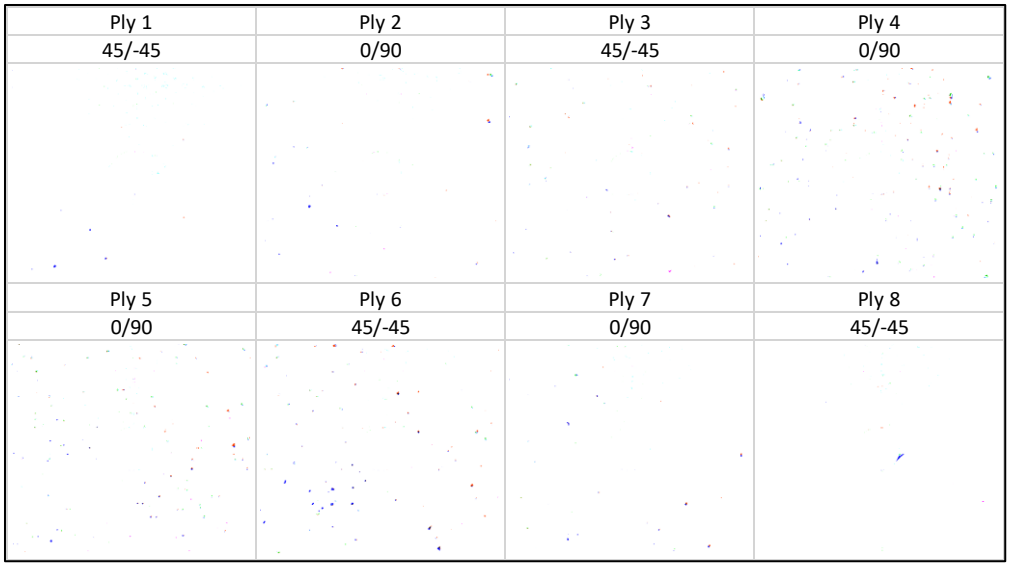


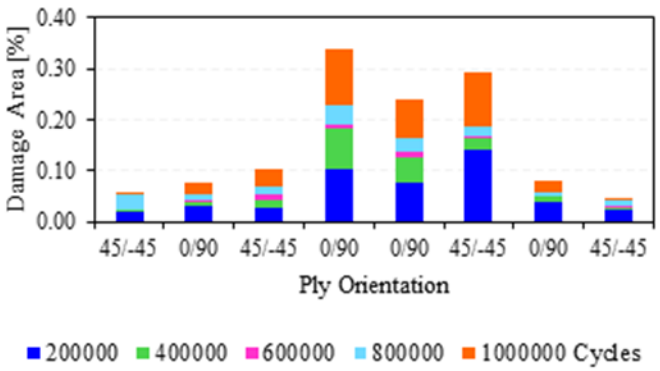


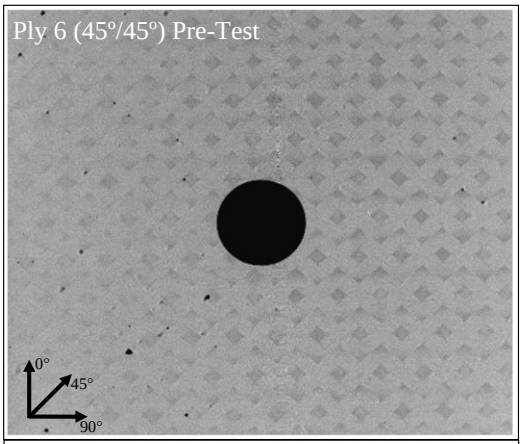
Specimen ID	MASC1-C1EO11-1K2
Test Method	OHT-T
Material System	T650 5320-1 8HS
Ply Layup	25/50/25
Number of Plies	8
Stress Ratio	0.1
% Stress	70% of Ultimate Stress
Final Cycles	1,000,000 (runout)
1) Increased frequency and size of porosities throughout the specimen.	

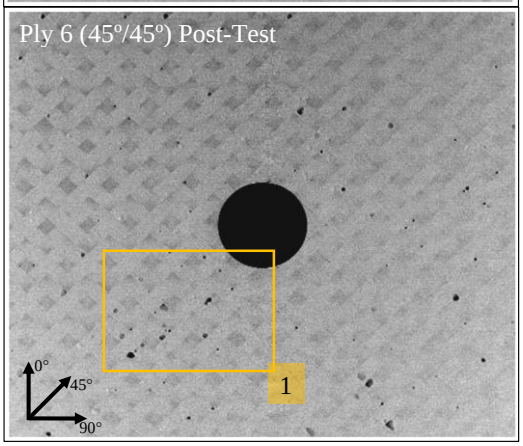
Figure B.61 – Ply-by-ply damage growth and area increase for T650/5320-1, 25/50/25, R=0.1, SL1.

DISTRIBUTION STATEMENT A.
Approved for public release: distribution is unlimited.





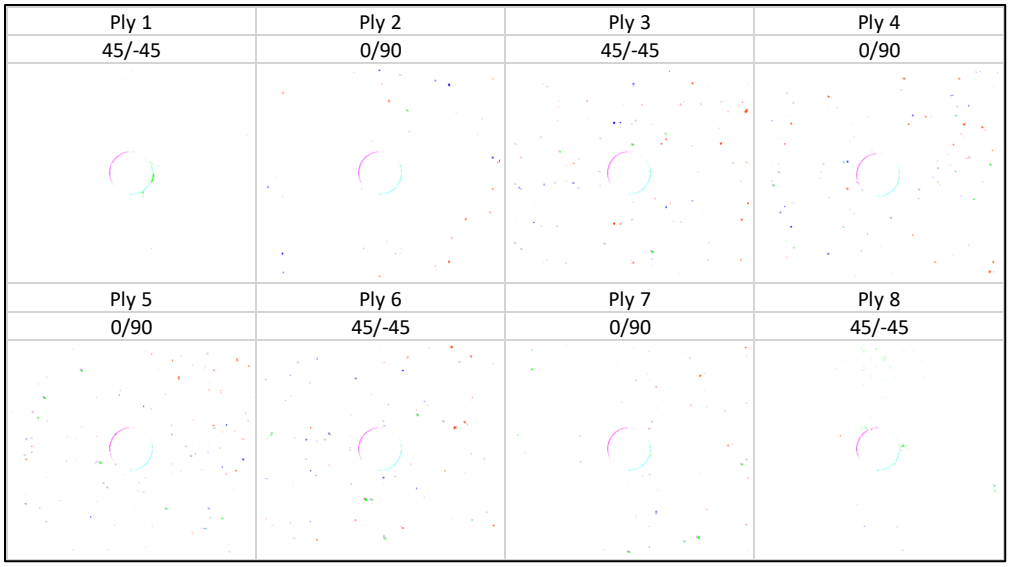


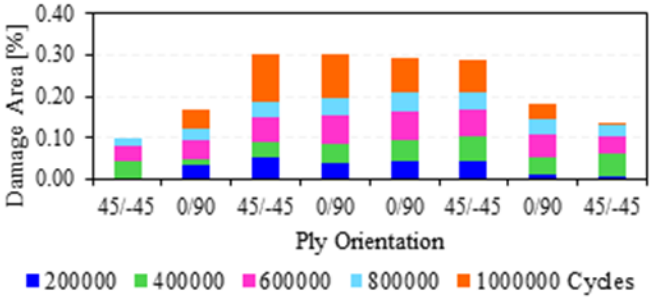


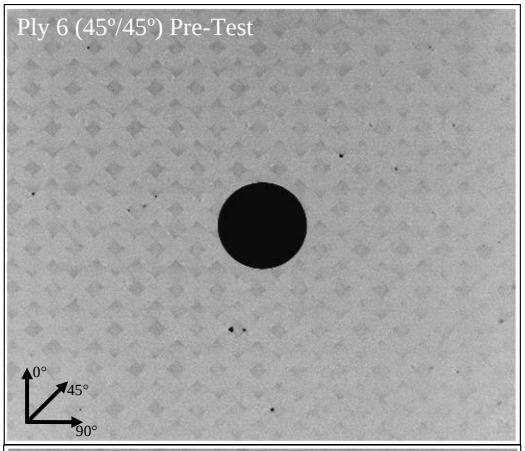
Specimen ID	MASC1-C2EO21-2K2
Test Method	OHT-T
Material System	T650 5320-1 8HS
Ply Layup	25/50/25
Number of Plies	8
Stress Ratio	0.1
% Stress	80% of Ultimate Stress
Final Cycles	1,000,000 (runout)
1) Increased frequency and size of porosities throughout the specimen.	

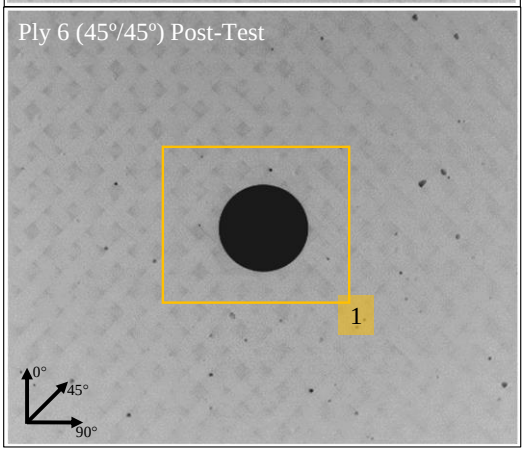
Figure B.62 – Ply-by-ply damage growth and area increase for T650/5320-1, 25/50/25, R=0.1, SL2.

DISTRIBUTION STATEMENT A.
Approved for public release: distribution is unlimited.









Specimen ID	MASC1-C3EO11-XX1
Test Method	OHT-T
Material System	T650 5320-1 8HS
Ply Layup	25/50/25
Number of Plies	8
Stress Ratio	0.1
% Stress	90% of Ultimate Stress
Final Cycles	1,000,000 (runout)
1) Minor delamination extending radially from the hole in all directions.	
Comments) Increased frequency and size of porosities throughout the specimen.	

Figure B.63 – Ply-by-ply damage growth and area increase for T650/5320-1, 25/50/25, R=0.1, SL3.

DISTRIBUTION STATEMENT A.
Approved for public release: distribution is unlimited.

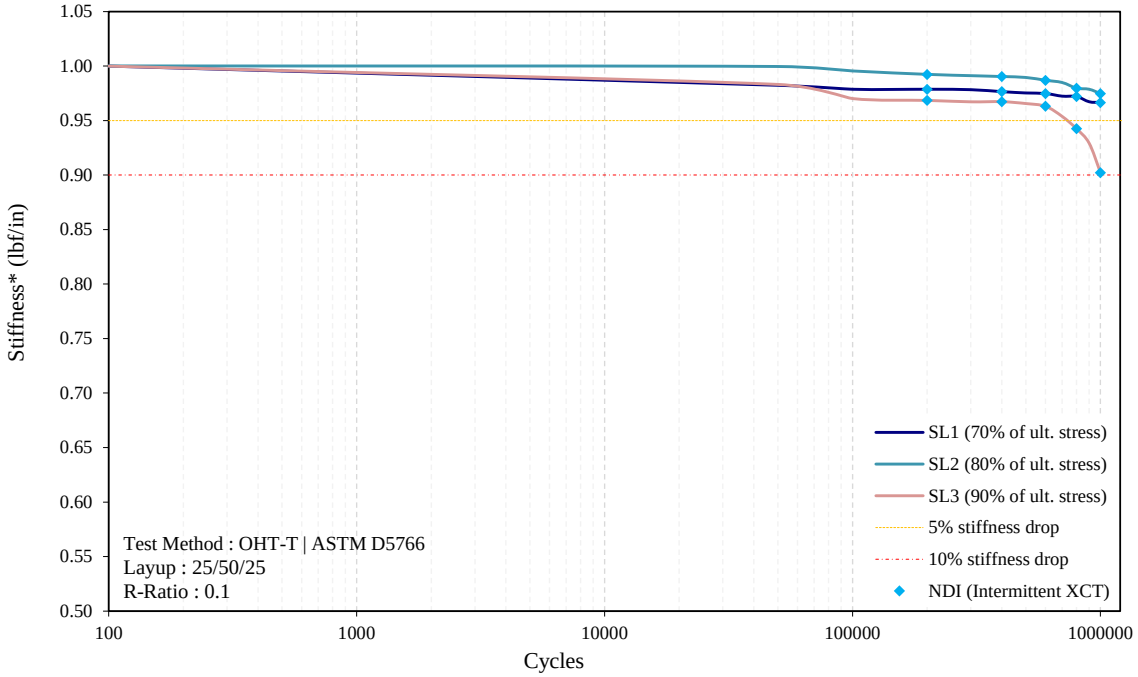
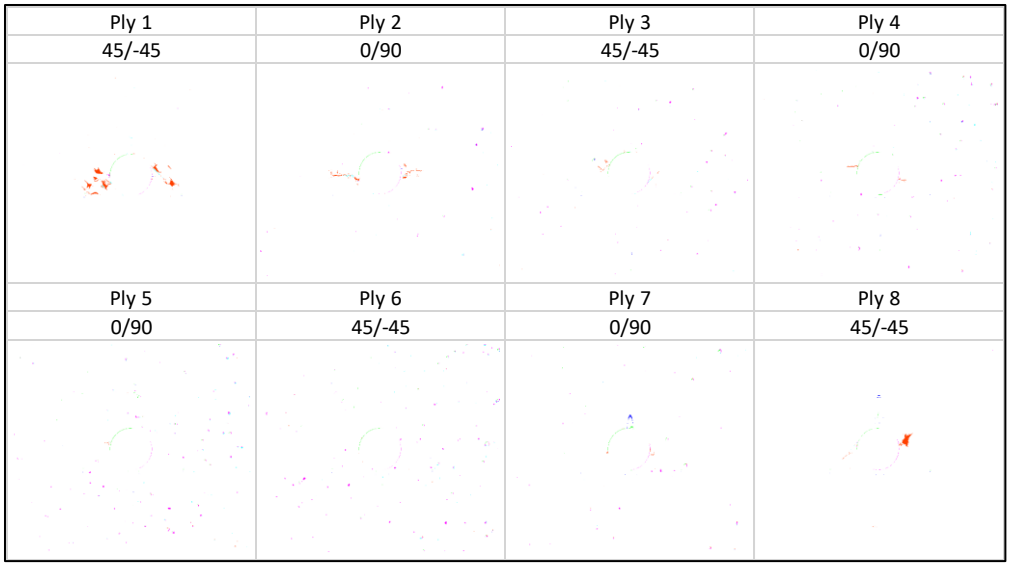
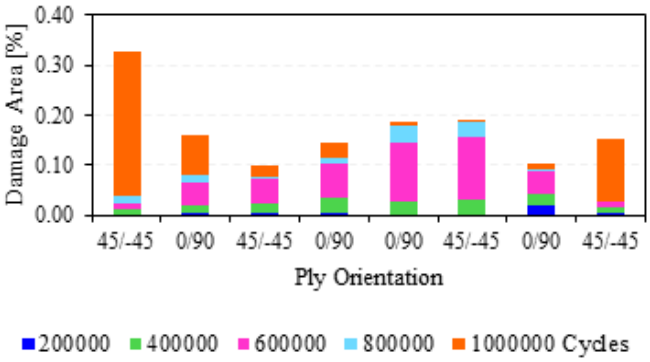
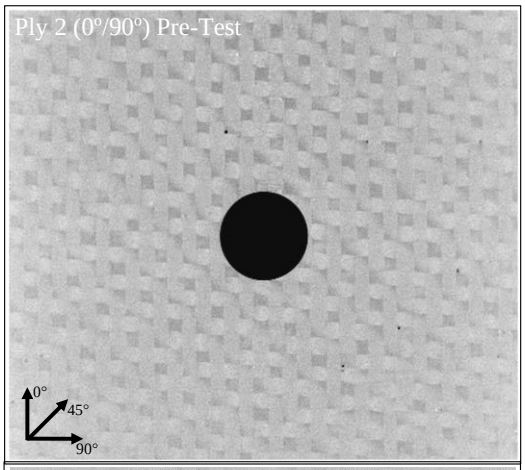


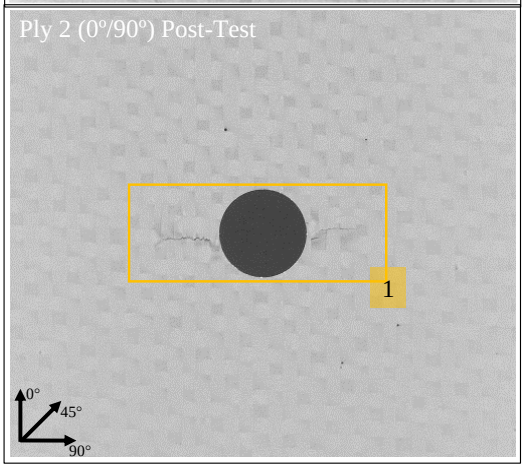
Figure B.64 – Apparent stiffness change during fatigue (normalized by initial compliance) for T650/5320-1 8HS, 25/50/25 layup, OH, R=0.1.

DISTRIBUTION STATEMENT A.
Approved for public release: distribution is unlimited.





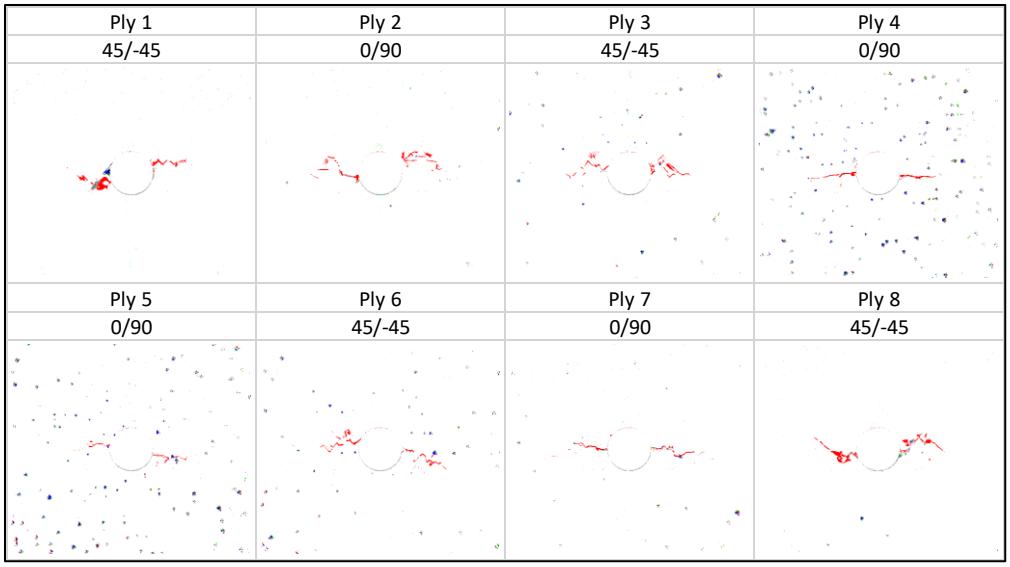


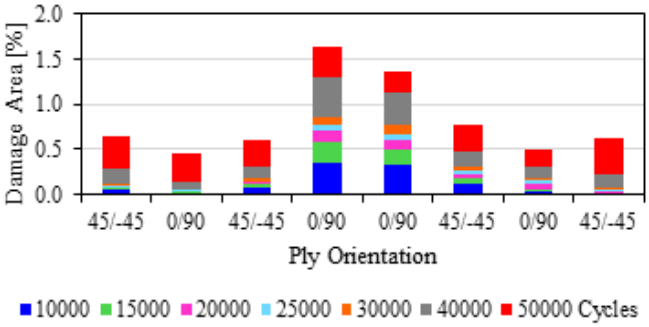


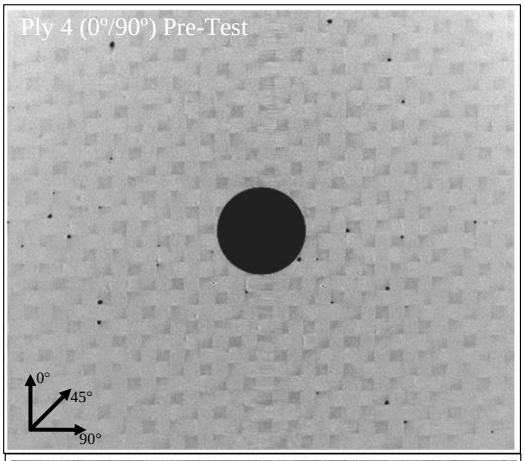
Specimen ID	MASC1-C1EO11-XX2
Test Method	OHC-C
Material System	T650 5320-1 8HS
Ply Layup	25/50/25
Number of Plies	8
Stress Ratio	5.0
% Stress	60% of Ultimate Stress
Final Cycles	1,000,000 (runout)
1)Fiber failure extending from the hole in both directions along the 90º direction.	

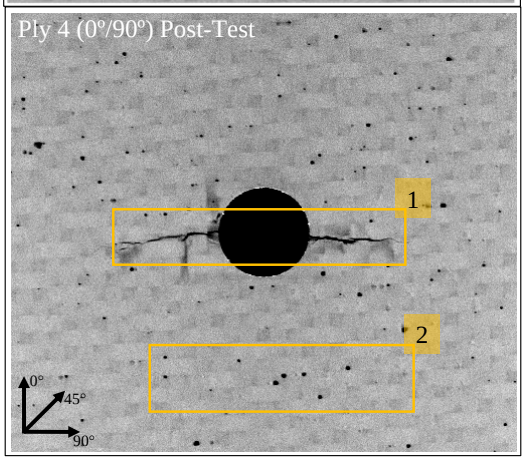
Figure B.65 – Ply-by-ply damage growth and area increase for T650/5320-1, 25/50/25, R=5, SL1.

DISTRIBUTION STATEMENT A.
Approved for public release: distribution is unlimited.





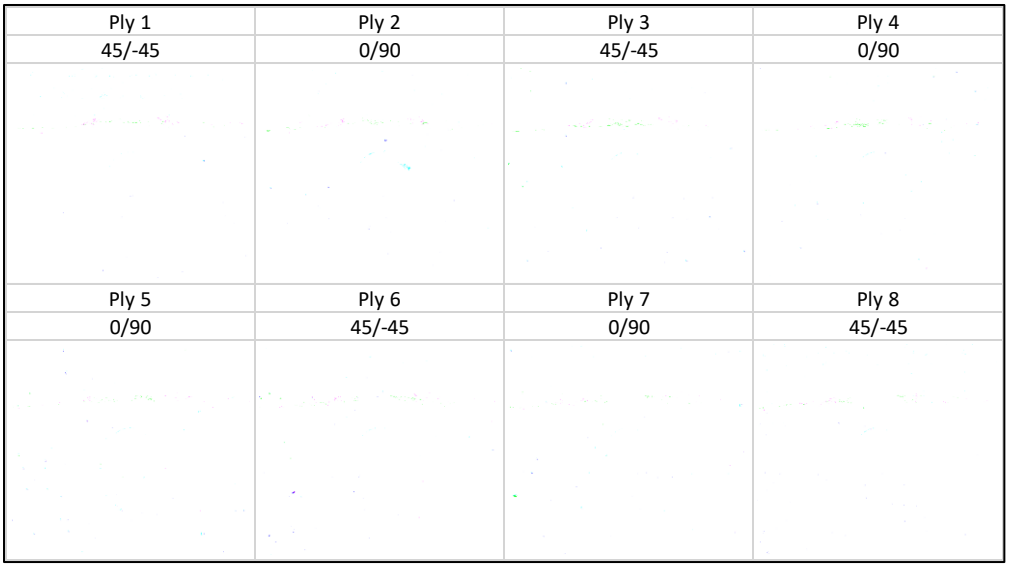


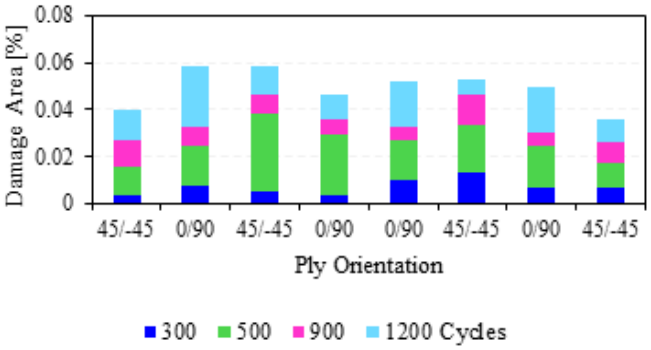


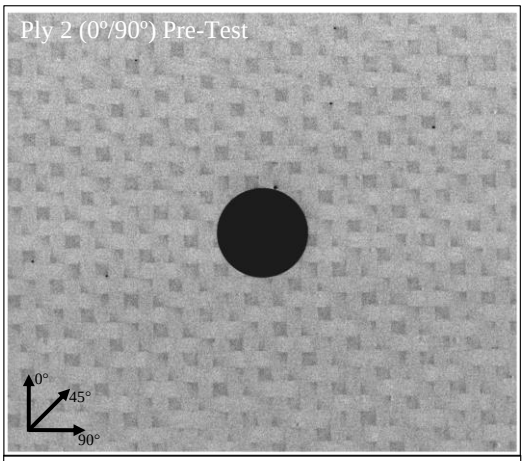
Specimen ID	MASC1-C2EO21-XX3
Test Method	OHC-C
Material System	T650 5320-1 8HS
Ply Layup	25/50/25
Number of Plies	8
Stress Ratio	5.0
% Stress	70% of Ultimate Stress
Final Cycles	50,717
1)Fiber failure extending from the hole in both directions along the 90º direction.	
2) Increased frequency and size of porosities throughout the specimen.	

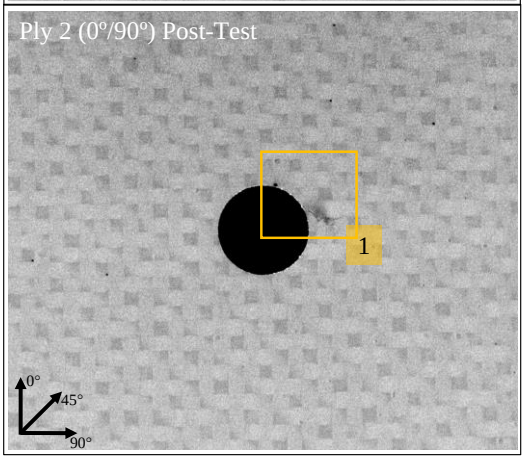
Figure B.66 – Ply-by-ply damage growth and area increase for T650/5320-1, 25/50/25, R=5, SL2.

DISTRIBUTION STATEMENT A.
Approved for public release: distribution is unlimited.









Specimen ID	MASC1-C3EO11-XX5
Test Method	OHC-C
Material System	T650 5320-1 8HS
Ply Layup	25/50/25
Number of Plies	8
Stress Ratio	5.0
% Stress	80% of Ultimate Stress
Final Cycles	1,495
1) Delamination and fiber failure near the hole extending horizontally.	

Figure B.67 – Ply-by-ply damage growth and area increase for T650/5320-1, 25/50/25, R=5, SL3.

DISTRIBUTION STATEMENT A.
Approved for public release: distribution is unlimited.

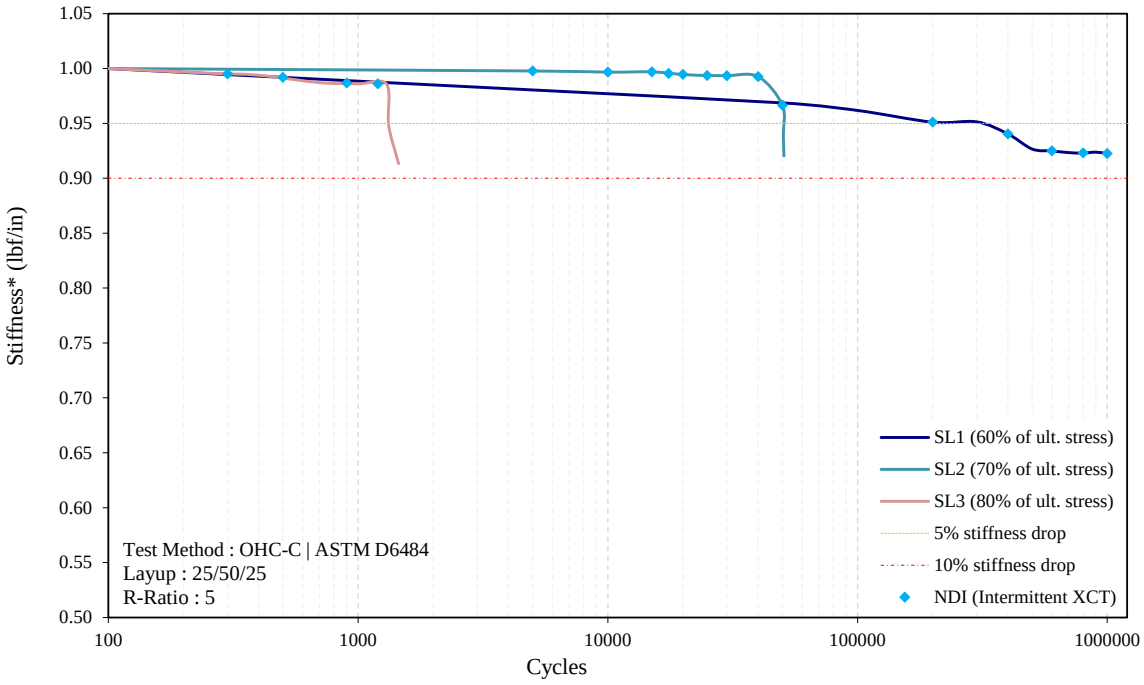
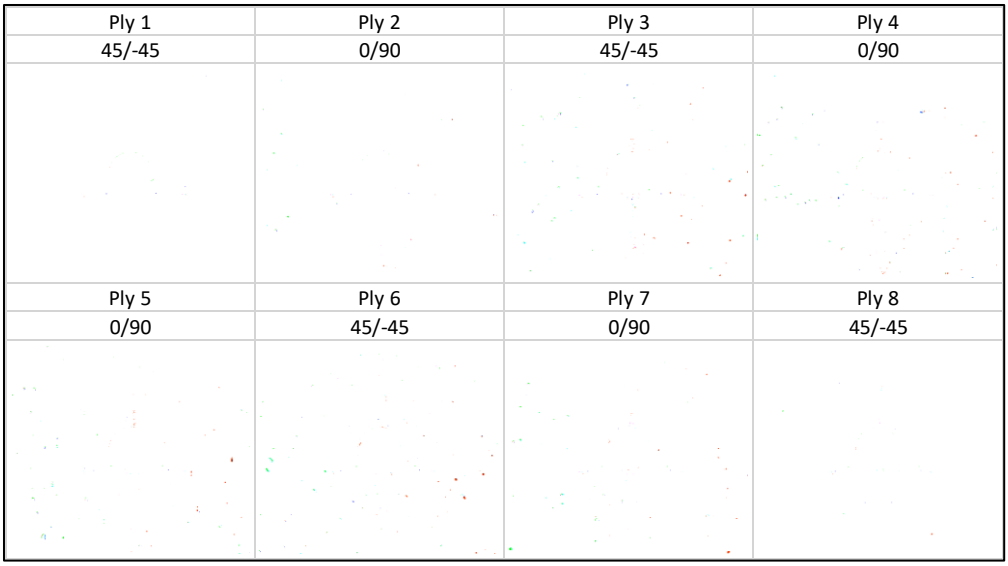
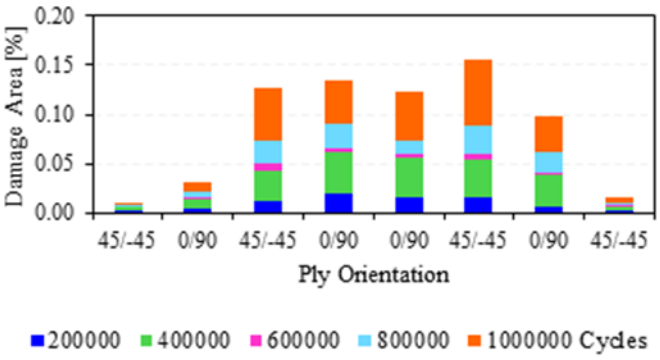
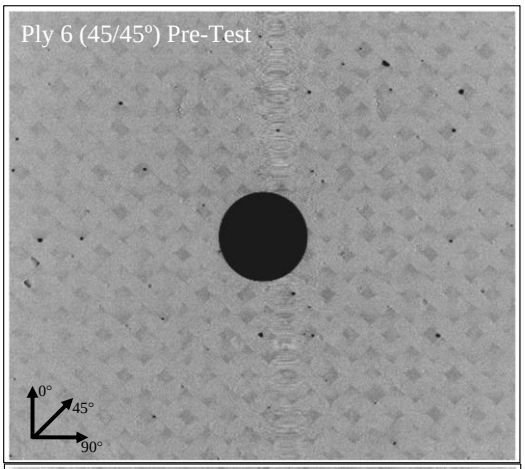


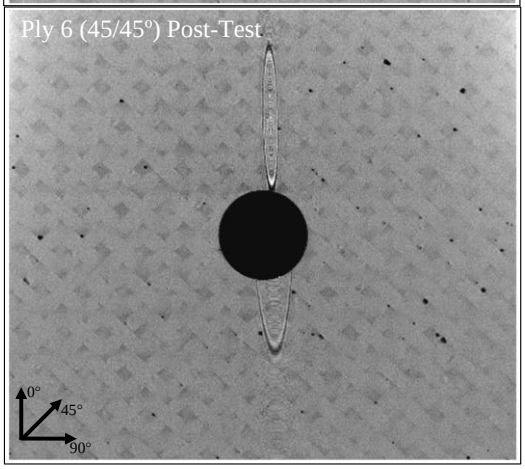
Figure B.68 – Apparent stiffness change during fatigue (normalized by initial compliance) for T650/5320-1 8HS, 25/50/25 layup, OHC-C, R=5.

DISTRIBUTION STATEMENT A.
Approved for public release: distribution is unlimited.





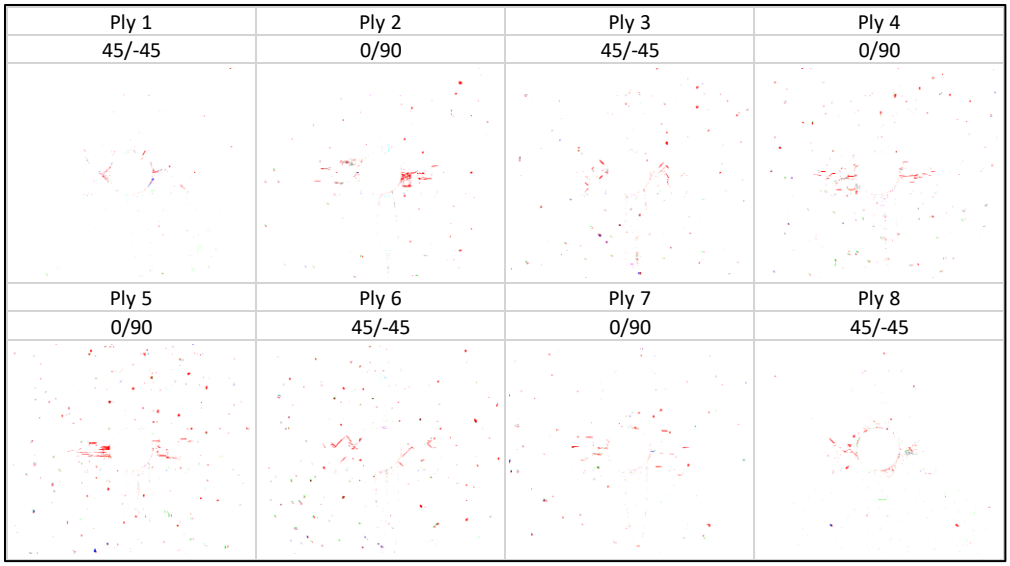


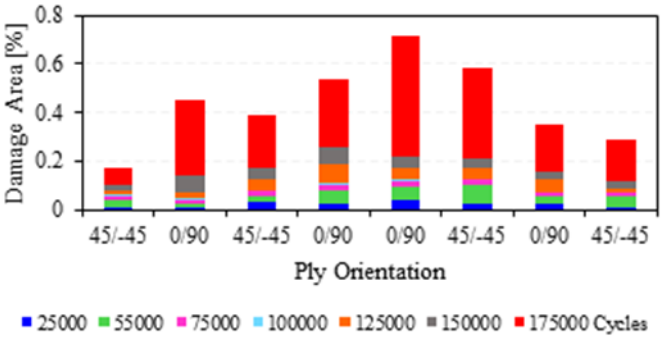


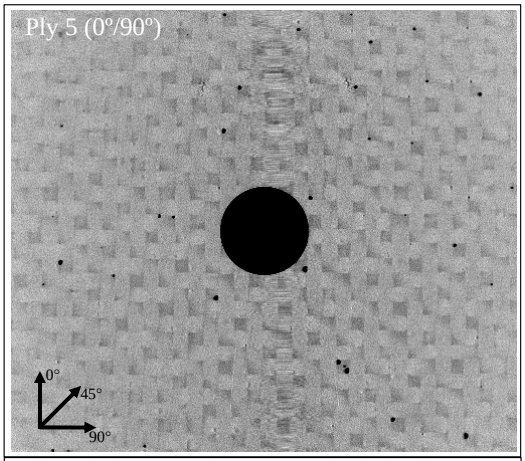
Specimen ID	MASC1-C1EO11-1M2
Test Method	OHC-T
Material System	T650 5320-1 8HS
Ply Layup	25/50/25
Number of Plies	8
Stress Ratio	-1.0
% Stress	40% of Ultimate Stress
Final Cycles	1,000,000 (runout)
Comments) Minor changes to porosities throughout the specimen.	

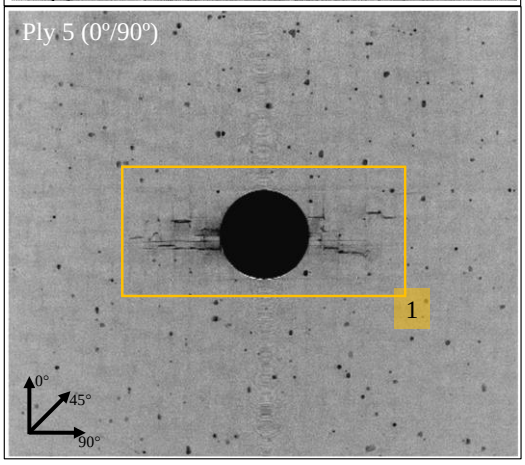
Figure B.69 – Ply-by-ply damage growth and area increase for T650/5320-1, 25/50/25, R=-1, SL1.

DISTRIBUTION STATEMENT A.
Approved for public release: distribution is unlimited.





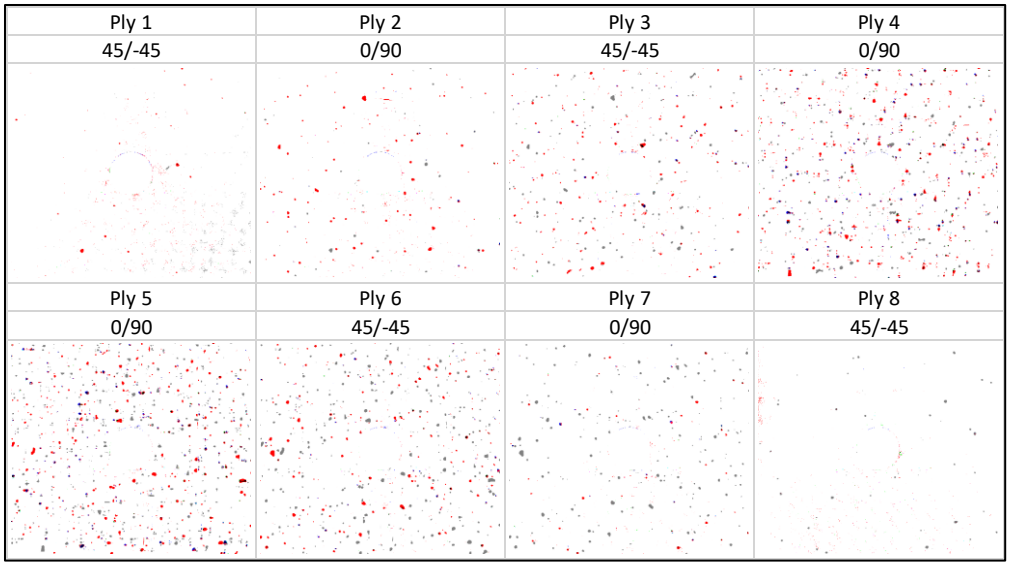


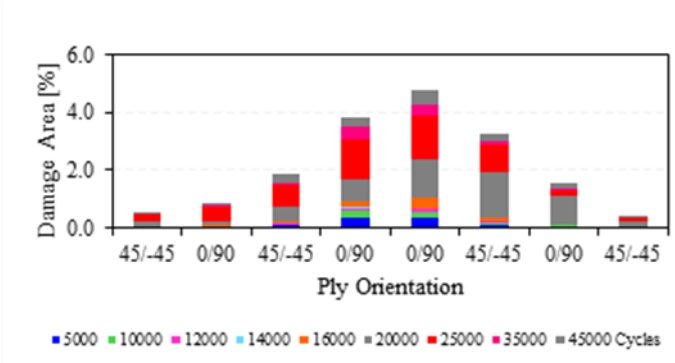


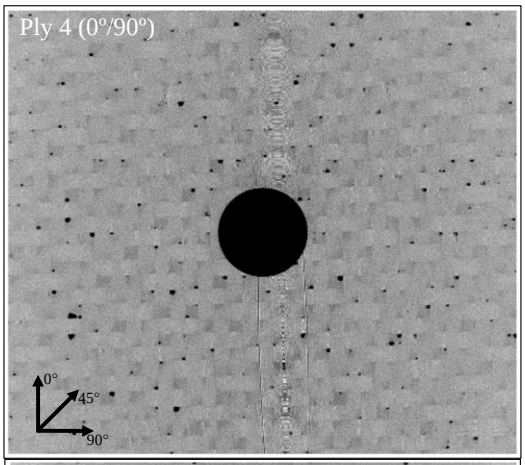
Specimen ID	MASC1-C3EO11-3M2
Test Method	OHC-T
Material System	T650 5320-1 8HS
Ply Layup	25/50/25
Number of Plies	8
Stress Ratio	-1.0
% Stress	55% of Ultimate Stress
Final Cycles	184,423
1)Several fiber failures extending from the hole in both directions along the 90º direction.	
Comments) Increased frequency and size of porosities throughout the specimen.	

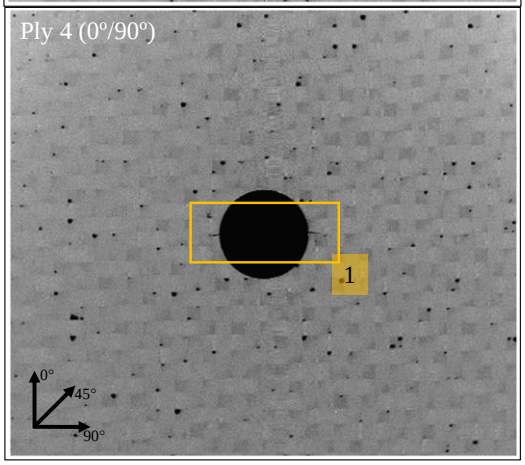
Figure B.70 – Ply-by-ply damage growth and area increase for T650/5320-1, 25/50/25, R=-1, SL2.

DISTRIBUTION STATEMENT A.
Approved for public release: distribution is unlimited.









Specimen ID	MASC1-C2EO21-2M2
Test Method	OHC-T
Material System	T650 5320-1 8HS
Ply Layup	25/50/25
Number of Plies	8
Stress Ratio	-1.0
% Stress	60% of Ultimate Stress
Final Cycles	54,218
1)Fiber failure extending from the hole in both directions along the 90° direction.	
Comments) Increased frequency and size of porosities throughout the specimen.	

Figure B.71 – Ply-by-ply damage growth and area increase for T650/5320-1, 25/50/25, R=-1, SL3.

DISTRIBUTION STATEMENT A.
Approved for public release: distribution is unlimited.

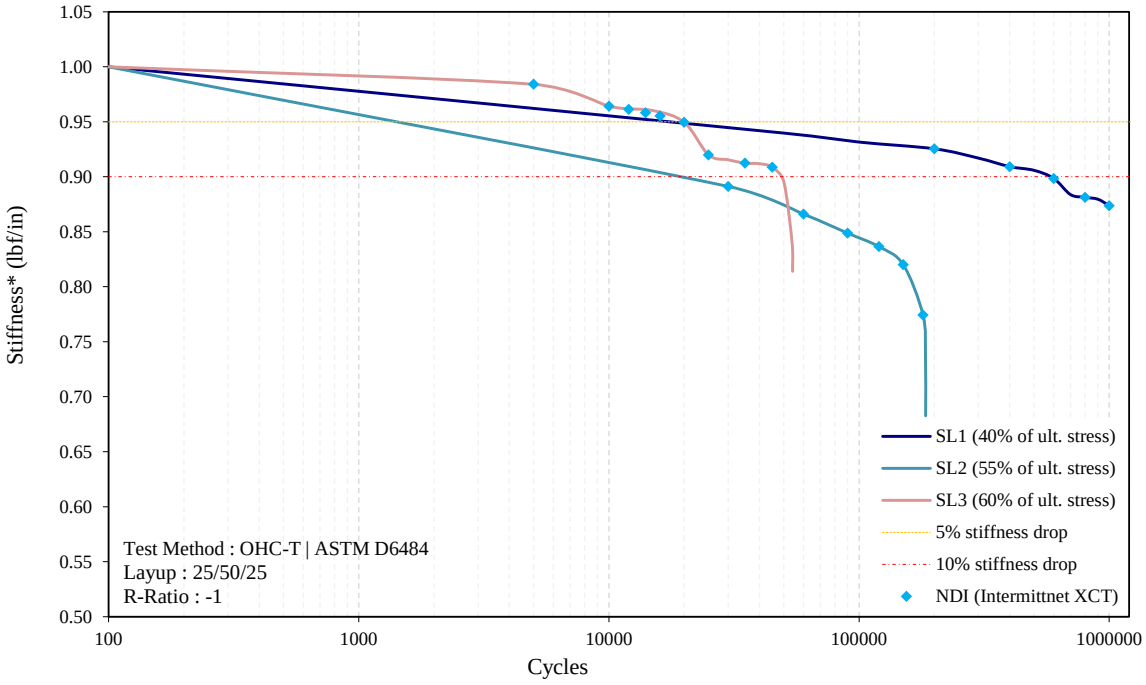


Figure B.72 – Apparent stiffness change during the tension fatigue (normalized by initial compliance) for T650/5320-1 8HS, 25/50/25 layup, OHC-T, R=-1.

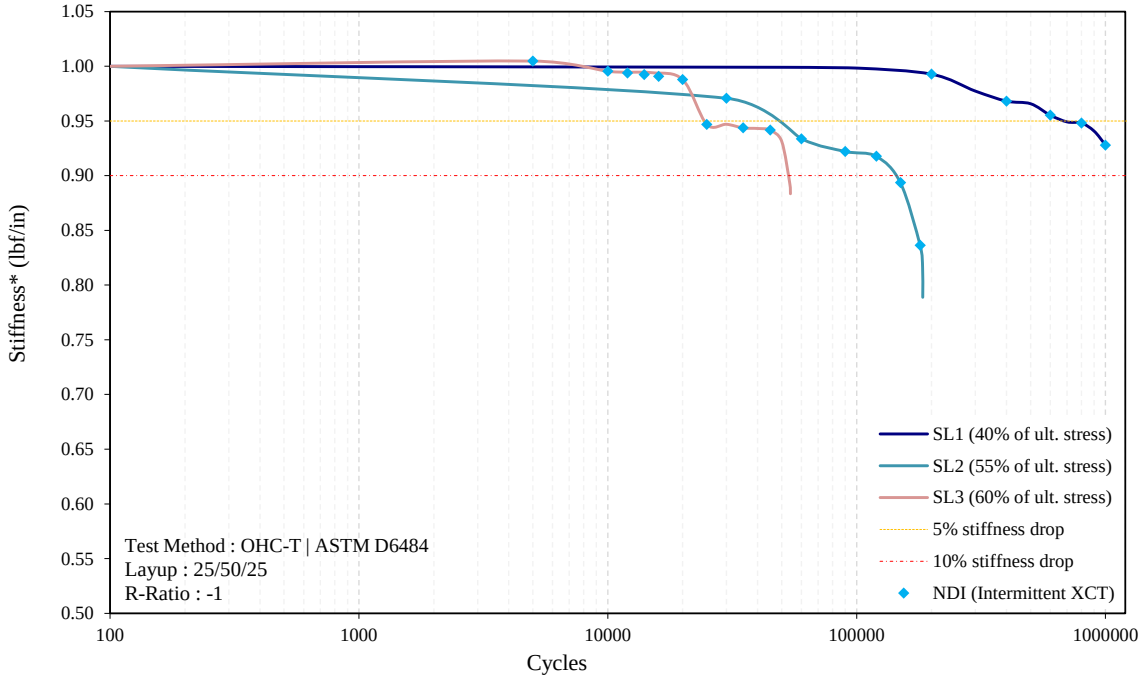


Figure B.73 – Apparent stiffness change during the compression fatigue (normalized by initial compliance) for T650/5320-1 8HS, 25/50/25 layup, OHC-T, R=-1.

DISTRIBUTION STATEMENT A.
Approved for public release: distribution is unlimited.

10/80/10 Open-Hole Test

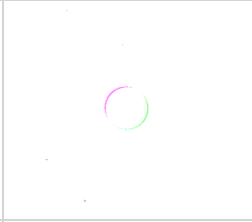
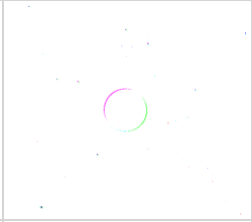
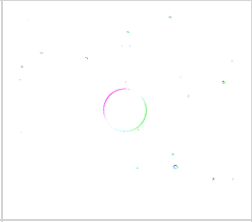
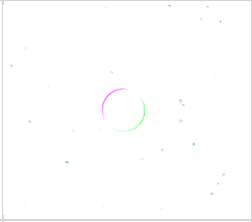
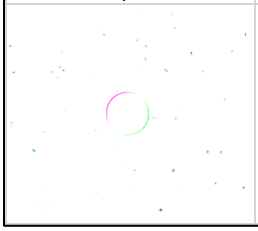
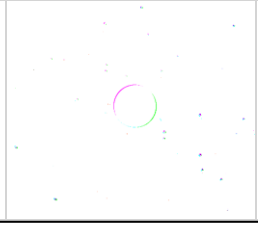
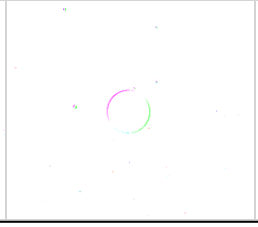
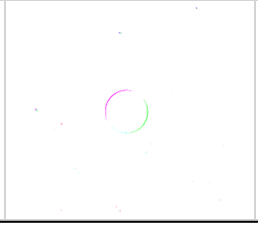
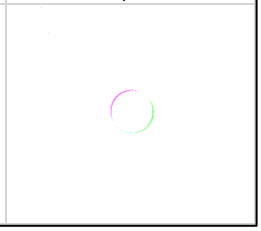
R=0.1, OHT-T → SL-1 (70%), SL-2 (80%), and SL-3 (90%)
R=5.0, OHC-C → Specimens: SL-1 (70%), SL-2 (80%), and SL-3 (90%)
R=-1, OHT-C → Specimens: SL-1 (35%), SL-2 (50%), and SL-3 (60%)

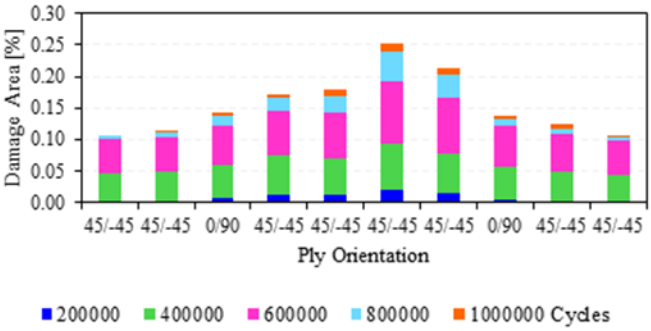
As seen above, three specimens were tested for each r-ratio at varying stress levels. Specimens were fatigued until failure or one-million cycles (runout) was achieved. In R=0.1 only SL-1 survived fatigue and developed a 6% decreased residual strength. SL-1 in this group did not demonstrate any signs of significant damage after fatigue (Figure Figure B.74). SL-2 and SL-3, displayed signs of fiber failure and delamination. SL-2 displayed the largest quantity of delamination near the fiber failures (Figure B.75) and SL-3 primarily displayed minor fiber failures (Figure B.76). In this group the majority of fiber failures were formed directly before failure with the fiber failures and delamination in this group leading to accelerated failure.

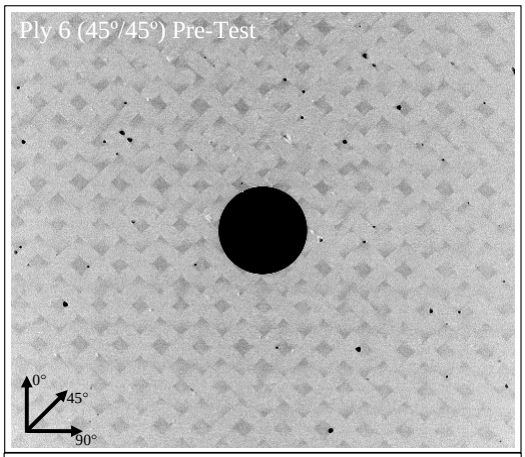
In R=5.0 SL-1 survived fatigue and developed a of 3% decrease in residual strength and displayed minor fiber failure on its 0°/90° plies (Figure B.78). SL-2 and SL-3 displayed fiber failure throughout all their plies directly through the hole in the 0° direction. In SL-2 cracks began propagating in the earliest stages of the fatigue (Figure B.79). In comparison, SL-3 formed the majority of fiber failures directly before the specimen failed (less than 3000 cycles before failure) (Figure Figure B.80). No specimens in this group display significant delamination.

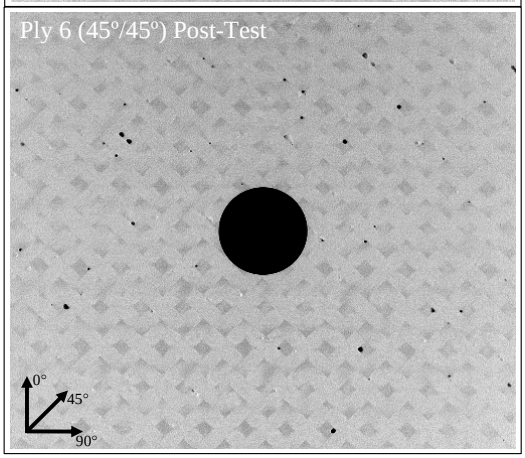
In R=-1 only SL-1 survived fatigue and developed a decrease of 9% in residual strength. After fatigue there was no significant damage visible within SL-1 (Figure B.82). SL-2 and SL-3 exhibited fiber failure and delamination in the region around the hole. In the case of SL-3 (Figure B.84), much more fiber failures were visible near the hole compared to SL-2 (Figure Figure B.83).

DISTRIBUTION STATEMENT A.
Approved for public release: distribution is unlimited.

Ply 1	Ply 2	Ply 3	Ply 4	Ply 5
45/-45	45/-45	0/90	45/-45	45/-45
				
Ply 6	Ply 7	Ply 8	Ply 9	Ply 10
45/-45	45/-45	0/90	45/-45	45/-45
				



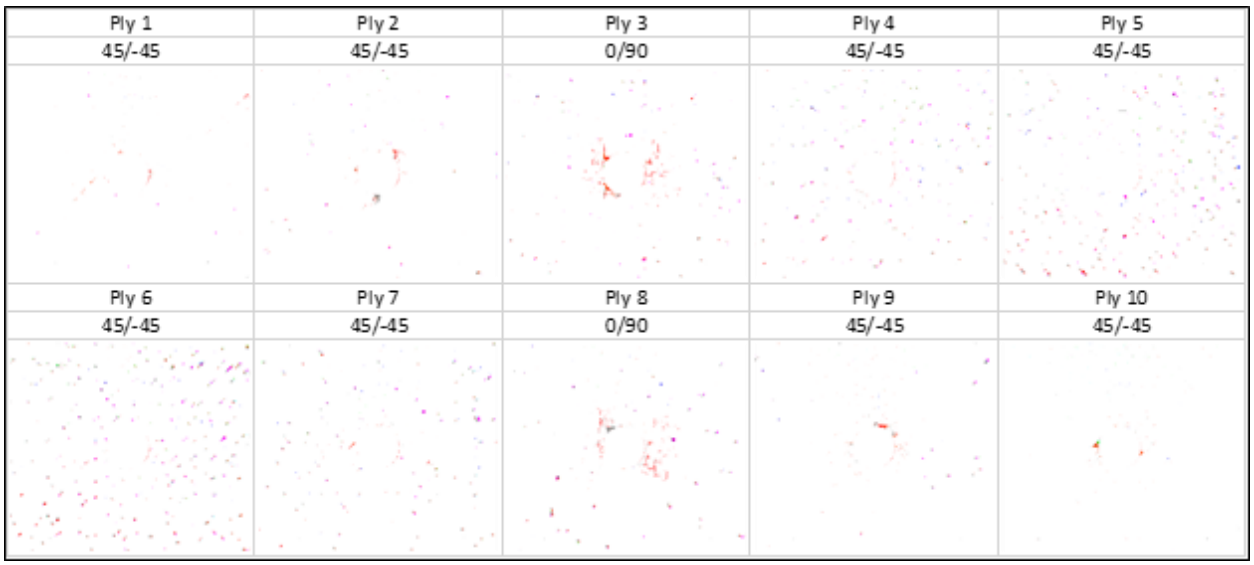


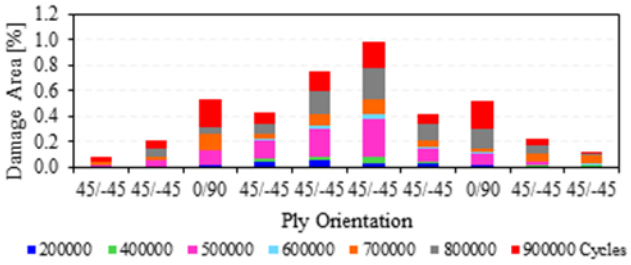


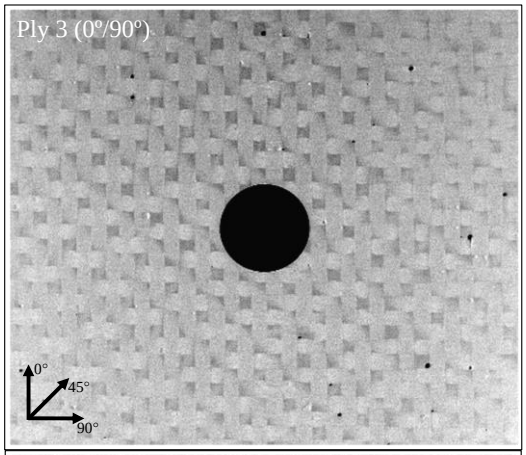
Specimen ID	MASC1-C1FO11-XX2
Test Method	OHT-T
Material System	T650 5320-1 8HS
Ply Layup	10/80/10
Number of Plies	10
Stress Ratio	0.1
% Stress	60% of Ultimate Stress
Final Cycles	1,000,000 (runout)
Comments) Minor changes to porosities throughout the specimen.	

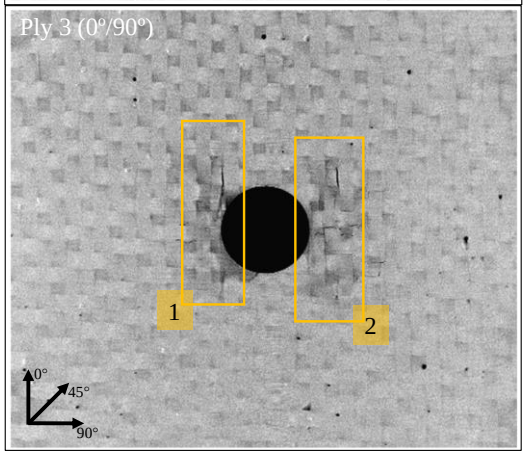
Figure B.74 – Ply-by-ply damage growth and area increase for T650/5320-1, 10/80/10, R=0.1, SL1.

DISTRIBUTION STATEMENT A.
Approved for public release: distribution is unlimited.





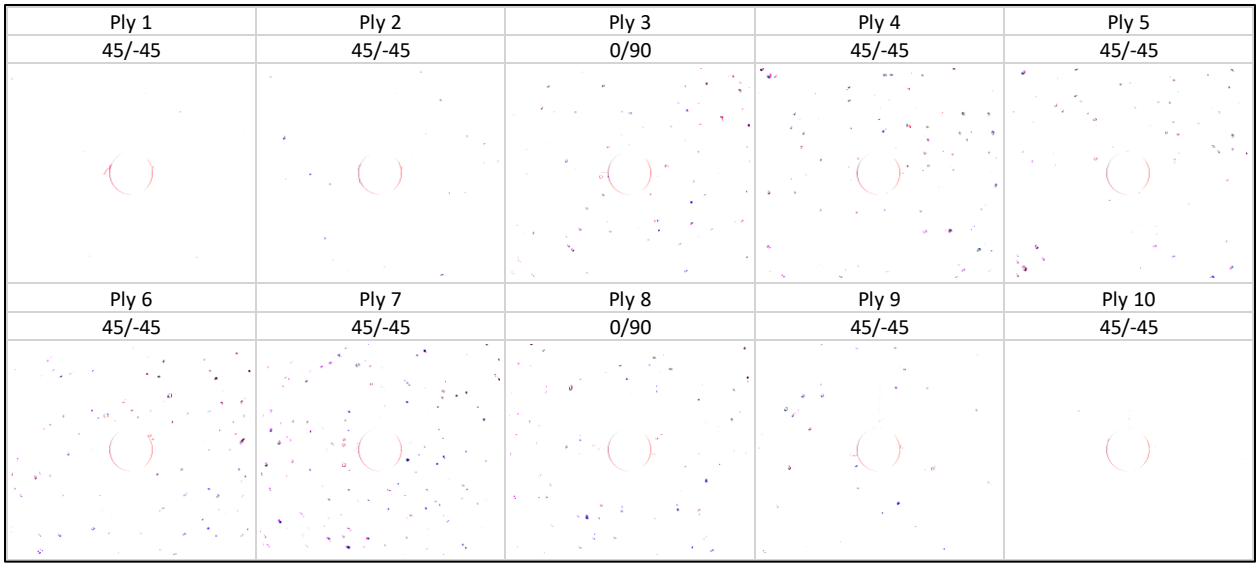


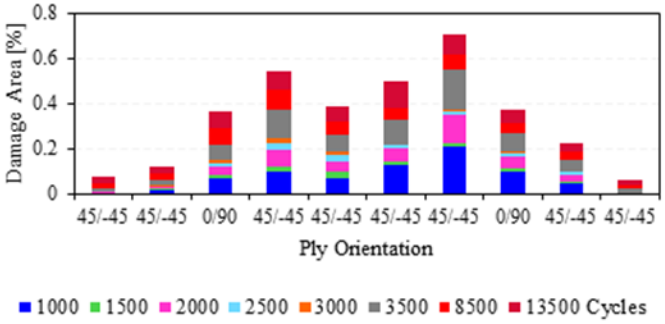


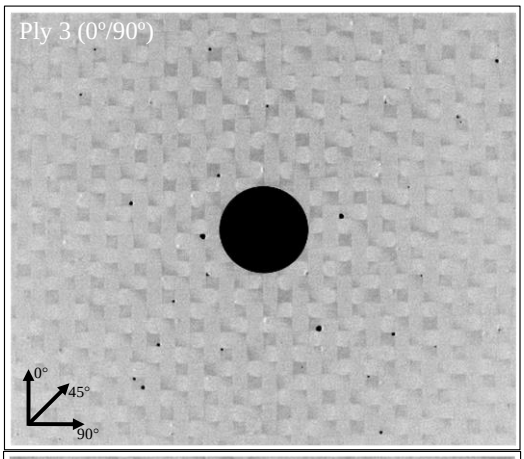
Specimen ID	MASC1-C2FO11-XX2
Test Method	OHT-T
Material System	T650 5320-1 8HS
Ply Layup	10/80/10
Number of Plies	10
Stress Ratio	0.1
% Stress	70% of Ultimate Stress
Final Cycles	902,330
1) Fiber failure extending tangentially from the hole in the 0° direction,	
2) Delamination surrounding fiber failures near the hole.	
Comments) Increased frequency and size of porosities throughout the specimen.	

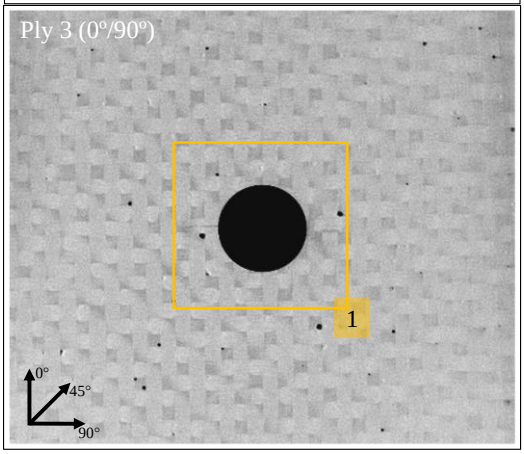
Figure B.75 – Ply-by-ply damage growth and area increase for T650/5320-1, 10/80/10, R=0.1, SL2.

DISTRIBUTION STATEMENT A.
Approved for public release: distribution is unlimited.









Specimen ID	MASC1-C3FO11-XX1
Test Method	OHT-T
Material System	T650 5320-1 8HS
Ply Layup	10/80/10
Number of Plies	10
Stress Ratio	0.1
% Stress	80% of Ultimate Stress
Final Cycles	16,958
1) Minor delamination extending radially from the hole in all directions.	
Comments) Minor changes to porosities throughout the specimen.	

Figure B.76 – Ply-by-ply damage growth and area increase for T650/5320-1, 10/80/10, R=0.1, SL3.

DISTRIBUTION STATEMENT A.
Approved for public release: distribution is unlimited.

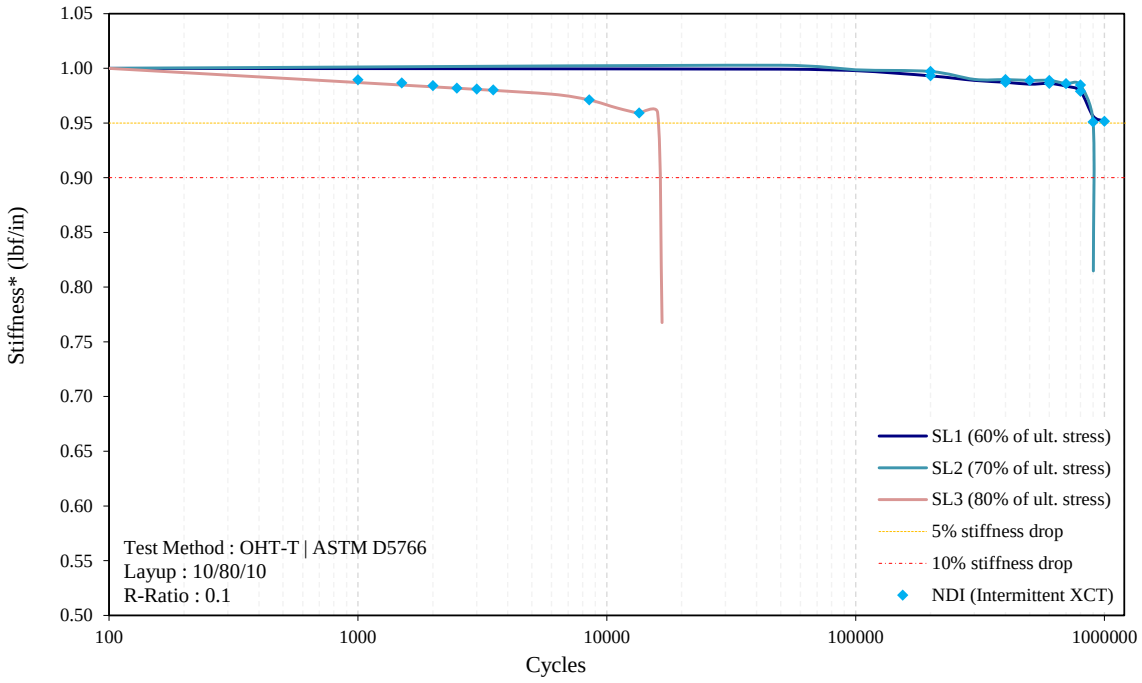
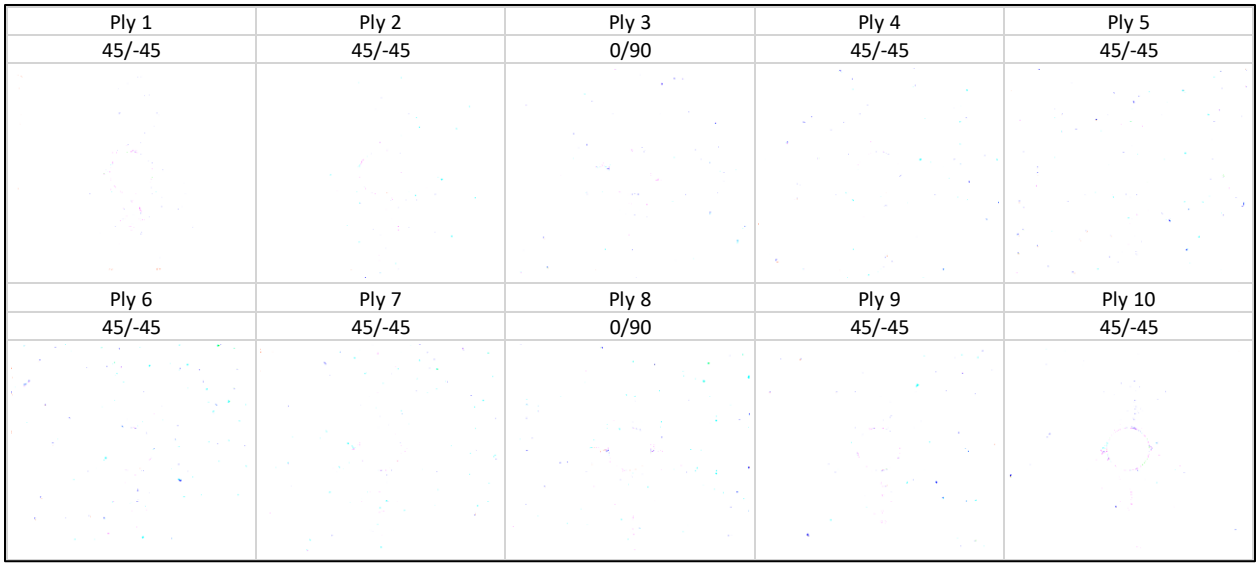
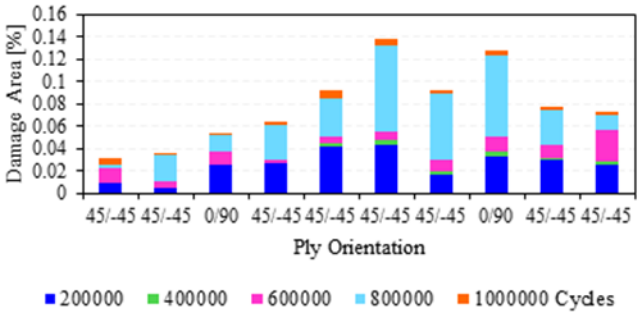
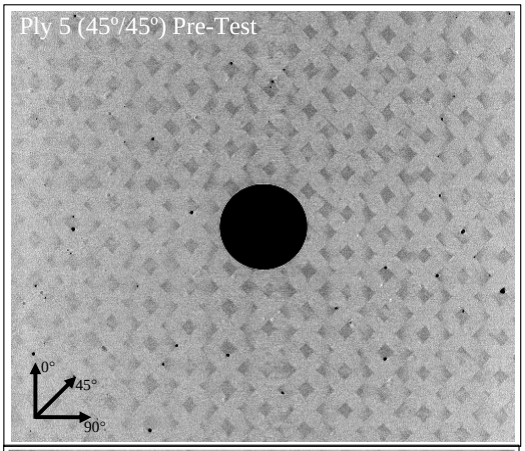


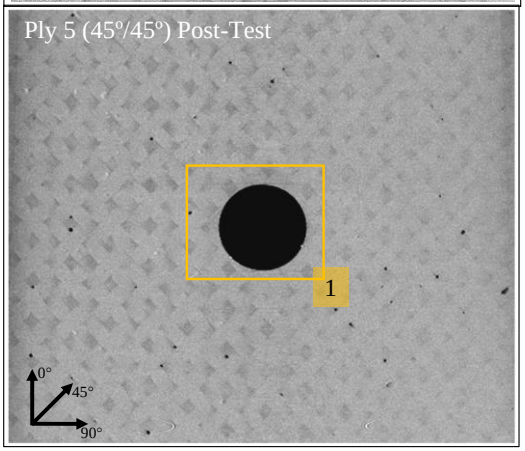
Figure B.77 – Apparent stiffness change during fatigue (normalized by initial compliance) for T650/5320-1 8HS, 10/80/10 layup, OHT-T, R=0.1.

DISTRIBUTION STATEMENT A.
Approved for public release: distribution is unlimited.





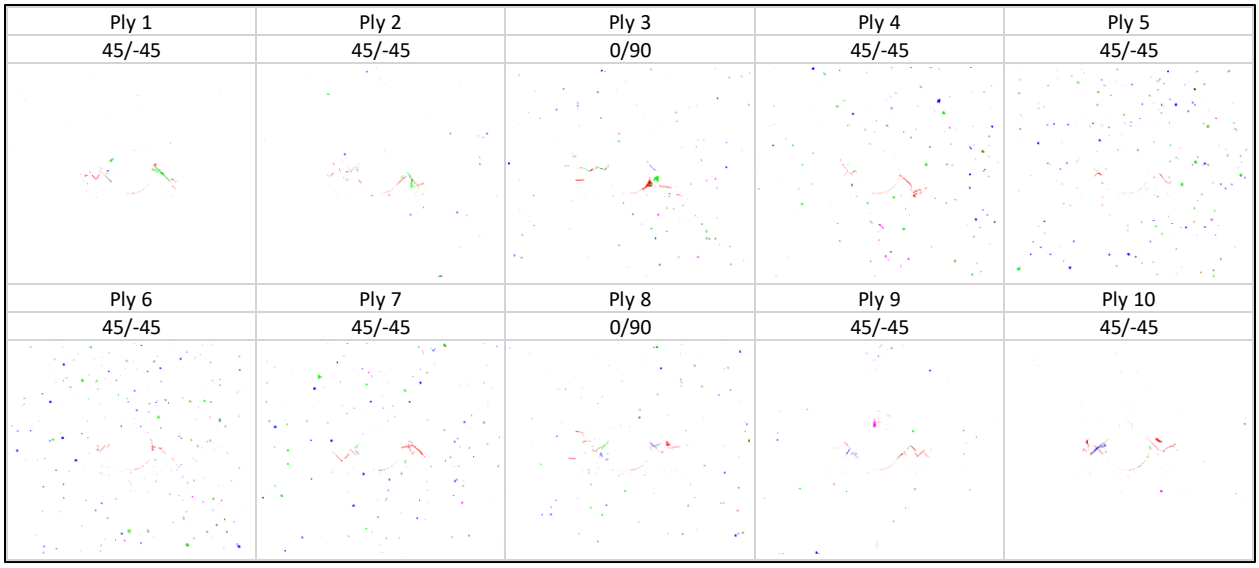


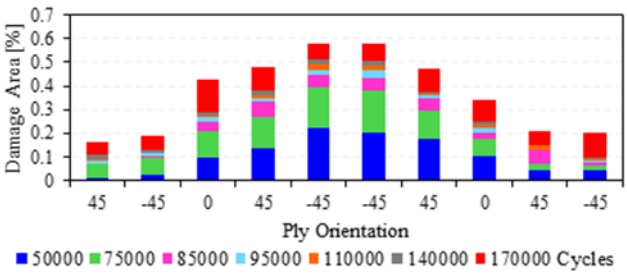


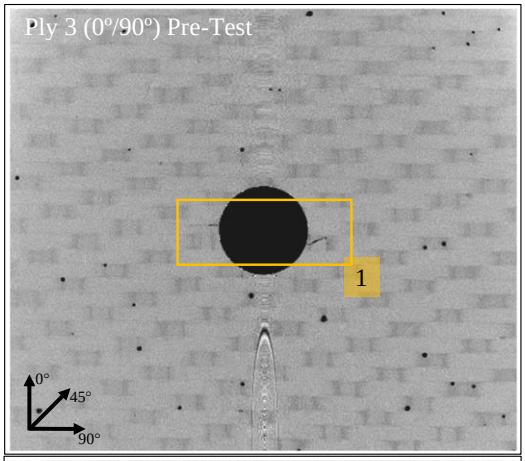
Specimen ID	MASC1-C1FO11-XX3
Test Method	OHC-C
Material System	T650 5320-1 8HS
Ply Layup	10/80/10
Number of Plies	10
Stress Ratio	5.0
% Stress	60% of Ultimate Stress
Final Cycles	1,000,000 (runout)
1) Minor delamination extending radially from the hole in all directions.	
Comments) Increased frequency and size of porosities throughout the specimen.	

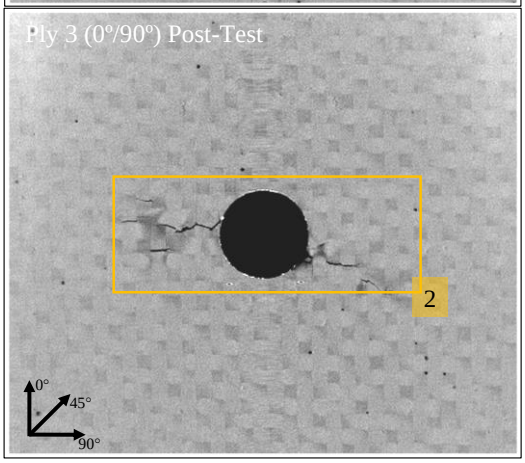
Figure B.78 – Ply-by-ply damage growth and area increase for T650/5320-1, 10/80/10, R=5, SL1.

DISTRIBUTION STATEMENT A.
Approved for public release: distribution is unlimited.





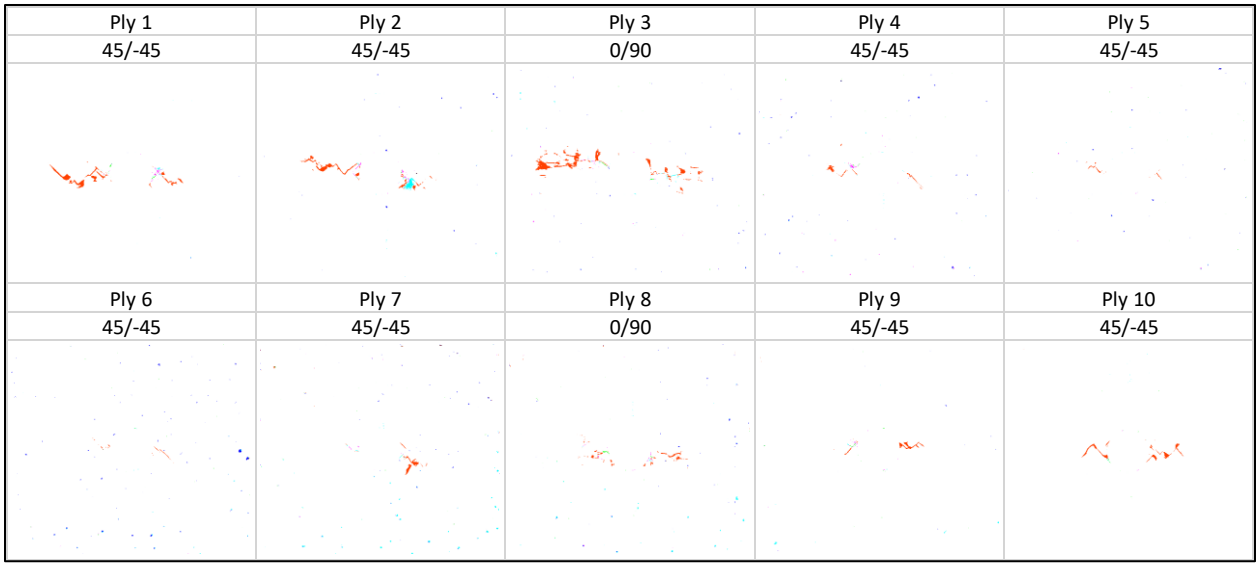


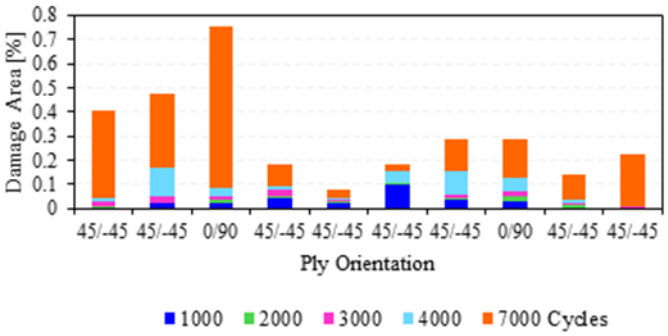


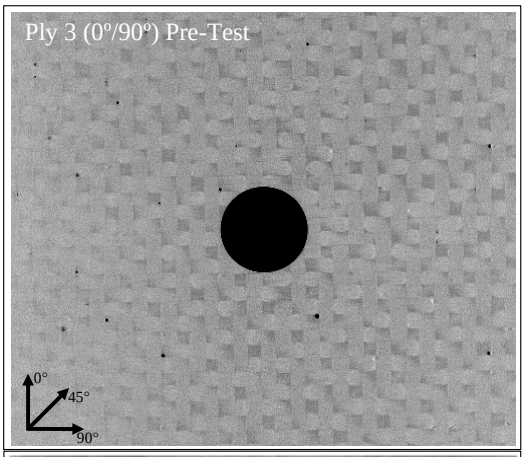
Specimen ID	MASC1-C2FO11-XX4
Test Method	OHC-C
Material System	T650 5320-1 8HS
Ply Layup	10/80/10
Number of Plies	10
Stress Ratio	5.0
% Stress	70% of Ultimate Stress
Final Cycles	189,953
1) Fibers damaged during machining processes extending into fiber failure.	
2) Fiber failure extending from the hole in both directions along the 90° direction.	
Comments) Increased frequency and size of porosities throughout specimen.	

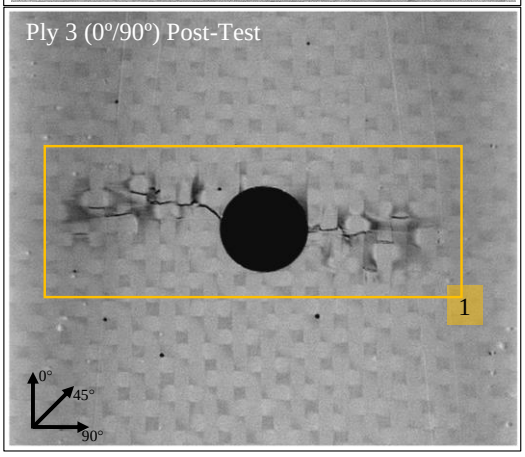
Figure B.79 – Ply-by-ply damage growth and area increase for T650/5320-1, 10/80/10, R=5, SL2.

DISTRIBUTION STATEMENT A.
Approved for public release: distribution is unlimited.









Specimen ID	MASC1-C3FO11-XX2
Test Method	OHC-C
Material System	T650 5320-1 8HS
Ply Layup	10/80/10
Number of Plies	10
Stress Ratio	5.0
% Stress	80% of Ultimate Stress
Final Cycles	7,301
1)Fiber failure extending from the hole in both directions along the 90° direction.	

Figure B.80 – Ply-by-ply damage growth and area increase for T650/5320-1, 10/80/10, R=5, SL3.

DISTRIBUTION STATEMENT A.
Approved for public release: distribution is unlimited.

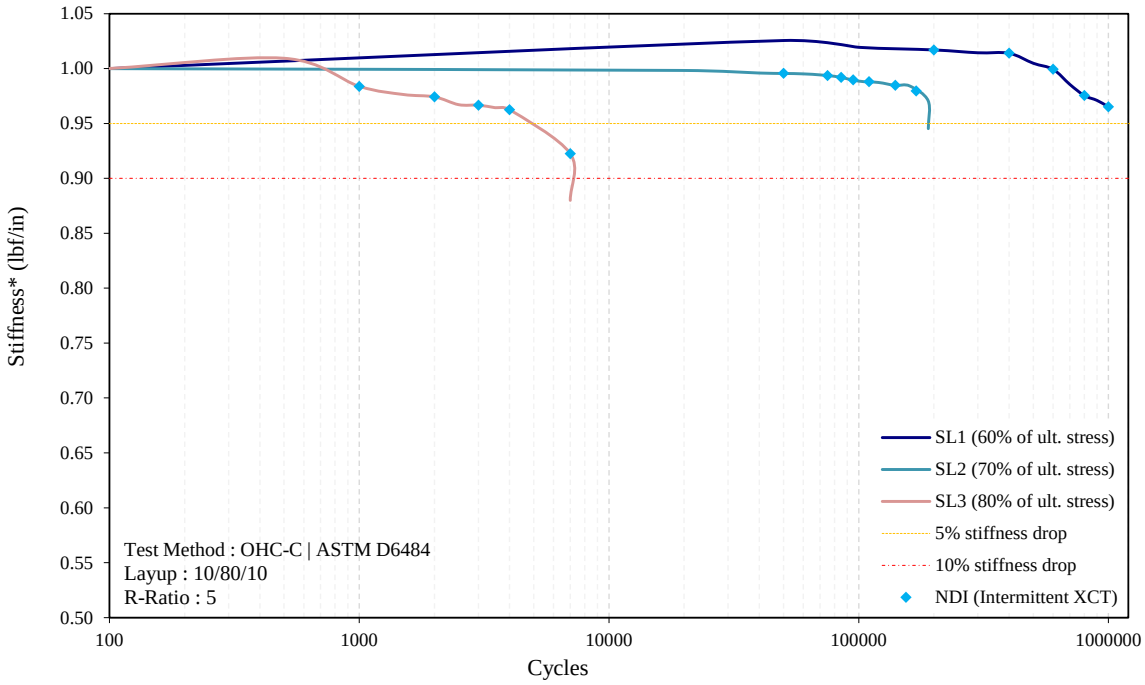
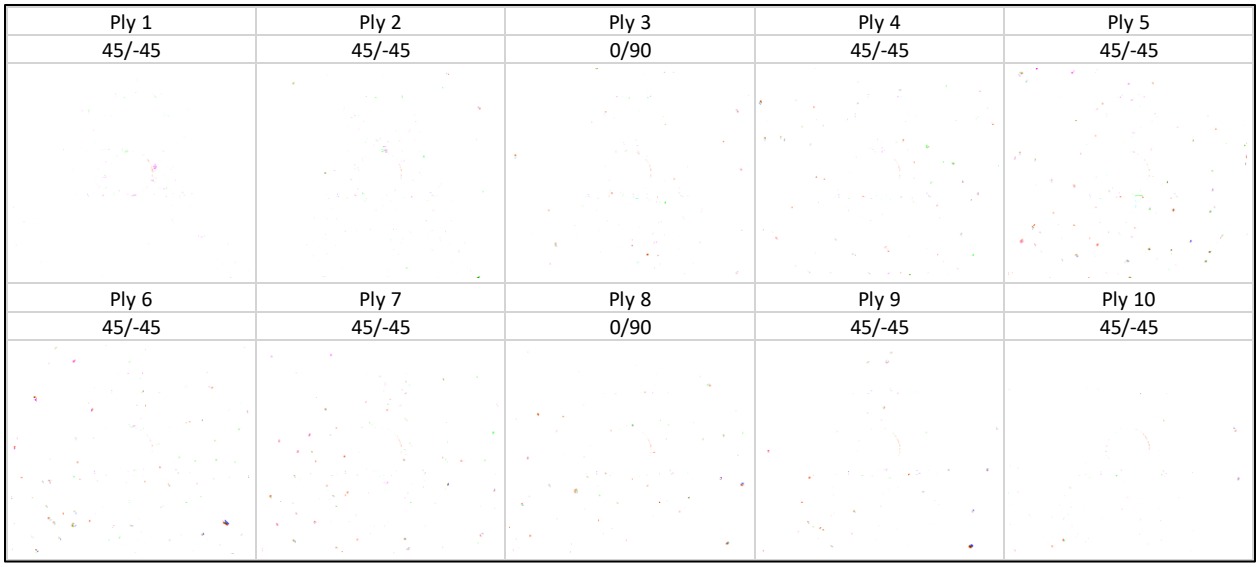
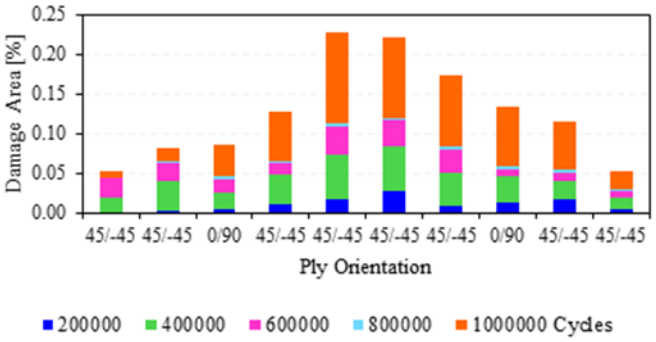
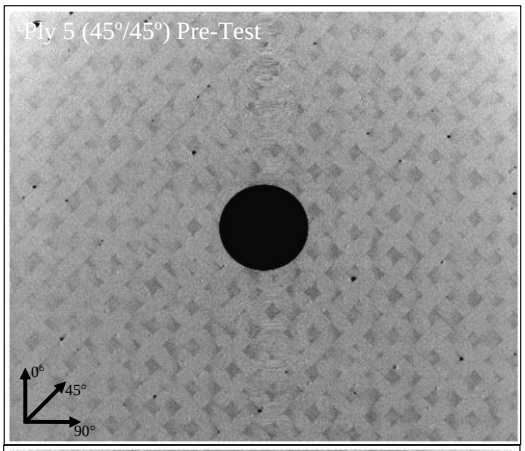


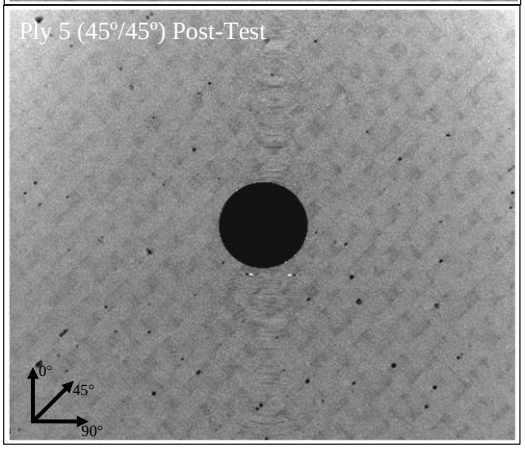
Figure B.81 – Apparent stiffness change during fatigue (normalized by initial compliance) for T650/5320-1 8HS, 10/80/10 layup, OHC-C, R=5.

DISTRIBUTION STATEMENT A.
Approved for public release: distribution is unlimited.





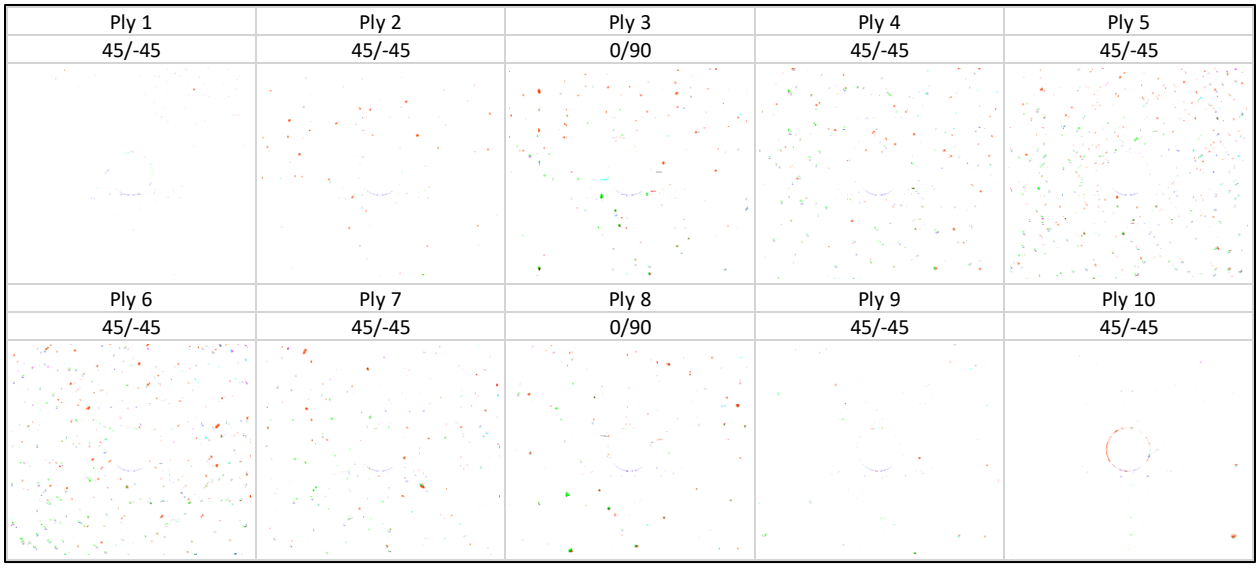


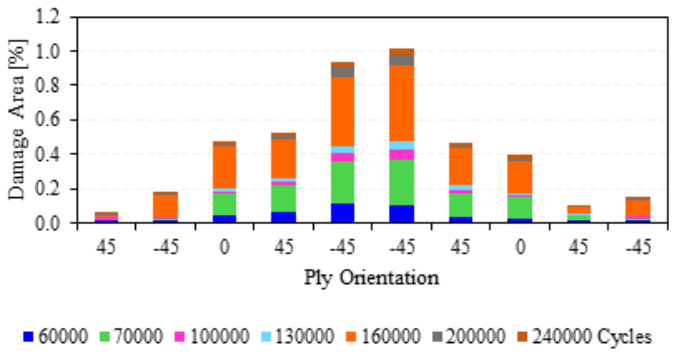


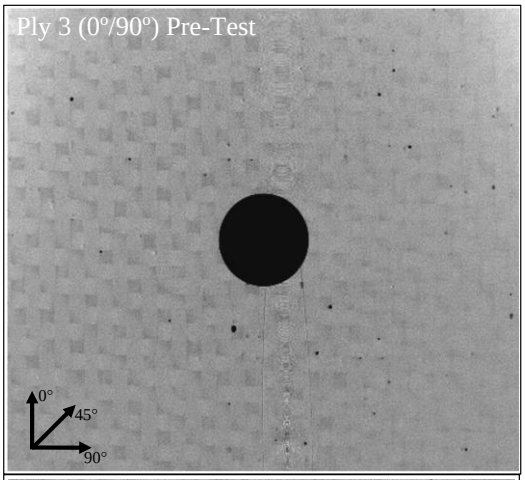
Specimen ID	MASC1-C1FO11-XX4
Test Method	OHC-T
Material System	T650 5320-1 8HS
Ply Layup	10/80/10
Number of Plies	10
Stress Ratio	-1.0
% Stress	35% of Ultimate Stress
Final Cycles	1,000,000 (runout)
Comments) Increased frequency and size of porosities throughout the specimen.	

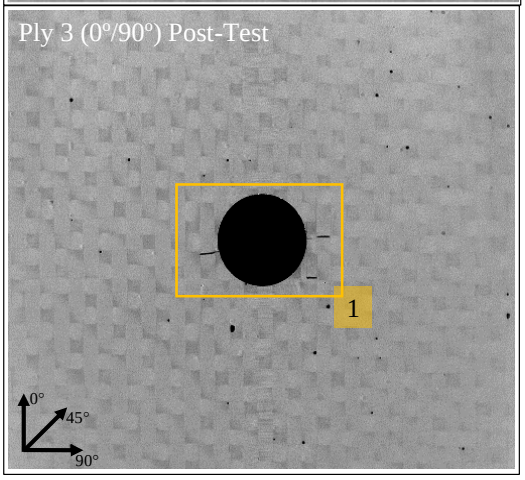
Figure B.82 – Ply-by-ply damage growth and area increase for T650/5320-1, 10/80/10, R=-1, SL1.

DISTRIBUTION STATEMENT A.
Approved for public release: distribution is unlimited.





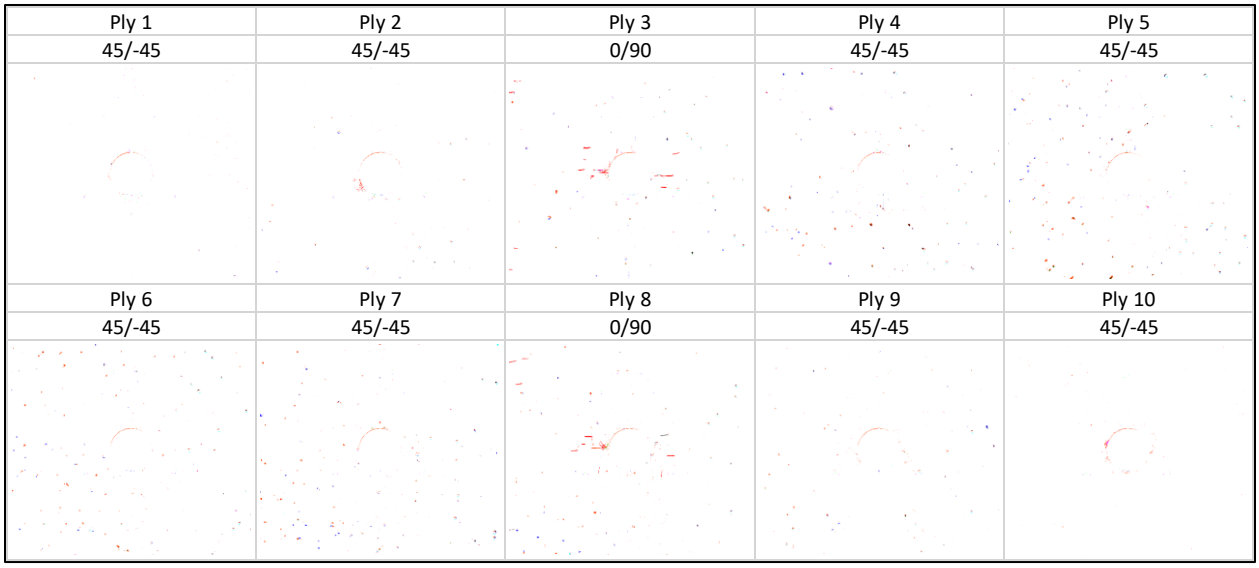


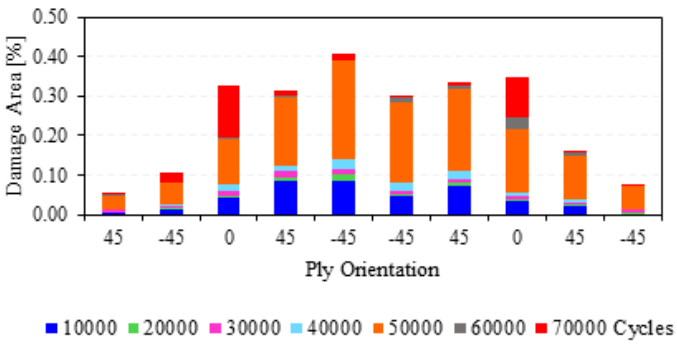


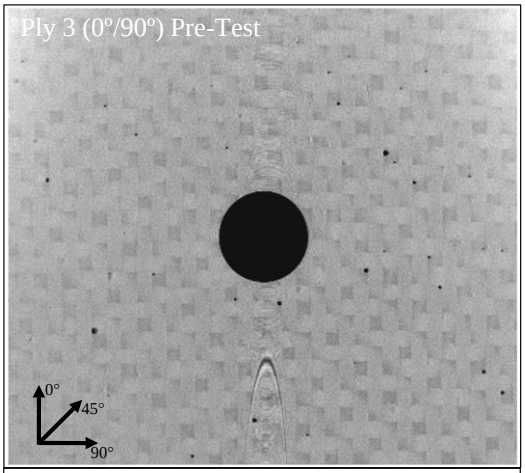
Specimen ID	MASC1-C2FO11-2M1
Test Method	OHC-T
Material System	T650 5320-1 8HS
Ply Layup	10/80/10
Number of Plies	10
Stress Ratio	-1.0
% Stress	45% of Ultimate Stress
Final Cycles	274,246
1)Fiber failure extending from the hole in both directions along the 90º direction.	
Comments) Increased frequency and size of porosities throughout the specimen.	

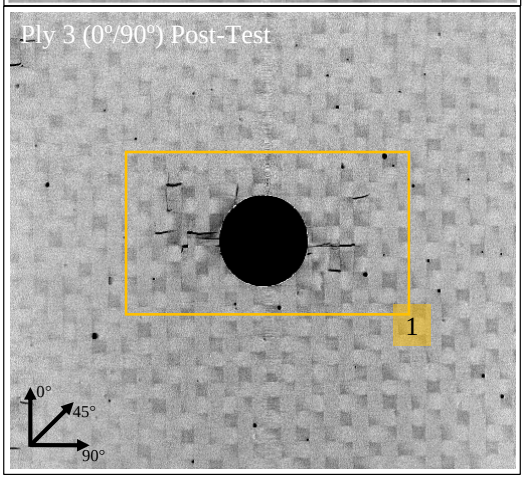
Figure B.83 – Ply-by-ply damage growth and area increase for T650/5320-1, 10/80/10, R=-1, SL2.

DISTRIBUTION STATEMENT A.
Approved for public release: distribution is unlimited.









Specimen ID	MASC1-C3FO11-3M2
Test Method	OHC-T
Material System	T650 5320-1 8HS
Ply Layup	10/80/10
Number of Plies	10
Stress Ratio	-1.0
% Stress	60% of Ultimate Stress
Final Cycles	70,596
1)Several fiber failures extending from the hole in both directions along the 90º direction.	
Comments) Increased frequency and size of porosities throughout the specimen.	

Figure B.84 – Ply-by-ply damage growth and area increase for T650/5320-1, 10/80/10, R=-1, SL3.

DISTRIBUTION STATEMENT A.
Approved for public release: distribution is unlimited.

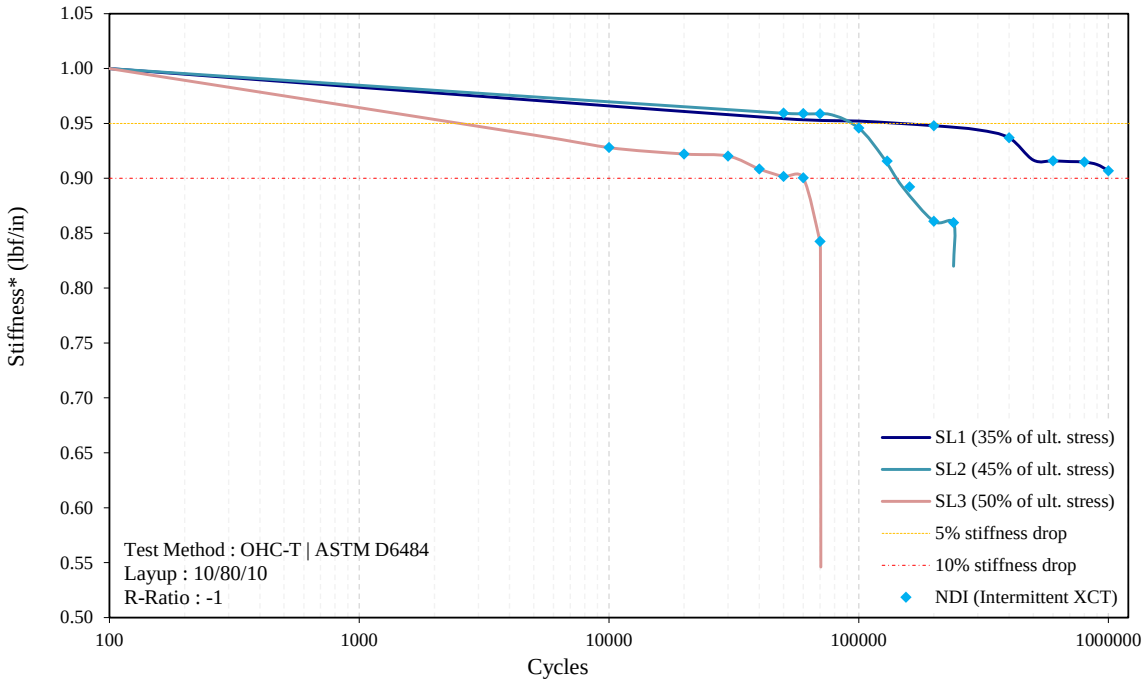


Figure B.85 – Apparent stiffness change during the tension fatigue (normalized by initial compliance) for T650/5320-1 8HS, 10/80/10 layup, OHC-T, R=-1.

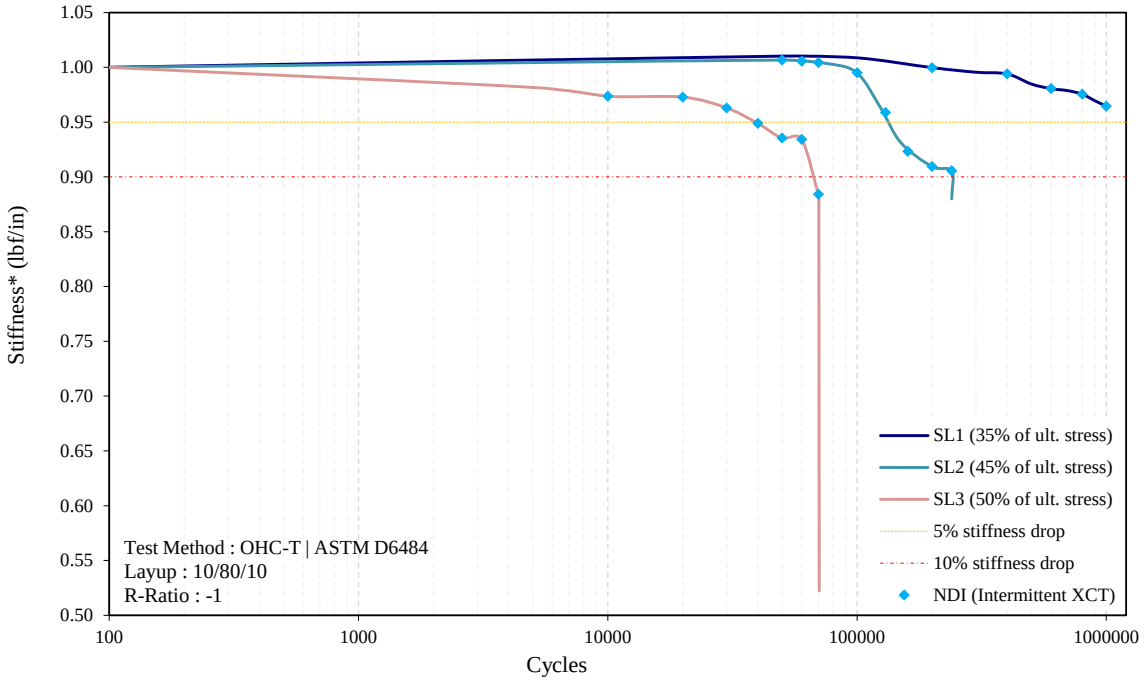


Figure B.86 – Apparent stiffness change during the compression fatigue (normalized by initial compliance) for T650/5320-1 8HS, 10/80/10 layup, OHC-T, R=-1.

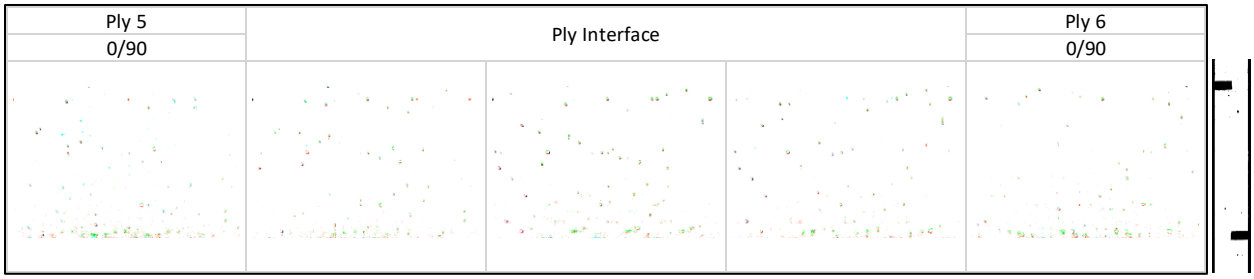
DISTRIBUTION STATEMENT A.
Approved for public release: distribution is unlimited.

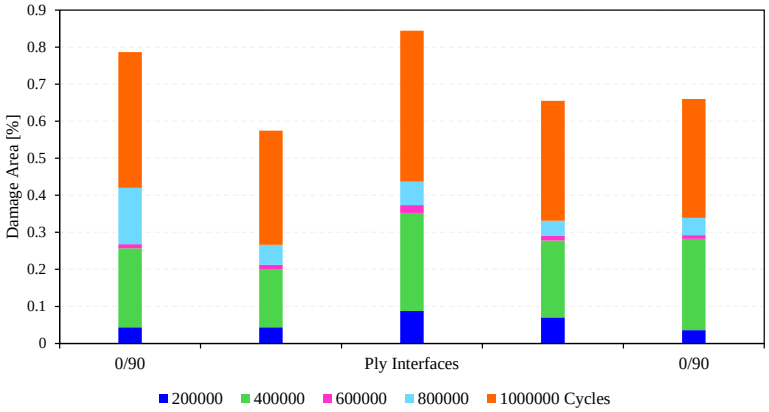
40/20/40 Double Notch Shear

R=0.1, OHT-T → Specimens: SL-1 (70%), SL-2 (80%), and SL-3 (90%)

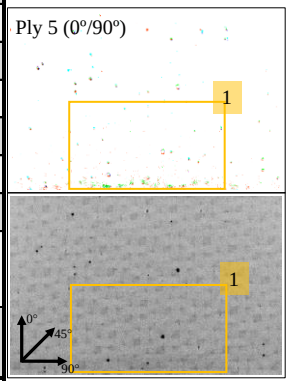
In the observance of progressive damage growth, three specimens were tested in R=0.1 at varying stress levels. Specimens were fatigued until failure or one-million cycles (runout) was achieved. For 40-20-40 only SL-1 survived fatigue and developed a 9% decrease in residual strength. All specimens in this group were cut evenly. In the T650 5320-1 8HS material system it is difficult to overcut the specimen and remain within tolerance. This is due to the relatively greater thickness of each ply in the layup. SL-1 displayed small areas of delamination near one notch (Figure B.87). SL-2 and SL-3 displayed even delamination through the gauge section with a slight increase closer to one notch (Figure Figure B.88 and Figure Figure B.89).

DISTRIBUTION STATEMENT A.
Approved for public release: distribution is unlimited.





Specimen ID	MASC1-C3GDII-XX6
Test Method	DNS
Material System	T650 5320-1 8HS
Ply Layup	40/20/40
Number of Plies	10
Stress Ratio	0.1
% Stress	30% of Ultimate Stress
Final Cycles	1,000,000 (runout)
Failure Mode	SHEAR
1) Minor damage across specimen, majority of damage near bottom notch.	
2) The notches were cut adequately.	



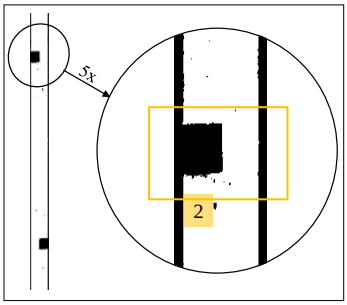
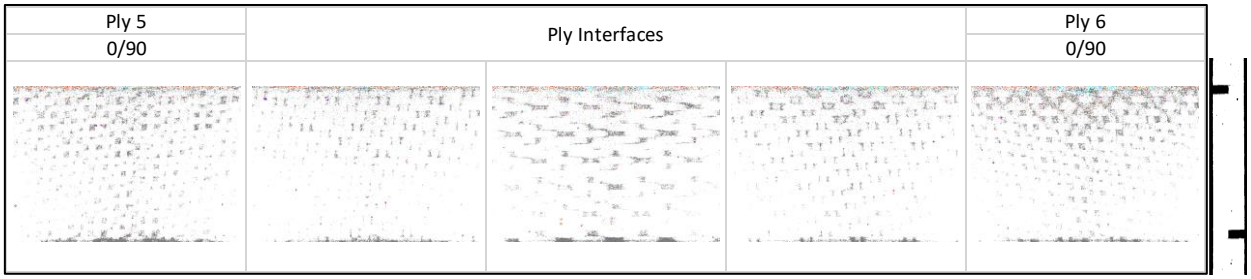
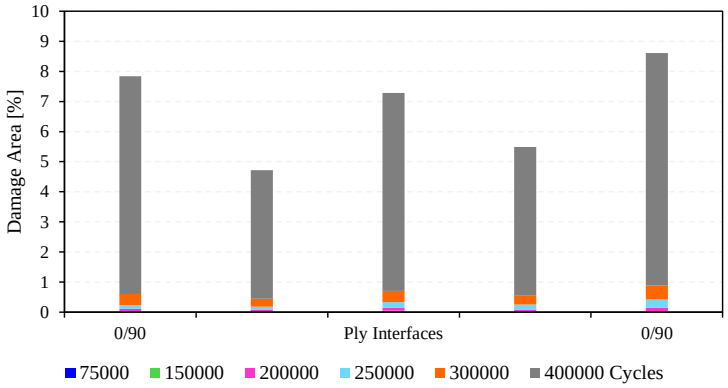


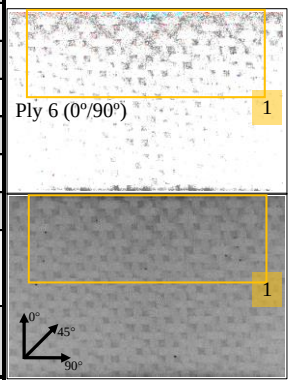
Figure B.87 – Shear gauge damage growth and area increase for T650 5320-1, 40/20/40, R=0.1, SL1.

DISTRIBUTION STATEMENT A.
Approved for public release: distribution is unlimited.





Specimen ID	MASC1-C1GD11-XX7
Test Method	DNS
Material System	T650 5320-1 8HS
Ply Layup	40/20/40
Number of Plies	10
Stress Ratio	0.1
% Stress	45% of Ultimate Stress
Final Cycles	420,485
Failure Mode	SHEAR
1) Majority of sheared area initiated from the upper notch.	
2) The notches were cut adequately.	



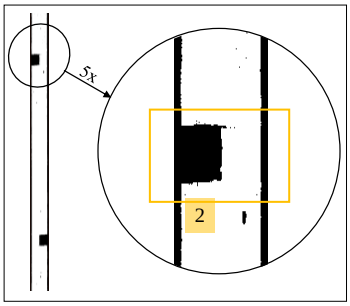
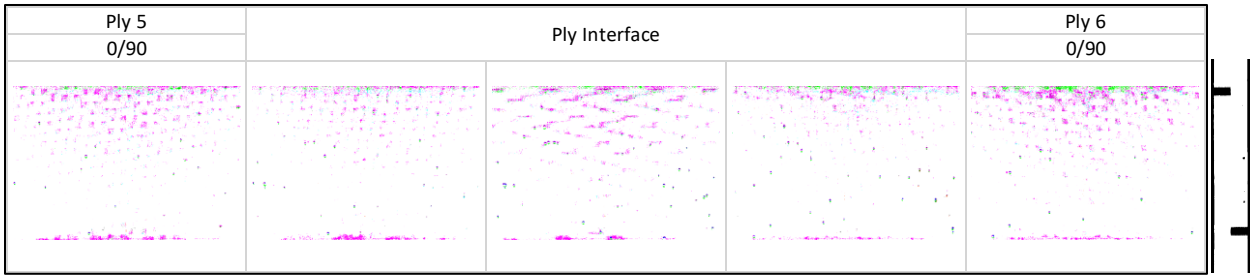
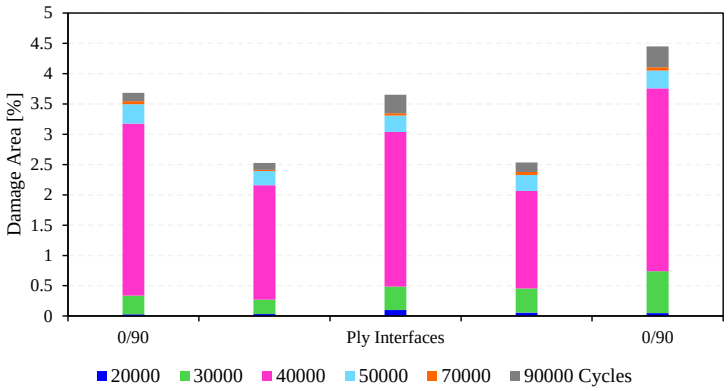


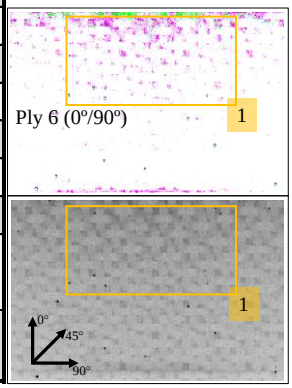
Figure B.88 – Shear gauge damage growth and area increase for T650 5320-1, 40/20/40, R=0.1, SL2.

DISTRIBUTION STATEMENT A.
Approved for public release: distribution is unlimited.





Specimen ID	MASC1-C2GD11-XX7
Test Method	DNS
Material System	T650 5320-1 8HS
Ply Layup	40/20/40
Number of Plies	10
Stress Ratio	0.1
% Stress	45% of Ultimate Stress
Final Cycles	98,487
Failure Mode	SHEAR
1) Majority of sheared area initiated from the upper notch.	
2) The notches were cut adequately.	



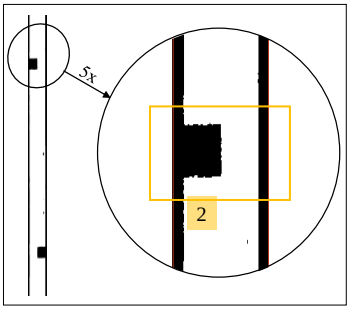


Figure B.89 – Shear gauge damage growth and area increase for T650 5320-1, 40/20/40, R=0.1, SL3.

DISTRIBUTION STATEMENT A.
Approved for public release: distribution is unlimited.

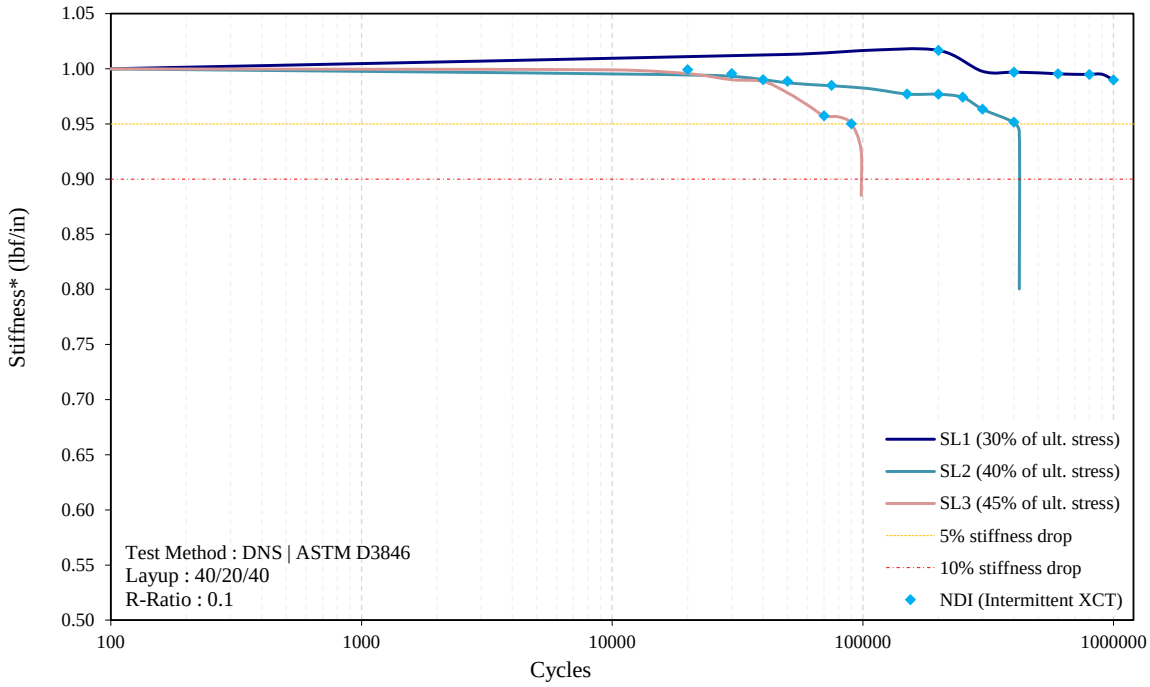


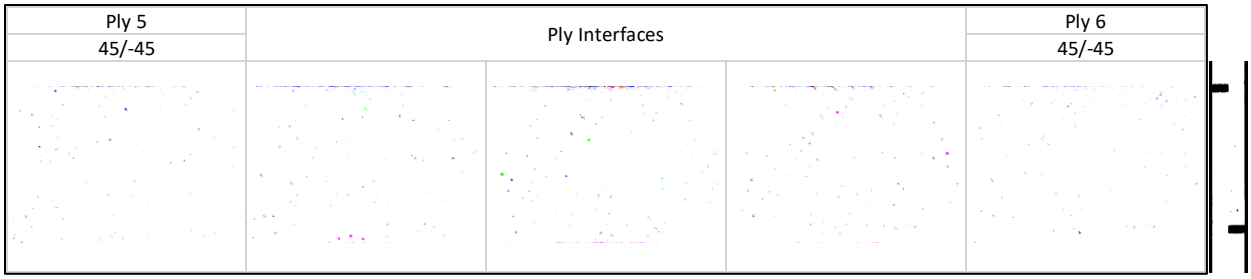
Figure B.90 – Apparent stiffness change during fatigue (normalized by initial compliance) for T650/5320-1 8HS, 40/20/40 layup, DNS, R=0.1.

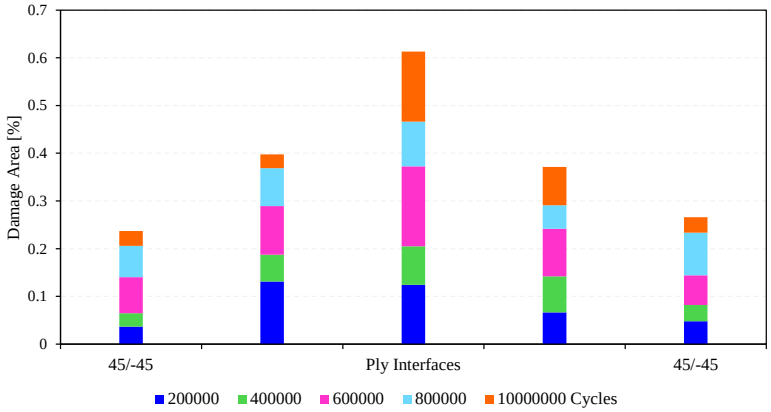
10/80/10 Double Notch Shear

R=0.1, OHT-T →Specimens: SL-1 (70%), SL-2 (80%), and SL-3 (90%)

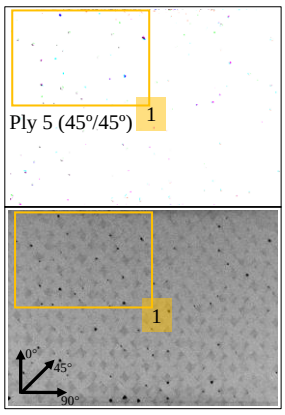
In the observance of progressive damage growth, three specimens were tested in R=0.1 at varying stress levels. Specimens were fatigued until failure or one-million cycles (runout) was achieved. For 10-80-10 only SL-1 survived fatigue and developed an average of 9% decreased residual strength. All specimens in this group were cut evenly. In the T650 5320-1 8HS material system it is difficult to overcut the specimen and remain within tolerance. This is due to the relatively greater thickness of each ply in the layup. SL-1 displayed very minor damage throughout the gauge section (Figure B.91). SL-2 displayed the largest amount of delamination extending from both notches. However, the majority of damage propagated from one notch (Figure B.92). SL-3 displayed a large amount of delamination however unlike SL-2 the sheared area extended evenly from both notches (Figure B.93).

DISTRIBUTION STATEMENT A.
Approved for public release: distribution is unlimited.





Specimen ID	MASC1-C1FD11-XX8
Test Method	DNS
Material System	T650 5320-1 8HS
Ply Layup	10/80/10
Number of Plies	10
Stress Ratio	0.1
% Stress	40% of Ultimate Stress
Final Cycles	1,000,000 (runout)
Failure Mode	SHEAR
1) Minor damage across specimen.	
2) The notches were cut adequately.	



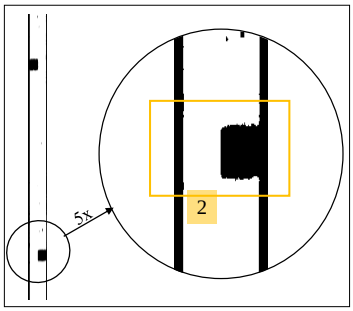
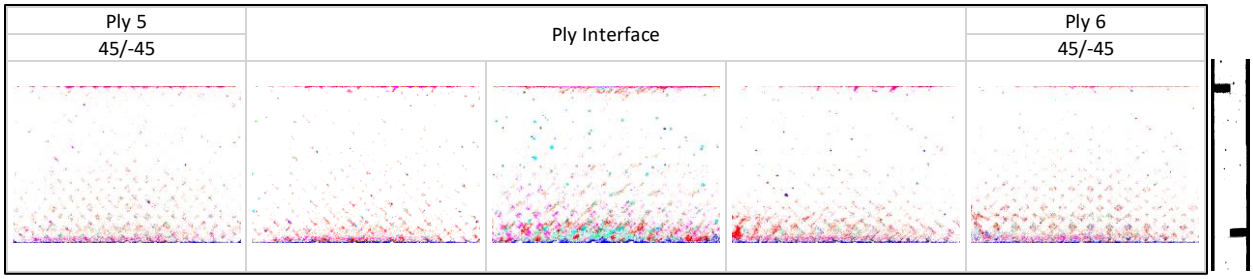
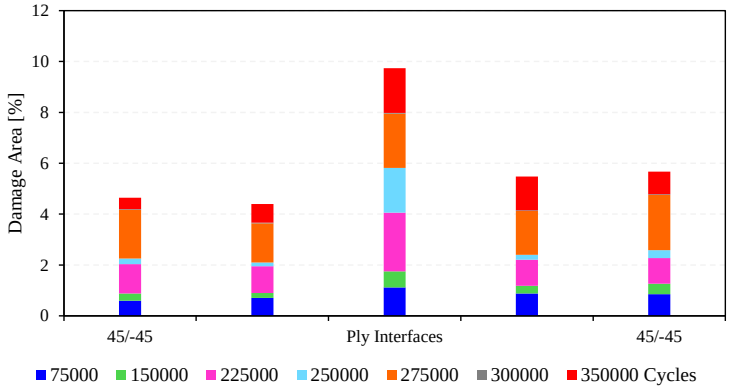


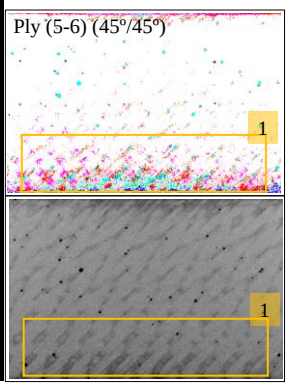
Figure B.91 – Shear gauge damage growth and area increase for T650 5320-1, 10/80/10, R=0.1, SL1.

DISTRIBUTION STATEMENT A.
Approved for public release: distribution is unlimited.





Specimen ID	MASC1-C3FD11-XX5
Test Method	DNS
Material System	T650 5320-1 8HS
Ply Layup	10/80/10
Number of Plies	10
Stress Ratio	0.1
% Stress	47.5% of Ultimate Stress
Final Cycles	374,237
Failure Mode	SHEAR
1) Increased signs of shearing near the top notch.	
2) The notches were cut adequately, initiation of the shear can be seen.	



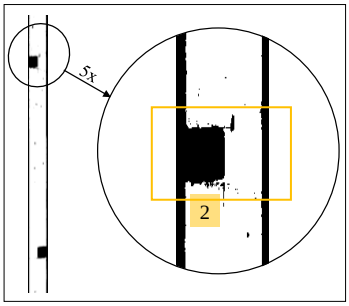
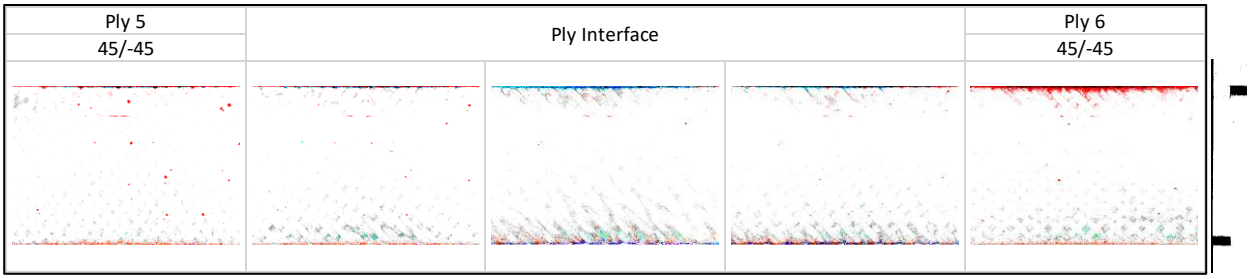
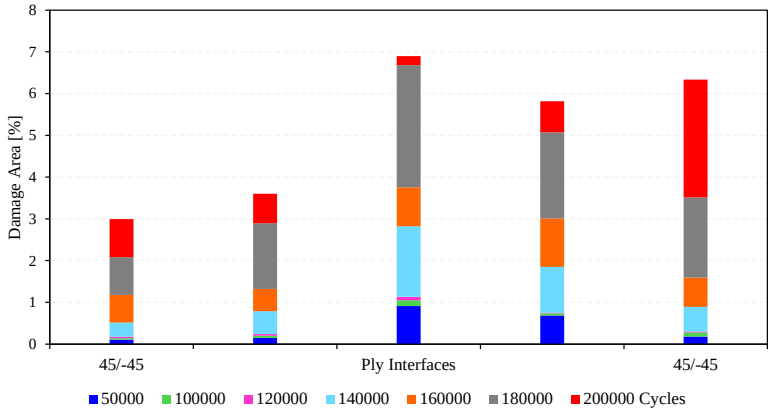


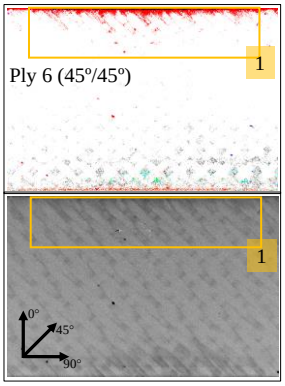
Figure B.92 – Shear gauge damage growth and area increase for T650 5320-1, 10/80/10, R=0.1, SL2.

DISTRIBUTION STATEMENT A.
Approved for public release: distribution is unlimited.





Specimen ID	MASC1-C2FD11-XX7
Test Method	DNS
Material System	T650 5320-1 8HS
Ply Layup	10/80/10
Number of Plies	10
Stress Ratio	0.1
% Stress	50% of Ultimate Stress
Final Cycles	201,556
Failure Mode	SHEAR
1) Manufacturing damage near the top notch.	
2) The notches were cut adequately, initiation of the shear can be seen.	



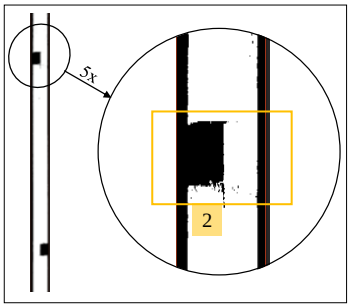


Figure B.93 – Shear gauge damage growth and area increase for T650 5320-1, 10/80/10, R=0.1, SL3.

DISTRIBUTION STATEMENT A.
Approved for public release: distribution is unlimited.

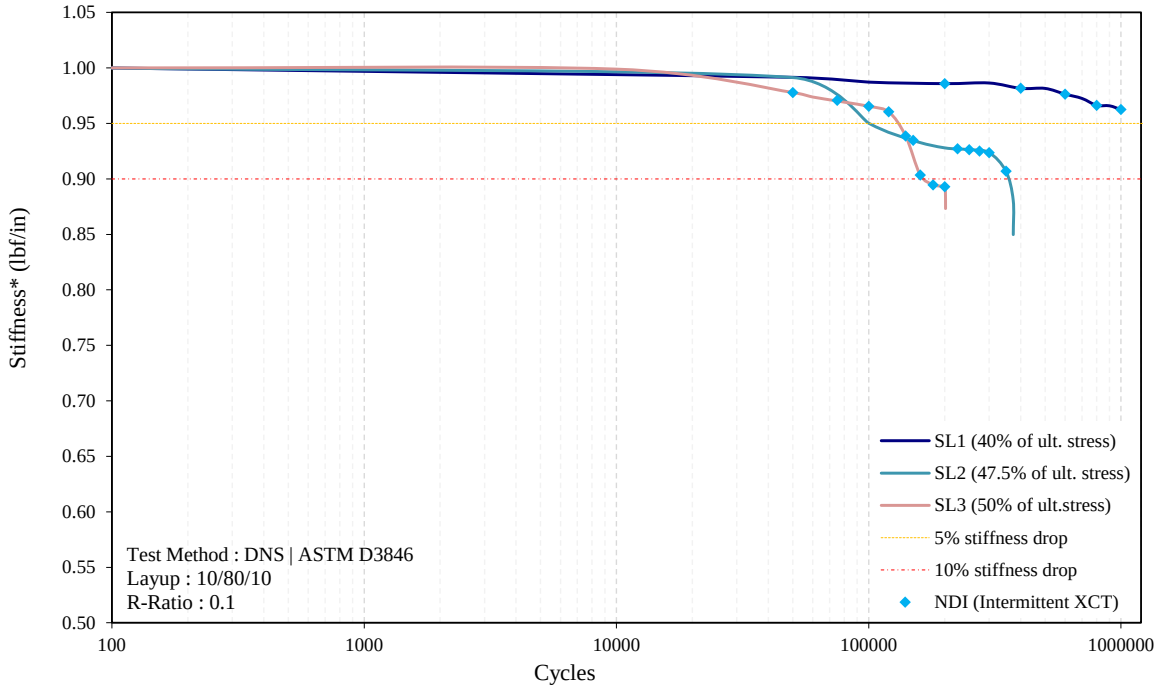


Figure B.94 – Apparent stiffness change during fatigue (normalized by initial compliance) for T650/5320-1 8HS, 10/80/10 layup, DNS, R=0.1.

A.6 Progressive Damage Growth for IM7/5250-4 UNI

This section includes IM7/5250-4 unidirectional laminates subjected to uniaxial tensile loading, considering three different layups, hard (50/40/10), quasi (25/50/25) and soft (10/80/10) as illustrated in Figure B.95. The laminates are composed of equal thickness lamina (CPT 0.0054”), 28 plies for hard layup and 24 plies for quasi and soft layups with stacking sequences $[45/0/-45/0_2/45/90/-45/0_2/45/0/-45/0]_s$, $[45/0/-45/90]_{3s}$ and $[45/-45/45/-45/90/-45/0/45/-45/45/-45/45]_s$ respectively.

50/40/10 Open-Hole Test

R=0.1, OHT-T → Specimens: SL-1 (70%), SL-2 (80%), and SL-3 (90%)
R=5.0, OHC-C → Specimens: SL-1 (75%), SL-2 (80%), and SL-3 (85%)
R=-1, OHC-T → Specimens: SL-1 (45%), SL-2 (55%), and SL-3 (60%)

Three specimens were tested for each r-ratio at varying stress levels and were fatigued until failure or one-million cycles (runout) was achieved. For R=0.1, all 3 specimens survived fatigue and developed an average of 31% increased residual strength. This was due to the stress relief that occurred when the outer plies and the regions above and below the hole became significantly delaminated in the 0° direction (Figure B.95). SL-2 and SL-3 displayed fiber failure above and

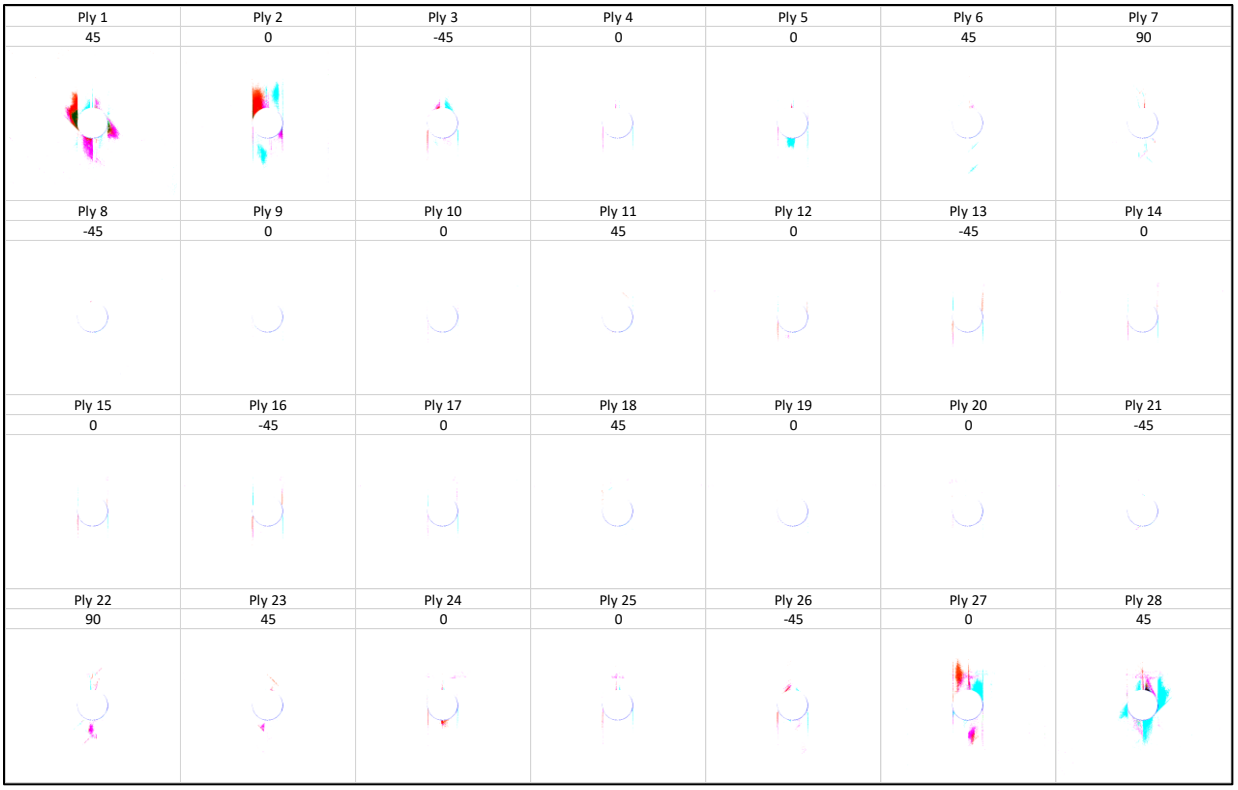
DISTRIBUTION STATEMENT A.
Approved for public release: distribution is unlimited.

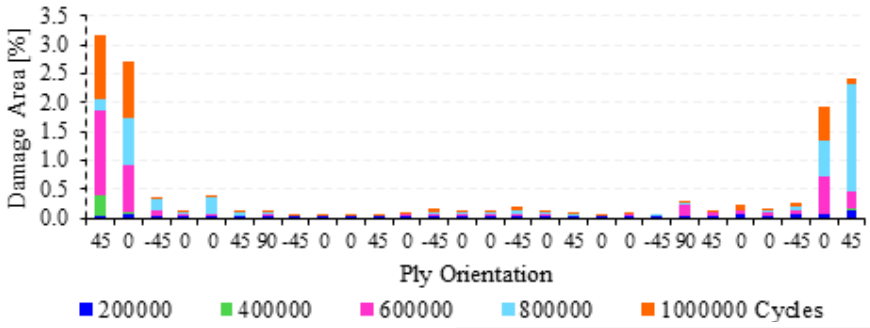
below the hole in the same region of delamination within the 90°plies. SL-2 and SL-3 uniquely displayed delamination propagating from the outer edges within their 90° and adjacent 45° plies (Figure B.96 and Figure B.97).

In R=5.0 only SL-1 achieved runout and had 3% increased residual strength (Figure B.99). SL-2 and SL-3 displayed significant fiber failure in the region around the hole (Figure B.100) while this group displayed negligible delamination after fatigue. The fiber failure begins on the outermost plies growing inward until the specimen reaches failure. The majority of fiber failures extended radially from the hole in the horizontal direction (Figure B.101) and this fiber failure in ultimately leads to an accelerated failure of the specimen.

In R=-1 only SL-1 achieved runout and developed a 32% decrease in residual strength. Despite the intense delamination and minor fiber failure around the hole, SL-1 did not display stress relief (Figure B.103). The majority of damage for this group of specimens was on the outer plies. SL-2 and SL-3 displayed critical damage on their inner 0° plies accelerating failure (Figure B.104). Although SL-3 survived further than SL-2, more critical fiber failures and delamination occurred in SL-3 (Figure B.105) providing minor stress relief to SL-3.

DISTRIBUTION STATEMENT A.
Approved for public release: distribution is unlimited.





Specimen ID	MASC1-A1DO11-3K2
Test Method	OHT-T
Material System	IM7 5250-4 UNI
Ply Layup	50/40/10
Number of Plies	28
Stress Ratio	0.1
% Stress	70% of Ultimate Stress
Final Cycles	1,000,000 (runout)
1) Fiber failure tangent to the hole extending vertically along the 0º direction.	
2) Delamination extending from the hole in 0º direction.	

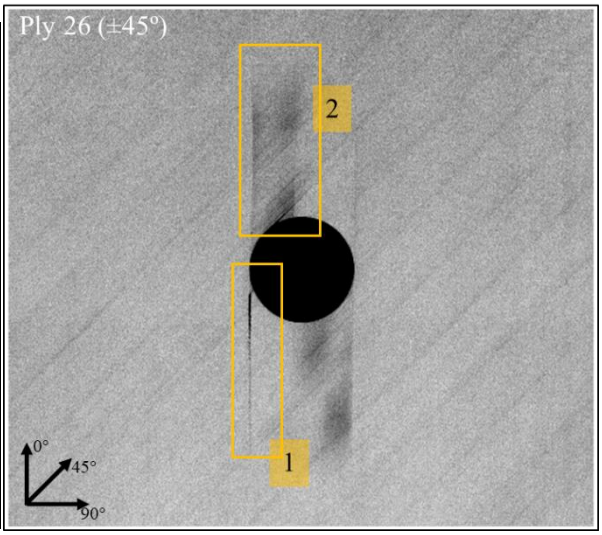
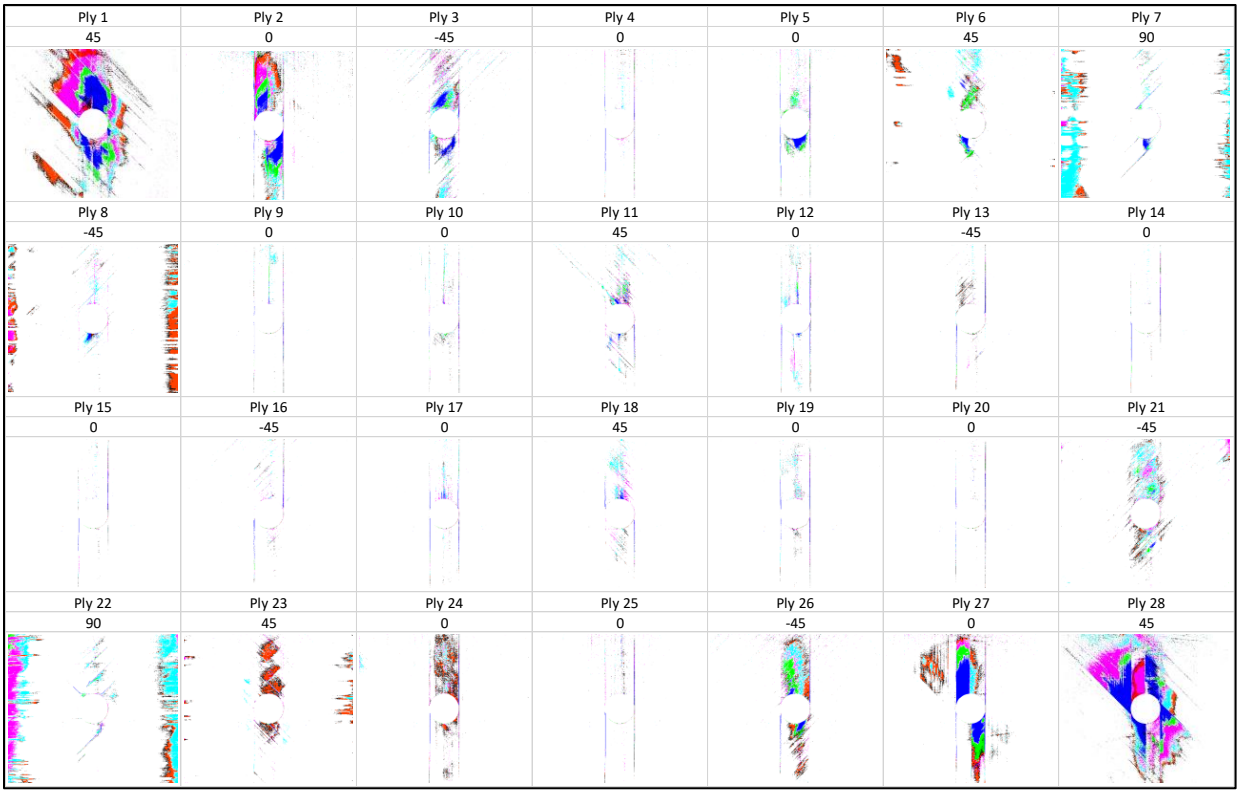
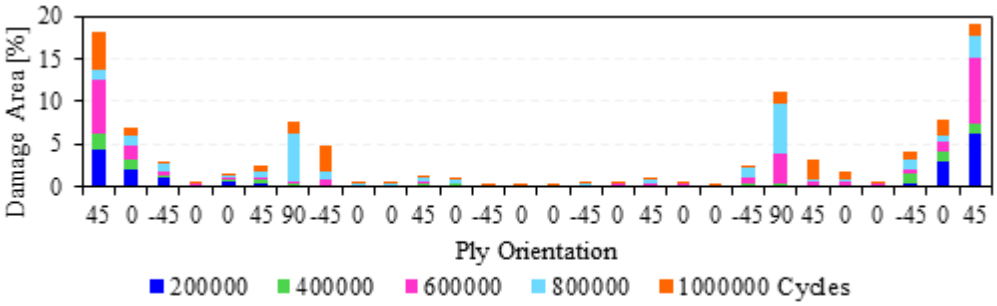


Figure B.95 – Ply-by-ply damage growth and area increase for IM7/5250-4, 50/40/10, R=0.1, SL1.

DISTRIBUTION STATEMENT A.
Approved for public release: distribution is unlimited.





Specimen ID	MASC1-A2DO11-2K1
Test Method	OHT-T
Material System	IM7 5250-4 UNI
Ply Layup	50/40/10
Number of Plies	28
Stress Ratio	0.1
% Stress	80% of Ultimate Stress
Final Cycles	1,000,000 (runout)
1) Delamination from the outer edge extending to the center along the 90° direction.	
2) Fiber failure above the hole (not formed from the hole) in the 45° direction.	
3) Fiber failure forming from the hole extending along the 45° direction.	

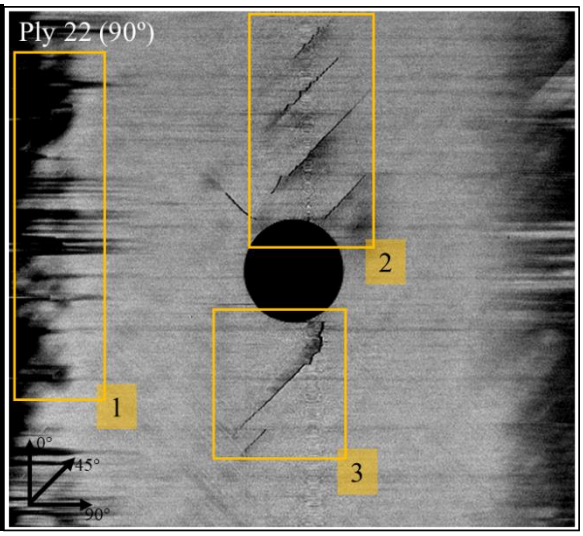
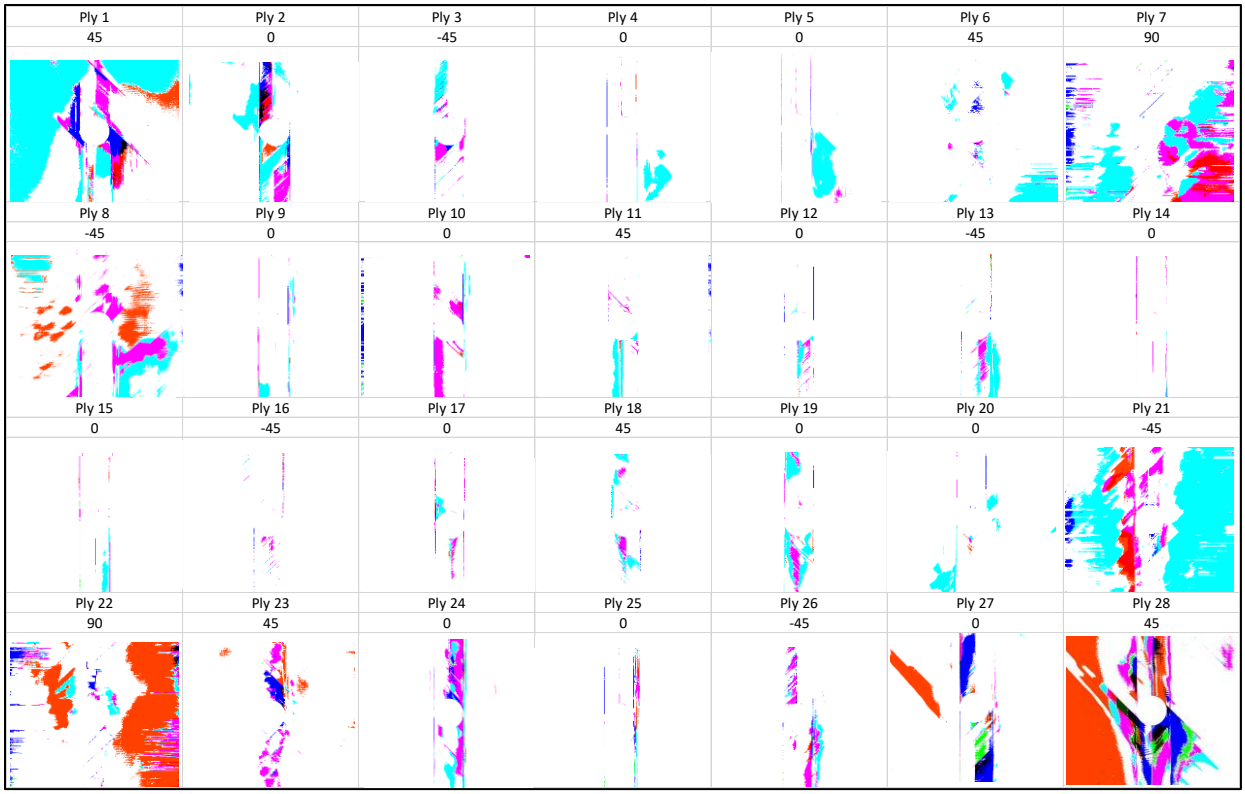
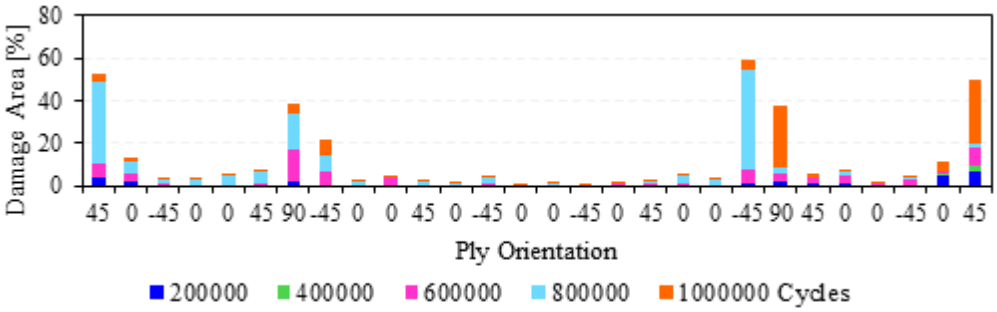


Figure B.96 – Ply-by-ply damage growth and area increase for IM7/5250-4, 50/40/10, R=0.1, SL2.

DISTRIBUTION STATEMENT A.
Approved for public release: distribution is unlimited.





Specimen ID	MASC1-A3DO11-3K1
Test Method	OHT-T
Material System	IM7 5250-4 UNI
Ply Layup	50/40/10
Number of Plies	28
Stress Ratio	0.1
% Stress	90% of Ultimate Stress
Final Cycles	1,000,000 (runout)
1) Separation of fibers extending from the outer edge inwards along the 90° direction.	
2) Fiber failure perpendicular to the 90° fibers extending from the hole in the 0° direction.	
3) Complete delamination of the outer edge to the center along the 90° direction.	

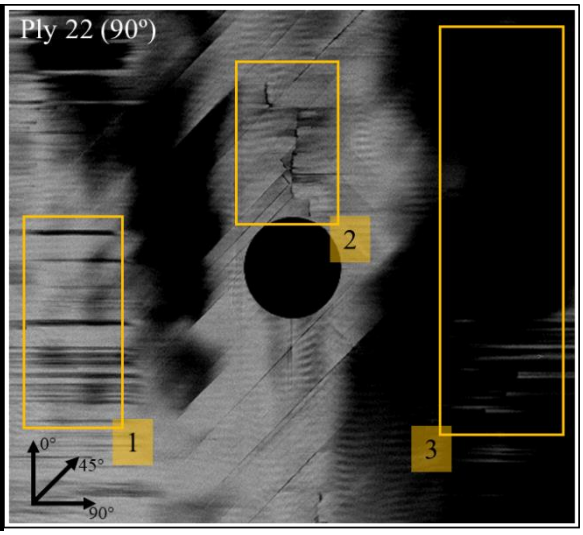


Figure B.97 – Ply-by-ply damage growth and area increase for IM7/5250-4, 50/40/10, R=0.1, SL3.

DISTRIBUTION STATEMENT A.
Approved for public release: distribution is unlimited.

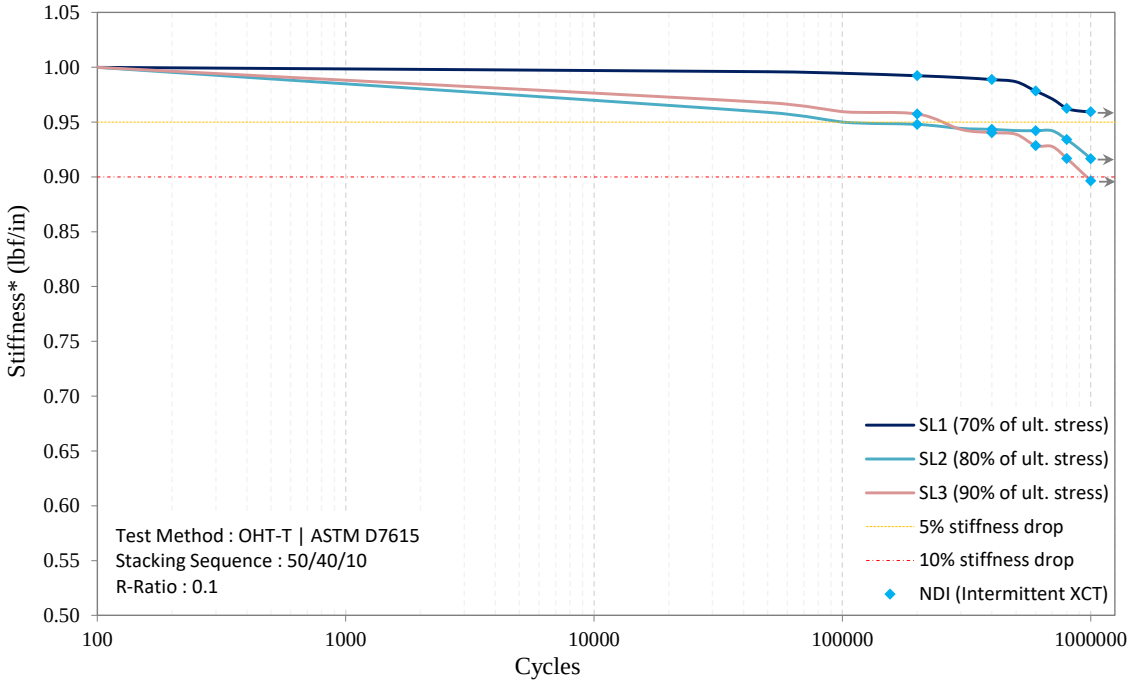
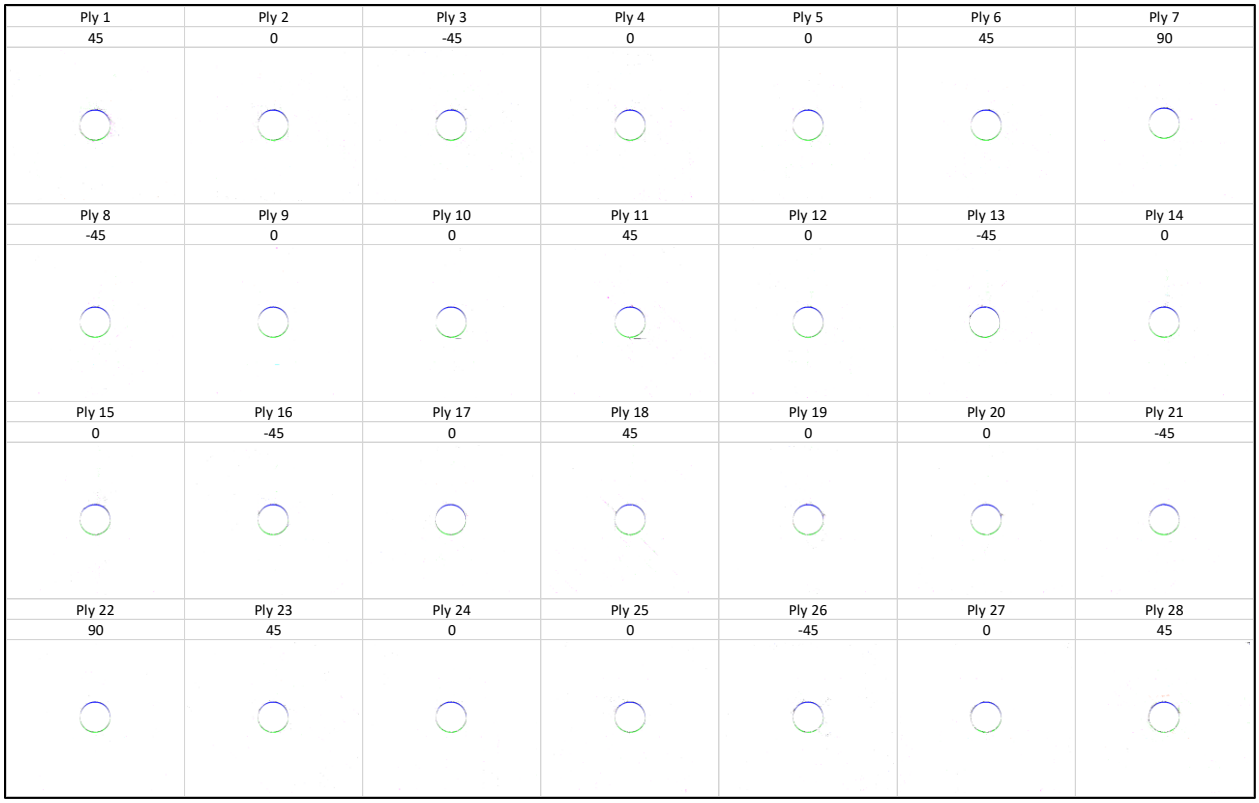
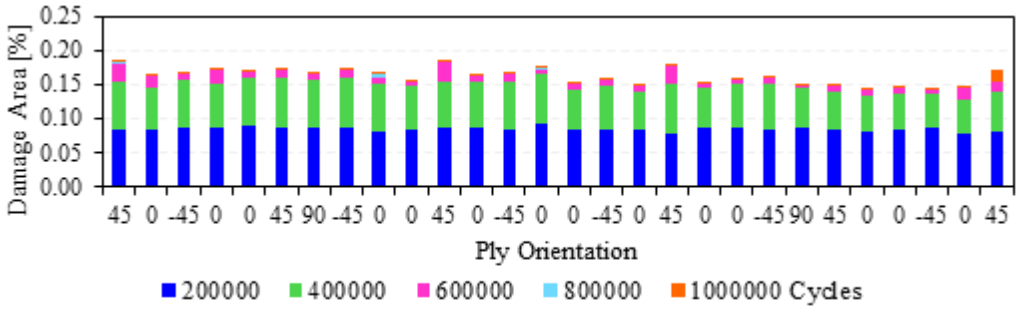


Figure B.98 – Apparent stiffness change during fatigue (normalized by initial compliance) for IM7/5250-4 UNI 50/40/10 layup, OHT-T, R=0.1.

DISTRIBUTION STATEMENT A.
Approved for public release: distribution is unlimited.





Specimen ID	MASC1-A2DO11-2L1
Test Method	OHC-C
Material System	IM7 5250-4 UNI
Ply Layup	50/40/10
Number of Plies	28
Stress Ratio	5.0
% Stress	75% of Ultimate Stress
Final Cycles	1,000,000 (runout)
1) Separation between the 45º fibers throughout the region near the hole.	
Comment) No significant damage after fatigue.	

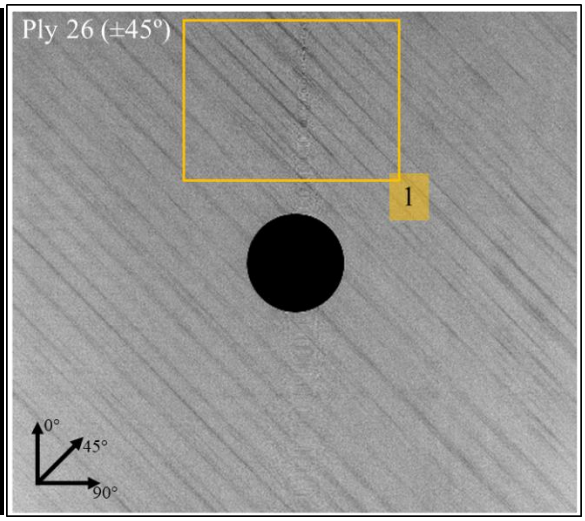
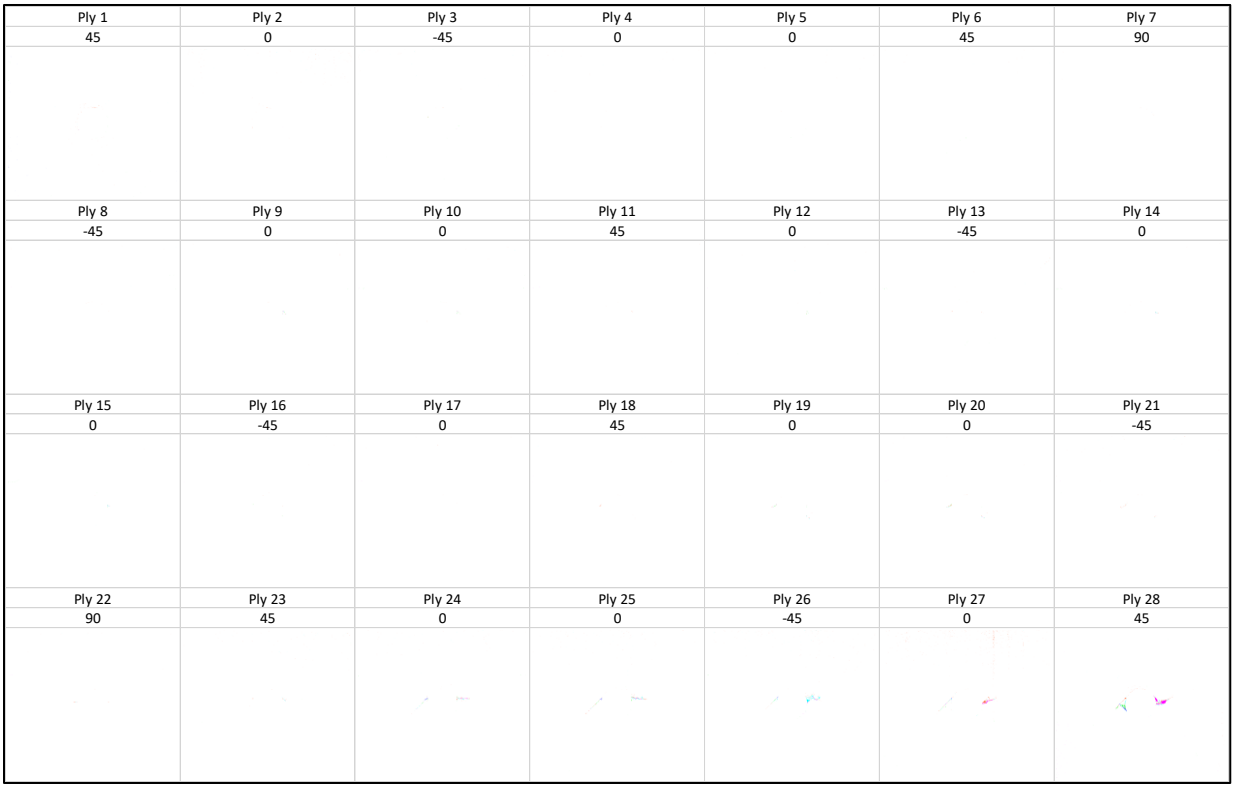
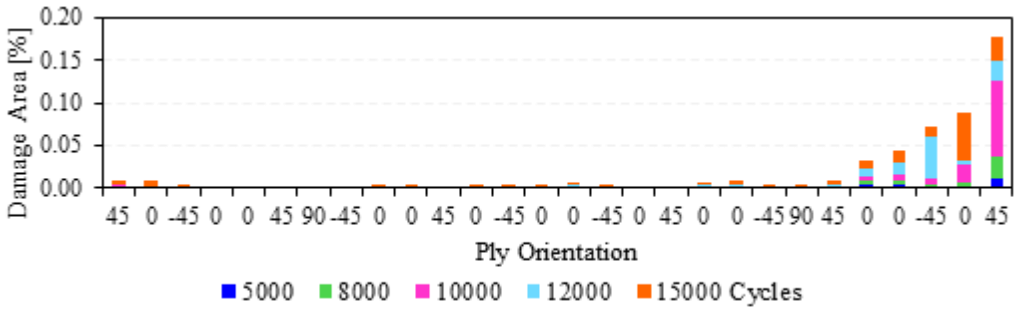


Figure B.99 – Ply-by-ply damage growth and area increase for IM7/5250-4, 50/40/10, R=5, SL1.

DISTRIBUTION STATEMENT A.
Approved for public release: distribution is unlimited.





Specimen ID	MASC1-A2DO11-XX6
Test Method	OHC-C
Material System	IM7 5250-4 UNI
Ply Layup	50/40/10
Number of Plies	28
Stress Ratio	5.0
% Stress	80% of Ultimate Stress
Final Cycles	16,751
1) Fiber separation between the 45º fibers extending radially from the hole.	
2) Fiber failure extending horizontally from the hole in the 90º direction.	

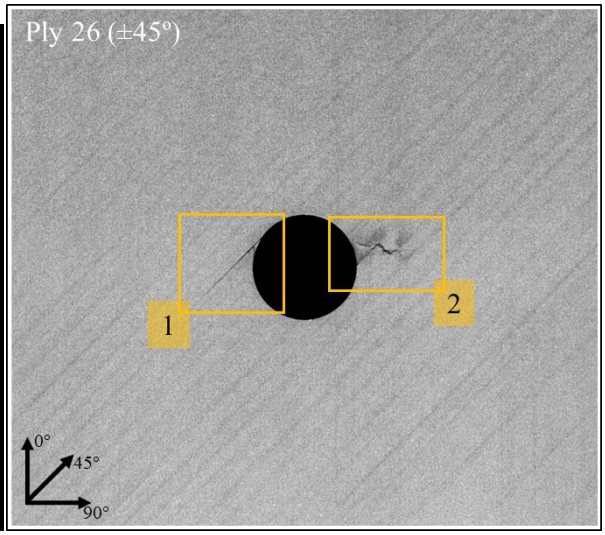
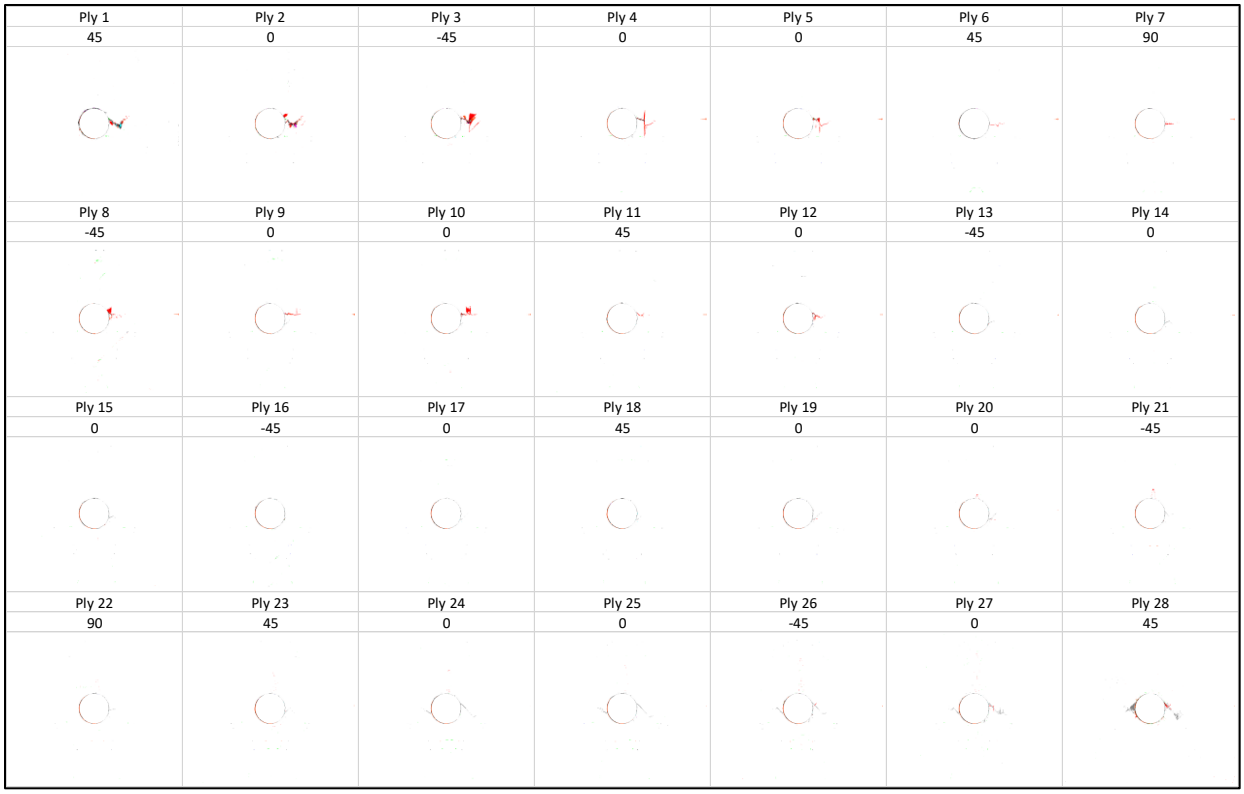
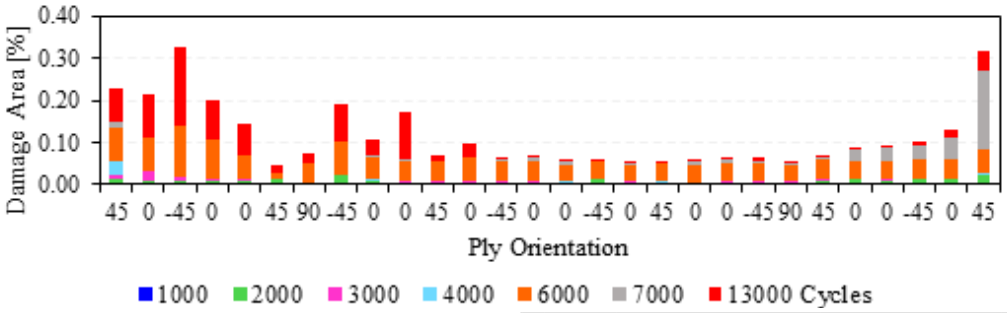


Figure B.100 – Ply-by-ply damage growth and area increase for IM7/5250-4, 50/40/10, R=5, SL2.

DISTRIBUTION STATEMENT A.
Approved for public release: distribution is unlimited.





Specimen ID	MASC1-A3DO11-3L1
Test Method	OHC-C
Material System	IM7 5250-4 UNI
Ply Layup	50/40/10
Number of Plies	28
Stress Ratio	5.0
% Stress	85% of Ultimate Stress
Final Cycles	14,657
1) Fiber failure extending horizontally from the hole in the 90º direction.	

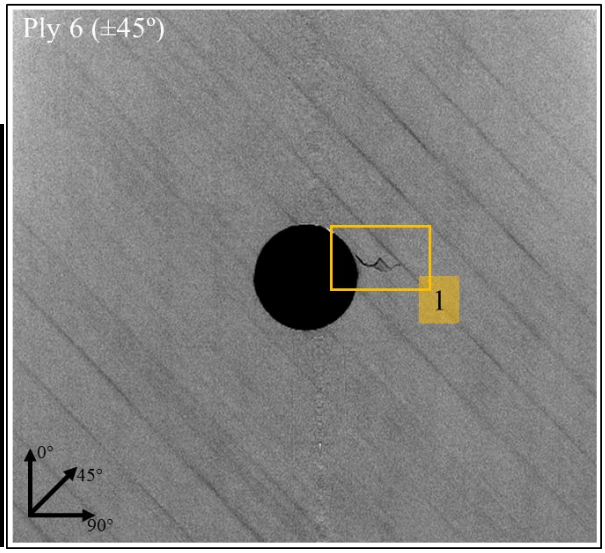


Figure B.101 – Ply-by-ply damage growth and area increase for IM7/5250-4, 50/40/10, R=5, SL3.

DISTRIBUTION STATEMENT A.
Approved for public release: distribution is unlimited.

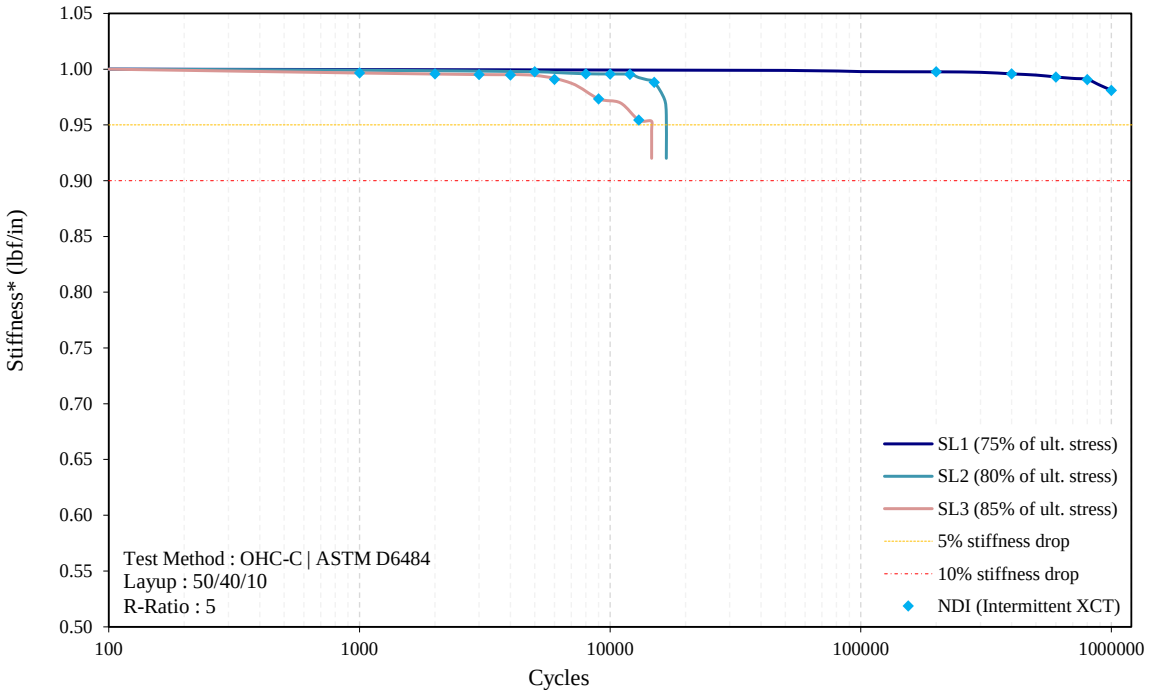
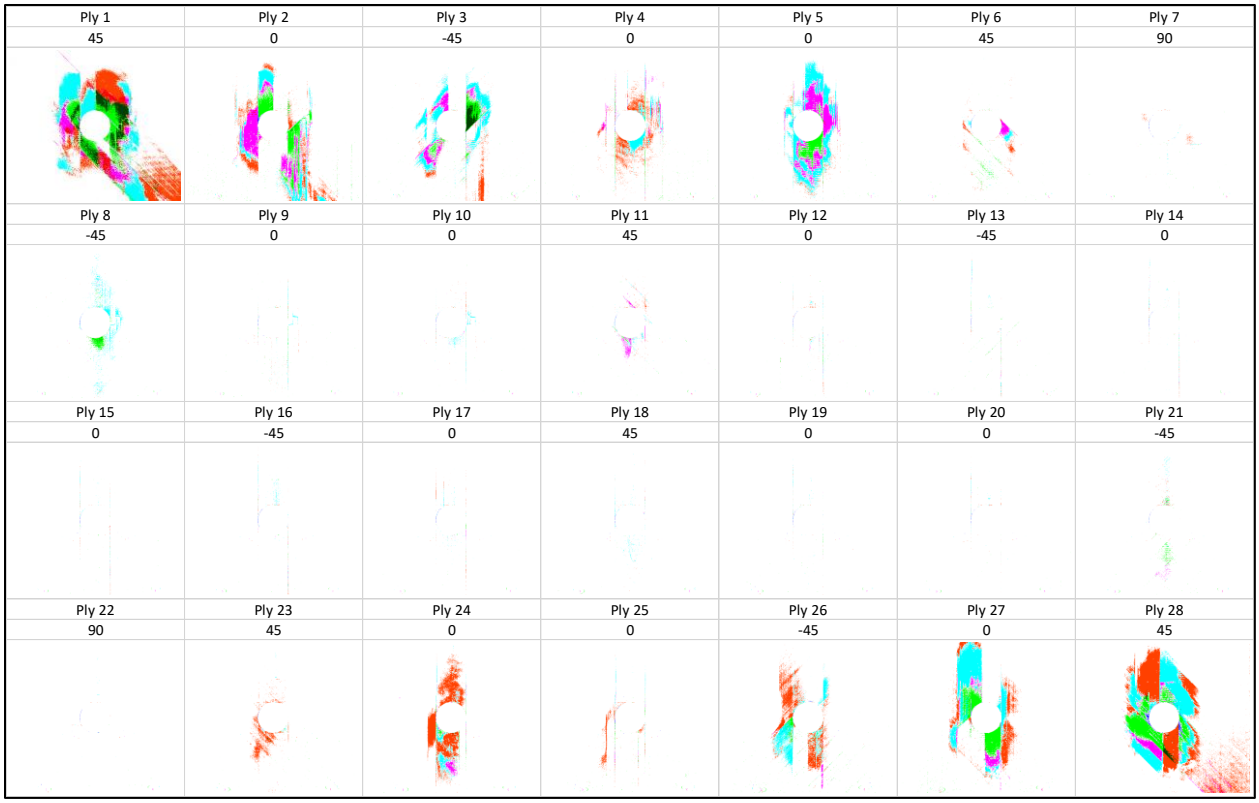
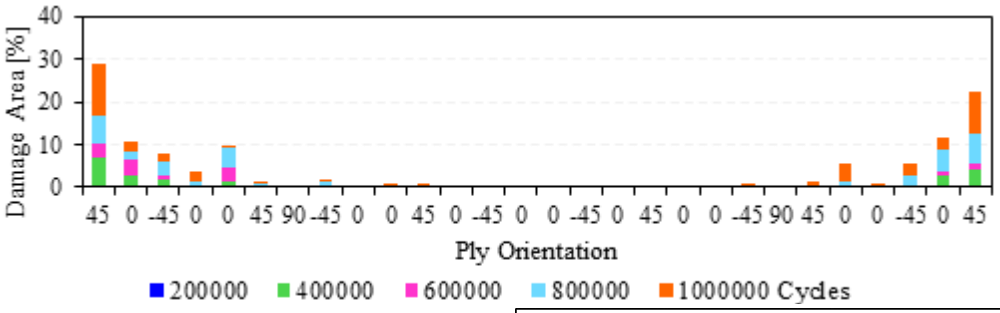


Figure B.102 – Apparent stiffness change during fatigue (normalized by initial compliance) for IM7/5250-4 UNI, 50/40/10 layup, OHT-T, R=5.

DISTRIBUTION STATEMENT A.
Approved for public release: distribution is unlimited.





Specimen ID	MASC1-A3DO11-3M1
Test Method	OHC-T
Material System	IM7 5250-4 UNI
Ply Layup	50/40/10
Number of Plies	28
Stress Ratio	-1.0
% Stress	45% of Ultimate Stress
Final Cycles	1,000,000 (runout)
1) Fiber failure extending tangentially from the hole in the 0° direction.	
2) Delamination extending from the hole vertically between the separated 0° fibers.	

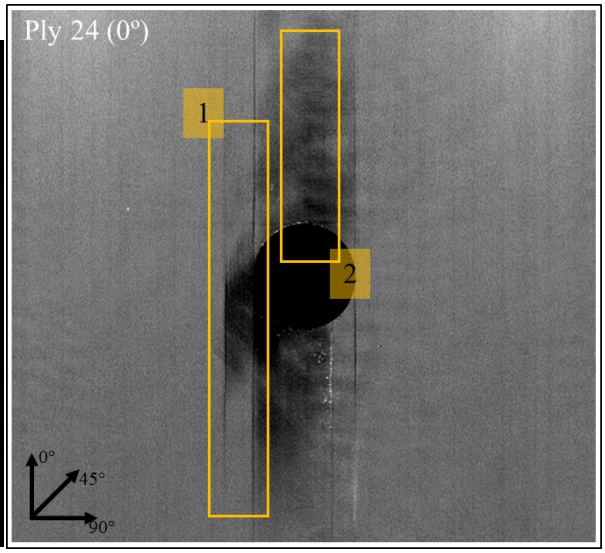
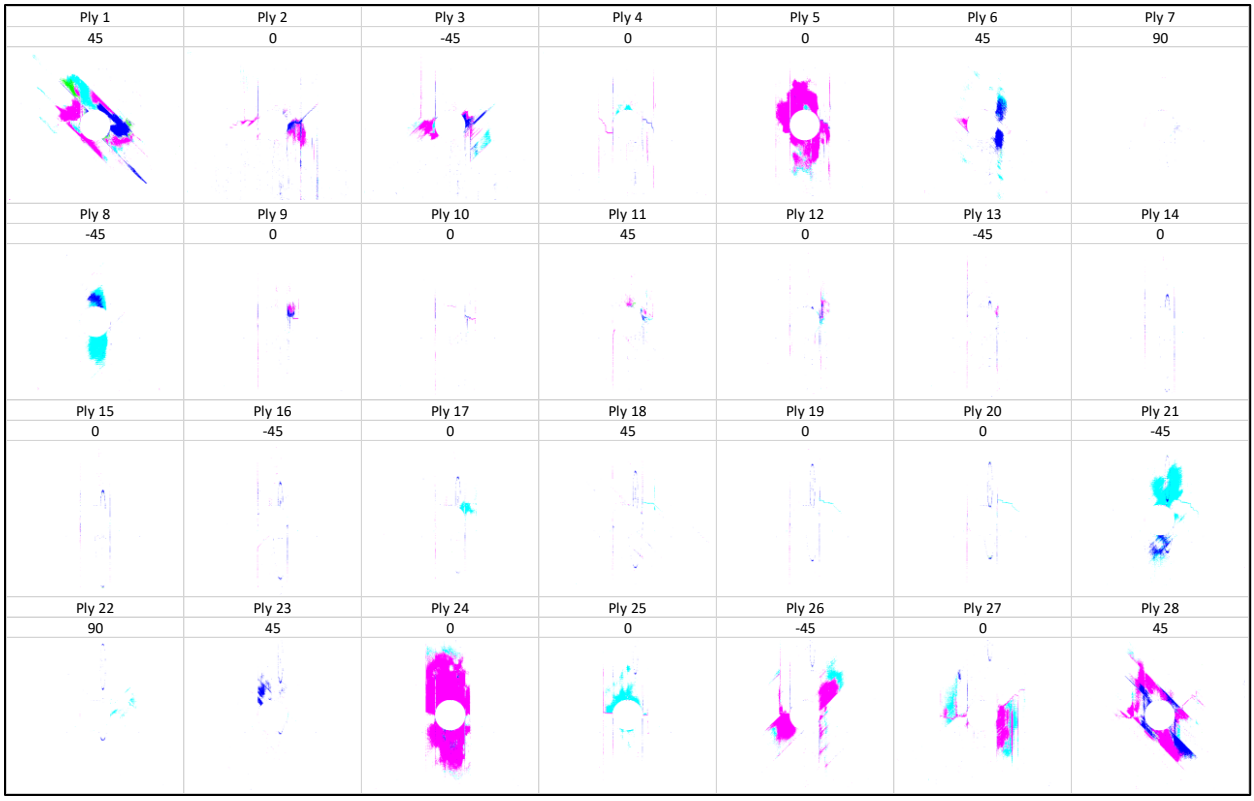
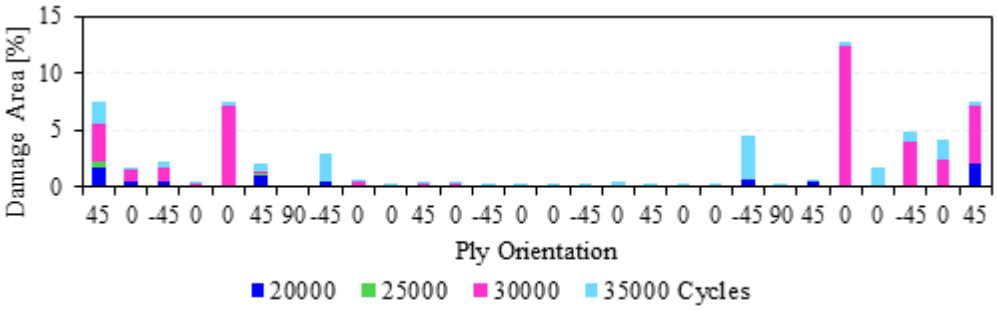


Figure B.103 – Ply-by-ply damage growth and area increase for IM7/5250-4, 50/40/10, R=-1, SL1.

DISTRIBUTION STATEMENT A.
Approved for public release: distribution is unlimited.





Specimen ID	MASC1-A2DO11-2M1
Test Method	OHC-T
Material System	IM7 5250-4 UNI
Ply Layup	50/40/10
Number of Plies	28
Stress Ratio	-1.0
% Stress	55% of Ultimate Stress
Final Cycles	35,325
1) Fiber failure extending tangentially from the hole in the 0° direction.	
2) Fiber failure propagating from the separation between the 0° fibers.	

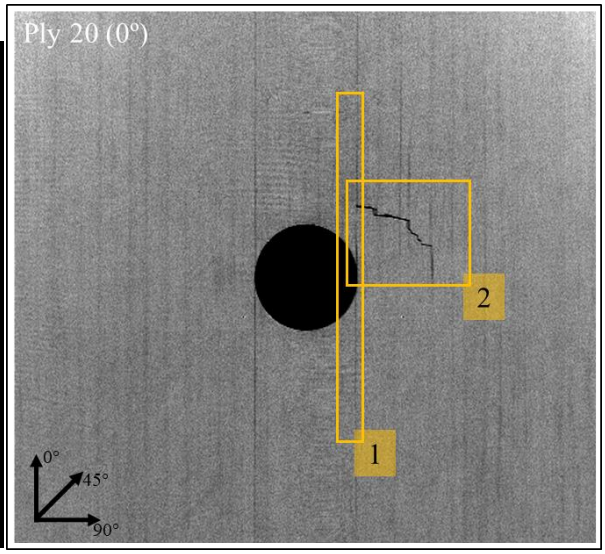


Figure B.104 – Ply-by-ply damage growth and area increase for IM7/5250-4, 50/40/10, R=-1, SL2.

DISTRIBUTION STATEMENT A.
Approved for public release: distribution is unlimited.

Continued…	MASC1-A2DO11-2M1
Test Method	OHC-T
Material System	IM7 5250-4 UNI
Ply Layup	50/40/10
Number of Plies	28
Stress Ratio	-1.0
% Stress	55% of Ultimate Stress
Final Cycles	35,325
1) Fiber failure extending from the separations between the 0° fibers.	

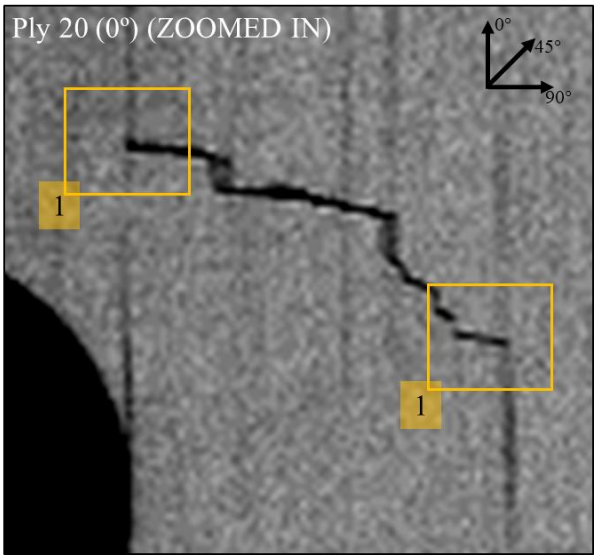
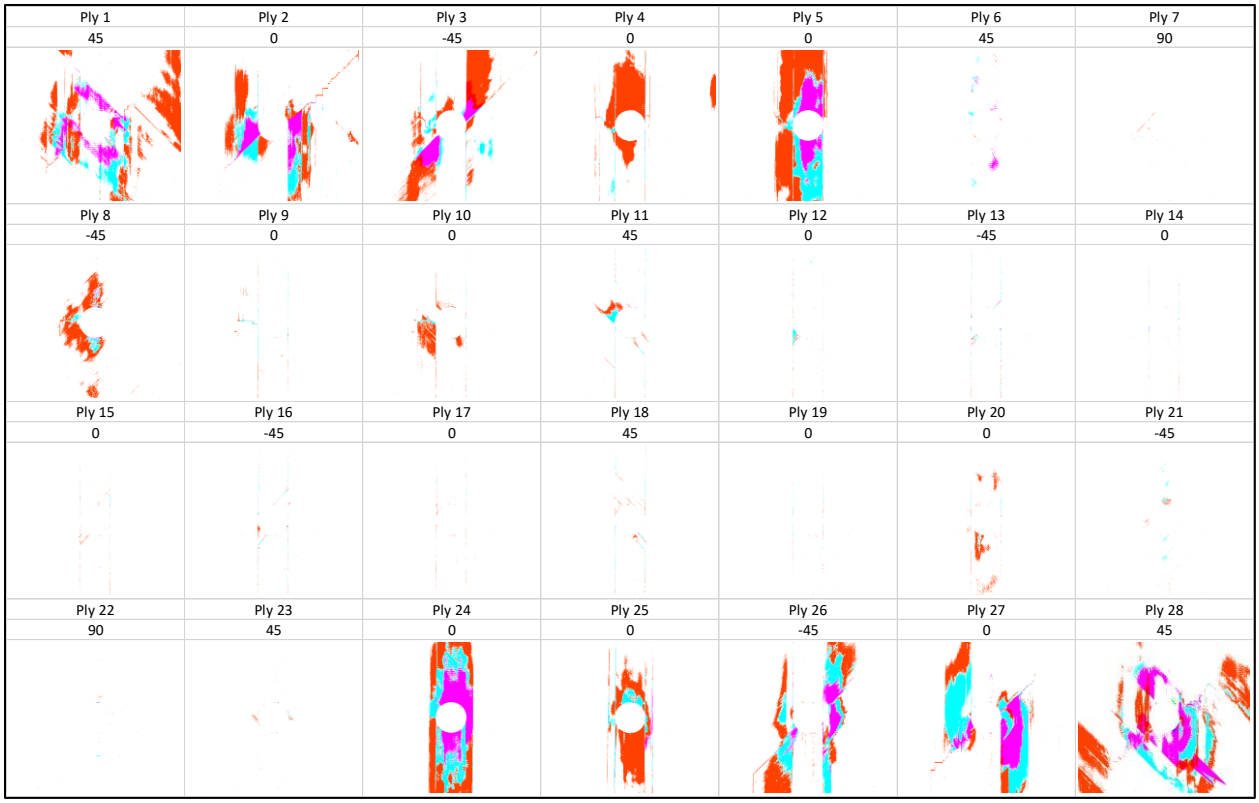
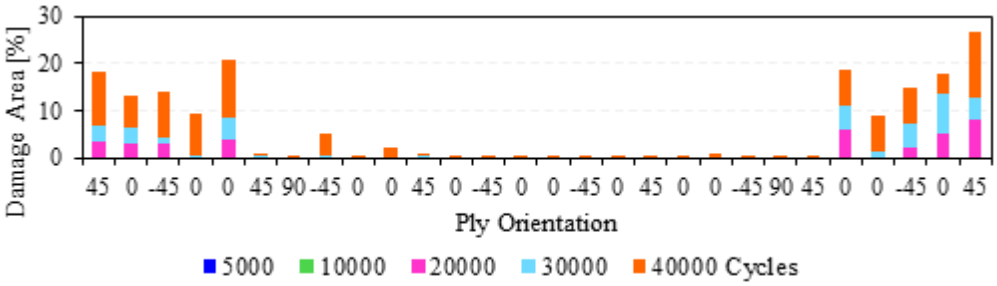


Figure B.104 – Ply-by-ply damage growth and area increase for IM7/5250-4, 50/40/10, R=-1, SL2(cont.).

DISTRIBUTION STATEMENT A.
Approved for public release: distribution is unlimited.





Specimen ID	MASC1-A1DO11-2K2
Test Method	OHC-T
Material System	IM7 5250-4 UNI
Ply Layup	50/40/10
Number of Plies	28
Stress Ratio	-1.0
% Stress	60% of Ultimate Stress
Final Cycles	42,762
1) Delamination of the 45° ply below the hole propagating from the vertical fiber failure.	
2) Fiber failure extending from the hole perpendicular to the 45° fibers.	
3) Fiber failure extending tangentially from the hole in the 0° direction.	
4)Fiber separation extending from the hole along the 45° direction.	

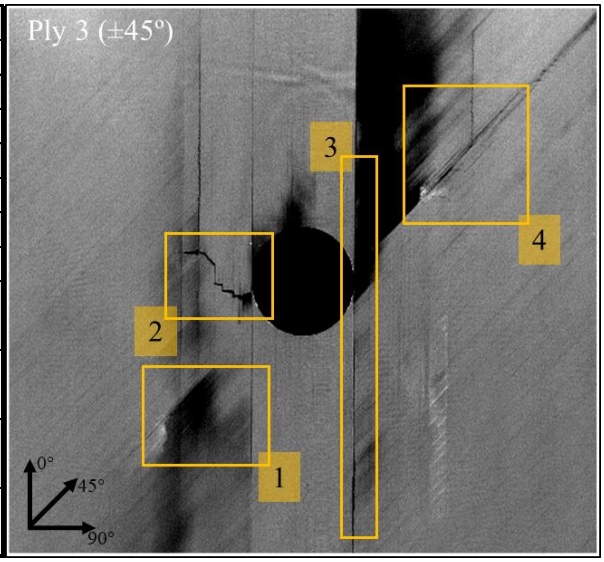


Figure B.105 – Ply-by-ply damage growth and area increase for IM7/5250-4, 50/40/10, R=-1, SL3.

DISTRIBUTION STATEMENT A.
Approved for public release: distribution is unlimited.

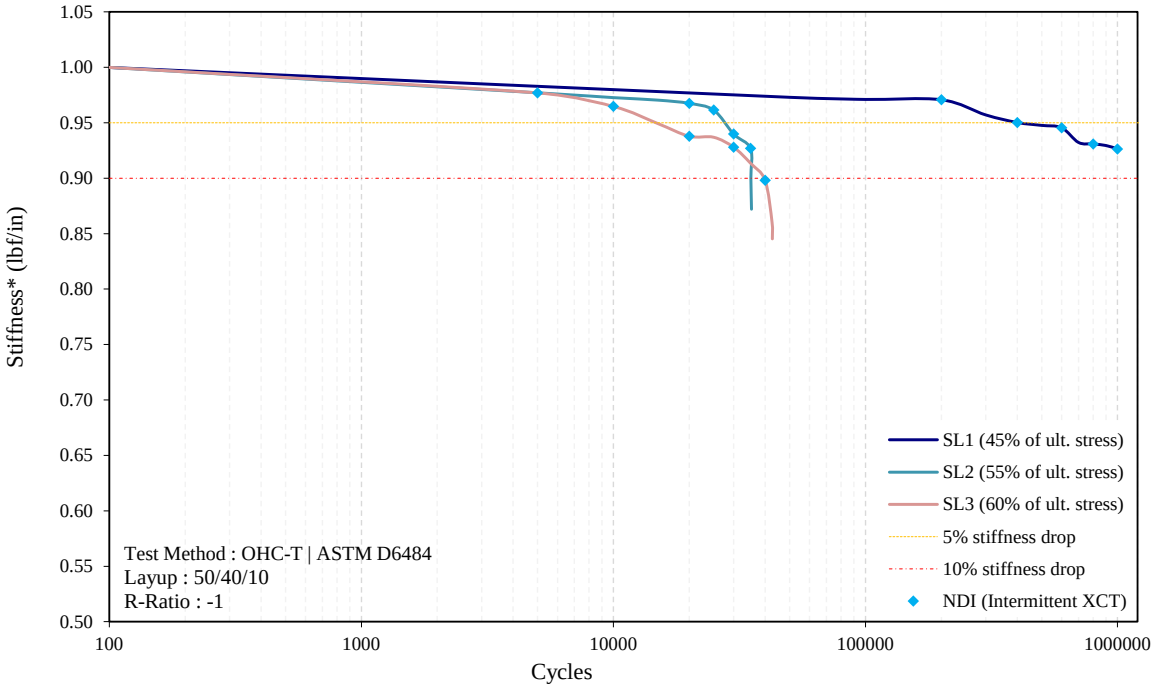


Figure B.106 – Apparent stiffness change during the tension fatigue (normalized by initial compliance) for IM7/5250-4 UNI, 50/40/10 layup, OHC-T, R= -1.

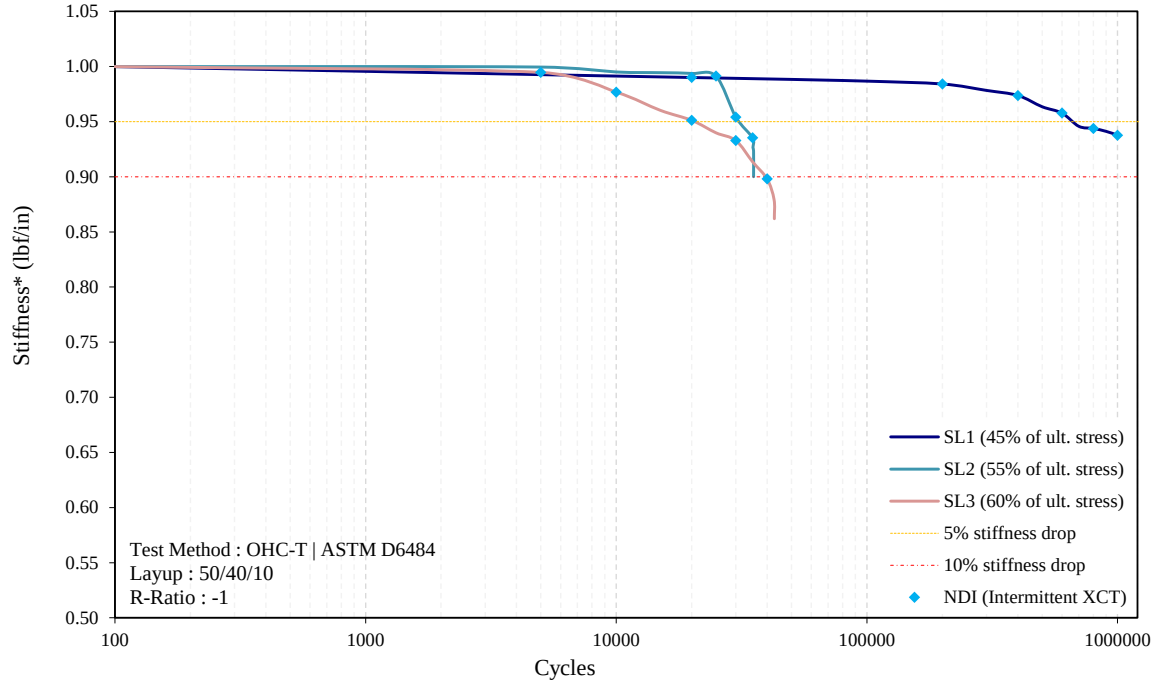


Figure B.107 – Apparent stiffness change during the compression fatigue (normalized by initial compliance) for IM7/5250-4 UNI, 50/40/10 layup, OHC-T, R=-1.

DISTRIBUTION STATEMENT A.
Approved for public release: distribution is unlimited.

25/50/25 Open-Hole Test

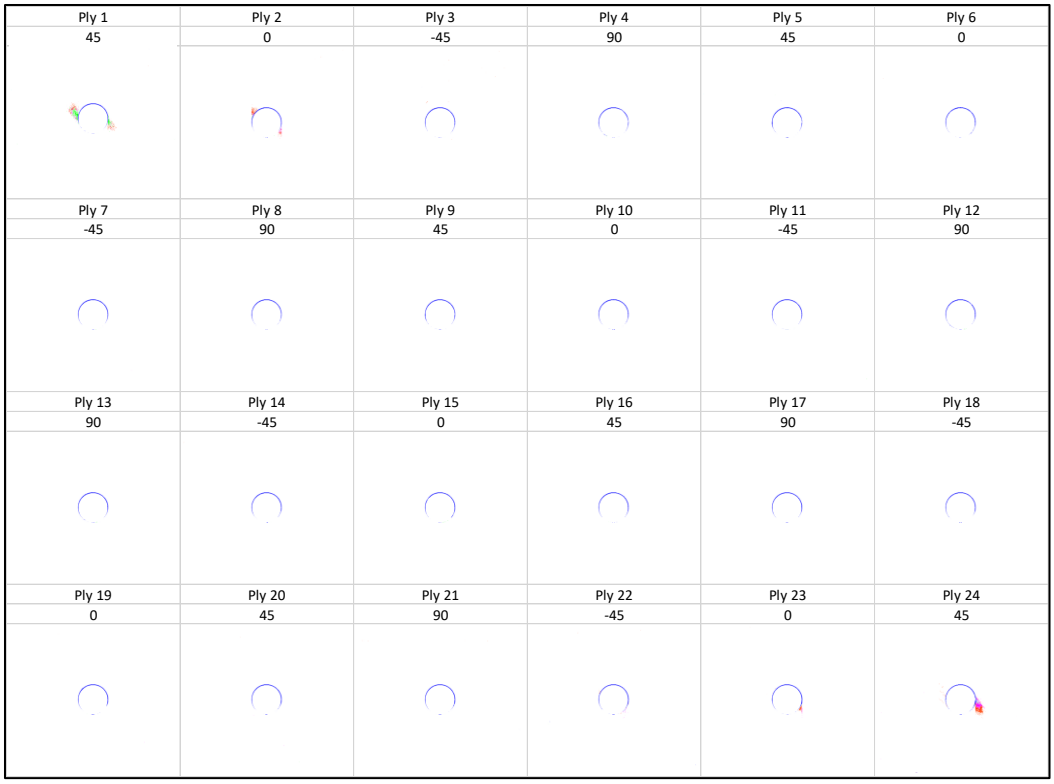
R=0.1, OHT-T → Specimens: SL-1 (70%), SL-2 (80%), and SL-3 (90%)
R=5.0, OHC-C → Specimens: SL-1 (60%), SL-2 (70%), and SL-3 (75%)
R=-1, OHT-C → Specimens: SL-1 (40%), SL-2 (50%), and SL-3 (55%)

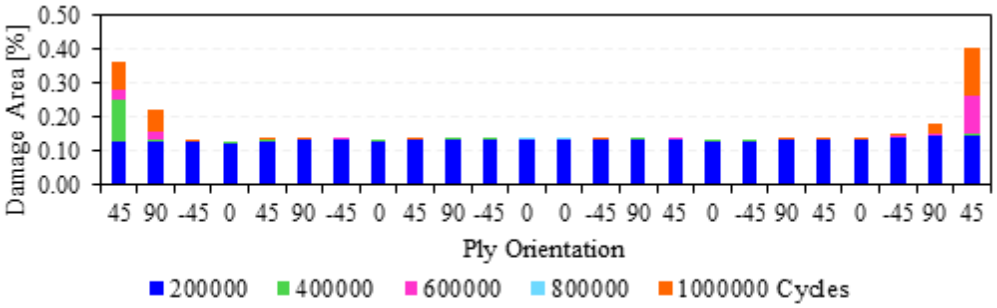
Three specimens were tested for each r-ratio at varying stress levels. Specimens were fatigued until failure or one-million cycles (runout) was achieved. For R=0.1 SL-1 and SL-2 survived fatigue and developed an average of 13% increased residual strength. SL-1 displayed no delamination or fiber failure (Figure B.108). SL-2 survived fatigue also, but displayed large amounts of delamination on its outer 45° plies near the hole. SL-2 also exhibited delamination initiating from the outer edges of the specimen growing towards the center (Figure B.109). The pattern of delamination experienced by SL-2 was also evident in SL-3. In addition, SL-3 also displayed fiber failure on the 90° and adjacent plies near the hole (Figure B.110).

In R=5.0 only SL-1 survived fatigue and developed an average of 3% decreased residual strength. SL-1 displayed no significant areas of delamination or fiber failure (Figure B.112). SL-3 and SL-2 displayed minimal delamination, however both specimens displayed fiber failure on their outermost 45° and 0° plies through the hole (Figure B.113). This damage was more apparent in SL-3 where the fiber failures spanned throughout the first and last 7 plies (Figure B.114).

In R=-1 only SL-1 survived fatigue and developed an average of 30% decreased residual strength. This large decrease of static strength was due to the large delamination near the hole on the first and last 3 plies of SL-1 (Figure B.116). All 3 specimens in this group displayed delamination on the outermost 3 plies centered about the hole. SL-2 and SL-3 failed because of the fiber failures that occurred through the hole (Figure B.117). Nearly all of the plies in SL-2 and SL-3 display fiber failure spanning from the hole to a nearby gap in the fibers (Figure Figure B.118).

DISTRIBUTION STATEMENT A.
Approved for public release: distribution is unlimited.





Specimen ID	MASC1-A1EO11-1K2
Test Method	OHT-T
Material System	IM7 5250-4 UNI
Ply Layup	25/50/25
Number of Plies	24
Stress Ratio	0.1
% Stress	70% of Ultimate Stress
Final Cycles	1,000,000 (runout)
1) Separation between the 45º fibers throughout the region near the hole.	
Comment) No significant damage after fatigue.	

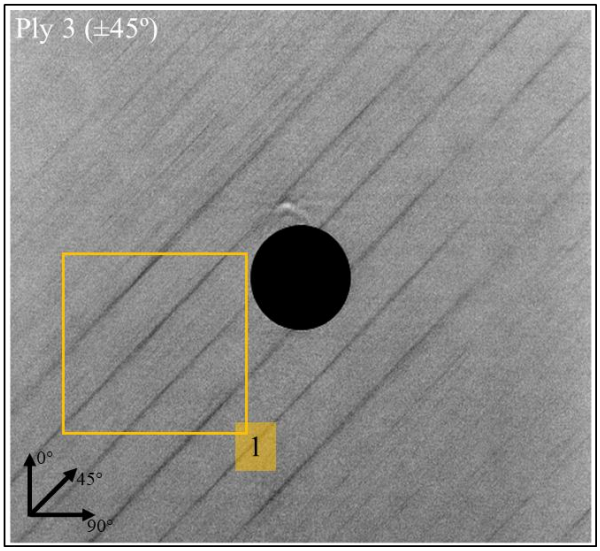
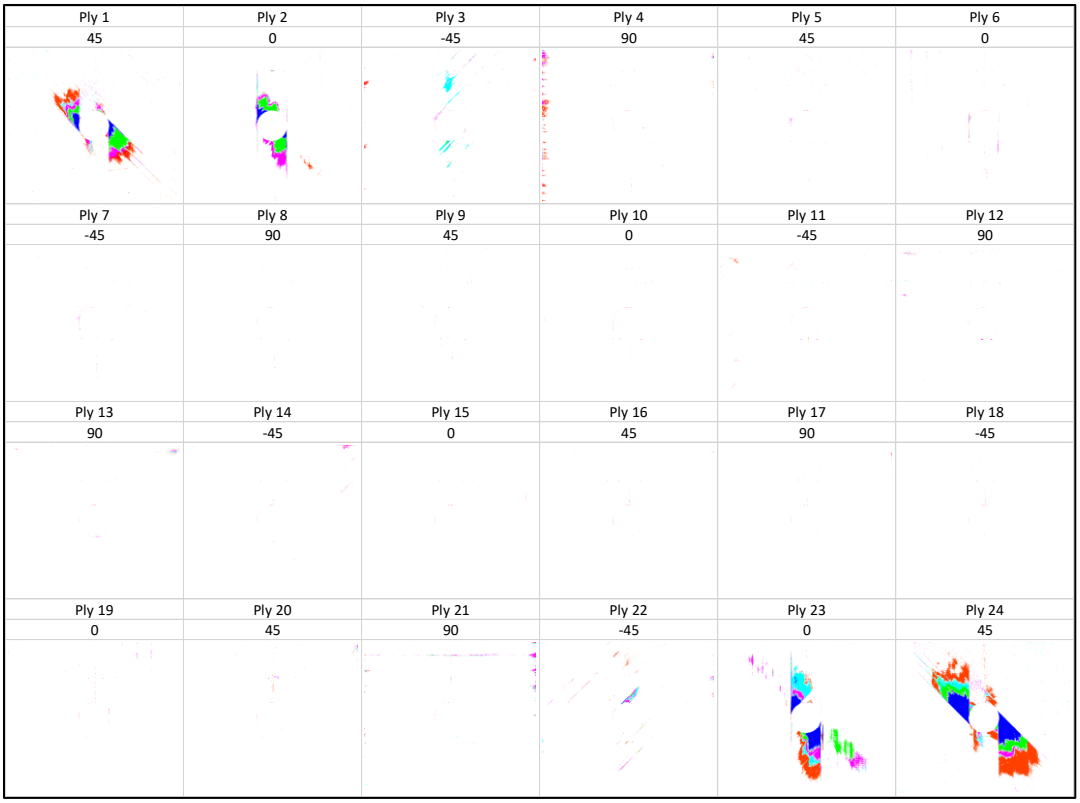
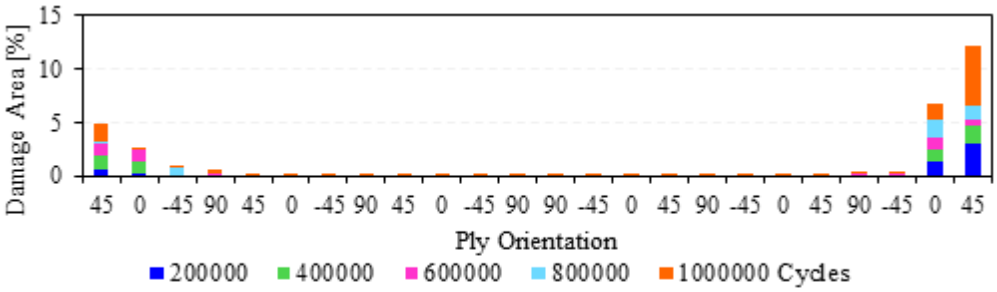


Figure B.108 – Ply-by-ply damage growth and area increase for IM7/5250-4, 25/50/25, R=0.1, SL1.

DISTRIBUTION STATEMENT A.
Approved for public release: distribution is unlimited.





Specimen ID	MASC1-A1EO11-2K1
Test Method	OHT-T
Material System	IM7 5250-4 UNI
Ply Layup	25/50/25
Number of Plies	24
Stress Ratio	0.1
% Stress	80% of Ultimate Stress
Final Cycles	1,000,000 (runout)
1) Separation between the 45° fibers throughout the region near the hole.	
2) Fiber failure forming from the hole extending along the 45° direction.	
3) Minor delamination from the outer edge to the center along the 90° direction.	

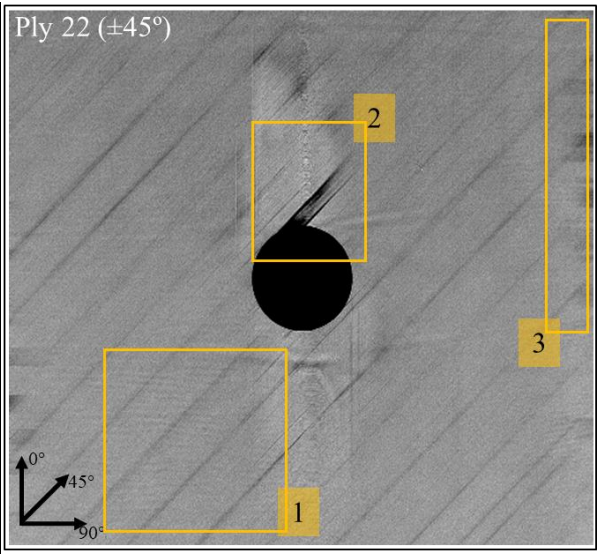
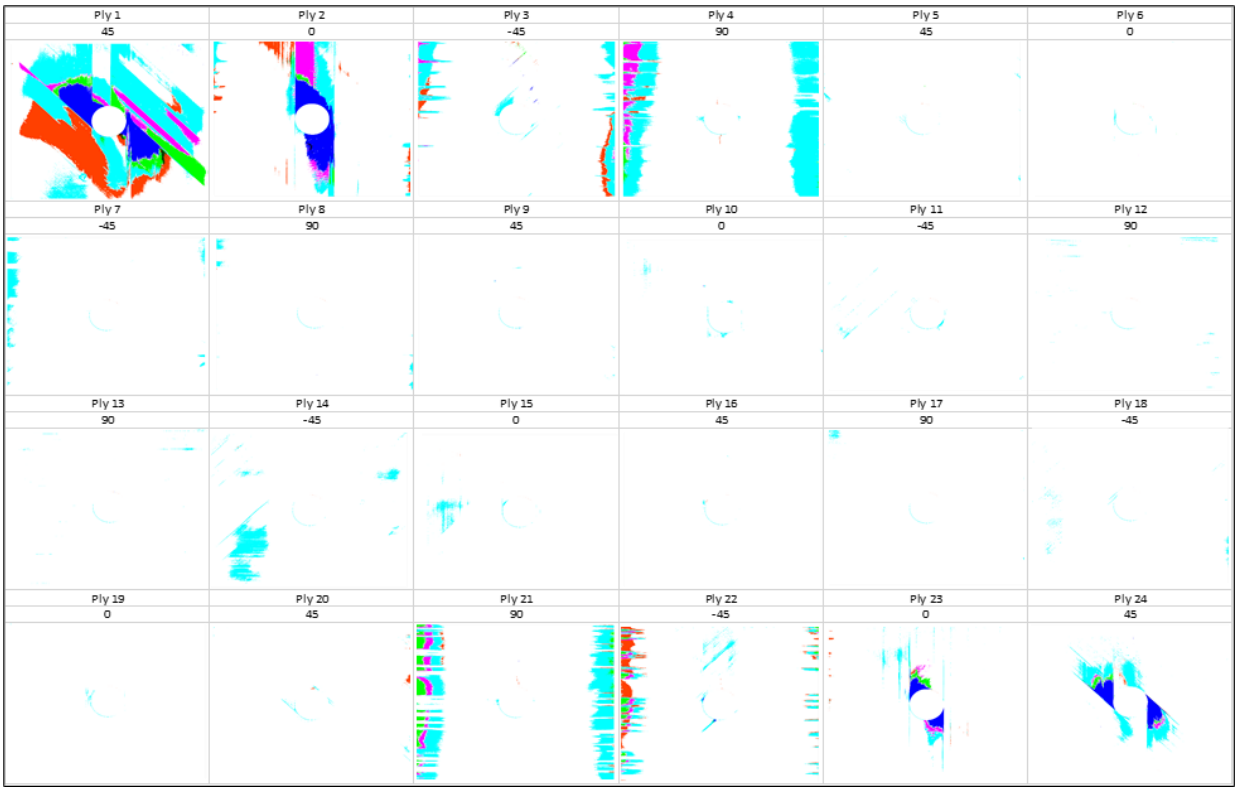
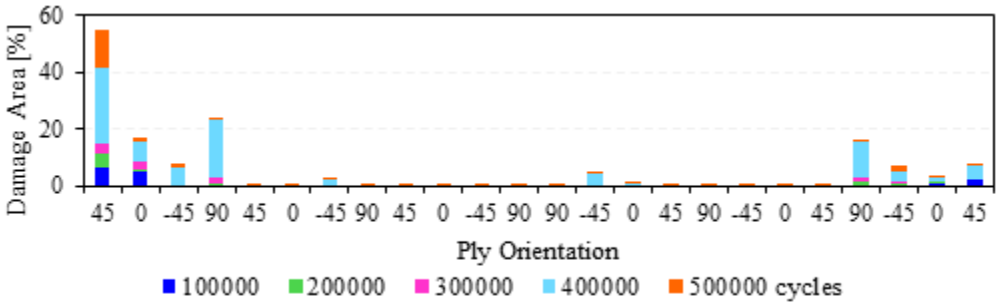


Figure B.109 – Ply-by-ply damage growth and area increase for IM7/5250-4, 25/50/25, R=0.1, SL2.

DISTRIBUTION STATEMENT A.
Approved for public release: distribution is unlimited.





Specimen ID	MASC1-A3EO11-3K1
Test Method	OHT-T
Material System	IM7 5250-4 UNI
Ply Layup	25/50/25
Number of Plies	24
Stress Ratio	0.1
% Stress	90% of Ultimate Stress
Final Cycles	605,661
1) Complete delamination of the outer edge to the center along the 90° direction.	
2) Fiber separation extending horizontally from the hole in the 90° direction	
3) Fiber failure extending from the hole perpendicular to the 90° fibers.	

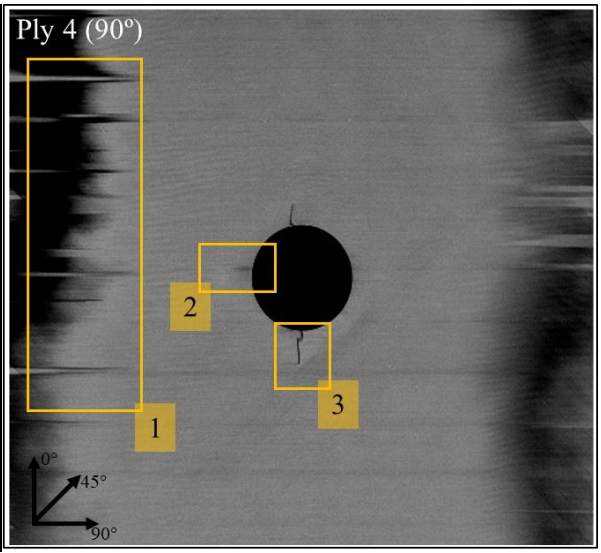


Figure B.110 – Ply-by-ply damage growth and area increase for IM7/5250-4, 25/50/25, R=0.1, SL3.

DISTRIBUTION STATEMENT A.
Approved for public release: distribution is unlimited.

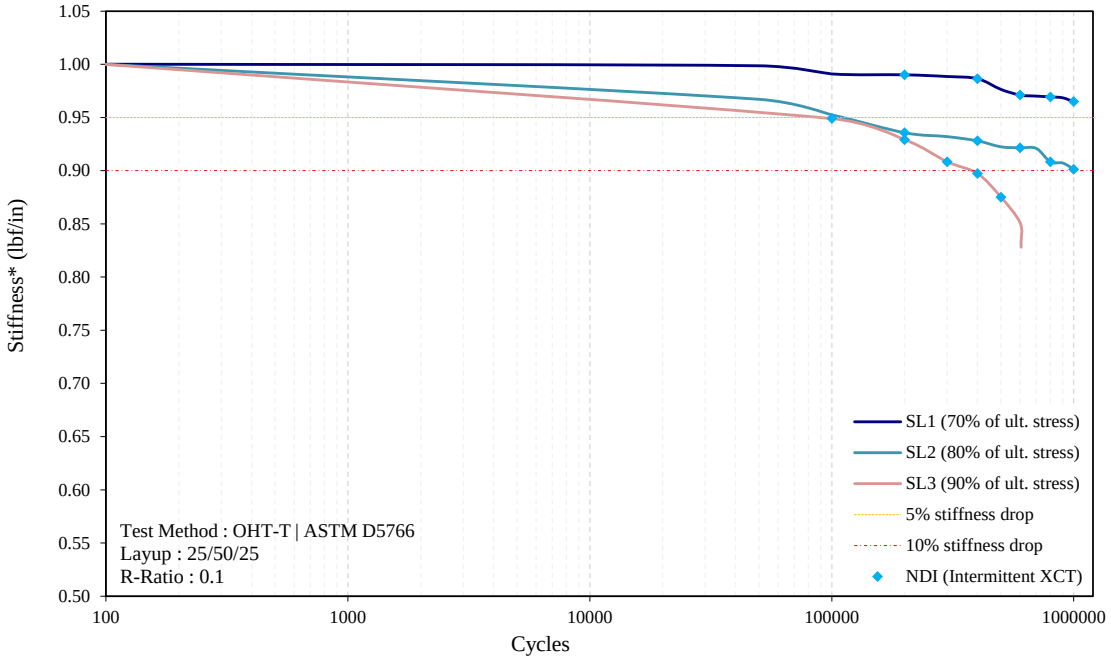
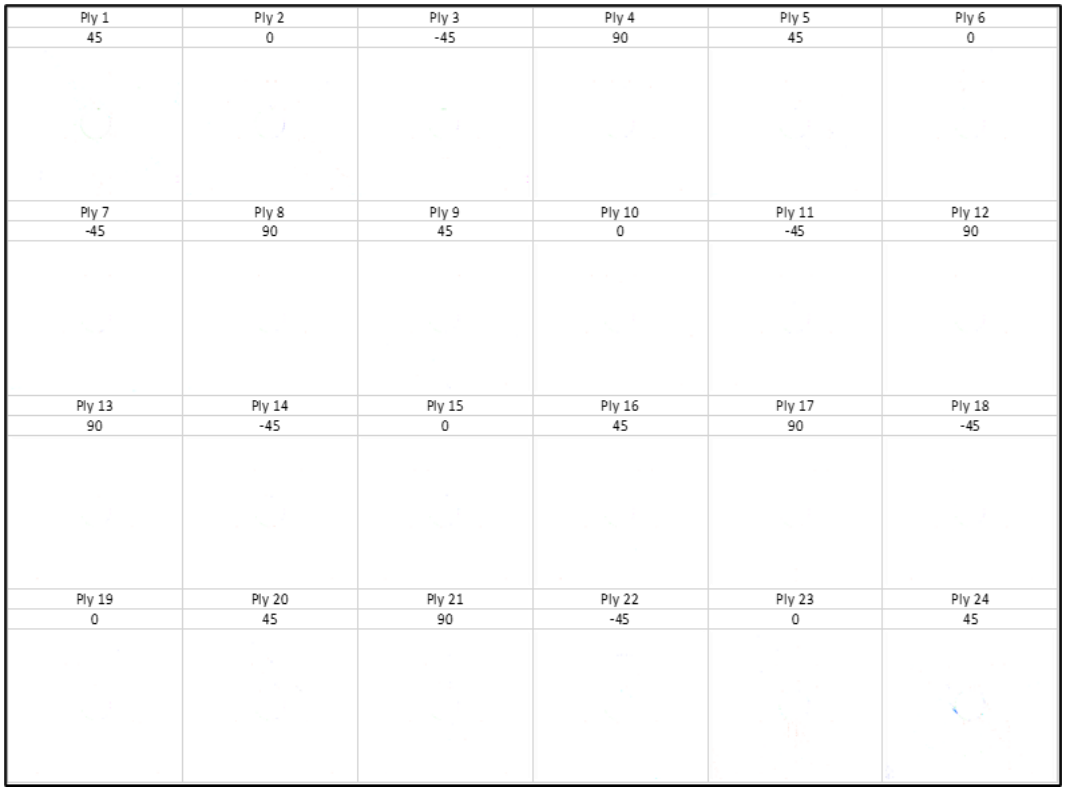
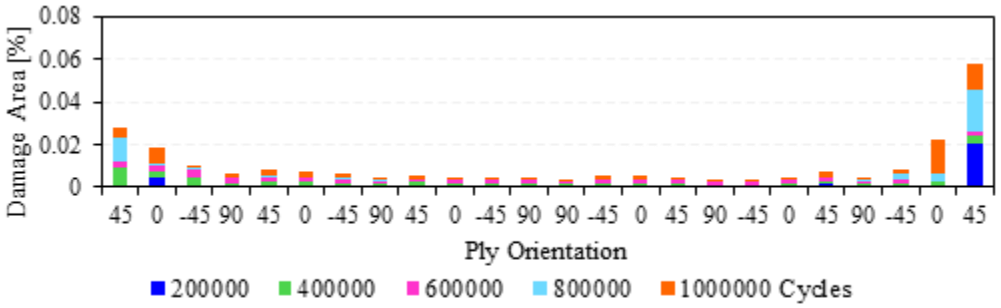


Figure B.111 – Apparent stiffness change during fatigue (normalized by initial compliance) for IM7/5250-4 UNI, 25/50/25 layup, OHT-T, R=0.1.

DISTRIBUTION STATEMENT A.
Approved for public release: distribution is unlimited.





Specimen ID	MASC1-A3EO11-XX2
Test Method	OHC-C
Material System	IM7 5250-4 UNI
Ply Layup	25/50/25
Number of Plies	24
Stress Ratio	5.0
% Stress	60% of Ultimate Stress
Final Cycles	1,000,000 (runout)
Comment) No significant damage after fatigue.	

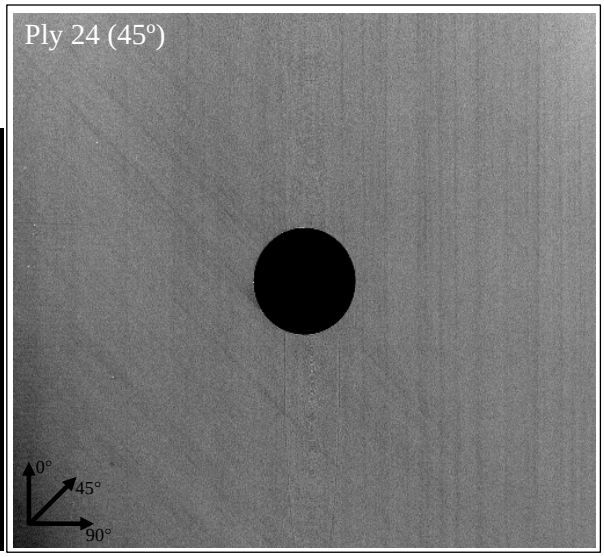
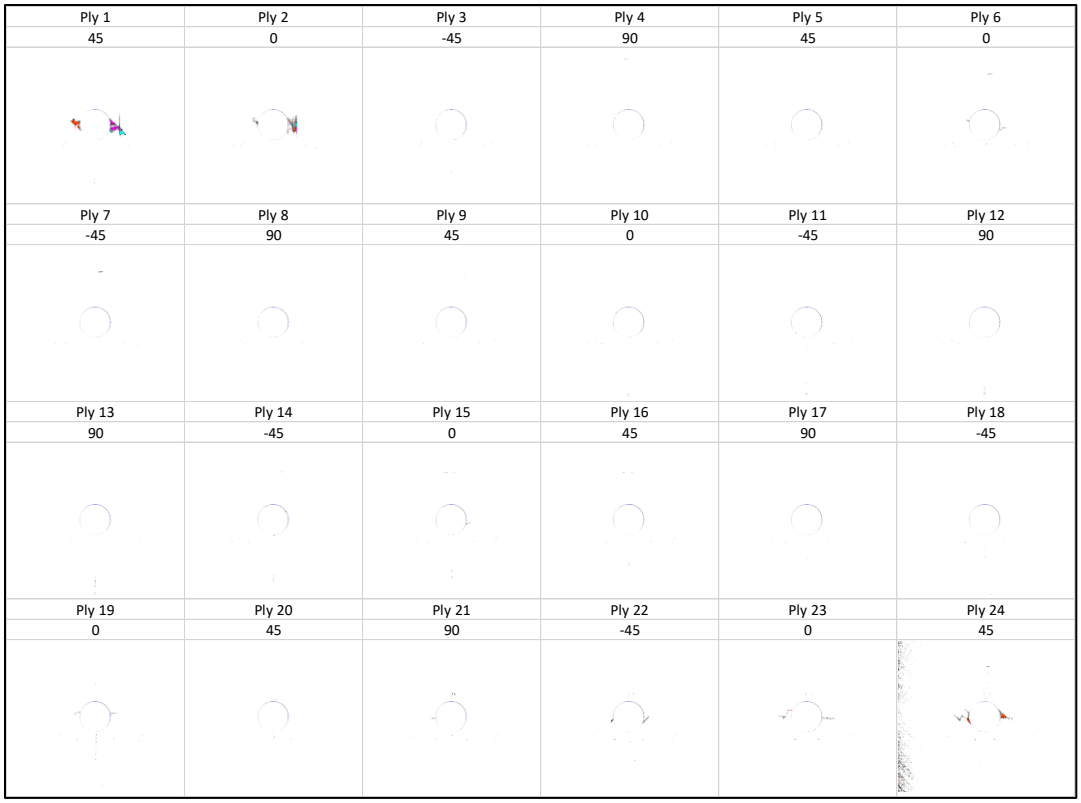
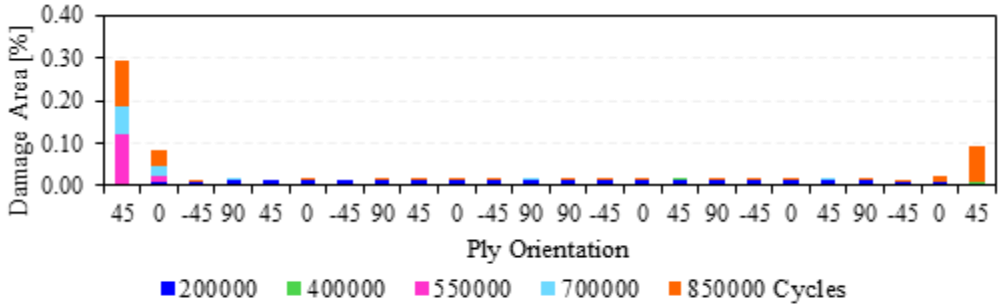


Figure B.112 – Ply-by-ply damage growth and area increase for IM7/5250-4, 25/50/25, R=5, SL1.

DISTRIBUTION STATEMENT A.
Approved for public release: distribution is unlimited.





Specimen ID	MASC1-A1EO11-1L1
Test Method	OHC-C
Material System	IM7 5250-4 UNI
Ply Layup	25/50/25
Number of Plies	24
Stress Ratio	5.0
% Stress	70% of Ultimate Stress
Final Cycles	949,923
1) Separation between the 0º fibers throughout the region near the hole.	
2) Fiber failure extending horizontally from the hole in the 90º direction.	

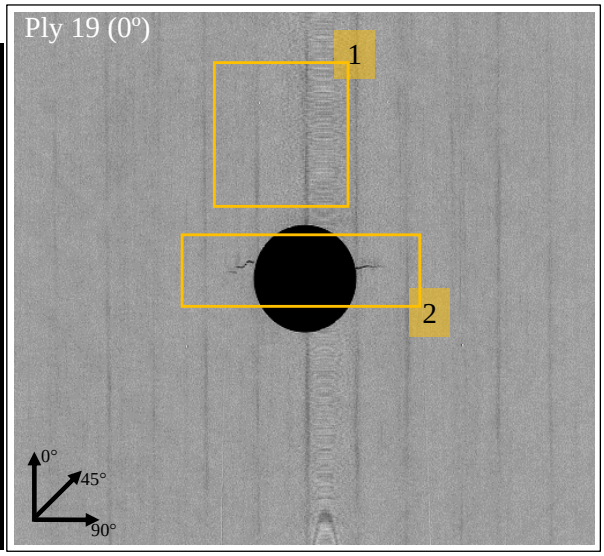
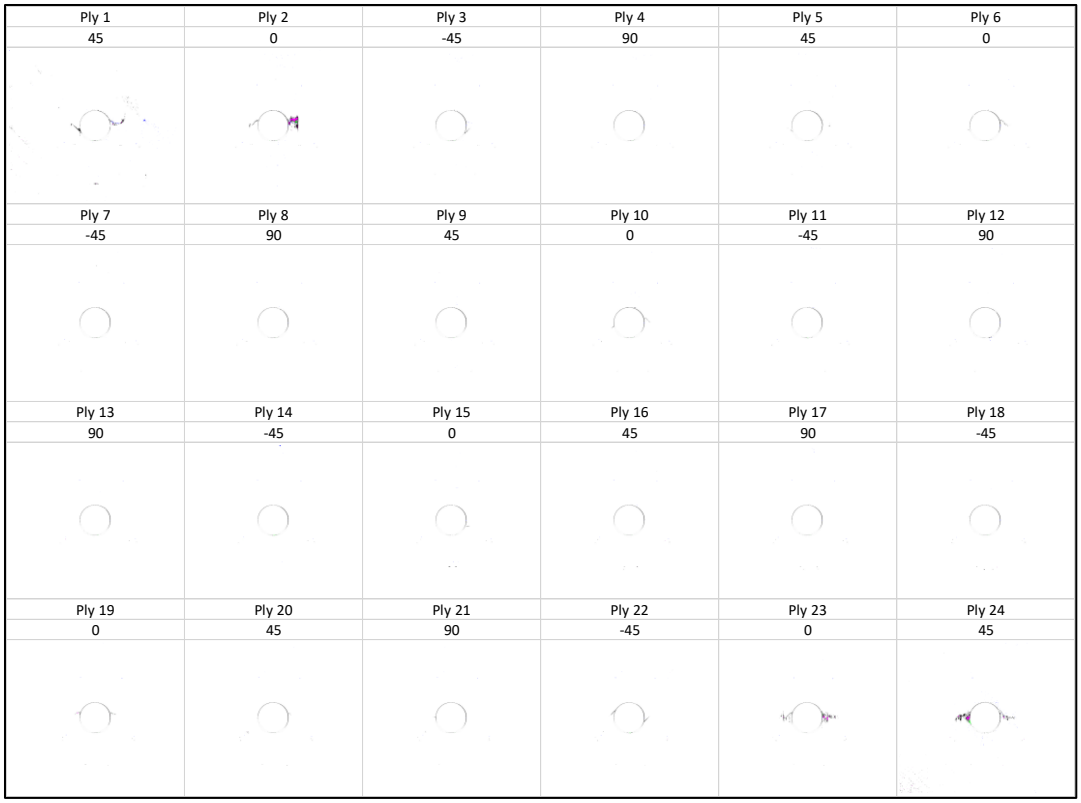
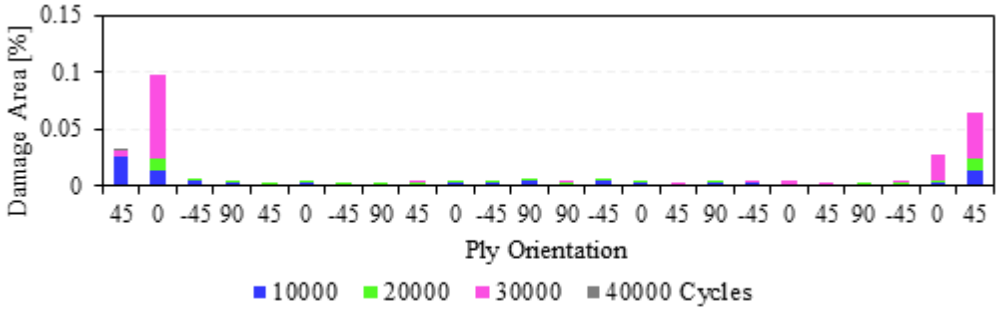


Figure B.113 – Ply-by-ply damage growth and area increase for IM7/5250-4, 25/50/25, R=5, SL2.

DISTRIBUTION STATEMENT A.
Approved for public release: distribution is unlimited.





Specimen ID	MASC1-A2EO11-2L1
Test Method	OHC-C
Material System	IM7 5250-4 UNI
Ply Layup	25/50/25
Number of Plies	24
Stress Ratio	5.0
% Stress	75% of Ultimate Stress
Final Cycles	46,829
1) Fiber failure extending horizontally from the hole in the 90º direction.	

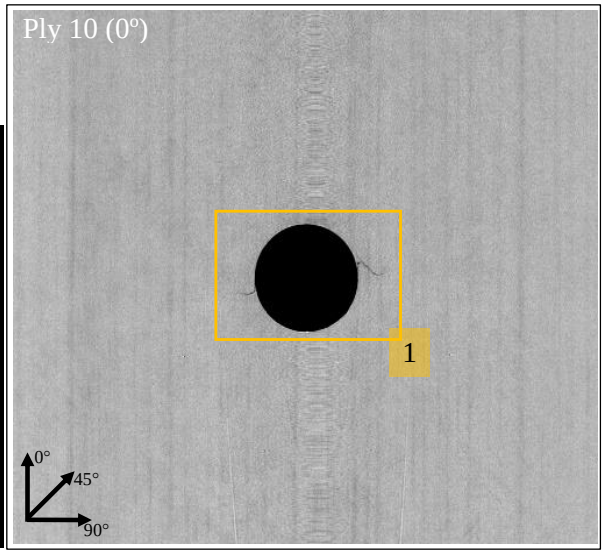


Figure B.114 – Ply-by-ply damage growth and area increase for IM7/5250-4, 25/50/25, R=5, SL3.

DISTRIBUTION STATEMENT A.
Approved for public release: distribution is unlimited.

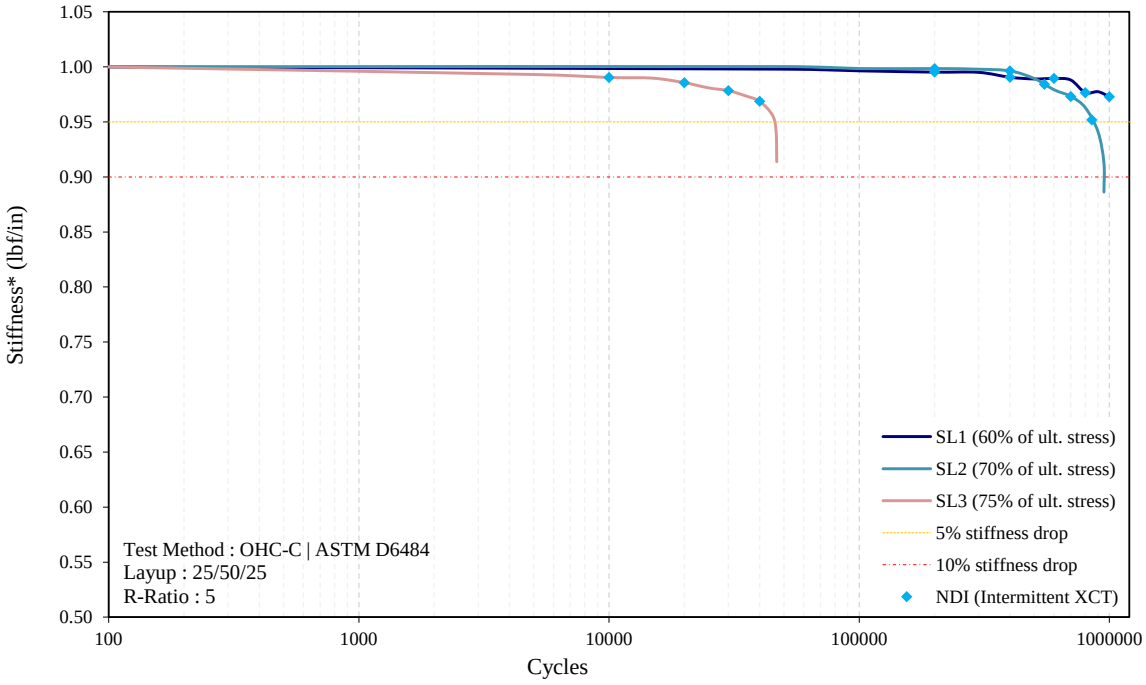
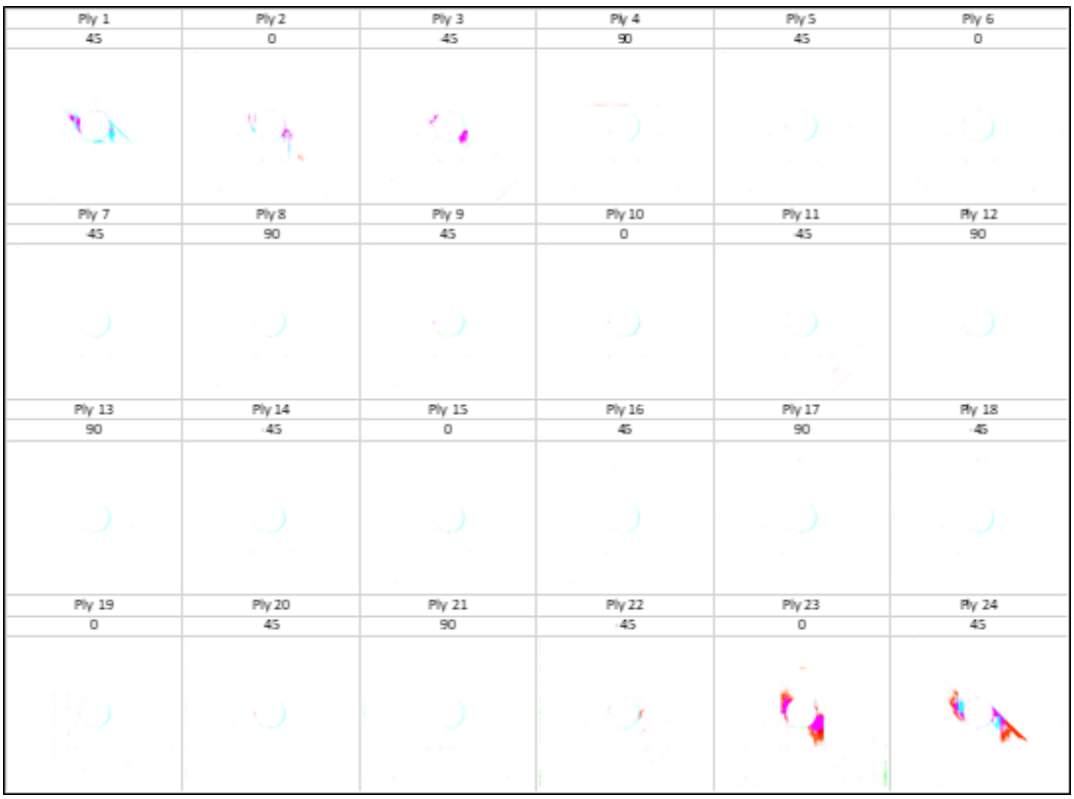
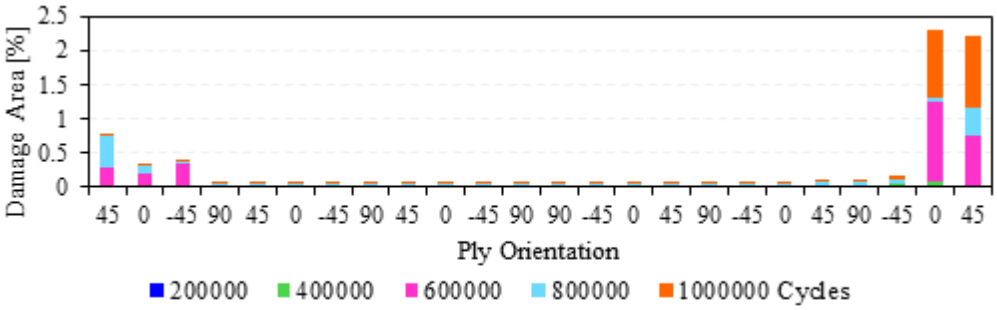


Figure B.115 – Apparent stiffness change during fatigue (normalized by initial compliance) for IM7/5250-4 UNI, 25/50/25 layup, OHC-C, R=5.

DISTRIBUTION STATEMENT A.
Approved for public release: distribution is unlimited.





Specimen ID	MASC1-A3EO11-3M1
Test Method	OHC-T
Material System	IM7 5250-4 UNI
Ply Layup	25/50/25
Number of Plies	24
Stress Ratio	-1.0
% Stress	40% of Ultimate Stress
Final Cycles	1,000,000 (runout)
1) Fiber failure horizontally extending from the hole leading to a large fiber separation.	

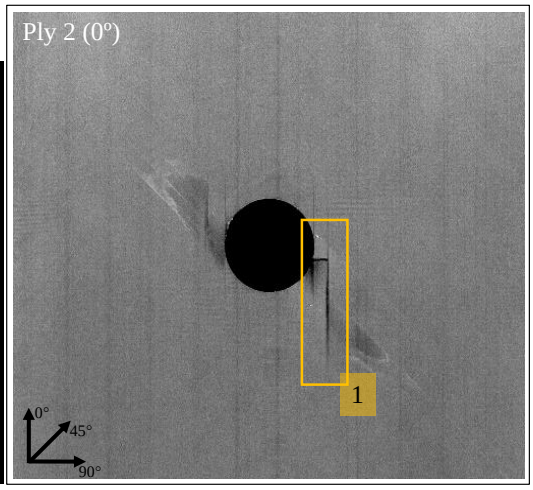
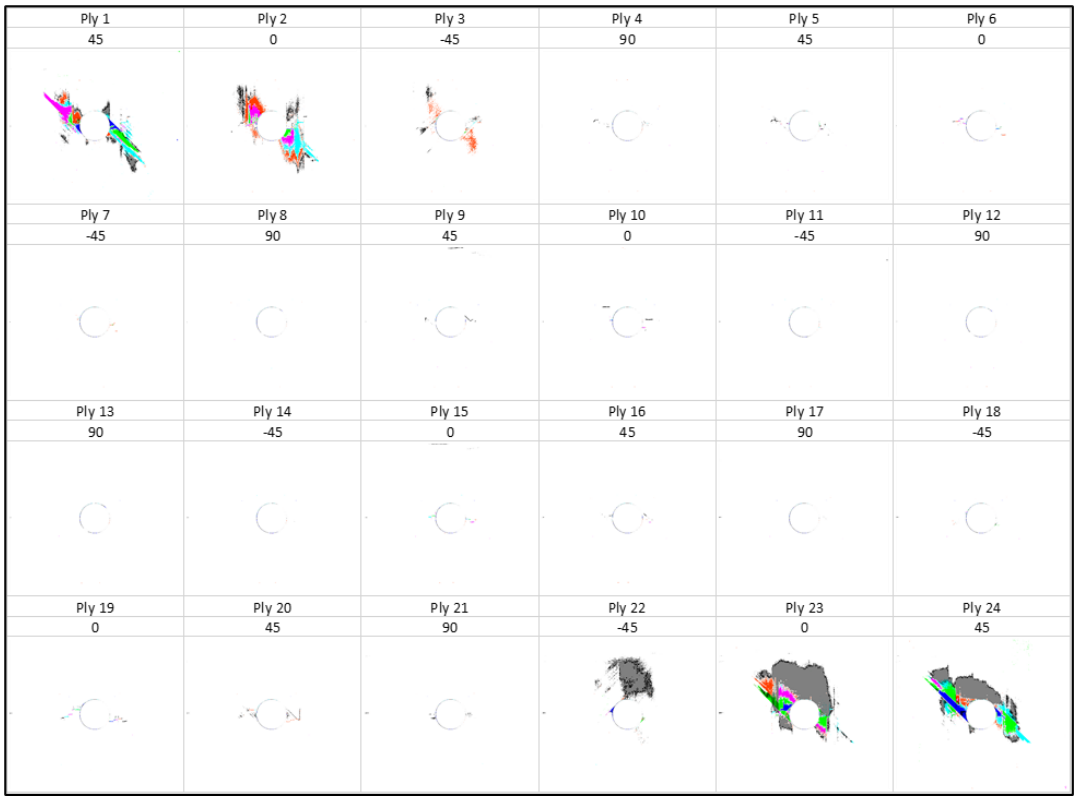
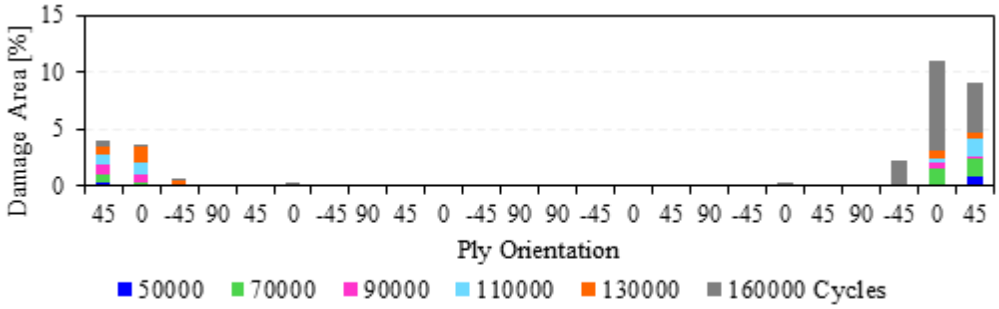


Figure B.116 – Ply-by-ply damage growth and area increase for IM7/5250-4, 25/50/25, R=-1, SL1.

DISTRIBUTION STATEMENT A.
Approved for public release: distribution is unlimited.





Specimen ID	MASC1-A1EO11-1M1
Test Method	OHC-T
Material System	IM7 5250-4 UNI
Ply Layup	25/50/25
Number of Plies	24
Stress Ratio	-1.0
% Stress	50% of Ultimate Stress
Final Cycles	172,295
1) Fiber failure extending horizontally from the hole, and extending from a fiber failure.	
2) Fiber failure extending from the outer edge in 0º direction towards the hole.	

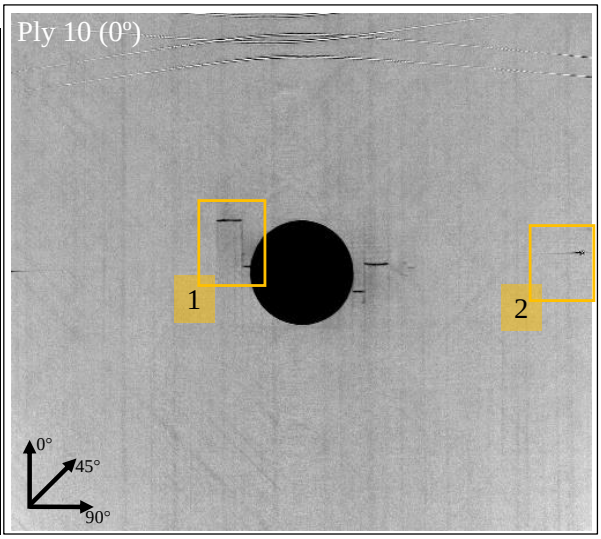
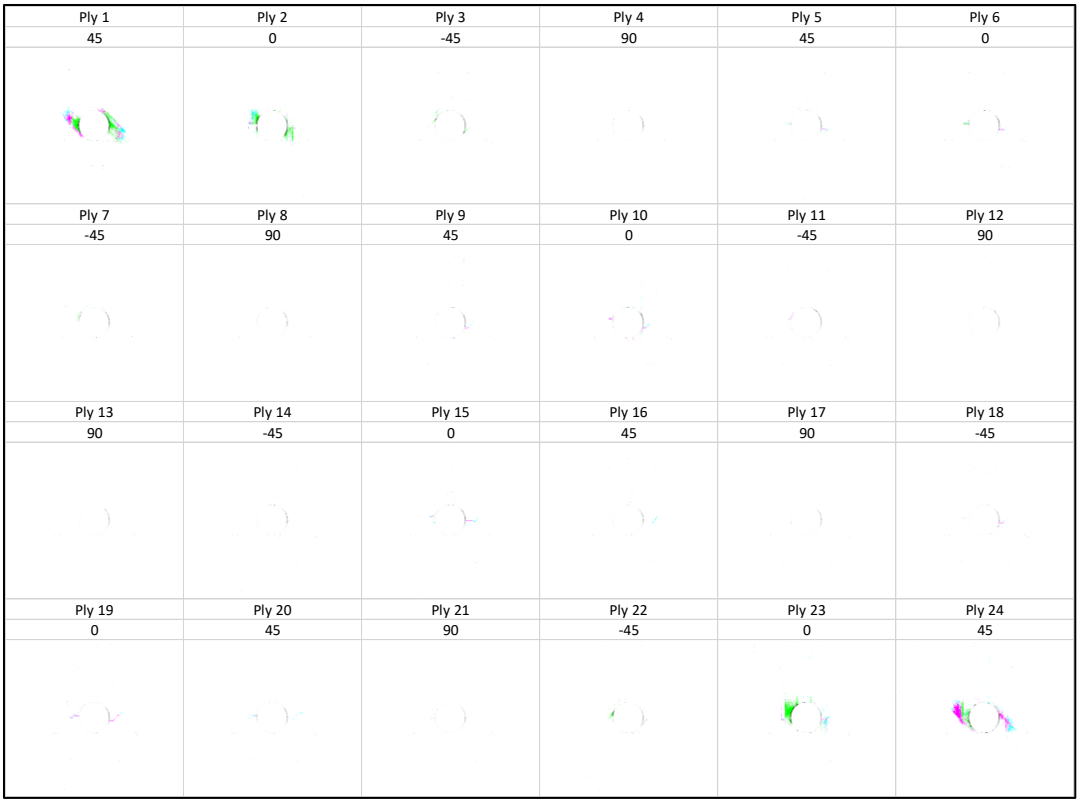
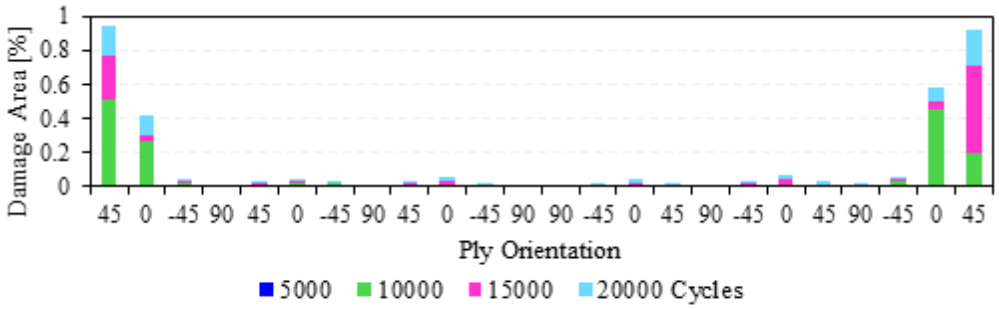


Figure B.117 – Ply-by-ply damage growth and area increase for IM7/5250-4, 25/50/25, R=-1, SL2.

DISTRIBUTION STATEMENT A.
Approved for public release: distribution is unlimited.





Specimen ID	MASC1-A2EO11-2M1
Test Method	OHC-T
Material System	IM7 5250-4 UNI
Ply Layup	25/50/25
Number of Plies	24
Stress Ratio	-1.0
% Stress	55% of Ultimate Stress
Final Cycles	24,404
1) Fiber failure extending horizontally from the hole in the 90º direction.	

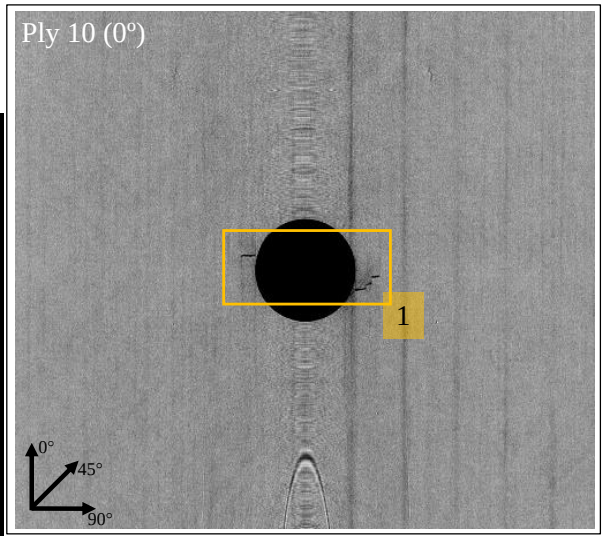


Figure B.118 – Ply-by-ply damage growth and area increase for IM7/5250-4, 25/50/25, R=-1, SL3.

DISTRIBUTION STATEMENT A.
Approved for public release: distribution is unlimited.

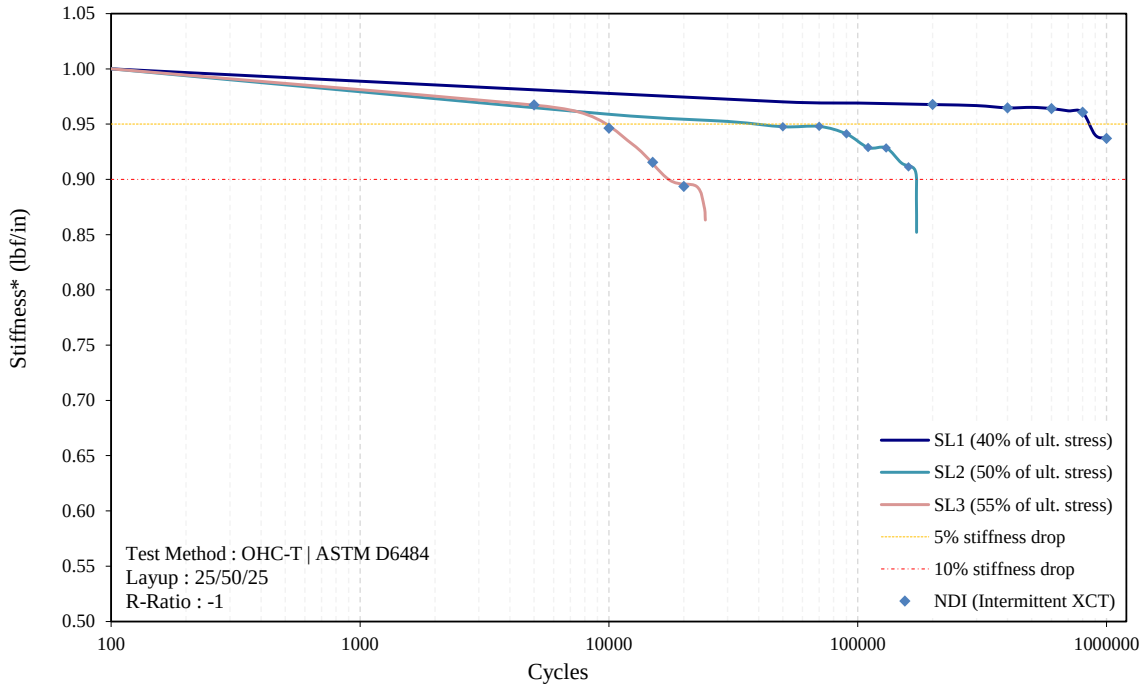


Figure B.119 – Apparent stiffness change during the tension fatigue (normalized by initial compliance) for IM7/5250-4 UNI, 25/50/25 layup, OHC-T, R=-1.

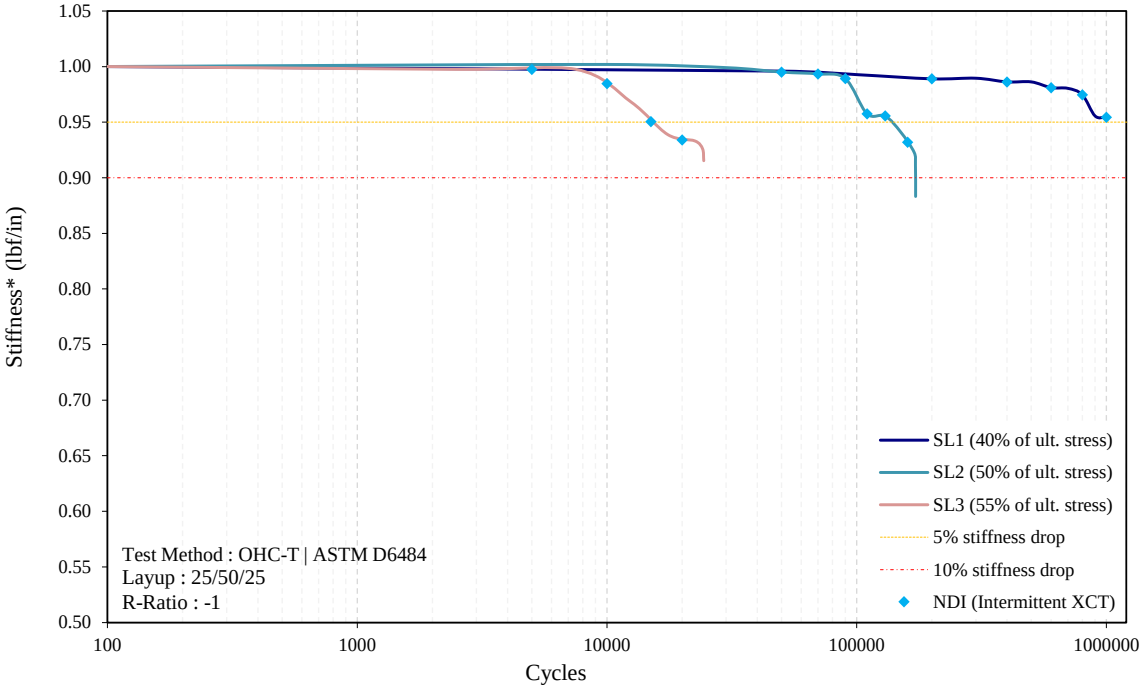


Figure B.120 – Apparent stiffness change during the compression fatigue (normalized by initial compliance) for IM7/5250-4 UNI, 25/50/25 layup, OHC-T, R=-1.

DISTRIBUTION STATEMENT A.
Approved for public release: distribution is unlimited.

10/80/10 Open-Hole Test

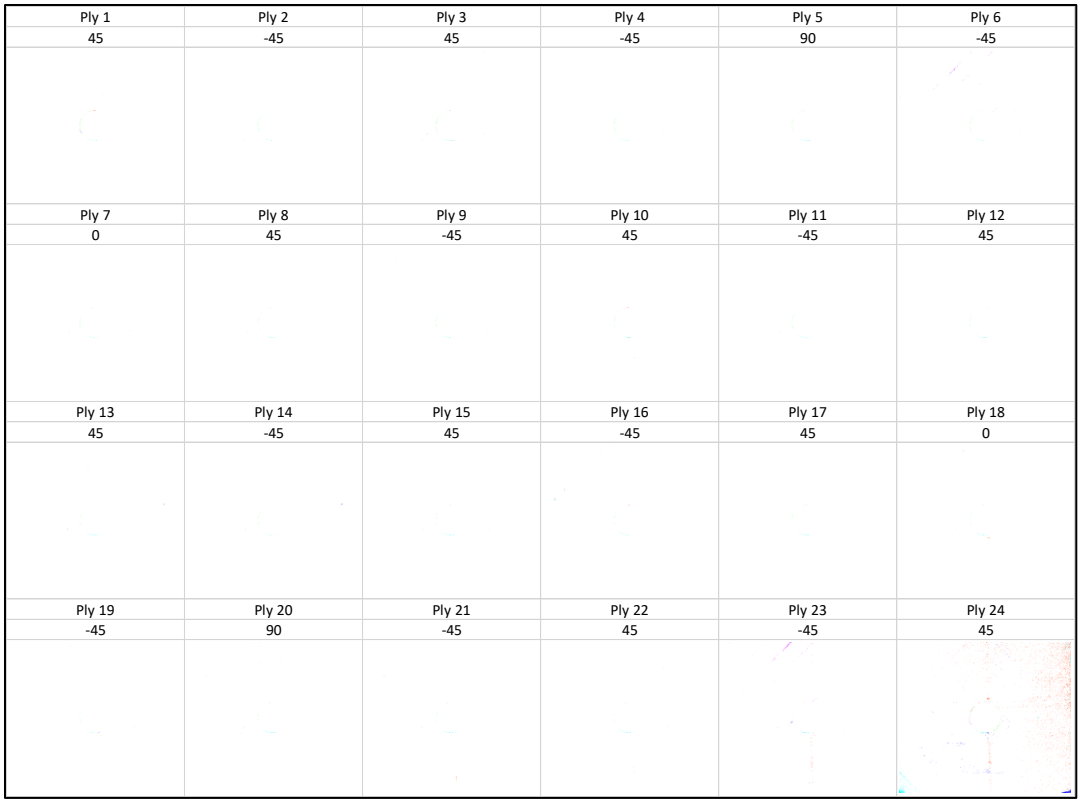
R=0.1, OHT-T → Specimens: SL-1 (60%), SL-2 (70%), and SL-3 (80%)
R=5.0, OHC-C → Specimens: SL-1 (65%), SL-2 (72.5%), and SL-3 (75%)
R=-1, OHT-C → Specimens: SL-1 (35%), SL-2 (45%), and SL-3 (50%)

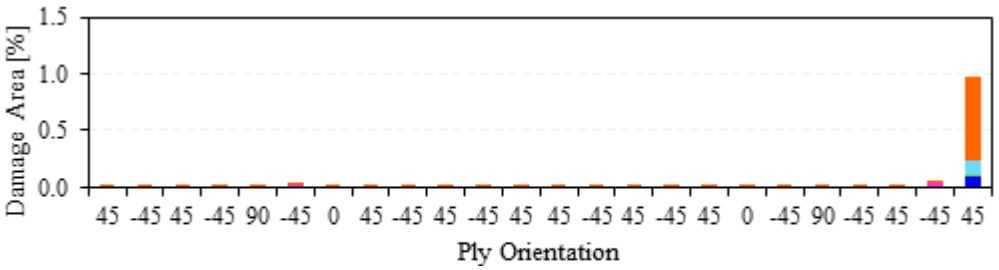
Three specimens were tested for each r-ratio at varying stress levels. Specimens were fatigued until failure or one-million cycles (runout) was achieved. For R=0.1 only SL-1 survived fatigue and developed an average of 3% decreased residual strength. SL-1 displayed minor damage throughout the specimen except on one of its outermost 45° plies (Figure Figure B.121). SL-2 displayed the greatest damage because the last scan was taken roughly 5,000 cycles before the specimen failed. SL-2 exhibits major delamination in the 45° direction through the hole throughout the majority of its damaged plies. SL-2 also displayed delamination that began on the outer edges of the specimen spreading towards the specimen's center (Figure B.122). In this group of specimens fiber-failure and delamination lead to accelerated failure. Due to the nature of this group, SL-3 displayed little damage in its latest scan (Figure B.123).

In R=5.0 only SL-1 survived fatigue and developed an average of 2% decreased residual strength. All 3 specimens demonstrate the same fiber failure within their 0° plies (Figure Figure B.125). However, in SL-2 and SL-3 the fiber failure extends to adjacent 45° and 90° plies (Figure Figure B.126). This fiber failure is apparent in SL-3, more than 14 plies demonstrate fiber failure through the hole (Figure B.127). This group of specimens did not display any significant delamination. Fiber failure in this group leads to accelerated failure of the specimen.

In R=-1 only SL-1 survived fatigue developing an average of 10% decreased residual strength (Figure B.129). The main form of damage in this group was the enlargement of spaces between fibers, primarily in the 45° plies (Figure B.130). Throughout all 3 specimens there was only minor delamination and fiber failure (Figure B.131). Fiber failure in this group leads to an accelerated failure of the specimen.

DISTRIBUTION STATEMENT A.
Approved for public release: distribution is unlimited.





Specimen ID	MASC1-A1FO11-1K1
Test Method	OHT-T
Material System	IM7 5250-4 UNI
Ply Layup	10/80/10
Number of Plies	24
Stress Ratio	0.1
% Stress	60% of Ultimate Stress
Final Cycles	1,000,000 (runout)
Comment) No significant damage after fatigue.	

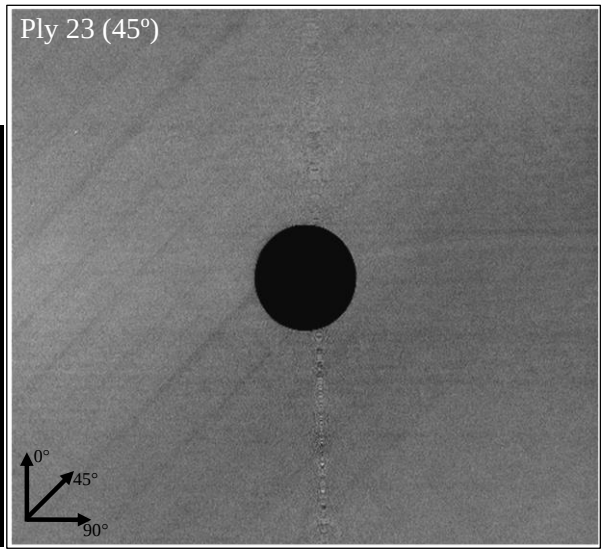
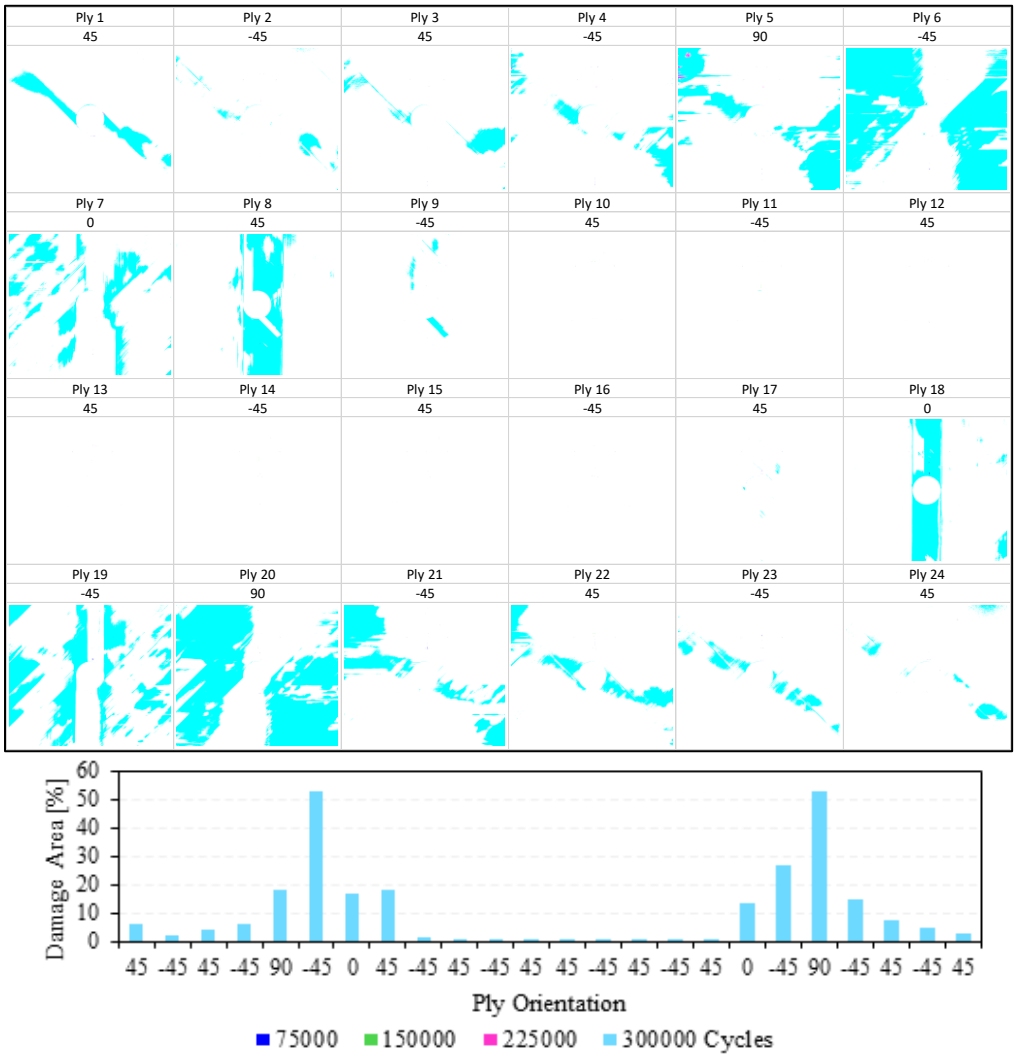


Figure B.121 – Ply-by-ply damage growth and area for IM7/5250-4, 10/80/10, R=0.1, SL1.

DISTRIBUTION STATEMENT A.
Approved for public release: distribution is unlimited.



Specimen ID	MASC1-A2FO11-2K1
Test Method	OHT-T
Material System	IM7 5250-4 UNI
Ply Layup	10/80/10
Number of Plies	24
Stress Ratio	0.1
% Stress	70% of Ultimate Stress
Final Cycles	305,951
1) Delamination from the outer edge to the center along the 45° direction.	
2) Delamination extending from the hole vertically in the 0º direction.	
3) Significant fiber separation between the 45º fibers in the 0º direction tangent to the hole.	

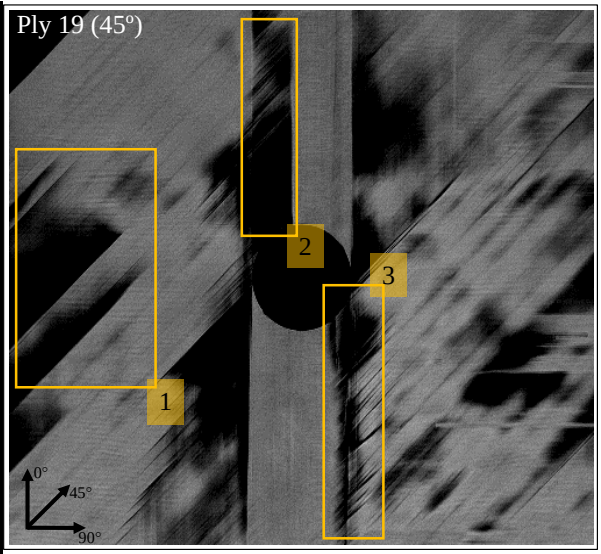
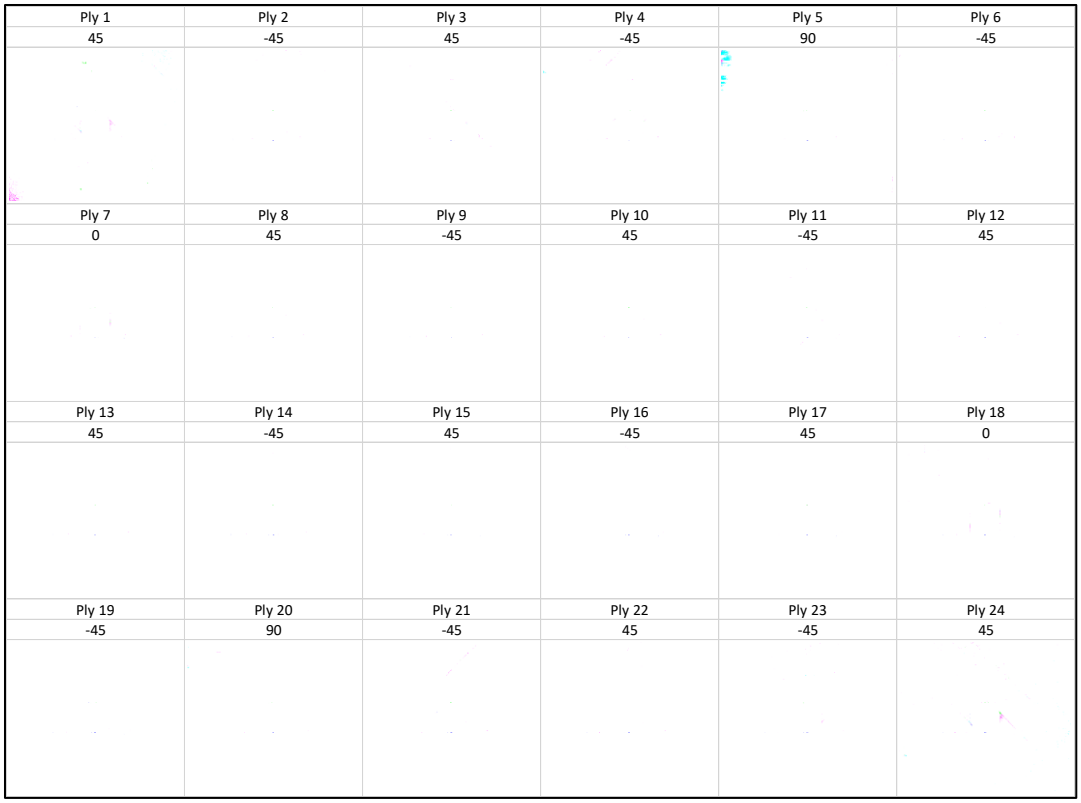
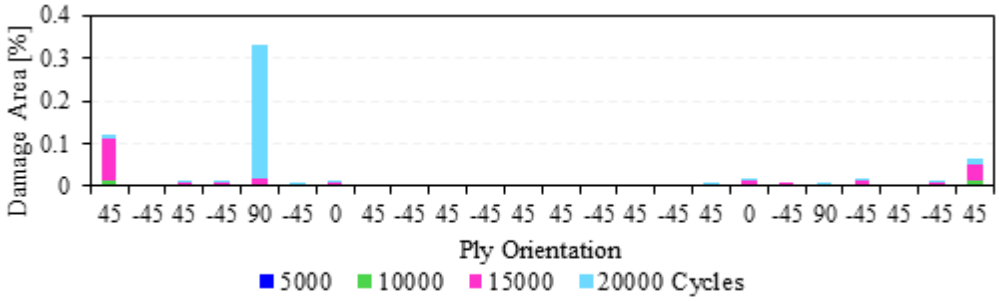
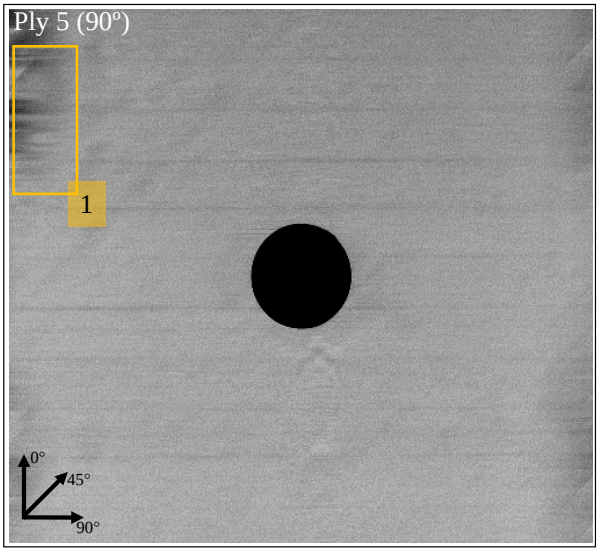


Figure B.122 – Ply-by-ply damage growth and area for IM7/5250-4, 10/80/10, R=0.1, SL2.

DISTRIBUTION STATEMENT A.
Approved for public release: distribution is unlimited.







Specimen ID	MASC1-A3FO11-3K1
Test Method	OHT-T
Material System	IM7 5250-4 UNI
Ply Layup	10/80/10
Number of Plies	24
Stress Ratio	0.1
% Stress	80% of Ultimate Stress
Final Cycles	29,600
1) Minor delamination from the outer edge to the center along the 90° direction.	

Figure B.123 – Ply-by-ply damage growth and area increase for IM7/5250-4, 10/80/10, R=0.1, SL3.

DISTRIBUTION STATEMENT A.
Approved for public release: distribution is unlimited.

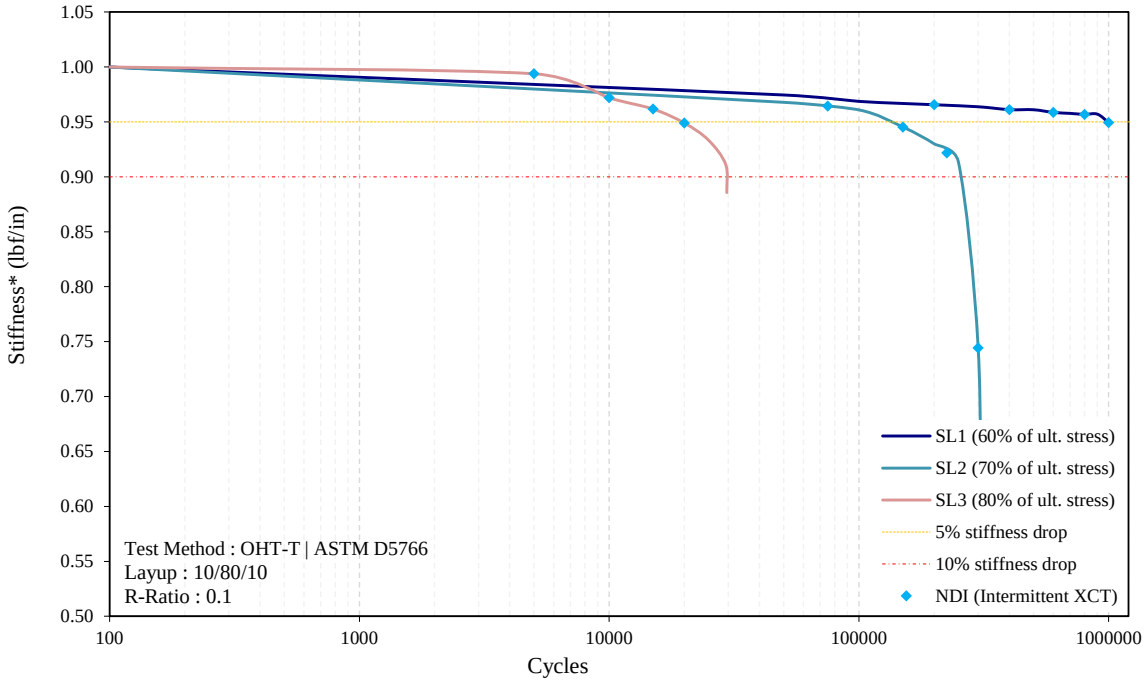
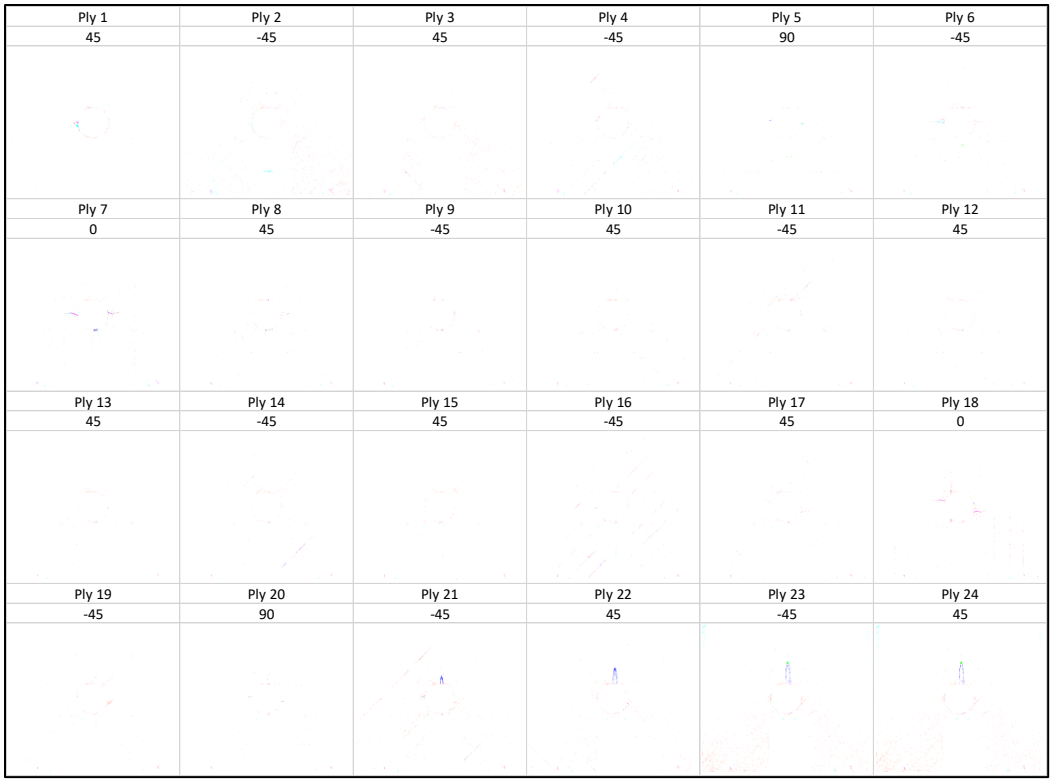
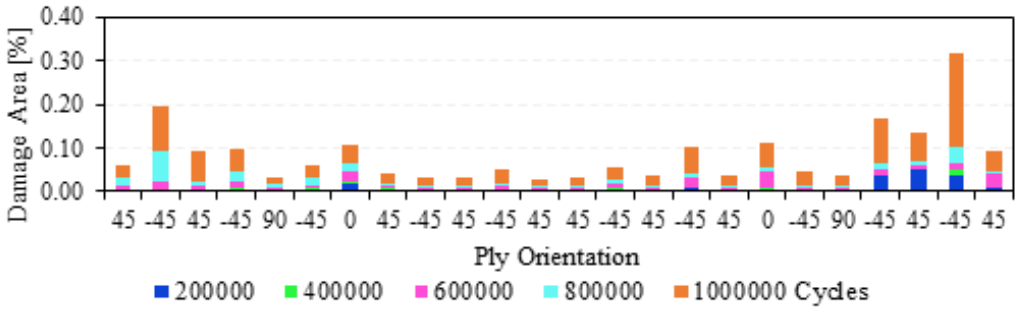


Figure B.124 – Apparent stiffness change during fatigue (normalized by initial compliance) for IM7/5250-4 UNI, 10/80/10 layup, OHT-T, R=0.1.

DISTRIBUTION STATEMENT A.
Approved for public release: distribution is unlimited.





Specimen ID	MASC1-A3FO11-3L1
Test Method	OHC-C
Material System	IM7 5250-4 UNI
Ply Layup	10/80/10
Number of Plies	24
Stress Ratio	5.0
% Stress	65% of Ultimate Stress
Final Cycles	1,000,000 (runout)
1) Fiber failure extending horizontally from the hole in the 90º direction.	

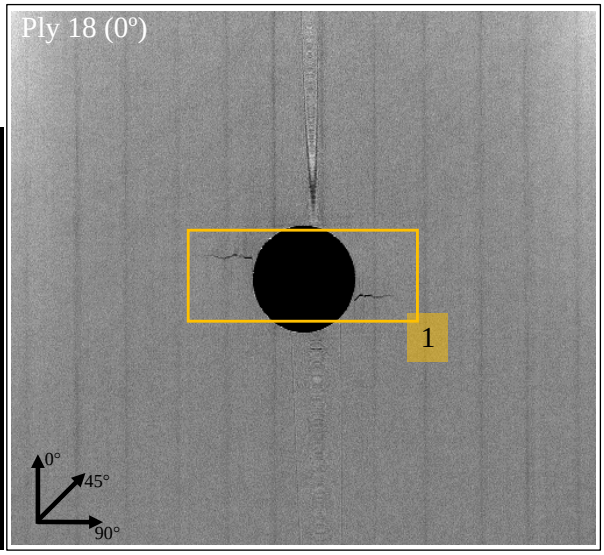
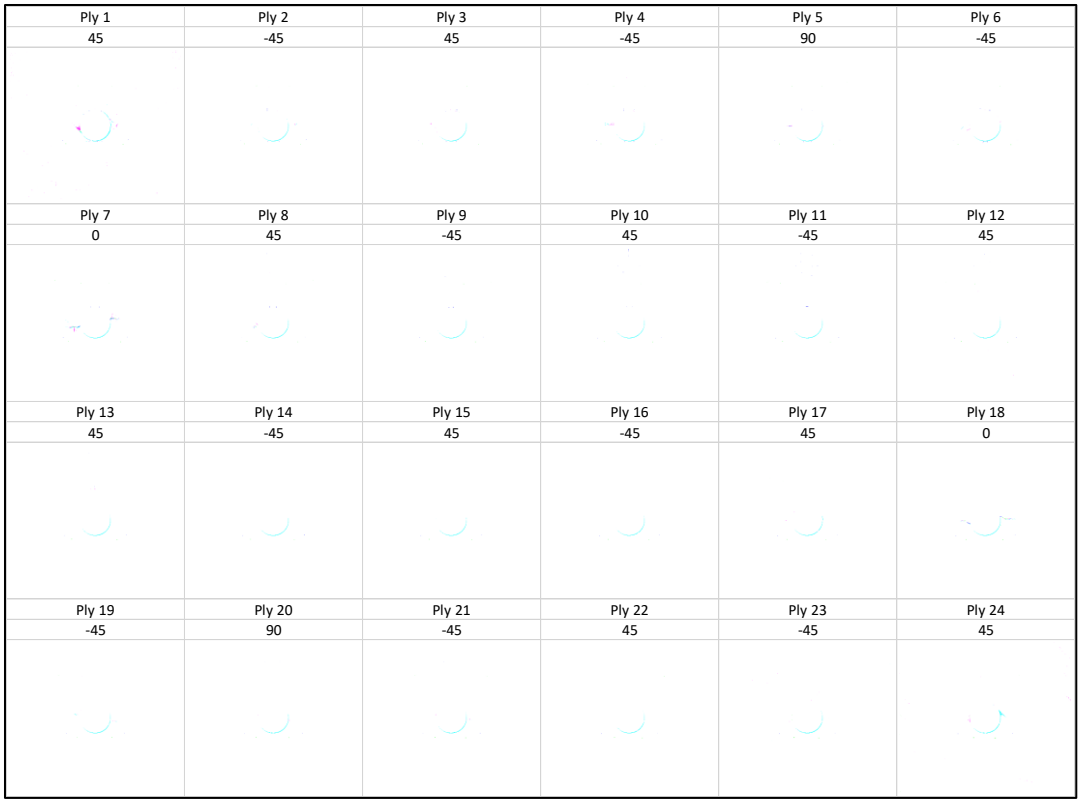
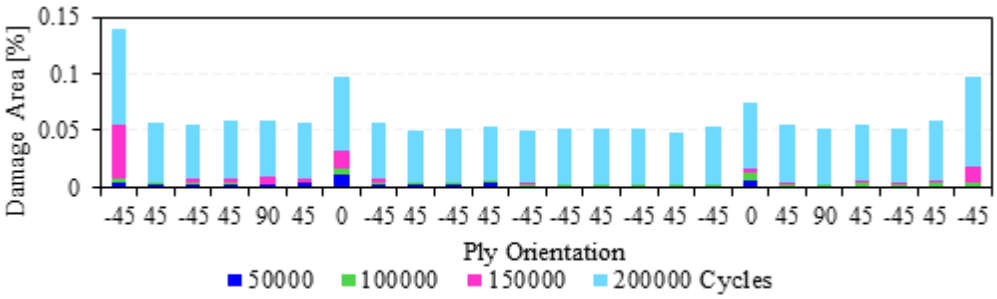


Figure B.125 – Ply-by-ply damage growth and area increase for IM7/5250-4, 10/80/10, R=5, SL1.

DISTRIBUTION STATEMENT A.
Approved for public release: distribution is unlimited.





Specimen ID	MASC1-A1FO11-XX2
Test Method	OHC-C
Material System	IM7 5250-4 UNI
Ply Layup	10/80/10
Number of Plies	24
Stress Ratio	5.0
% Stress	72.5% of Ultimate Stress
Final Cycles	292,567
1) Fiber failure extending horizontally from the hole in the 90º direction.	

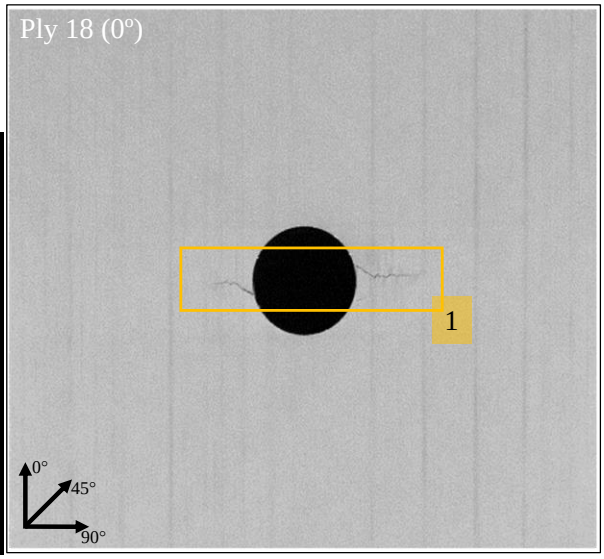
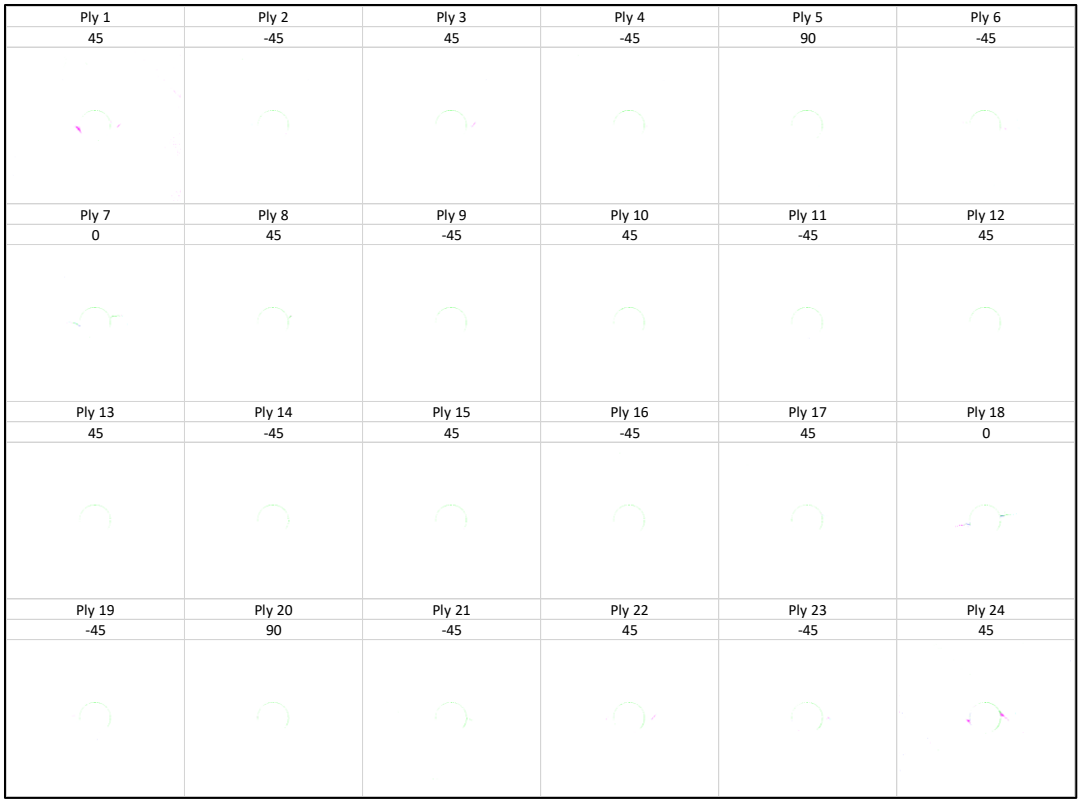
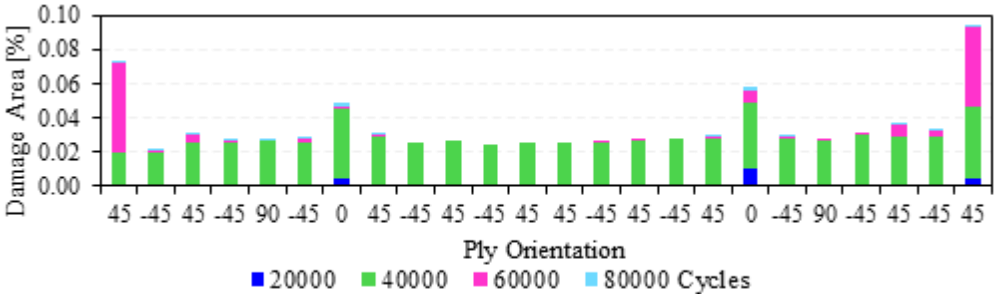


Figure B.126 – Ply-by-ply damage growth and area increase for IM7/5250-4, 10/80/10, R=5, SL2.

DISTRIBUTION STATEMENT A.
Approved for public release: distribution is unlimited.





Specimen ID	MASC1-A2FO11-XX1
Test Method	OHC-C
Material System	IM7 5250-4 UNI
Ply Layup	10/80/10
Number of Plies	24
Stress Ratio	5.0
% Stress	75% of Ultimate Stress
Final Cycles	99,110
1) Fiber failure extending horizontally from the hole in the 90º direction.	

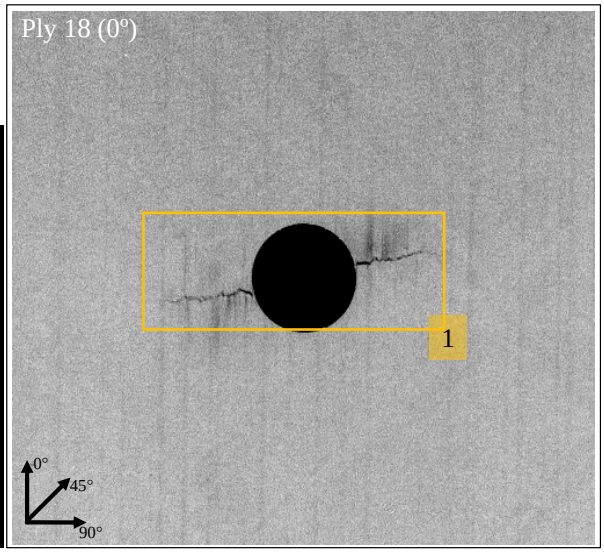


Figure B.127 – Ply-by-ply damage growth and area increase for IM7/5250-4, 10/80/10, R=5, SL3.

DISTRIBUTION STATEMENT A.
Approved for public release: distribution is unlimited.

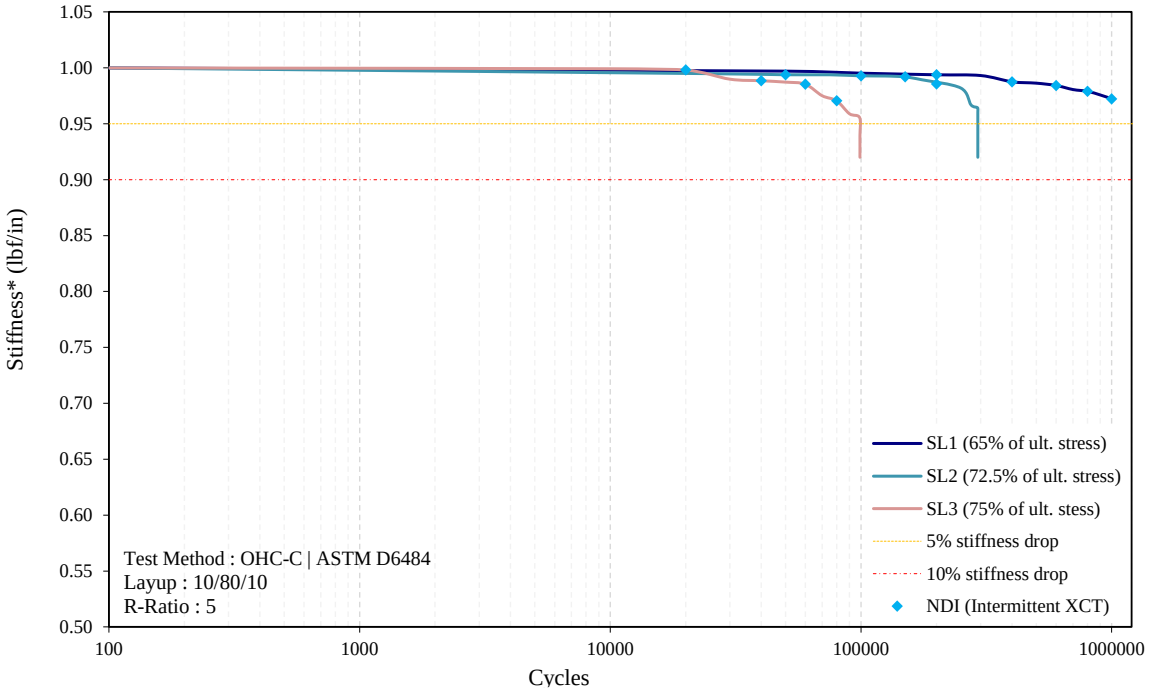
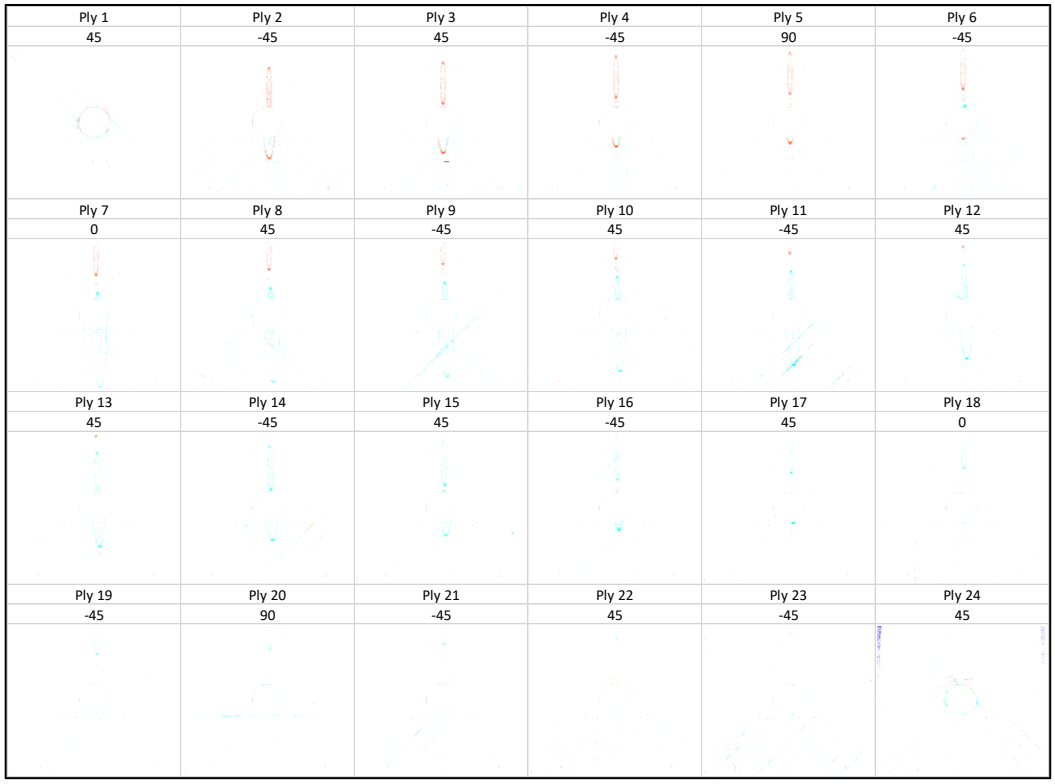
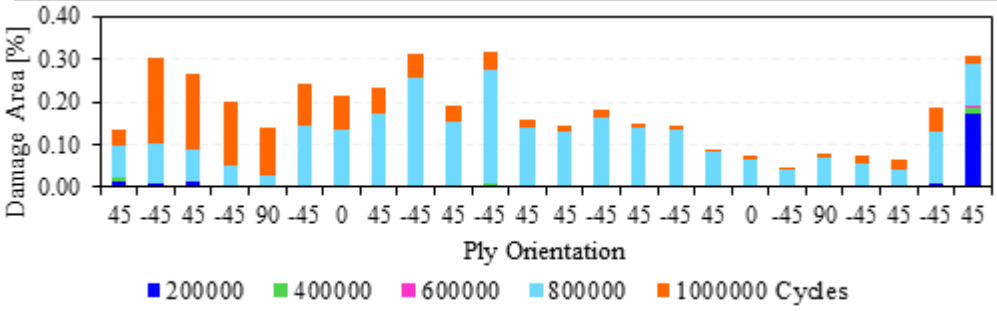


Figure B.128 – Apparent stiffness change during fatigue (normalized by initial compliance) for IM7/5250-4 UNI, 10/80/10 layup, OHC-C, R=5.

DISTRIBUTION STATEMENT A.
Approved for public release: distribution is unlimited.





Specimen ID	MASC1-A1FO11-1M1
Test Method	OHC-T
Material System	IM7 5250-4 UNI
Ply Layup	10/80/10
Number of Plies	24
Stress Ratio	-1.0
% Stress	35% of Ultimate Stress
Final Cycles	1,000,000 (runout)
1) Separation between the 45º fibers throughout the region near the hole.	
Comment) No significant damage after fatigue.	

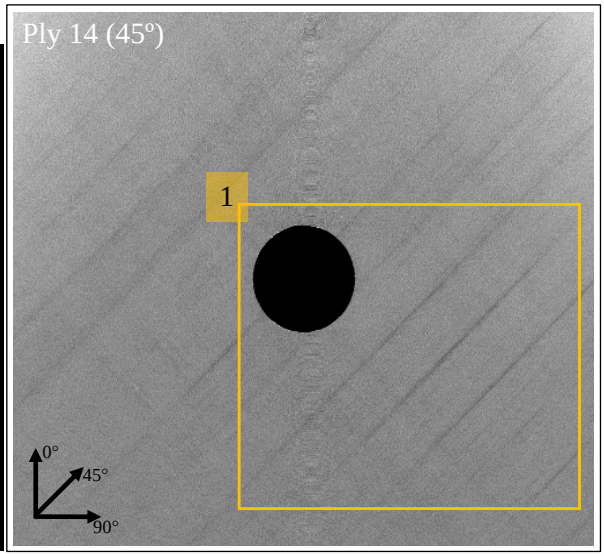
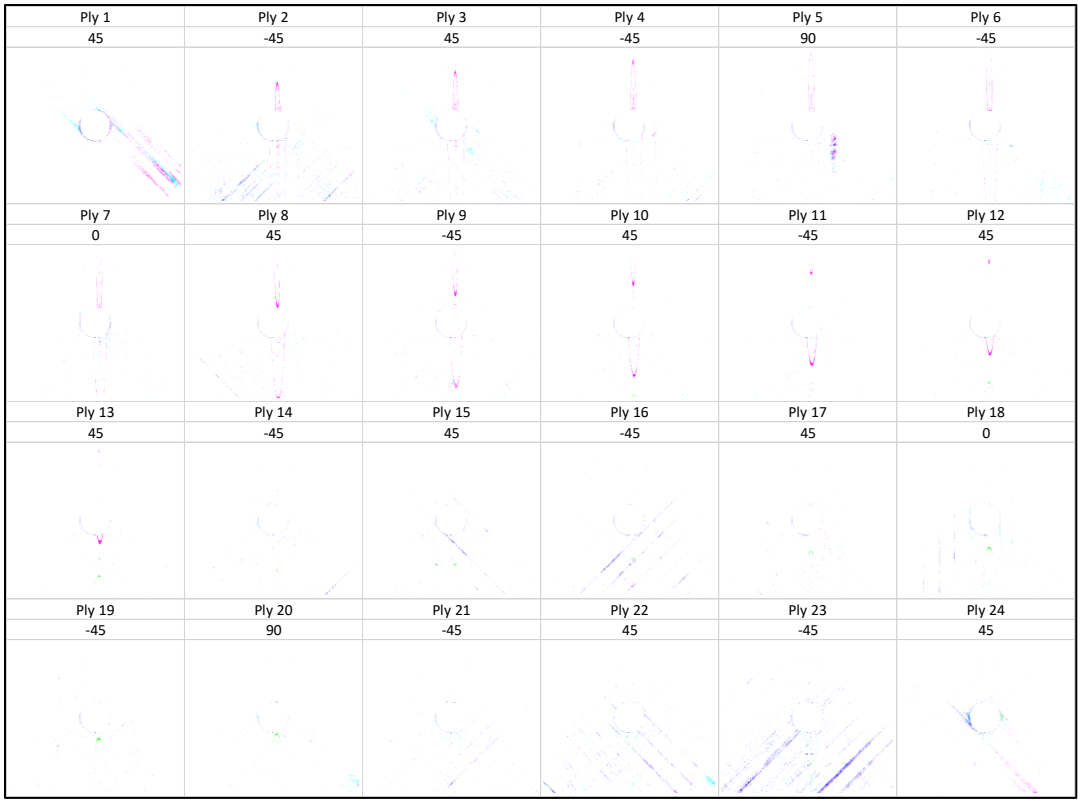
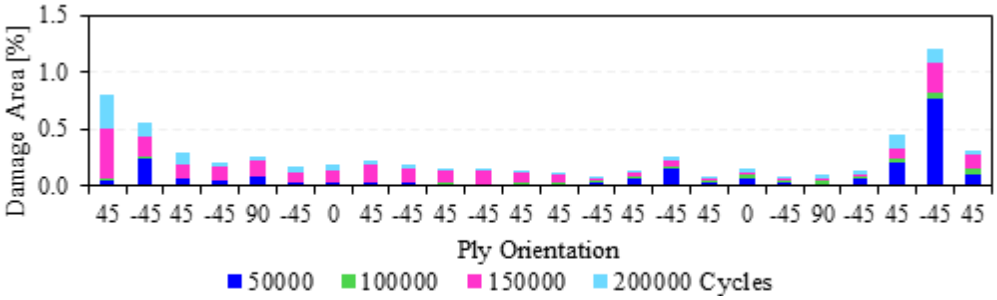


Figure B.129 – Ply-by-ply damage growth and area increase for IM7/5250-4, 10/80/10, R=-1, SL1.

DISTRIBUTION STATEMENT A.
Approved for public release: distribution is unlimited.





Specimen ID	MASC1-A2FO11-2M1
Test Method	OHC-T
Material System	IM7 5250-4 UNI
Ply Layup	10/80/10
Number of Plies	24
Stress Ratio	-1.0
% Stress	45% of Ultimate Stress
Final Cycles	226,324
1) Separation between the 45º fibers throughout the region near the hole.	
Comment) No significant damage after fatigue.	

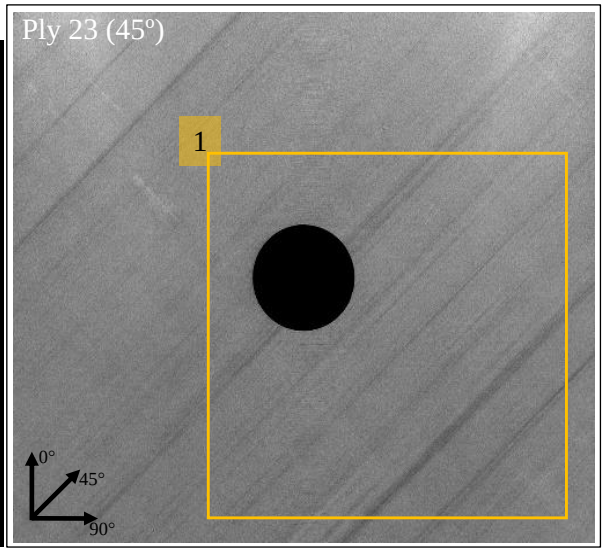
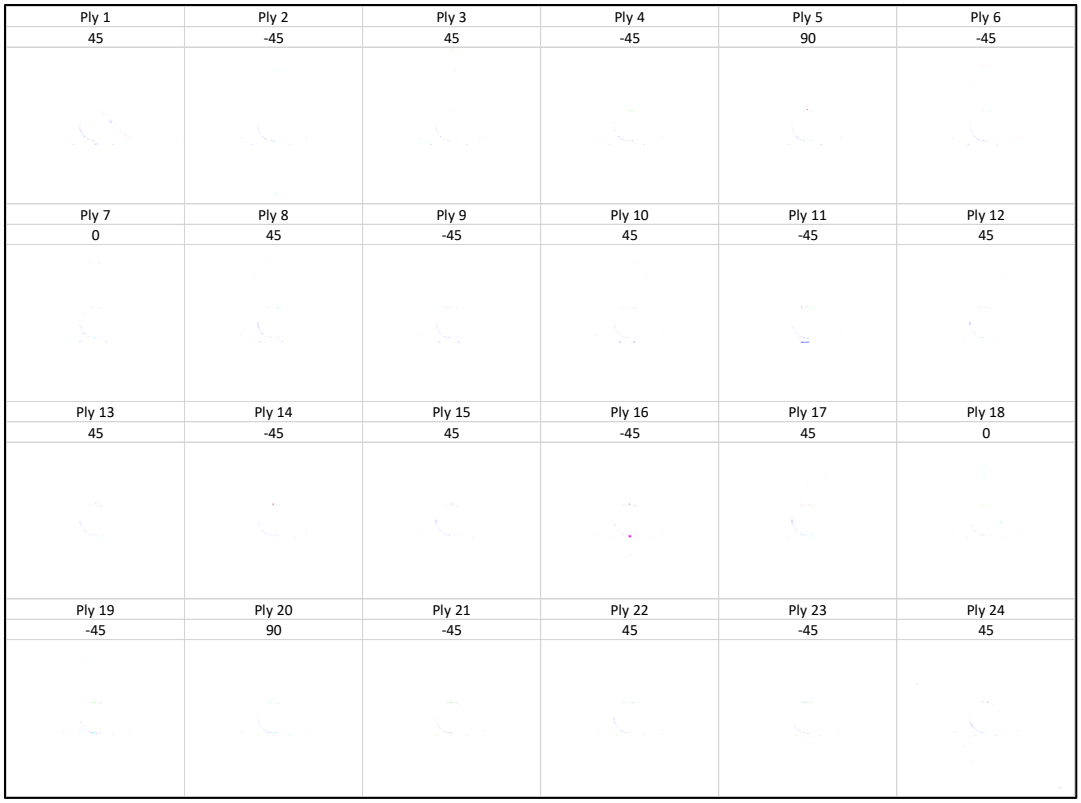
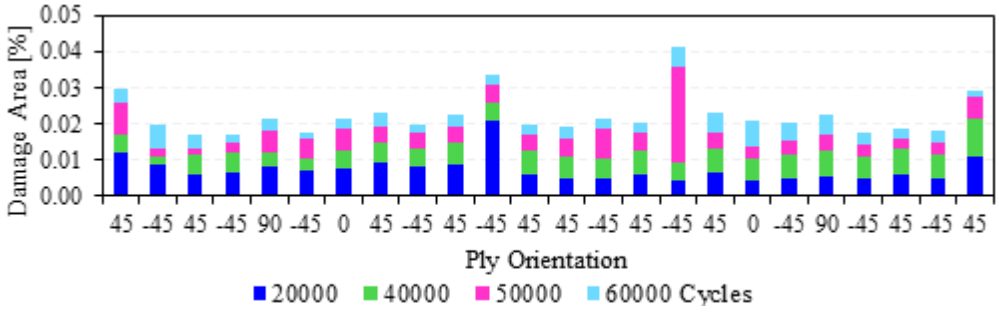


Figure B.130 – Ply-by-ply damage growth and area for IM7/5250-4, 10/80/10, R=-1, SL2.

DISTRIBUTION STATEMENT A.
Approved for public release: distribution is unlimited.





Specimen ID	MASC1-A3FO11-XX1
Test Method	OHC-T
Material System	IM7 5250-4 UNI
Ply Layup	10/80/10
Number of Plies	24
Stress Ratio	-1.0
% Stress	50% of Ultimate Stress
Final Cycles	68,544
1) Fiber failure extending horizontally from the hole in the 90º direction.	
2) Artifact from scanning processes.	

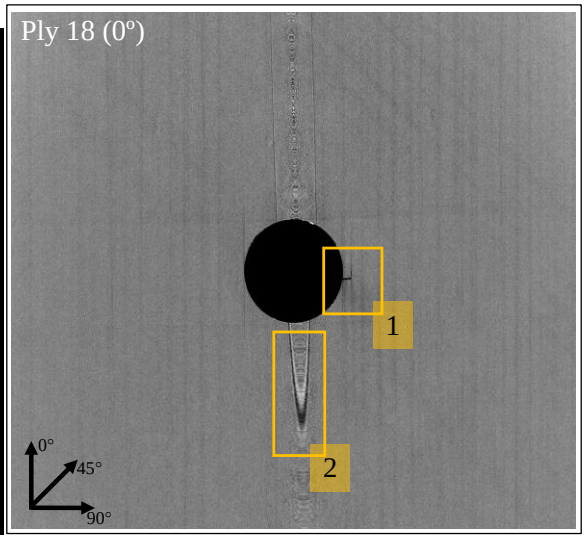


Figure B.131 – Ply-by-ply damage growth and area increase for IM7/5250-4, 10/80/10, R=-1, SL3.

DISTRIBUTION STATEMENT A.
Approved for public release: distribution is unlimited.

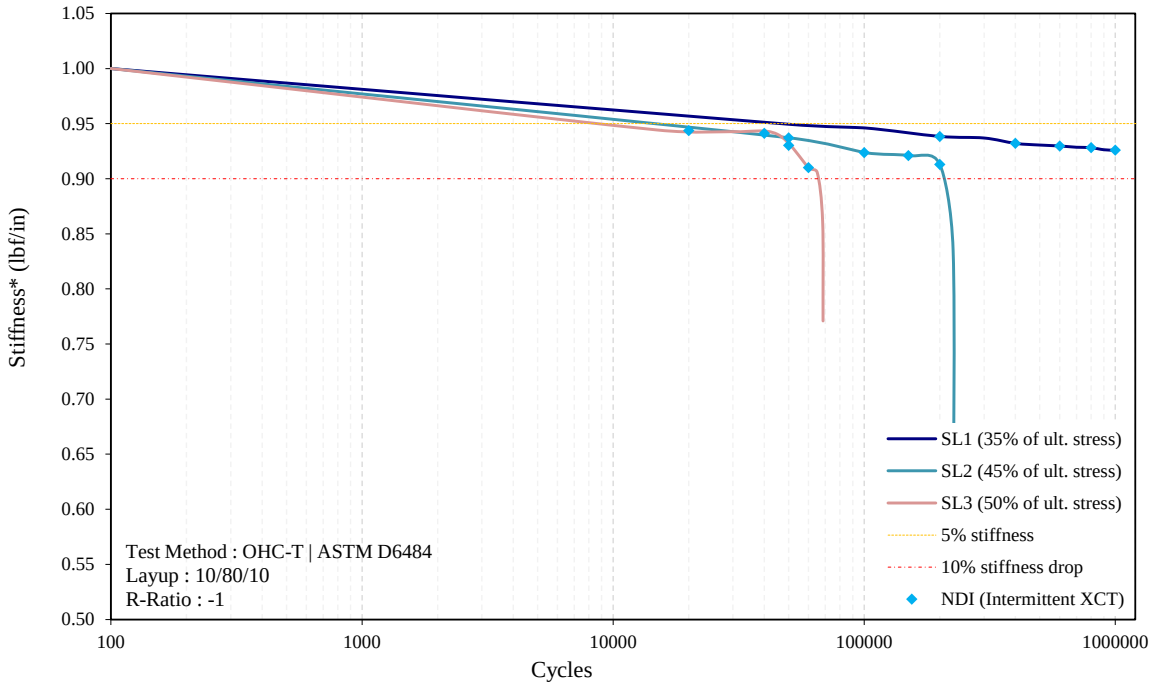


Figure B.132 – Apparent stiffness change during the tension fatigue (normalized by initial compliance) for IM7/5250-4 UNI, 10/80/10 layup, OHC-T, R=-1.

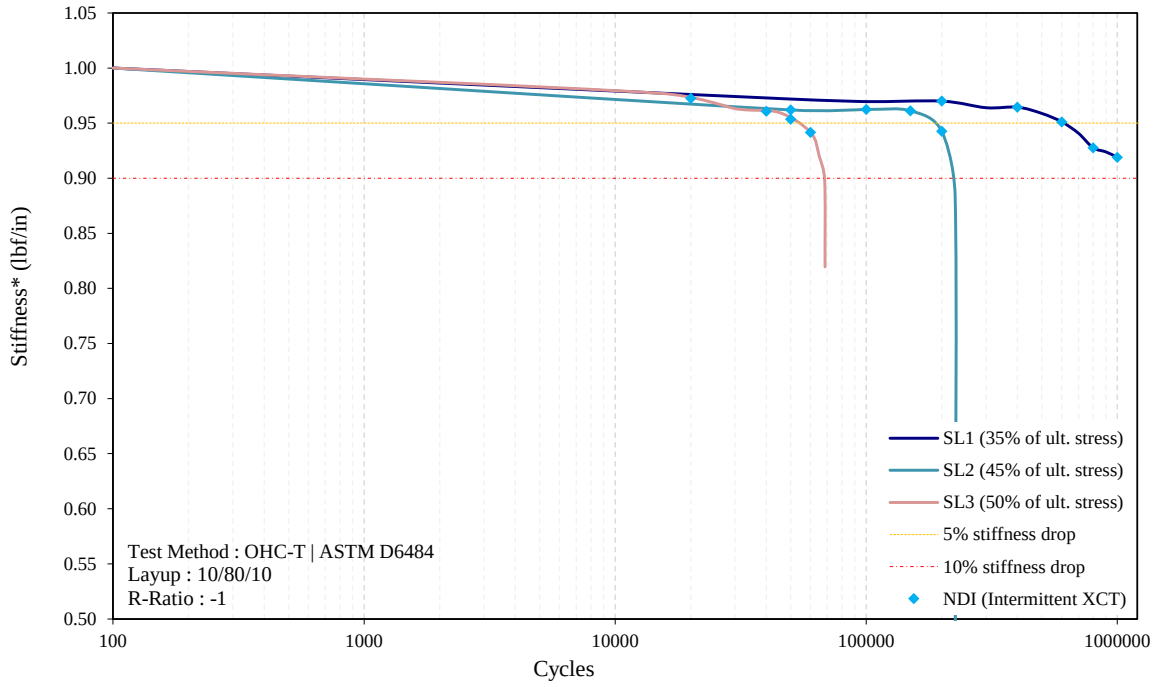


Figure B.133 – Apparent stiffness change during the compression fatigue (normalized by initial compliance) for IM7/5250-4 UNI, 10/80/10 layup, OHC-T, R=-1.

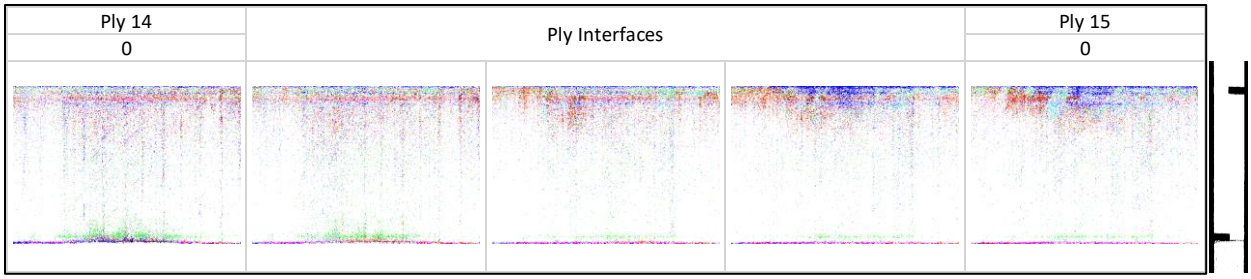
DISTRIBUTION STATEMENT A.
Approved for public release: distribution is unlimited.

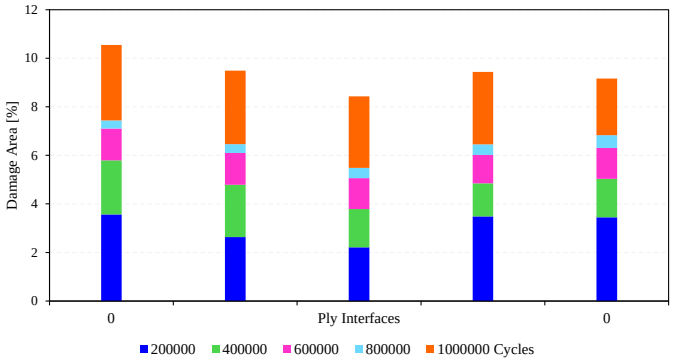
50/40/10 Double Notch Shear

R=0.1, OHT-T → Specimens: SL-1 (40%), SL-2 (45%), and SL-3 (50%)

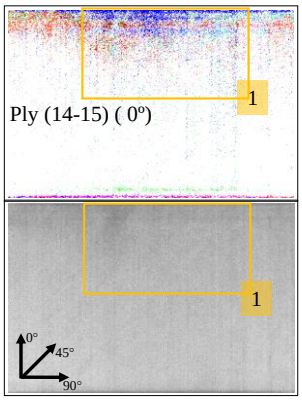
Three specimens were tested in R=0.1 at varying stress levels. Specimens were fatigued until failure or one-million cycles (runout) was achieved. For 50-40-10 only SL-1 survived fatigue and developed an average of 8% decreased residual strength. SL-1 displayed a large sheared area between the 14^{th} and 15^{th} plies with an uneven concentration of delamination opposite to the overcut notch (Figure B.134). SL-2 displayed a similar amount of sheared area, there was an uneven concentration of delamination opposite to the overcut notch (Figure B.135). SL-3 displayed a very concentrated region of delamination initiating from one notch, this specimen's notches were cut within tolerance, and were cut evenly (Figure B.136).

DISTRIBUTION STATEMENT A.
Approved for public release: distribution is unlimited.





Specimen ID	MASC1-A1DD11-1K2
Test Method	DNS
Material System	IM7 5250-4 UNI
Ply Layup	50/40/10
Number of Plies	24
Stress Ratio	0.1
% Stress	40% of Ultimate Stress
Final Cycles	1,000,000 (runout)
Failure Mode	SHEAR
1) Sheared area on the 45° ply near the notch on one side.	
2) The notch was overcut, stress was not concentrated in the designed shear plane.	



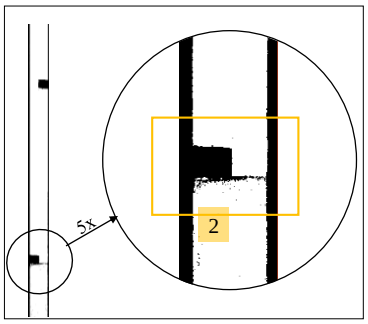
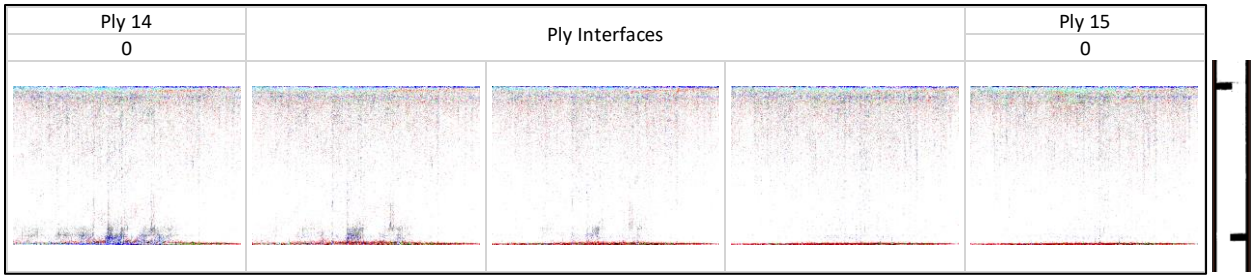
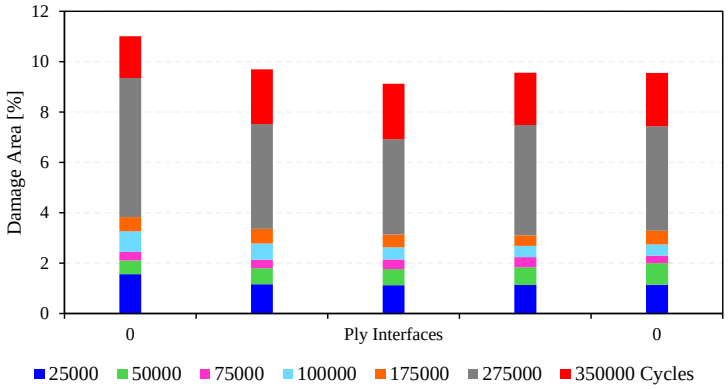


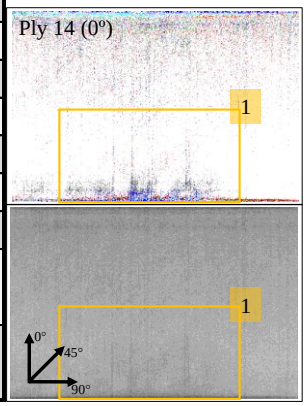
Figure B.134 – Shear gauge damage growth and area increase for IM7/5250-4, 50/40/10, R=0.1, SL1.

DISTRIBUTION STATEMENT A.
Approved for public release: distribution is unlimited.





Specimen ID	MASC1-A2DD11-2K2
Test Method	DNS
Material System	IM7 5250-4 UNI
Ply Layup	50/40/10
Number of Plies	24
Stress Ratio	0.1
% Stress	45% of Ultimate Stress
Final Cycles	392,877
Failure Mode	SHEAR
1) Damaged area in this region was uneven, most likely due to the overcut notch.	
2) The notch was overcut, stress was not concentrated in the designed shear plane.	



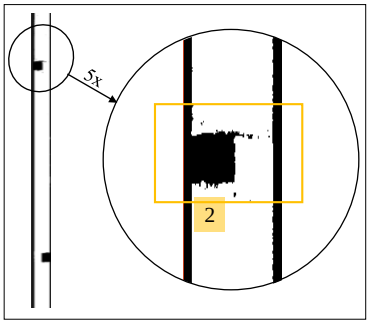
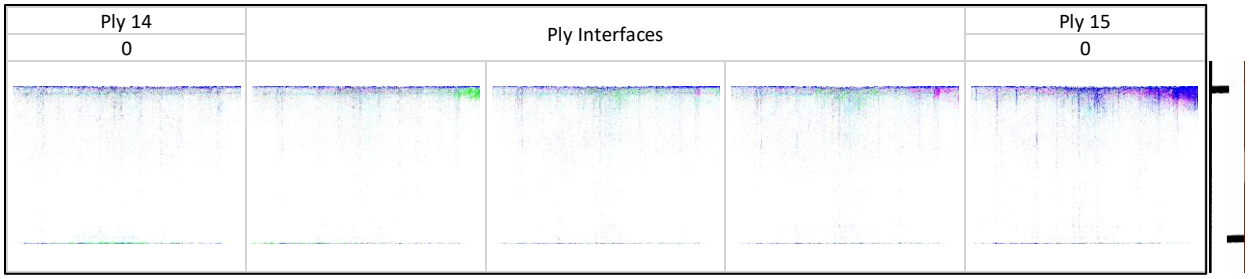
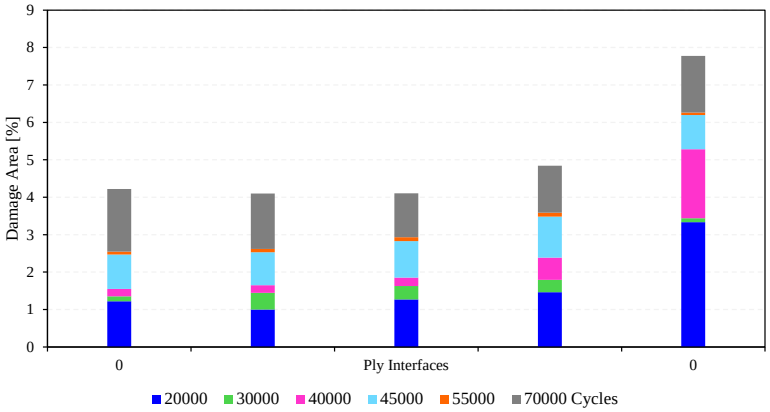


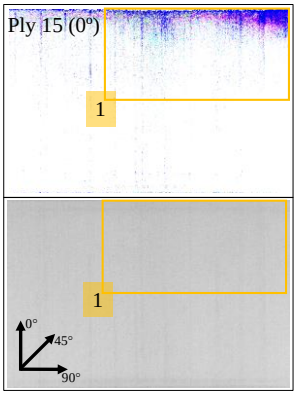
Figure B.135 – Shear gauge damage growth and area increase for IM7/5250-4, 50/40/10, R=0.1, SL2.

DISTRIBUTION STATEMENT A.
Approved for public release: distribution is unlimited.





Specimen ID	MASC1-A3DD11-3K2
Test Method	DNS
Material System	IM7 5250-4 UNI
Ply Layup	50/40/10
Number of Plies	24
Stress Ratio	0.1
% Stress	50% of Ultimate Stress
Final Cycles	63,250
Failure Mode	SHEAR
1) Majority of sheared area initiated from only one notch.	
2) The notch was cut adequately.	



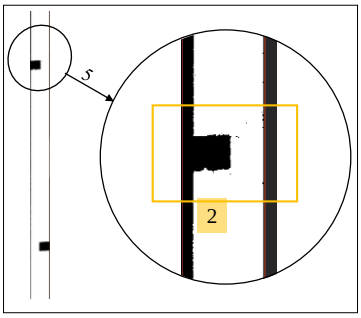


Figure B.136 – Shear gauge damage growth and area increase for IM7/5250-4, 50/40/10, R=0.1, SL3.

DISTRIBUTION STATEMENT A.
Approved for public release: distribution is unlimited.

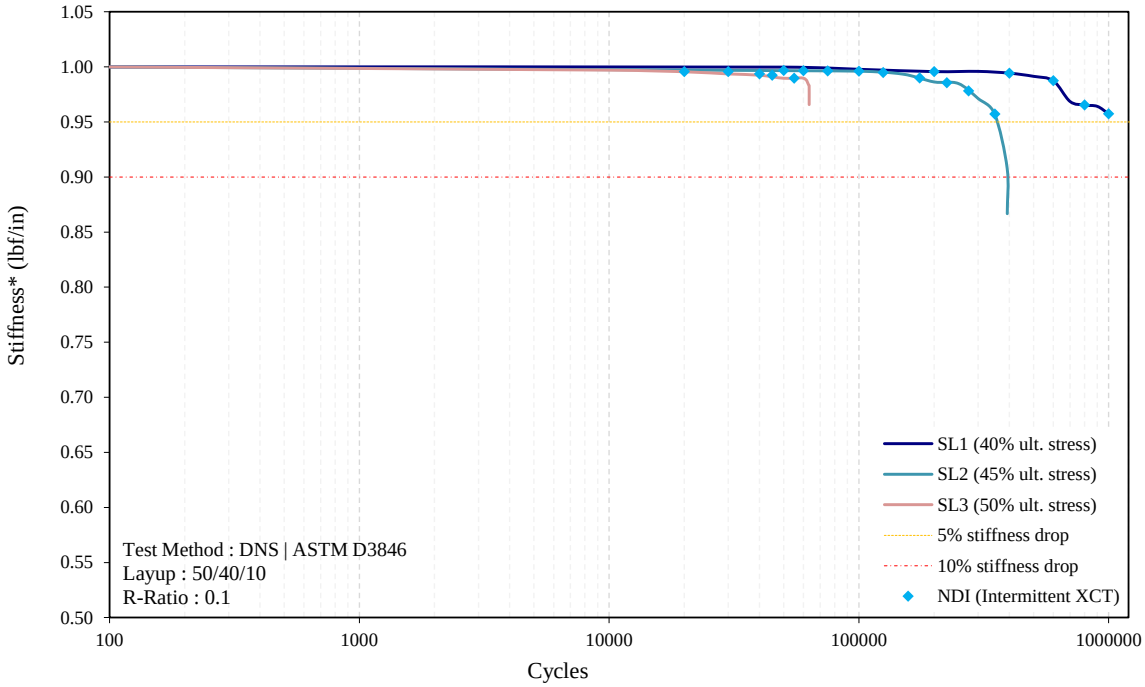


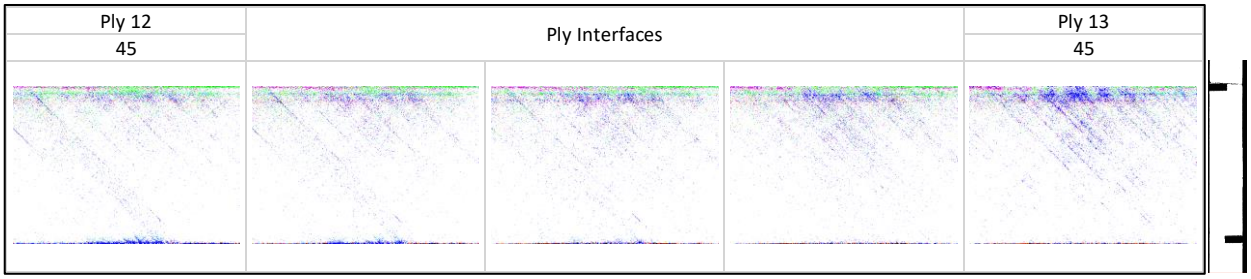
Figure B.137 - Apparent stiffness change during fatigue (normalized by initial compliance) for IM7 5250-4 UNI, 50/40/10 layup, DNS, R= 0.1.

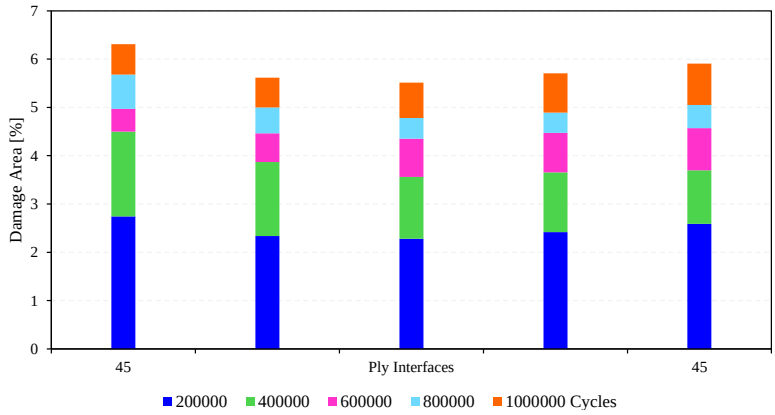
10/80/10 Double Notch Shear

R=0.1, OHT-T → Specimens: SL-1 (45%), SL-2 (50%), and SL-3 (55%)

Three specimens were tested in R=0.1 at varying stress levels. Specimens were fatigued until failure or one-million cycles (runout) was achieved. For 10-80-10 only SL-1 survived fatigue and developed an average of 2% decreased residual strength. SL-1 displayed the majority of its sheared area closest to the notch that exhibits signs of being overcut (Figure B.138). SL-2 again displayed the majority of its sheared area closest to the notch that was overcut (Figure B.139). SL-3 was cut evenly and displayed no signs of being overcut, delamination in the gauge area uniquely began from both notches (Figure B.140).

DISTRIBUTION STATEMENT A.
Approved for public release: distribution is unlimited.





Specimen ID	MASC1-A1FD11-1K2
Test Method	DNS
Material System	IM7 5250-4 UNI
Ply Layup	10/80/10
Number of Plies	24
Stress Ratio	0.1
% Stress	45% of Ultimate Stress
Final Cycles	1,000,000 (runout)
Failure Mode	Shear
1) Damage within the 45° ply near the notch on one side.	
2) The notch was overcut, stress was not concentrated in the designed shear plane.	

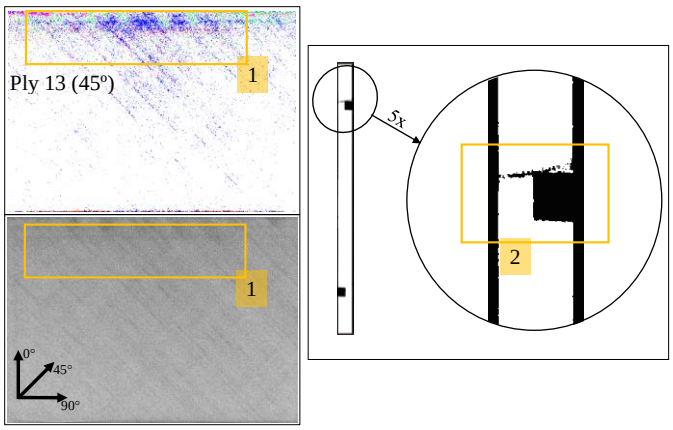
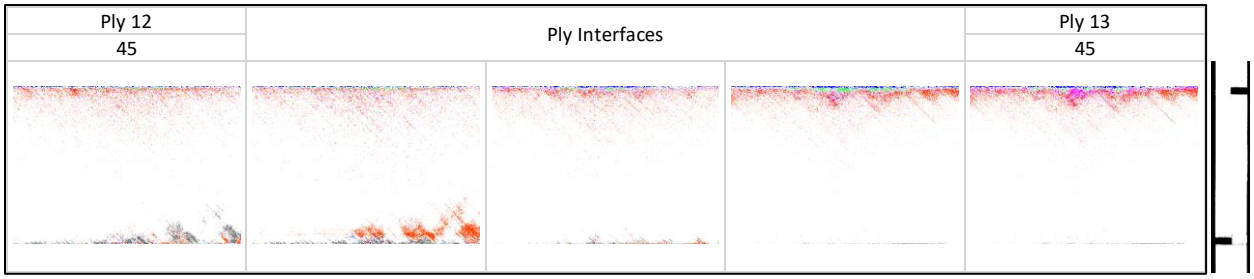
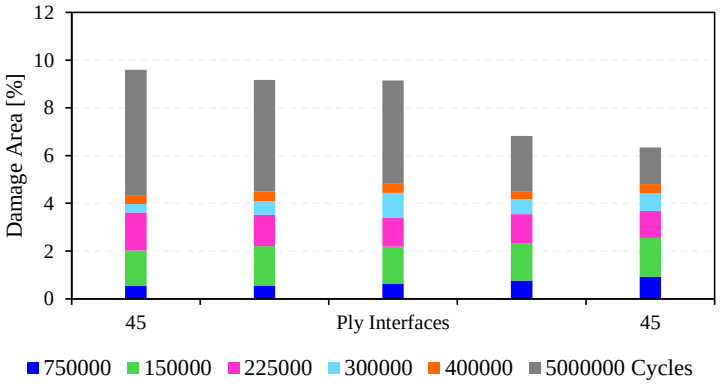


Figure B.138 – Shear gauge damage growth and area increase for IM7/5250-4, 10/80/10, R=0.1, SL1.

DISTRIBUTION STATEMENT A.
Approved for public release: distribution is unlimited.





Specimen ID	MASC1-A3FD11-3K2
Test Method	DNS
Material System	IM7 5250-4 UNI
Ply Layup	10/80/10
Number of Plies	24
Stress Ratio	0.1
% Stress	50% of Ultimate Stress
Final Cycles	501,674
Failure Mode	SHEAR
1) Increased signs of shear near the overcut notch.	
2) The notch was overcut, stress was not concentrated in the designed shear plane.	

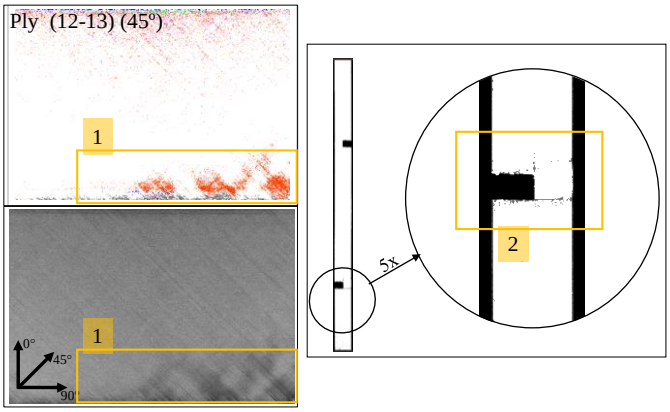
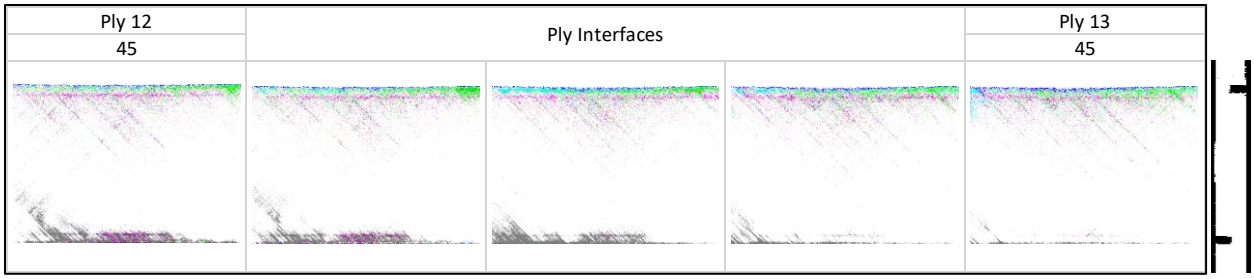
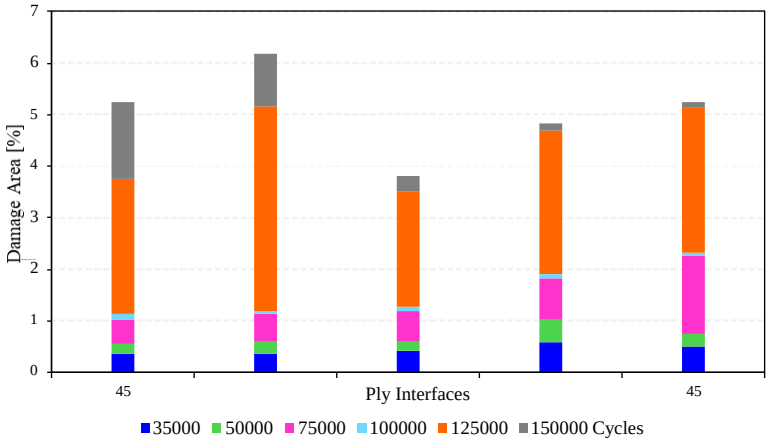


Figure B.139 – Shear gauge damage growth and area increase for IM7/5250-4, 10/80/10, R=0.1, SL2.

DISTRIBUTION STATEMENT A.
Approved for public release: distribution is unlimited.





Specimen ID	MASC1-A2FD11-2K2
Test Method	DNS
Material System	IM7 5250-4 UNI
Ply Layup	10/80/10
Number of Plies	24
Stress Ratio	0.1
% Stress	55% of Ultimate Stress
Final Cycles	162,259
Failure Mode	SHEAR
1) Signs of shearing initiated from the notches extending inwards.	
2) The notch was cut adequately.	

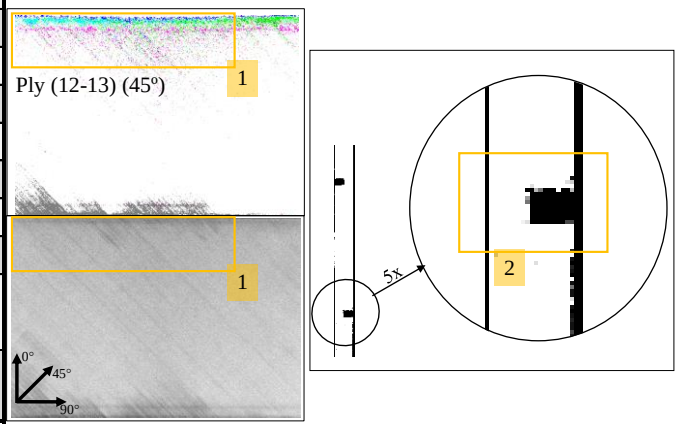


Figure B.140 – Shear gauge damage growth and area increase for IM7/5250-4, 10/80/10, R=0.1, SL3.

DISTRIBUTION STATEMENT A.
Approved for public release: distribution is unlimited.

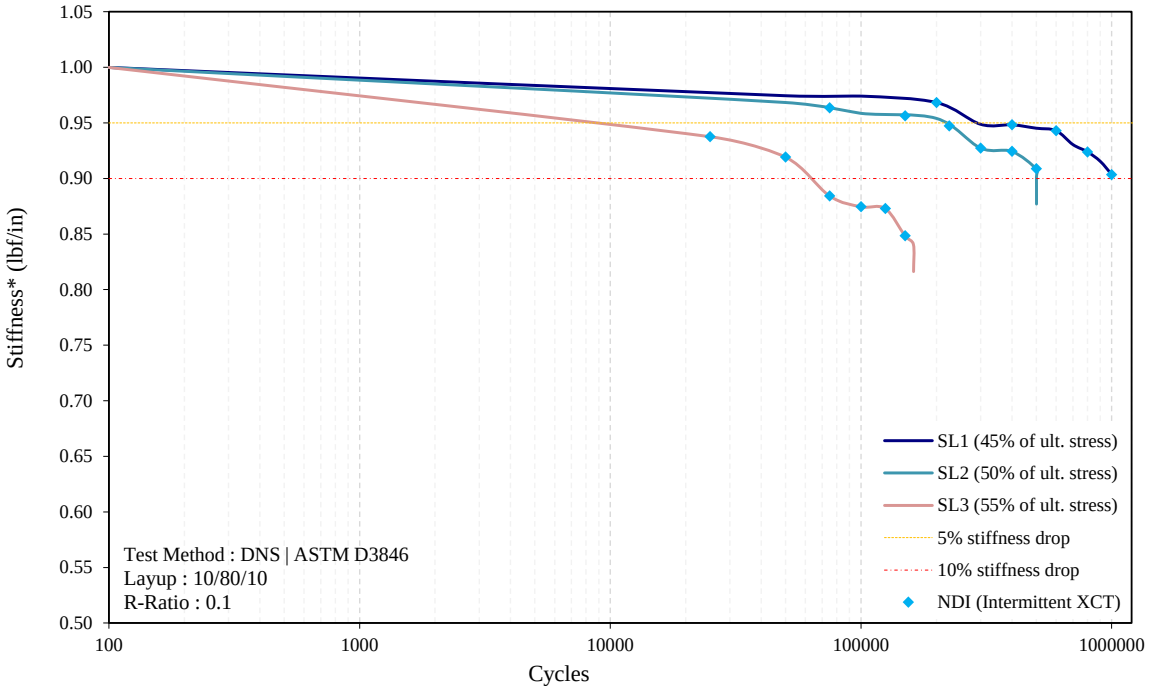


Figure B.141 – Apparent stiffness change during fatigue (normalized by initial compliance) for IM7 5250-4 UNI, 10/80/10 layup, DNS, R= 0.1.

DISTRIBUTION STATEMENT A.
Approved for public release: distribution is unlimited.

LIST OF SYMBOLS, ABBREVIATIONS, AND ACRONYMS

AFRL	Air Force Research Laboratory
AGATE	Advanced General Aviation Transport Experiments
AMCSC	Advanced Material Characterization and Structural Certification
AMIS	Automated Microscopic Inspection System
ASTM	American Society for Testing and Materials
BBT	Building-Blocks of Testing
BMI	Bismaleimide
BSAM	B-Spline Analysis Method
CAI	Compression after Impact
CBS	Curved Beam Strength
CDFS	Compression-Dominant Fatigue Spectrum
CFRP	Carbon Fiber-Reinforced Polymer
CMC	Ceramic Matrix Composites
CT	Computed Tomography
CTE	Coefficient of Thermal Expansion
CV	Coefficient of Variation
DaDT	Durability and Damage Tolerance
DIC	Digital Image Correlation
DLT	Design Lifetime
DMA	Dynamic Mechanical Analysis
DNS	Double-Notch Shear
DOD	Department of Defense
DSC	Differential Scanning Calorimetry
DSG	Design Service Goal
DSS	Deferred Severity Spectrum
EPC	Extended Post-Cure
FAA	Federal Aviation Administration
ILT	Interlaminar Tension
IW	Individual Weibull
JAMS	Joint Advanced Materials and Structures Center of Excellence
JW	Joint Weibull
LEF	Load-Enhancement Factor
LF	Load Factor
LOV	Limit of Validity
MASC	Modeling for Affordable, Sustainable Composites
MED	Multiple Element Damage
MLE	Maximum Likelihood Estimation
MLSP	Modal Life Shape Parameters
MSD	Multiple Site Damage

DISTRIBUTION STATEMENT A.
Approved for public release: distribution is unlimited.

MSSP	Modal Static Shape Parameter
MTS	Material Test Systems
NASA	National Aeronautics and Space Administration
NCAMP	National Center for Advanced Materials Performance
NCAT	National Center for Aviation Training
NDI	Nondestructive Inspection
NIAR	National Institute for Aviation Research
OEM	Original Equipment Manufacturer
OH	Open Hole
OHC	Open-Hole Compression
OHC-C	Open-Hole Compression-Compression
OHC-T	Open-Hole Compression-Tension
OHT	Open-Hole Tension
OHT-T	Open-Hole Tension-Tension
PDA	Progressive Damage Growth Analysis
PTFE	Polytetrafluoroethylene
RRX	Rank Regression in X
RS	Residual Strength
RTD	Room-Temperature Dry
RXCC	Composites Branch, Structural Materials Division, Materials and Manufacturing Directorate
Rx-FEM	Regularized Extended Finite Element Methodology
S	Sendeckyj
SACC	Scatter Analysis Computer Code
SBS	Short-Beam Shear
SL	Stress Level
SN	Stress to Number of Cycles
ST	Strength Tracking
TC	Type Certificate
TDFS	Tension-Dominant Fatigue Spectrum
Tg	Glass Transition Temperature
TTU	Through-Transmission Ultrasonic
UNI	Unidirectional Layup
UT	Ultrasonic Testing
V&V	Verification and Validation
WFD	Widespread Fatigue Damage
WSU	Wichita State University
XCT	X-Ray Computed Tomography

DISTRIBUTION STATEMENT A.
Approved for public release: distribution is unlimited.